Dissertation zur Erlangung des Doktorgrades
der Fakultät für Chemie und Pharmazie
der Ludwig-Maximilians-Universität München

Size-Induced Rate Accelerations in Organocatalysis

Benjamin Pölloth

aus Neumarkt i. d. Opf., Deutschland

2020

Erklärung

Diese Dissertation wurde im Sinne von § 7 der Promotionsordnung vom 28. November 2011 von Herrn Prof. Dr. Hendrik Zipse betreut.

Eidesstattliche Versicherung

Diese Dissertation wurde eigenständig und ohne unerlaubte Hilfe erarbeitet.

München, 11.09.2020

....
Benjamin Pölloth

Dissertation eingereicht am 17.07.2020

1. Gutachter: Prof. Dr. Hendrik Zipse

2. Gutachter: Prof. Dr. Burkhard König

Mündliche Prüfung am 08.09.2020

Acknowledgment

List of publications

Parts of this thesis have been published as follows:

Marta Marín-Luna[‡], Benjamin Pölloth[‡], Fabian Zott, and Hendrik Zipse* "**Size-dependent rate acceleration in the silylation of secondary alcohols: the bigger the faster**" *Chem. Sci.*, **2018**, *9*, 6509 – 6515.

Benjamin Pölloth, Ieva Teikmane, Stefan Schwarzer, Hendrik Zipse* "**Development of a Modular Online Video Library for the Introductory Organic Chemistry Laboratory**" *J. Chem. Ed.,* **2020**, *97*, 338 – 343.

Benjamin Pölloth, Stefan Schwarzer, Hendrik Zipse* "**Student Individuality Impacts Use and Benefits of an Online Video Library for the Organic Chemistry Laboratory**" *J. Chem. Ed.,* **2020**, *97*, 328 – 337.

Benjamin Pölloth, Mukund P. Sibi, and Hendrik Zipse* "**The Size-Accelerated Kinetic Resolution of Secondary Alcohols**" *Angewandte Chemie International Edition,* **2020**, *in review. Manuscript ID: 202011687.*

[‡]Authors declare equal contribution; *corresponding author.

Table of Contents

x

This thesis comprises two main parts:

Part I: Size-Induced Rate Accelerations in Organocatalysis.

Experimental and theoretical physical-organic studies.

Part II: An Online Video Library for the Organic Chemistry Laboratory.

Empirical studies.

Summary

Steric effects through sizeable moieties are commonly attributed to be mainly repulsive in organic chemistry. However, the size of molecules also significantly influences the strength of dispersion forces. Transition state theory implicates that reaction rates should be accelerated if the transition state is stabilized, e.g. through dispersion energy. Thus, in here the influence of large aromatic moieties on the reaction rates of several organocatalysed protecting group reactions is investigated.

Chapter 2. Chemoselectivity in the Silylation of Aliphatic and Aromatic Alcohols.

Competition experiments of aromatic and aliphatic alcohols in the uncatalysed and Lewis base-catalysed silylation of primary and secondary alcohols were studied. While aromatic alcohols were found to react notably faster than comparable aliphatic alcohols with aromatic silyl chlorides, further variation of substrates and a correlation with computed reaction free energies indicate that relative rates are mainly dominated by the presence of unfavourable γ-CH-bonds. Smaller dispersion-related accelerations were observed. However, the model system was found to be not suitable for quantitative investigation of dispersive interactions, while the comparison of substrates with aromatic moieties of increasing size seems more promising as their structural geometry is retained.

Chapter 3. Size-Dependent Rate Acceleration in the Silylation of Secondary Alcohols: the Bigger the Faster.[1]

Relative rates for the reaction of secondary alcohols carrying large aromatic moieties with silyl chlorides carrying equally large substituents have been determined in organic solvents. Introducing matching pairs of big dispersion energy donor (DED) groups enhanced rate constants up to four times, notably depending on the hydrogen bond donor ability of the solvent. A linear correlation between computed dispersion

energy contributions to the stability of the silyl ether products and experimental relative rate constants was found. These results indicate a cooperation between solvophobic effects and DED-groups in the kinetic control of silylation reactions.
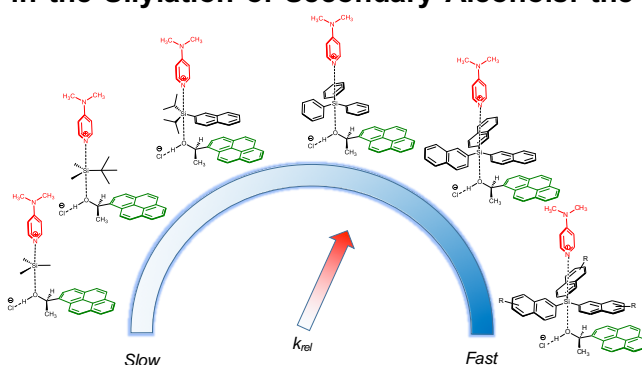
Chapter 4. Rate Accelerations in the Lewis Acid-Catalysed Hydrosilylation of Ketones.
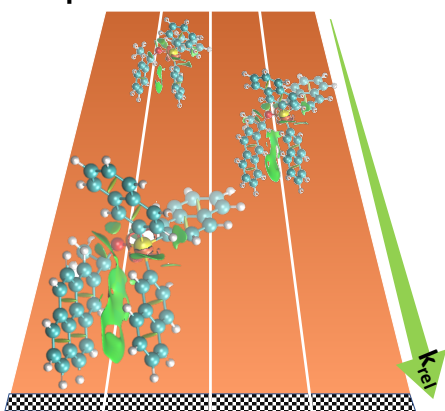
Are the observed rate accelerations in the silylation of secondary alcohols specific for this reaction type or rather a general phenomenon? To investigate this question, size-effects were also studied for the hydrosilylation of ketones by Lewis acid $B(C_6F_5)_3$. This reaction type yields the same products as the silylation of alcohols, but substrates and catalysts are from different compound classes. Indeed, relative rates were accelerated through the introduction of sizeable groups by a factor of up to four. The choice of the solvent was found to be critical for the extent of these size-effects. The crucial but hardly predictable role of solvents remains thus the major challenge to make use of attractive interaction in a targeted manner for selective reactions. A correlation of experimental relative rates and stabilization of reaction products by computed

---

dispersion contributions was found. This supports the hypothesis, that increasing molecule moieties can generally accelerate reactions through stabilizing dispersive interactions.

Chapter 5 and 6. The Size-Accelerated Kinetic Resolution of Secondary Alcohols.[2]
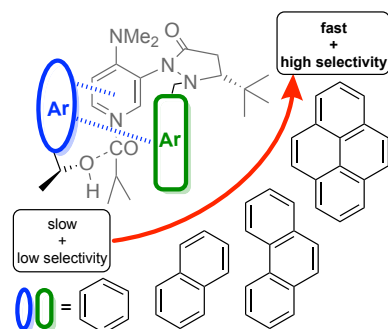
The selectivity of kinetic resolution (KR) experiments may either result from accelerating the transformation of the major enantiomer through attractive non-covalent interactions (NCIs), or from retarding the transformation of the minor isomer through repulsive steric forces. The investigation of size-effects in the silylation based KR of secondary alcohols was found to be difficult due to the proposed transition state structure. Thus, the factors responsible for the acylation-based KR by chiral pyridine derivatives were elucidated by measurements of relative rates for a set of substrates of systematically increasing size using accurate competitive linear regression analyses. Increasing the side chain size from phenyl to pyrenyl results in a rate acceleration of more than 40 for the major enantiomer. Based on this observation a new catalyst with increased steric bulk has been designed that gives enantioselectivity values of up to $s = 250$. Extensive conformational analysis of the relevant transition states indicates that alcohol attack to the more crowded side of the acyl-catalyst intermediate is favoured due to stabilizing CH-π interactions. Experimental and theoretical results imply that enantioselectivity enhancements result from accelerating the transformation of the major enantiomer through attractive NCIs rather than retarding the transformation of the minor isomer through repulsive steric forces.

Chapter 8 and 9. Empirical Studies on an Online Video Library for the Organic Chemistry Laboratory.[3]

A modular and target-group oriented online video library with 48 videos was developed and produced in order to reduce the complexity of an introductory organic chemistry laboratory class. The library comprises three different types of videos: "Tutorials" explaining fundamental laboratory techniques, "Don'ts" pointing students in a humorous way to typical mistakes, and videos demonstrating complete syntheses in a "Step-by-Step" fashion. The principles, development, production, and presentation of this video library are described. The online video library was used intensively by bachelor-level students before and throughout an introductory organic chemistry laboratory course, when presented and assigned to the experiments appropriately. An empirical study ($N = 103$) revealed that the utilization of videos and preferences for video types depend crucially on individual student characteristics, such as gender, study course, intrinsic motivation, and the self-perception of conscientiousness. Student assessment of the video library, a positive impact on students' self-concept of ability, and an increase of knowledge in know-how tests on laboratory techniques of up to 100% indicate the benefits of the online video library on students' cognitive, affective, and psychomotor learning in a laboratory course.

[2] Submitted to *Angewandte Chemie International Edition* with manuscript ID 202011687 (© 2020 Wiley VCH).
[3] Reprinted with permission from *J. Chem. Ed.,* **2020**, *97*, 338 – 343 and *J. Chem. Ed.,* **2020**, *97*, 328 – 337. Copyright (2020) American Chemical Society.

Part I: Size-Induced Rate Accelerations in Organocatalysis.

Experimental and theoretical physical-organic studies.

Chapter 1. Introduction

1.1. Non-Covalent Interactions

Without non-covalent interactions (NCIs) neither condensed phase would exist nor life would be possible as – for example – the structure and function of DNA and proteins crucially depend on NCIs.[1] In general, all interactions between atoms and molecules – covalent as well as non-covalent – originate in a single fundamental force, the electromagnetic force.[2] While covalent bonds arise from the electromagnetic attraction of atoms sharing electrons, NCIs do not involve shared electrons and are therefore in general much weaker. Nonetheless, the accumulation of weak forces results in significant attractive interactions notably depending on the size of a molecule. Despite these facts, the influence of sizeable groups, that is steric effects, are often understood as purely repulsive.[3] The attractive component, in contrast, was largely overlooked in organic chemistry.[4] Hence, this thesis describes investigations on how far attractive steric effects can accelerate organocatalysed reactions.

1.1.1. Dispersion Forces

In the 1870s, van der Waals already discovered that real gases show a different behaviour than it would be expected for ideal gases. Based on these findings he postulated – in a time where it was not even commonly accepted that matter is built from particles – attractive forces between all types of atoms or molecules including non-polar species and rare gases.[1, 5] While attractive forces of dipole molecules with each other, ions or induced dipoles were easily rationalized by matters of electromagnetic attractions, for weakly- or non-polar substances the origin of this attraction was much more controversial. Debye[6] proposed 1920 that every molecule can be polarized through the contact with a dipole molecule. While dipole-dipole forces can be both, repulsive or attractive depending on the orientation of the dipole moments to each other, the resulting force of induced dipoles and inducing dipoles is always attractive. The strength of these forces notably depend on the polarizability of involved molecules.[6] However, the gas phase behaviour of non-polar molecules implicated some kind of attractive forces. Due to the lack of a better explanation, a quadrupole moment was proposed for all kinds of atoms and molecules.[7] This hypothesis was eventually disproved by wave mechanics. For example, the quadrupole moment of the hydrogen molecule is way too small to explain the experimentally measured attractive forces and for noble gases no dipole or quadrupole moment was found at all.[7] It was the development of quantum mechanics, that allowed Fritz London to describe these forces in a comprehensive manner. London described that due to the zero-point motion of every system, electron distribution within a molecule varies in every instance leading to temporarily dipoles. The generated electric field of these instantaneous dipoles then induces other dipoles and attractive interactions arise that London called dispersion force.[7-8] Due to these important findings, the attractive component of van der Waals interactions is

known nowadays as "London dispersion".[9] Feynman eventually refined that not the attraction of the two temporary dipoles results in attractive forces, "but rather the attraction of each nucleus for the distorted charge distribution of its *own* electrons."[10] Thus, the origins of London dispersion forces can also be understood in analogy to covalent bonds as accumulation of electron density between attracted nuclei in a bond critical point.[11] However, their strength depends on the distance R between atoms by R^{-6} and their attraction radius is thus notably larger than in covalent interactions where forces decline exponentially. Moreover, in contrast to forces between permanent dipoles, these forces are not temperature dependent.[12] It is only due to London dispersion forces that non-polar compounds and even rare gases can be liquified. Consequently, estimating the strength of dispersion forces allows to predict boiling points quite accurately.[2] While the strength of a single dispersion interaction is quite small, their ubiquitous number and constant attractive nature make them the dominant force even between polar molecules.[2]

1.1.2. Attractive and Repulsive Steric Interactions

Obviously, not all interactions of atoms and molecules are attractive. The counterpart of attractive dispersion forces is the Pauli repulsion, that arises if electron clouds overlap and the Pauli exclusion principle forces electrons in energetically less favourable states.[13] These forces are extremely strong at small atom distances, but their strength eventually decreases sharply at longer distance of the two interacting nuclei. Based on the localized nature of these repulsion forces, the van der Waals radius of atoms and molecules is defined. Thus, the total potential *w* between two neutral atoms with a distance *r* is approximated by the Lennard-Jones-Potential (**Figure 1.1**) with ϵ defined as the depth of the potential well (Eq. 1). σ is there in the distance, where attractive and repulsive interactions cancel each other resulting in zero interaction of the two atoms.[2, 14]

$$w(r) = 4\epsilon\left[\left(\frac{\sigma}{r}\right)^{12} - \left(\frac{\sigma}{r}\right)^{6}\right] \qquad \text{Eq. 1}$$
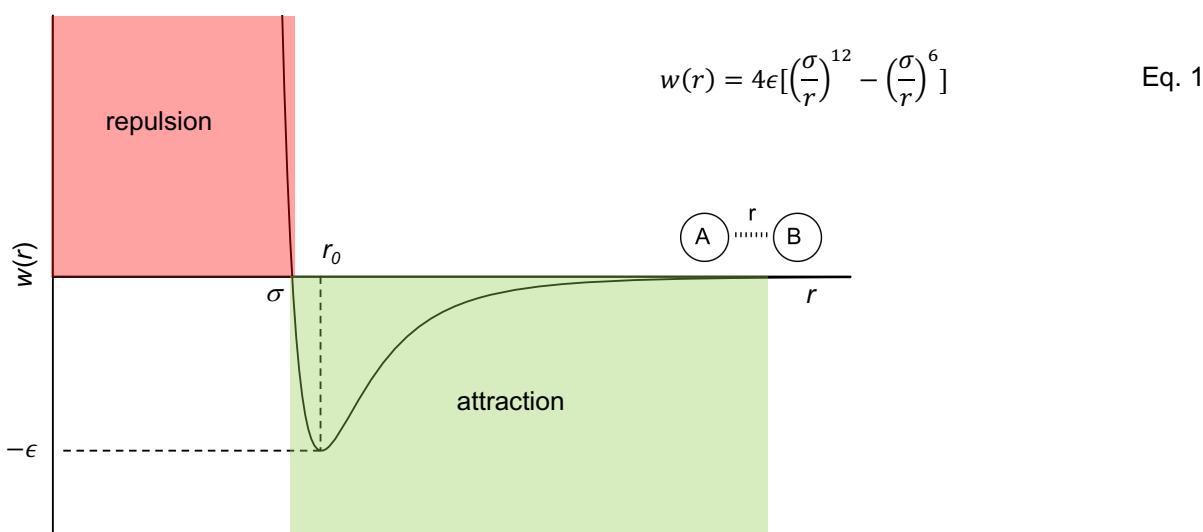
Figure 1.1. The Lennard-Jones-Potential *w(r)* as a function of the distance *r* of two rare gas molecules A and B as described by Eq. 1.[14a]

In molecular chemistry, repulsive interactions do not only arise within the van der Waals radii of two groups. Additionally, molecular vibrations can be affected by repulsive effects and thus influence thermodynamic corrections in an unfavourable manner.[15] Steric effects in chemistry are thus always an equilibrium of attractive and repulsive forces. Especially in molecular organic chemistry with sizeable moieties, steric forces are a central element controlling stability, reactivity and catalysis. However, steric effects in organic chemistry are commonly seen as mainly repulsive while attractive dispersion forces are underestimated.[4] Only recently the attractive component of steric effects was reconsidered. For example, dimers of adamantyl-derivatives have the longest ever synthesized, stable aliphatic C-C-bond and Schreiner *et al.*[16] showed that this bond is stabilized by dispersion forces of the very bulky substituents. Several outstanding reviews in the early 2010s highlighted the often overseen crucial role of attractive NCIs for example in asymmetric catalysis[17] or in the structure and reactivity of organic compounds.[4, 9] Several of the important findings from the area of asymmetric organocatalysis are further discussed below.

1.1.3. Classification of Non-Covalent Interactions
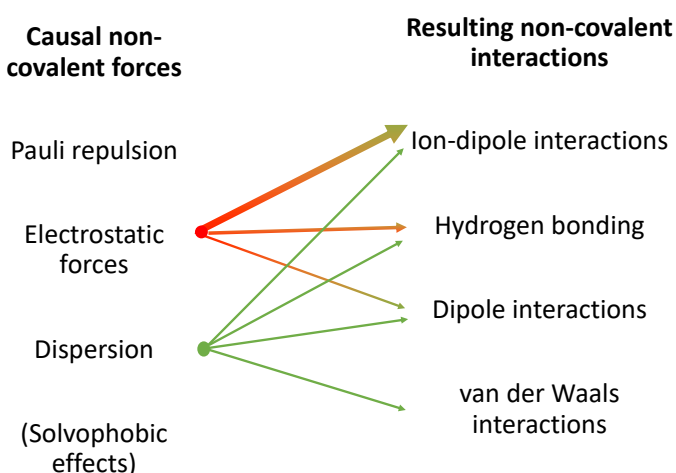
Figure 1.2. Non-covalent forces and a categorization scheme for NCIs based on the weight of electrostatic forces as displayed by the weight of the arrows.

In principle, all NCIs root in the interplay of three forces: Pauli repulsion, repulsive or attractive electrostatic forces and attractive dispersion forces. It should be noted, that the term electrostatic forces refers here (and very commonly in literature) to interactions involving permanent dipoles or quadrupoles, even if all of the forces somehow rely on electromagnetic interactions. In solution phase, additionally solvophobic effects play a role on NCIs (see below). Based on the nature of interacting particles and the strength of electrostatic forces, different classes of NCI are commonly distinguished (see **Figure 1.2**). Unfortunately, this classification is not always very stringent and cause and effects, that is the causal forces and resulting geometries, are often mixed. The strongest NCIs involve charged species like, for example, ion-ion or ion-dipole forces with a strong electrostatic component.[18] Classically, hydrogen bonds are defined as interactions of the type X-

H—Y of electronegative atoms X and Y like F, O, and N.[4] Stabilization enthalpy for the interactions of these strongly polarized bonds is commonly between $10 - 40$ kJ mol^{-1} and thus approximately a tenth of a covalent bond.[2] Due to their relative strength, classic hydrogen bonds were the first NCIs whose role in organic reactions was re-investigated.[19] At the time, hydrogen bonds are defined much broader including various types of CH-X and even CH-n (lone pair) or CH-π (aromatic systems) interactions.[4] Interactions of dipoles involve an orientation and induction effect where the electrostatic component can be both, attractive or repulsive. Hence, Israelachvili states that "[d]ispersion forces generally exceed the dipole-dependent induction and orientation forces except for small highly polar molecules, such as water."[2, 9] Finally, interactions of non-polar molecules are generally known as van der Waals interactions. Within this categorisation scheme it is not meaningful to consider interactions involving aromatic moieties as a special type of NCIs, as depending on the nature of the interacting particles and the aromatic substituents the weight of dispersion and electrostatic forces can differ dramatically. Thus, for all classes of NCIs (see **Figure 1.2**) interactions involving aromatic moieties are known. The herein (and also elsewhere frequently) used term "aromatic interactions" should thus not be misunderstood in terms of a special kind of NCI or even force between π-systems but rather as a collective term for all NCIs involving aromatic moieties. **Figure 1.3** gives an overview of different types, but also geometrical arrangements of so-called aromatic interactions.
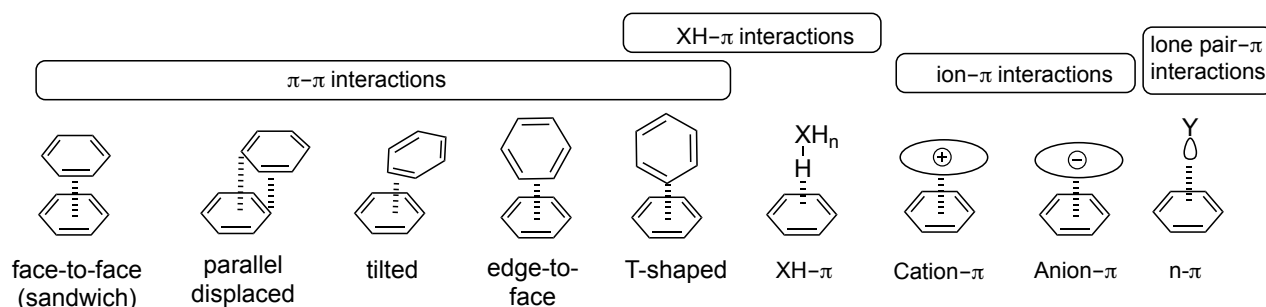
Figure 1.3. Types and different geometrical arrangements of NCIs involving aromatic moieties.

A big experimental advantage of aromatic interactions is, that aromatic moieties can be readily enlarged without losing control on the geometry of the molecule as it is the case when flexible aliphatic side chains are extended. Thus, the influence of the size of aromatic systems on steric interactions can be investigated systematically. As this approach was mainly chosen in the herein reported investigations, the different types of non-covalent interactions involving aromatic moieties are discussed in detail.

1.1.4. π-π Interactions

Despite the fact that NCIs of molecules with aromatic rings were some of the first NCIs to be discovered, surprisingly their exact nature is still not fully elucidated.[20] This may be due to the fact that several factors like electrostatic forces, dispersion and in solution phase solvophobic effects

contribute to these interactions. Their individual influence is often difficult to distinguish. Furthermore, especially π-π interactions comprise a wide variety of geometries and subtypes as shown in **Figure 1.3**.[21] High level quantum chemistry calculations (CCSD(T)/CBS) of the benzene dimer indicate that the face-to-face π-π-stacking orientation (7.6 kJ mol^{-1} in the benzene dimer) is energetically less favourable than parallel displaced (11.5 kJ mol^{-1}) or T-shaped geometries (11.6 kJ mol^{-1}).[22] This can be rationalized by the quadrupole moment of aromatic rings: above and below the ring plane a negative partial charge occurs while the edges of the ring are partially positive charged.[23] Thus, the electrostatic forces are repulsive for face-to-face aligned aromatic rings, while they are attractive for the other orientations.[20] The fact that, despite repulsive electrostatics, even a face-to-face stacking geometry of two benzene monomers is energetically stabilized highlights the major role of London dispersion forces. Note, that accordingly the term "π-π-stacking interaction" can be misunderstood as it implies a direct interaction of the delocalized electrons that would be primarily repulsive.[23a] With this limitation in mind, the term π-π interaction is used herein for the ease of discussion to describe NCIs involving two neutral aromatic rings. The recent discussion on the role of substituents at the aryl rings provides good insights into the nature of aromatic interactions: Hunter and Sanders[23b] proposed that electron-withdrawing groups would lower the electron density of the π-system and thus reduce their repulsion forces. The strength of π-π interactions is then expected to rise for electron-withdrawing group and vice-versa to be weakened if electron-donating substituents are present.[20, 23b] In disagreement with that purely electrostatic view of π-π interactions it was found that both electron-withdrawing and electron-donating substituents further stabilize aromatic interactions.[24] Thus, Wheeler and Houk[25] proposed a direct interaction of the substituents with the unsubstituted aryl ring. Indeed, interaction energies of substituted aryl to aryl (Ar-X—Ar) systems correlate with interaction energies for systems where the substituted aryl rest is replaced by a hydrogen atom (H-X—Ar).[25-26] Due to findings like this and due to numerous high-accuracy computational studies it is "now generally accepted that dispersion plays a major role in the attractive nature of π-π interactions".[27] Therefore, one could ask in how far "special noncovalent π-π stacking interactions really exist."[28] Grimme elucidated that the strength of aromatic-aromatic interactions is similar to interactions involving comparable saturated rings in small systems. Only if more than 10 carbon atoms are involved the strength of π-π interactions is increased disproportionately. This can be rationalized by a decrease of Pauli repulsion through a further delocalisation of repulsive electron clouds. Nonetheless, "normal" dispersion forces are by far the dominant term in π-π interactions.[28] Accordingly, Wheeler and Bloom[29] showed that the presence of a delocalised electron system is not essential for interactions of two aromatic moieties as the interaction energies are comparable to structurally similar (that is planar) but non-aromatic systems.[26a, 29]

1.1.5. Cation-π Interactions

Regarding the negative quadrupole moment above and below the aromatic ring plane it should not come as a surprise that cation-π interactions are within the strongest known NCIs with a magnitude comparable to hydrogen bonds or ion pairs.[30] Besides their relative strength they are much more directed and enhanced by strong electrostatic effects as compared to π-π interactions of neutral compounds. Cation-π interactions were first reported for alkali metal cations and benzene[31] but attraction to all kinds of cations were found later on (for comprehensive reviews see references [30a, 32]). The recognition of cations in proteins is commonly based on cation-π interactions in "aromatic boxes" of tryptophan, tyrosine and phenylalanine.[33] Of special interest in organocatalysis is the interaction of a neutral aromatic ring with a positively charged (hetero)arene, e.g. pyridinium.[32b] Shimizu *et al.*[34] used a molecular balance to account for the higher stabilization energy for cationic N-heterocyclic arenes. Yamada *et al.*[35] measured with a molecular seesaw balance that the pyridinium-phenyl interaction is around 6.1 kJ mol^{-1} more favourable than phenyl-phenyl stacking in chloroform, with this preference being notably decreased in other solvents. It should be noted that the design of both balances forces aromatic rings into face-to-face stacking geometries. While this conformation is clearly favourable for cation-π interactions from an electrostatic point of view,[30a] it is unfavourable for π-π interactions as discussed above.

1.1.6. Other Aromatic Interactions

XH-π interactions comprise interactions of aromatic rings with aliphatic and aromatic CH-bonds (the latter being equivalent to T-shaped aromatic-aromatic interactions) but also various heteroatom-hydrogen bonds. CH-π interactions are clearly dominated by dispersion forces and can be understood as weak hydrogen bonds.[4] They play an important role in nature for example in enzyme-carbohydrate recognition.[36] A more detailed discussion for this type of interaction is found in Chapter 2 of this thesis. Anion-π and lone-pair-π interaction are somehow counterintuitive to the negative quadrupole moment above and below the planes of aromatic rings, but lead nonetheless to stabilizing interactions and are most commonly found for electron-deficient aromatic systems.[27] As anion-π, n-π and XH-π interactions only play a minor role in this work the interested reader is referred to the literature [4, 27, 37].

1.1.7. NCIs in Solution

Solvation of molecules is based on the same forces that were discussed for NCIs above – that is orientation and induction effects of polar molecules and dispersion. From a different point of view, one could simply describe solvation as a network of non-covalent solvent-solute interactions. This puts a major burden on NCIs in solution phase: Every newly built solute-solute interaction comes at the price of abandoning solvent-solute interactions. This is especially true for dispersion interactions

as they distribute to all NCIs. While in gas-phase calculations stabilization energies of several kJ mol^{-1} for dispersion interactions are commonly determined, the picture in solution is very different. For example, dispersive forces can be attenuated in organic solvents like DCM by 70%.[38] Several authors therefore question whether dispersion would even play a role at all for molecular recognition in solution.[39] Instead, the solvophobic effect was proposed as the main driving force for aromatic-aromatic interactions in solvents. If the interaction of solvent molecules with each other is preferable over solvent-solute interactions, the accumulation of large aromatic moieties is also energetically favourable due to reinforced solvent-solvent interactions. Moreover, it is very difficult to experimentally distinguish dispersion forces and solvophobic effects as both arise from an increase of interacting solute surfaces. Therefore, the behaviour of molecular balances in different solvents was investigated. The underlying hypothesis is that the strength of solvophobic effects is a function of the forces among solvent molecules. The effects of increasing the strength of solvent-solvent-interactions – as described by the cohesive energy density (*ced*)[40] – on the thermodynamic equilibrium were then used to estimate the strength of solvophobic interactions. Accordingly, Cubberley and Iverson[41] showed that the self-association constants of foldamers in various solvents correlate with the *ced* of the solvents and concluded that they are strongly dominated by solvophobic interactions. Shimizu *et al.*[42] investigated the effects of the increased polarizability of aromatic systems on the interaction energies with a phenyl moiety. It was concluded that solvophobic effects dominate while dispersion forces still play a role but are diminished by one order of magnitude in solution as compared to gas phase. Cockroft *et al.*[43] compared alkyl-alkyl-stacking with (similar sized but less polarizable) perfluoro analogues in different solvents. Dispersion was found to be the main term for the self-association of alkyl chains in apolar or fluorous solvents, while solvophobic effects dominated in polar solvents.[43] In most of these studies only systems with small non-covalent contact areas were investigated. Cockroft *et al.*[44] thus systematically increased aromatic moieties and observed a notable growth of stacking energies for supramolecular complexes. These increases were found to correlate well with calculated dispersion contributions but only to a minor extent with the change of solvent-accessible area. Thus, especially in big systems, dispersion can still govern aromatic stacking in organic solvents. However, in all studies stabilizing effects were found to be dramatically reduced as compared to gas-phase calculations. Wheeler stated accordingly: "Despite this recent progress in understanding the nature of noncovalent interactions involving aromatic rings, many questions remain. The most pressing of these involves the effects of solvent, since the vast majority of computational studies of these interactions have involved gas-phase models."[21]

1.1.8. The Role of NCIs in Asymmetric Organocatalysis

The holy grail of organic chemistry is to perform reactions in such a selective way that only a specific group of a specific stereoisomer of one specific compound reacts. Nature achieves this goal for many reactions through enzymatic catalysis.[45] Accordingly, the development of organocatalysis

(for an introduction see below) opened a multitude of new opportunities for selective synthesis. Hence, the IUPAC named 2019 asymmetric organocatalysis as one of "ten chemical innovations that will change our world."[46] As selectivity in enzymatic catalysis is known to mainly rely on a network of attractive NCIs,[45] it is not surprising that attempts to better understand the role of steric interaction in asymmetric organocatalysis are prominent and will help in further developing the field. Very early examples for the use of attractive interactions were reported for enantioselective Diels-Alder reactions by Hawkins[47] or Corey[48]. Corey[19a] explained the enantioselectivity of chiral boron Lewis acids by hydrogen bonding. In a 2001 computational study, Noyori[49] showed that enantioselectivity in hydrogenation reactions originates from attractive NCIs of an edge-to-face stacking geometry. For the famous Sharpless oxidation no correlation between the steric hindrance at the binding site was found whereas higher rates were observed for aromatic substrates as compared to aliphatic ones.[50] Fuji[51] examined in detail the change in conformation through loading of a DMAP-derived catalyst (induced-fit model) and provided an insightful model of the closed conformation in which attractive interactions between pyridinium ring and naphthyl moiety predict the structure. Despite these prominent findings the role of sizeable groups was in general rather seen in "blocking" one side of the catalyst,[52] while the role of attractive interactions was commonly limited to determine the structure of the (loaded) catalyst but neglected in the rate- and structure-determining transition state involving the substrate.[53] A major change happened through the reinvestigation of the origins of enantioselectivity, for example, in prominent reviews of Jacobsen,[17a] Houk[17b] or Schreiner[9]. Jacobsen thus stated: "The question of whether selectivity is achieved primarily through stabilizing or destabilizing interactions represents a fundamental difference in the way macromolecular and small molecule catalysts are thought to operate."[17a] This development was enabled as discussed below to a large extent through the improvements of theoretical methods in describing non-covalent interactions properly. In the last decade, a large number of asymmetric reactions was thus re-analysed mainly by computational methods.[54] This development is perhaps best illustrated by a recent example: The design principle for various biaryl based catalyst by the List group with outstanding reactivities in diverse fields of organocatalysis was to create an "extremely sterically demanding chiral cavity"[55] and a further increase of moieties around the reaction centre was found to improve enantioselectivity notably.[55-56] However, a closer analysis of the catalyst-reagent complex by other groups pointed towards a notable influence of dispersion forces.[9, 54f] Very recently, a computational study highlighted that the stereoselectivity in an asymmetric Diels-Alder reaction with that catalyst type is induced by dispersion forces of the substrate and the crowded reaction centre – with List being co-author of the study.[57]

1.2. NCIs in Computational Chemistry

The discussed evolution of the perception of dispersion forces was very prominently induced by recent developments in computational chemistry. As wavefunction-based *ab initio* methods converge to the exact solution of the Schrödinger equation,[58] also dispersion forces can be

theoretically calculated exactly. However, very elaborate methods are needed to approach this goal. The "gold standard" of quantum chemical methods, coupled cluster theory with single, double and perturbative triple excitations (CCSD(T)) describes dispersion interactions properly.[59] Unfortunately, the computational cost of CCSD(T) scales with the atom number N of a system by N^7 which only allows calculations for small systems.[58] Thus, in general cheaper methods are used, most commonly density functional theory (DFT) methods. These methods, however, cannot describe dispersion interactions adequately: In DFT methods the exchange-correlation functional is approximated as a local function of electron density. This local and static treatment of electron density does not include fluctuation of electrons and polarization of atoms – the reasons for London dispersion forces.[9, 60] While short-range interactions of atoms are described well in DFT methods long-range interactions are accordingly underestimated and the R^{-6} dependency of dispersion interactions is not reflected in energies.[61] As dispersion interactions were generally regarded as negligible and in turn did not show up in calculations this failure was tolerated over decades. Only in the mid 2000s major attempts were undertaken in order to fix this shortcoming. The most commonly used DFT-D corrections calculate pairwise dispersion energies depending on the distance r_{AB} of two atoms A and B and use the additivity of dispersion forces as shown in Eq. 2.[9, 62] As C_6^{AB} is a semi empirical descriptor of dispersion interactions for atom pairs A and B, computational costs for that kind of dispersion correction are very small. Prominent examples are Grimme's DFT-D and D2 corrections.[63]

$$E_{disp} = -\frac{1}{2} \sum_{A,B} \frac{C_6^{AB}}{R_{AB}^6}$$

Eq. 2

The Grimme-D3 correction further improved the calculation of dispersion energies by considering the molecular environment of each atom (mainly number of neighbouring atoms) through the implementation of specifically pre-calculated C_6^{AB}.[64] These factors are non-empirical but computed for all elements in differently coordinated hydrides and are accurate to approx. 5%.[65] Due to this high precision and low computational cost the Grimme-D3 correction became a frequently used tool in computational chemistry. On the other hand, important progress was achieved for exact wavefunction-based methods as well. A prominent example is the development of domain based local pair natural orbital (DLPNO) methods by Neese *et al.*[66] Here, electron pair correlation energies are estimated in a first step. Based on these energies the electron pairs are classified as weak or strong. Correlation energies for strong pairs are explicitly calculated while an estimated correction term is added for weak pairs. This procedure reduces the size-dependence of computational costs dramatically to near linear scaling. Despite these approximations, the differences in obtained reaction energies, as compared to full CCSD(T) calculations, are typically below 1 kcal mol^{-1}.[58, 67] The synchronicity of the outlined developments in computational chemistry and the rediscovery of the impact of dispersion interactions is no coincidence. In contrast, the newly developed methods allowed interpretation of experimental results by means of dispersive interaction, while impressive results from the experimental side motivated the improvement of

computational handling of dispersion interactions.[9] Moreover, the increased accuracy of these methods also revealed the above discussed fact that calculated (gas-phase) dispersion interactions are commonly up to an order of magnitude stronger than in experiments performed in solution phase.

1.3. Organocatalysed Protecting Group Reactions

Protecting group reactions are ideal model reactions for physical organic studies for several reasons: The reactions generally proceed smoothly and without side products.[68] Also, the broad variety of available substrates and reaction conditions allows to systematically change parameters.[69] Moreover, mechanisms and properties of protecting group reactions are in general investigated in detail and therefore allow to test hypotheses in a very targeted manner. Thus, in this thesis organocatalysed protecting group reactions are employed as model reactions. Therefore, this chapter provides some glances on protecting group chemistry, the concept of organocatalysis and important mechanisms of Lewis base-catalysed reactions. As it is impossible to give a comprehensive overview of these broad topics in the framework of this thesis, only specific aspects that are relevant herein are highlighted.

1.3.1. Protecting Group Chemistry

Targeted organic syntheses, for example, in natural product syntheses often demands the chemo-, regio- and stereoselective reaction of molecules bearing diverse functional groups. Thus, it is very common practice to use protecting groups to avoid unwanted side-reactions.[68] Protecting groups should thus be easily addable and selectively removable, but also form adducts that are stable to common reaction conditions.[69] Among the most common groups to be protected are alcohols, that are in general either protected as ester, ethers, or silyl ethers (see **Figure 1.4**).[69]
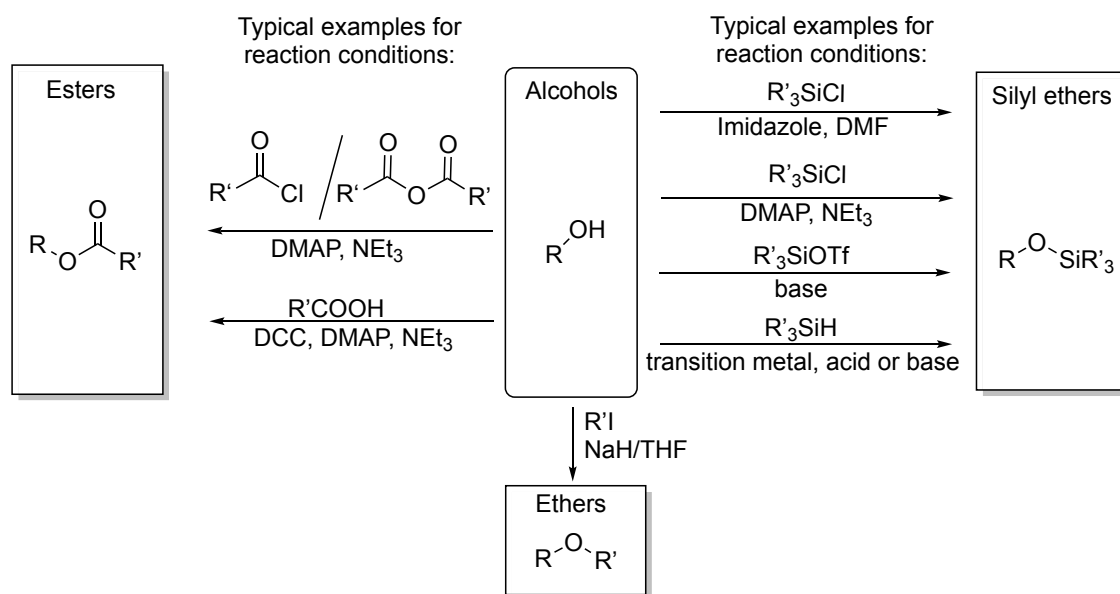
Figure 1.4. Overview of important protecting groups for the hydroxy group. Examples for reaction conditions are chosen based on their relevance for this work.

Acyl group transfer and the class of esters play an outstanding role in biochemistry as well as in protecting group chemistry.[70] A multitude of different methods for the synthesis of esters is known.[69] A prominent role plays the Lewis base-catalysed acylation with acid chlorides or anhydrides, that will be discussed below. While the direct acylation with carboxylic acids usually demands forcing reaction conditions, their activation through carbodiimids like dicyclohexylcarbodiimid (DCC) in Steglich-type esterification is another synthetically important pathway.[71] Another very commonly used alcohol protecting group are silyl ethers. The introduction of *tert*-butyldimethylsilyl chloride (TBDMSCl) with imidazole in DMF as a protecting group was reported 1972 by Corey *et al.*[72] The procedure was refined for the usage of DMAP or other Lewis bases later on.[73] Silyl substrates with very good leaving groups like triflate readily form silyl ethers, even in the absence of catalysts if a Brønsted base is present.[74] Also, silanes can be used for a broad range of reaction conditions including transition-metal, Brønsted acid or Brønsted base catalysis.[75] Silyl ethers can be cleaved by acid or base catalysed hydrolysis or under very mild conditions by the use of tetra-*n*-butylammonium fluoride (TBAF).[69] A broad variety of silylation reagents is known including trialkyl substituted silyl chlorides, e.g. TBDMSCl, trimethylsilyl chloride (TMSCl), triisopropylsilyl chloride (TIPSCl), and aryl-substituted silyl chlorides like dimethylphenylsilyl chloride (DMPSCl) or triphenylsilyl chloride (TPSCl).[69] The corresponding silyl ethers differ dramatically in stability and reactivity and thus allow tailor-made applications as protecting groups.[76]

1.3.2. Organocatalysis
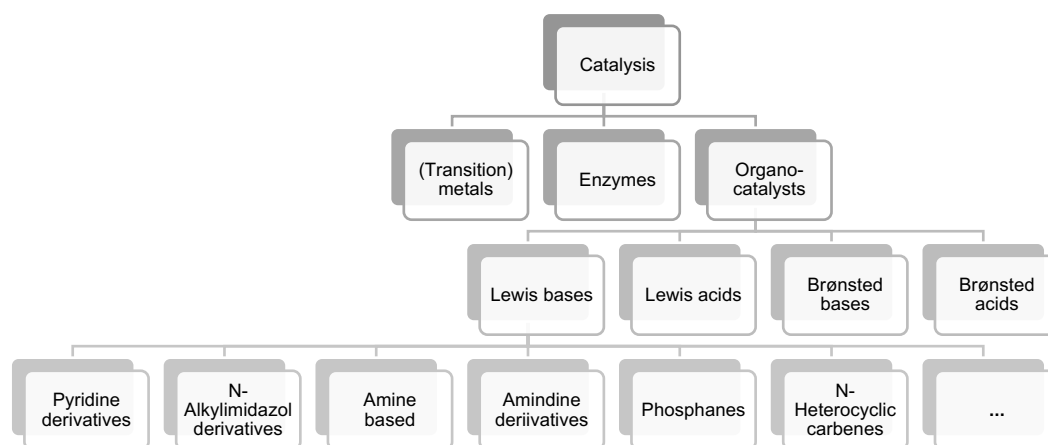
Figure 1.5. Hierarchy of catalysis types with examples of commonly used Lewis base catalysts.[70]

Organocatalysis, "the use of small organic molecules to catalyse organic transformations"[77] is still a young field of organic chemistry. This is somehow surprising, as already in the 19th century Liebig[78] used acetaldehyde as catalyst for the synthesis of oxamide from cyan and water and, for example, Lewis acid catalysis was commonly utilized in various reaction types.[79] Nonetheless, no unifying concept of organocatalysis was developed until the late 1990s and especially asymmetric

catalysis was generally restricted to enzymatic or transition metal catalysis.[80] However, after the enormous potential of organocatalysis became obvious the amount of research and number of publications in this field of research unfolded rapidly after 2000.[77, 81] Organocatalysts can be further classified by their function in the catalytic cycle: Proton donating or accepting catalysts are described as Brønsted acids or bases while electron pair donating or accepting catalysts are known as Lewis base and acid catalysts.[80, 82] Lewis base catalysts comprise, inter alia, a broad variety of tertiary amines, N-arenes, phosphanes, and N-heterocyclic carbenes (some important classes are shown in **Figure 1.5**).[70, 82] In most of the projects herein 4-dimethylaminopyrdine (DMAP) derivatives are used. An example for Lewis acid catalysis is presented for the hydrosilylation of ketones (for further discussion see Chapter 4).

1.3.3. DMAP Derivatives as Lewis Base Catalysts
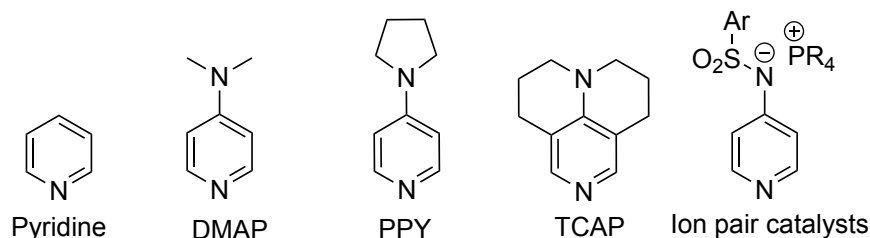
Figure 1.6. Pyridine, DMAP, and several DMAP-derived organocatalysts.

In the late 1960s DMAP-catalysed acylation reactions were described independently by the Steglich[83] and Litvinenko[84] group for the first time. They found its activity superior to that of pyridine which was known to aid the acylation of alcohols since the end of the 19th century.[85] Further notable improvements of catalytic reactivity were found for 4-pyrrolidinopyridin (PPY)[86] and 9-azajulolidine (TCAP), the latter with a catalytic activity roughly 6 – 10 times faster than DMAP.[87] This trend in catalytic activity from pyridine to TCAP can be rationalized by the increasing stabilization of the cationic acylated pyridinium moiety. The impact of better electron-donating groups on the 4-amino nitrogen atom enables its lone pair to further stabilize the acylated intermediate by $n_N \rightarrow \pi^*$ interactions.[88] This interaction and thus overall nucleophilicity is further improved by conformational fixation of the substituent in 4-position.[87, 89] Indeed, the catalytic activity of different aminopyridines was found to correlate well with calculated methyl or acetyl cation affinities reflecting the stability of the acylated pyridinium derivatives.[90] Recently, Helberg and Zipse[91] reported that pyridinyl amide ion pairs show an even higher catalytic activity in the reaction of isocyanates with alcohols. Further investigations of this promising catalyst class have to be undertaken to elucidate its scope. DMAP-based catalysts are characterised by a high versatility towards synthetic modifications enabling chiral structures for enantioselective catalysis. Important milestone were the development of planar-chiral DMAP derivatives through π complexation to a metal fragment ML_n by the Fu group[52a, 52c, 92] and the C-2 substituted chiral DMAP employing a Lewis acid co-catalyst derivative

developed by Vedejs *et al.*[93] Since then, a broad variety of chiral DMAP derivatives were found to be effective organocatalysts for enantioselective reactions.[70, 94] Due to the decreased catalytic activity of C-2-substituted DMAP derivatives[82] the introduction of the chirality at the C-2 position is rather rare.[95] Chiral elements are most commonly introduced at the C-3, for example by Spivey[96], Yamada[97], Connon[98] or Sibi[99] but also at the C-4 position, e.g. in studies of Fuji[100], Kawabata[101], and recently by Suga[102].

1.3.4. Mechanisms of DMAP-Catalysed Acylation and Silylation of Alcohols
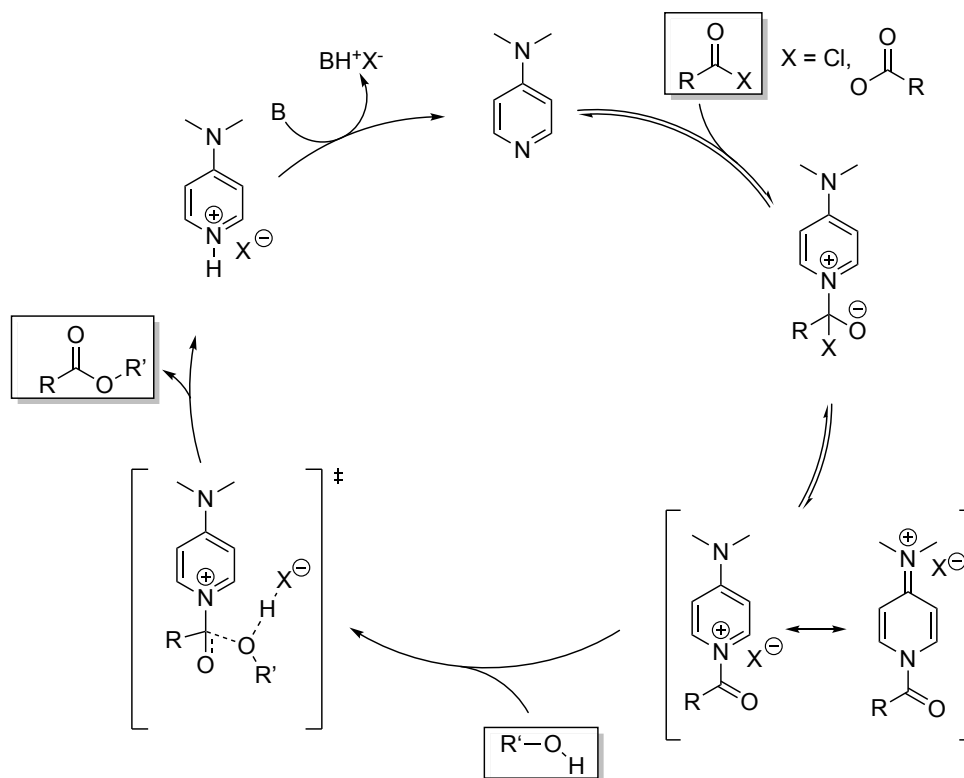
Figure 1.7. The mechanism of the DMAP-catalysed esterification of alcohols by acid chlorides or anhydrides with auxiliary base B.[88, 94a, 103]

The generally accepted mechanism of the DMAP-catalysed acylation of alcohols is shown in **Figure 1.7**.[88, 94a, 103] In a first step DMAP is acylated, typically by an acid chloride or anhydride. After elimination of the leaving group the acyl pyridinium intermediate is formed, whose stability for different catalysts was discussed above. In the transition state, the alcohol attacks the activated acyl moiety. Especially in the case of anhydrides, the counterion is usually hydrogen bonded to one the pyridinium hydrogen atoms.[103] The hydroxyl proton is removed by the counterion and the ester product is released. In this step the auxiliary base (typically a tertiary amine) is not involved as reaction rates are independent of an increase of amine concentration above one equivalent.[103] Finally, protonated DMAP catalyst is recovered by the auxiliary base. In general, the addition of the alcohol to the acyl pyridinium is the rate limiting step.[103] However, for some 3-substituted DMAP derivatives the loading of the catalyst was found to be rate determining.[54g] An alternative pathway

with DMAP acting as Brønsted base was discussed, but computational studies proved it to be unlikely and no correlation of experimental half-lives and the pK_a of the catalyst was found.[103-104]
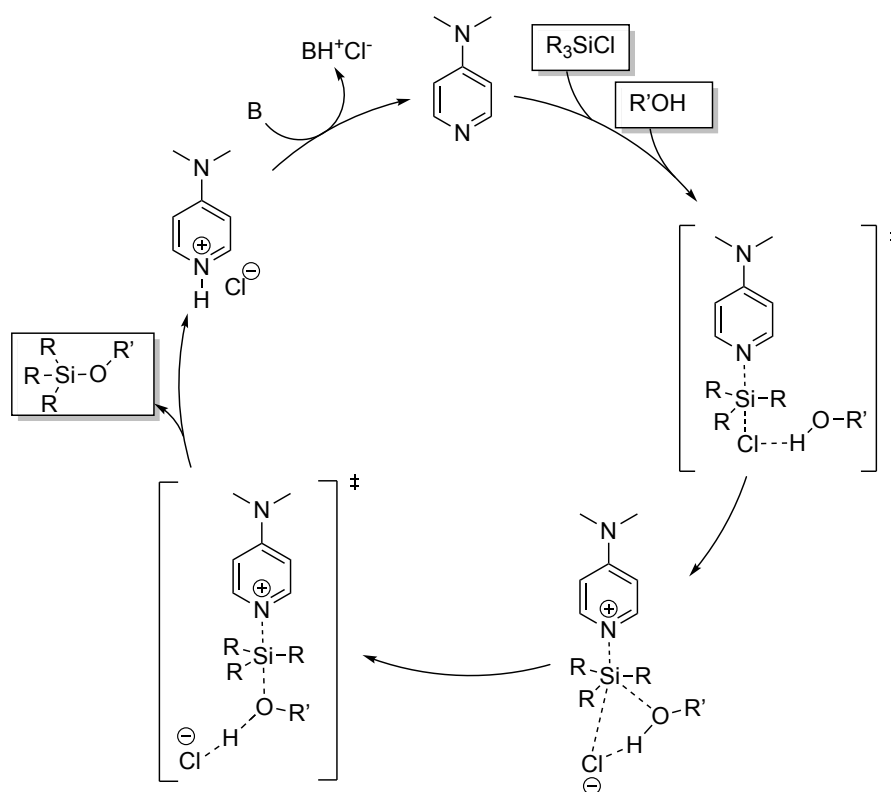
Figure 1.8. The proposed mechanism for the DMAP-catalysed silylation of alcohols by silyl chlorides with auxiliary base B.[105]

DMAP derivatives were also found to be suitable catalysts for the silylation of alcohols. As described above, the silylation of alcohols with silyl chlorides mediated by amine bases has a prominent place in the standard toolbox of organic synthesis.[69] However, the mechanism is of this reaction is less elucidated as compared to acylation reactions. The proposed mechanism shown in **Figure 1.8**[105] resembles the proposed mechanism for DMAP-catalysed acylation reaction and occurs via two S_N2Si[106] reaction steps. In the first step, the Lewis base attacks the silyl chloride to yield a pyridinium intermediate. A similar intermediate was already proposed by Hernandez in the first description of DMAP-catalysed silylation reaction.[73a] In the second S_N2Si reaction the Si-O-bond is formed and the hydroxyl proton is transferred to the counterion or the auxiliary base. Mechanistic studies showed that an auxiliary base is crucial for the recovery of Lewis base catalysts and that relative catalytic activities of different Lewis base catalysts are comparable to those reported above for acylation reactions.[73b] Wiskur *et al.*[107] reported a rate increase through introduction of electron-withdrawing groups in triarylsilyl chlorides. This agrees with the depicted mechanism as the nucleophilic attack of DMAP should be favoured by electron-deficient silyl atoms. Recently however, Zipse *et al.*[105] found two distinct correlations of relative rates and Hammett parameters describing the electronic properties of alcohol substituents and accordingly suggested a change in mechanism. Computational studies showed that at least for the silylation with TBDMSCl the general base

pathway is energetically comparable to the nucleophilic pathway.[105] In how far this is also true for triaryl-substituted silyl chlorides has still to be elucidated.

1.4. Aims of this Thesis

The literature overview above illustrates how the size of molecules can impact reactions, inter alias, by means of Pauli repulsion, electrostatic and dispersion forces. Most of the quoted studies used elaborated computational methods, thermodynamic equilibria (e.g. in molecular balances) or (enantio-)selectivity values comparing two species. However, significant effects of molecule size should be expected for the stability of transition state structures and according to the transition state theory thus on reaction rates itself. Despite this assumption, experimental studies on the influence of sizeable groups on reaction kinetics are still rare. The central goal of the work presented in this thesis is thus to elucidate how large groups influence the reaction rates in organocatalysed reactions. The focus is set on aromatic interactions as they can induce archetypical NCIs and the increase of aromatic surfaces does in general not induce major conformational changes. As these rate differences in solution are expected to be rather small, competition experiments with a reference compound were chosen as the main experimental tool. The setup of two (or more) species reacting in the same batch allows identical reaction conditions and a quite accurate determination of relative rates (different methods are presented and evaluated in Chapter 6). All reactions are some kind of organocatalysed protecting group reactions. First, rate differences in the silylation of aromatic alcohols as compared to aliphatic alcohols are researched. Eventually, size-induced rate accelerations for aromatic compounds were investigated more detailed in the Lewis base-catalysed silylation of secondary alcohols and the Lewis acid-catalysed hydrosilylation of ketones. Finally, the origin of enantioselectivity in kinetic resolution reactions was elucidated and the gained insights were employed to develop a catalyst system with improved enantioselectivity.

1.5. References

[1]   P. Hobza, D. Müller-Dehlefs, *Non-covalent Interactions: Theory and Experiment*, Royal Society of Chemistry, Cambridge, **2010**.
[2]   J. N. Israelachvili, *Intermolecular and Surface Forces*, 3 ed., Elsevier, Burlington, **2011**.
[3]   M. S. Sigman, J. J. Miller, *J. Org. Chem.* **2009**, *74*, 7633-7643.
[4]   O. Takahashi, Y. Kohno, M. Nishio, *Chem. Rev.* **2010**, *110*, 6049-6076.
[5]   J. D. van der Waals, *Over de continuïteit van den gas - en vloeistoftoestand.*, Sijthoff, **1873**.
[6]   P. Debye, *Physik. Z.* **1920**, *21*, 178-187.
[7]   F. London, *Z. Phys.* **1930**, *63*, 245-279.
[8]   R. Eisenschitz, F. London, *Z. Phys.* **1930**, *60*, 491-527.
[9]   J. P. Wagner, P. R. Schreiner, *Angew. Chem. Int. Ed.* **2015**, *54*, 12274-12296.
[10]   R. P. Feynman, *Phys. Rev.* **1939**, *56*, 340-343.
[11]   R. F. Bader, *J. Phys. Chem. A* **2010**, *114*, 7431-7444.
[12]   F. London, *Trans. Faraday Soc.* **1937**, *33*, 8-26.
[13]   J. A. Rackers, J. W. Ponder, *J. Chem. Phys.* **2019**, *150*, 084104.
[14]   a) J. M. Parson, P. E. Siska, Y. T. Lee, *J. Chem. Phys.* **1972**, *56*, 1511-1516; b) J. E. Jones, *Proc. R. Soc. London, Ser. A* **1924**, *106*, 463-477.
[15]   A. Milo, E. N. Bess, M. S. Sigman, *Nature* **2014**, *507*, 210-214.
[16]   P. R. Schreiner, L. V. Chernish, P. A. Gunchenko, E. Y. Tikhonchuk, H. Hausmann, M. Serafin, S. Schlecht, J. E. Dahl, R. M. Carlson, A. A. Fokin, *Nature* **2011**, *477*, 308-311.
[17]   a) R. R. Knowles, E. N. Jacobsen, *Proc. Natl. Acad. Sci. USA* **2010**, *107*, 20678-20685; b) E. H. Krenske, K. N. Houk, *Acc. Chem. Res.* **2013**, *46*, 979-989.
[18]   B. Linder, *Elementary physical chemistry*, World Scientific Publishing, Hackensack, **2011**.
[19]   a) E. J. Corey, J. J. Rohde, *Tetrahedron Lett.* **1997**, *38*, 37-40; b) A. G. Doyle, E. N. Jacobsen, *Chem. Rev.* **2007**, *107*, 5713-5743.
[20]   J. W. Hwang, P. Li, K. D. Shimizu, *Org. Biomol. Chem.* **2017**, *15*, 1554-1564.
[21]   S. E. Wheeler, J. W. Bloom, *J. Phys. Chem. A* **2014**, *118*, 6133-6147.
[22]   M. O. Sinnokrot, C. D. Sherrill, *J. Phys. Chem. A* **2006**, *110*, 10656-10668.
[23]   a) C. R. Martinez, B. L. Iverson, *Chem. Sci.* **2012**, *3*, 2191; b) C. A. Hunter, J. K. M. Sanders, *J. Am. Chem. Soc.* **1990**, *112*, 5525-5534.
[24]   M. O. Sinnokrot, C. D. Sherrill, *J. Am. Chem. Soc.* **2004**, *126*, 7690-7697.
[25]   S. E. Wheeler, K. N. Houk, *J. Am. Chem. Soc.* **2008**, *130*, 10854-10855.
[26]   a) S. E. Wheeler, *Acc. Chem. Res.* **2013**, *46*, 1029-1038; b) J. Hwang, P. Li, W. R. Carroll, M. D. Smith, P. J. Pellechia, K. D. Shimizu, *J. Am. Chem. Soc.* **2014**, *136*, 14060-14067.
[27]   A. J. Neel, M. J. Hilton, M. S. Sigman, F. D. Toste, *Nature* **2017**, *543*, 637-646.
[28]   S. Grimme, *Angew. Chem. Int. Ed.* **2008**, *47*, 3430-3434.
[29]   J. W. Bloom, S. E. Wheeler, *Angew. Chem. Int. Ed.* **2011**, *50*, 7847-7849.
[30]   a) C. R. Kennedy, S. Lin, E. N. Jacobsen, *Angew. Chem. Int. Ed.* **2016**, *55*, 12596-12624; b) J. P. Gallivan, D. A. Dougherty, *J. Am. Chem. Soc.* **2000**, *122*, 870-874.
[31]   J. Sunner, K. Nishizawa, P. Kebarle, *J. Phys. Chem.* **1981**, *85*, 1814-1820.
[32]   a) A. S. Mahadevi, G. N. Sastry, *Chem. Rev.* **2013**, *113*, 2100-2138; b) S. Yamada, *Chem. Rev.* **2018**, *118*, 11353-11432.
[33]   a) F. D. Toste, M. S. Sigman, S. J. Miller, *Acc. Chem. Res.* **2017**, *50*, 609-615; b) K. D. Daze, F. Hof, *Acc. Chem. Res.* **2013**, *46*, 937-945.
[34]   P. Li, C. Zhao, M. D. Smith, K. D. Shimizu, *J. Org. Chem.* **2013**, *78*, 5303-5313.
[35]   S. Yamada, N. Yamamoto, E. Takamori, *J. Org. Chem.* **2016**, *81*, 11819-11830.
[36]   Z. R. Laughrey, S. E. Kiehna, A. J. Riemen, M. L. Waters, *J. Am. Chem. Soc.* **2008**, *130*, 14625-14633.
[37]   J. W. Bloom, R. K. Raju, S. E. Wheeler, *J. Chem. Theory Comput.* **2012**, *8*, 3167-3174.
[38]   R. Pollice, M. Bot, I. J. Kobylianskii, I. Shenderovich, P. Chen, *J. Am. Chem. Soc.* **2017**, *139*, 13126-13140.
[39]   a) L. Yang, C. Adam, G. S. Nichol, S. L. Cockroft, *Nat. Chem.* **2013**, *5*, 1006-1010; b) C. A. Hunter, *Chem. Sci.* **2013**, *4*, 834-848; c) K. D. Shimizu, *Nat. Chem.* **2013**, *5*, 989-990.
[40]   L. Yang, C. Adam, S. L. Cockroft, *J. Am. Chem. Soc.* **2015**, *137*, 10084-10087.
[41]   M. S. Cubberley, B. L. Iverson, *J. Am. Chem. Soc.* **2001**, *123*, 7560-7563.
[42]   J. Hwang, B. E. Dial, P. Li, M. E. Kozik, M. D. Smith, K. D. Shimizu, *Chem. Sci.* **2015**, *6*, 4358-4364.
[43]   C. Adam, L. Yang, S. L. Cockroft, *Angew. Chem. Int. Ed.* **2015**, *54*, 1164-1167.
[44]   L. Yang, J. B. Brazier, T. A. Hubbard, D. M. Rogers, S. L. Cockroft, *Angew. Chem. Int. Ed.* **2016**, *55*, 912-916.
[45]   S. J. Benkovic, S. Hammes-Schiffer, *Science* **2003**, *301*, 1196-1202.
[46]   F. Gomollón-Bel, *Chem. Int.* **2019**, *41*, 12-17.
[47]   J. M. Hawkins, S. Loren, *J. Am. Chem. Soc.* **1991**, *113*, 7794-7795.
[48]   E. J. Corey, T. P. Loh, *J. Am. Chem. Soc.* **1991**, *113*, 8966-8967.
[49]   M. Yamakawa, I. Yamada, R. Noyori, *Angew. Chem. Int. Ed.* **2001**, *40*, 2818-2821.
[50]   H. C. Kolb, P. G. Andersson, K. B. Sharpless, *J. Am. Chem. Soc.* **1994**, *116*, 1278-1291.
[51]   T. Kawabata, M. Nagato, K. Takasu, K. Fuji, *J. Am. Chem. Soc.* **1997**, *119*, 3169-3170.
[52]   a) J. C. Ruble, G. C. Fu, *J. Org. Chem.* **1996**, *61*, 7230-7231; b) J. C. Ruble, H. A. Latham, G. C. Fu, *J. Am. Chem. Soc.* **1997**, *119*, 1492-1493; c) G. C. Fu, *Acc. Chem. Res.* **2000**, *33*, 412-420.
[53]   S. Yamada, K. Yamashita, *Tetrahedron Lett.* **2008**, *49*, 32-35.
[54]   a) S. Y. Park, J. W. Lee, C. E. Song, *Nat. Commun.* **2015**, *6*, 7512; b) R.-Z. Liao, S. Santoro, M. Gotsev, T. Marcelli, F. Himo, *ACS Catalysis* **2016**, *6*, 1165-1171; c) M. Raynal, P. Ballester, A. Vidal-Ferran, P. W. van Leeuwen, *Chem. Soc. Rev.* **2014**, *43*, 1660-1733; d) T. Geiger, A. Haupt, C. Maichle-Mossmer, C. Schrenk, A. Schnepf, H. F. Bettinger, *J. Org. Chem.* **2019**, *84*, 10120-10135; e) T. J. Seguin, T. Lu, S. E. Wheeler, *Org. Lett.* **2015**, *17*, 3066-3069; f) S. E. Wheeler, T. J. Seguin, Y. Guan, A. C. Doney, *Acc. Chem. Res.* **2016**, *49*, 1061-1069; g) R. Maji, H. Ugale, S. E. Wheeler, *Chem. Eur. J.* **2019**, *25*, 4452-4459.
[55]   I. Coric, B. List, *Nature* **2012**, *483*, 315-319.
[56]   a) P. Garcia-Garcia, F. Lay, P. Garcia-Garcia, C. Rabalakos, B. List, *Angew. Chem. Int. Ed.* **2009**, *48*, 4363-4366; b) L. Kotzner, M. J. Webber, A. Martinez, C. De Fusco, B. List, *Angew. Chem. Int. Ed.* **2014**, *53*, 5202-5205; c) T. Gatzenmeier, M. van Gemmeren, Y. Xie, D. Hofler, M. Leutzsch, B. List, *Science* **2016**, *351*, 949-952; d) T. Gatzenmeier, M. Turberg, D. Yepes, Y. Xie, F. Neese, G. Bistoni, B. List, *J. Am. Chem. Soc.* **2018**, *140*, 12671-12676.
[57]   D. Yepes, F. Neese, B. List, G. Bistoni, *J. Am. Chem. Soc.* **2020**, *142*, 3613-3625.
[58]   M. Sparta, F. Neese, *Chem. Soc. Rev.* **2014**, *43*, 5032-5041.
[59]   E. G. Hohenstein, C. D. Sherrill, *Wiley Interdiscip. Rev. Comput. Mol. Sci.* **2012**, *2*, 304-326.
[60]   a) S. Kristyán, P. Pulay, *Chem. Phys. Lett.* **1994**, *229*, 175-180; b) J. Pérez-Jordá, A. D. Becke, *Chem. Phys. Lett.* **1995**, *233*, 134-137.
[61]   S. Grimme, *WIREs Comput. Mol. Sci.* **2011**, *1*, 211-228.
[62]   J. Klimes, A. Michaelides, *J. Chem. Phys.* **2012**, *137*, 120901.
[63]   a) S. Grimme, *J. Comput. Chem.* **2004**, *25*, 1463-1473; b) S. Grimme, *J. Comput. Chem.* **2006**, *27*, 1787-1799.
[64]   S. Grimme, J. Antony, S. Ehrlich, H. Krieg, *J. Chem. Phys.* **2010**, *132*, 154104.
[65]   S. Grimme, A. Hansen, J. G. Brandenburg, C. Bannwarth, *Chem. Rev.* **2016**, *116*, 5105-5154.
[66]   a) C. Riplinger, B. Sandhoefer, A. Hansen, F. Neese, *J. Chem. Phys.* **2013**, *139*, 134101; b) C. Riplinger, F. Neese, *J. Chem. Phys.* **2013**, *138*, 034106.
[67]   D. G. Liakos, M. Sparta, M. K. Kesharwani, J. M. Martin, F. Neese, *J. Chem. Theory Comput.* **2015**, *11*, 1525-1539.
[68]   J. Clayden, N. Greeves, S. Warren, *Organic Chemistry*, OUP, Oxford, **2012**.
[69]   P. G. M. Wuts, T. W. Greene, *Greene's Protective Groups in Organic Synthesis*, John Wiley & Sons, Hoboken, **2006**.
[70]   C. E. Muller, P. R. Schreiner, *Angew. Chem. Int. Ed.* **2011**, *50*, 6012-6042.
[71]   B. Neises, W. Steglich, *Angew. Chem. Int. Ed.* **1978**, *17*, 522-524.
[72]   E. J. Corey, A. Venkateswarlu, *J. Am. Chem. Soc.* **1972**, *94*, 6190-6191.

[73]   a) S. K. Chaudhary, O. Hernandez, *Tetrahedron Lett.* **1979**, *20*, 99-102; b) P. Patschinski, C. Zhang, H. Zipse, *J. Org. Chem.* **2014**, *79*, 8348-8357.
[74]   P. Li, J. Li, F. Arikan, W. Ahlbrecht, M. Dieckmann, D. Menche, *J. Org. Chem.* **2010**, *75*, 2429-2444.
[75]   A. Weickgenannt, M. Oestreich, *Chem. Asian J.* **2009**, *4*, 406-410.
[76]   G. van Look, G. Simchen, J. Heberle, *Silylating Agents*, Fluka Chemie AG, Buchs, **1995**.
[77]   D. W. MacMillan, *Nature* **2008**, *455*, 304-308.
[78]   J. von Liebig, *Annalen der Chemie und Pharmacie* **1860**, *113*, 246-247.
[79]   A. Corma, H. Garcia, *Chem. Rev.* **2003**, *103*, 4307-4365.
[80]   B. List, *Chem. Rev.* **2007**, *107*, 5413-5415.
[81]   K. A. Ahrendt, C. J. Borths, D. W. C. MacMillan, *J. Am. Chem. Soc.* **2000**, *122*, 4243-4244.
[82]   E. Vedejs, S. E. Denmark, *Lewis Base Catalysis in Organic Synthesis*, Wiley-VCH, Weinheim, **2016**.
[83]   W. Steglich, G. Höfle, *Angew. Chem.* **1969**, *81*, 1001-1001.
[84]   L. M. Litvinenko, A. I. Kirichenko, *Dokl. Akad. Nauk. SSSR* **1967**, *176*, 97 - 100.
[85]   A. Einhorn, F. Hollandt, *Justus Liebig's Annalen der Chemie* **1898**, *301*, 95-115.
[86]   G. Höfle, W. Steglich, H. Vorbrüggen, *Angew. Chem. Int. Ed.* **1978**, *17*, 569-583.
[87]   M. R. Heinrich, H. S. Klisa, H. Mayr, W. Steglich, H. Zipse, *Angew. Chem. Int. Ed.* **2003**, *42*, 4826-4828.
[88]   A. C. Spivey, S. Arseniyadis, *Angew. Chem. Int. Ed.* **2004**, *43*, 5436-5441.
[89]   H. Mayr, T. Bug, M. F. Gotta, N. Hering, B. Irrgang, B. Janker, B. Kempf, R. Loos, A. R. Ofial, G. Remennikov, H. Schimmel, *J. Am. Chem. Soc.* **2001**, *123*, 9500-9512.
[90]   a) E. Larionov, F. Achrainer, J. Humin, H. Zipse, *ChemCatChem* **2012**, *4*, 559-566; b) E. Larionov, H. Zipse, *Wiley Interdiscip. Rev. Comput. Mol. Sci.* **2011**, *1*, 601-619.
[91]   J. Helberg, T. Ampssler, H. Zipse, *J. Org. Chem.* **2020**, *85*, 5390-5402.
[92]   J. C. Ruble, J. Tweddell, G. C. Fu, *J. Org. Chem.* **1998**, *63*, 2794-2795.
[93]   E. Vedejs, X. Chen, *J. Am. Chem. Soc.* **1996**, *118*, 1809-1810.
[94]   a) H. Mandai, K. Fujii, S. Suga, *Tetrahedron Lett.* **2018**, *59*, 1787-1803; b) R. Gurubrahamam, Y.-S. Cheng, W.-Y. Huang, K. Chen, *ChemCatChem* **2016**, *8*, 86-96.
[95]   E. Y. Yazıcıoğlu, C. Tanyeli, *Tetrahedron: Asymmetry* **2012**, *23*, 1694-1699.
[96]   A. C. Spivey, D. P. Leese, F. Zhu, S. G. Davey, R. L. Jarvest, *Tetrahedron* **2004**, *60*, 4513-4525.
[97]   S. Yamada, T. Misono, Y. Iwai, *Tetrahedron Lett.* **2005**, *46*, 2239-2242.
[98]   O. Gleeson, R. Tekoriute, Y. K. Gun'ko, S. J. Connon, *Chem. Eur. J.* **2009**, *15*, 5669-5673.
[99]   G. Ma, J. Deng, M. P. Sibi, *Angew. Chem. Int. Ed.* **2014**, *53*, 11818-11821.
[100]   T. Kawabata, K. Yamamoto, Y. Momose, H. Yoshida, Y. Nagaoka, K. Fuji, *Chem. Commun.* **2001**, 2700-2701.
[101]   T. Kawabata, R. Stragies, T. Fukaya, Y. Nagaoka, H. Schedel, K. Fuji, *Tetrahedron Lett.* **2003**, *44*, 1545-1548.
[102]   H. Mandai, K. Fujii, H. Yasuhara, K. Abe, K. Mitsudo, T. Korenaga, S. Suga, *Nat. Commun.* **2016**, *7*, 11297.
[103]   S. Xu, I. Held, B. Kempf, H. Mayr, W. Steglich, H. Zipse, *Chem. Eur. J.* **2005**, *11*, 4751-4757.
[104]   E. Larionov, M. Mahesh, A. C. Spivey, Y. Wei, H. Zipse, *J. Am. Chem. Soc.* **2012**, *134*, 9390-9399.
[105]   M. Marin-Luna, P. Patschinski, H. Zipse, *Chem. Eur. J.* **2018**, *24*, 15052-15058.
[106]   a) M. A. van Bochove, F. M. Bickelhaupt, *Eur. J. Org. Chem.* **2008**, *2008*, 649-654; b) T. A. Hamlin, M. Swart, F. M. Bickelhaupt, *ChemPhysChem* **2018**, *19*, 1315-1330.
[107]   R. K. Akhani, M. I. Moore, J. G. Pribyl, S. L. Wiskur, *J. Org. Chem.* **2014**, *79*, 2384-2396.

Chapter 2. Chemoselectivity in the Silylation of Aliphatic and Aromatic Alcohols.

Benjamin Pölloth, and Hendrik Zipse
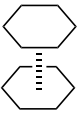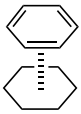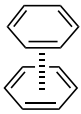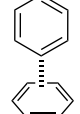
Unpublished Results

Author contributions: B.P. and H.Z. conceived the study. The experimental study was performed by B.P. A few results from the bachelor thesis of Stefan Weitl, who worked under the supervision of B.P., are reported. All of these results were reanalysed by B.P. and are explicitly marked. The computational study was performed by B.P. The manuscript was written by B.P.

2.1. Introduction

The stability of biologically very important carbohydrate-protein binding is mainly achieved by attractive interactions of aromatic amino acid moieties and aliphatic carbohydrates. Waters *et al.*[1] investigated a β-hairpin structure in an aqueous solution with a prominent tryptophan carbohydrate interaction. While replacing tryptophan by naphthyl did not change the free folding energy notably (approx. -4 kJ mol^{-1}) it was lowered to only -0.7 kJ mol^{-1} by substitution with phenyl and even turned out to be destabilizing if a cyclohexyl moiety was used instead. This finding illustrates exemplary the role of attractive non-covalent interactions (NCIs) between aromatic and aliphatic moieties.[2] Therefore, the question whether NCIs between two aromatic moieties are special as compared to interactions involving aliphatic moieties was investigated. Grimme[3] argued that attractive forces between two aromatic moieties mainly arises from conventional dispersion interactions. Only in bigger aromatic system (>10 carbons) long-rang correlation effects of non-local electrons lead to a disproportionate increase of interaction energy that cannot be found for saturated interactions. Bloom and Wheeler[4] showed that also aromaticity itself does not stabilize aromatic-aromatic interactions in a specific way. The interaction energy between a planar non-aromatic benzene-analogue and benzene is even more stabilizing than the corresponding aromatic-aromatic interaction.

Table 2.1. Literature interaction energies [kJ mol^{-1}] for dimers of cyclohexane and benzene on different levels of theory.

B2PLYP-D/TZV(2d,p)[3]	-12.92		-10.95	-11.79
CCSD(T)/CBS[5]	-10.95	-13.67[6]	-11.41	-11.87
M06-2X/cc-pVTZ//M06-2X/6-31G* [7]	-8.57	-13.38	-10.99	
E_{disp}[a] PBE0/cc-pVDZ[7]	-15.76	-18.43	-33.98	

[a]Dispersion energy as determined by symmetry adapted perturbation theory (SAPT) on DFT level

In theoretical studies dimers of cyclohexane and benzene are often used as model system to quantify interactions involving aromatic and/or aliphatic moieties (see **Table 2.1**). In early DFT studies the interaction energy of a cyclohexane dimer was found to be higher than in the benzene dimer.[3] However, results with coupled cluster methods and complete basis set extrapolation – the golden standard of quantum chemistry[8] – show that the interaction energy of two benzene rings is slightly higher as compared to the interaction energy of two cyclohexane molecules. The preferable conformation for a pair of two benzene rings was found to be T-shaped (and thus CH-π interactions), while the face-to-face stacking conformation becomes eventually more stabilizing for bigger aromatic systems.[5] Surprisingly, the highest interaction energy was found between cyclohexane and benzene.[6-7] Symmetry adapted perturbation theory (SAPT)[9] analysis revealed, however, that stabilization by dispersion energy is notably higher in the benzene dimer as compared to dimers involving cyclohexane. Stacking energies of the latter interactions are dominated by electrostatic

forces.[4] Another important difference is that the strength of π-π interactions is much better preserved by horizontal displacement of one aromatic moiety than for interactions with an aliphatic moiety.[10] Consequently, the radius of attraction is bigger for aromatic-aromatic interactions. As ideal distances are much harder to realize in real chemical structures than in theoretical simulations this could explain the prominent role of π-π interactions. A common strategy to test, whether specific C-H-bonds are involved in NCI, is to replace relevant hydrogen atoms by fluorine atoms.[11] As the exposed radii of covalently bonded hydrogen and fluorine atoms is comparable (0.11 nm resp. 0.14 nm)[12] no major change of geometry is expected through the substitution of hydrogen by fluorine. However, due to the strong electronegativity of fluorine atoms the strength of CF-π interactions is negligible.[13] By exchanging the CH proton for a fluorine atom it could be shown, for example, that chiral recognition of amino acid derivatives with a synthetic receptor mainly depends on the weak aliphatic CH-π interaction with tryptophan.[11c]

Based on the different interaction energies of the benzene dimer and the cyclohexane-benzene-dimer we wondered in how far these differences could be used as a control element in reactions of aromatic and aliphatic compounds. As a model system we chose the silylation of alcohols. The mechanism of Lewis base-catalysed silylation reactions is discussed in the introduction of this thesis. The therein proposed transition state respectively the transition state for the uncatalysed S_N2Si silylation could possibly be stabilized or destabilized through interactions of the substituents of the silyl chloride and of the alcohol. This could alter relative rates and result in different product ratios if a sub-stochiometric ratio of silyl chloride is used (see **Scheme 2.1**). We thus used pairs of aromatic and aliphatic alcohols of comparable size to study their relative rates in competition experiments.
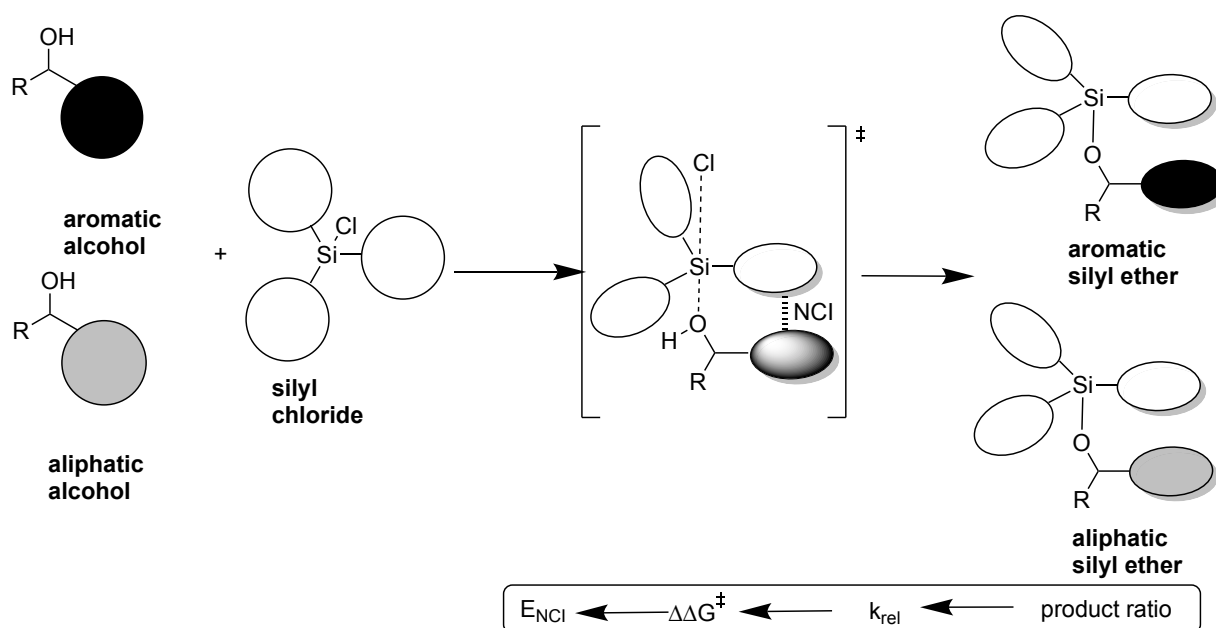
Scheme 2.1. Conceptual idea for the study to estimate relative strengths of interactions between two aromatic moieties as compared to aliphatic-aromatic interactions. In the silylation of aromatic and aliphatic alcohols, NCIs could stabilize the transition state, accelerate reactions and thus lead to differences in product ratios.

2.2. Results and Discussion

2.2.1. Experimental Procedures

1 : 1 competition experiments of aliphatic and aromatic alcohols with different concentrations of silyl chloride were performed. Analysis was performed via ^{1}H-NMR or GC analysis (for details see SI). Selectivity s in this project is defined relative to the rate of the aliphatic alcohol if not stated differently (Eq. 2.1).

$$s = \frac{k(alc_{aromatic})}{k(alc_{aliphatic})} \qquad \text{Eq. 2.1}$$

From the experimental chemoselectivity of reactants and products conversion and selectivity was calculated by Kagan's formula (Eq. 2.3 and Eq. 2.2).[14]

$$conv = \frac{C_{alcohols}}{C_{alcohols} + C_{ethers}} \qquad \text{Eq. 2.2}$$

$$s = \frac{ln(1 - conv(1 + C_{ethers}))}{ln(1 - conv(1 - C_{ethers}))} \qquad \text{Eq. 2.3}$$

As a model system for the investigation of relative rates of aromatic versus aliphatic alcohols the silylation of benzyl alcohol (**1a**) and cyclohexylmethanol (**2a**) with triphenylsilyl chloride (TPSCl, **3a**) in the presence of triethylamine (**4**) was studied (**Scheme 2.2**). Phenyl and cyclohexyl moieties are chosen as minimal aromatic and aliphatic systems. Due to identical carbon counts in both systems it was hypothesized that the reactivity of both alcohols in silylation reactions is comparable.
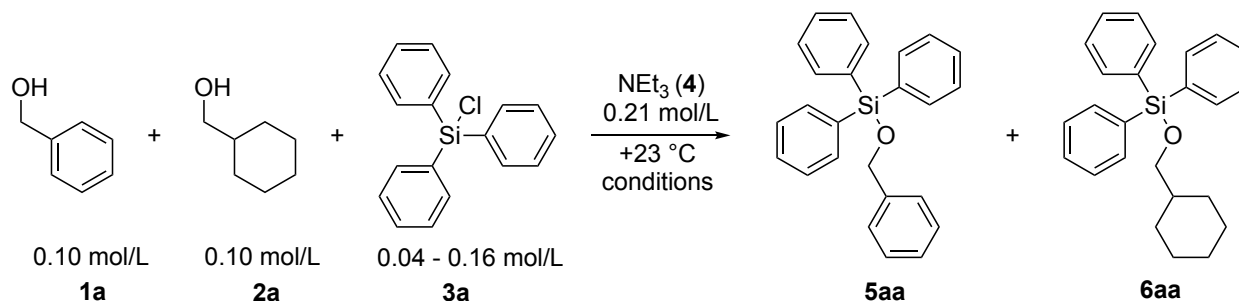
Scheme 2.2. Model system for competition experiments to determine the selectivity of the silylation of aliphatic and aromatic alcohols.

2.2.2. Investigation of Reaction Conditions for Primary Alcohols

In the reaction presented in **Scheme 2.2** primary alcohol **1a** reacts around 6.5 times faster than primary aliphatic alcohol **2a**. This value could be reproduced within the typical error margin several times and for different concentrations of silyl chloride (see **Figure 2.1** red squares). The (uncatalysed) reaction mixture was found to be stable over months so that product distribution is under clear kinetic control. Regarding the hypothesis based on the higher interaction energies for phenyl-cyclohexyl as compared to phenyl-phenyl pairs, both the magnitude and the direction of the observed selectivity are surprising. Very likely there are other factors included in controlling relative rates of **1a** to **2a**. This could comprise differences in the reactivity of the hydroxy group due to acidity or nucleophilicity or further steric effects – that can be both, attractive or repulsive. In a first step, the influence of solvents and catalyst concentrations on the selectivity was investigated.

Table 2.2. Selectivity values determined by competition experiments for the reaction shown in **Scheme 2.2** (T = +23 °C, 1.05 eq NEt$_3$ (**4**)).

solvent	catalyst	$s = \dfrac{k(\mathbf{1a})}{k(\mathbf{2a})}$
CDCl$_3$	-	6.5±0.5
DCM	-	4.2±0.1[a]
THF	-	4.1±0.2[a]
CDCl$_3$	10% TCAP **7**	1.7±0.2
CDCl$_3$	10% TCAP **7**[b]	1.5±0.2[b]
CDCl$_3$	5% TCAP **7**	1.8±0.3
CDCl$_3$	2.5% TCAP **7**	2.1±0.2

TCAP **7**
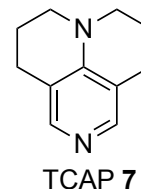
[a]determined from repeated measurements at 50% conversion. [b] Silyl chloride stock solution added by syringe pump over a period of 30 mins.

Table 2.2 shows that the selectivity value is strongly dependent on reaction conditions. The use of other solvents than CDCl$_3$ lowers selectivity notably. However, the number of experimental solvent-dependent selectivity values does not allow a more detailed discussion. Interestingly, catalysis with 9-azajulolidine (TCAP, **7**) lowers the selectivity dramatically and almost identical reaction rates for both alcohols are observed. Selectivity decreases further with increasing catalyst concentration.

$$C_{ether} = \frac{[5aa]-[6aa]}{[5aa]+[6aa]}$$
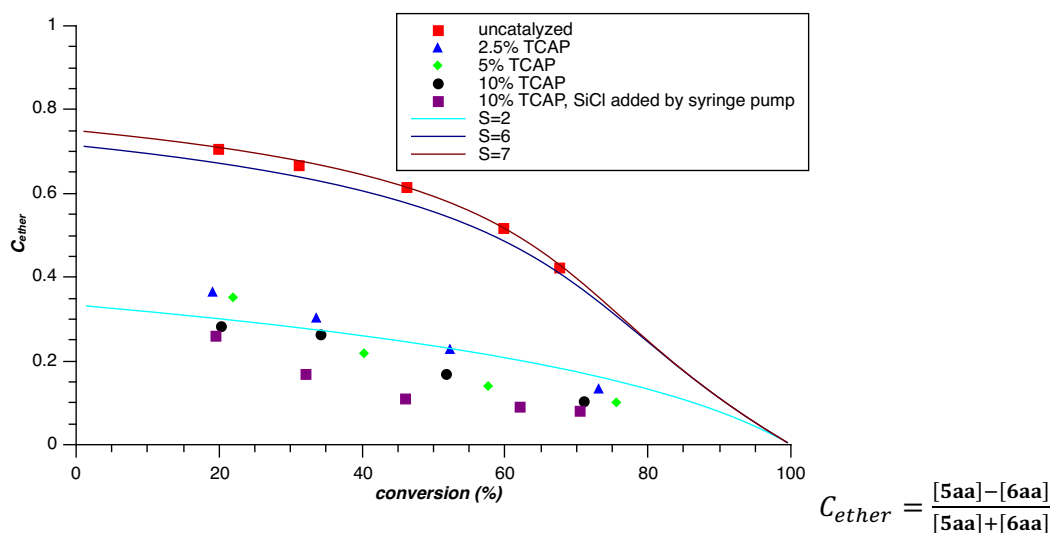
Figure 2.1. Plot of experimental chemoselectivity C_{ether} values vs. conversion for the reaction in **Scheme 2.2**. The curves show expected conversion vs. chemoselectivity for a given selectivity value as simulated by CoPaSi[15]. The plot was created with QTIplot.[16]

Figure 2.1 shows, that experimental chemoselectivity values for the catalysed reactions at different conversion values do not fit the simulated curves for a given selectivity value. Indeed, observed selectivity decreases with relative concentration of silyl chloride **3a**, to the most extent for low catalyst loadings. This indicates a competition of an uncatalysed and a catalysed pathway.[17] As the selectivity of the uncatalysed pathway was determined to be s = 6.5, the selectivity of the catalysed pathway has to be close to 1. With higher catalyst concentration the catalysed pathway becomes more dominant and thus overall selectivity is lowered. This effect is even more pronounced if the silyl chloride was added slowly over the period of 30 mins using a syringe pump

(see **Figure 2.1** purple squares). A possible explanation could comprise the very high reactivity of primary alcohols with aromatic silyl chlorides catalysed by the very active Lewis base TCAP (**7**).[18] The Hammond-postulate implies that the transition state (TS) for the very fast catalysed reaction occurs early and the structure of the alcohol reagent impacts thus the structure of the TS to a lesser extent than in the uncatalysed reaction. Then distances of alcohol and silyl chloride moieties in the TS would be longer and the impact of (attractive and repulsive) steric interactions lower. A similar influence of absolute reaction rate on selectivity was found for the silylation of primary versus secondary alcohol[19] and for kinetic resolution reactions based on silylation reactions.[20] It should be emphasized that a general reactivity-selectivity principle itself is not a meaningful physical-organic concept.[21] Another explanation could be based on the observation that long-term experiments (see Chapter 2.4.5) showed that especially the primary aromatic silyl ether **5aa** is unstable in the presence of TCAP (**7**). Thus, thermodynamic processes like a re-etherfication or a selective deprotection could also influence product ratios. Due to those uncertainties the silylation of primary alcohols was always conducted uncatalysed in the following. Catalysed reactions were only used for secondary alcohols that react much slower and result in stable product mixtures.

2.2.3. Variation of Silyl Chlorides

In a first step to elucidate the origin of the 6.5 times faster reaction of **1a** compared to **2a** the reaction was repeated with different silyl chlorides (see **Table 2.3**). In a preliminary project[22] dimethylphenylsilyl chloride (DMPSCl, **3b**) was utilized in a comparable reaction setup. Interestingly, relative rates of the alcohols are similar to those with TPSCl (**3a**). It is thus unlikely, that a general steric hindrance of aliphatic alcohol **2a** is the main reason for the selectivity. If that were true the replacement of two phenyl groups by small methyl groups should reduce steric strain dramatically and relative rates of **2a** should increase. In sharp contrast, in reactions with *tert*-butyldimethylsilyl chloride (TBDMSCl, **3c**) the selectivity is inverted and aliphatic alcohol **2a** reacts twice as fast as aromatic alcohol **1a**. The most likely explanation is that two rigid aromatic moieties can be easier arranged in a favourable geometry towards each other while the same is true for two flexible aliphatic groups. However, this arrangement seems to be more difficult for geometrically different aromatic and aliphatic groups. As described above substitution of hydrogen atoms with fluorine can give insights in how far CH-π interactions are active in molecular recognition. Thus, hydrogen was systematically exchanged by fluorine in silyl chlorides **3d** - **3f**. Selectivity was notably lowered to *s* = 4.0 – 4.5 for *para*- and *meta*-substituted silyl chloride **3d** and **3e** but not affected by *ortho*-substitution in **3f**. Increased electron density is likely to increase reaction rates, like Wiskur *et al.*[20] showed for **3d**. However, if electronic effects were mainly responsible for a change in selectivity a prominent difference in relative rates for *para*- and *meta*-substituted silyl chlorides should be expected as the relevant Hammett parameters differ dramatically (σ_m(F) = 0.34, σ_p(F) = 0.06)[23]. Hammett parameter for *ortho*-position are not available as commonly steric effects are predominant to electronic effects.[24] Based on these results, it could be hypothesized that the

observed decrease of selectivity is due to smaller attractive CH-π interactions involving the *para*- and *meta*-hydrogen atoms but the results are not clear enough for a detailed discussion.

Table 2.3. Selectivity values determined by competition experiments with different silyl chlorides.

N°		SiCl	Si$_{ar}$	Si$_{al}$	$s = \dfrac{k(\textbf{1a})}{k(\textbf{2a})}$
1	R^1, R^2 = (phenyl)	3a	5aa	6aa	6.5±0.5
2	R^1 = (phenyl) R^2 = CH$_3$	3b	5ab	6ab	6.4±0.3[22]
3	R^1 = (tert-butyl) R^2 = CH$_3$	3c	5ac	6ac	0.54±0.1[a]
4	R^1, R^2 = (4-F-phenyl)	3d	5ad	6ad	4.0±0.6
5	R^1, R^2 = (3-F-phenyl)	3e	5ae	6ae	4.5±0.5
6	R^1, R^2 = (2-F-phenyl)	3f	5af	6af	6.6±0.3
7	R^1, R^2 = (2-naphthyl)	3g	5ag	6ag	7.1±0.6[a]

[a]Raw NMR data were experimental determined by S. Weitl[25] under the supervision of B. Pölloth. The herein reported data are fully re-analysed as described in Chapter 2.4.3.

If attractive π-π interactions were responsible for the selectivity of the reaction, increasing the aromatic surface should further accelerate the reaction of the aromatic alcohol. Indeed, utilizing tris(2-naphthyl)silyl chloride (TNpSCl, **3g**) enhanced the selectivity slightly. However, the change of relative rate is very small and within experimental error. The reliability of selectivity measurements is higher for smaller selectivity values.[26] Thus, 2-naphthylmethanol (**1b**) was used as a reagent that is very similar to **1a** but π-π interactions should be strengthened by bigger aromatic surfaces.

Table 2.4. Selectivity values determined by competition experiments with 2-naphthylmethanol **1b**. Raw NMR data were experimental determined by S. Weitl[25] under the supervision of B. Pölloth. The herein reported data are fully re-analysed as described in Chapter 2.4.3.

N°			Alc2	SiCl	Si1	Si2	$s = \dfrac{k(1b)}{k(alc2)}$
1	$R_{alc} =$ phenyl	$R^1 =$ *tert*-butyl, $R^2 = CH_3$	1a	3c	5bc	5ac	0.99±0.01
2	$R_{alc} =$ phenyl	$R^1, R^2 =$ phenyl	1a	3a	5ba	5aa	1.13±0.03
3	$R_{alc} =$ phenyl	$R^1, R^2 =$ naphthyl	1a	3g	5bg	5ag	1.24±0.02
4	$R_{alc} =$ cyclohexyl	$R^1, R^2 =$ phenyl	2a	3a	5ba	6aa	6.5±0.2
5	$R_{alc} =$ cyclohexyl	$R^1, R^2 =$ naphthyl	2a	3g	5bg	6ag	7.5±0.3
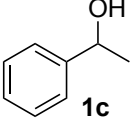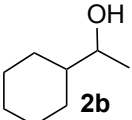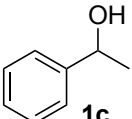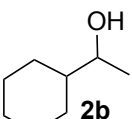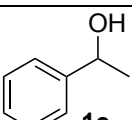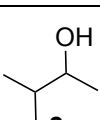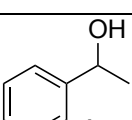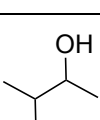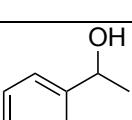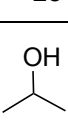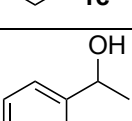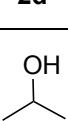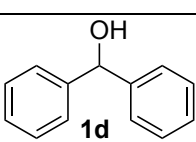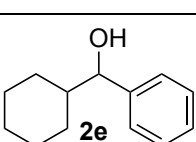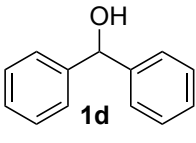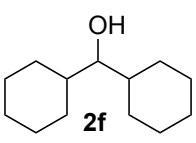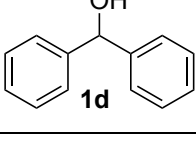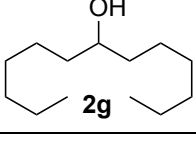
Standard deviations for competition experiments between **1b** and **1a** in **Table 2.4** clearly reflect that the obtained relative rates are more reliable than those for the higher selectivity values reported above. While **1b** and **1a** react with non-aromatic TBDMSCl (**3c**) with similar rates, increasing the aromatic moiety on the silyl chloride side leads to an increase of relative rates of the bigger alcohol **1b**. Thus, attractive π-π interactions notably affect the selectivity. However, these increases of selectivity are too small to be reliably determined in competition experiments of **1b** and aliphatic **2a** (**Table 2.4**, line 4 and 5). The approach to use systematically growing aromatic moieties on very similar aromatic reagents to estimate the influence of π-π interactions is therefore very promising and was further explored in Chapter 3 of this thesis. All in all, the experiments with different silyl chlorides on primary alcohols indicate that the geometry of interacting reagents notably impacts selectivity. From an experimental point of view, several disadvantages of the silylation of primary alcohols as a model system for physical-organic studies were recognized during this project: Absolute reaction rates are very high and full conversion is achieved for the uncatalysed reaction in seconds. Hence, a notable part of the reaction already happens during the process of adding the reagent to the reaction mixture. This makes strict control of reaction conditions like temperature and concentrations much more difficult and the process of adding reagents could influence rates notably. Moreover, the notable background reaction as described above makes analysis of the

catalysed reaction very difficult. To avoid these problems in the subsequent alternation of substrates the silylation of secondary alcohols was investigated.

2.2.4. Secondary Alcohols

Relative rates for secondary alcohols were determined by the same protocol as described before. Systematic changes of both moieties of the alcohols were used to gain further insights into the origins of the observed selectivity. In a first step the reactivity of aromatic and aliphatic secondary alcohols **1c** and **2b** in the absence of (attractive or repulsive) steric interactions was controlled by the use of small trimethylsilyl chloride (TMSCl, **3h**). Reactions were catalysed by 4-dimethylaminopyridine (DMAP, **8**). 1-Phenylethanol (**1c**) and 1-cyclohexylethanol (**2b**) react indeed with almost identical rates with TMSCl (**3h**). This allows to exclude the hypothesis that different acidities or nucleophilicities of the hydroxy group are the main factor influencing rates. However, with TPSCl (**3a**) the aromatic alcohol **1c** reacts roughly four times faster than the aliphatic alcohol **2b**. This relative acceleration is somewhat smaller than in the uncatalysed reaction of primary alcohol **1a** ($s = 6.5$) but notably bigger than in the catalysed reaction of primary alcohols. Subsequently, 1-cyclohexylethanol (**2b**) was systematically deconstructed. Removing parts of the ring structure leads to *sec*-isoamyl alcohol (**2c**). Interestingly, relative rates with TMSCl (**3h**, $s = 1.4$) and TPSCl (**3a**, $s = 4.1$) with **2c** are similar to those of **2b**. The smallest possible secondary alcohol derived from **2b** is isopropanol (**2d**), that reacts three times faster with TMSCl (**3h**) than **1c**, **2b** and **2c**. The significant structural differences of the smallest possible secondary alcohol **2d** as compared to the other alcohols seems to notably affect its reactivity. However, if aromatic TPSCl (**3a**) is used relative rates for **1c** were increased by a factor of 2.1 relative to the reaction with TMSCl (**3h**). Finally, the second methyl group was replaced by bigger moieties. In these experiments TCAP (**7**) was used instead of DMAP (**8**). Based on the proposed mechanism and results of earlier studies this should not affect selectivity.[18] First, the methyl group in **1c** resp. **2b** was replaced by a phenyl group leading to **1d** resp. **2e**. Very interestingly, this change did not affect selectivity values at all. However, adding a second cyclohexyl group to **2c** (= **2f**) led to an extraordinary drop of its reactivity. The obtained product and reactant ratios are beyond the accuracy limits of ^{1}H-NMR spectroscopy. Thus, analysis was performed by GC analysis. However, selectivity values higher than 200 cannot be reliably determined by single point competitions.[26-27] For a detailed discussion on limitations and alternatives to determine selectivity values in highly selective reactions see Chapter 6 of this thesis. Even competitions of **2f** with slower alcohols **2g** and **2e** as well as the uncatalysed reaction of **1d** and **2f** lead to selectivity values beyond the scope of analytical methods. Nonetheless, it can be stated that **2f** reacts at least 200 times slower than alcohols **1d** and **2e**. Finally, opening the two cyclohexyl rings of **2f** leads to tridecan-7-ol **2g**. This very flexible molecule reacted 1.9 times slower than aromatic alcohol **1d** – a similar accelerations as found in competition experiments of **1c** and **2d** between small TMSCl (**3h**) to TPSCl (**3a**).

Table 2.5. Selectivity values determined by competition experiments with secondary alcohols.

N°	Alc1	Alc2	SiCl	Si1	Si2	cat.	$s = \dfrac{k(1x)}{k(2x)}$
1	**1c**	**2b**	$R^5 = CH_3$	**3h**	**5ch**	**6bh**	DMAP (**8**) (10%)	**1.1±0.03**
2	**1c**	**2b**	$R^5 =$	**3a**	**5ca**	**6ba**	DMAP (**8**) (10%)	**3.8±0.1**
3	**1c**	**2c**	$R^5 = CH_3$	**3h**	**5ch**	**6ch**	DMAP (**8**) (10%)	**1.4±0.1**
4	**1c**	**2c**	$R^5 =$	**3a**	**5ca**	**6ca**	DMAP (**8**) (10%)	**4.1±0.3**
5	**1c**	**2d**	$R^5 = CH_3$	**3h**	**5ch**	**6dh**	DMAP (**8**) (10%)	**0.36±0.01**
6	**1c**	**2d**	$R^5 =$	**3a**	**5ca**	**6da**	DMAP (**8**) (10%)	**0.73±0.01**
7	**1d**	**2e**	$R^5 =$	**3a**	**5da**	**6ea**	TCAP (**7**) (10%)	**4.0±0.1**
8	**1d**	**2f**	$R^5 =$	**3a**	**5da**	**6fa**	TCAP (**7**) (10%)	**>200**
9	**1d**	**2g**	$R^5 =$	**3a**	**5da**	**6ga**	TCAP (**7**) (10%)	**1.9±0.1**

Even if not all effects can be fully rationalized, several trends are apparent from this reaction series:

1. Similar rates with small TMSCl (**3h**) for aromatic **1c** and aliphatic **2b**, **2c**: The reactivity of the alcohol group (e.g. due to differences in acidity or nucleophilicity) is not the main factor for selectivities in this project as it should impact relative rates with TMSCl (**3h**) in a similar way as those with TPSCl (**3a**).

2. Structures with saturated branches in β-position to the hydroxy group (**2b**, **2e**, and **2c**) react roughly four times slower with TPSCl (**3a**) than comparable aromatic alcohols (**1c**, **1d**), if two saturated β-branches are introduced (**2f**) rates are lowered by a factor of at least 200: Especially the latter observation indicates that neighbouring CH-bonds parallel to the hydroxy group notably lower reactivity. That can be rationalized by geometrical dispositions. Literature crystal structures[28] as presented in **Figure 2.2** show that tetrahedral groups shield the hydroxy group in **2f** from all directions, while planar moieties in **1d** demand less space.
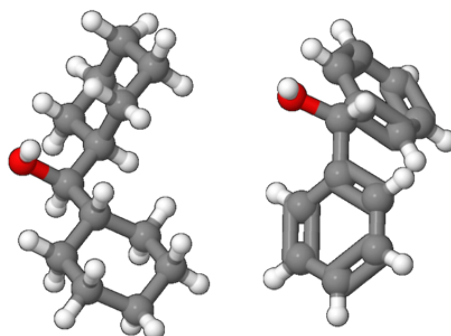
Figure 2.2. Crystal structures for **2f**[29] and **1d**[30] as reported in the CCDC-database.

3. All reactions with a pair of aromatic substituents on the alcohol and the silyl chloride show significantly higher reaction rates; including β-branch-free isopropanol (**2d**) (as compared to its reaction with TMSCl **3h**) and tridecan-7-ol (**2g**): It is reasonable to assume that this acceleration by a factor of roughly two is related to stabilizing π-π interactions. However, for a more detailed inspection of these rate accelerations other experimental approaches should be chosen (see Chapter 3).

2.2.5. Computational Study

For a further analysis of the origins of chemoselectivity a computational study was performed on the secondary silyl ethers. Conformational search for reactants and products was performed with Maestro, optimization was done at the SMD(CHCl$_3$)/B3LYP-D3/6-311+G(2d)/6-31+G(d) level of theory, followed by single point calculations for the best conformer at the DLPNO-CCSD(T)/def2-TZVPP level. **Table 2.6** shows reaction free energies for the reactions depicted above.

Table 2.6. Reaction free energies at different levels of theories for the depicted reactions. Additionally, the difference of Grimme-D3 dispersion correction is shown. All energy differences are reported kJ mol^{-1}.

Reaction	SMD(CHCl$_3$)/B3LYP-D3/6-311+G(2d)/6-31+G(d)[a]			DLPNO-CCSD(T)/def2-TZVPP//SP[b]
	ΔG_{298} (best conformer)	ΔG_{298} (Boltzmann averaged)	$\Delta E_{Grimme-D3}$	ΔG_{298} (best conformer)
1c + 3a → 5ca + HCl	+12.9	+12.3	-23.0	+7.2
2b + 3a → 6ba + HCl	+13.5	+12.6	-23.2	+9.2
2c + 3a → 6ca + HCl	+15.6	+15.2	-18.3	+11.3
2d + 3a → 6da + HCl	+15.3	+15.1	-11.9	+9.4
1d + 3a → 5da + HCl	+6.9	+6.7	-27.6	+0.7
2e + 3a → 6ea + HCl	+9.9	+10.0	-30.6	+6.5
2f + 3a → 6fa + HCl	+11.9	+11.8	-36.3	+11.1

[a] H,(C,O): 6-31+G(d); Si,Cl: 6-311+G(2d) [b] SMD(CHCl$_3$) solvation energy added

All reactions were found to be endergonic in agreement with other studies.[31] The driving force for these silylation reactions is accordingly the strongly exergonic reaction of side-product hydrogen chloride and the auxiliary base triethyl amine (**4**). This also explains why the reaction basically stops if the auxiliary base is used in an under-stochiometric ratio.[18] Analysis of the contribution of Grimme-D3 dispersion correction to reaction free energies clearly shows that in the course of all reactions additional dispersive interactions are generated. Unsurprisingly, a clear trend is visible with the lowest gain of dispersion energy for the formation of isopropanol silyl ether **6da** and *sec*-isoamyl alcohol silyl ether **6ca**. In the case of 1-cyclohexylethanol (**2b**) and 1-phenylethanol (**1c**) the gain of dispersion energy is basically the same. However, for alcohols doubly-substituted with bulky groups the gain of dispersion energy increases from double phenyl-substituted **1d** via mixed-substituted **2e** to doubly cyclohexyl-substituted alcohol **2f** by roughly 10 kJ mol^{-1}. This agrees with the discussed literature trends and clearly indicates that the major rate deviances between aromatic and aliphatic alcohols cannot be solely attributed to dispersion forces. Subsequently, we tried to relate experimental and computational results. In principle the Eyring equation (Eq. 2.1) allows to correlate relative rates and the difference of free energy of the related transition states $\Delta\Delta G^{\ddagger}$ by Eq. 2.2.

$$k = \frac{k_B T}{h} \cdot e^{-\frac{\Delta G^{\ddagger}}{RT}}$$
Eq. 2.1

$$\Delta\Delta G^{\ddagger} = RT \ln(s)$$
Eq. 2.2

Unfortunately, the computational costs for optimization and identification of the best transition states are usually very high. The Marcus theory, however, proposes that the activation free energy and the reaction free energy are related and for similar reactions a correlation can be expected.[32] In this manner we calculated the expected relative barriers from the selectivity values obtained

experimentally by Eq. 2.2. Indeed, the expected trends for $\Delta\Delta G^{\ddagger}_{298}$ are reflected in the differences of reaction free energies at DLPNO-CCSD(T)/ def2-TZVPP level of theory except for the reaction with isopropanol (**2c**) that was already found above to be too different from the other alcohols (see reaction rates with TMSCl **3h**. Unfortunately, the small number of data points does not allow a more detailed analysis. $\Delta\Delta G_{298}$ was further decomposed into solvation energies, thermal correction to free energy and total electronic energies (**Table 2.7**).

Table 2.7. Differences of reaction free energies and decomposition into its contributors.

Name	$\Delta\Delta G^{\ddagger}_{298}$ expected (Eq. 2.2)	SMD(CHCl$_3$)/B3LYP-D3/ 6-311+G(2d)/6-31+G(d)[a]			DLPNO-CCSD(T)/ def2-TZVPP//SP	
		$\Delta\Delta G_{298}$	$\Delta\Delta E$ (solvation energy)	$\Delta\Delta E_{298}$ (thermal correction)	$\Delta\Delta E$	$\Delta\Delta G^{b}_{298}$
ΔG(**6ba**) - ΔG (**5ca**)	+3.3	+0.3	+1.1	+3.6	-2.6	+2.1
ΔG(**6ca**) - ΔG (**5ca**)	+3.5	+3.0	+1.2	+3.2	-0.2	+4.2
ΔG(**6da**) - ΔG (**5ca**)	-0.8	+2.9	+0.7	-1.7	+3.3	+2.3
ΔG(**6fa**) - ΔG (**5da**)	+13.1	+5.2	+4.3	+7.9	-1.8	+10.4
ΔG(**6ea**) - ΔG (**5da**)	+3.4	+3.4	+1.8	+3.2	+0.7	+5.8

[a]H(C,O): 6-31+G(d); Si,Cl: 6-311+G(2d) [b] SMD(CHCl$_3$) solvation energy added

Table 2.8. Structures of the best conformers of silyl ethers. Pictures were generated with CYLview.[33]

5ca	**6ca**	**6ba**
5da	**6ea**	**6fa**
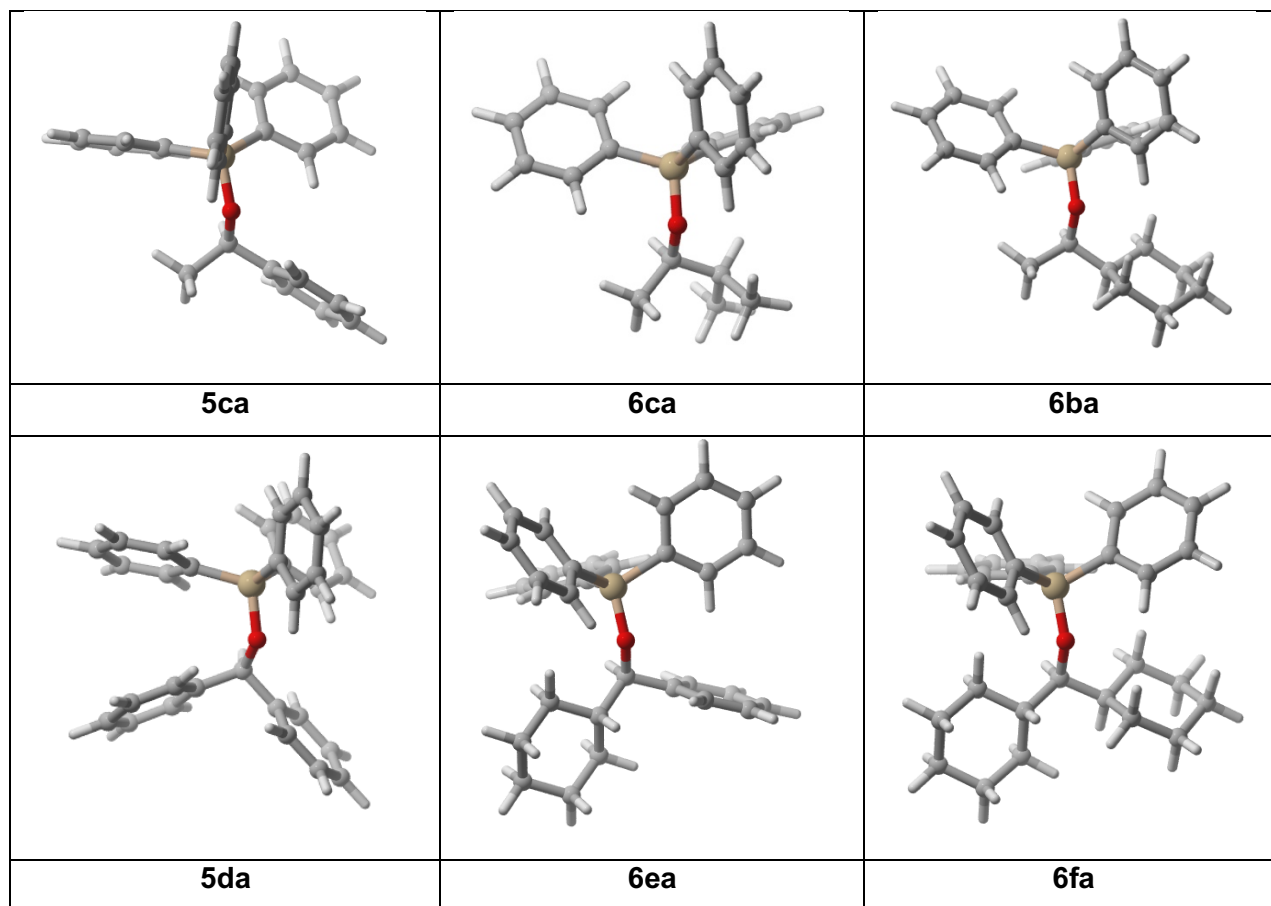
Surprisingly, no major differences are present in reaction electronic energies at single point level for the different alcohols. Reaction electronic energies are even slightly more favourable for the reactions involving cyclohexyl groups. This again confirms theoretical results on better stabilization energies for a mixed aromatic-aliphatic stacking. Hence, differences in reaction free energies are mainly caused by differences in solvation energy and especially very unfavourable thermal corrections to 298 K for mixed aromatic-aliphatic silyl ether. The latter one will notably depend on the geometry of investigated systems. Steric unfavourable geometries are generally characterized by a restriction of molecular vibrations. Accordingly, Sigman *et al.*[34] proposed to use molecular vibrations as descriptor for spatial interactions. Structures for the best conformers are depicted in **Table 2.8**. Various stacking interactions can be found throughout the conformers. For silyl ethers with aliphatic moieties conformational fixed γ-CH-bonds parallel to the C-O-bond can be seen in **6ca**, **6ba**, **6ea**, and to the highest extent in **6fa**.

2.3. Conclusion

Phenyl-substituted primary and secondary alcohols react up to 8 times faster with triarylsilyl chlorides than their aliphatic analogues. Increasing the aromatic surface of the silyl chloride further accelerated aromatic alcohols. In contrast, for silyl chlorides without aromatic groups similar rates were obtained for aromatic and aliphatic alcohols. In the case of bulky TBDMSCl (**3c**) even the aliphatic alcohol reacted faster. In reactions with aromatic silyl chlorides relative rates decrease with the number of possible 1,5-interactions of the hydroxy group. Accordingly, relative rates for dicyclohexylmethanol (**2f**) were at least 200 times slower than for diphenylmethanol (**1c**). However, an acceleration of aromatic alcohols by a factor of two could be also observed relative to unhindered alcohols. Thus, selectivity is induced by an interplay of attractive and unfavourable non-covalent interactions. Relative rates were found to correlate with reaction free energies. In accordance with literature reports, the gain of dispersion energy was found to be higher in the formation of aliphatic-aromatic silyl ethers than for aromatic-aromatic silyl ethers. The differences in reaction free energies are, however, not the result of differences in electronic energies, but reflect differences in solvation and vibrational energies. Relative rates are accordingly not governed as hypothesized by the different strength of NCIs between aromatic and aliphatic moieties as compared to two aromatic ones but prominently by geometrical properties of the reacting partners. These results indicate that for a quantitative analysis of attractive dispersive interactions reagents should be investigated that are geometrically and electronically as similar as possible. For example, secondary alcohols with systematically increasing aromatic surfaces seem to be suitable model reagents for quantifying rate accelerations through attractive interactions.

2.4. Experimental Methods and Data for Competition Experiments

2.4.1. Experimental Protocol for Competition Experiments

R^1, R^3, R^5, R^6 = hydrocarbon
R^2, R^4 = hydrogen or hydrocarbon
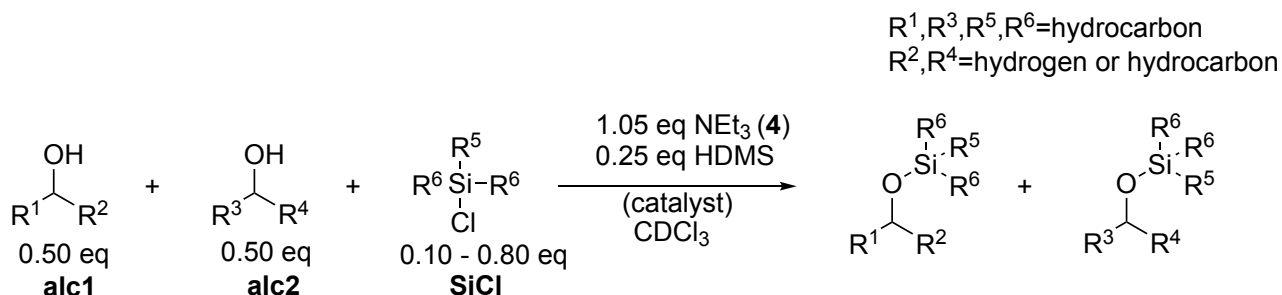
Scheme 2.3. Experimental setup of competition experiments.

General methods: All calibrated flasks, stirring bars, GC vials, NMR tubes and other equipment were oven-dried at 110 °C overnight prior to use and were evacuated and purged with nitrogen three times prior to use. Solutions were transferred using Hamilton syringes, that were dried under vacuum and flushed with nitrogen. Preparation of stock solutions and reaction setup in the GC vials was performed under nitrogen atmosphere. CDCl$_3$ and triethylamine (**4**) were freshly distilled from CaH$_2$ prior to use.

Typical procedure for uncatalysed reactions: For the preparation of stock solution A a 1 : 1 mixture of the two alcohols (each 0.20 mol/L, 0.50 eq), triethylamine (**4**, 0.42 mol/L, 1.05 eq) and internal standard hexadimethylsilane (**9**, 0.10 mol/L, 0.25 eq) are weighed into a calibrated flask and filled with CDCl$_3$. Stock solution B is similarly prepared from the corresponding silyl chloride. Subsequently diluted stock solutions B$_x$ containing various concentrations (0.04 mol/L, 0.10 eq to 0.32 mol/L, 0.80 eq) of silyl chloride are prepared from B and CDCl$_3$. 0.5 mL of A and diluted stock solution B$_x$ are mixed in a GC vial equipped with a stirring bar, capped and stirred. The temperature is controlled in a GC-vial holder connected to the circuit of a cryostat at +23 °C. After the stated amount of time, 0.6 mL of reaction mixture are transferred into a NMR tube and a ^{1}H-NMR is recorded. To the remaining solution in the GC vial 1 mL of dry DCM is added and a gas chromatogram is measured.

Typical procedure for catalysed reactions: Three stock solutions instead of two were prepared as explained above: Stock solution A contains mixtures 1 : 1 of the two alcohols (each 0.30 mol/L, 0.50 eq), triethylamine (**4**, 0.63 mol/L, 1.05 eq) and internal standard hexadimethylsilane (**9**, 0.10 mol/L, 0.17 eq), stock B various concentrations of silyl chloride and stock C the relevant concentration of catalyst. 0.5 mL of each stock solution is transferred to the GC vial yielding the same concentration of 0.10 mol/L per alcohol in the reaction mixture. All following steps were performed similarly to uncatalysed reactions. Note that for all competition experiments with trinaphthylsilyl chloride (**3g**), *tert*-butyldimethylsilyl chloride (**3c**) or with 2-naphthylmethanol (**1b**) concentrations were one third of the above stated (0.033 mol/L of each alcohol in reaction mixture)

due to solubility reasons. Competition experiments of **1a** and **2a** with **3a** at both concentrations indicate that this change in concentration does not affect selectivity.

2.4.2. Analysis of NMR Spectra
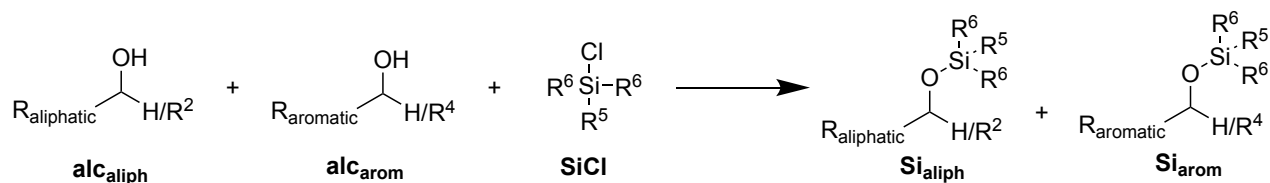
Scheme 2.4. Competition experiment of an aliphatic alcohol **alc$_{aliph}$** and an aromatic alcohol **alc$_{arom}$**.

Typical reaction mixture of a competition experiment of aliphatic and aromatic alcohol as shown in **Scheme 2.4** contains four species of interest: the two unreacted alcohols and the two formed silyl ethers. Reaction mixtures were analysed by ^{1}H-NMR and/or by gas chromatography. ^{1}H-NMR spectra are recorded on a 400 MHz machine. Automated phase correction and a Bernstein polynomial fit with polynomial order 3 is applied. The α hydrogen atoms of alcohol respectively silyl ether are integrated and absolute integral values are used for further calculation.
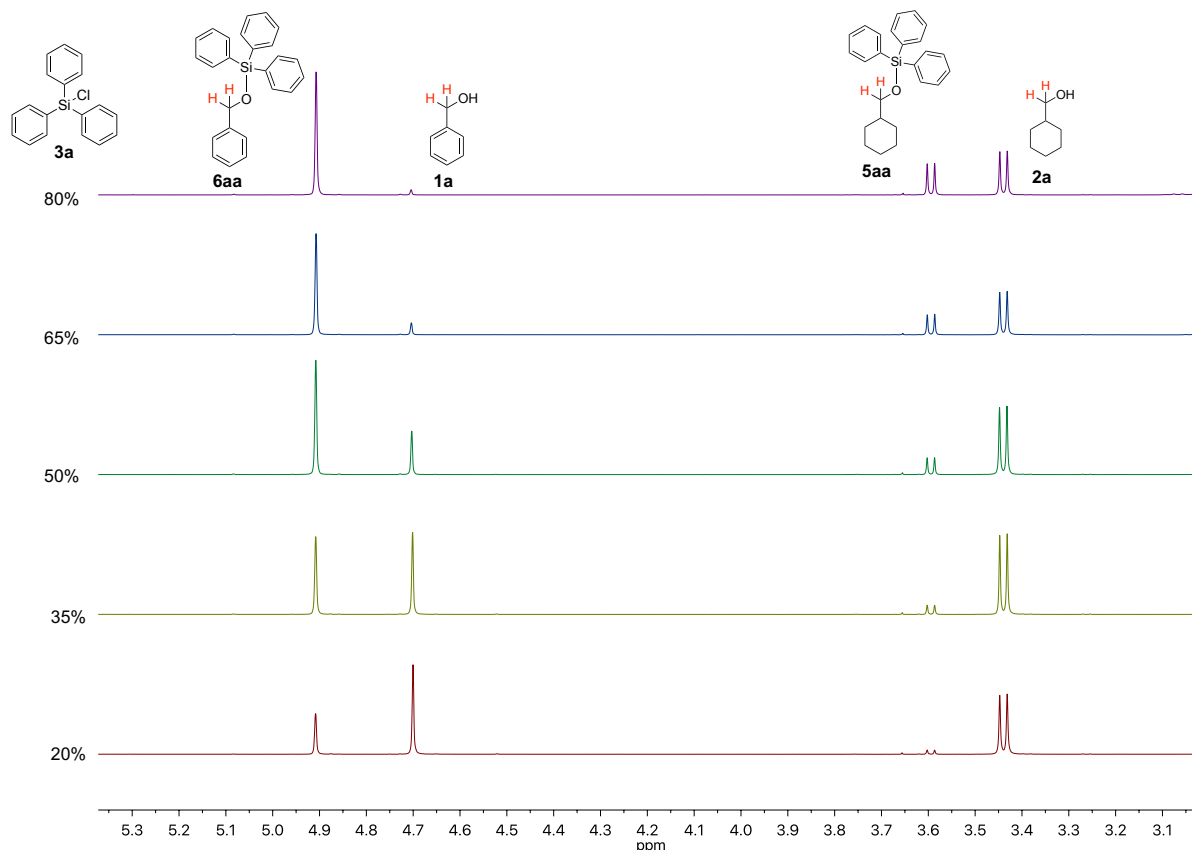
Figure 2.3. Representative example for ^{1}H-NMR analysis of a competition experiment of alcohol **1a** and **2a** with silyl chloride **3a**. The signal of the red marked α hydrogen atoms of alcohol respectively silyl ether are integrated.

2.4.3. Calculation of Selectivity Values
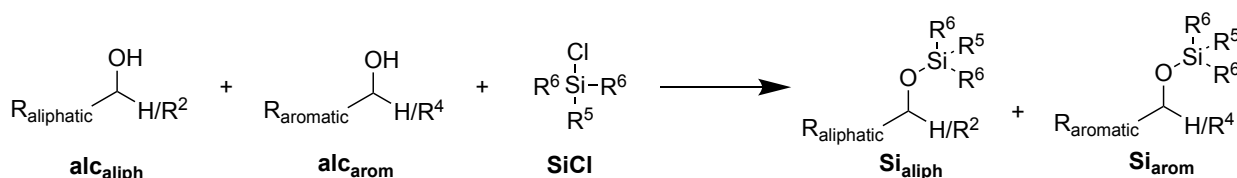
Scheme 2.5. Competition experiment of an aliphatic alcohol **alc_aliph** and an aromatic alcohol **alc_arom**.

Selectivity for competition experiments as shown in **Scheme 2.5** is defined as the reaction rate ratio of aromatic alcohol **alc_arom** relative to aliphatic alcohol **alc_aliph** as shown in Eq. 2.4. In experiments of two aliphatic or two aromatic alcohols the selectivity is defined separately.

$$s = \frac{k(alc_{aromatic})}{k(alc_{aliphatic})}$$

Eq. 2.4

The chemoselectivity C of alcohols and silyl ether products is defined analogously to enantiomeric excess by Eq. 2.6 and Eq. 2.7. As the calculation of chemoselectivity values assume a perfect 1 : 1 ratio of both alcohols, a correction factor f describing the initial ratio of the two alcohols (Eq. 2.5) is introduced to equilibrate minor experimental deviations.

$$f = \frac{[\mathbf{Si_{arom}}] + [\mathbf{alc_{arom}}]}{[\mathbf{Si_{aliph}}] + [\mathbf{alc_{aliph}}]}$$

Eq. 2.5

$$C_{ether} = \frac{[\mathbf{Si_{arom}}] - [\mathbf{Si_{aliph}}] \cdot f}{[\mathbf{Si_{arom}}] + [\mathbf{Si_{aliph}}] \cdot f}$$

Eq. 2.6

$$C_{alcohols} = \frac{[\mathbf{alc_{aliph}}] \cdot f - [\mathbf{alc_{arom}}]}{[\mathbf{alc_{aliph}}] \cdot f + [\mathbf{alc_{arom}}]}$$

Eq. 2.7

For the calculation of conversion *conv* and selectivity *s* Eq. 2.8 and Eq. 2.9 as developed by Kagan and Fiaud[14] for kinetic resolution reactions were used. For a detailed discussion of different methods to determine selectivity see Chapter 6 of this thesis.

$$s = \frac{ln(1 - conv(1 + C_{ethers}))}{ln(1 - conv(1 - C_{ethers}))}$$

Eq. 2.8

$$conv = \frac{C_{alcohols}}{C_{alcohols} + C_{ethers}}$$

Eq. 2.9

2.4.4. GC Analysis

As an independent analysis method several competition experiments were also analysed by gas chromatography (GC). Intermediate concentrations were analysed by a flame ionization detector (FID). As the effective carbon number is the same for aromatic and aliphatic alcohols resp. silyl ethers in competition experiments FID areas can be compared directly without a calibration curve.[35] This correlation of relative FID area and relative concentration of alcohols resp. silyl ether was confirmed by FID analysis of standard solutions with known ratios of species. It is important to note that FID areas of alcohols cannot be directly compared to areas of silyl ethers. GC analysis is by far more sensitive than ^{1}H-NMR and thus especially important for high selectivity values if

concentrations of the slow reacting species (resp. reactant of fast reacting species) are too small for NMR analysis. As this is especially important in this project for secondary alcohols the reaction in **Scheme 2.6** is shown as a representative example. The GC spectra shown in **Figure 2.4** are analysed in **Table 2.9** as described above. No correction factor is used in GC analysis. **Table 2.10** gives data for ^{1}H-NMR analysis of the same experiment. Both analysis methods lead to the same selectivity value. Also, for the competition experiments with fluorinated silyl chlorides both GC and NMR analysis gave comparable selectivity values (see **Table 2.11** and **Table 2.12**). If not stated differently, selectivity values are reported based on ^{1}H-NMR analysis.
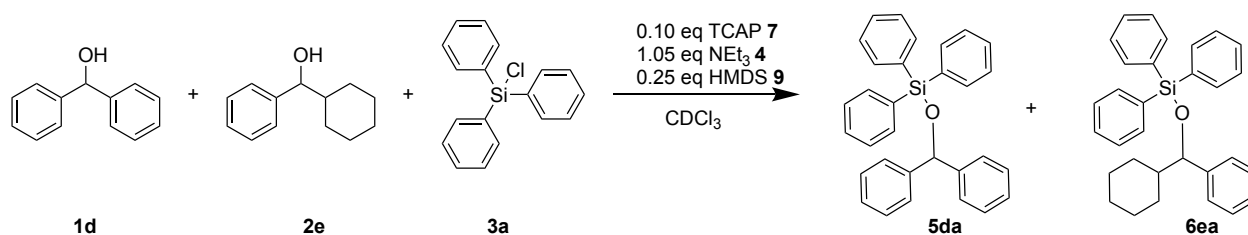
Scheme 2.6. Competition experiment of **2e** and **1d** with silyl chloride **3a**.
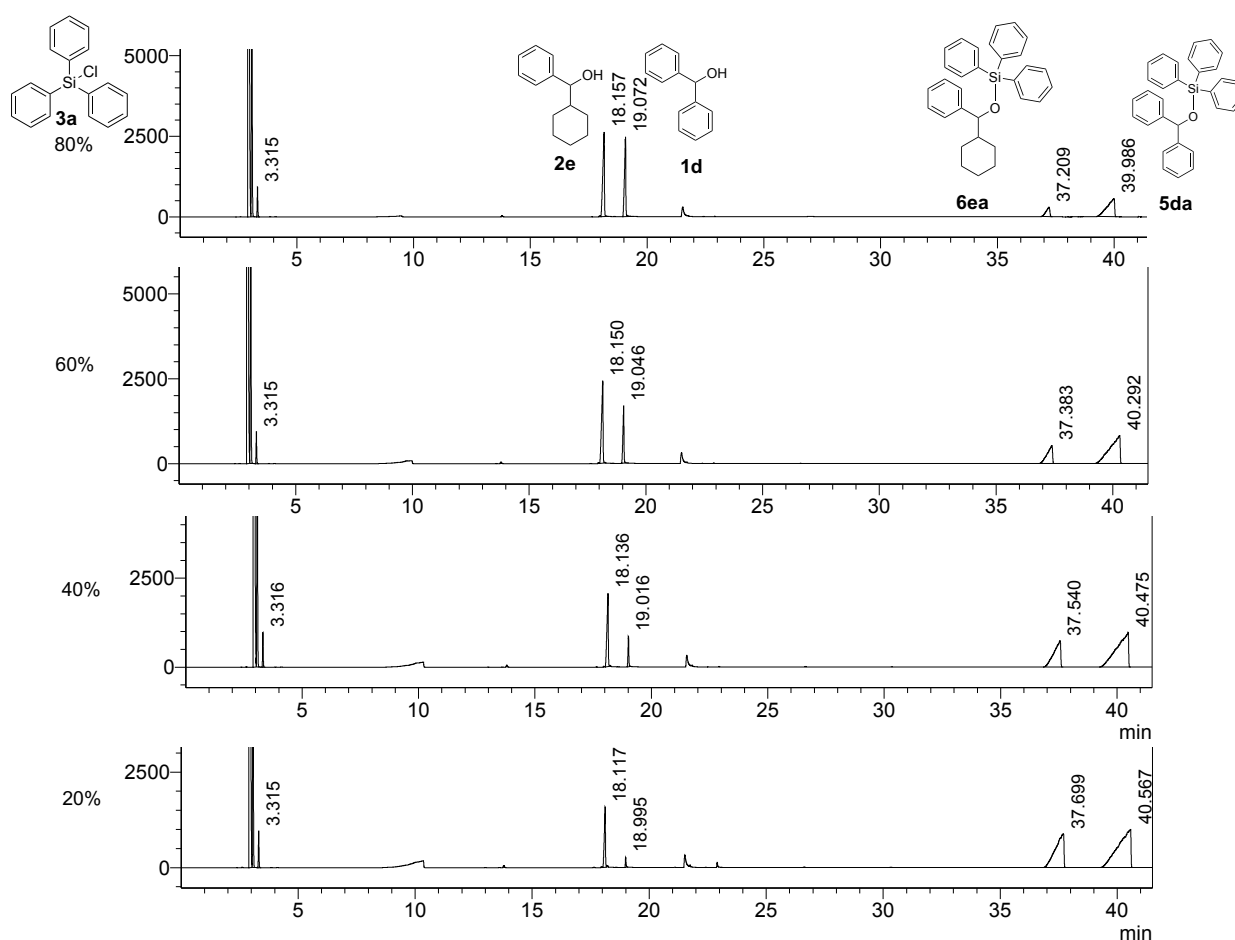
Figure 2.4. Representative example for GC analysis of a competition experiment of alcohol **2e** and **1d** with silyl chloride **3a** as shown in **Scheme 2.6**. Signals are measured by FID, intensities are reported in mV. The broadness of the peaks of silyl ether products is unavoidable due to their high molar mass.

Table 2.9. GC analysis of the competition experiment shown in **Scheme 2.6** (for relevant GC spectra see **Figure 2.4**).

% of 3a	GC-FID area [mV]				Chemoselectivity C		conv	s	averaged	
	2e	1d	6ea	5da	silyl ethers	alcohols			s	St.Dev
20	12214990	9820431	3234946	12385061	0.58579455	0.10866863	15.65%	4.26	**4.00**	**0.18**
40	10666713	5324862	8273058	24451278	0.49437886	0.33404158	40.32%	4.05		
60	8295959	2064096	14862067	33368117	0.38370266	0.60152798	61.05%	3.95		
80	5432307	530567	22154424	37238329	0.25396878	0.8220432	76.40%	3.76		

Table 2.10. ^{1}H-NMR integrals of the competition experiment shown in **Scheme 2.6**.

% of 3a	^{1}H-NMR integral				Chemoselectivity C		conv	s	averaged	
	2e	1d	6ea	5da	silyl ethers	alcohols			s	St.Dev
20	10920	24510	2921	32509	10920	24510	19.53%	4.28	**4.04**	**0.14**
40	18645	11968	6418	24195	18645	11968	40.94%	3.99		
60	25239	4869	11237	18872	25239	4869	60.57%	3.90		
80	28683	971	17028	12626	28683	971	77.07%	4.00		

2.4.5.Stability of Reaction Mixtures and Reliability of Measured Selectivity Values

The analysis of reaction mixtures of competition experiments for the determination of relative rates is only meaningful if no equilibration process after the reaction alters the ratios of reactants and products. Thus, the long-term stability was controlled through repeated GC analysis of the same sample (alcohols **1a** and **2a** with silyl chloride **3a**) over the period of 1.5 months. Ratios were found to be constant over that time for uncatalysed primary alcohol reaction mixtures and for all mixtures with secondary alcohols (see detailed information in Chapter 3). However, in reactions catalysed by 10% TCAP (**7**) the concentration of aromatic silyl ether **5aa** decreased by 53% over 28 days, while the concentration of the corresponding primary alcohol **1a** increased by 47%. The ratio of aliphatic alcohol **2a** to silyl ether **6aa** only changed slightly in the same time. Comparable but smaller effects were also found in experiments with less catalyst loading but not in uncatalysed reactions. The catalyst therefore seems to mediate the deprotection reaction of primary aromatic silyl ether. Due to several side products and the long reactions times the deprotection does not seem to be a useful reaction nor suitable for detailed kinetic measurements. Because of these findings together with the above reported irregularities in catalysed reactions, only the uncatalysed silylation of primary alcohols as investigated, while in all catalysed reactions secondary alcohols were used, as in these cases no side reactions occured.

The reliability of all experiments was controlled by the correction factor and by fitting of experimental values with simulated turnover-curves for a given selectivity value. Selectivity curves were simulated as described in Chapter 3.

2.4.6. Integral Tables of Competition Experiments

Table 2.11. ^{1}H-NMR data for competition experiments for the silylation of aromatic (arom.) and aliphatic (aliph.) alcohols with specified silyl chloride (SiCl) as outlined above. Raw absolute integrals are reported, chemoselectivity was calculated by Eq. 2.6 resp. Eq. 2.7, conversion by Eq. 2.8, selectivity values by Eq. 2.9. The last row reports mean of selectivity over all measurement points and standard deviation (std. dev.).

Arom. alcohol	Aliph. alcohol	SiCl	conditions[a]	% SiCl[b]	raw absolute integrals ^{1}H-NMR				Chemoselectivity		conversion	Selectivity	
					Arom. Si-ether	Arom. alcohol	Aliph. Si-ether	Aliph. alcohol	C_{ether}	$C_{alcohol}$			mean ± std. dev.
1a	2a	3a	-	10%	26838	113705	5473	137155	0.67	0.09	11.47%	5.42	6.5±0.5
				30%	43435	69839	8570	103558	0.67	0.20	22.99%	6.08	
				50%	79445	25563	20651	80874	0.58	0.53	48.00%	6.21	
				10%	29851	116867	4883	141143	0.72	0.10	11.84%	6.69	
				30%	67772	82041	12606	133399	0.68	0.25	26.94%	6.67	
				50%	98808	36253	25541	104531	0.58	0.50	46.40%	6.02	
				20%	4169	8103	697	11258	0.71	0.18	19.90%	6.91	
				35%	5779	5341	1119	9730	0.67	0.30	31.14%	6.74	
				50%	8325	2824	1907	8781	0.61	0.53	46.26%	6.99	
				65%	9027	926	2708	6653	0.52	0.77	59.81%	6.96	
				80%	9606	369	3746	5887	0.42	0.89	67.59%	6.70	
1a	2a	3a	solvent DCM	50%	95218	34297	32480	86636	0.46	0.47	50.39%	4.17	4.2±0.04
				50%	101153	38517	33820	95439	0.47	0.46	49.29%	4.25	
1a	2a	3a	solvent THF	50%	74324	36387	27440	81851	0.46	0.39	46.12%	3.85	4.1±0.2
				50%	94634	43022	33513	100733	0.47	0.41	46.86%	4.05	
				50%	103280	41752	34140	105444	0.49	0.45	47.84%	4.44	
1a	2a	3a	10% **7**	20%	5256	12040	2940	14352	0.28	0.09	23.70%	1.94	1.7±0.2

Arom. alcohol	Aliph. alcohol	SiCl	conditions[a]	% SiCl[b]	raw absolute integrals ^{1}H-NMR				Chemoselectivity		conversion	Selectivity	
					Arom. Si-ether	Arom. alcohol	Aliph. Si-ether	Aliph. alcohol	C_{ether}	$C_{alcohol}$			mean ± std. dev.
				40%	9397	11311	6189	14560	0.21	0.12	37.60%	1.71	
1a	2a	3a	10% 7	60%	9240	7522	7861	9046	0.08	0.09	50.81%	1.28	
				20%	25878	73769	14384	84886	0.28	0.07	20.23%	1.92	
				40%	42091	55572	24376	72898	0.26	0.14	34.08%	1.95	
				60%	57711	37828	40678	54130	0.17	0.18	51.66%	1.65	
				80%	74978	20828	60106	34401	0.10	0.25	70.93%	1.51	
1a	2a	3a	10% 7, SiCl added via syringe pump (30 mins)	20%	26416	81303	15452	92612	0.26	0.06	19.41%	1.82	1.5±0.2
				35%	40685	67760	28704	79431	0.17	0.08	32.03%	1.52	
				50%	54880	51803	43921	63799	0.12	0.10	46.11%	1.38	
				65%	71977	34779	60665	46518	0.09	0.14	62.01%	1.34	
				80%	80301	25479	69015	37143	0.08	0.18	70.46%	1.36	
1a	2a	3a	5% 7	20%	39178	93511	18948	114657	0.35	0.10	21.85%	2.29	1.8±0.3
				40%	63948	66332	41424	90099	0.22	0.15	40.29%	1.78	
				60%	59743	31152	45255	46291	0.14	0.19	57.58%	1.57	
				80%	68464	13851	55834	26362	0.10	0.31	75.55%	1.57	
1a	2a	3a	2.5% 7	20%	27501	77955	12756	92171	0.36	0.09	19.12%	2.33	2.1±0.2
				40%	40455	51987	21642	71029	0.30	0.15	33.56%	2.16	
				60%	58841	32657	36645	53929	0.23	0.25	52.38%	1.99	
				80%	75296	15525	56894	32987	0.13	0.36	73.10%	1.76	
1a	2a	3c	-	20%	10728	75411	15099	70380	-0.17	-0.03	15.06%	0.68	0.54±0.1
				35%	17883	59633	28255	47225	-0.24	-0.10	30.25%	0.56	

Arom. alcohol	Aliph. alcohol	SiCl	conditions[a]	% SiCl[b]	raw absolute integrals ^{1}H-NMR				Chemoselectivity		conversion	Selectivity	
					Arom. Si-ether	Arom. alcohol	Aliph. Si-ether	Aliph. alcohol	C_{ether}	$C_{alcohol}$			mean ± std. dev.
				50%	26039	50965	43163	35231	-0.24	-0.19	44.44%	0.52	
1a	2a	3c	-	65%	27704	44465	46178	25487	-0.25	-0.27	51.41%	0.47	
				80%	36938	32002	57306	11629	-0.22	-0.47	68.36%	0.43	
				20%	11188	81841	14465	76152	-0.14	-0.02	13.99%	0.74	
				35%	17447	65490	25792	53624	-0.21	-0.08	26.76%	0.60	
				50%	25738	58977	41648	39886	-0.25	-0.17	40.73%	0.51	
				65%	34254	49384	56115	25089	-0.26	-0.31	55.03%	0.45	
				80%	34829	33185	55813	15915	-0.21	-0.37	64.51%	0.48	
1a	2a	3d	-	10%	31705	119384	10785	146979	0.51	0.08	13.91%	3.33	4.0±0.6
				30%	28105	52361	6910	75285	0.61	0.17	21.67%	4.89	
				50%	74532	55804	21232	110156	0.56	0.32	36.67%	4.81	
				70%	90597	28121	33580	85510	0.46	0.50	52.26%	4.35	
				10%	19687	87467	5880	103393	0.55	0.07	11.88%	3.67	
				30%	33103	67317	10393	91121	0.53	0.14	21.60%	3.70	
				50%	56307	44606	20272	81110	0.47	0.29	37.90%	3.66	
				70%	54699	22226	23539	56304	0.41	0.42	50.29%	3.55	
1a	2a	3e	-	20%	42588	104414	12529	132539	0.54	0.13	18.80%	3.79	4.5±0.5
				35%	66172	84694	18148	129369	0.56	0.22	28.08%	4.40	
				55%	89907	45592	28226	102625	0.51	0.40	43.96%	4.48	
				10%	13040	107138	3748	122694	0.57	0.04	6.91%	3.82	
				30%	30635	84350	7372	115550	0.63	0.12	16.32%	5.01	
				50%	48623	35617	15525	79862	0.56	0.33	37.00%	4.85	

					raw absolute integrals ^{1}H-NMR				Chemoselectivity		conversion	Selectivity	
Arom. alcohol	Aliph. alcohol	SiCl	conditions[a]	% SiCl[b]	Arom. Si-ether	Arom. alcohol	Aliph. Si-ether	Aliph. alcohol	C_{ether}	$C_{alcohol}$			mean ± std. dev.
				70%	58478	12386	25222	57876	0.46	0.60	56.44%	4.82	
1a	2a	3f	-	20%	32329	66320	6245	94386	0.68	0.16	19.49%	6.20	6.6±0.3
				40%	59879	39654	12797	88028	0.65	0.37	36.43%	6.78	
				60%	71141	35169	16672	90122	0.62	0.44	41.26%	6.52	
				80%	95167	2004	41514	56625	0.40	0.93	70.12%	7.06	
1a	2a	3g	-	20%	50943	163161	9622	206981	0.69	0.11	14.12%	5.98	7.1±0.6
				35%	91856	118548	17121	198045	0.69	0.24	25.81%	6.92	
				50%	124247	63704	25885	164055	0.66	0.44	39.87%	7.38	
				65%	3379	596	931	3077	0.57	0.67	54.13%	7.18	
				80%	3913	154	1591	2451	0.42	0.88	67.78%	6.55	
				20%	1260	3141	193	4784	0.76	0.15	16.26%	8.52	
				35%	2142	2425	433	4731	0.70	0.27	27.64%	7.23	
				50%	2315	1308	563	3632	0.65	0.41	38.66%	7.07	
				65%	2718	756	772	3297	0.61	0.58	48.61%	7.25	
				80%	2816	501	929	3047	0.57	0.67	54.13%	7.10	
1b	1a	3c	-	20%	15196	64957	16025	68970	0.00	0.00	18.91%	1.01	0.99±0.01
				35%	26520	56577	28059	59754	0.00	0.00	31.93%	1.00	
				50%	33267	42718	35064	44976	0.00	0.00	43.79%	1.00	
				65%	41528	34109	44498	35240	-0.01	-0.01	55.35%	0.98	
				80%	40750	27729	43643	28602	-0.01	-0.01	59.96%	0.98	
				20%	18064	93737	18427	96100	0.00	0.00	16.12%	1.00	

Arom. alcohol	Aliph. alcohol	SiCl	conditions[a]	% SiCl[b]	raw absolute integrals ^{1}H-NMR				Chemoselectivity		conversion	Selectivity	
					Arom. Si-ether	Arom. alcohol	Aliph. Si-ether	Aliph. alcohol	C_{ether}	$C_{alcohol}$			mean ± std. dev.
				35%	27929	64856	29431	66834	-0.01	0.00	30.34%	0.98	
				50%	35422	44654	37225	45367	-0.01	-0.01	44.65%	0.97	
				65%	46665	33535	48816	34467	0.00	-0.01	58.40%	0.99	
				80%	54516	24106	57761	24071	-0.01	-0.02	69.96%	0.97	
1b	1a	3a	-	20%	1681	6224	1533	6585	0.06	0.01	20.07%	1.14	1.13±0.03
				35%	2750	5322	2544	6052	0.07	0.03	31.84%	1.19	
				50%	2816	2926	2663	3294	0.05	0.04	46.87%	1.14	
				65%	4583	2782	4639	3282	0.03	0.05	60.39%	1.10	
				80%	3654	1219	3580	1423	0.02	0.06	73.27%	1.10	
1b	1a	3g	-	20%	755	3697	671	3942	0.08	0.01	15.75%	1.18	1.24±0.02
				35%	1355	3045	1207	3500	0.09	0.04	28.22%	1.24	
				50%	1908	2300	1746	2719	0.07	0.05	42.22%	1.22	
				65%	2251	2261	2078	2766	0.08	0.07	46.39%	1.23	
				80%	2074	1392	1908	1786	0.07	0.09	55.74%	1.26	
				20%	1098	4981	930	5491	0.11	0.02	16.27%	1.27	
				35%	852	1906	753	2159	0.09	0.04	28.38%	1.23	
				50%	1155	1469	1033	1738	0.08	0.06	40.65%	1.24	
				65%	2757	2096	2536	2565	0.07	0.08	53.26%	1.22	
				80%	104697	62321	97895	82778	0.07	0.10	58.43%	1.26	
1b	2a	3a	-	20%	2257	3785	414	5601	0.69	0.20	22.12%	6.56	6.5±0.2
				35%	2802	2027	610	4323	0.65	0.35	35.20%	6.57	

					raw absolute integrals ¹H-NMR				Chemoselectivity		conversion	Selectivity	
Arom. alcohol	Aliph. alcohol	SiCl	conditions[a]	% SiCl[b]	Arom. Si-ether	Arom. alcohol	Aliph. Si-ether	Aliph. alcohol	C_{ether}	$C_{alcohol}$			mean ± std. dev.
				50%	3816	993	1012	3875	0.59	0.59	50.03%	6.80	
				65%	4415	358	1601	3183	0.47	0.80	62.98%	6.36	
				80%	4654	110	2179	2688	0.37	0.92	71.23%	6.34	
1b	2a	3g	-	20%	1115	3702	167	4892	0.75	0.11	13.23%	7.82	7.5±0.3
				35%	2261	2327	433	4446	0.69	0.28	29.08%	7.30	
				50%	2332	1200	541	3338	0.65	0.43	39.99%	7.19	
				65%	2461	1294	512	3538	0.68	0.43	39.09%	7.88	
				80%	2932	520	870	3000	0.58	0.67	53.71%	7.43	
1c	2b	3h	10% 8	20%	3901	13818	3735	14246	0.03	0.01	21.39%	1.07	1.1±0.03
				35%	6579	12082	6311	13256	0.04	0.02	33.75%	1.12	
				50%	8943	7725	8536	8722	0.04	0.04	51.56%	1.13	
1c	2b	3a	10% 8	20%	13461	19836	4401	30219	0.52	0.19	26.57%	3.81	3.8±0.1
				35%	19232	13690	7597	27421	0.46	0.31	40.06%	3.59	
				50%	24256	8248	9871	23370	0.43	0.47	52.16%	3.89	
1c	2c	3h	10% 8	20%	3029	15717	2185	16068	0.15	0.02	14.06%	1.38	1.4±0.1
				35%	4407	15705	3324	16201	0.13	0.03	19.47%	1.33	
				50%	6338	6144	5297	7585	0.11	0.09	45.95%	1.34	
				20%	1532	4027	935	4209	0.21	0.06	22.87%	1.61	
				35%	2105	3380	1490	3798	0.15	0.08	33.28%	1.46	
1c	2c	3a	10% 8	20%	11891	19681	2971	26881	0.58	0.18	23.81%	4.51	4.1±0.3

Arom. alcohol	Aliph. alcohol	SiCl	conditions[a]	% SiCl[b]	raw absolute integrals ^{1}H-NMR				Chemoselectivity		conversion	Selectivity	mean ± std. dev.
					Arom. Si-ether	Arom. alcohol	Aliph. Si-ether	Aliph. alcohol	C_{ether}	$C_{alcohol}$			
				35%	18063	15255	5757	25492	0.49	0.28	36.32%	3.84	
				50%	22065	8842	8038	21562	0.45	0.44	49.27%	3.95	
1c	2d	3h	10% 8	20%	559	5297	1258	3748	-0.45	-0.09	17.34%	0.35	0.36±0.01
				50%	1833	3921	3374	1853	-0.34	-0.32	48.21%	0.37	
				65%	2678	3115	4455	965	-0.28	-0.50	64.21%	0.36	
1c	2d	3a	10% 8	20%	1315	5628	1542	4715	-0.13	-0.04	21.79%	0.74	0.73±0.01
				30%	1851	5170	2149	4146	-0.13	-0.06	30.25%	0.73	
				50%	2590	3373	2922	2403	-0.12	-0.11	49.15%	0.72	
				70%	3782	1659	3991	957	-0.07	-0.22	75.08%	0.72	
1d	2e	3a	10% 7	20%	10920	24510	2749	30599	0.58	0.14	19.53%	4.28	4.0±0.1
				40%	18645	11968	6117	23057	0.49	0.34	40.94%	3.99	
				60%	25239	4869	10774	18095	0.38	0.59	60.57%	3.90	
				80%	28683	971	16208	12018	0.25	0.86	77.07%	4.00	
1d	2g	3a	10% 7	20%	7928	22942	3841	25464	0.32	0.08	19.39%	2.11	1.9±0.1
				40%	14160	14439	8395	19568	0.25	0.16	39.77%	1.91	
				60%	19927	8003	12994	13723	0.19	0.28	59.99%	1.88	
				80%	24693	3232	18258	8350	0.13	0.46	78.52%	1.86	

[a]Only deviations from standard conditions ($CDCl_3$, +23 °C, 1.1 eq NEt_3, no catalyst) are reported. [b]Relative to the total concentration of both alcohols.

Table 2.12. GC integral data for selected competition experiments for the silylation of aromatic (arom.) and aliphatic (aliph.) alcohols with specified silyl chloride (SiCl) as outlined above. Raw absolute integrals are reported, chemoselectivity was calculated by Eq. 2.6 resp. Eq. 2.7, conversion by Eq. 2.8, selectivity values by Eq. 2.9. The last row reports mean of selectivity over all measurement points and standard deviation (std. dev.).

Arom. alcohol	Aliph. alcohol	SiCl	cond-itions[a]	% SiCl[b]	Arom. Si-ether	Arom. alcohol	Aliph. Si-ether	Aliph. alcohol	C_{ether}	$C_{alcohol}$	conversion	Selectivity	mean ± std. dev.
					raw absolute integrals GC-FID				Chemoselectivity		conversion	Selectivity	
1a	**2a**	**3d**	-	10%	1166699	694631	237933	1001770	0.62	0.25	29.16%	5.37	**4.9±0.9**
				30%	425226	163287	205461	841470	0.61	0.45	42.29%	6.27	
				50%	777689	175775	1702362	4681654	0.47	0.63	57.50%	5.06	
				70%	1315240	413100	1182666	4292388	0.57	0.52	47.89%	6.00	
				10%	1977778	1599001	456496	1696082	0.58	0.11	15.53%	4.12	
				30%	1750186	1133442	839952	2831613	0.54	0.21	28.28%	4.14	
				50%	1252161	536320	1385434	3885253	0.47	0.40	45.77%	4.08	
				70%	1323089	425274	2455267	6029209	0.42	0.51	54.94%	3.97	
1a	**2a**	**3e**	-	20%	1009539	567456	453234	1485352	0.53	0.28	34.49%	4.28	**4.6±0.7**
				35%	815045	315949	682491	2377126	0.55	0.44	44.34%	5.30	
				55%	744138	157378	1218240	3672791	0.50	0.65	56.46%	5.70	
				10%	1883789	1546186	179267	827779	0.64	0.10	13.26%	5.08	
				30%	1554333	1112131	416581	1627347	0.59	0.17	21.87%	4.58	
				50%	1520671	655294	1371826	3803062	0.47	0.40	45.84%	4.02	
				70%	1108033	311241	2236610	4746374	0.36	0.56	60.97%	3.56	
1a	**2a**	**3f**	-	20%	7187316	5407094	1742414	10401421	0.71	0.14	16.54%	6.85	**6.7±0.2**
				40%	6599421	2944526	3904075	18863616	0.66	0.38	36.82%	6.98	
				60%	6909658	2667559	5474433	22962559	0.61	0.44	41.87%	6.41	
				80%	4272602	204961	13723703	31620791	0.39	0.91	69.71%	6.54	
1d	**2e**	**3a**	10% 7	20%	12214990	9820431	3234946	12385061	0.59	0.11	15.65%	4.26	**4.0±0.2**
				40%	10666713	5324862	8273058	24451278	0.49	0.33	40.32%	4.05	

Arom. alcohol	Aliph. alcohol	SiCl	cond-itions[a]	% SiCl[b]	Arom. Si-ether	Arom. alcohol	Aliph. Si-ether	Aliph. alcohol	C_{ether}	$C_{alcohol}$			mean ± std. dev.
					raw absolute integrals GC-FID				Chemoselectivity		conversion	Selectivity	
				60%	8295959	2064096	14862067	33368117	0.38	0.60	61.05%	3.95	
				80%	5432307	530567	22154424	37238329	0.25	0.82	76.40%	3.76	
1d	**2f**	**3a**	-		3679125	1699287	15818	4474095	0.99	0.37	27.05%	405.97	**340.5±50.4**
					3452764	719785	36329	6546465	0.99	0.65	39.84%	356.77	
				20%	15217010	9648206	58435	15385856	0.99	0.22	18.41%	327.81	
				40%	15502026	3808758	156919	30270541	0.99	0.61	37.96%	358.81	
				60%	14824088	24218	968455	38443647	0.95	1.00	51.18%	252.91	
1d	**2f**	**3a**	10% **7**	20%	14793892	9085866	75998	16499387	0.99	0.24	19.44%	274.28	**270.7±3.6**
				40%	15066049	2549045	268591	33567674	0.98	0.71	41.93%	267.02	
1d	**2g**	**3a**	10% **7**	20%	10550706	10272608	5576318	10196697	0.29	0.01	4.36%	1.85	**1.9±0.1**
				40%	8920710	6778913	12035366	20303890	0.26	0.14	34.79%	1.92	
				60%	6484458	3648647	18595936	28468955	0.21	0.28	57.16%	1.96	
				80%	4119058	1332040	25662369	34523900	0.15	0.51	77.64%	2.04	
1d	**2g**	**3a**	10% **7**	20%	4721839	8176621	8247254	54271	0.99	0.27	21.35%	197.46	**207.9±10.4**
				40%	835378	7692684	19584571	223052	0.98	0.80	45.13%	218.30	

[a]Only deviations from standard conditions (CDCl₃, +23 °C, 1.1 eq NEt₃, no catalyst) are reported. [b]Relative to the total concentration of both alcohols.

2.5. Synthetic Procedures and Compound Characterizations

2.5.1. General Synthetic Procedures

General methods: All reactions sensitive to air and moisture were proceeded under a nitrogen atmosphere and the glassware as well as magnetic stir bars were dried overnight in a dry oven at 110°C.

Solvents, reagents, and catalysts: All reagents and solvents were purchased from the companies TCI, Sigma Aldrich or Fisher Scientific. $CDCl_3$ was freshly distilled from calcium hydride (CaH_2) under nitrogen atmosphere. All reagents were used without further purification, if not mentioned otherwise. All air- or water-sensitive reagents were stored under nitrogen.

Chromatography: Silica gel for column chromatography was purchased from Acros Organics (mesh 35-70). Thin-layer chromatography was performed by using TLC plates purchased by Merck (silica gel 60 F254, thickness 0.2 mm).

NMR spectroscopy: All ^1H, ^{13}C and ^{19}F-NMR spectra were recorded by a Varian INOVA 400 or a Bruker BioSpin NanoBay 400 machine in $CDCl_3$ at 23 °C. ^1H spectra were recorded at 400 MHz, ^{13}C-NMR spectra respectively at 101 MHz and ^{19}F spectra at 377 MHz. The ^{29}Si-NMR spectra were recorded with Bruker 400 TR or JEOL 400 machine at 79 MHz. The chemical shifts for ^1H, ^{13}C and ^{29}Si are reported in ppm (δ), relative to the chemical shift of tetramethylsilane (TMS). The chemical shifts of ^{19}F-NMR spectra are reported in ppm (δ), relative to the chemical shift of $CFCl_3$. For ^1H and ^{13}C spectra the resonance of $CHCl_3$ at δ = 7.26 ppm resp. δ = 77.16 ppm was used as an internal reference. Spectra were imported and processed in the MestreNova 12.0.4 program. For ^1H-NMR spectra multiplicity (d=doublet, t=triplet, q=quartet, dd=doublet of doublets, m=multiplet), coupling constants J, and number of protons are reported. For ^{13}C-NMR spectra doublets (d) due to coupling with fluorine are reported.

Mass spectrometry: Electron ionization (EI) HRMS spectra were recorded on a Thermo Finnigan LTQ FT machine of the MAT 95 type with a direct exposure probe (DEP) and electron impact ionization (EI, 70 eV). For electrospray ionization (ESI) spectra a Thermo Finnigan LTQ FT Ultra Fourier Transform Ion Cyclotron Resonance Mass Spectrometer was utilized.

Infrared spectroscopy: Infrared (IR) spectra were measured at FT-IR Perkin Elmer Spectrum BXII/1000 with Smiths ATR.

Melting points: Melting point were measure at a Büchi M560 and are stated uncorrected.

2.5.2. Silanes and Silyl Chlorides

GP1a: Synthesis of silanes[20]

CAUTION: Washing and removing of solvents from lithium salts has to be performed extremely carefully and under full exclusion of air and water. Especially drying of lithium salts has to be strictly prevented as dry halogen-lithium salts tend to be explosive.[36] Thus, it is strongly recommended to use GP1b or a Grignard reaction[31] for the synthesis of silanes instead. 10 mmol of adequate iodo- or bromofluorobenzene are put into an oven-dried 3-neck flask and solved under N_2 in 20 mL of freshly distilled pentane. 5.1 mL of 2 M *n*-butyl-lithium solution in THF (1.02 eq) are slowly dropped in and the mixture is stirred for 1.5 hours. Solids are allowed to settle on the ground of the flask and the supernatant is carefully removed via syringe and directly quenched with ethanol. The solid is washed with pentane (2 x 5 mL) and 10 mL of pentane are added. 300 μL of trichlorosilane (3.0 mmol, 0.30 eq) in 5 mL pentane are slowly added and stirred overnight. The reaction mixture is transferred into test tubes and centrifuged. The supernatant is collected under N_2 and the solid is washed with pentane (2 x 5 mL). The combined liquid phases are quenched through addition of trimethylsilyl chloride and the solvent is removed under reduced pressure. The crude product is purified by Kugelrohr-distillation.

GP1b: Synthesis of silanes[37]

20 mmol of adequate bromofluorobenzene are put into an oven-dried 3-neck flask with internal thermometer, solved under N_2 in 30 mL of dry THF and cooled to -78 °C. 8.8 mL of 2.5 M *n*-butyl-lithium solution in THF (1.1 eq) are slowly dropped in while keeping the temperature of the mixture below -50 °C. After stirring the mixture for 2 hours at -78 °C a solution of 605 μL (812 mg, 6.0 mmol, 0.30 eq) of trichlorosilane in 5 mL pentane is slowly dropped in. The solution is allowed to warm to room temperature and stirred overnight. The reaction mixture is then cooled again to 0 °C and quenched through addition of ammonium chloride solution. The mixture is filtered, extracted with EtOAc (3 x 15 mL) and washed with saturated NH_4Cl solution. The combined organic phases are dried over $MgSO_4$, filtered and the solvent is removed under reduced pressure. The crude product is purified by recrystallization from hexanes.

GP2: Chlorination of silanes[20]

The corresponding silane is solved in a Schlenk flask under N_2 atmosphere in 10 mL of dry tetrachloromethane. An excess of sulfuryl chloride are added and stirred under reflux. Solvent and remaining reagents are removed in vacuo and collected in an additional liquid nitrogen cooling trap. The product is precipitated through addition of dry pentane and isolated by Schlenk filtration. It is crucial to perform all reaction and purification steps under strict exclusion of moisture and air.

Synthesis and characterisation of tri(naphthyl)silane **10g** and corresponding silyl chloride **3g** is reported in Chapter 3.[31]

Tris(4-fluorophenyl)silane 10d
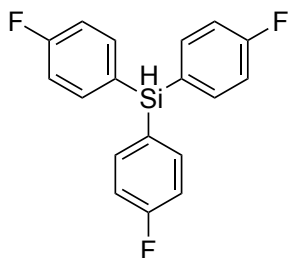
Following GP1a (*please note safety instructions above*) starting from 2.22 g 1-Iodo-4-fluorobenzene (10 mmol) yields 616 mg (1.96 mmol, 65%) of **10d** as colourless liquid. Analytical data are in agreement with literature data.[20]

1H NMR (400 MHz, CDCl$_3$) δ 7.56 – 7.47 (m, 6H), 7.16 – 7.06 (m, 6H), 5.46 (s, 1H) ppm. **13C NMR** (101 MHz, CDCl$_3$) δ 164.5 (d), 137.8 (d), 128.5 (d), 115.7 (d) ppm. **19F NMR** (377 MHz, CDCl$_3$) δ -109.99 ppm.

Tris(4-fluorophenyl)silyl chloride 3d
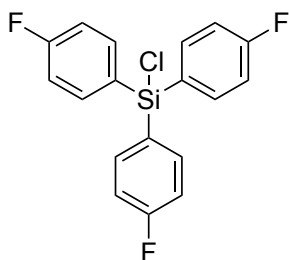
616 mg (1.96 mmol, 1.0 eq) of **10d** and 792 μL (1.32 g, 9.8 mmol, 5 eq) of SO$_2$Cl$_2$ were reacted for 4 hours according to GP2 yielding 578 mg (1.65 mmol, 85%) of **3d** as white crystals. Analytical data are in agreement with literature data.[20]

1H NMR (400 MHz, CDCl$_3$) δ 7.60 – 7.42 (m, 6H), 7.08 – 6.97 (m, 6H) ppm. **13C NMR** (101 MHz, CDCl$_3$) δ 164.9 (d), 137.5 (d), 128.3 (d), 115.8 (d) ppm. **19F NMR** (377 MHz, CDCl$_3$) δ -108.31 ppm.

Tris(3-fluorophenyl)silane 10e
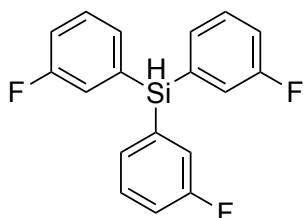
Following GP1a (*please note safety instructions above*) starting from 1.75 g 1-bromo-3-fluorobenzene (10 mmol) yields 579 mg (1.84 mmol, 61%) of **10e** as colourless liquid.

1H NMR (400 MHz, CDCl$_3$) δ 7.45 – 7.36 (m, 3H), 7.32 (m, 3H), 7.23 (m, 3H), 7.14 (m, 3H), 5.46 (s, 1H) ppm. **13C NMR** (101 MHz, CDCl$_3$) δ 162.8 (d), 135.0 (d), 131.4 (d), 130.3 (d), 122.1 (d), 117.5 (d) ppm. **19F NMR** (377 MHz, CDCl$_3$) δ -112.54 ppm. **29Si NMR** (79 MHz, CDCl$_3$) δ -18.17 ppm. **HRMS** (70 eV, EI) m/z calc. for C$_{18}$H$_{12}$F$_3$Si [M-H]$^+$ 313.0655; found 313.0655.

Tris(3-fluorophenyl)silyl chloride 3e
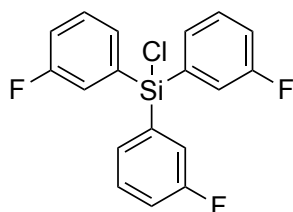
337 mg (1.07 mmol, 1.0 eq) of **10e** and 1.08 mL (1.44 g, 10.7 mmol, 10 eq) of SO$_2$Cl$_2$ were reacted for 24 hours according to GP2. The crude product was purified by Kugelrohr-distillation yielding 257 mg (0.74 mmol, 69%) of **3e** as colourless liquid.

1H NMR (400 MHz, CDCl$_3$) δ 7.49 – 7.38 (m, 6H), 7.37 – 7.29 (m, 3H), 7.25 – 7.18 (m, 3H) ppm. **13C NMR** (101 MHz, CDCl$_3$) δ 162.8 (d), 134.7 (d), 130.9 (d), 130.5 (d), 121.7 (d), 118.5 (d) ppm. **19F NMR** (377 MHz, CDCl$_3$) δ -111.83 ppm. **29Si NMR** (79 MHz, CDCl$_3$) δ -14.47 ppm. **HRMS** (70 eV, EI) m/z calc. for C$_{18}$H$_{13}$F$_3$SiCl [M]$^+$ 348.0343; found 348.0336.

Tris(2-fluorophenyl)silane 10f
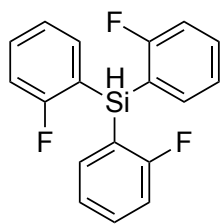
Following GP1a starting from 3.5 g 1-bromo-3-fluorobenzene (20 mmol, 1.0 eq) yields 1.42 g (1.84 mmol, 61%) of **10f** as white crystals.

mp +76 °C. **^{1}H NMR** (600 MHz, CDCl$_3$) δ 7.51 – 7.44 (m, 3H), 7.44 – 7.39 (m, 3H), 7.17 (t, J = 7.3 Hz, 3H), 7.08 (d, J = 8.5 Hz, 3H), 5.75 (q, J = 3.1 Hz, 1H) ppm. **^{13}C NMR** (151 MHz, CDCl$_3$) δ 167.4 (d), 137.4 (d), 133.0 (d), 124.4 (d), 118.4 (d), 115.1 (d) ppm. **^{19}F NMR** (377 MHz, CDCl$_3$) δ -98.28 ppm. **^{29}Si NMR** (79 MHz, CDCl$_3$) δ -32.27 ppm. **HRMS** (70 eV, EI) m/z calc. for C$_{18}$H$_{13}$F$_3$Si [M]$^+$ 314.0733; found 314.0734. **IR** ν = 3071 (w), 2200 (m, Si-H), 1436 (s), 1198 (s), 759 (vs) cm^{-1}.

Tris(2-fluorophenyl)silyl chloride 3f
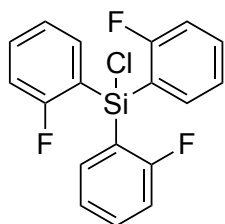
1.14 g (3.64 mmol, 1.0 eq) of **10f** and 1.83 mL (2.46 g, 18.2 mmol, 5.0 eq) of SO$_2$Cl$_2$ were reacted for 16 hours according to GP2 yielding 1.27 g (3.65 mmol, quantitative) of **3f** as white crystals.

mp +92 °C. **^{1}H NMR** (400 MHz, CDCl$_3$) δ 7.66 – 7.51 (m, 6H), 7.33 – 7.27 (m, 3H), 7.13 (t, J = 8.1 Hz, 3H) ppm. **^{13}C NMR** (101 MHz, CDCl$_3$) δ 167.1 (d), 136.7 (d), 133.9 (d), 124.5, 119.1 (d), 115.5 (d) ppm. **^{19}F NMR** (377 MHz, CDCl$_3$) δ -96.96 ppm. **HRMS** (70 eV, EI) m/z calc. for C$_{18}$H$_{13}$F$_3$SiCl [M]$^+$ 348.0343; found 348.0335. **IR** ν = 3070 (w), 1601 (s), 1434 (s), 1206 (s), 756 (vs) cm^{-1}.

2.5.3. Alcohols

2-Naphthylmethanol 1b
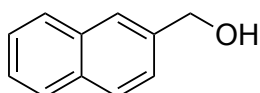
4.30 g (25 mmol, 1.0 eq) of 2-naphthoic acid is solved in 100 mL of dry THF and cooled to 0 °C. 2.85 g (75 mmol, 3.0 eq) of LiAlH$_4$ is added in portions and the reaction mixture is stirred overnight at rt. The reaction mixture is cooled to 0 °C again, carefully quenched through addition of water and extracted with DCM (3 x 10 mL). The combined organic phases are dried over natrium sulfate, filtered and the solvent is removed under reduced pressure. Purification by column chromatography (silica, hexanes/EtOAc = 2/1) yields beige crystals (2.98 g, 18.8 mmol, 75%). Analytic data are in accordance with literature values.[38]

^{1}H NMR (200 MHz, CDCl$_3$) δ 7.88 – 7.79 (m, 4H), 7.54 – 7.45 (m, 3H), 4.86 (s, 2H), 1.83 (s, 1H, OH) ppm. **^{13}C NMR** (101 MHz, CDCl$_3$) δ 138.4, 133.5, 133.1, 128.5, 128.0, 127.8, 126.3, 126.0, 125.6, 125.3, 65.6 ppm. **HRMS** (70 eV, EI) m/z calc. for C$_{11}$H$_{10}$O [M]$^+$ 158.0726; found 158.0724.

GP3: Grignard reactions

33 mmol (1.1 eq) of magnesium turnings are covered with 5 ml of dry THF in a 3-neck flask. 30 mmol (1.0 eq) of corresponding bromo-hydrocarbon are solved in 7 mL of dry THF. One tenth of the solution is added. After the Grignard reaction has started the remaining solution is slowly dropped into the reaction mixture. After stirring for 2 hours 1.0 eq of corresponding aldehyde in 3 mL THF are slowly added at 0 °C. The reaction mixture is heated to reflux for 2 hours. After cooling

down, the mixture is quenched with ice water and concentrated hydrochloric acid is carefully added to remove magnesium hydroxide. The mixture is extracted with EtOAc (3 x 15 mL), the combined organic layers dried over MgSO$_4$, filtered and the solvent is removed under reduced pressure.

Cyclohexylphenylmethanol 2e
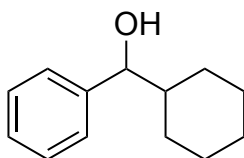
802 mg magnesium turnings, 4.71 g (30 mmol, 1.0 eq) of bromobenzene and 3.36 g (30 mmol, 1.0 eq) cyclohexanecarbaldehyde in 3 mL THF were used in a Grignard reaction following GP3. Purification by column chromatography (silica, hexanes/EtOAc = 9/1) yields white crystals (3.9 g, 20.5 mmol, 68%).

Analytic data are in accordance with literature values.[39]

^{1}H NMR (200 MHz, CDCl$_3$) δ 7.45 – 7.18 (m, 5H), 4.37 (d, J = 7.1 Hz, 1H), 1.98 (d, J = 12.3 Hz, 1H), 1.89 – 1.48 (m, 4H), 1.48 – 0.68 (m, 6H) ppm.

Tridecan-7-ol 2g
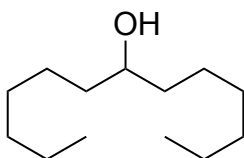
802 mg (33 mmol, 1.1 eq) magnesium turnings, 4.21 mL (4.95 g, 30 mmol, 1.0 eq) of 1-bromohexane and 4.23 mL (3.42 g, 30 mmol, 1.0 eq) heptanal in 3 mL THF were used in a Grignard reaction following GP3. Recrystallisation from pentane at -20 °C yields white crystals (3.70 g, 18.3 mmol, 60.8%).

Analytic data are in accordance with literature values.[40]

^{1}H NMR (400 MHz, CDCl$_3$) δ 3.57 (dt, J = 7.1, 4.1 Hz, 1H), 1.48 – 1.17 (m, 20H), 0.93 – 0.79 (m, 6H) ppm. **^{13}C NMR** (101 MHz, CDCl$_3$) δ 72.1, 37.6, 32.0, 29.5, 25.8, 22.8, 14.2 ppm. **HRMS** (70 eV, EI) m/z calc. for C$_{13}$H$_{28}$O [M-H]$^+$ 199.2056; found 199.2057.

2.5.4. Silyl Ethers

GP4: Silylation of alcohols

1.0 eq of alcohol, 1.2 eq of triethylamine **4**, 0.10 eq of DMAP **8** and 1.2 eq of corresponding silyl chloride are solved in an oven-dried flask under N$_2$ atmosphere in dry THF and stirred. After full conversion of the alcohol as monitored by TLC the reaction is quenched through addition of water and extracted with EtOAc (3 x 15 mL), washed with brine, dried over MgSO$_4$, filtered and the solvent is removed under vacuum. Purification is done by column chromatography, quantitative thin-layer chromatography or recrystallisation.

Synthesis, analytical data and spectra for silyl ether **5ag**, **5ac**, **5ba**, **5bg**, **5bc**, **6ag**, **6ac** are reported in the bachelor thesis of S. Weitl,[25] those for silyl ethers **5ca** and **5ch** in Chapter 3.[31] Analytical data of silyl ethers **6da**[41], **6dh**[42], **6ch**[43] and **6bh**[44] were in accordance with literature values.

(Phenylmethoxy)triphenylsilane 5aa
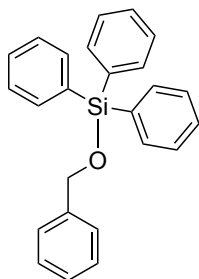
Synthesized according to GP4 from **1a** and **3a**, purified by column chromatography (silica, hexanes/EtOAc = 19/1) yielding white crystals (86%). Analytical data are in accordance with literature.[45]

mp +88 °C. **^{1}H NMR** (400 MHz, CDCl$_3$) δ 7.75 (d, J = 8.1 Hz, 6H), 7.55 – 7.49 (m, 3H), 7.49 – 7.42 (m, 8H), 7.39 (t, J = 7.6 Hz, 2H), 7.32 (t, J = 7.2 Hz, 1H), 4.99 (s, 2H) ppm. **^{13}C NMR** (101 MHz, CDCl$_3$) δ 140.7, 135.6, 135.6, 135.5, 134.1, 130.2, 128.4, 128.1, 128.1, 128.0, 127.2, 126.5, 65.7 ppm. **HRMS** (70 eV, EI) m/z calc. for C$_{25}$H$_{22}$OSi [M]$^+$ 366.1434; found 366.1453.

(Phenylmethoxy)tris(4-fluorophenyl)silane 5ad
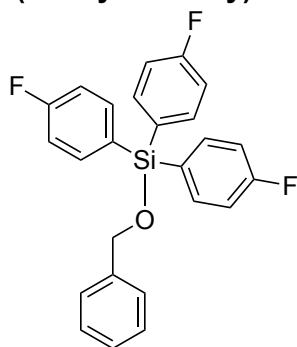
Synthesized according to GP4 from **1a** and **3d**, purified by recrystallization from hexanes/EtOAc = 19/1 yielding white crystals (76%).

mp +87 °C. **^{1}H NMR** (400 MHz, CDCl$_3$) δ 7.45 – 7.37 (m, 6H), 7.36 – 7.26 (m, 8H), 7.22 – 7.11 (m, 3H), 4.91 (s, 2H) ppm. **^{13}C NMR** (101 MHz, CDCl$_3$) δ 162.8 (d), 139.9, 135.9 (d), 131.0 (d), 130.2 (d), 128.5, 127.6, 126.6, 121.7 (d), 117.8 (d), 66.1 ppm. **^{19}F NMR** (377 MHz, CDCl$_3$) δ -112.46 ppm. **^{29}Si NMR** (79 MHz, CDCl$_3$) δ -14.18 ppm. **HRMS** (70 eV, EI) m/z calc. for C$_{25}$H$_{19}$F$_3$OSi [M]$^+$ 420.1152; found 420.1176.

(Phenylmethoxy)tris(3-fluorophenyl)silane 5ae
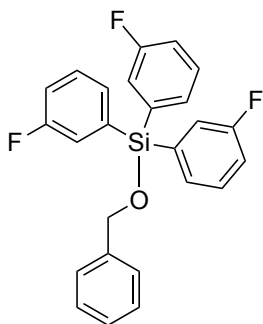
Synthesized according to GP4 from **1a** and **3e**, purified by column chromatography (silica, hexanes) yielding a colourless oil (36%).

^{1}H NMR (200 MHz, CDCl$_3$) δ 7.50 – 7.26 (m, 14H), 7.26 – 7.08 (m, 3H), 4.91 (s, 2H) ppm. **^{13}C NMR** (101 MHz, CDCl$_3$) δ 164.5 (d), 137.6 (d), 137.2 (d), 130.4 (d), 129.4, 128.5, 127.5, 126.6, 115.6 (d), 115.4 (d), 65.9 ppm. **^{19}F NMR** (377 MHz, CDCl$_3$) δ -109.36 ppm. **^{29}Si NMR** (79 MHz, CDCl$_3$) δ -18.25 ppm. **HRMS** (70 eV, EI) m/z calc. for C$_{25}$H$_{19}$F$_3$OSi [M]$^+$ 420.1152; found 420.1163.

(Phenylmethoxy)tris(2-fluorophenyl)silane 5af
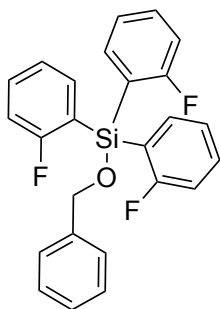
Synthesized according to GP4 from **1a** and **3f**, purified by column chromatography (silica, hexanes/EtOAc = 19/1) yielding white crystals (56%).

mp +85 °C. **^{1}H NMR** (400 MHz, CDCl$_3$) δ 7.65 – 7.50 (m, 6H), 7.47 (d, J = 7.4 Hz, 2H), 7.40 (dd, J = 8.2, 6.8 Hz, 2H), 7.36 – 7.29 (m, 1H), 7.26 (t, J = 7.3 Hz, 3H), 7.13 (t, J = 8.3 Hz, 3H), 5.09 (s, 2H) ppm. **^{13}C NMR** (101 MHz, CDCl$_3$) δ 167.2 (d), 140.5, 137.0 (d), 133.1 (d), 128.3, 127.2, 126.6, 124.4, 120.1 (d), 115.1 (d), 66.2 ppm. **^{19}F NMR** (377 MHz, CDCl$_3$) δ -97.86 ppm. **HRMS** (70 eV,

EI) m/z calc. for $C_{25}H_{19}F_3OSi$ [M]$^+$ 420.1152; found 420.1145. **IR** ν = 3065 (w), 1428 (s), 1059 (s), 695 (vs) cm^{-1}.

(Diphenylmethoxy)triphenylsilane 5da
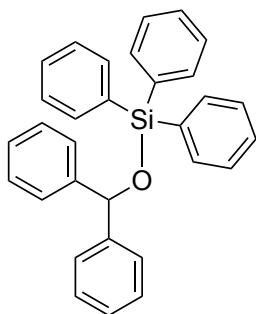
Synthesized according to GP4 from **1d** and **3a**, purified by column chromatography (silica, hexanes/EtOAc = 19/1) yielding a white solid (44%). **mp** +103 °C. **^{1}H NMR** (400 MHz, CDCl$_3$) δ 7.54 (dd, *J* = 8.0, 1.4 Hz, 6H), 7.44 – 7.37 (m, 3H), 7.35 – 7.27 (m, 10H), 7.25 – 7.14 (m, 6H), 5.93 (s, 1H) ppm. **^{13}C NMR** (101 MHz, CDCl$_3$) *δ* 144.5, 135.6, 134.3, 130.0, 128.3, 127.8, 127.1, 126.7, 77.9 ppm. **^{29}Si NMR** (79 MHz, CDCl$_3$) δ -11.88 ppm. **HRMS** (70 eV, EI) m/z calc. for $C_{31}H_{26}OSi$ [M]$^+$ 442.1747; found 442.1740. **IR** ν = 3065 (w), 1428 (s), 1059 (s), 695 (vs) cm^{-1}.

(Cyclohexylmethoxy)triphenylsilane 6aa
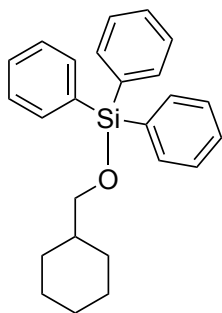
Synthesized according to GP4 from **2a** and **3a**, purified by column chromatography (silica, hexanes/EtOAc = 19/1) yielding white crystals (50%). Analytical data are in accordance with literature.[46]

mp +54 °C. **^{1}H NMR** (400 MHz, CDCl$_3$) δ 7.70 – 7.63 (m, 6H), 7.51 – 7.36 (m, 9H), 3.63 (d, J = 6.4 Hz, 2H), 1.88 – 1.55 (m, 6H), 1.36 – 1.09 (m, 3H), 0.96 (qd, J = 12.3, 3.2 Hz, 2H) ppm.**^{13}C NMR** (101 MHz, CDCl$_3$) *δ* 135.6, 134.7, 130.0, 127.9, 69.5, 40.5, 29.9, 26.8, 26.1 ppm. **HRMS** (70 eV, EI) m/z calc. for $C_{25}H_{28}OSi$ [M]$^+$ 372.1904; found 372.1910.

(Cyclohexylmethoxy)tris(4-fluorophenyl)silane 6ad
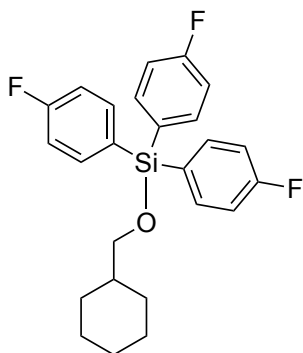
Synthesized according to GP4 from **2a** and **3d**, purified by column chromatography (silica, hexanes/EtOAc = 19/1) yielding a colourless oil (59%).

^{1}H NMR (400 MHz, CDCl$_3$) δ 7.61 – 7.50 (m, 6H), 7.16 – 7.05 (m, 6H), 3.54 (d, J = 6.3 Hz, 2H), 1.79 – 1.62 (m, 5H), 1.59 – 1.49 (m, 1H), 1.28 – 1.13 (m, 3H), 0.97 – 0.85 (m, 2H) ppm. **^{13}C NMR** (101 MHz, CDCl$_3$) *δ* 164.3 (d), 137.3 (d), 129.7 (d), 115.2 (d), 69.4, 40.3, 29.7, 26.6, 25.8 ppm. **^{19}F NMR** (377 MHz, CDCl$_3$) *δ* -109.89 ppm. **MS** (70 eV, EI) 330.22 [M – C_6H_5F]$^+$, 313.15 [M – CyHexMeO]$^+$, 235.09 [M – 2 C_6H_5F]$^+$.

(Cyclohexylmethoxy)tris(3-fluorophenyl)silane 6ae
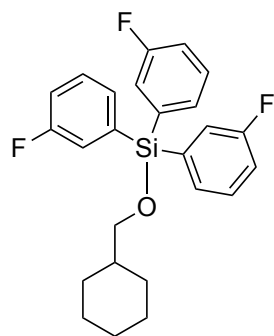
Synthesized according to GP4 from **2a** and **3e**, purified by Kugelrohr distillation yielding a colourless oil (19%).

^{1}H NMR (400 MHz, CDCl$_3$) δ 7.44 – 7.31 (m, 6H), 7.28 - 7.25 (m, 3H), 7.18 – 7.11 (m, 3H), 3.57 (d, J = 6.3 Hz, 2H), 1.79 – 1.63 (m, 5H), 1.31 – 1.08 (m, 4H), 0.98 – 0.87 (m, 2H) ppm. **^{13}C NMR** (101 MHz, CDCl$_3$) δ 162.7 (d), 136.5, 131.0 (d), 130.1 (d), 121.7 (d), 117.6 (d), 69.8, 40.4, 29.8, 26.7, 26.0 ppm. **^{19}F NMR** (377 MHz, CDCl$_3$) δ -112.76 ppm. **HRMS** (70 eV, EI) m/z calc. for C$_{25}$H$_{25}$F$_3$OSi [M]$^+$ 426.1621; found 426.1635. **IR** ν = 3065 (w), 1428 (s), 1059 (s), 695 (vs) cm^{-1}.

(Cyclohexylmethoxy)tris(2-fluorophenyl)silane 6af
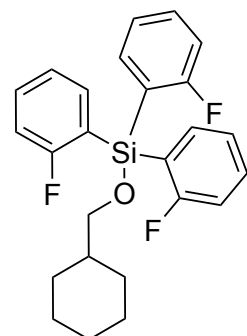
Synthesized according to GP4 from **2a** and **3f**, purified by column chromatography (silica, hexanes/EtOAc = 19/1) yielding white crystals (54%). **mp** +77 °C. **^{1}H NMR** (400 MHz, CDCl$_3$) δ 7.56 – 7.40 (m, 6H), 7.18 (td, J = 7.4, 0.9 Hz, 3H), 7.04 (t, J = 8.3 Hz, 3H), 3.68 (d, J = 6.3 Hz, 2H), 1.87 – 1.56 (m, 6H), 1.33 – 1.04 (m, 3H), 0.94 (m, 2H) ppm. **^{13}C NMR** (101 MHz, CDCl$_3$) δ 167.2 (d), 137.0 (d), 132.9 (d), 124.2, 120.6 (d), 115.1 (d), 70.0, 40.3, 29.8, 26.8, 26.1 ppm. **^{19}F NMR** (377 MHz, CDCl$_3$) δ -97.95 ppm. **HRMS** (ESI) m/z calc. for C$_{25}$H$_{25}$F$_3$OSi [M+H]$^+$ 427.1700; found 427.1698. **IR** ν = 3065 (w), 1428 (s), 1059 (s), 695 (vs) cm^{-1}.

(Cyclohexylethoxy)triphenylsilane 6ba
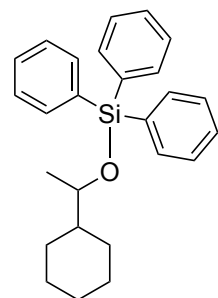
Synthesized according to GP4 from **2b** and **3a**, purified by quantitative thin layer chromatography (silica, hexanes/EtOAc = 19/1) yielding a colourless oil (39%). **^{1}H NMR** (400 MHz, CDCl$_3$) δ 7.64 (dd, J = 7.9, 1.5 Hz, 6H), 7.47 – 7.33 (m, 9H), 3.86 – 3.71 (m, 1H), 1.84 – 1.58 (m, 5H), 1.42 – 0.91 (m, 9H) ppm. **^{13}C NMR** (101 MHz, CDCl$_3$) δ 135.7, 135.4, 129.9, 127.8, 74.1, 45.5, 28.8, 28.4, 26.9, 26.6, 26.5, 20.4 ppm. **HRMS** (70 eV, EI) m/z calc. for C$_{26}$H$_{30}$OSi [M]$^+$ 386.2060; found 386.2065.

((3-Methylbutan-2-yl)oxy)triphenylsilane 6ca
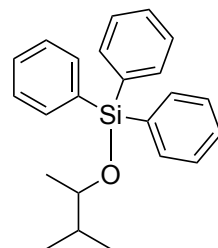
Synthesized according to GP4 from **2c** and **3a**, purified by quantitative thin layer chromatography (silica, hexanes/EtOAc = 19/1) yielding a colourless oil (33%). **^{1}H NMR** (400 MHz, CDCl$_3$) δ 7.67 (d, J = 7.3 Hz, 6H), 7.55 – 7.35 (m, 9H), 3.84 (p, J = 6.1, 5.7 Hz, 1H), 1.84 – 1.65 (m, 1H), 1.21 – 1.08 (m, 3H), 1.00 – 0.80 (m, 6H) ppm. **^{13}C NMR** (101 MHz, CDCl$_3$) δ 135.7, 135.4, 129.9, 127.8, 74.4, 35.2, 19.7, 18.3, 17.8 ppm. **HRMS** (70 eV, EI) m/z calc. for C$_{23}$H$_{26}$OSi [M]$^+$ 346.1747; found 346.1735.

(Cyclohexylphenylmethoxy)triphenylsilane 6ea
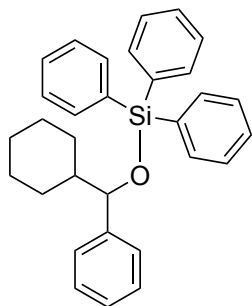
Synthesized according to GP4 from **2e** and **3a**, purified by column chromatography (silica, hexanes/EtOAc = 19/1) yielding a white solid (70%). **^{1}H NMR** (400 MHz, CDCl$_3$) δ 7.50 (dd, J = 4.4, 2.4 Hz, 6H), 7.42 – 7.36 (m, 3H), 7.34 – 7.27 (m, 6H), 7.22 – 7.12 (m, 5H), 4.53 (d, J = 6.6 Hz, 1H), 1.96 (d, J = 12.8 Hz, 1H), 1.73 – 1.51 (m, 4H), 1.40 (d, J = 13.9 Hz, 1H), 1.19 – 0.75 (m, 5H) ppm. **^{13}C NMR** (101 MHz, CDCl$_3$) δ 143.1, 135.7, 134.8, 129.8, 127.7, 127.5, 127.0, 81.1, 46.1, 29.4, 29.0, 26.6, 26.3 ppm.

(Dicyclohexylmethoxy)triphenylsilane 6fa
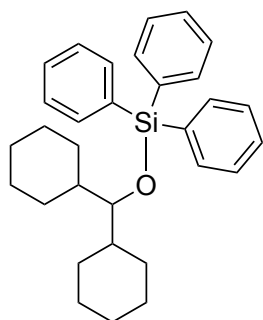
Synthesized according to GP4 from **2f** and **3a**, purified by column chromatography (silica, hexanes/EtOAc = 19/1) yielding a white solid (31%). **mp** +107 °C. **^{1}H NMR** (400 MHz, CDCl$_3$) δ 7.68 – 7.62 (m, 6H), 7.43 – 7.32 (m, 9H), 3.26 (t, J = 4.9 Hz, 1H), 1.79 (d, J = 12.8 Hz, 2H), 1.67 – 1.56 (m, 5H), 1.52 – 1.24 (m, 5H), 1.20 – 0.95 (m, 10H) ppm. **^{13}C NMR** (101 MHz, CDCl$_3$) δ 135.9, 129.7, 127.7, 83.3, 41.4, 30.3, 28.6, 26.8, 26.5 ppm. **^{29}Si NMR** (79 MHz, CDCl$_3$) δ -15.24 ppm. **HRMS** (70 eV, EI) m/z calc. for C$_{31}$H$_{38}$OSi [M]$^+$ 454.2686; found 454.2685. **IR** ν = 2918 (w), 1427 (m), 1020 (s), 702 (vs) cm^{-1}.

(7-Tridecanyloxy)triphenylsilane 6ga
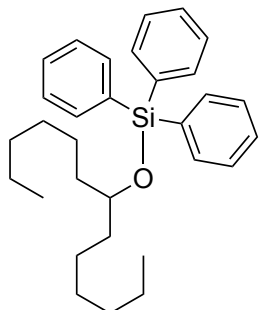
Synthesized according to GP4 from **2g** and **3a**, purified by column chromatography (silica, hexanes/EtOAc = 19/1) yielding a white solid (88%). **^{1}H NMR** (400 MHz, CDCl$_3$) δ 7.69 – 7.52 (m, 6H), 7.52 – 7.27 (m, 9H), 3.84 (p, J = 5.8 Hz, 1H), 1.67 – 1.39 (m, 5H), 1.39 – 1.05 (m, 15H), 0.86 (t, J = 7.1 Hz, 6H) ppm. **^{13}C NMR** (101 MHz, CDCl$_3$) δ 135.7, 135.4, 129.9, 127.8, 73.9, 36.9, 31.9, 29.5, 25.3, 22.7, 14.2 ppm. **MS** (70 eV, EI) 373.24 [M − C$_6$H$_{13}$]$^+$, 259.06 [C$_{13}$H$_{27}$O]$^+$, 199.02 [SiPh$_3$]$^+$.

2.6. Computational Methods and Data

2.6.1. Theoretical Methods

Geometry optimizations and vibrational frequency calculations were performed with the B3LYP-D3 hybrid functional[47] in combination with the 6-31+G(d) (for H, C, and O atoms) and 6-311+G(2d) basis set (for Si and Cl atoms).[48] Solvent effects for chloroform have been calculated with the SMD continuum solvation model.[49] Thermochemical corrections to 298.15 K have been calculated for all minima from unscaled vibrational frequencies obtained at this same level. Initial search of conformational space of every compound was performed with Maestro.[50] If the number of conformers was too high in regard to computational costs redundant conformers were eliminated (maximum atom deviation 0.5 Å) with Maestro. All conformers were then optimized and confirmed to be stationary points by the absence of imaginary frequencies. For the best conformer single point energies were calculated at the DLPNO-CCSD(T)/def2-TZVPP//SMD(CHCl$_3$)/B3LYP-D3/6-311+G(2d)/6-31+G(d) level[51] level with auxiliary basis set def2-TZVPP/C.[52] This combination was found in previous studies to perform well for this kind of systems.[31, 53]. G_{298} were calculated through addition of thermal correction and solvation factors obtained as the difference between the energies computed at B3LYP-D3/6-311+G(2d)/6-31+G(d) in solution and in gas phase. All calculations have been performed with Gaussian 09[54] and ORCA version 4.0.[55]

2.6.2. Tables of Energies, Enthalpies and Free Energies.

Table 2.13. Energies, enthalpies, free energies and Grimme-D3 correction (in Hartree) for all conformers at SMD(CHCl$_3$)/B3LYP-D3/6-311+G(2d)/6-31+G(d) level of theory. Enthalpy and free energy differences are reported relative the best conformer.

compound	filename	E_{tot}	H_{298}	G_{298}	*Grimme-D3*	ΔH_{298}	ΔG_{298}
1c	roh1_1	-386.128464	-385.957847	-386.000431	-0.013565	0.0	0.0
1c	roh1_2	-386.126712	-385.956315	-385.999667	-0.013401	4.0	2.0
1c	roh1_5	-386.126402	-385.955725	-385.998036	-0.013839	5.6	6.3
1c	roh1_4	-386.126553	-385.955745	-385.997964	-0.013618	5.5	6.5
1c	roh1_3	-386.126553	-385.955744	-385.997961	-0.013618	5.5	6.5
1c	roh1_6	-386.126711	-385.957261	-385.997631	-0.013397	1.5	7.4
1d	Ph2OH_2	-577.878008	-577.651355	-577.703029	-0.021416	0.0	0.0
1d	Ph2OH_4	-577.877335	-577.650611	-577.702120	-0.021801	2.0	2.4
2b	CyEtOH_2	-389.760105	-389.518234	-389.562845	-0.022995	0.0	0.0
2b	CyEtOH_1	-389.760241	-389.518113	-389.562701	-0.022865	0.3	0.4
2b	CyEtOH_5	-389.760039	-389.518137	-389.562666	-0.022711	0.3	0.5
2b	CyEtOH_3	-389.759946	-389.517874	-389.562443	-0.023101	0.9	1.1
2b	CyEtOH_4	-389.759892	-389.517804	-389.562293	-0.023216	1.1	1.4
2b	CyEtOH_6	-389.759476	-389.517492	-389.561977	-0.022865	1.9	2.3
2b	CyEtOH_9	-389.759847	-389.517658	-389.561880	-0.023172	1.5	2.5
2b	CyEtOH_10	-389.759475	-389.517364	-389.561808	-0.023072	2.3	2.7

compound	filename	E_{tot}	H_{298}	G_{298}	Grimme-D3	ΔH_{298}	ΔG_{298}
2b	CyEtOH_7	-389.759724	-389.517411	-389.561662	-0.023375	2.2	3.1
2b	CyEtOH_12	-389.757273	-389.515014	-389.559359	-0.023782	8.5	9.2
2b	CyEtOH_8	-389.757261	-389.514812	-389.558844	-0.023996	9.0	10.5
2b	CyEtOH_13	-389.754150	-389.511780	-389.555857	-0.024164	16.9	18.3
2b	CyEtOH_14	-389.752758	-389.510421	-389.554846	-0.024204	20.5	21.0
2c	samOH_1	-273.011614	-272.837655	-272.877925	-0.013742	0.1	0.0
2c	samOH_5	-273.011521	-272.837673	-272.877784	-0.013614	0.1	0.4
2c	samOH_4	-273.011591	-272.837699	-272.877749	-0.013874	0.0	0.5
2c	samOH_3	-273.011257	-272.837336	-272.877605	-0.014032	1.0	0.8
2c	samOH_2	-273.011387	-272.837550	-272.877593	-0.013955	0.4	0.9
2c	samOH_9	-273.011436	-272.837488	-272.877530	-0.013989	0.6	1.0
2c	samOH_7	-273.010848	-272.837076	-272.877417	-0.013719	1.6	1.3
2c	samOH_6	-273.011164	-272.837244	-272.877404	-0.014177	1.2	1.4
2c	samOH_8	-273.011069	-272.837154	-272.877209	-0.013896	1.4	1.9
2d	iprOH_1	-194.376887	-194.262586	-194.296387	-0.006500	0.1	0.0
2d	iprOH_2	-194.376997	-194.262614	-194.296319	-0.006366	0.0	0.2
2d	iprOH_3	-194.376997	-194.262614	-194.296319	-0.006366	0.0	0.2
2d	iprOH_4	-194.374704	-194.261448	-194.294456	-0.006233	3.1	5.1
2e	PhCyOH_3	-581.513517	-581.215338	-581.268150	-0.031214	0.0	0.0
2e	PhCyOH_2	-581.512504	-581.214350	-581.267352	-0.031479	2.6	2.1
2e	PhCyOH_4	-581.512761	-581.214444	-581.267021	-0.032425	2.3	3.0
2e	PhCyOH_6	-581.511379	-581.213239	-581.266055	-0.032342	5.5	5.5
2e	PhCyOH_1	-581.511602	-581.213359	-581.266028	-0.031432	5.2	5.6
2f	Cy2OH_2	-585.143669	-584.773927	-584.828533	-0.041146	0.0	0.0
2f	Cy2OH_6	-585.143212	-584.773383	-584.828096	-0.040740	1.4	1.1
2f	Cy2OH_5	-585.143212	-584.773383	-584.828094	-0.040740	1.4	1.2
2f	Cy2OH_3	-585.143598	-584.773752	-584.828015	-0.040884	0.5	1.4
2f	Cy2OH_4	-585.143598	-584.773752	-584.828015	-0.040884	0.5	1.4
2f	Cy2OH_9	-585.141263	-584.771135	-584.825050	-0.042385	7.3	9.1
2f	Cy2OH_7	-585.140986	-584.770857	-584.824770	-0.042178	8.1	9.9
2f	Cy2OH_8	-585.140986	-584.770855	-584.824768	-0.042178	8.1	9.9
3a	ph3sicl_04	-1444.848706	-1444.554639	-1444.624661	-0.035166	2.4	0.0
3a	ph3sicl_05	-1444.848714	-1444.554539	-1444.622493	-0.035177	2.7	5.7
3a	ph3sicl_02	-1444.848703	-1444.555560	-1444.621933	-0.035160	0.0	7.2
5ca	Ph1_9	-1370.140385	-1369.688211	-1369.774605	-0.055644	1.4	0.0
5ca	Ph1_3	-1370.140686	-1369.688732	-1369.774046	-0.058089	0.0	1.5
5ca	Ph1_5	-1370.140573	-1369.688603	-1369.773885	-0.058310	0.3	1.9
5ca	Ph1_4	-1370.140545	-1369.688532	-1369.773462	-0.058453	0.5	3.0
5ca	Ph1_8	-1370.140545	-1369.688530	-1369.773439	-0.058452	0.5	3.1

compound	filename	E_{tot}	H_{298}	G_{298}	Grimme-D3	ΔH_{298}	ΔG_{298}
5ca	Ph1_7	-1370.140695	-1369.688633	-1369.773221	-0.058192	0.3	3.6
5ca	Ph1_6	-1370.140695	-1369.688633	-1369.773213	-0.058195	0.3	3.7
5ca	Ph1_2	-1370.140229	-1369.688145	-1369.773113	-0.058105	1.5	3.9
5da	Ph2OTPS_18	-1561.892145	-1561.384037	-1561.479470	-0.067347	1.5	0.0
5da	Ph2OTPS_20	-1561.892032	-1561.383914	-1561.479348	-0.066679	1.8	0.3
5da	Ph2OTPS_23	-1561.892057	-1561.383897	-1561.478902	-0.066831	1.9	1.5
5da	Ph2OTPS_1	-1561.892543	-1561.384415	-1561.478719	-0.067811	0.5	2.0
5da	Ph2OTPS_17	-1561.892683	-1561.384402	-1561.478325	-0.067656	0.6	3.0
5da	Ph2OTPS_15	-1561.891776	-1561.383490	-1561.477353	-0.067125	2.9	5.6
5da	Ph2OTPS_5	-1561.892150	-1561.383912	-1561.477250	-0.067977	1.8	5.8
5da	Ph2OTPS_19	-1561.891794	-1561.384613	-1561.475573	-0.066777	0.0	10.2
5da	Ph2OTPS_10	-1561.891796	-1561.384612	-1561.475497	-0.066786	0.0	10.4
6ba	CyTPS_3	-1373.773141	-1373.249285	-1373.336774	-0.066750	1.0	0.0
6ba	CyTPS_1	-1373.773475	-1373.249674	-1373.336711	-0.067444	0.0	0.2
6ba	CyTPS_8	-1373.773153	-1373.249376	-1373.336548	-0.067478	0.8	0.6
6ba	CyTPS_9	-1373.773142	-1373.249271	-1373.336251	-0.066926	1.1	1.4
6ba	CyTPS_2	-1373.772948	-1373.249231	-1373.336173	-0.066875	1.2	1.6
6ba	CyTPS_5	-1373.772200	-1373.248284	-1373.334613	-0.064788	3.6	5.7
6ba	CyTPS_4	-1373.772200	-1373.248284	-1373.334612	-0.064788	3.6	5.7
6ba	CyTPS_11	-1373.771396	-1373.247560	-1373.334123	-0.066353	5.6	7.0
6ba	CyTPS_19	-1373.771509	-1373.247631	-1373.332941	-0.069804	5.4	10.1
6ba	CyTPS_6	-1373.772709	-1373.249664	-1373.332863	-0.067019	0.0	10.3
6ba	CyTPS_10	-1373.771979	-1373.247785	-1373.332639	-0.070219	5.0	10.9
6ba	CyTPS_15	-1373.769097	-1373.245206	-1373.331949	-0.066975	11.7	12.7
6ba	CyTPS_7	-1373.771267	-1373.248463	-1373.331541	-0.066017	3.2	13.7
6ba	CyTPS_17	-1373.768364	-1373.244296	-1373.330091	-0.069699	14.1	17.5
6ba	CyTPS_21	-1373.765665	-1373.241574	-1373.329622	-0.066927	21.3	18.8
6ba	CyTPS_16	-1373.768652	-1373.244343	-1373.329032	-0.072114	14.0	20.3
6ba	CyTPS_20	-1373.765431	-1373.242222	-1373.325571	-0.065707	19.6	29.4
6ba	CyTPS_22	-1373.761969	-1373.239000	-1373.323510	-0.064671	28.0	34.8
6ca	samTPX_3	-1257.023711	-1256.568094	-1256.651056	-0.055990	0.6	0.0
6ca	samTPX_2	-1257.023836	-1256.568241	-1256.650796	-0.056340	0.2	0.7
6ca	samTPX_4	-1257.023239	-1256.567579	-1256.650784	-0.055169	2.0	0.7
6ca	samTPX_1	-1257.024022	-1256.568332	-1256.650662	-0.057179	0.0	1.0
6ca	samTPX_6	-1257.022851	-1256.567266	-1256.650617	-0.054838	2.8	1.2
6ca	samTPX_7	-1257.022484	-1256.566879	-1256.650146	-0.056276	3.8	2.4
6ca	samTPX_5	-1257.022151	-1256.566588	-1256.649629	-0.056134	4.6	3.7
6ca	samTPX_9	-1257.022328	-1256.566551	-1256.648725	-0.056426	4.7	6.1
6ca	samTPX_10	-1257.021593	-1256.566001	-1256.648490	-0.058282	6.1	6.7

compound	filename	E_{tot}	H_{298}	G_{298}	Grimme-D3	ΔH_{298}	ΔG_{298}
6ca	samTPX_11	-1257.020820	-1256.565124	-1256.647792	-0.057265	8.4	8.6
6ca	samTPX_12	-1257.020229	-1256.564426	-1256.647136	-0.056315	10.3	10.3
6ca	samTPX_13	-1257.020325	-1256.564552	-1256.647092	-0.055201	9.9	10.4
6da	iprOTPS_4	-1178.387240	-1177.991395	-1178.069641	-0.046033	0.9	0.0
6da	iprOTPS_3	-1178.387283	-1177.991339	-1178.068897	-0.046116	1.1	2.0
6da	iprOTPS_2	-1178.387712	-1177.991746	-1178.068395	-0.046294	0.0	3.3
6ea	PhCyOTPS_10	-1565.527740	-1564.947881	-1565.043447	-0.077946	4.2	0.0
6ea	PhCyOTPS_5	-1565.527246	-1564.947353	-1565.043159	-0.077821	5.6	0.8
6ea	PhCyOTPS_1	-1565.527551	-1564.947635	-1565.042394	-0.079110	4.9	2.8
6ea	PhCyOTPS_4	-1565.527018	-1564.947061	-1565.041946	-0.079210	6.4	3.9
6ea	PhCyOTPS_2	-1565.527018	-1564.947061	-1565.041934	-0.079208	6.4	4.0
6ea	PhCyOTPS_12	-1565.526291	-1564.946264	-1565.041572	-0.078221	8.5	4.9
6ea	PhCyOTPS_11	-1565.528356	-1564.949493	-1565.041494	-0.078314	0.0	5.1
6ea	PhCyOTPS_18	-1565.528357	-1564.949493	-1565.041488	-0.078312	0.0	5.1
6ea	PhCyOTPS_13	-1565.528357	-1564.949493	-1565.041484	-0.078314	0.0	5.2
6ea	PhCyOTPS_7	-1565.528357	-1564.949494	-1565.041480	-0.078315	0.0	5.2
6ea	PhCyOTPS_3	-1565.528357	-1564.949494	-1565.041480	-0.078314	0.0	5.2
6ea	PhCyOTPS_21	-1565.526746	-1564.947027	-1565.041346	-0.078876	6.5	5.5
6ea	PhCyOTPS_17	-1565.526619	-1564.946885	-1565.041140	-0.079629	6.8	6.1
6ea	PhCyOTPS_20	-1565.526990	-1564.947088	-1565.040880	-0.078895	6.3	6.7
6ea	PhCyOTPS_19	-1565.526209	-1564.947237	-1565.038895	-0.077154	5.9	12.0
6ea	PhCyOTPS_6	-1565.526180	-1564.947297	-1565.038527	-0.078828	5.8	12.9
6ea	PhCyOTPS_8	-1565.526184	-1564.947294	-1565.038485	-0.078831	5.8	13.0
6fa	Cy2OTPS_1	-1569.158916	-1568.507370	-1568.603082	-0.090359	0.0	0.0
6fa	Cy2OTPS_6	-1569.155610	-1568.503930	-1568.600696	-0.088260	9.0	6.3
6fa	Cy2OTPS_14	-1569.155288	-1568.503516	-1568.600452	-0.088242	10.1	6.9
6fa	Cy2OTPS_15	-1569.155356	-1568.503525	-1568.600311	-0.088170	10.1	7.3
6fa	Cy2OTPS_5	-1569.155275	-1568.503531	-1568.599902	-0.088289	10.1	8.3
6fa	Cy2OTPS_8	-1569.155513	-1568.503831	-1568.599704	-0.091018	9.3	8.9
6fa	Cy2OTPS_17	-1569.155114	-1568.503347	-1568.599462	-0.088521	10.6	9.5
6fa	Cy2OTPS_3	-1569.155109	-1568.503398	-1568.599331	-0.088616	10.4	9.8
6fa	Cy2OTPS_4	-1569.155109	-1568.503396	-1568.599326	-0.088610	10.4	9.9
HCl	hcl_1	-460.834150	-460.824373	-460.845585	-0.000003	0.0	0.0

Table 2.14. Boltzmann averaged free energies at SMD(CHCl₃)/B3LYP-D3/6-311+G(2d)/6-31+G(d) level of theory, single point gas phase total energies at B3LYP-D3/6-311+G(2d)/6-31+G(d) and at DLPNO-CCSD(T)/def2-TZVPP level for the best conformers. Free energy at single point level of theory was obtained through addition of solvation energy and thermal corrections from SMD(CHCl₃)/B3LYP-D3/6-311+G(2d)/6-31+G(d) level frequency calculation. All energies are reported in Hartree.

compound	SMD(CHCl₃)/B3LYP-D3/6-311+G(2d)/6-31+G(d)	B3LYP-D3/6-311+G(2d)/6-31+G(d)	DLPNO-CCSD(T)/def2-TZVPP//SP	
	G_{298} (Boltzmann averaged)	E_{tot} (gas)	E_{tot}	$G_{298}{}^b$
1c	-385.999830	-386.114812	-385.419682	-385.305301
1d	-577.702778	-577.858446	-576.792892	-576.637475
2b	-389.562399	-389.747786	-389.047685	-388.862744
2c	-272.877625	-273.002263	-272.525603	-272.401265
2d	-194.296261	-194.368653	-194.044554	-193.972288
2e	-581.267567	-581.496205	-580.425021	-580.196966
2f	-584.828137	-585.127445	-584.051190	-583.752278
3a	-1444.624341	-1444.824957	-1442.511231	-1442.310935
5ca	-1369.773912	-1370.110809	-1367.602349	-1367.266145
5da	-1561.478984	-1561.856349	-1558.977657	-1558.600778
6ba	-1373.336366	-1373.745327	-1371.231356	-1370.822803
6ca	-1256.650581	-1256.998882	-1254.708341	-1254.360515
6da	-1178.069251	-1178.363347	-1176.225978	-1175.932272
6ea	-1565.042497	-1565.494892	-1562.609512	-1562.158067
6fa	-1568.602382	-1569.128112	-1566.236658	-1565.711628
HCl	-460.845585	-460.829022	-460.330801	-460.347364

ᵃC,H,O: 6-31+G(d); Si, Cl: 6-311+G(2d) ᵇsolvation energy added

2.7. NMR Spectra of Products
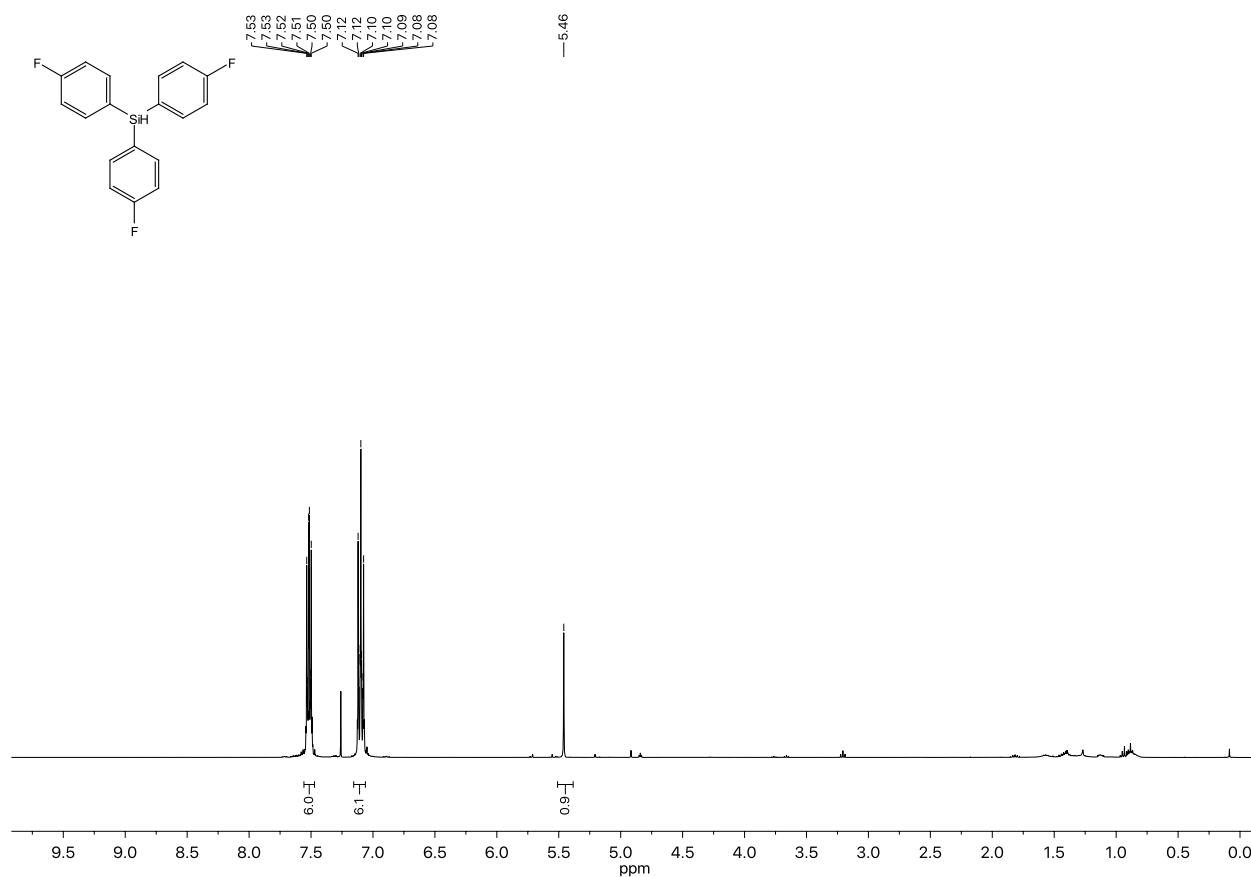
Figure 2.5. ^{1}H-NMR spectrum of **10d**.
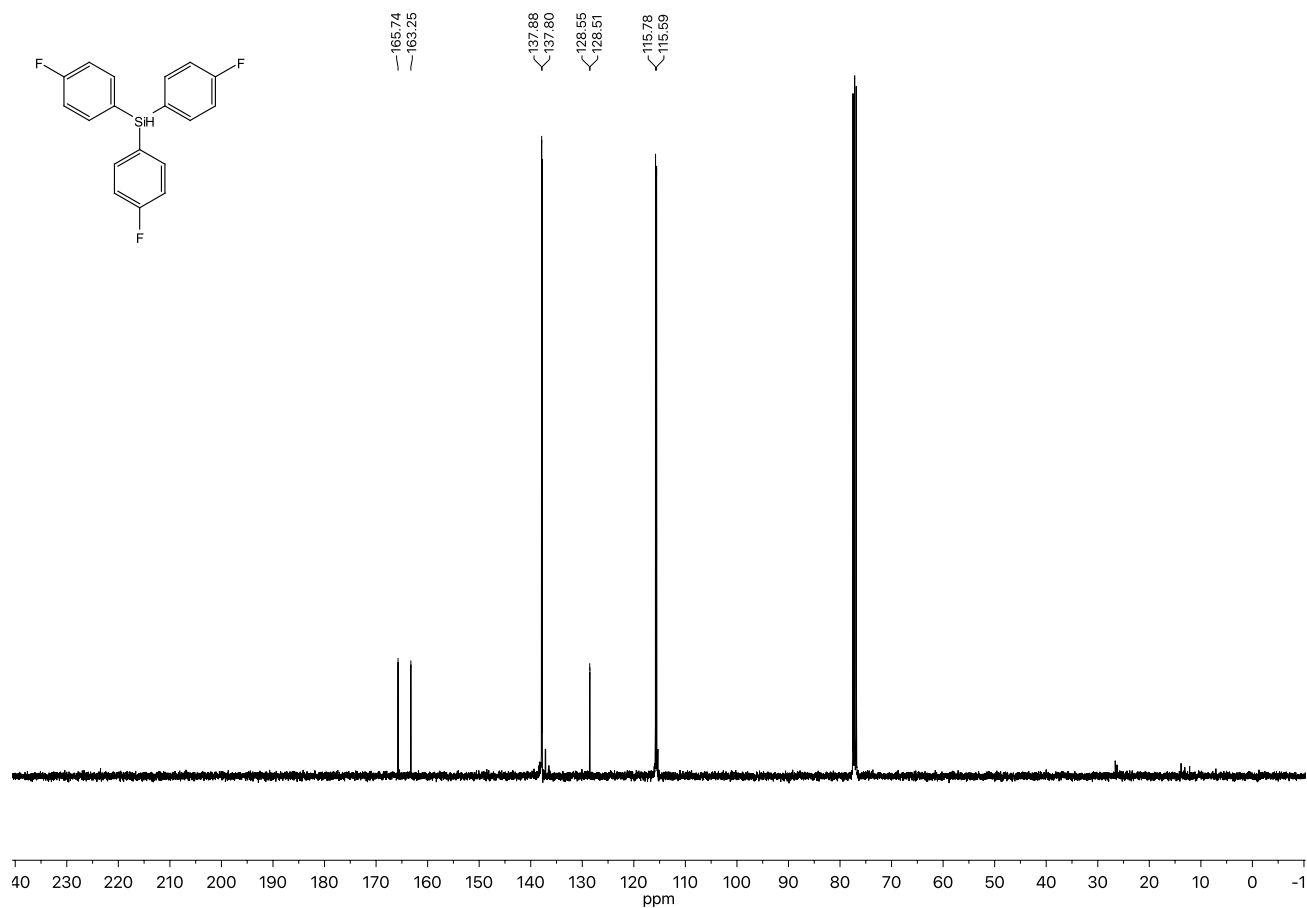
Figure 2.6. ^{13}C-NMR spectrum of **10d**.
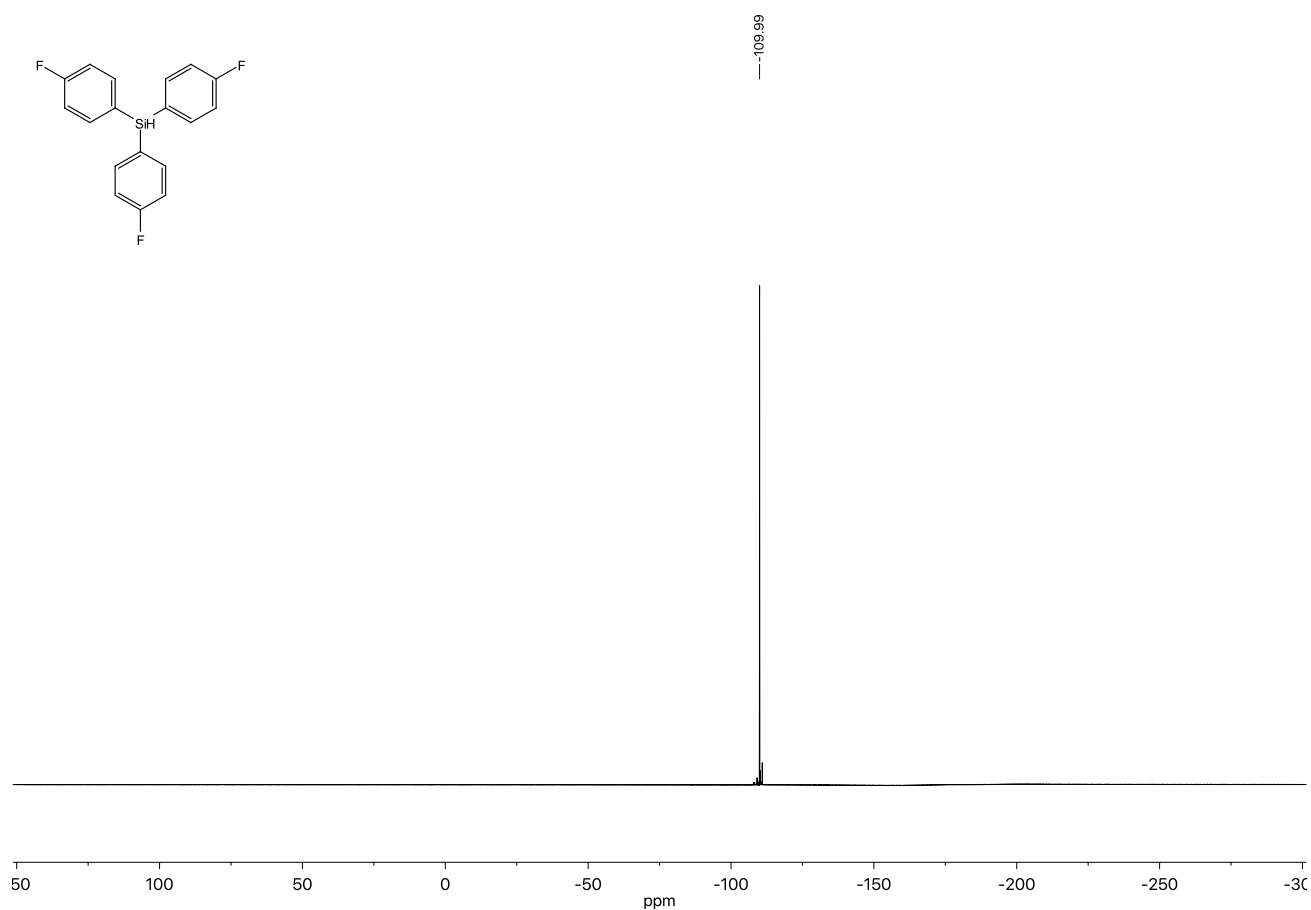
Figure 2.7. ^{19}F-NMR spectrum of **10d**.
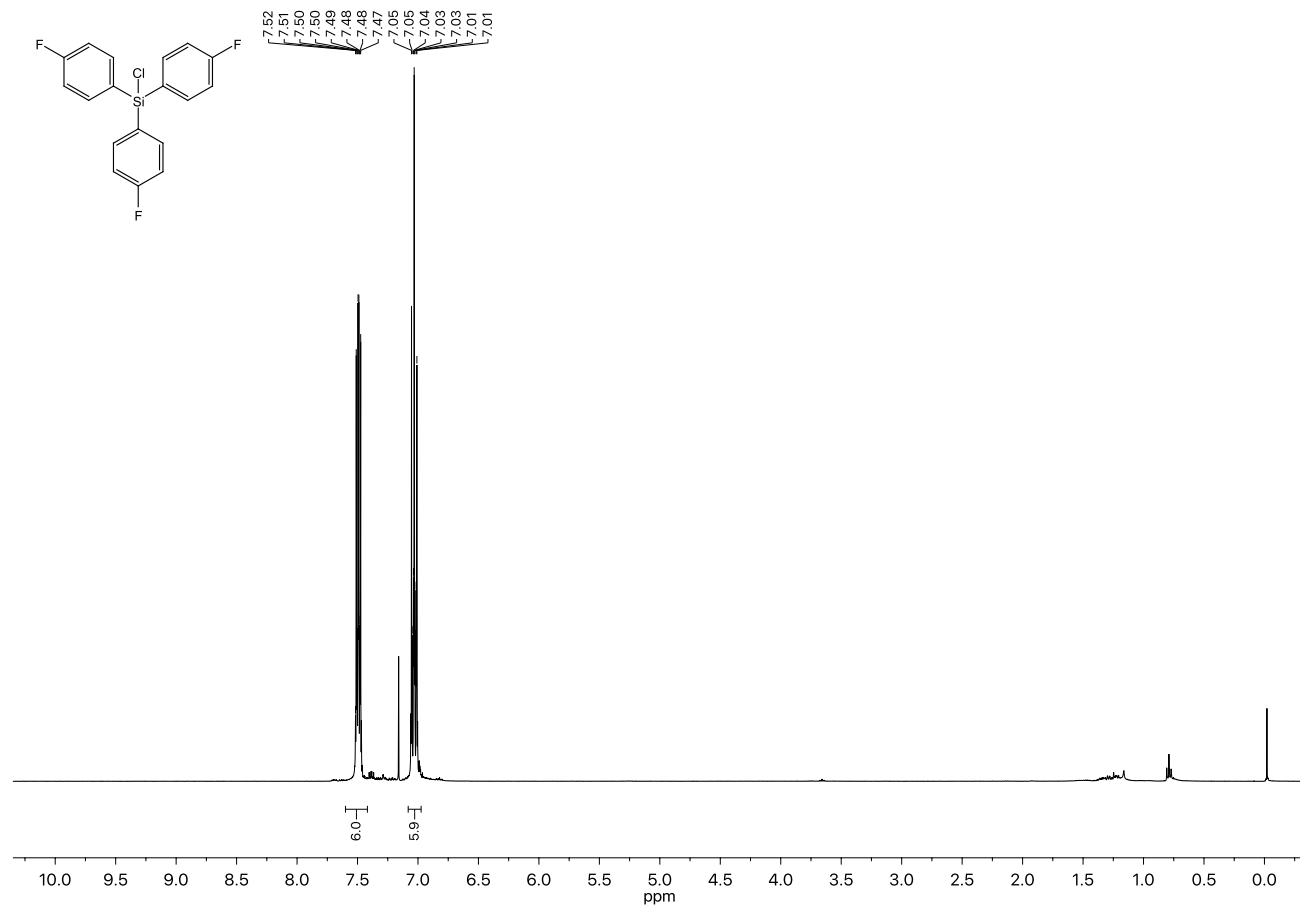
Figure 2.8. ^{1}H-NMR spectrum of **3d**.
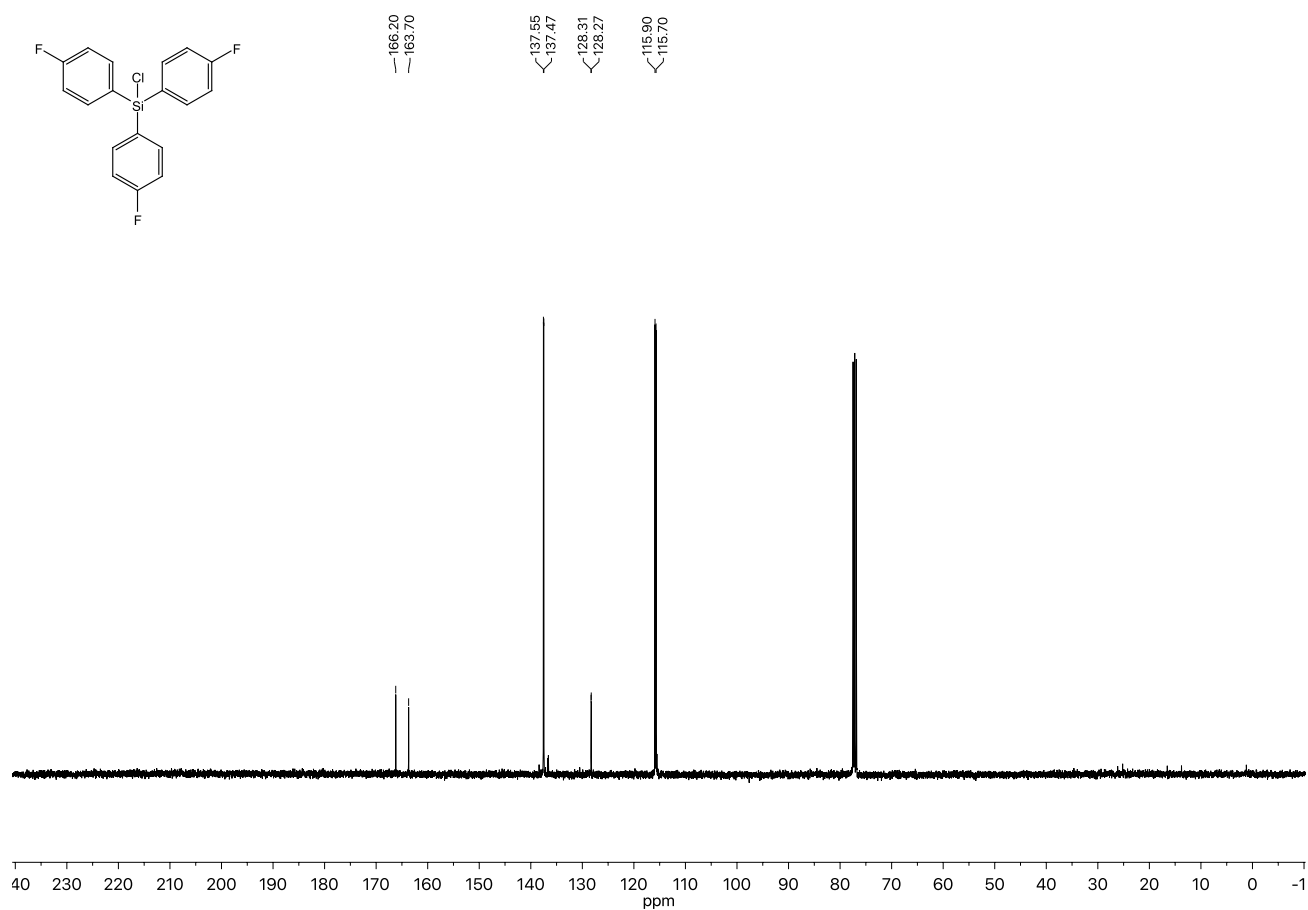
Figure 2.9. ^{13}C-NMR spectrum of **3d**.
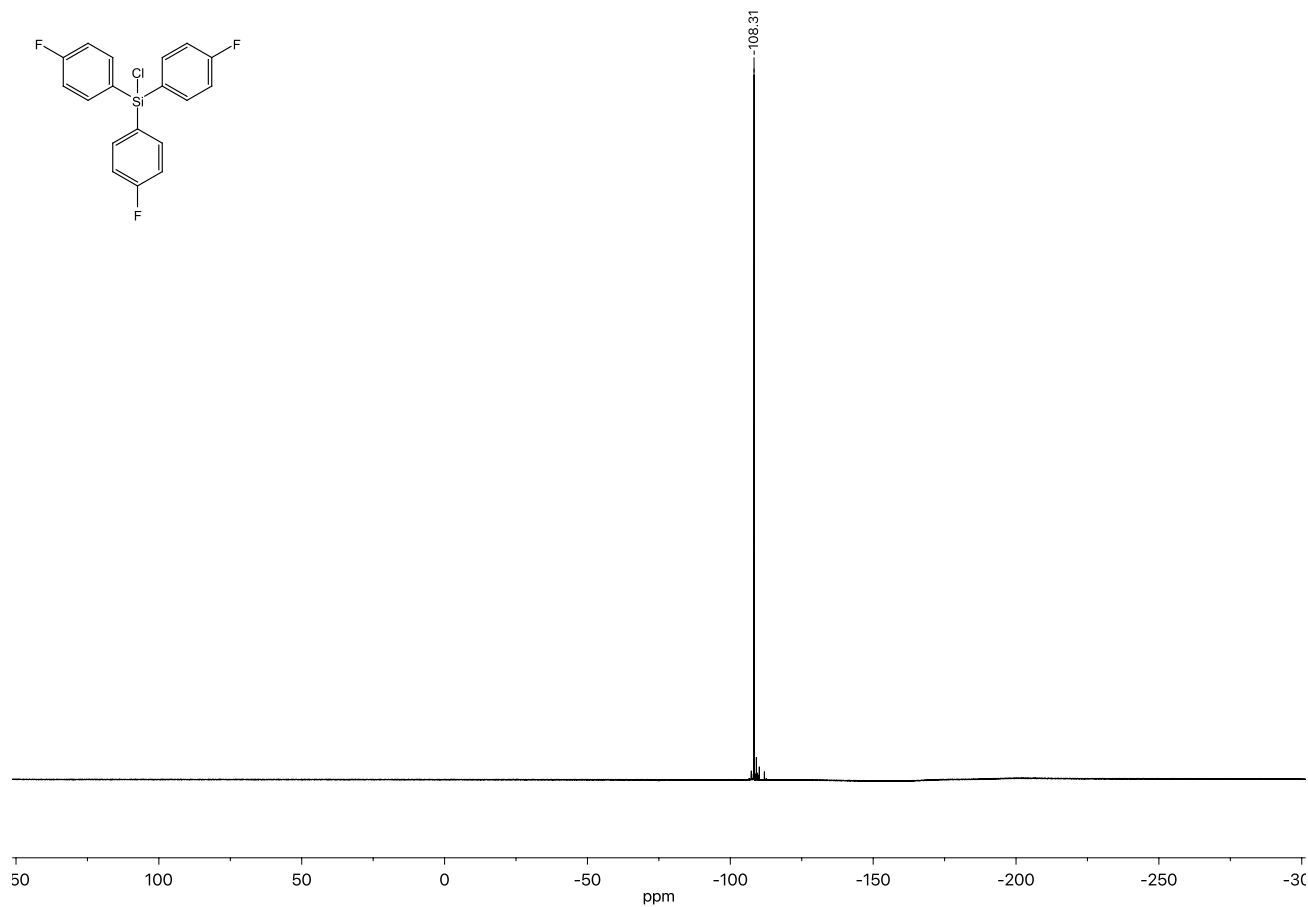
Figure 2.10. ^{19}F-NMR spectrum of **3d**.
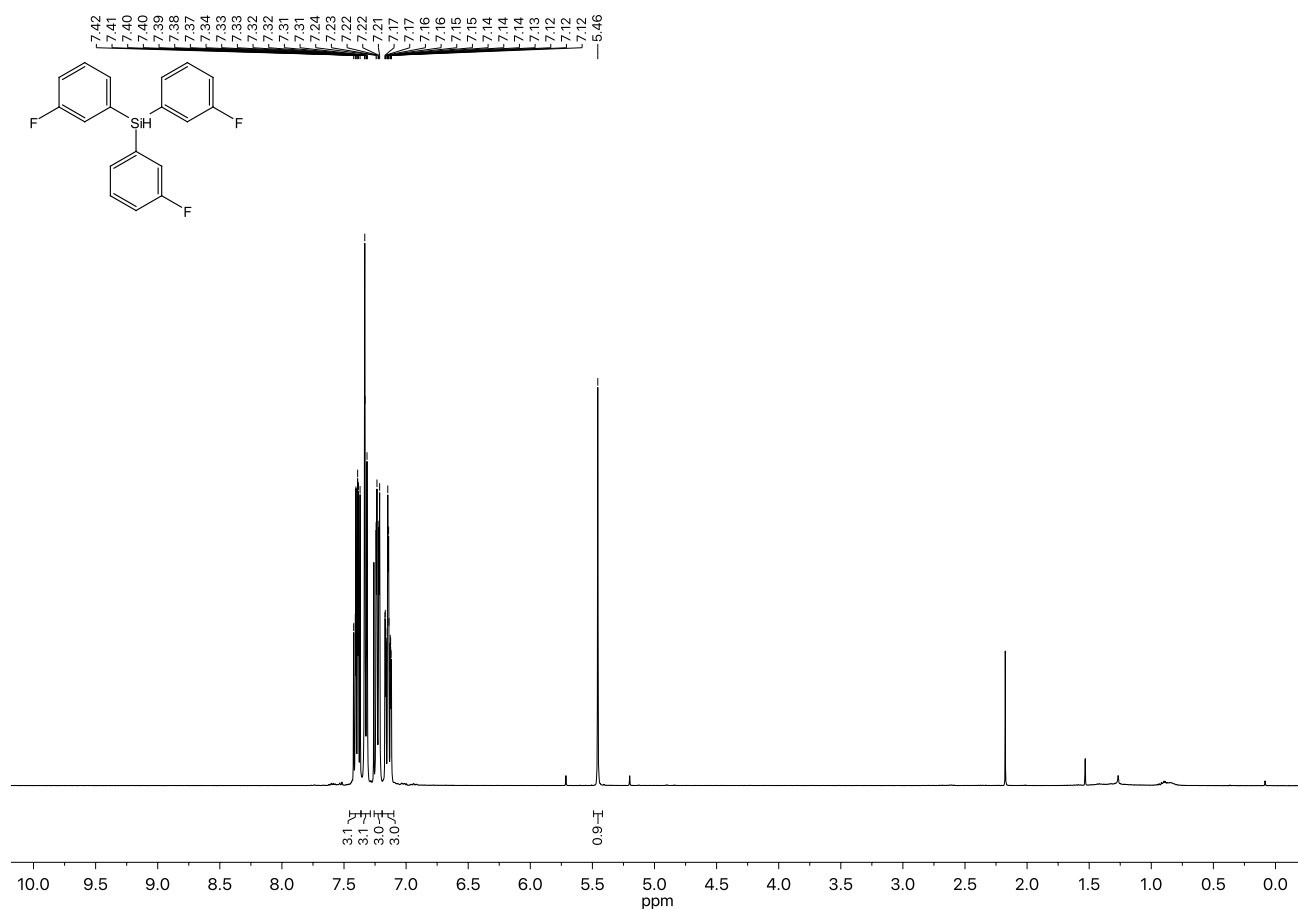
Figure 2.11. ^{1}H-NMR spectrum of **10e**.
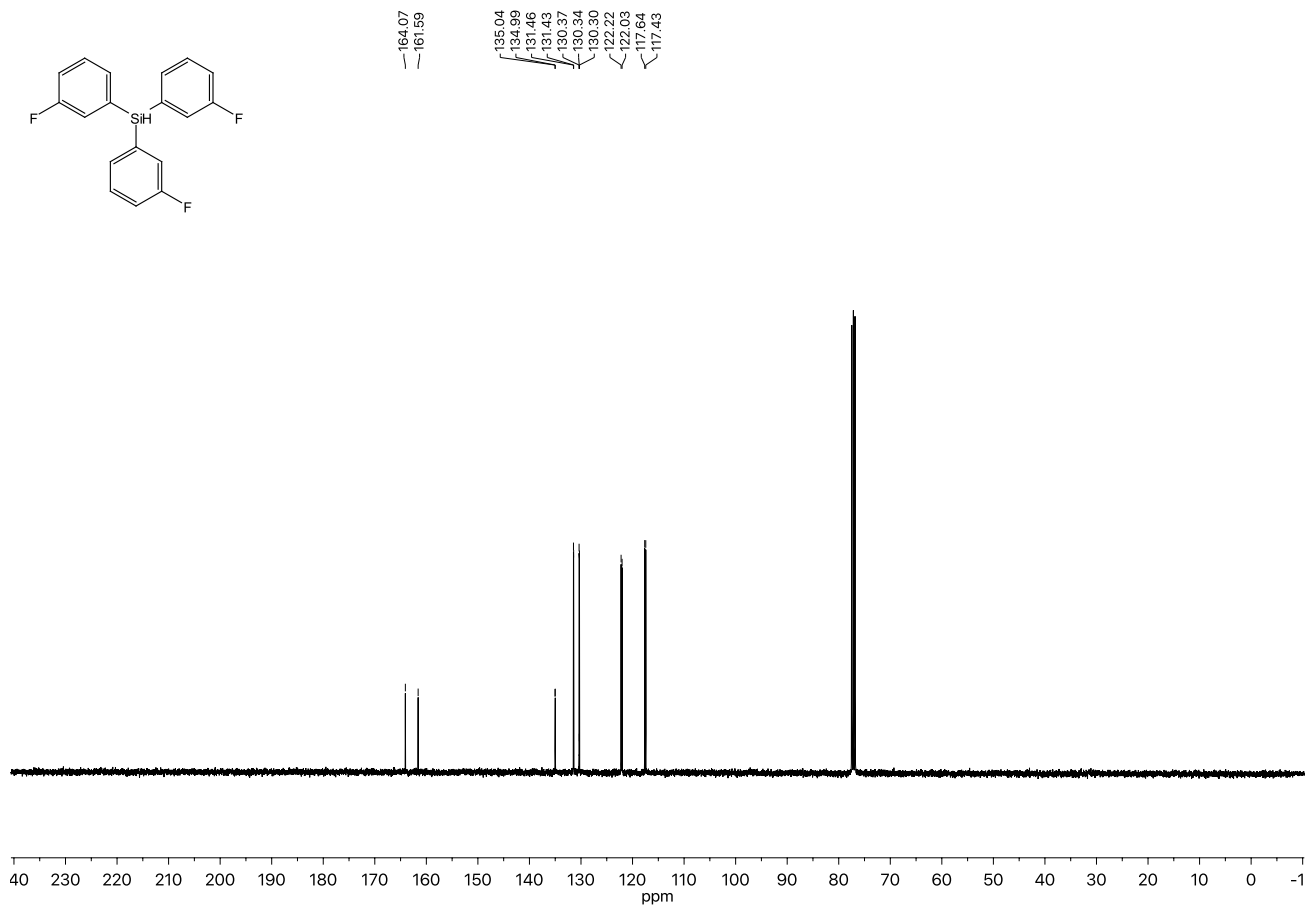
Figure 2.12. ^{13}C-NMR spectrum of **10e**.
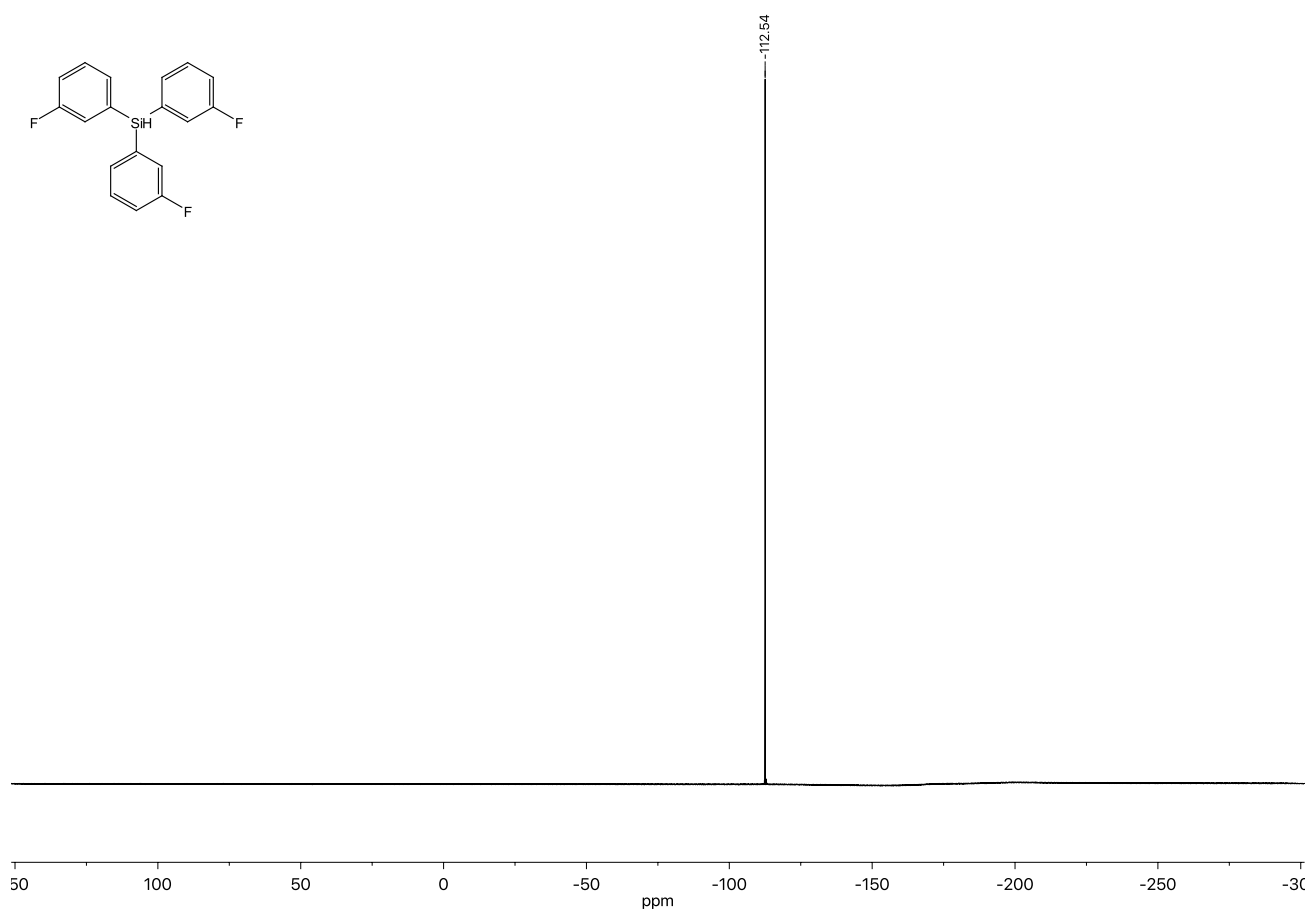
Figure 2.13. ¹⁹F-NMR spectrum of **10e**.
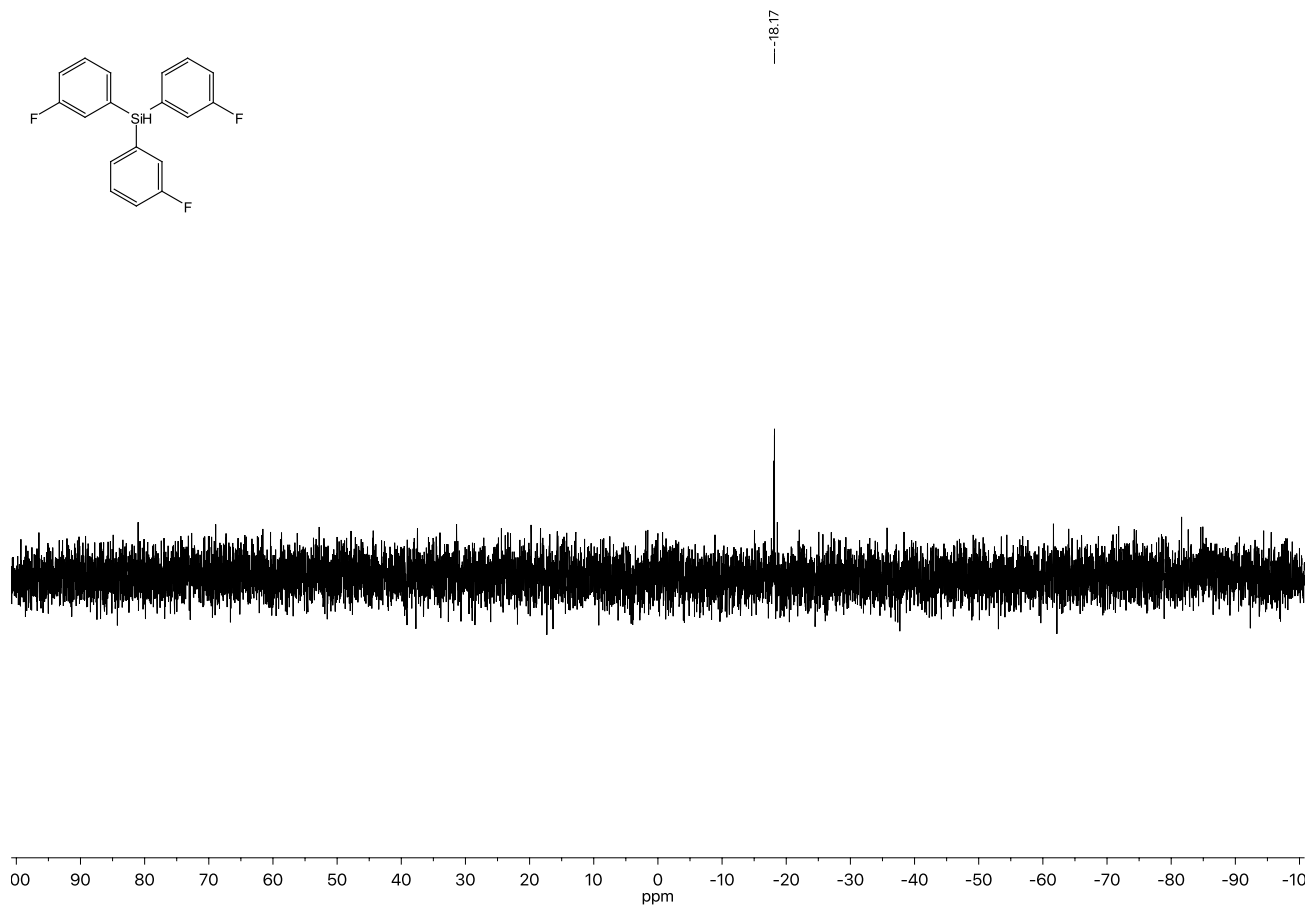
Figure 2.14. ²⁹Si-NMR spectrum of **10e**.
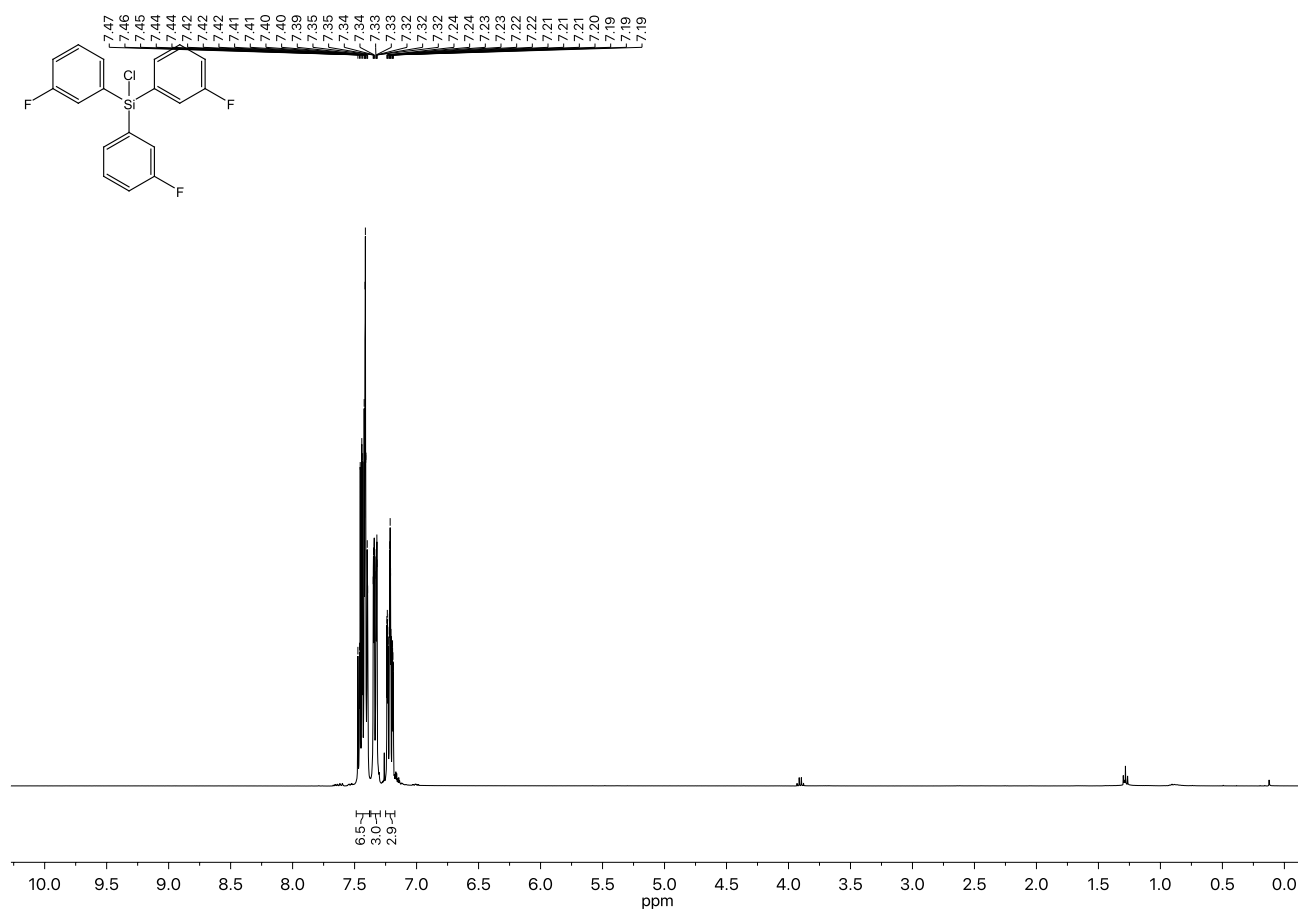
Figure 2.15. ^{1}H-NMR spectrum of **3e**.
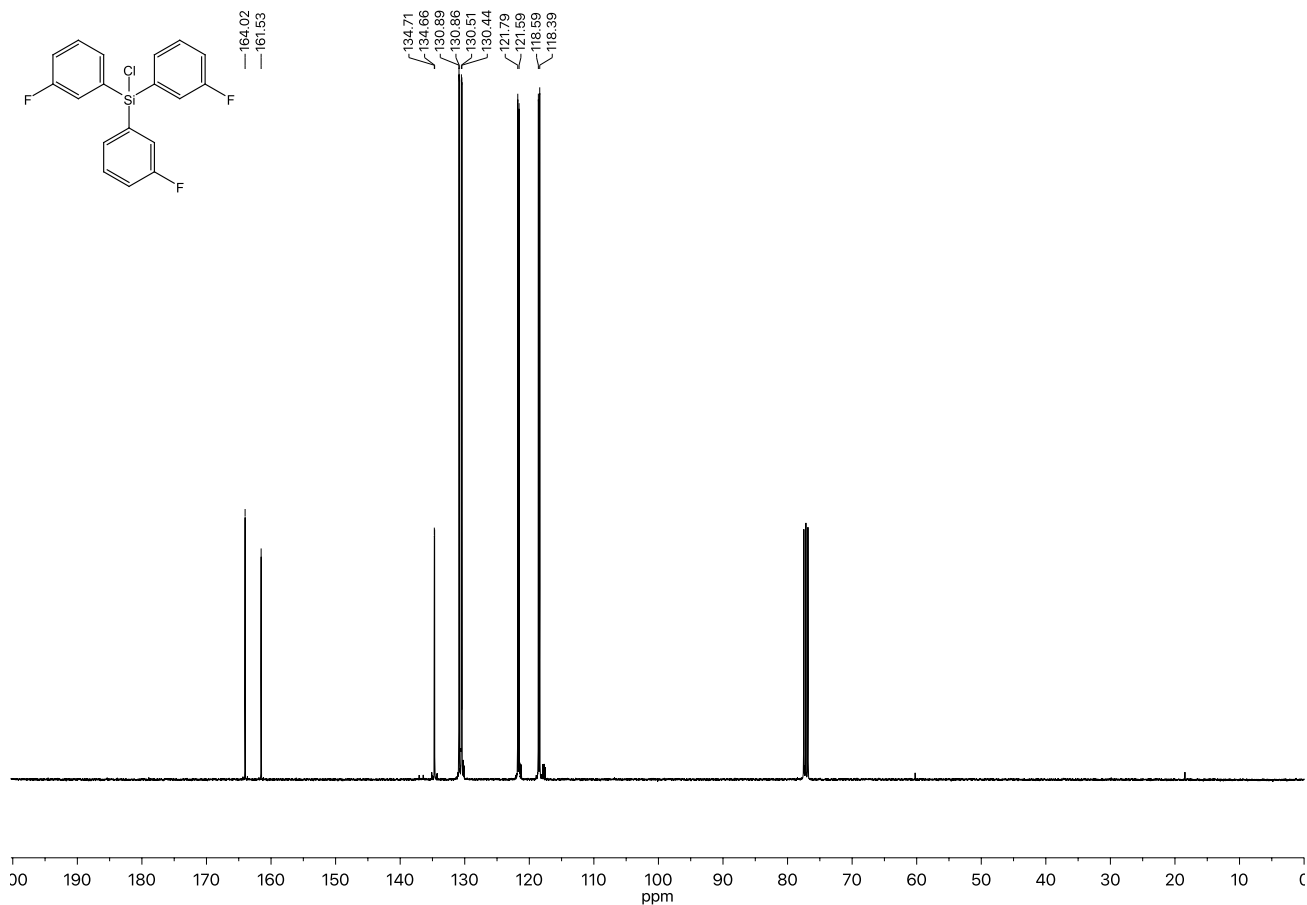
Figure 2.16. ^{13}C-NMR spectrum of **3e**.
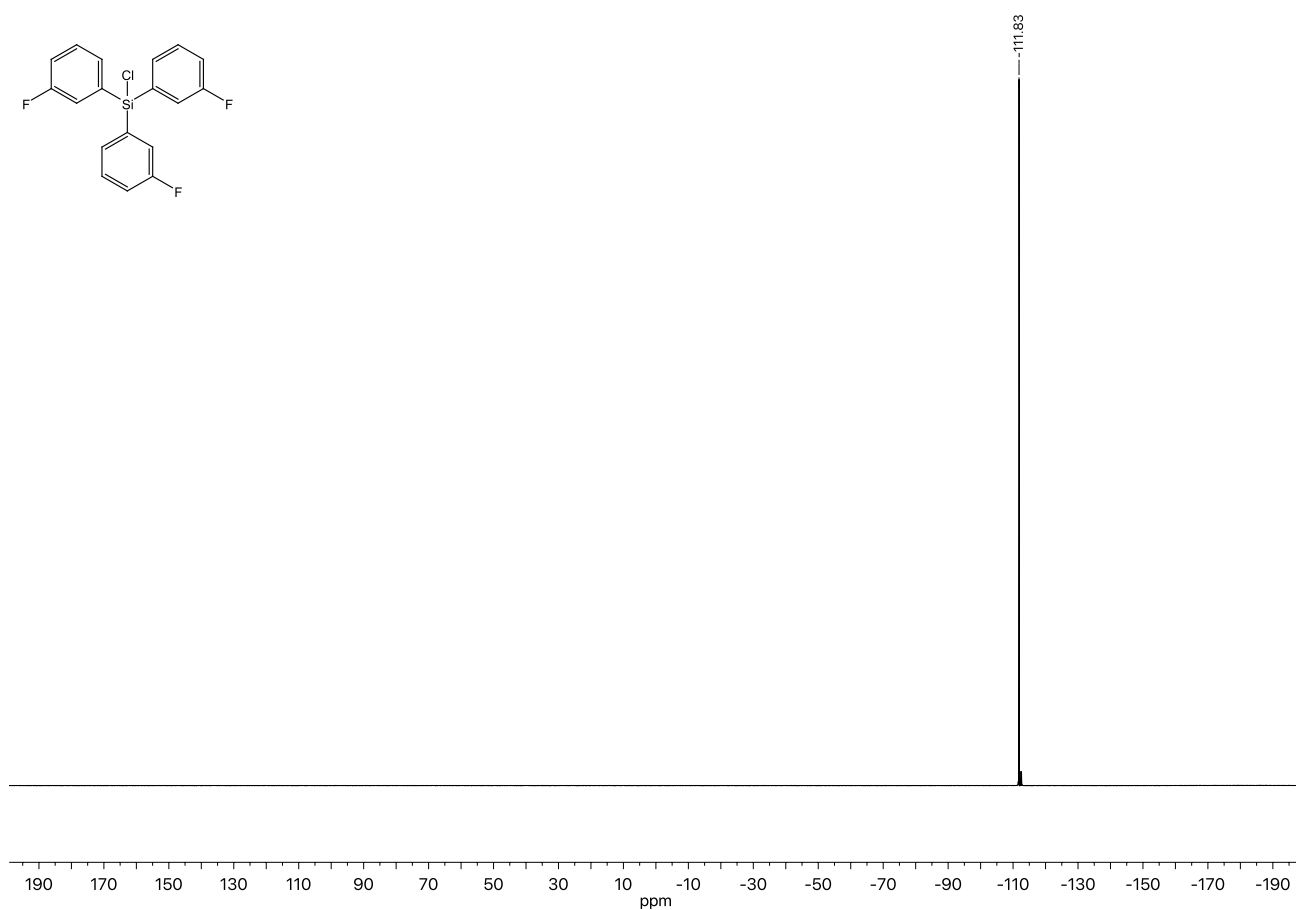
Figure 2.17. ^{19}F-NMR spectrum of **3e**.
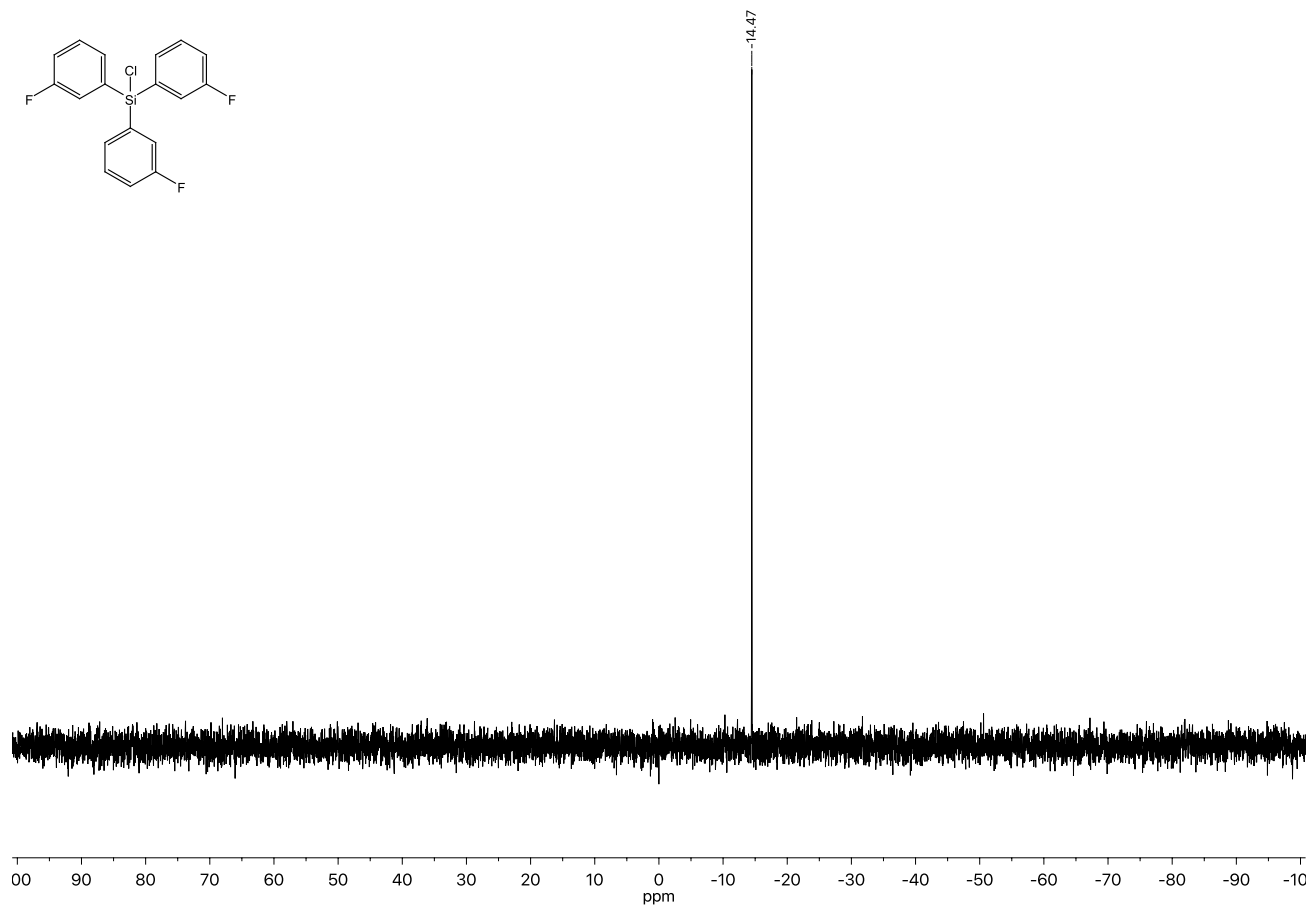
Figure 2.18. ^{29}Si-NMR spectrum of **3e**.
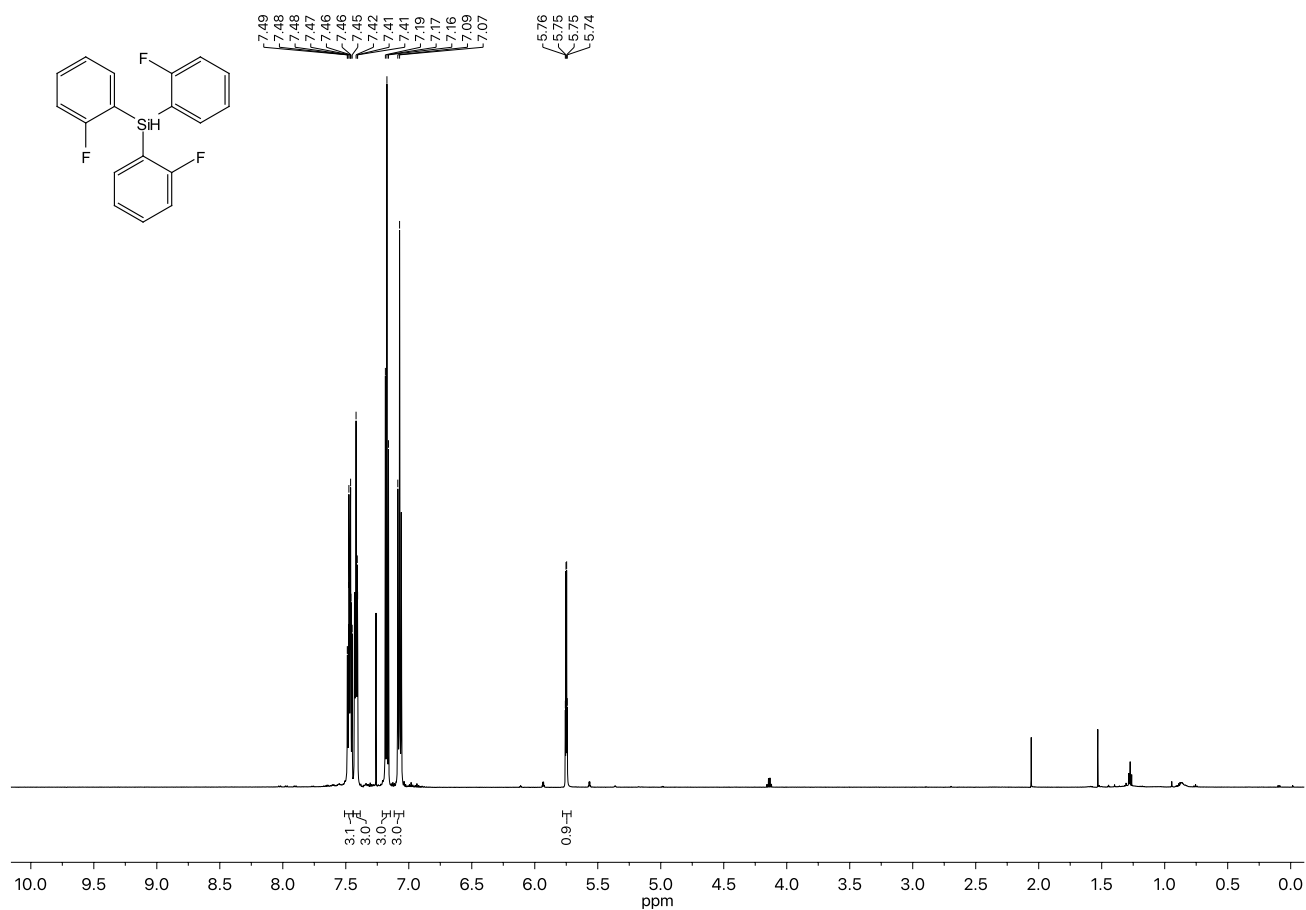
Figure 2.19. ¹H-NMR spectrum of **10f**.
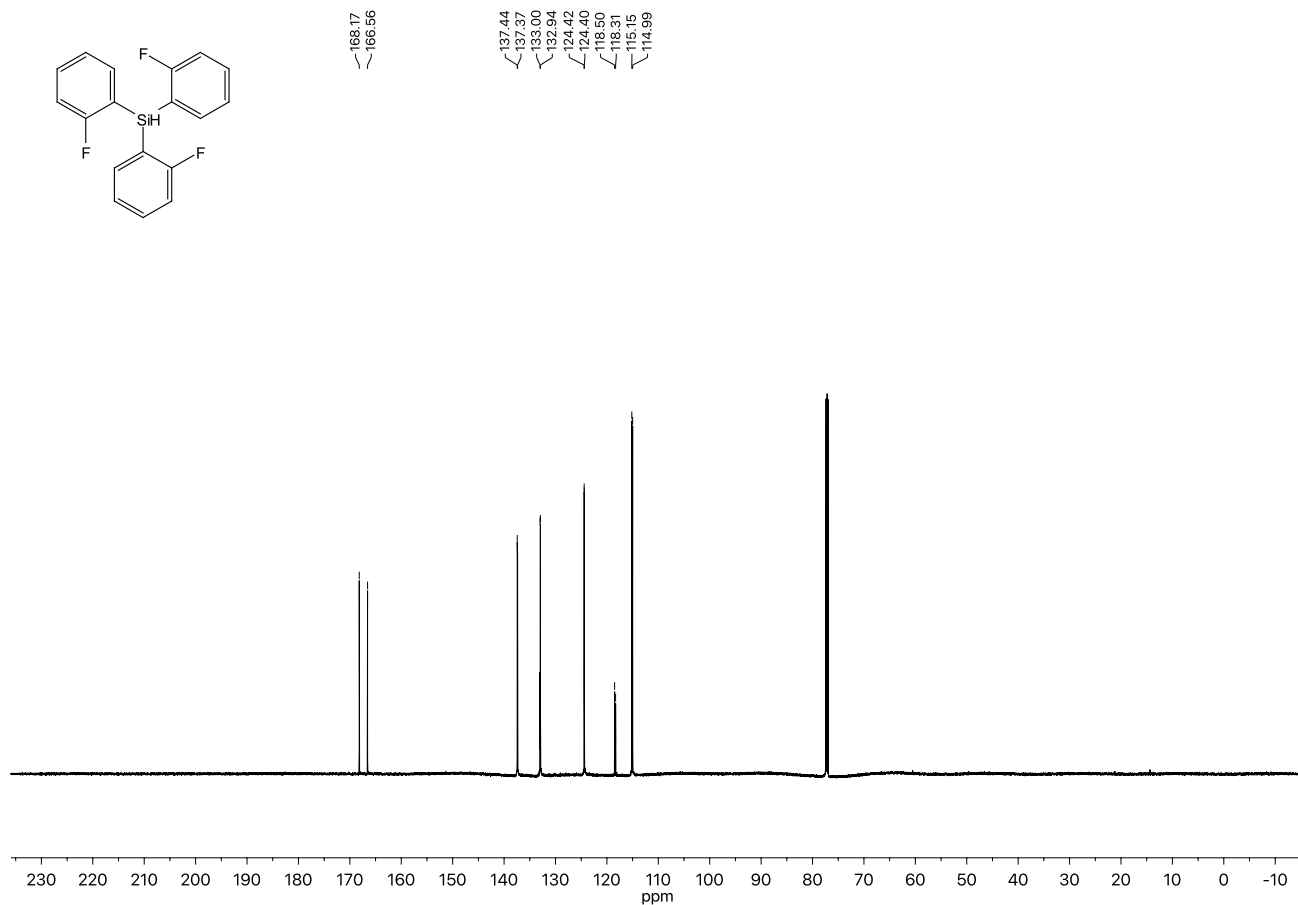
Figure 2.20. ¹³C-NMR spectrum of **10f**.
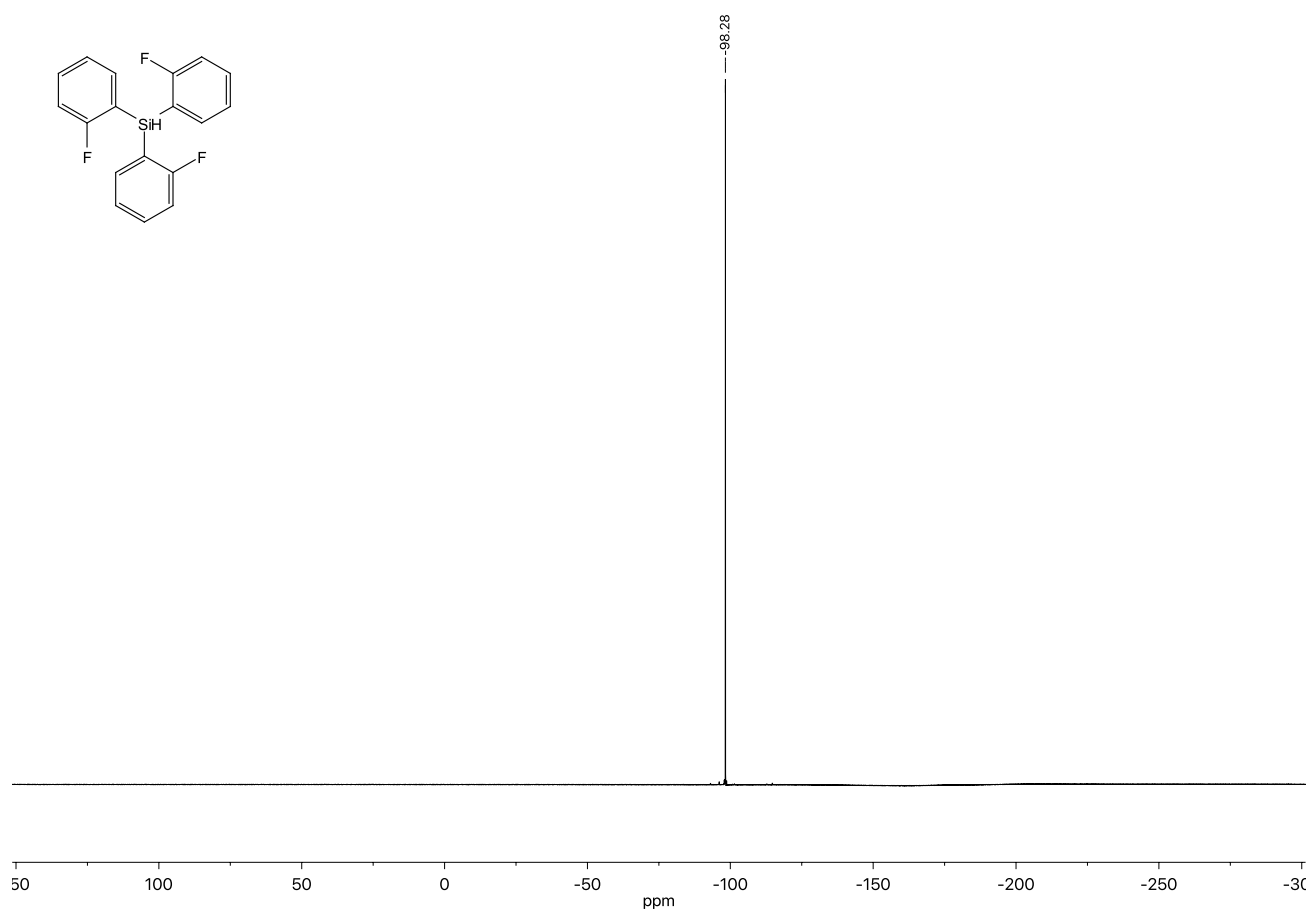
Figure 2.21. ^{19}F-NMR spectrum of **10f**.
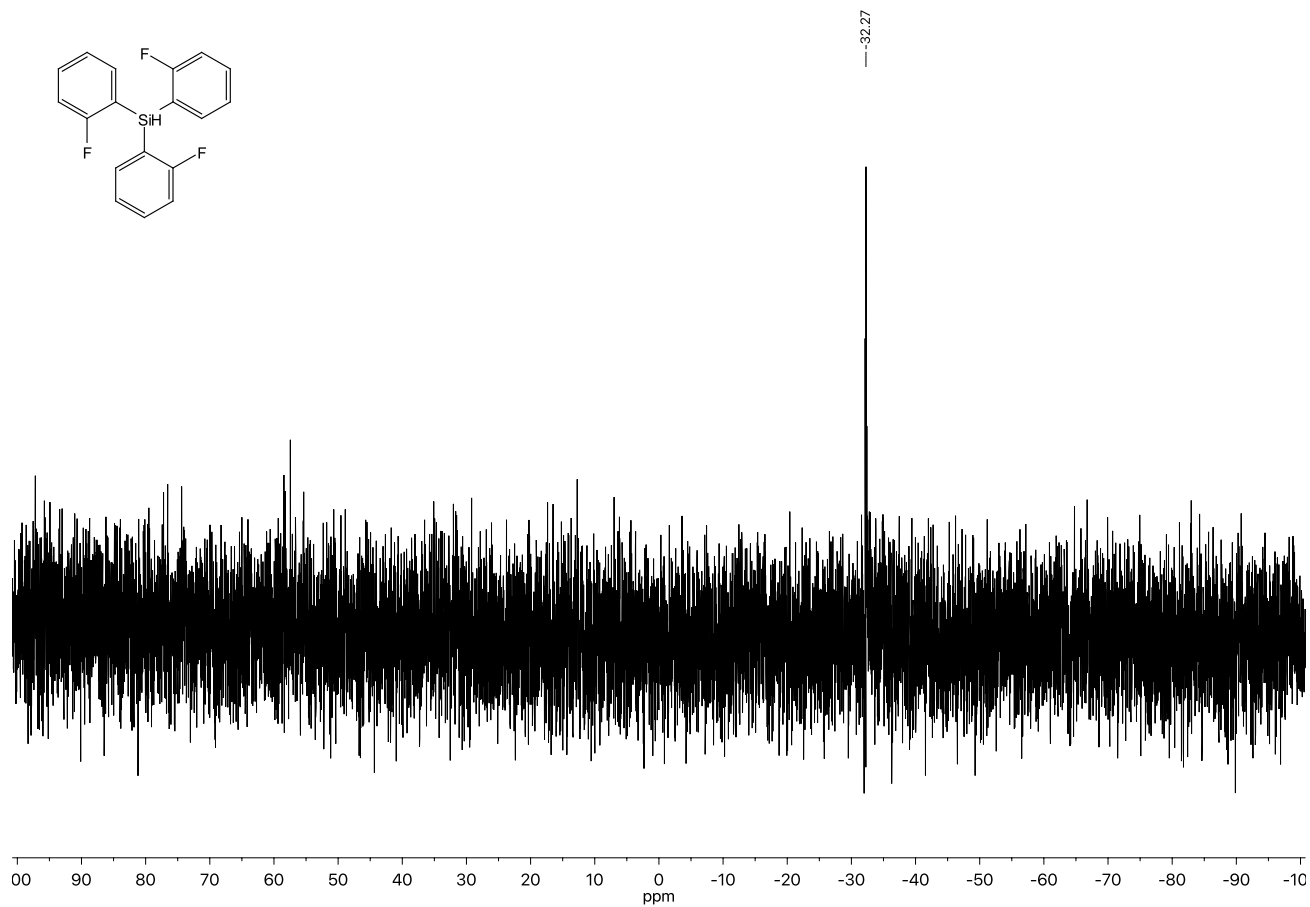
Figure 2.22. ^{29}Si-NMR spectrum of **10f**.
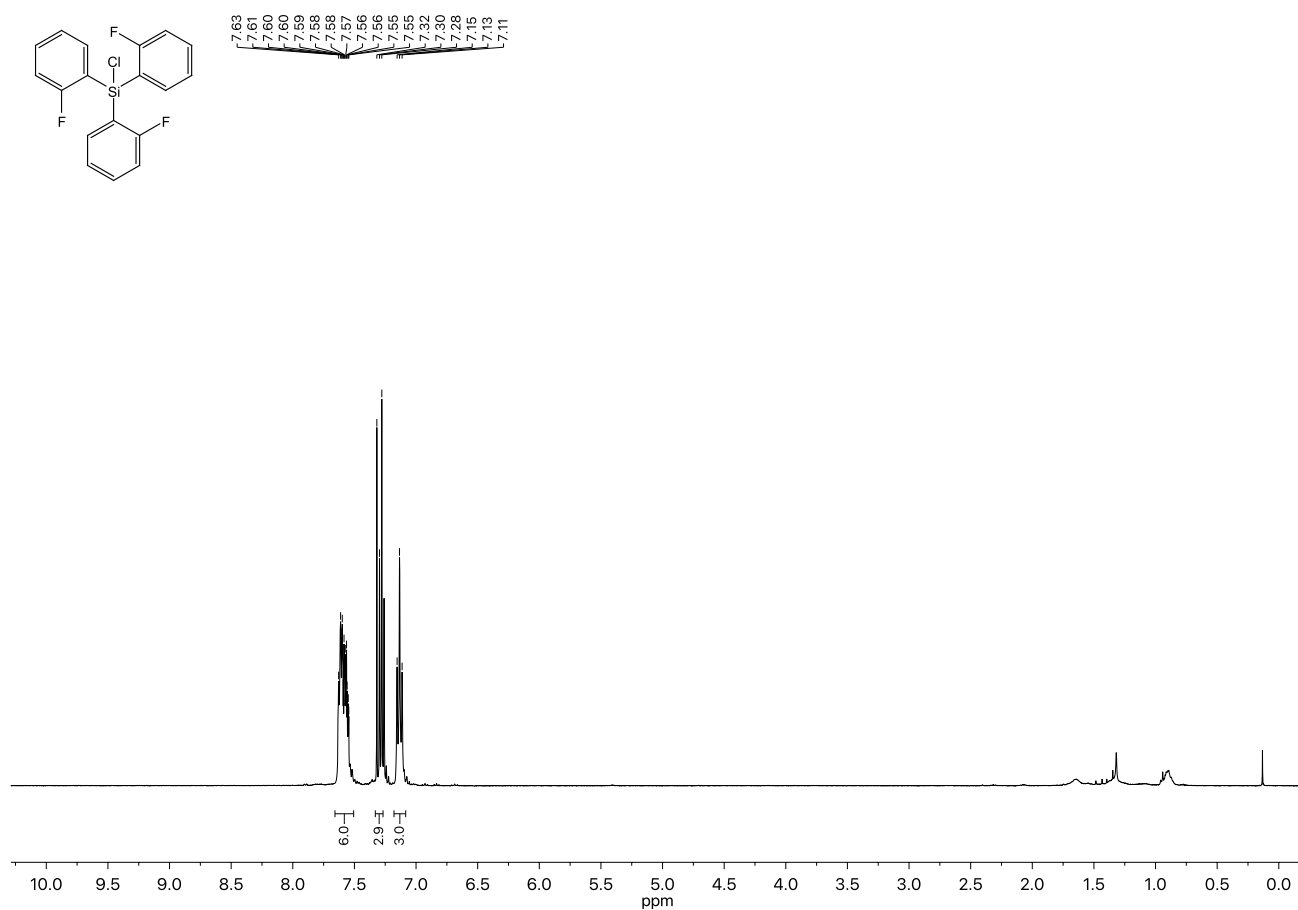
Figure 2.23. ^{1}H-NMR spectrum of **3f**.
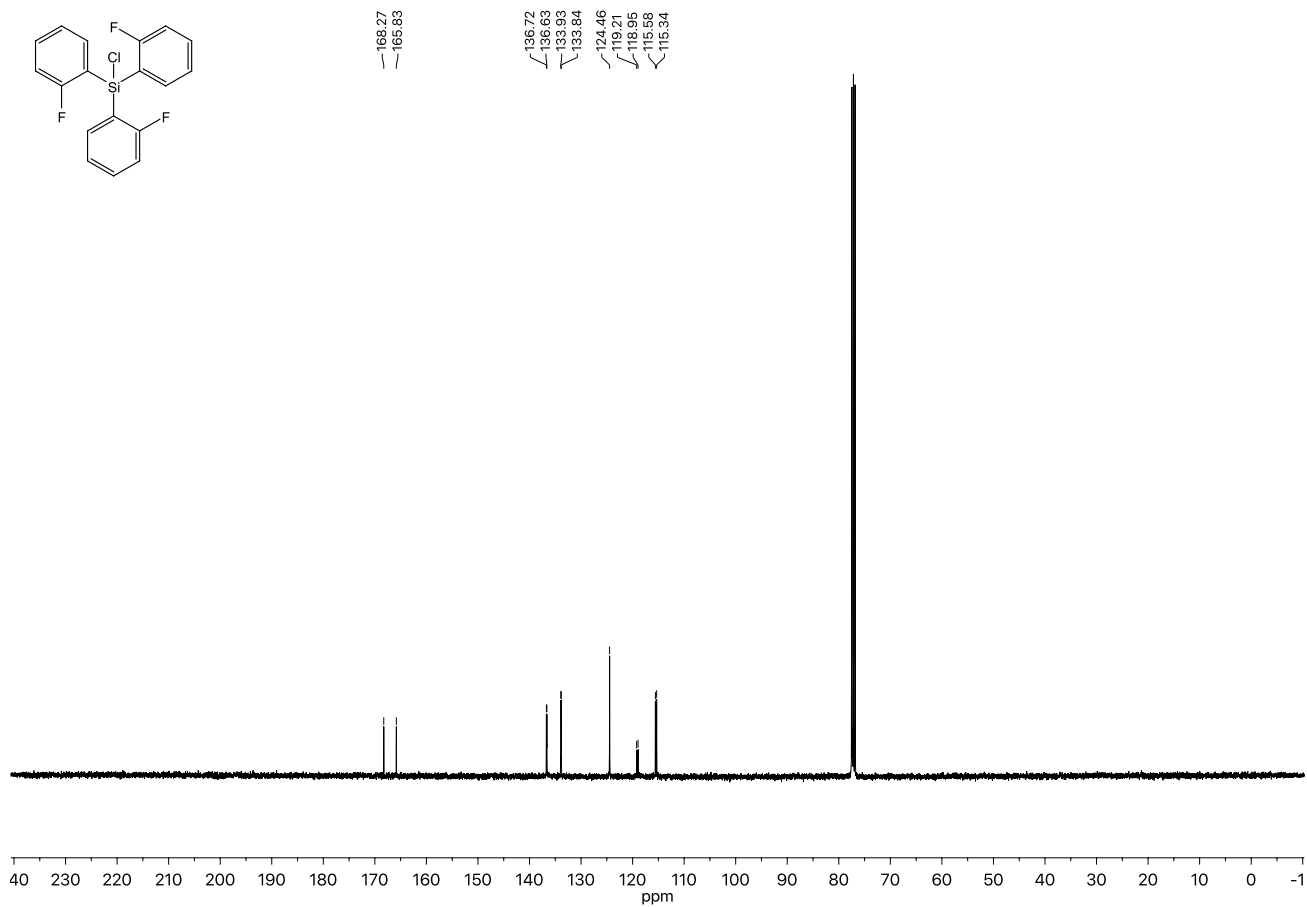
Figure 2.24. ^{13}C-NMR spectrum of **3f**.
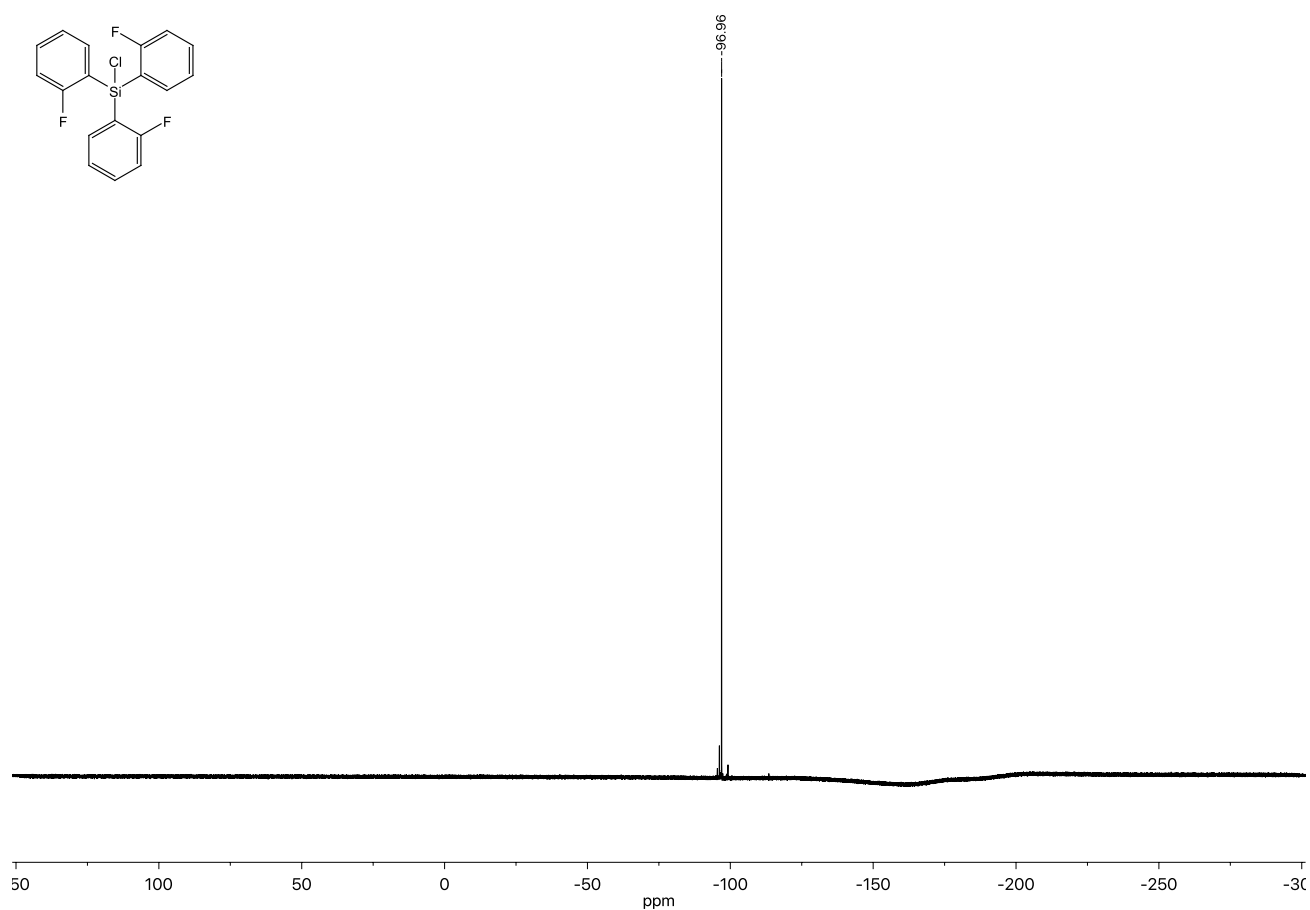
Figure 2.25. ^{19}F-NMR spectrum of **3f**.
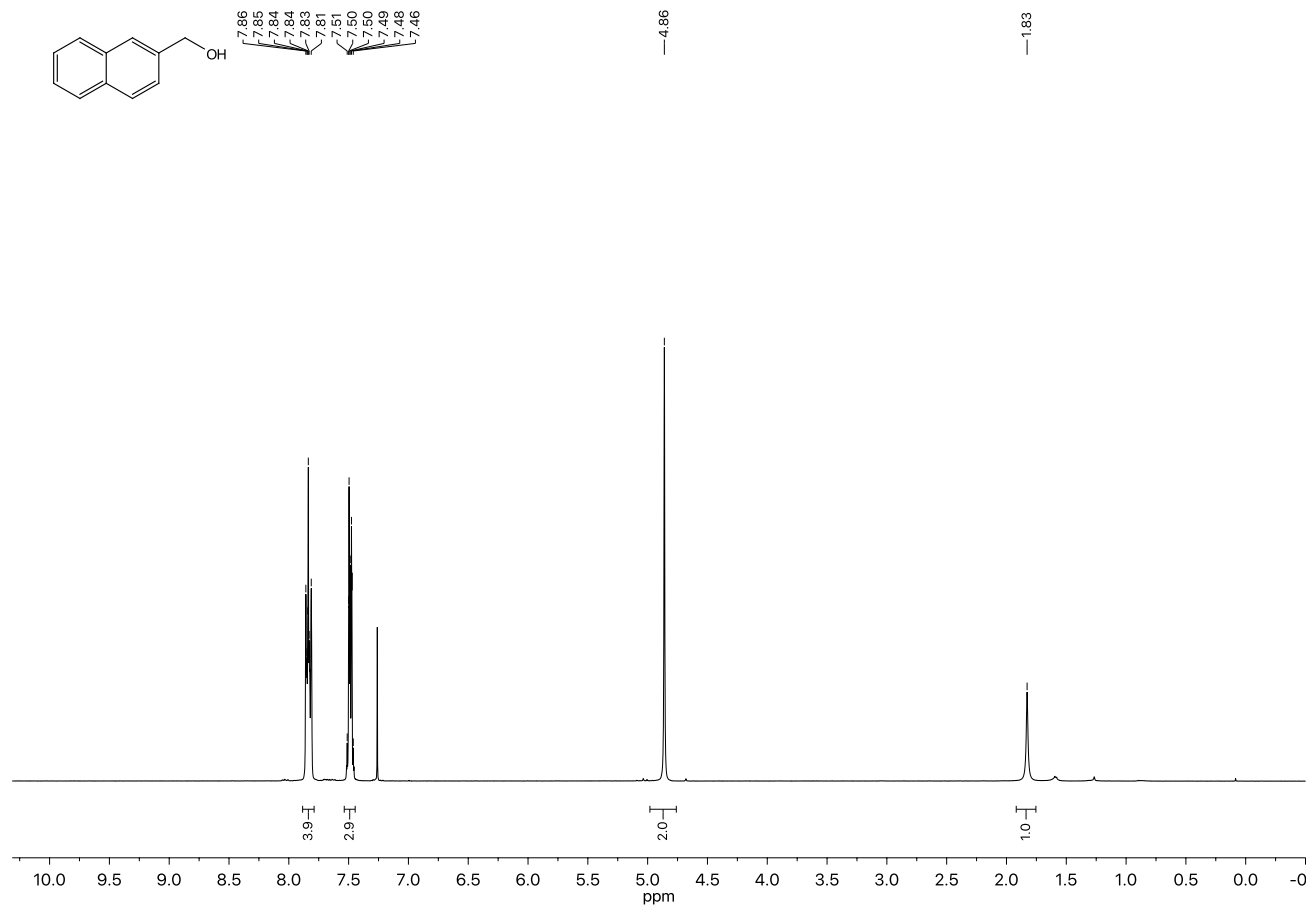
Figure 2.26. ^{1}H-NMR spectrum of **1b**.
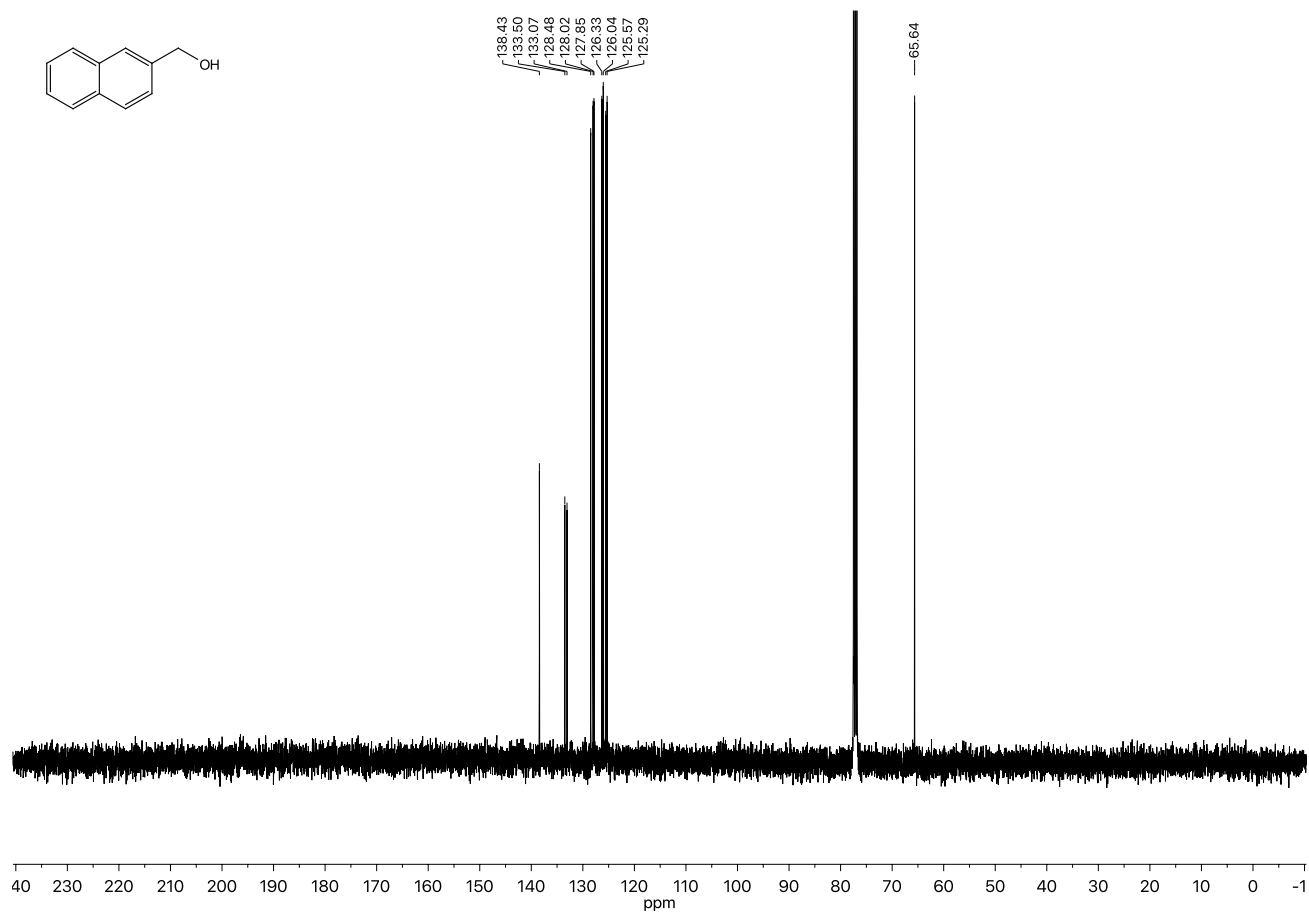
Figure 2.27. ^{13}C-NMR spectrum of **1b**.
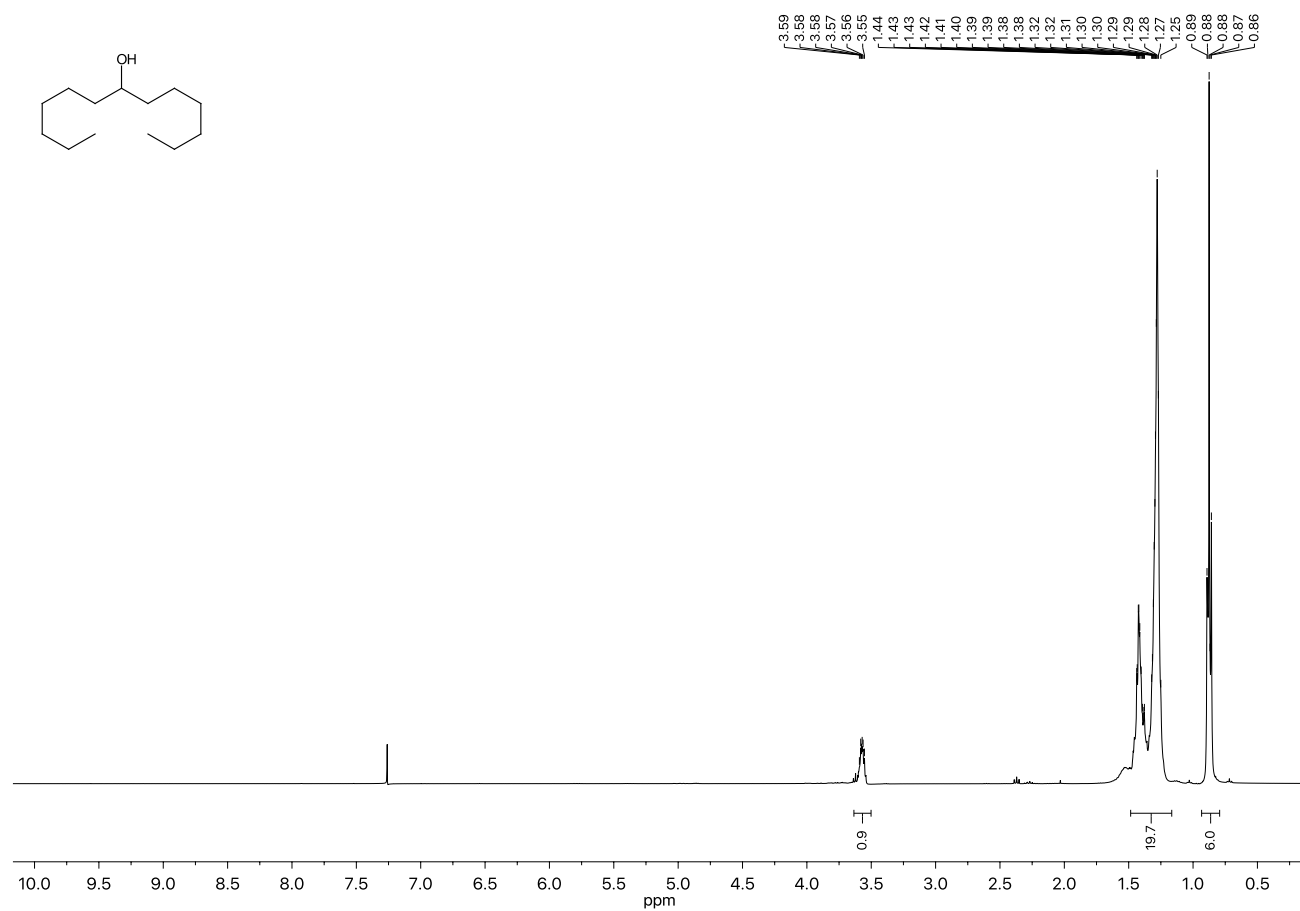
Figure 2.28. ^{1}H-NMR spectrum of **2g**.
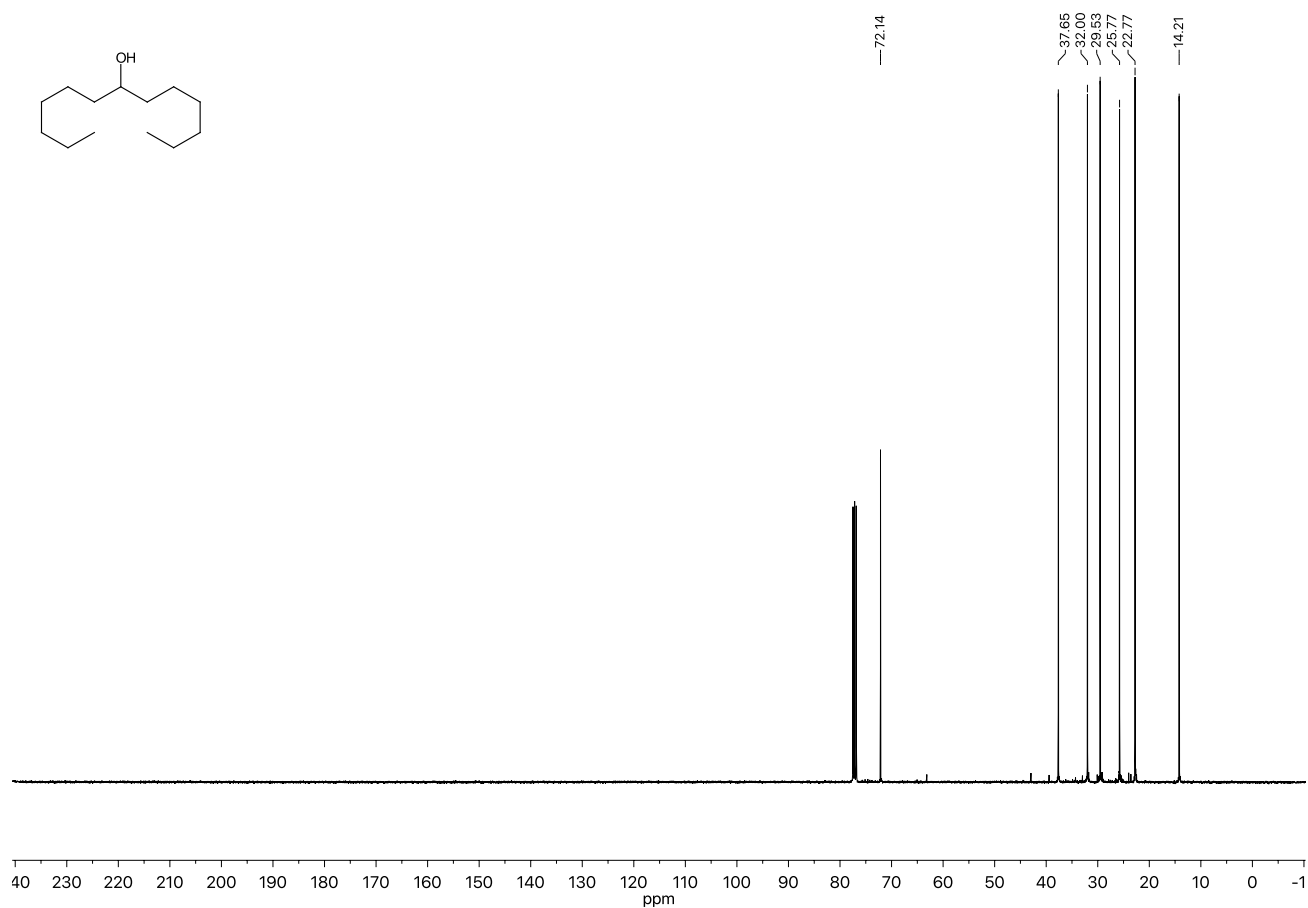
Figure 2.29. ^{13}C-NMR spectrum of **2g**.
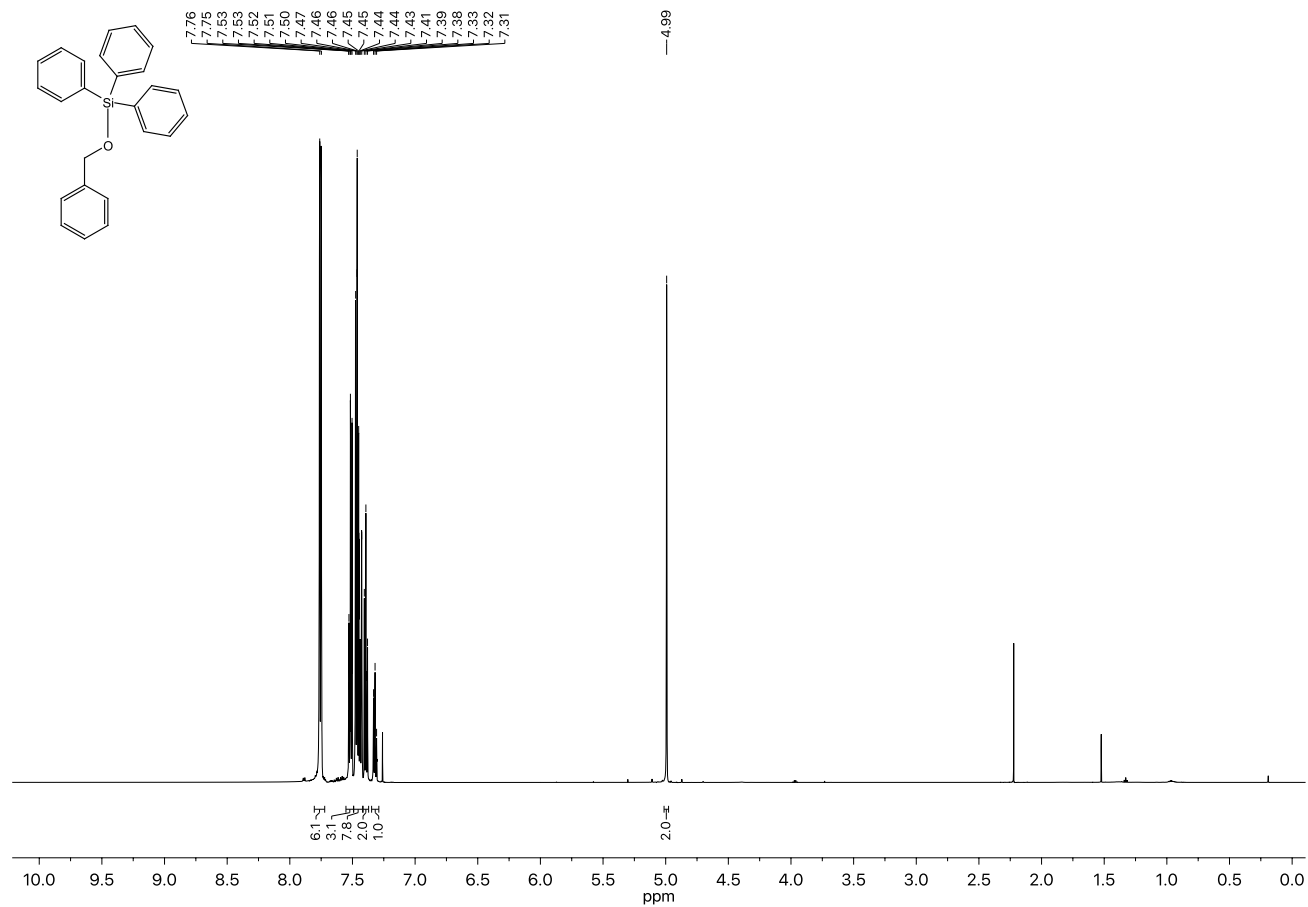
Figure 2.30. ^{1}H-NMR spectrum of **5aa**.
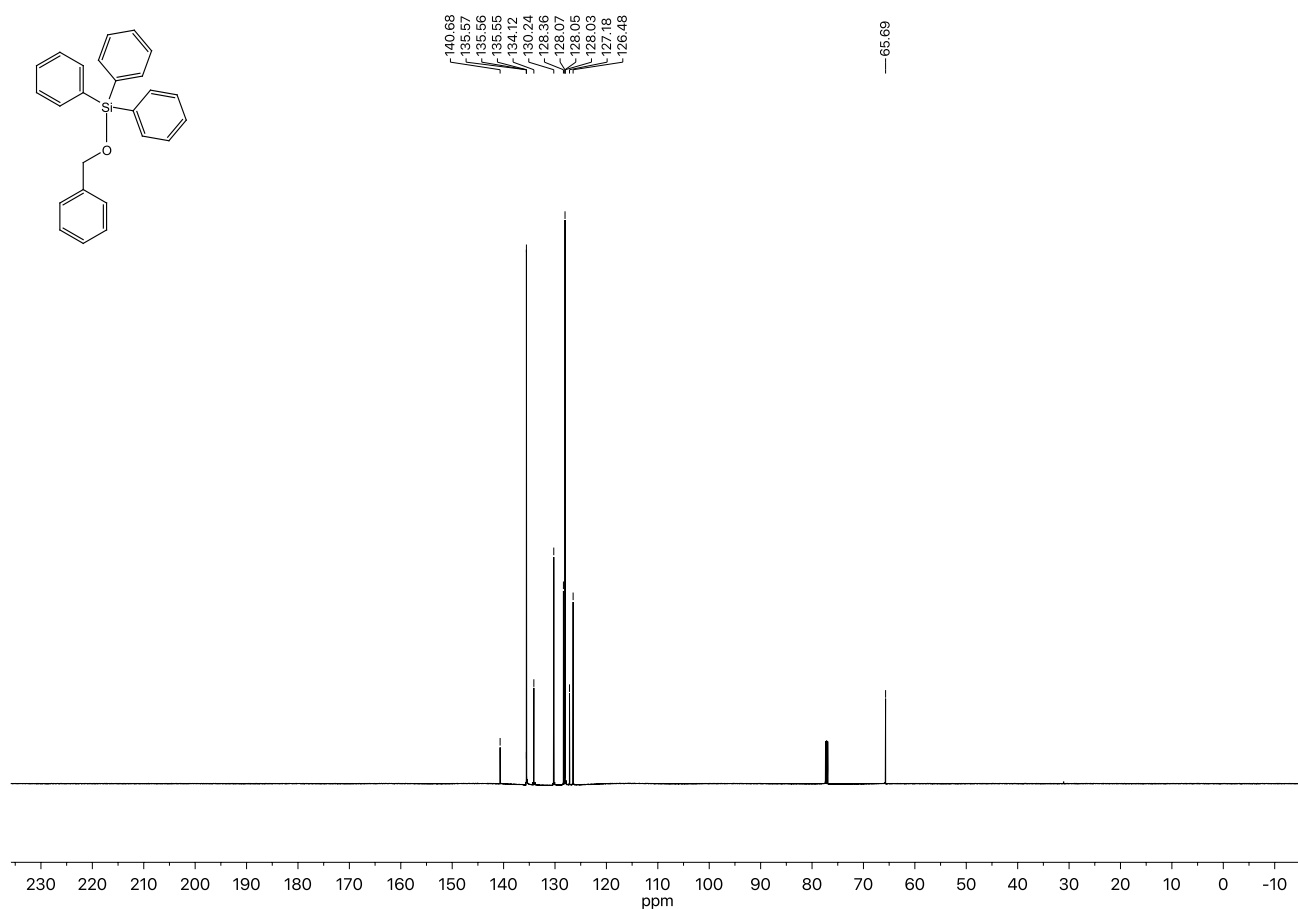
Figure 2.31. ^{13}C-NMR spectrum of **5aa**.
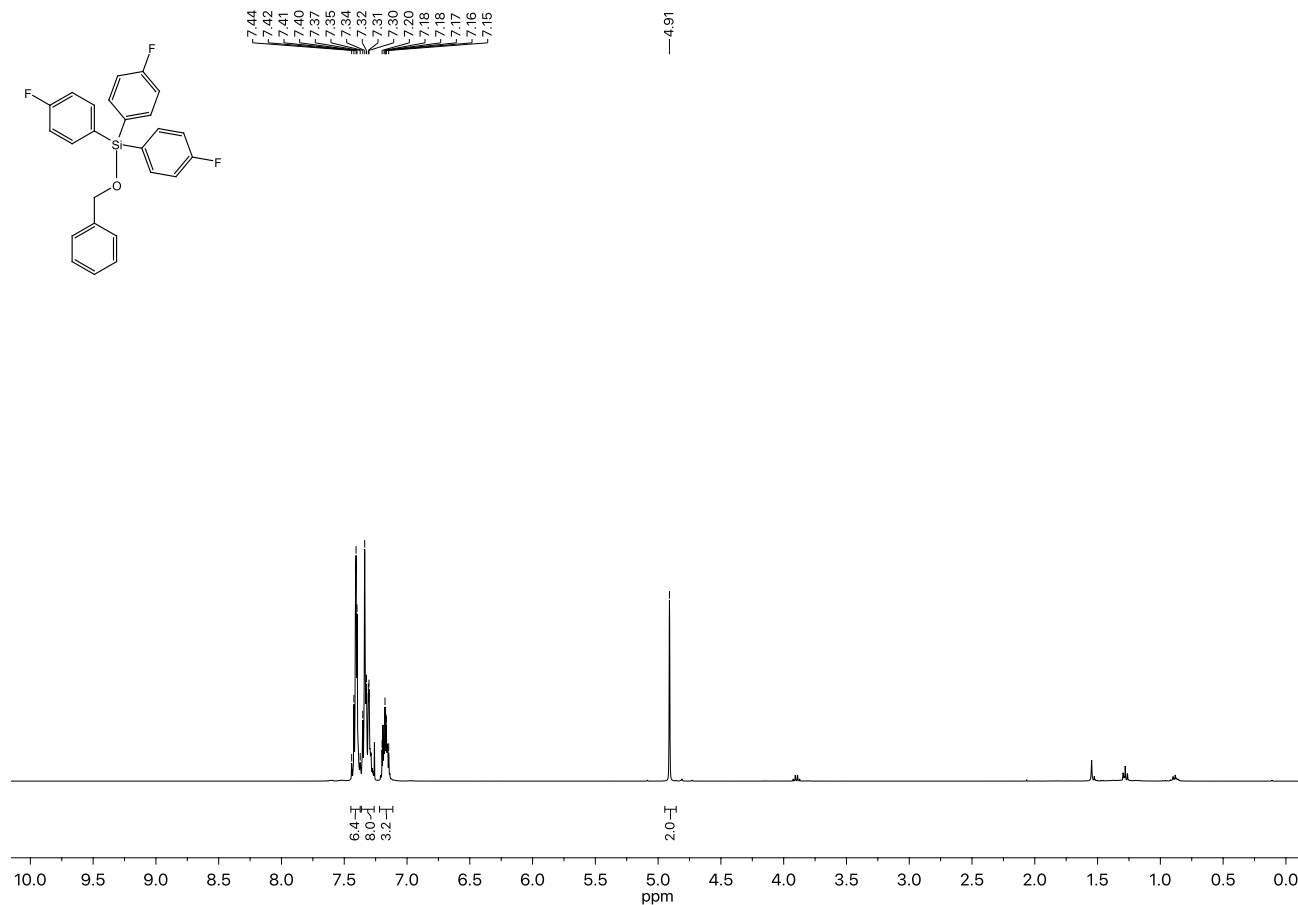
Figure 2.32. ^{1}H-NMR spectrum of **5ad**.
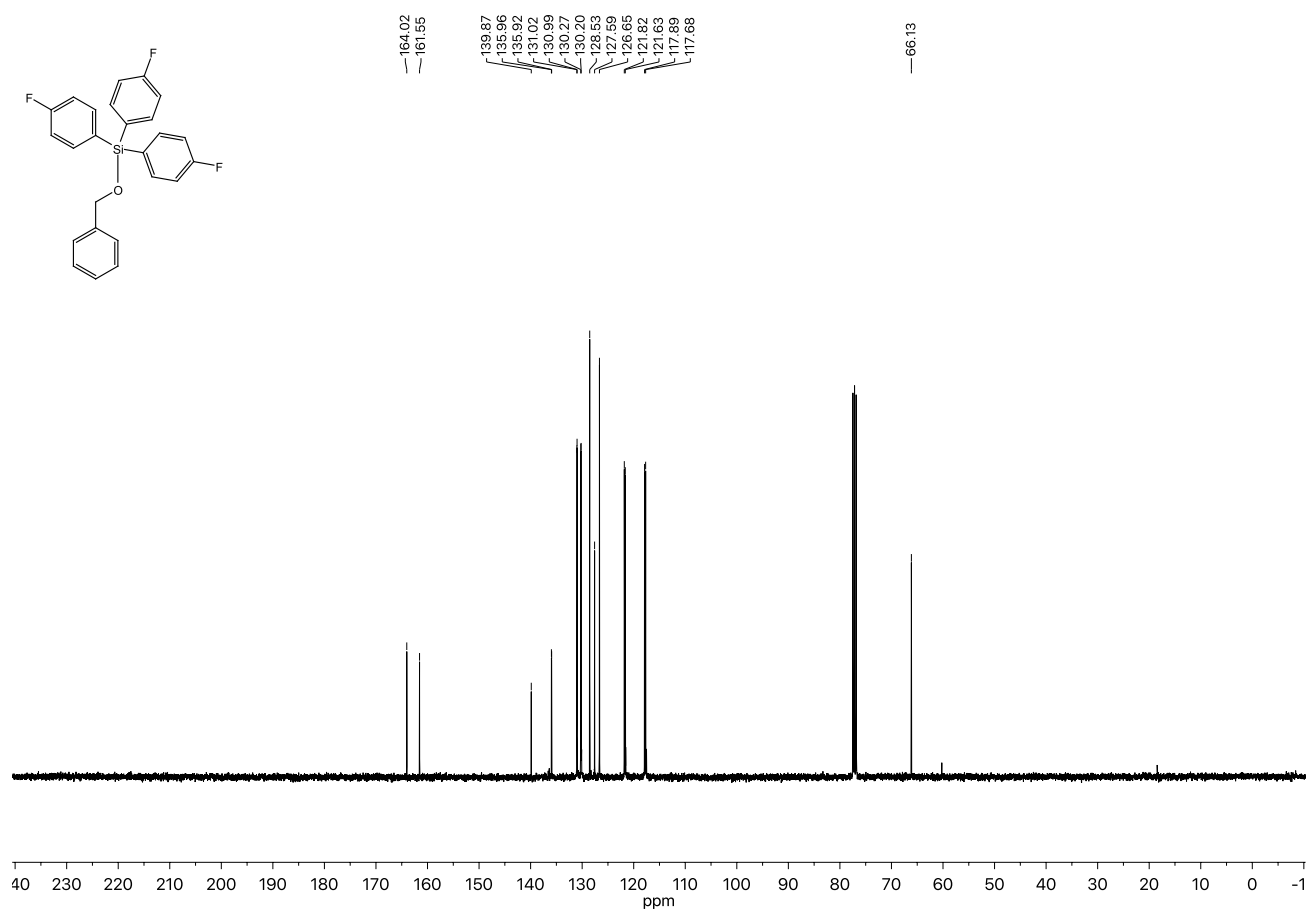
Figure 2.33. ^{13}C-NMR spectrum of **5ad**.
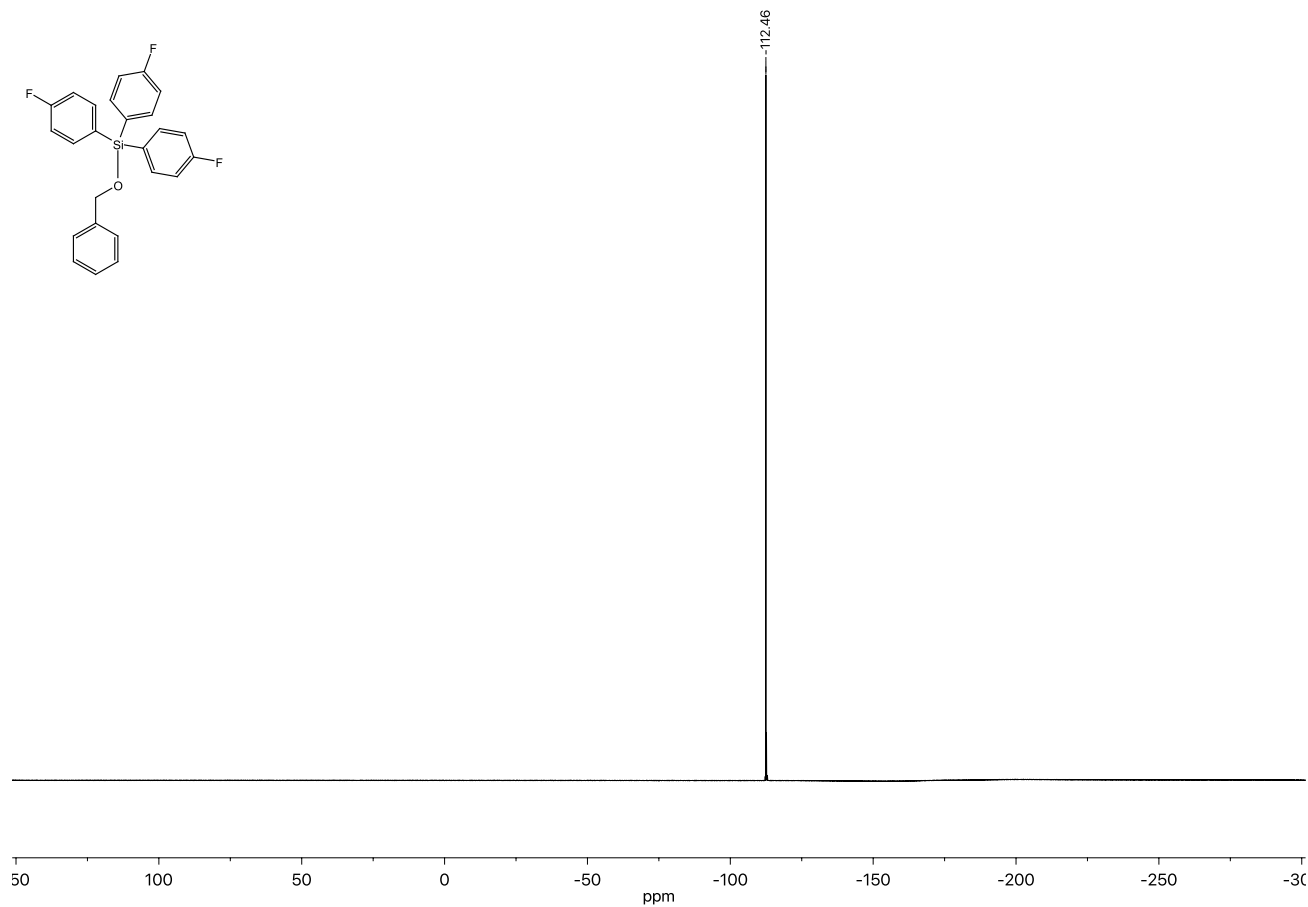
Figure 2.34. ^{19}F-NMR spectrum of **5ad**.
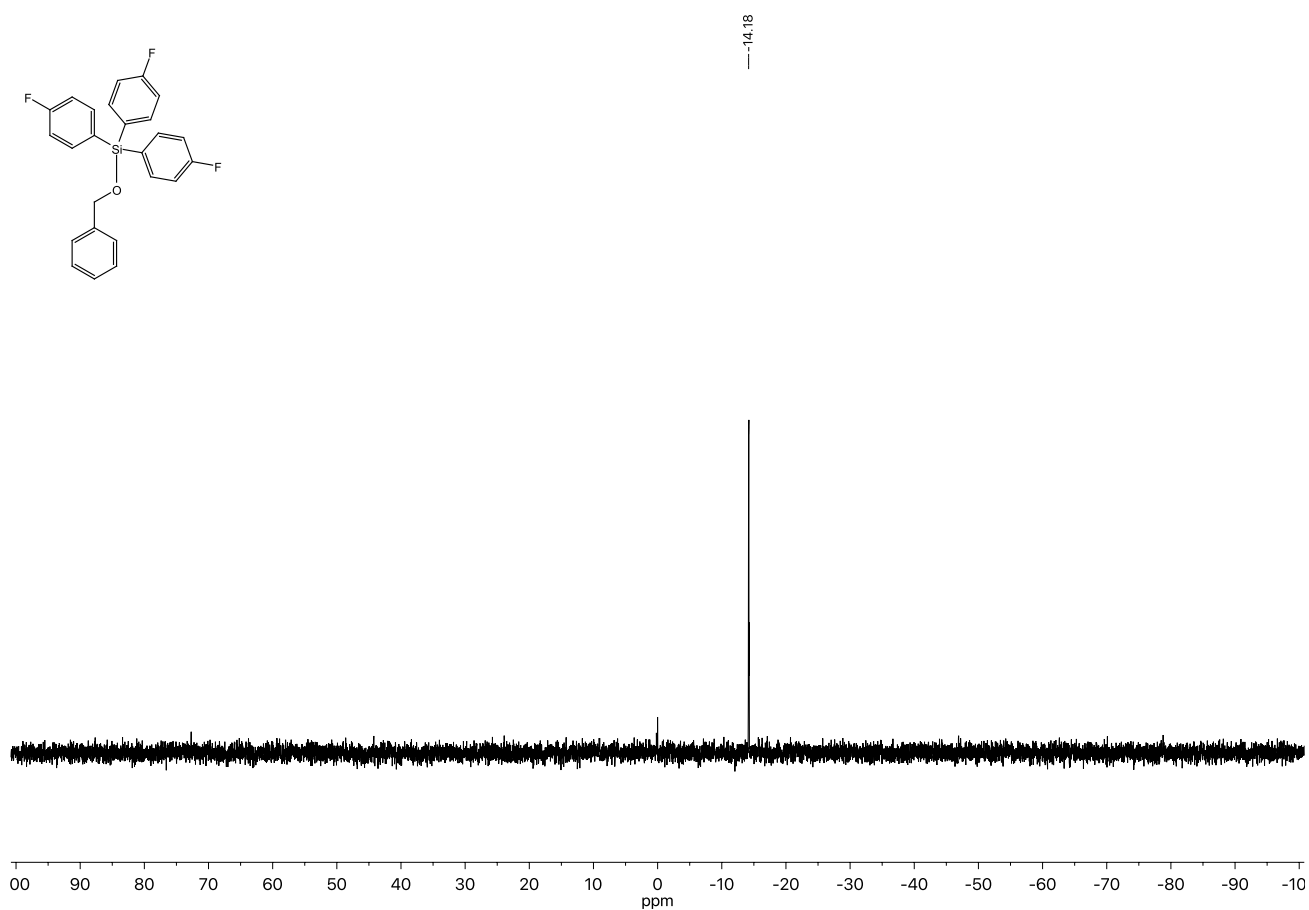
Figure 2.35. ^{29}Si-NMR spectrum of **5ad**.
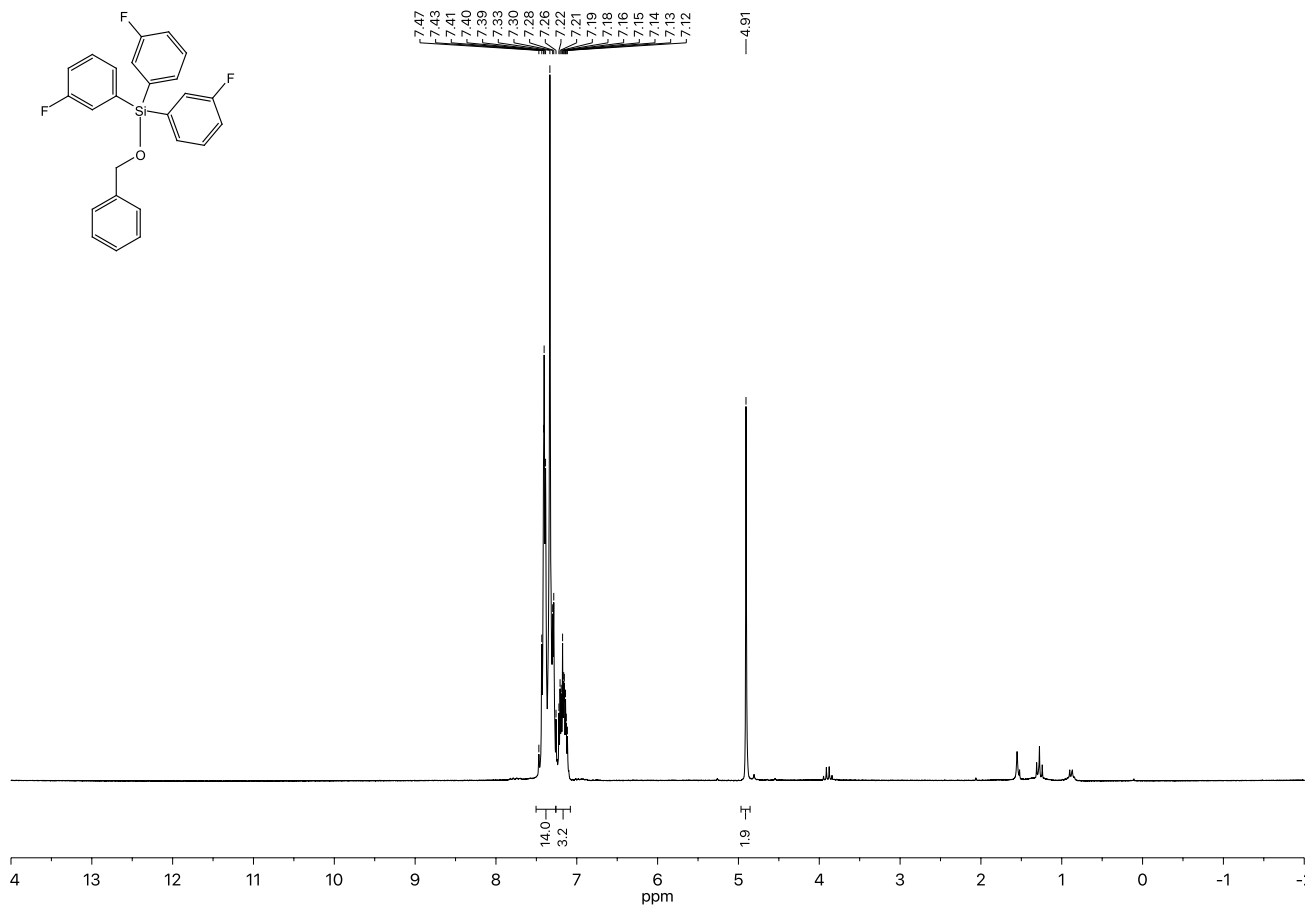
Figure 2.36. ^{1}H-NMR spectrum of **5ae**.
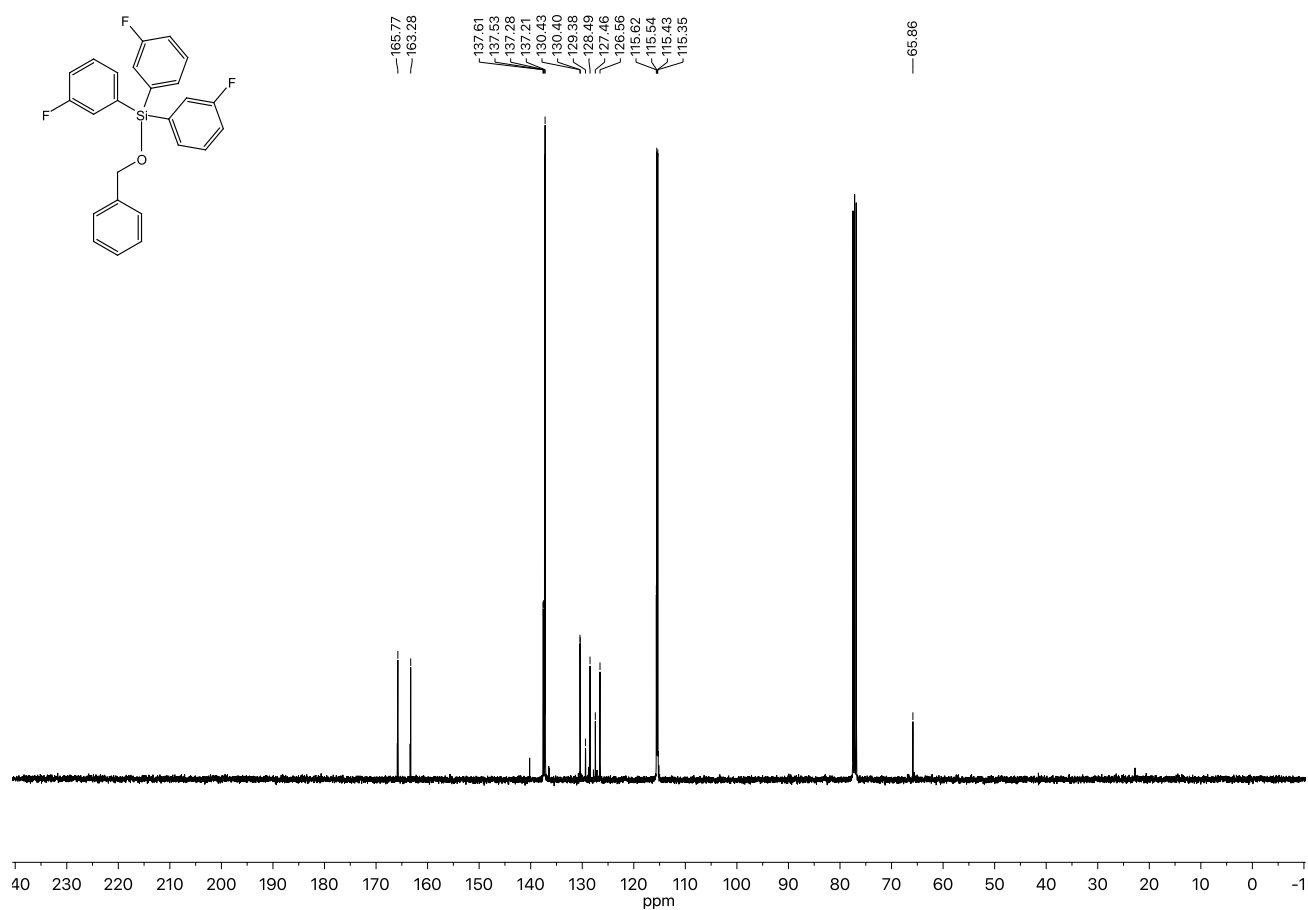
Figure 2.37. ^{13}C-NMR spectrum of **5ae**.
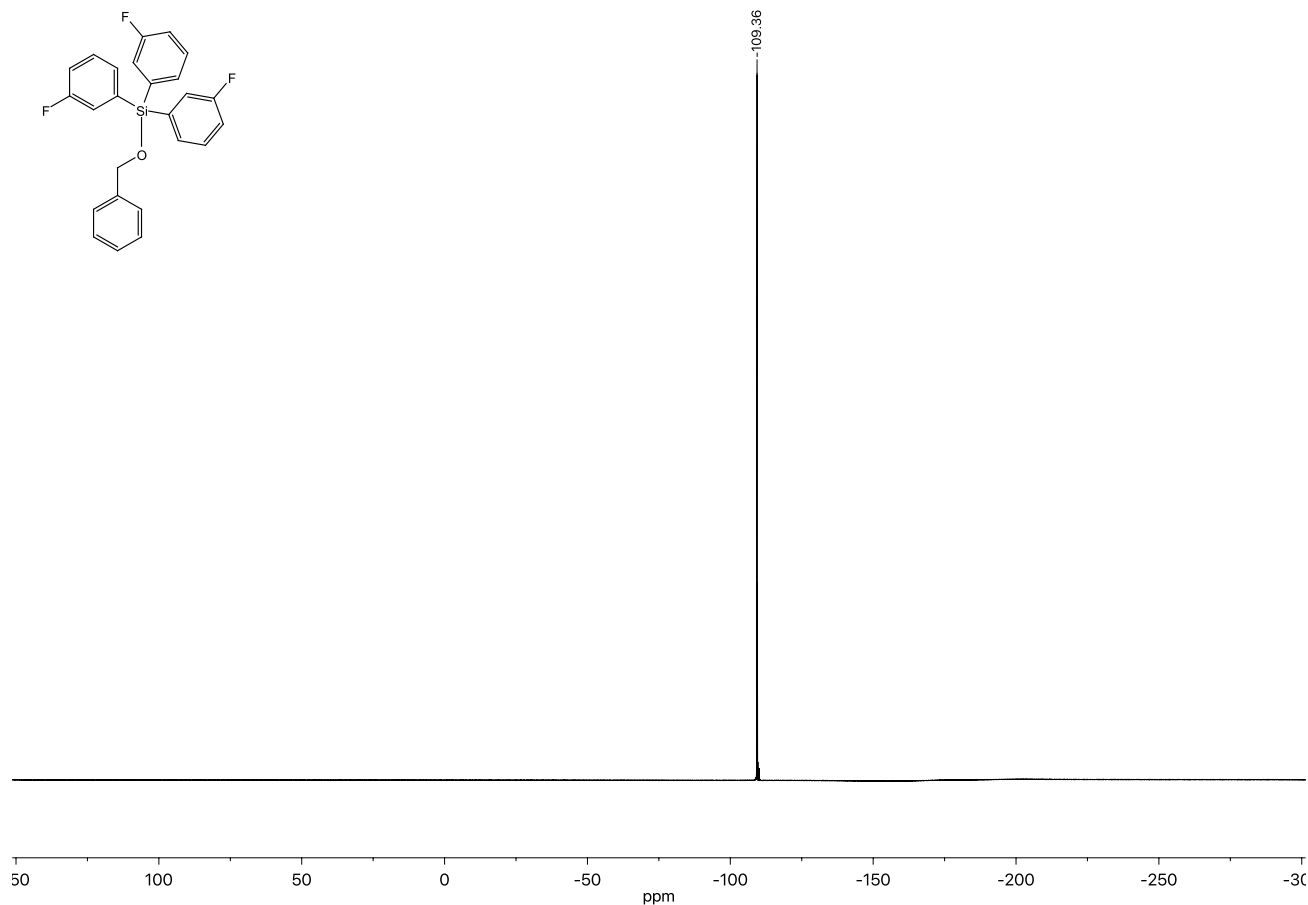
Figure 2.38. ^{19}F-NMR spectrum of **5ae**.
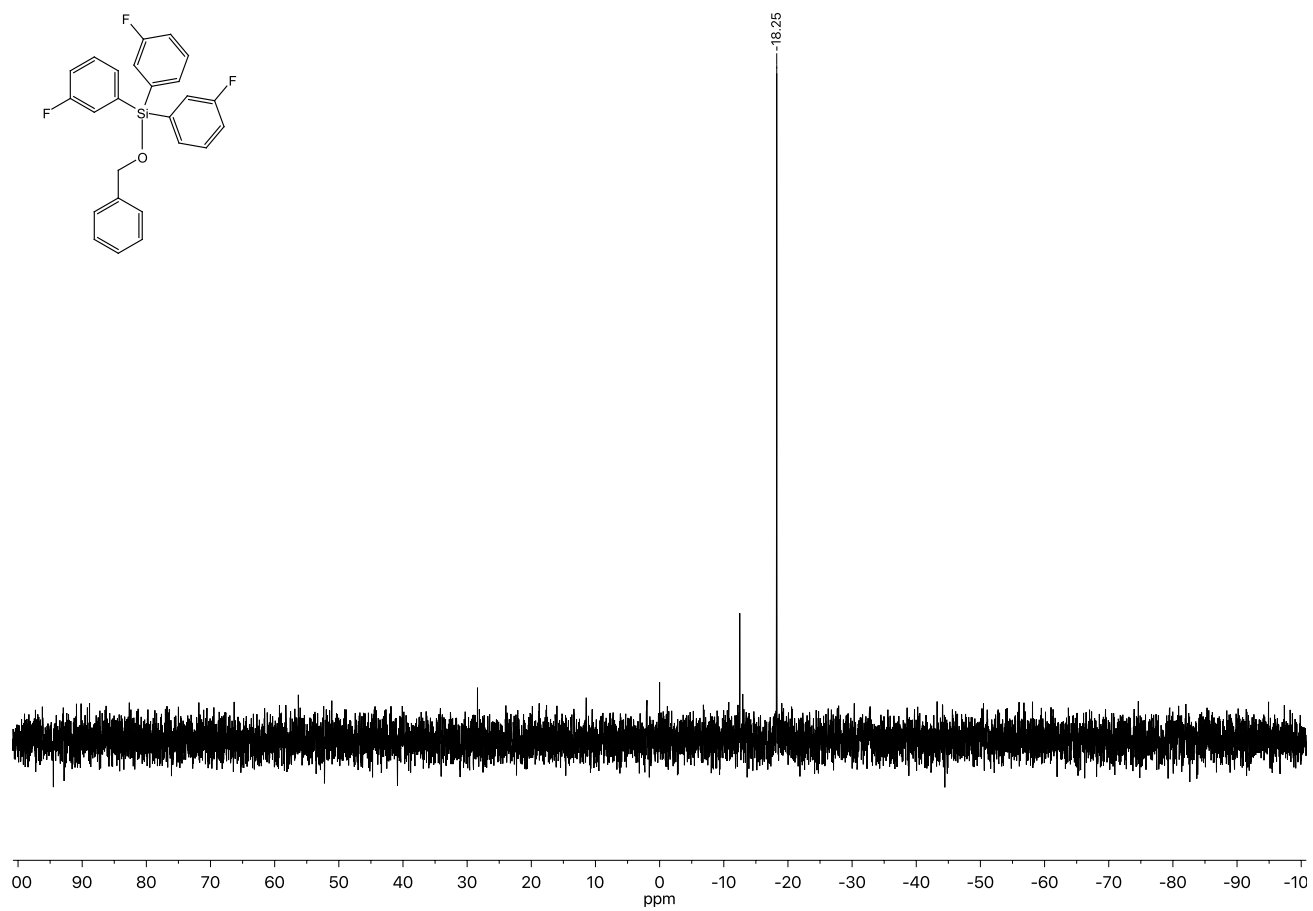
Figure 2.39. ^{29}Si-NMR spectrum of **5ae**.
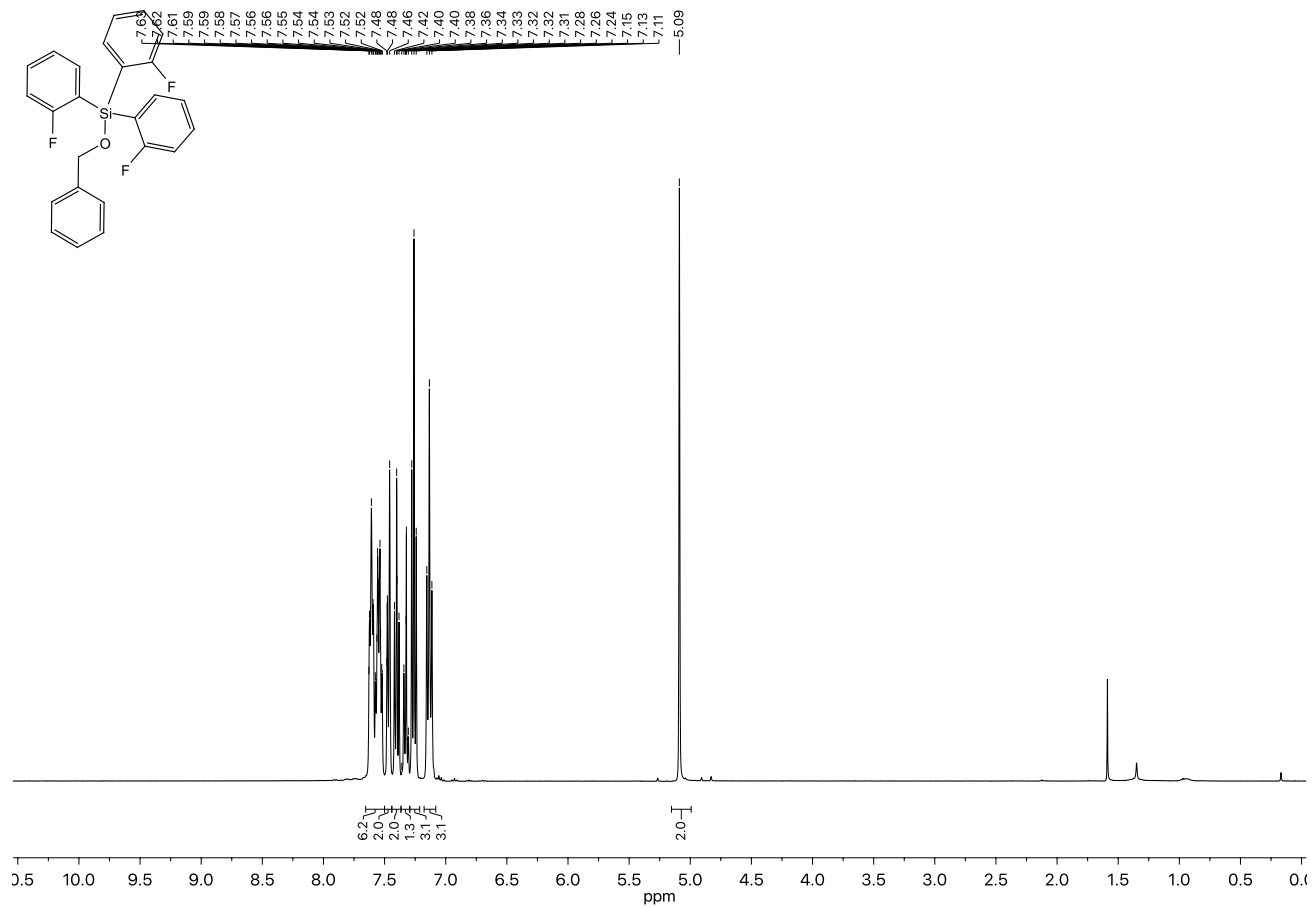
Figure 2.40. ^{1}H-NMR spectrum of **5af**.
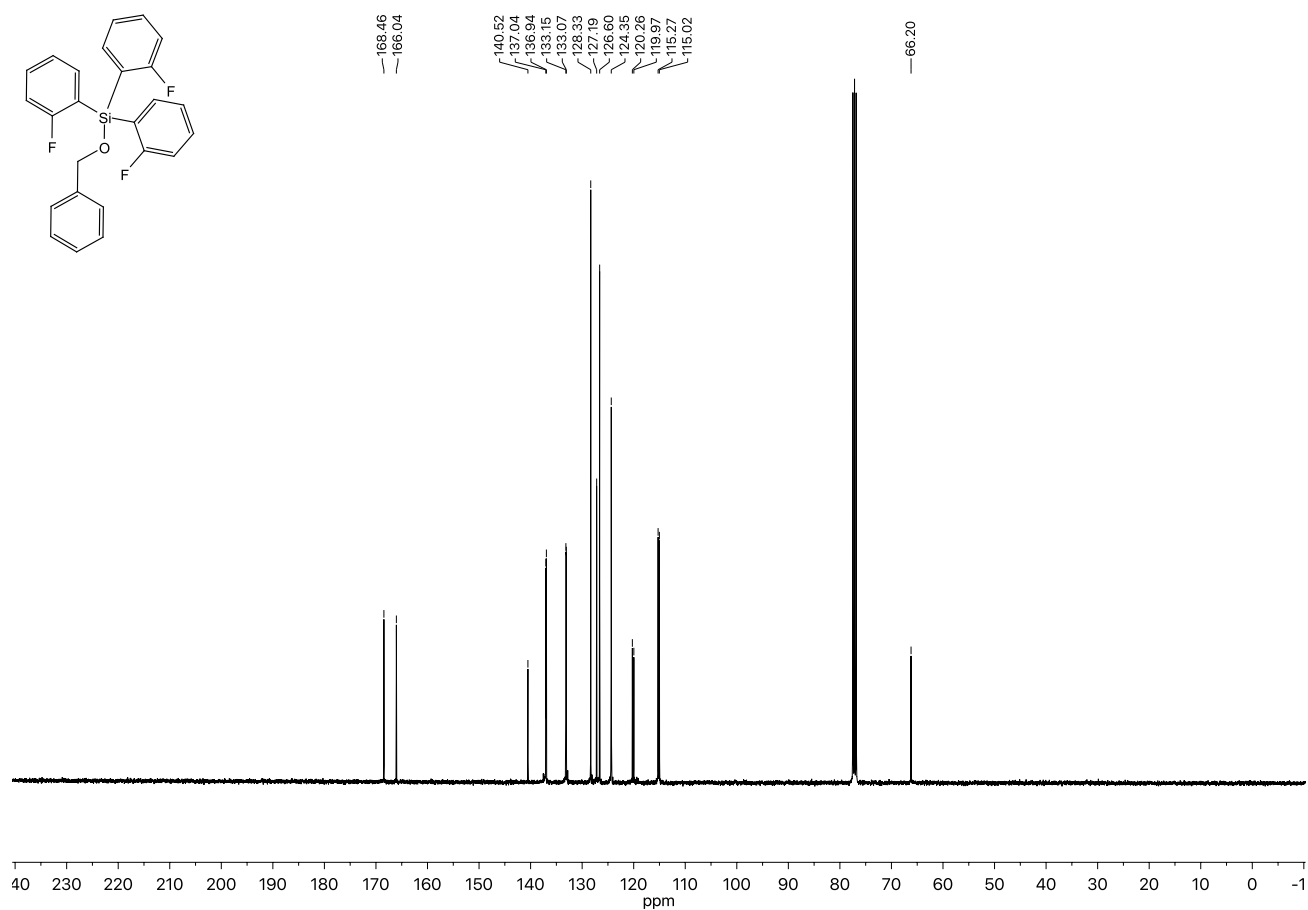
Figure 2.41. ^{13}C-NMR spectrum of **5af**.
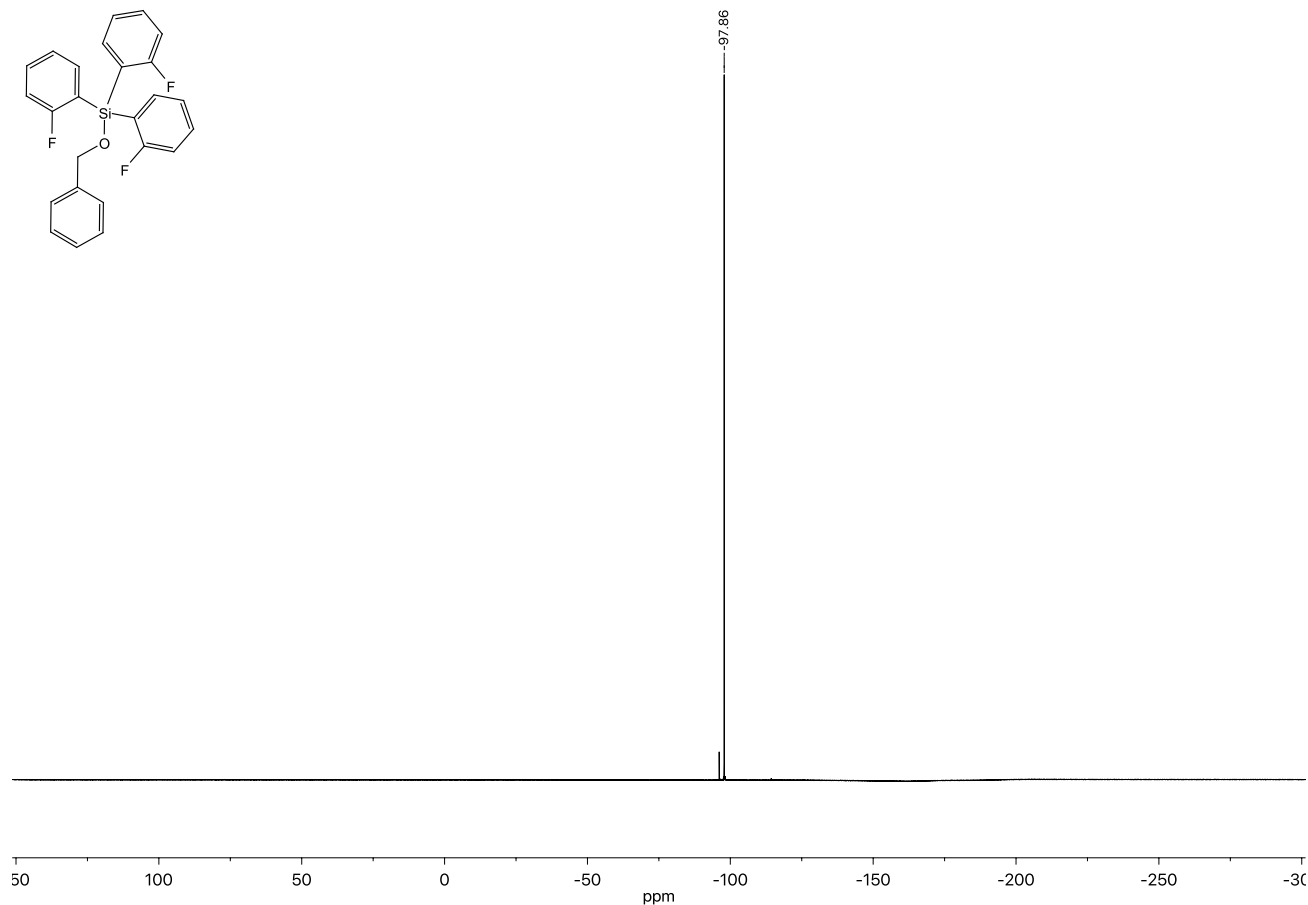
Figure 2.42. ^{19}F-NMR spectrum of **5af**.
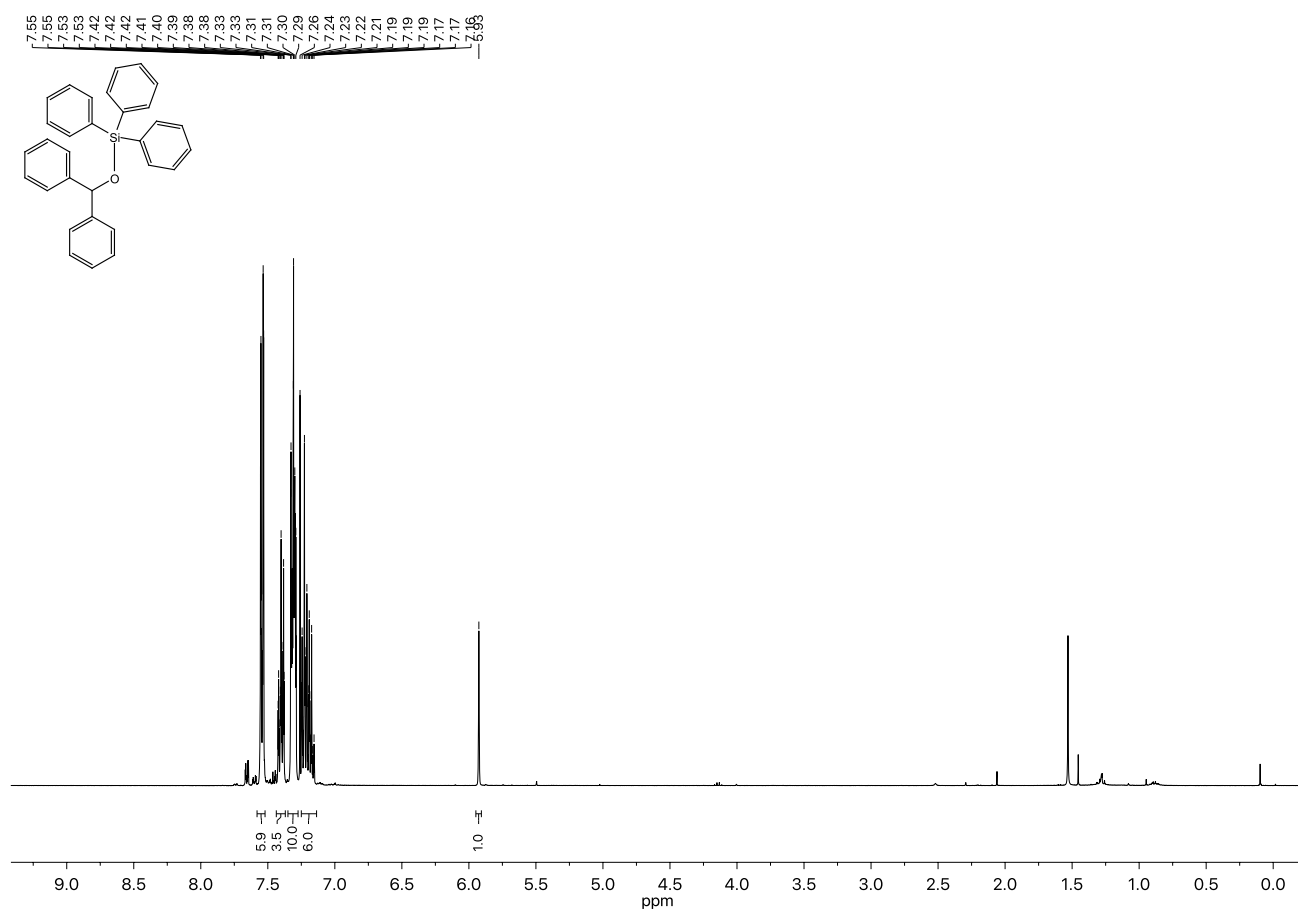
Figure 2.43. ^{1}H-NMR spectrum of **5da**.
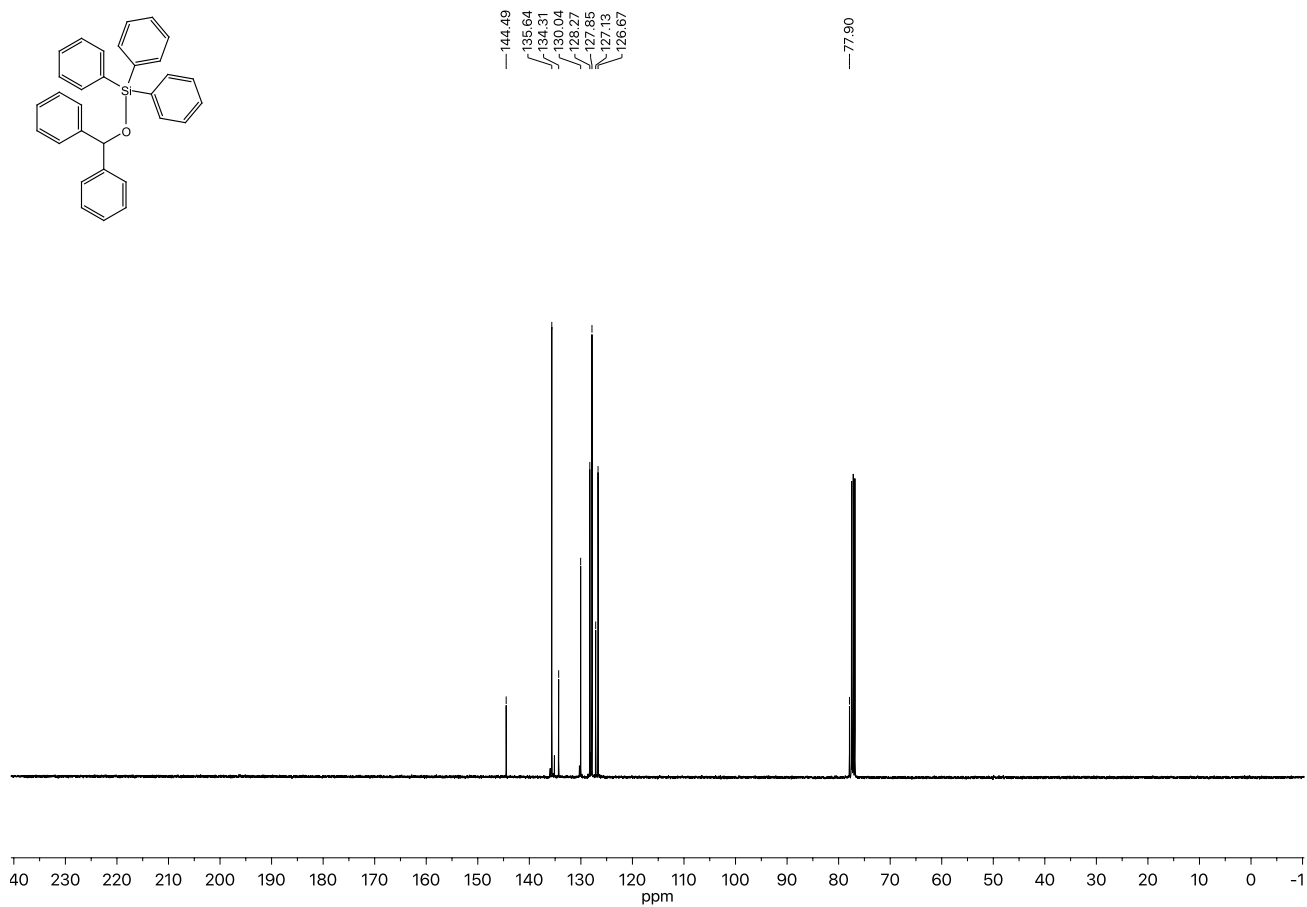
Figure 2.44. ^{13}C-NMR spectrum of **5da**.
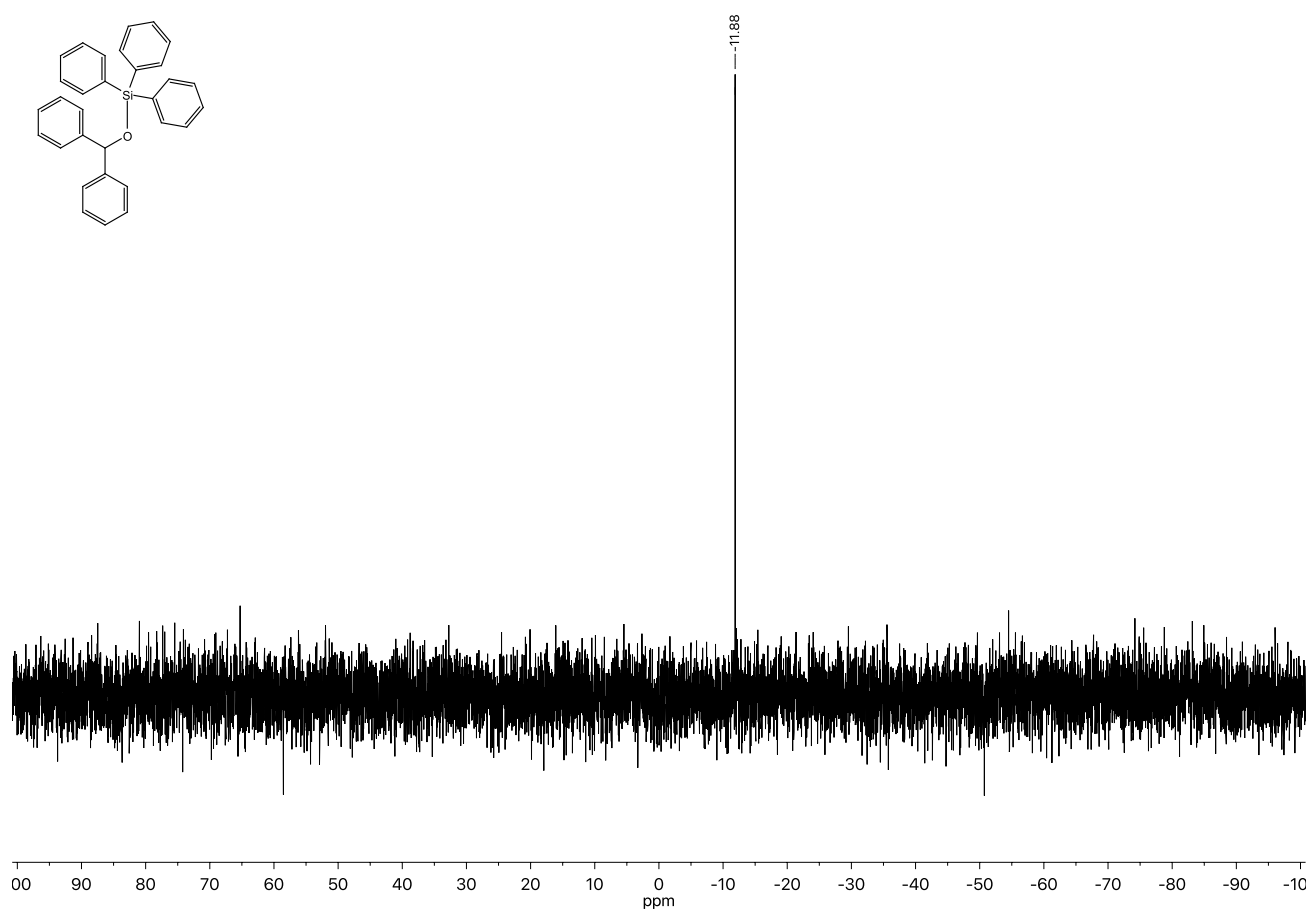
Figure 2.45. ^{29}Si-NMR spectrum of **5da**.
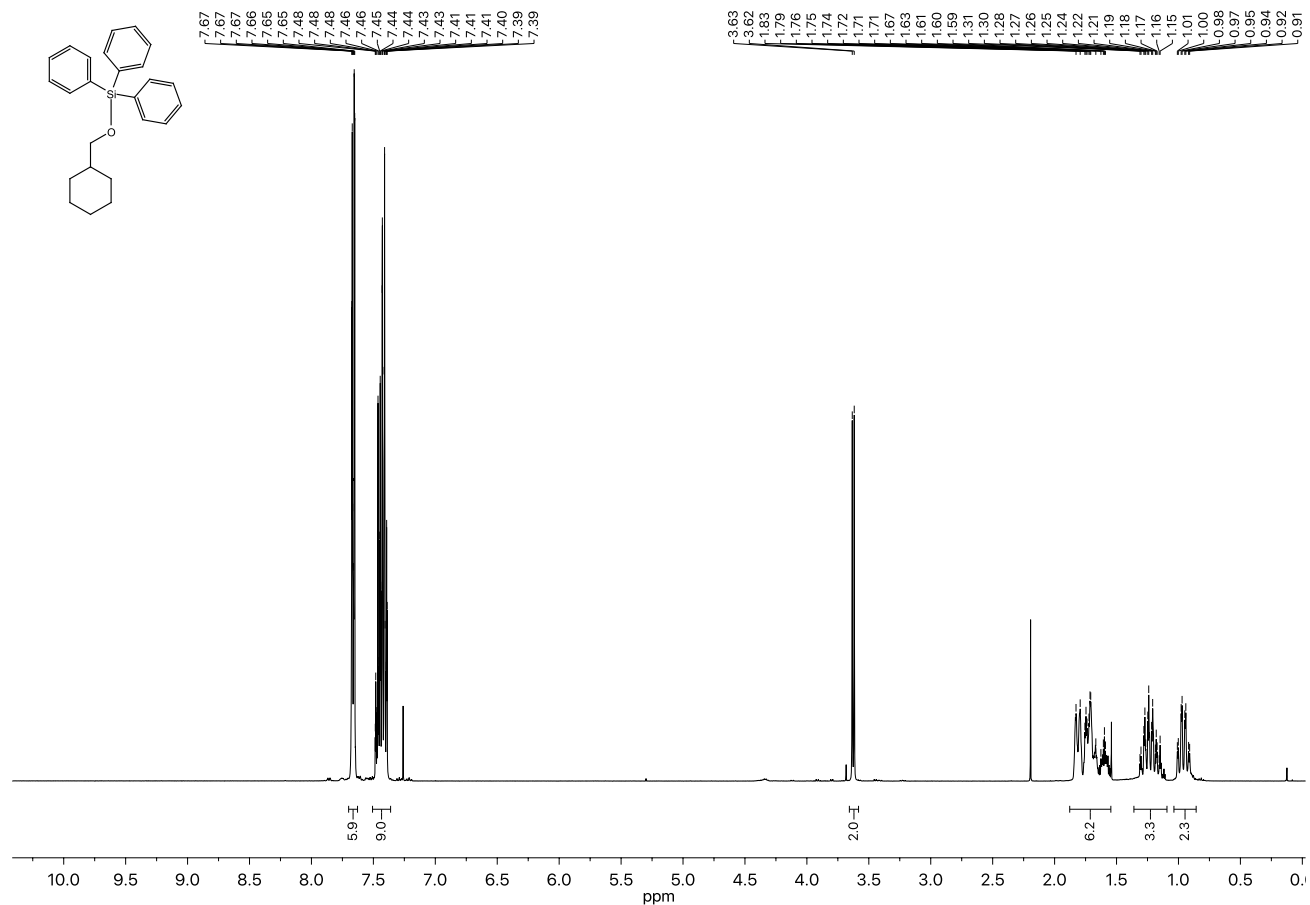
Figure 2.46. ^{1}H-NMR spectrum of **6aa**.
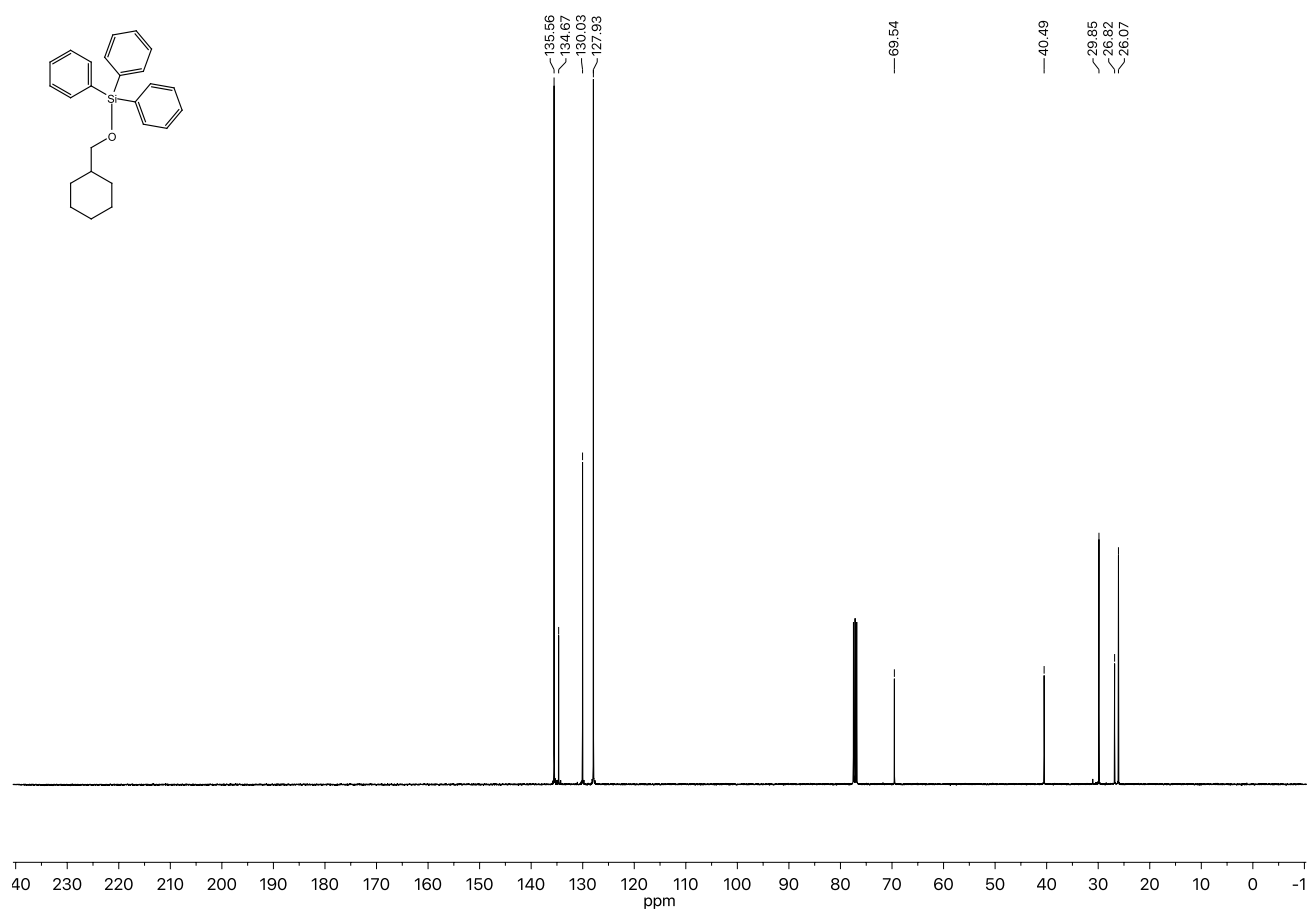
Figure 2.47. ^{13}C-NMR spectrum of **6aa**.
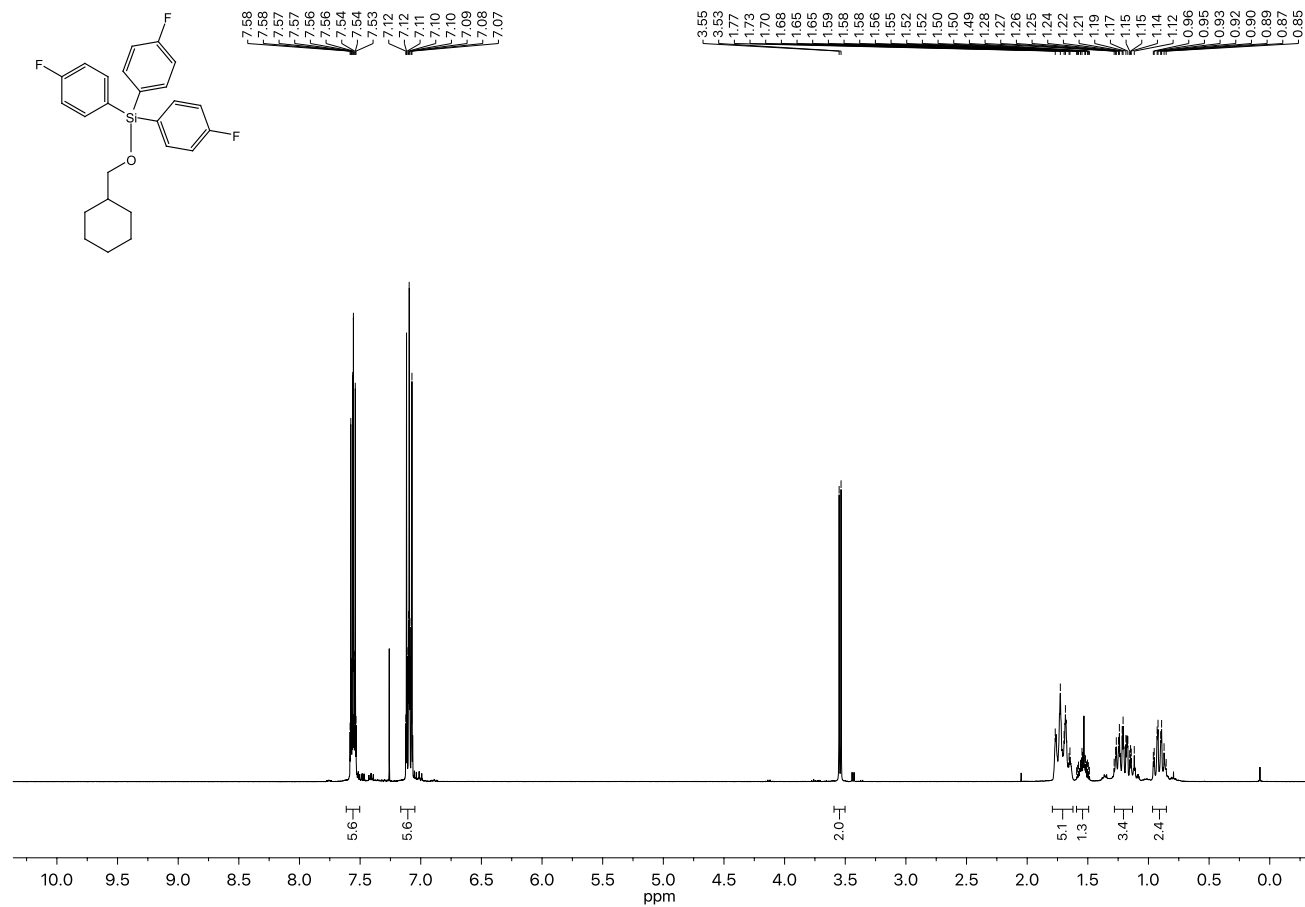
Figure 2.48. ^{1}H-NMR spectrum of **6ad**.
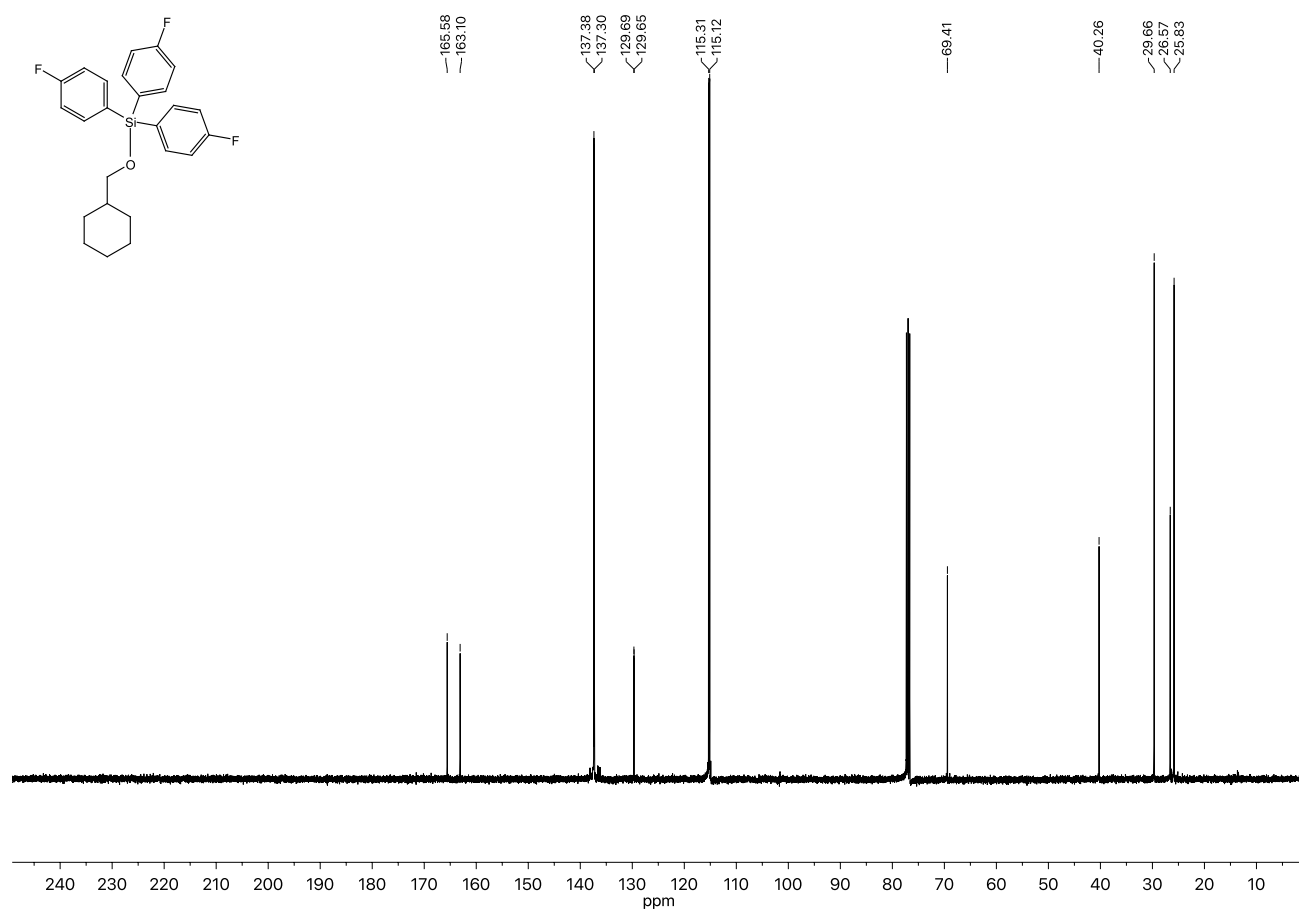
Figure 2.49. ^{13}C-NMR spectrum of **6ad**.
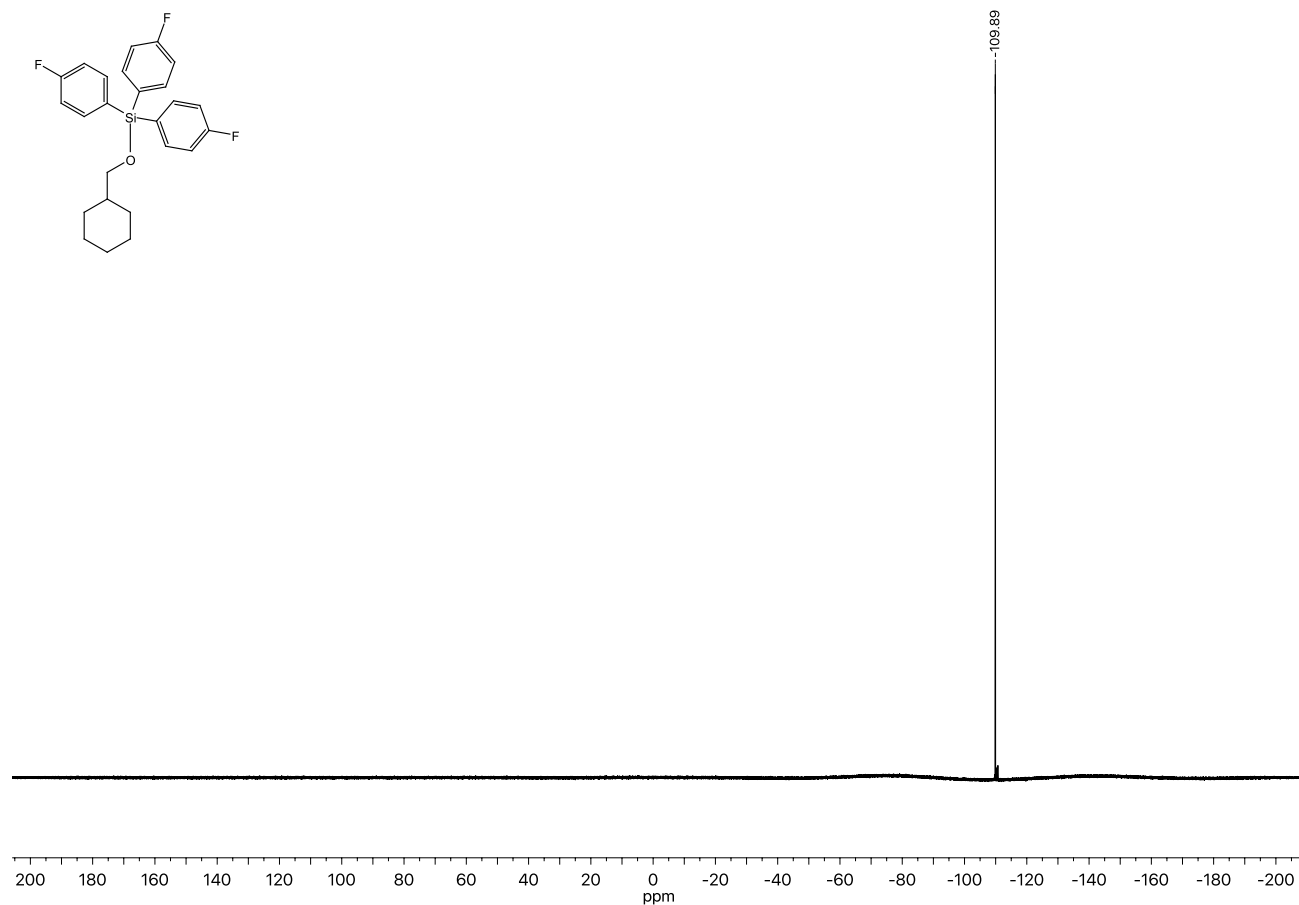
Figure 2.50. ^{19}F-NMR spectrum of **6ad**.
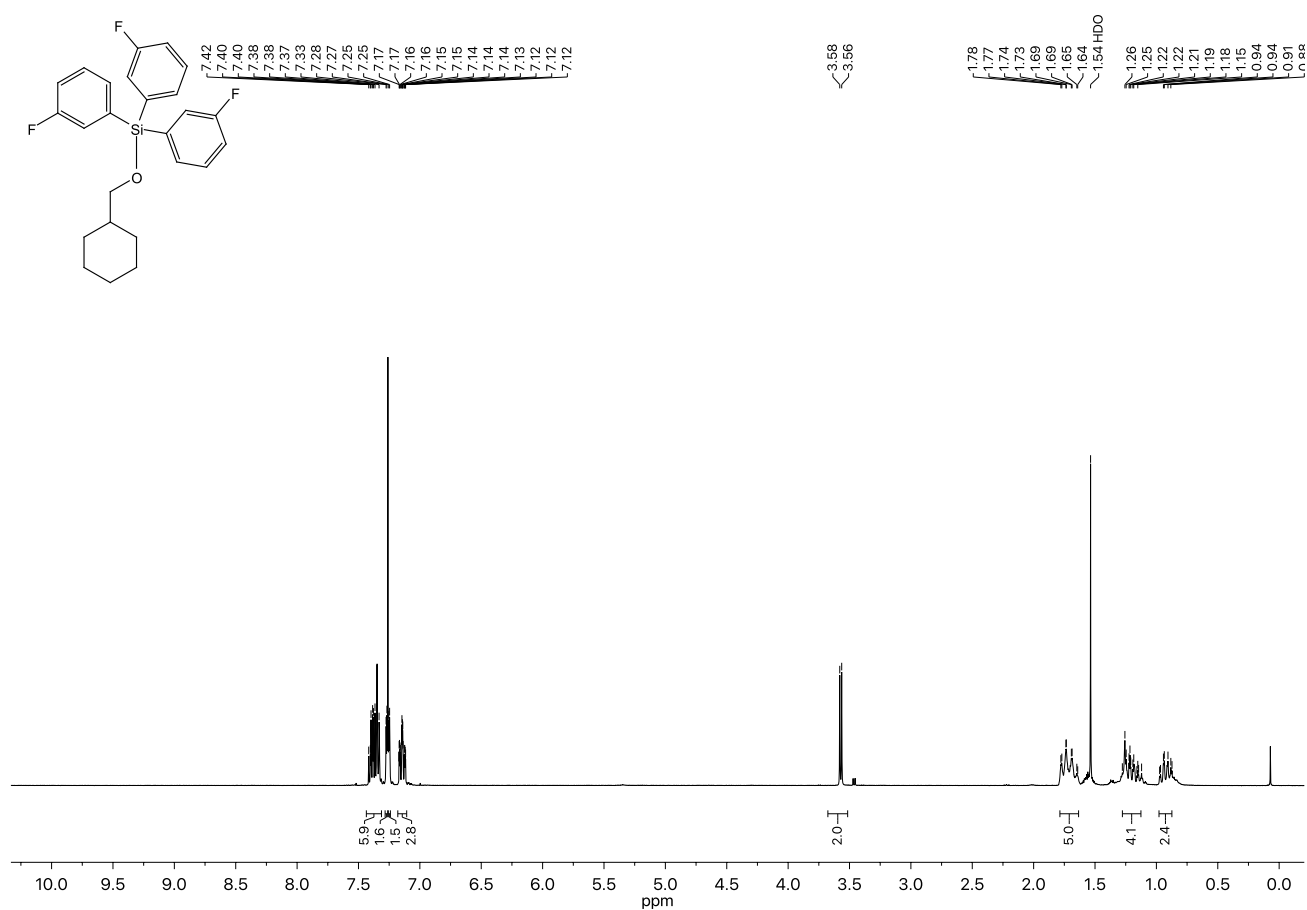
Figure 2.51. ^{1}H-NMR spectrum of **6ae**.
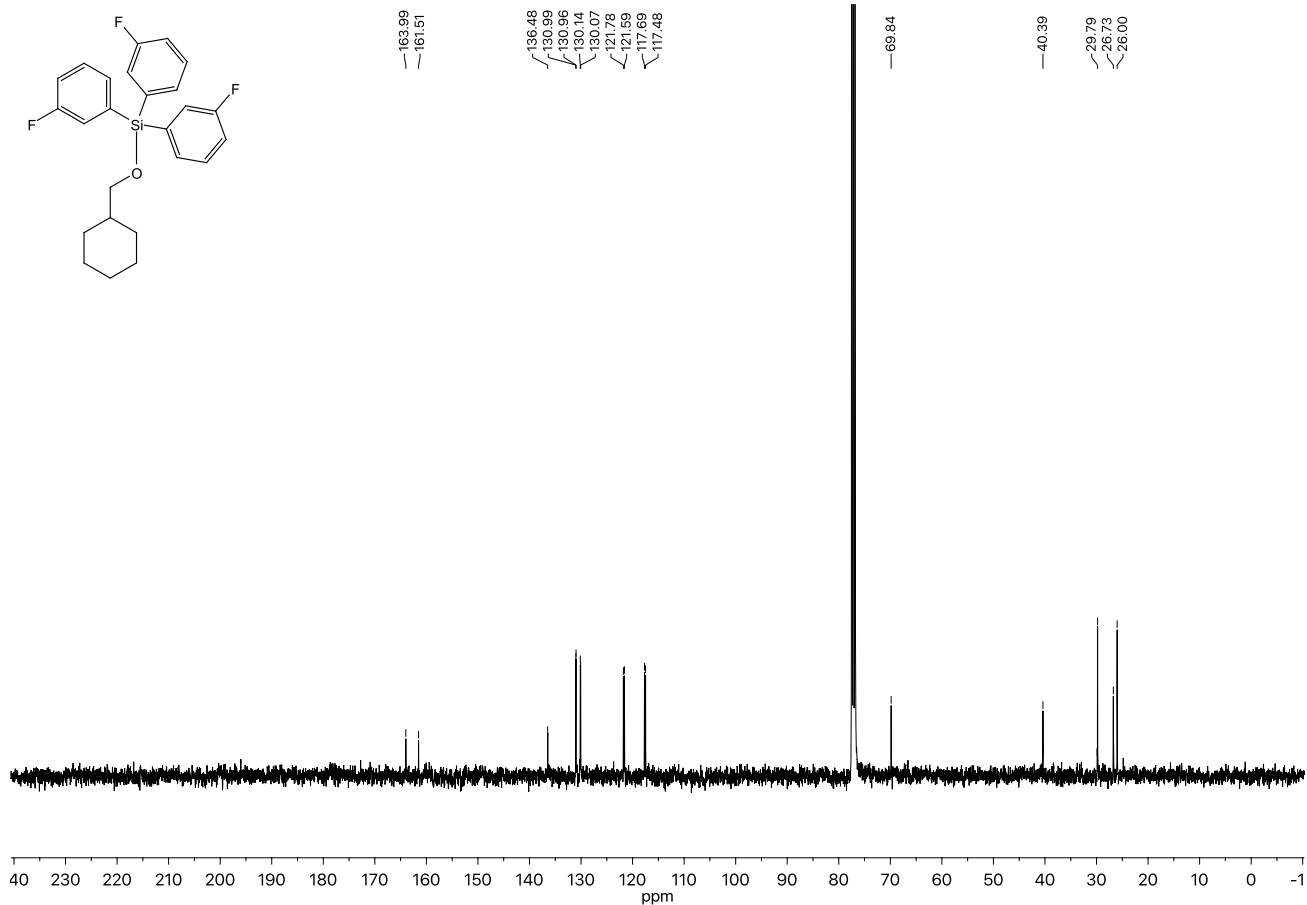
Figure 2.52. ^{13}C-NMR spectrum of **6ae**.
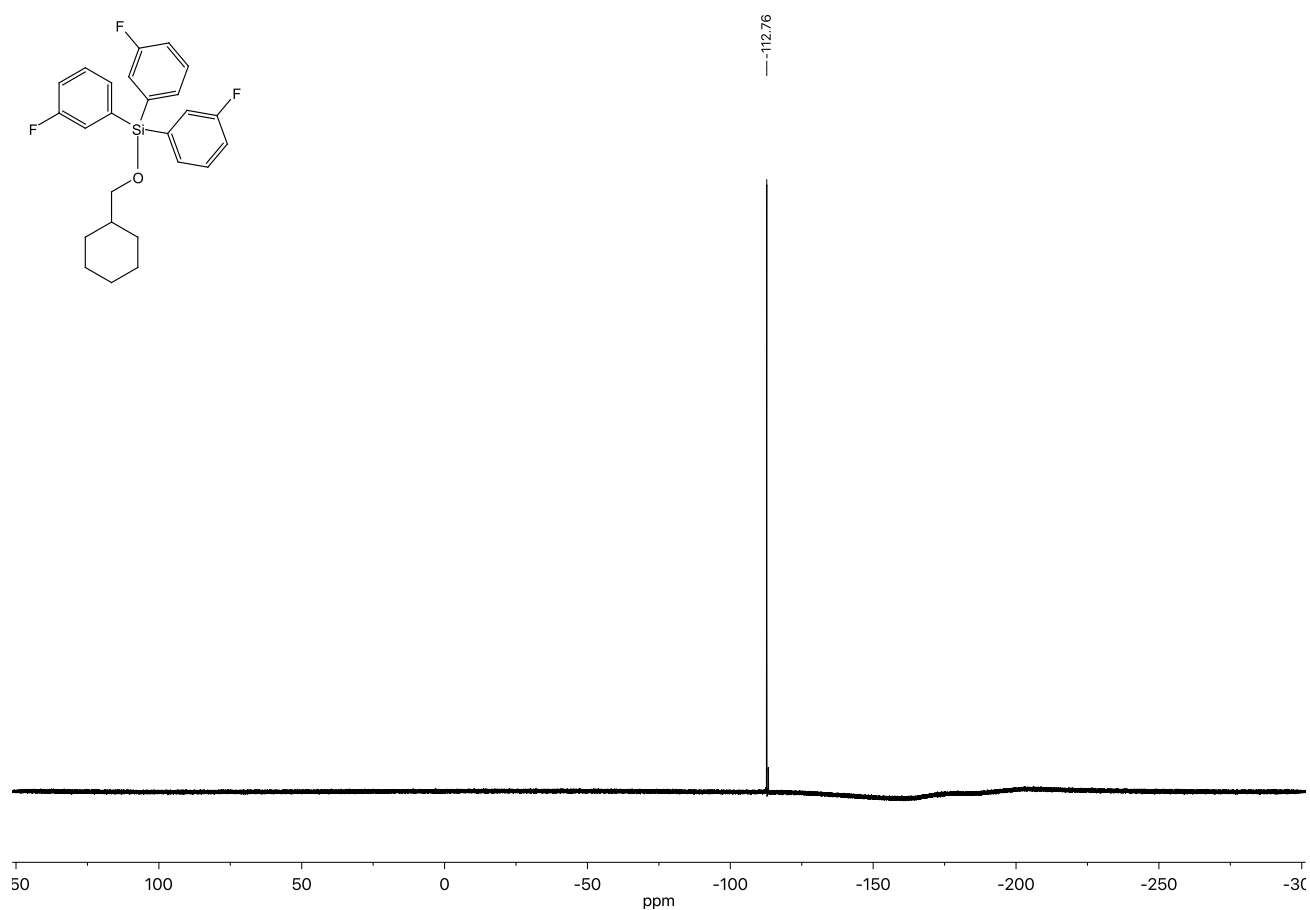
Figure 2.53. ^{19}F-NMR spectrum of **6ae**.
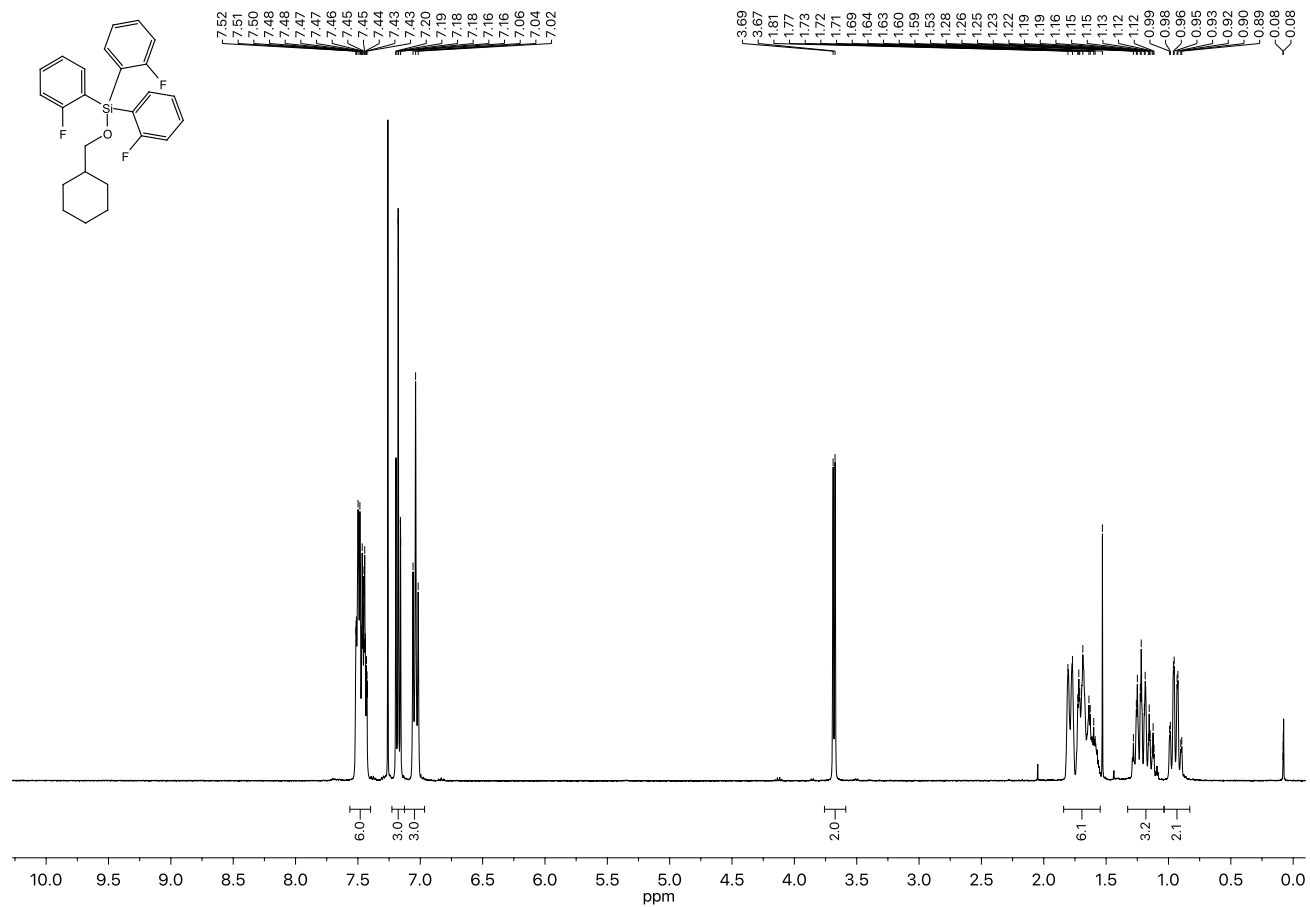
Figure 2.54. ^{1}H-NMR spectrum of **6af**.
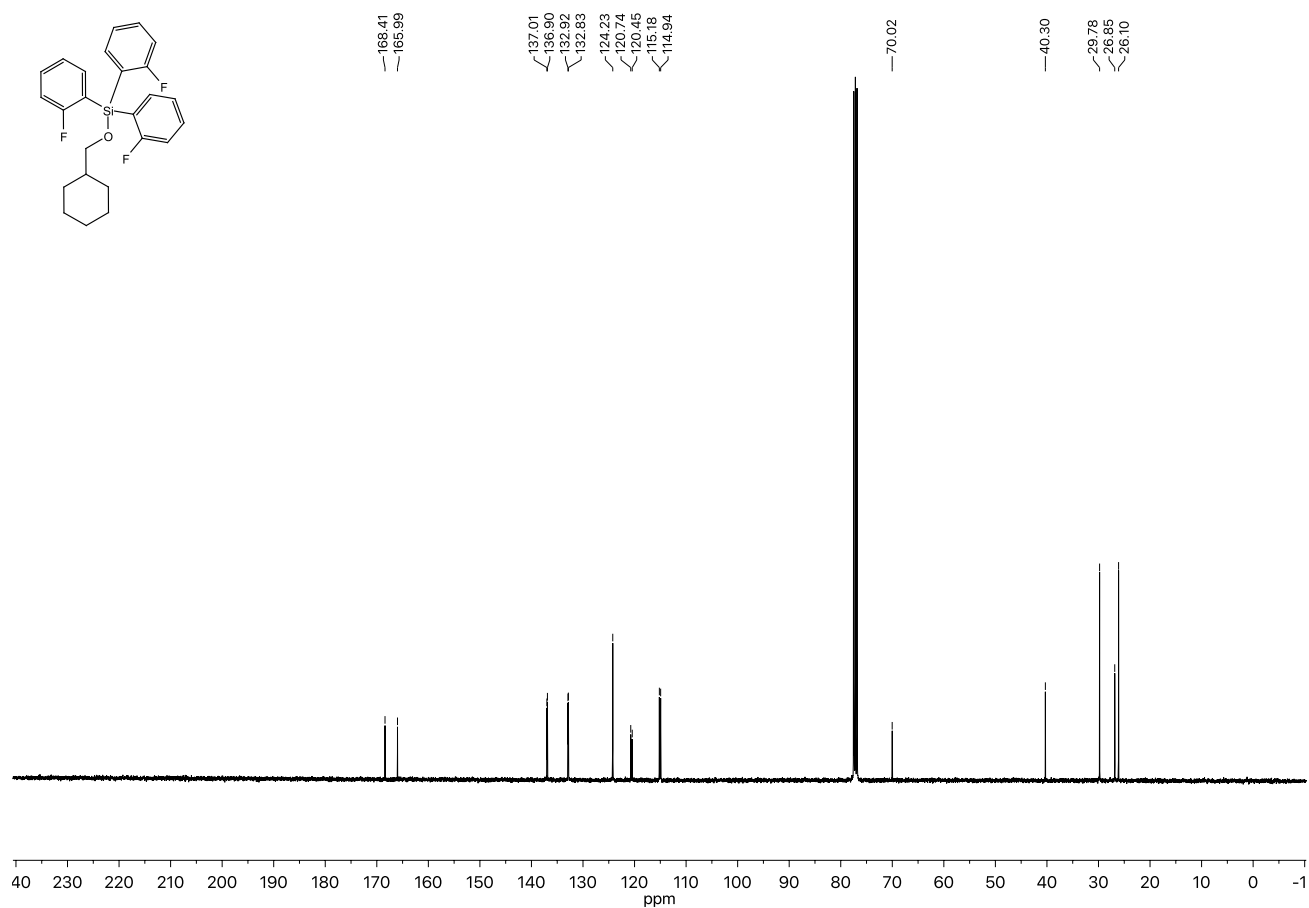
Figure 2.55. ^{13}C-NMR spectrum of **6af**.
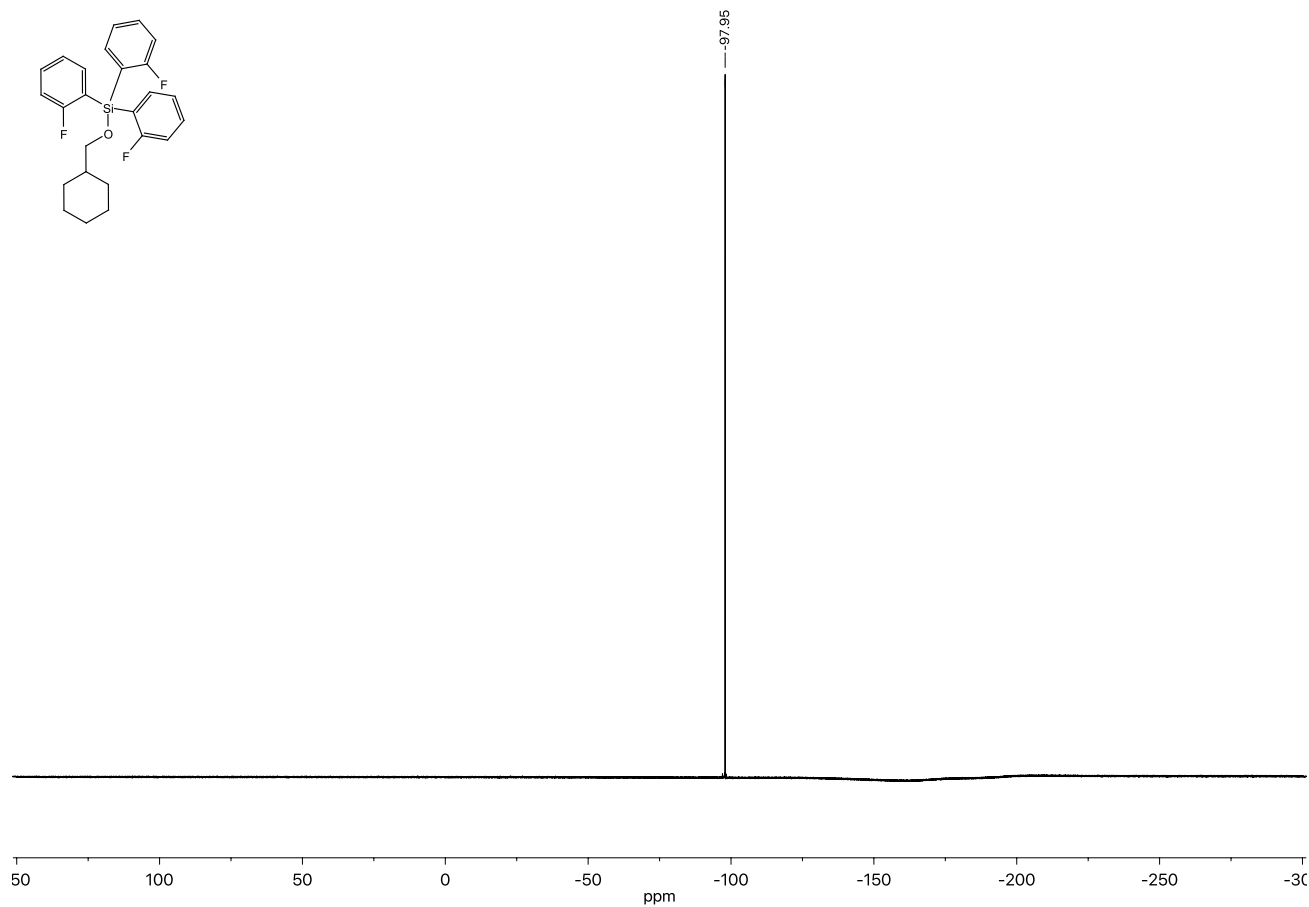
Figure 2.56. ^{19}F-NMR spectrum of **6af**.
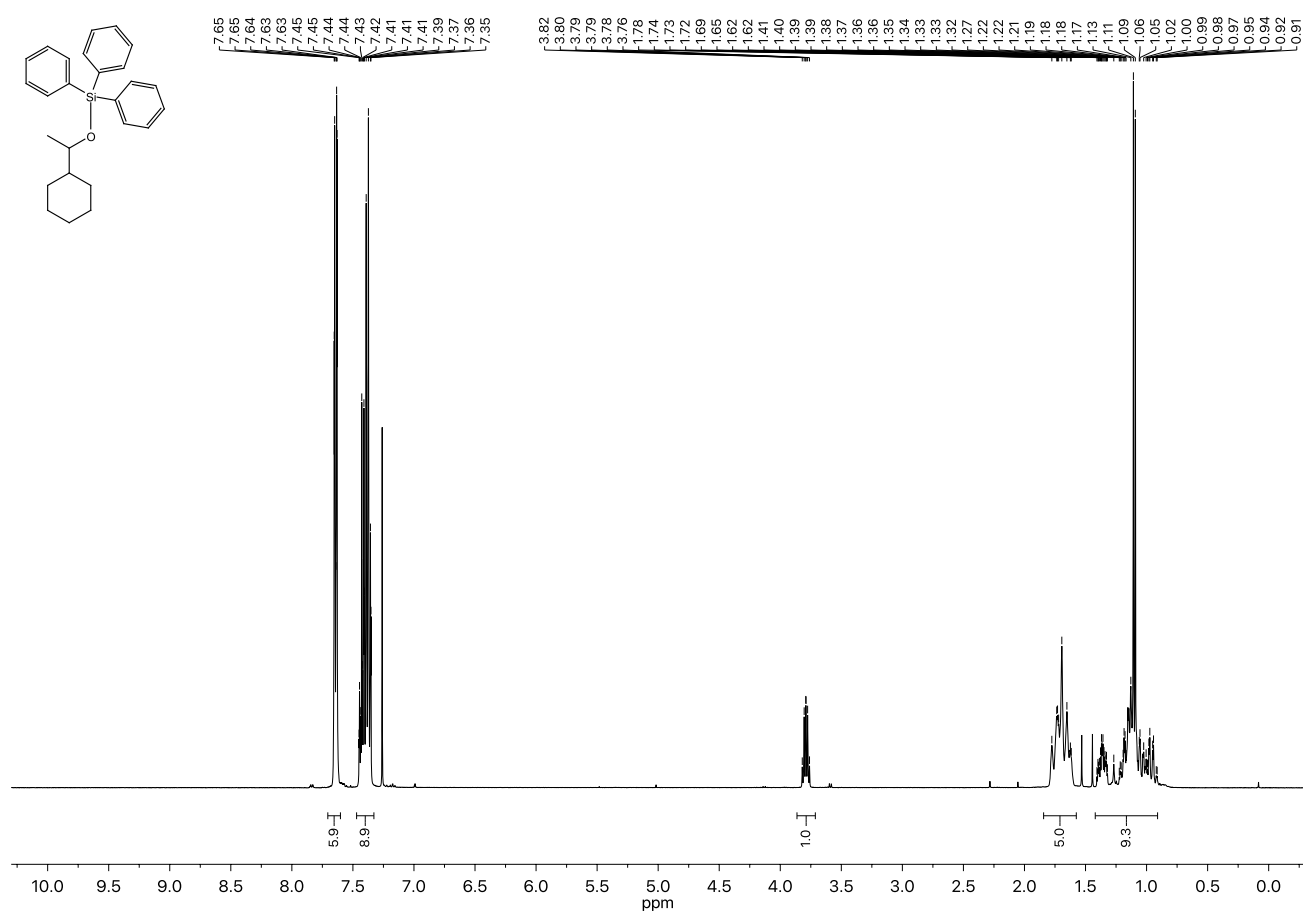
Figure 2.57. ^{1}H-NMR spectrum of **6ba**.
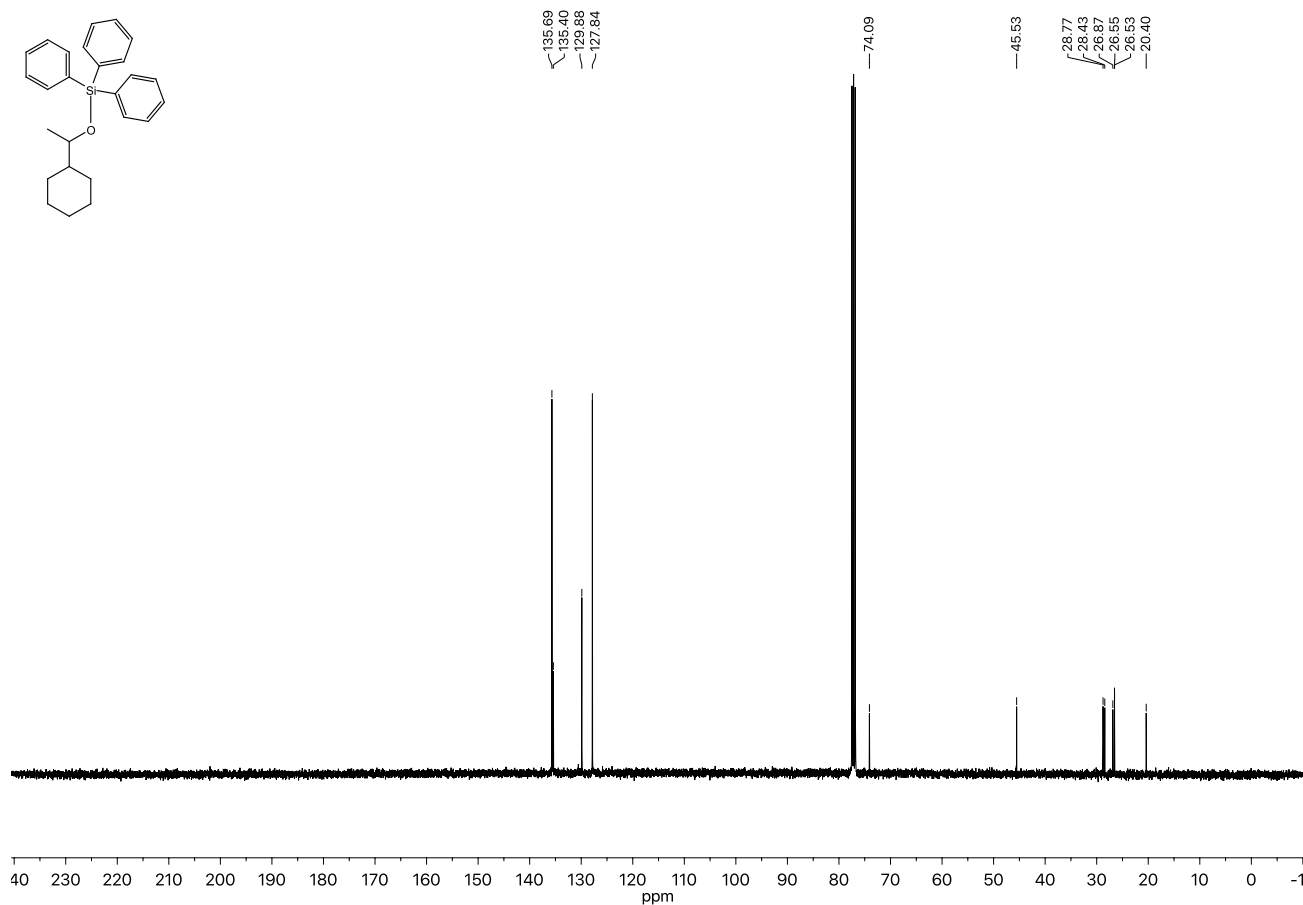
Figure 2.58. ^{13}C-NMR spectrum of **6ba**.
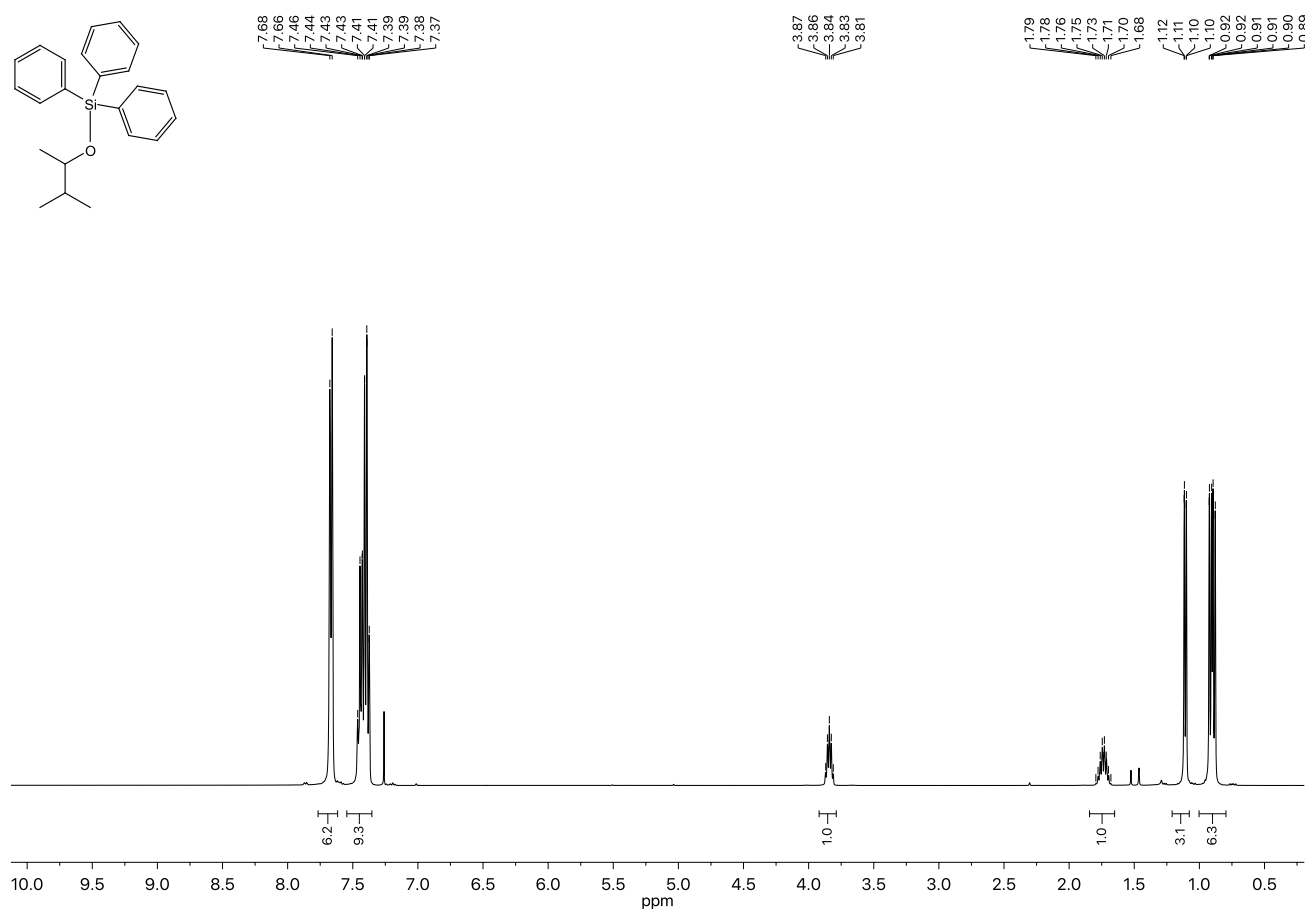
Figure 2.59. ^{1}H-NMR spectrum of **6ca**.
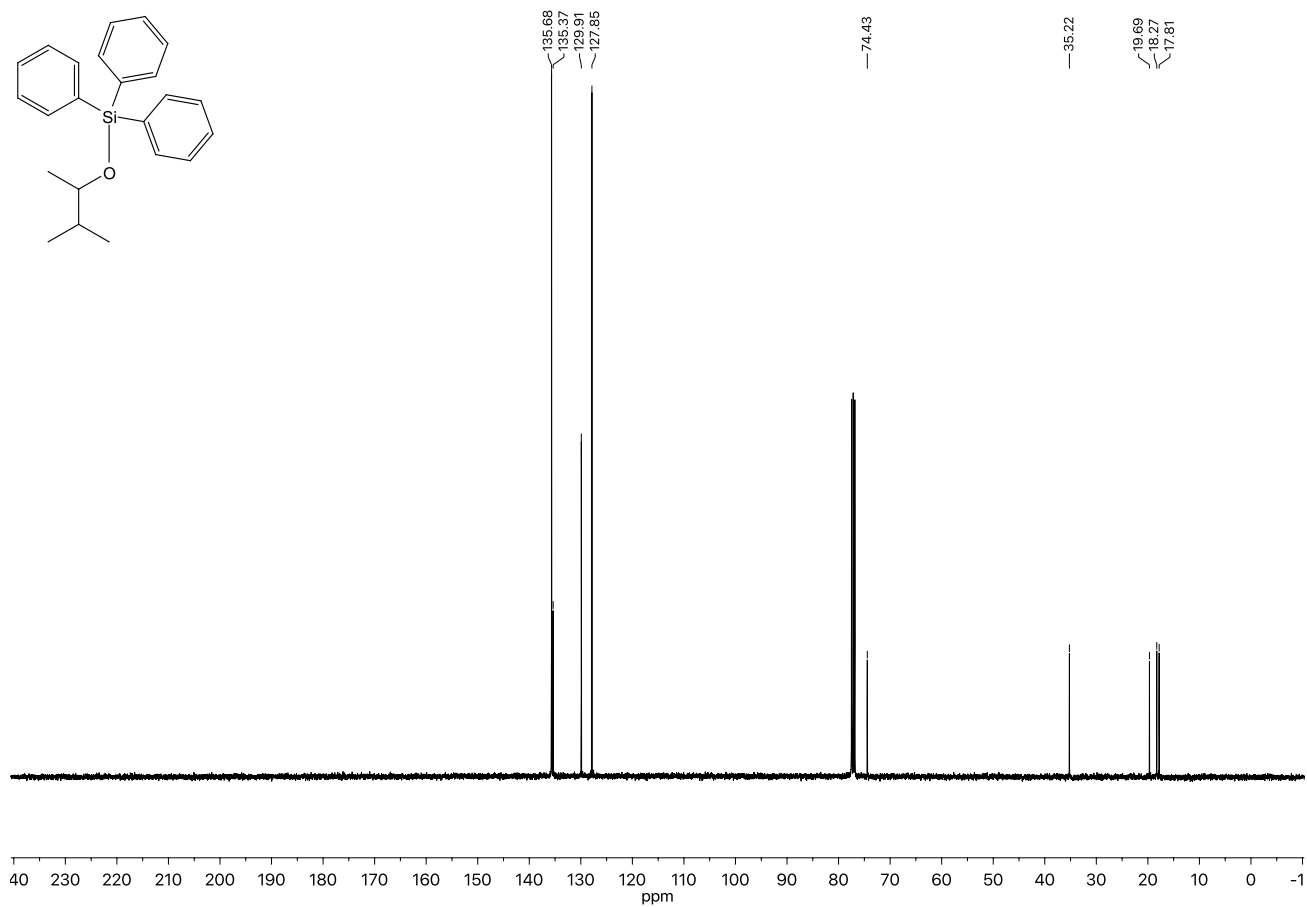
Figure 2.60. ^{13}C-NMR spectrum of **6ca**.
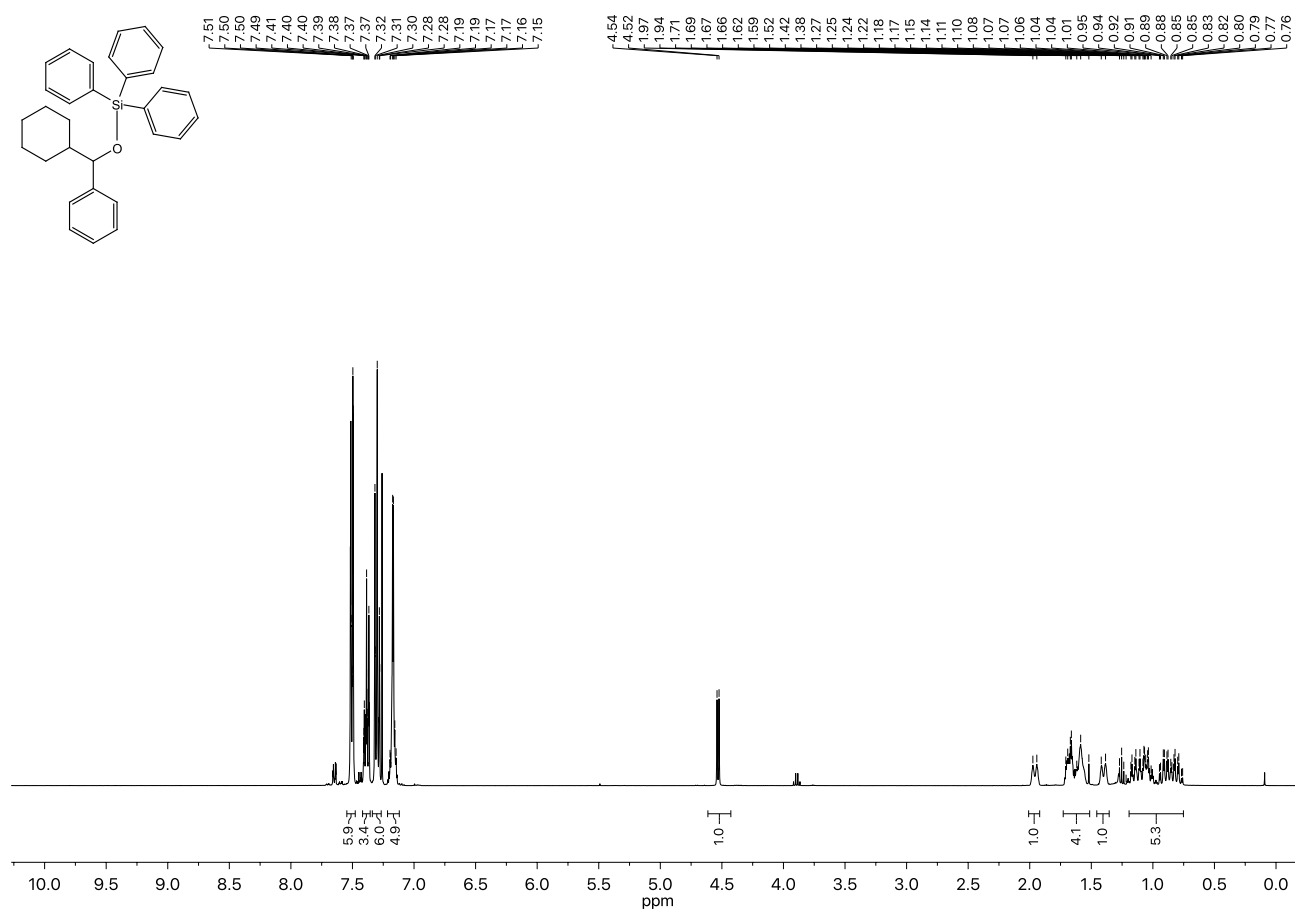
Figure 2.61. ¹H-NMR spectrum of **6ea**.
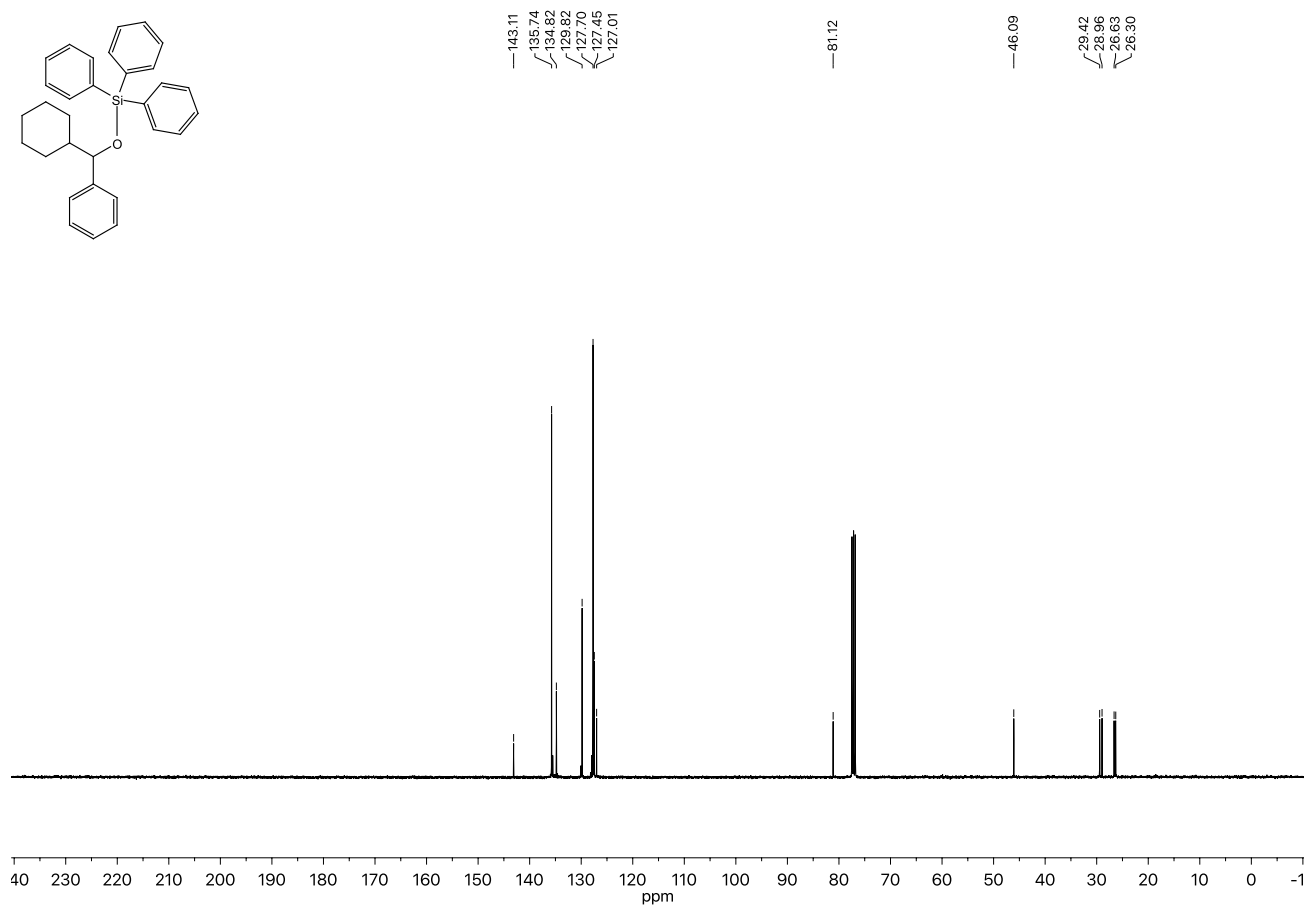
Figure 2.62. ¹³C-NMR spectrum of **6ea**.
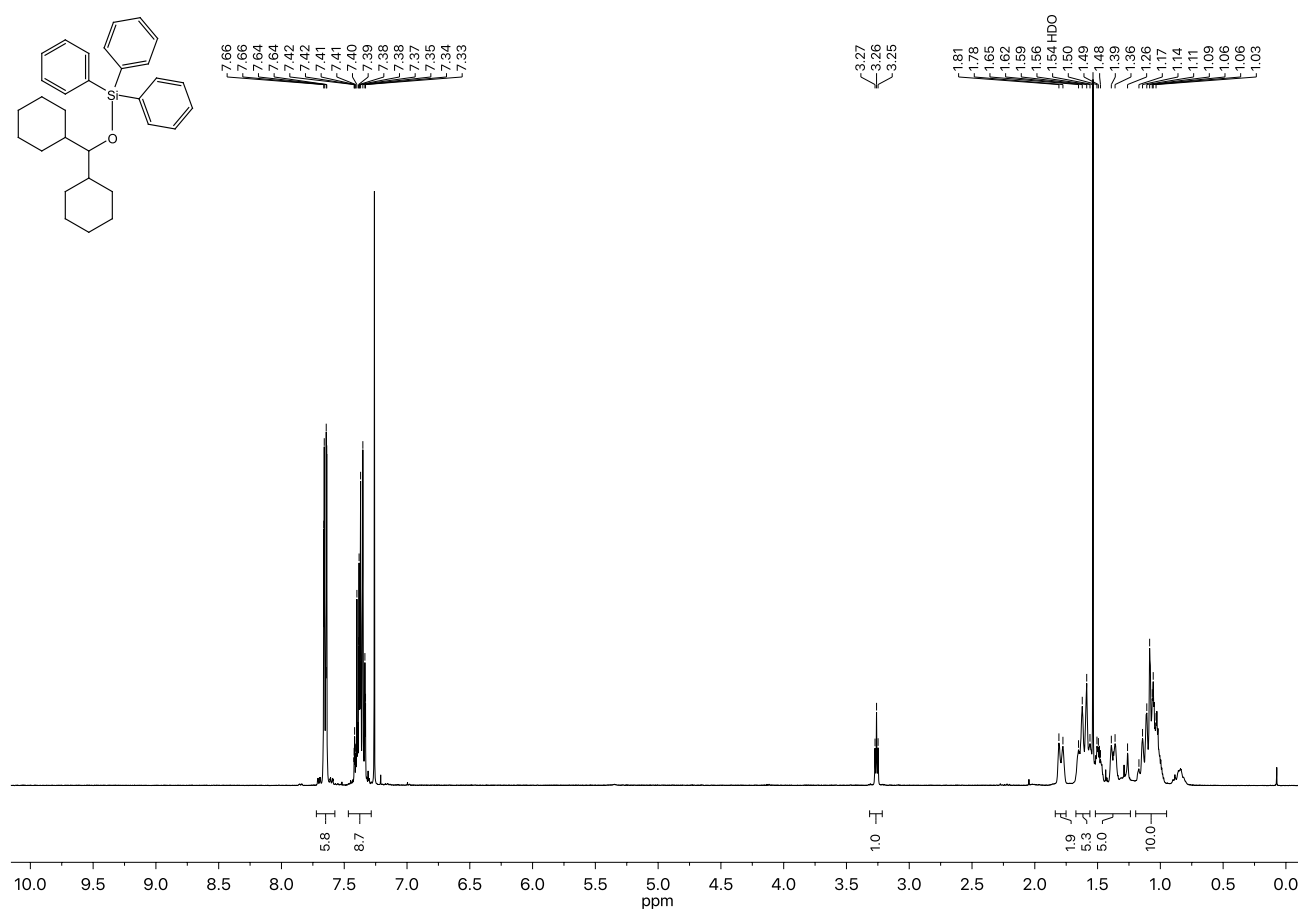
Figure 2.63. ^{1}H-NMR spectrum of **6fa**.
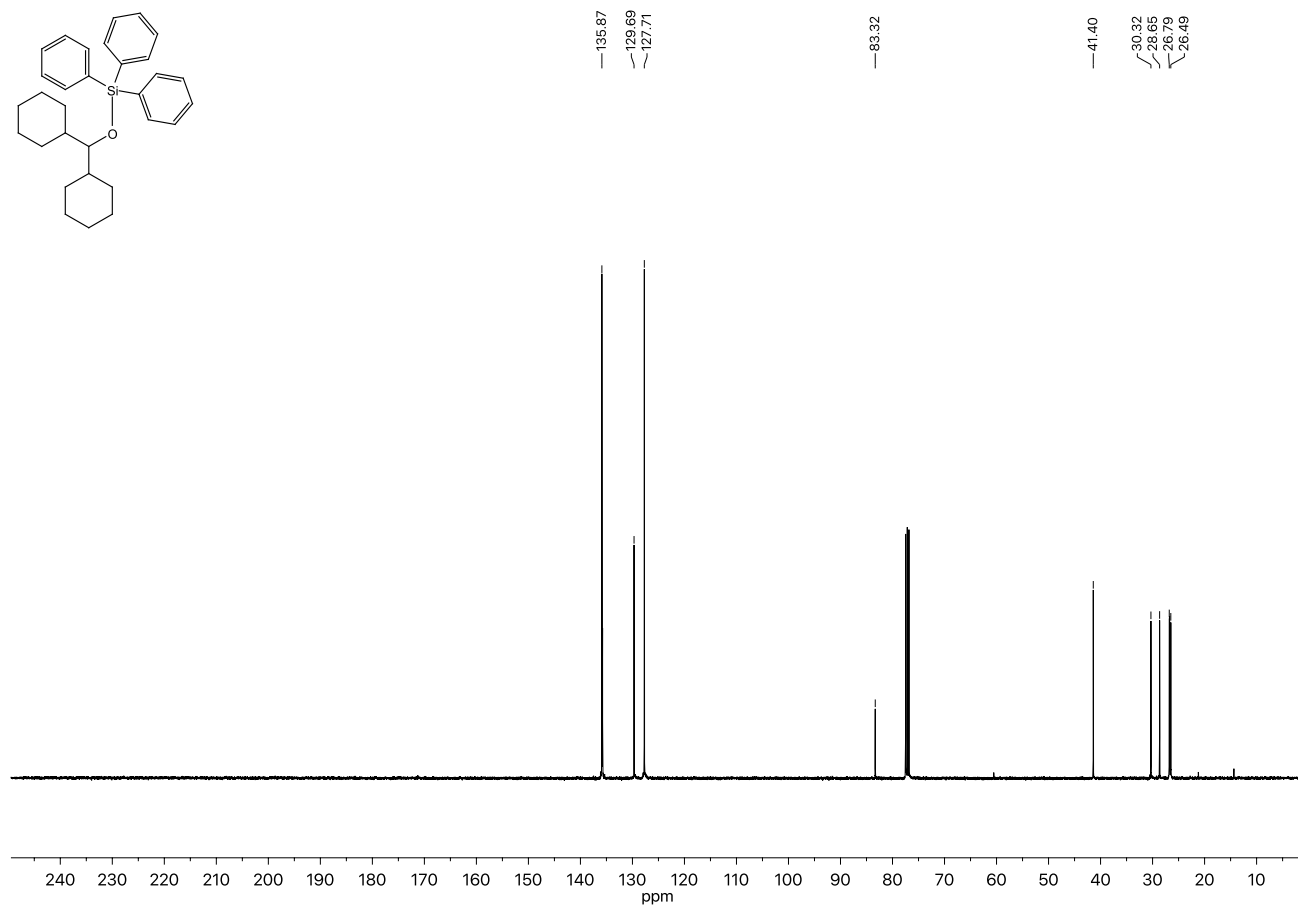
Figure 2.64. ^{13}C-NMR spectrum of **6fa**.
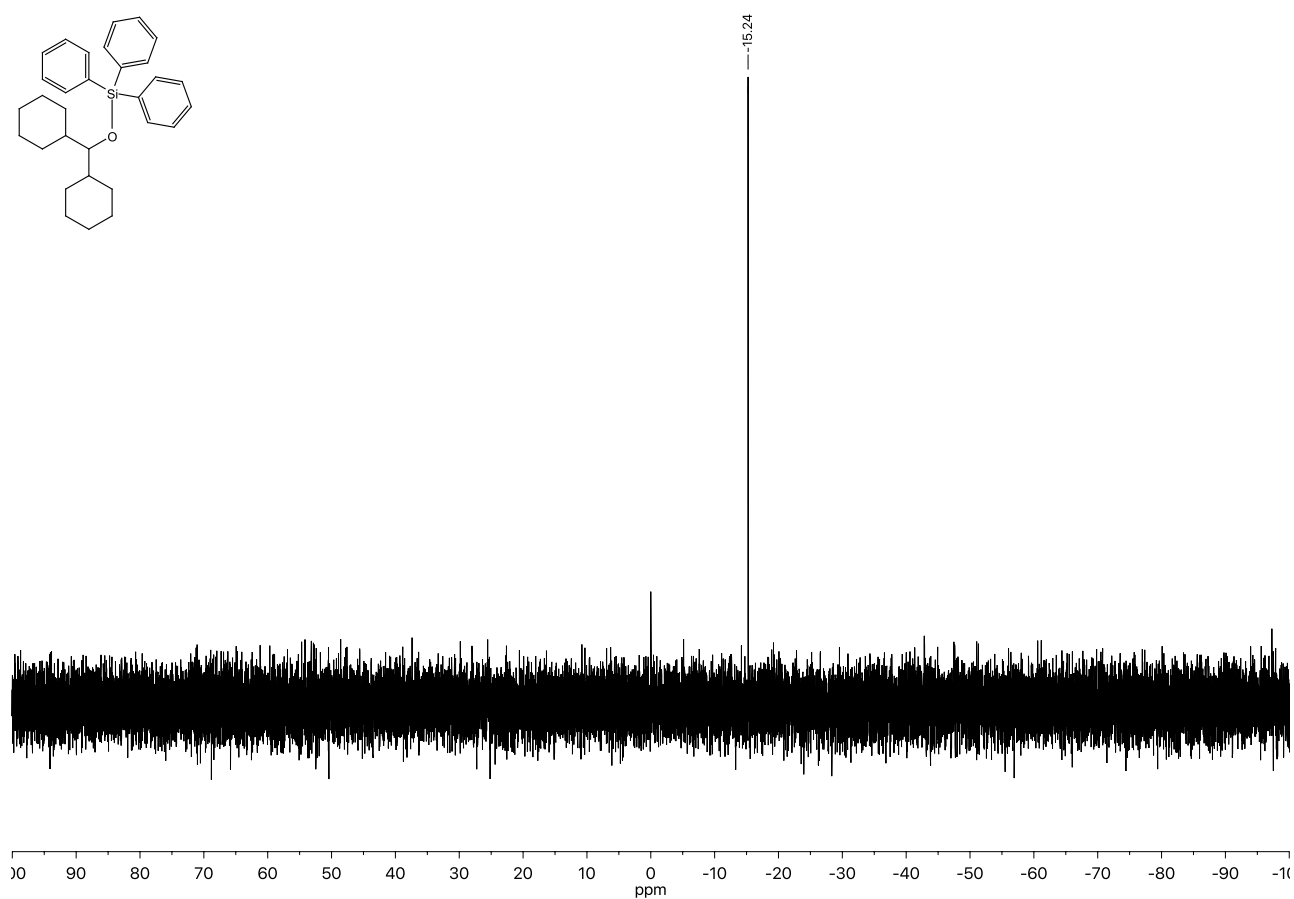
Figure 2.65. ^{29}Si-NMR spectrum of **6fa**.
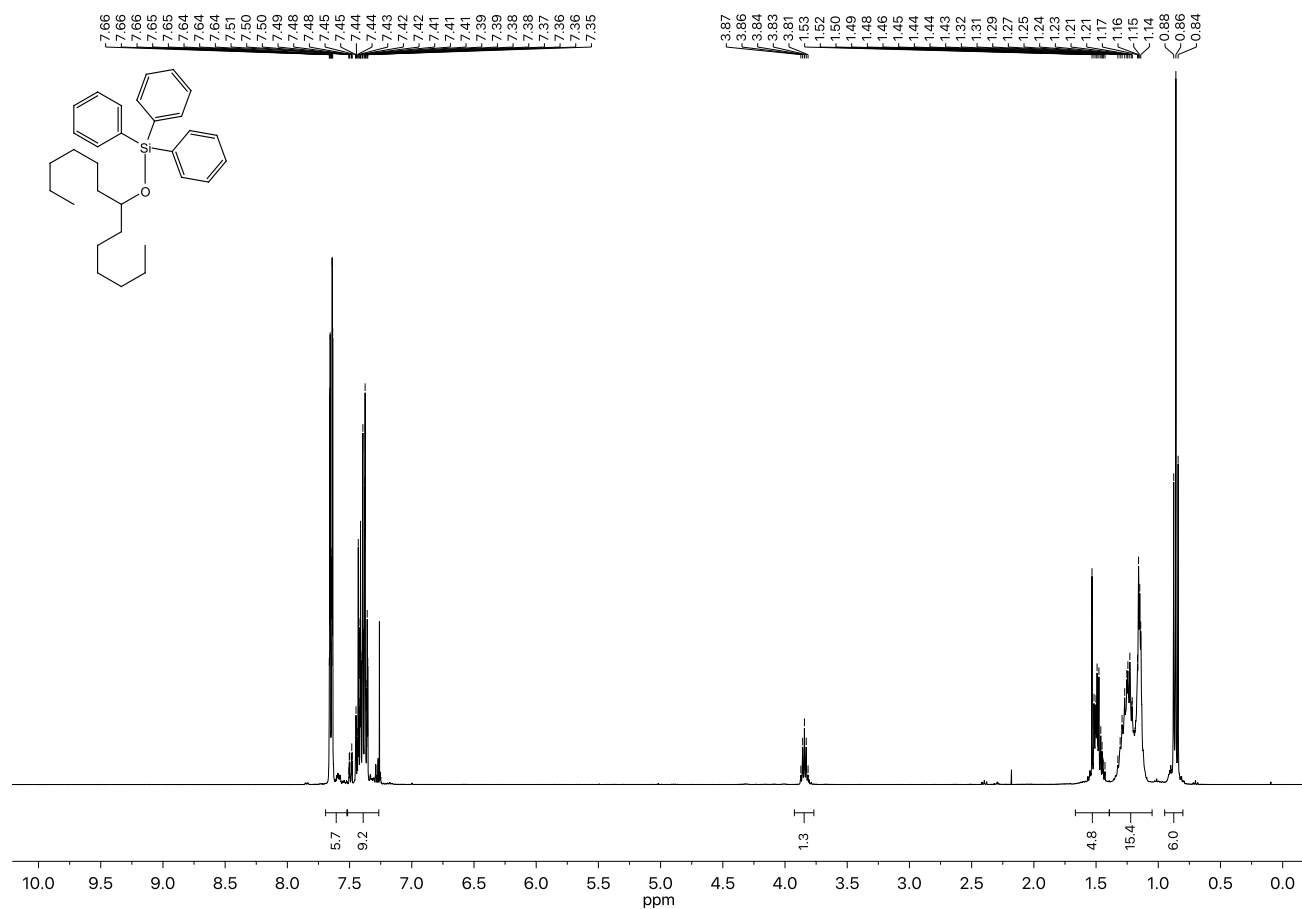
Figure 2.66. ^{1}H-NMR spectrum of **6ga**.
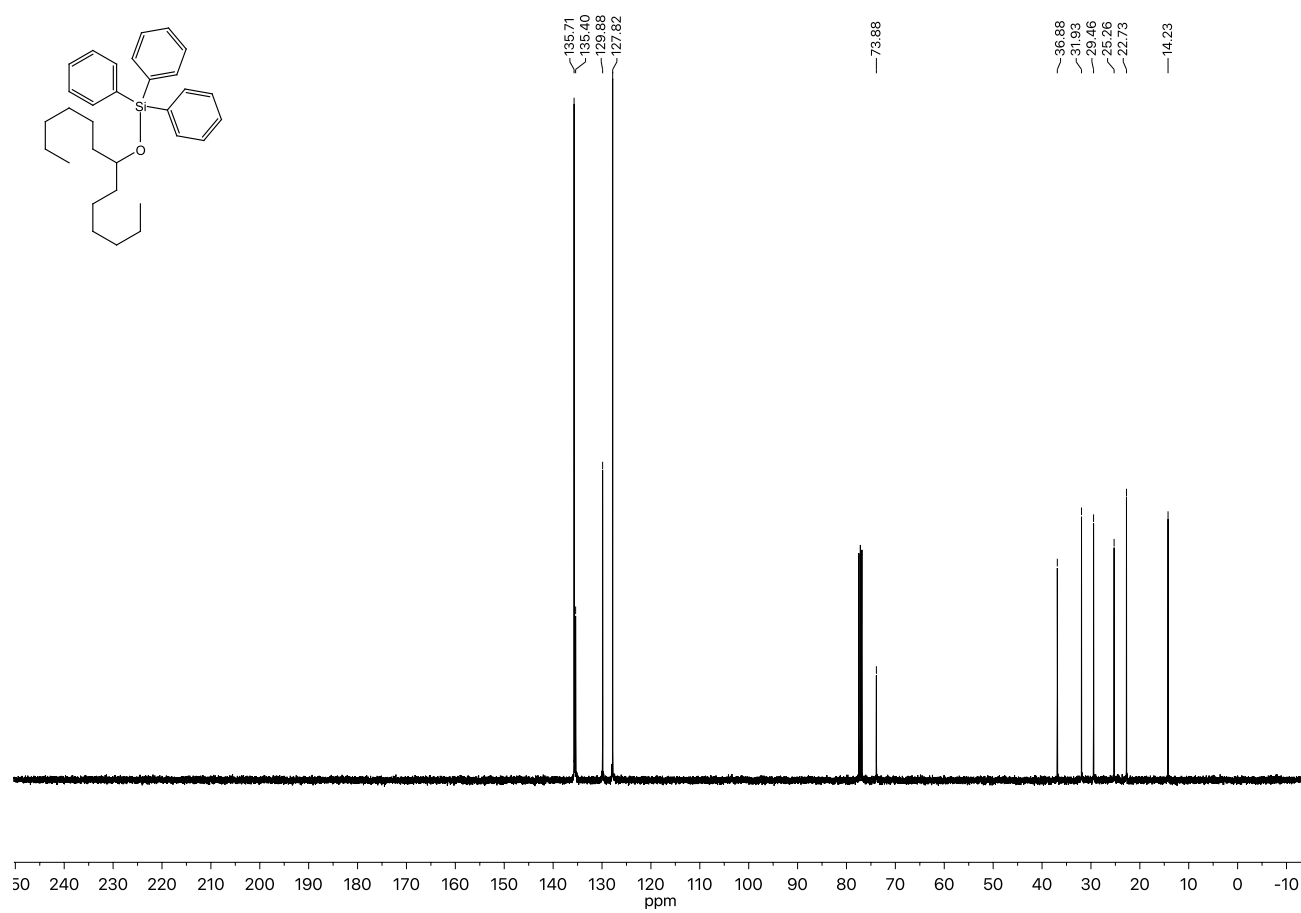
Figure 2.67. ^{13}C-NMR spectrum of **6ga**.

2.8. References

[1]   Z. R. Laughrey, S. E. Kiehna, A. J. Riemen, M. L. Waters, *J. Am. Chem. Soc.* **2008**, *130*, 14625-14633.
[2]   a) E. H. Krenske, K. N. Houk, *Acc. Chem. Res.* **2013**, *46*, 979-989; b) A. J. Neel, M. J. Hilton, M. S. Sigman, F. D. Toste, *Nature* **2017**, *543*, 637-646; c) O. Takahashi, Y. Kohno, M. Nishio, *Chem. Rev.* **2010**, *110*, 6049-6076.
[3]   S. Grimme, *Angew. Chem. Int. Ed.* **2008**, *47*, 3430-3434.
[4]   J. W. Bloom, S. E. Wheeler, *Angew. Chem. Int. Ed.* **2011**, *50*, 7847-7849.
[5]   K. S. Kim, S. Karthikeyan, N. J. Singh, *J. Chem. Theory Comput.* **2011**, *7*, 3471-3477.
[6]   D. B. Ninkovic, D. Z. Vojislavljevic-Vasilev, V. B. Medakovic, M. B. Hall, E. N. Brothers, S. D. Zaric, *Phys. Chem. Chem. Phys.* **2016**, *18*, 25791-25795.
[7]   J. R. Premkumar, D. Umadevi, G. N. Sastry, *Indian J. Chem.* **2014**, *53A*, 958 - 991.
[8]   J. Rezac, K. E. Riley, P. Hobza, *J. Chem. Theory Comput.* **2011**, *7*, 2427-2438.
[9]   T. M. Parker, L. A. Burns, R. M. Parrish, A. G. Ryno, C. D. Sherrill, *J. Chem. Phys.* **2014**, *140*, 094106.
[10]   D. B. Ninkovic, J. P. Blagojevic Filipovic, M. B. Hall, E. N. Brothers, S. D. Zaric, *ACS Cent. Sci.* **2020**, *6*, 420-425.
[11]   a) A. Matsushima, T. Fujita, T. Nose, Y. Shimohigashi, *J. Biochem.* **2000**, *128*, 225-232; b) Y. Nakagawa, K. Irie, R. C. Yanagita, H. Ohigashi, K. Tsuda, *J. Am. Chem. Soc.* **2005**, *127*, 5746-5747; c) R. Carrillo, M. Lopez-Rodriguez, V. S. Martin, T. Martin, *Angew. Chem. Int. Ed.* **2009**, *48*, 7803-7808.
[12]   J. N. Israelachvili, *Intermolecular and Surface Forces*, 3 ed., Elsevier, Burlington, **2011**.
[13]   H. Adams, S. L. Cockroft, C. Guardigli, C. A. Hunter, K. R. Lawson, J. Perkins, S. E. Spey, C. J. Urch, R. Ford, *Chembiochem* **2004**, *5*, 657-665.
[14]   H. B. Kagan, J. C. Fiaud, *Top. Stereochem.* **1988**, *18*, 249-300.
[15]   S. Hoops, S. Sahle, R. Gauges, C. Lee, J. Pahle, N. Simus, M. Singhal, L. Xu, P. Mendes, U. Kummer, *Bioinformatics* **2006**, *22*, 3067-3074.
[16]   I. Vasilief, QtiPlot 0.9.8.9, **2011**.
[17]   J. Helberg, M. Marin-Luna, H. Zipse, *Synthesis* **2017**, *49*, 3460-3470.
[18]   P. Patschinski, C. Zhang, H. Zipse, *J. Org. Chem.* **2014**, *79*, 8348-8357.
[19]   P. Patschinski, H. Zipse, *Org. Lett.* **2015**, *17*, 3318-3321.
[20]   R. K. Akhani, M. I. Moore, J. G. Pribyl, S. L. Wiskur, *J. Org. Chem.* **2014**, *79*, 2384-2396.
[21]   H. Mayr, A. R. Ofial, *Angew. Chem. Int. Ed.* **2006**, *45*, 1844-1854.
[22]   H. Laqua, *Quantifizierung dispersiver Wechselwirkungen - Vergleich der Selektivitäten von primären Alkoholen mit gesättigten und ungesättigten Ringsystemen*, bachelor thesis, LMU München (Munich), **2015**.
[23]   C. Hansch, A. Leo, R. W. Taft, *Chem. Rev.* **1991**, *91*, 165-195.
[24]   M. T. Tribble, J. G. Traynham, *J. Am. Chem. Soc.* **1969**, *91*, 379-388.
[25]   S. Weitl, *Untersuchung des Einflusses der London-Dispersion auf die Selektivität von Silylierungsreaktionen primärer Alkohole*, Bachelor thesis, LMU München (Munich), **2017**.
[26]   M. D. Greenhalgh, J. E. Taylor, A. D. Smith, *Tetrahedron* **2018**, *74*, 5554-5560.
[27]   H. F. Klare, M. Oestreich, *Angew. Chem. Int. Ed.* **2007**, *46*, 9335-9338.
[28]   P. Sgarabotto, F. Ugozzoli, S. Sorriso, Z. Malarski, *Acta Cryst. C* **1988**, *44*, 671-673.
[29]   P. Sgarabotto, F. Ugozzoli, S. Sorriso, Z. Malarski, CCDC 1165726, **1989**.
[30]   S. Ebbinghaus, D. Abeln, M. Epple, CCDC 108059, **2000**.
[31]   M. Marin-Luna, B. Pölloth, F. Zott, H. Zipse, *Chem. Sci.* **2018**, *9*, 6509-6515.
[32]   F. A. Carey, R. J. Sundberg, *Advanced Organic Chemistry, Part A: Structure and Mechanisms*, Springer, New York, **2007**.
[33]   C. Y. Legault, CYLview 1.0b, Université de Sherbrooke, **2009**.
[34]   A. Milo, E. N. Bess, M. S. Sigman, *Nature* **2014**, *507*, 210-214.
[35]   A. R. Katritzky, E. S. Ignatchenko, R. A. Barcock, V. S. Lobanov, M. Karelson, *Anal. Chem.* **1994**, *66*, 1799-1807.
[36]   T. J. Cleij, J. K. King, L. W. Jenneskens, *Chem. Mater.* **2000**, *12*, 84-89.
[37]   L. Hevesi, M. Dehon, R. Crutzen, A. Lazarescu-Grigore, *J. Org. Chem.* **1997**, *62*, 2011-2017.
[38]   D. Y. Ong, Z. Yen, A. Yoshii, J. Revillo Imbernon, R. Takita, S. Chiba, *Angew. Chem. Int. Ed.* **2019**, *58*, 4992-4997.
[39]   S. Crook, N. J. Parr, J. Simmons, S. Jones, *Tetrahedron: Asymmetry* **2014**, *25*, 1298-1308.
[40]   G. Nagarjuna, A. Kumar, A. Kokil, K. G. Jadhav, S. Yurt, J. Kumar, D. Venkataraman, *J. Mater. Chem.* **2011**, *21*, 16597-16602.
[41]   N. Luo, J. Liao, L. Ouyang, H. Wen, Y. Zhong, J. Liu, W. Tang, R. Luo, *Organometallics* **2019**, *39*, 165-171.
[42]   R. R. Dey, B. Paul, S. S. Dhar, S. Bhattacharjee, *Chem. Lett.* **2014**, *43*, 1545-1547.
[43]   A. A. Krolevets, V. V. Antipova, A. G. Popov, A. V. Adamov, *J. Gen. Chem. USSR* **1988**, *58*, 2023-2030.
[44]   A. Simonneau, J. Friebel, M. Oestreich, *Eur. J. Org. Chem.* **2014**, *2014*, 2077-2083.
[45]   N. A. DeLucia, N. Das, A. K. Vannucci, *Org. Biomol. Chem.* **2018**, *16*, 3415-3418.
[46]   E. Vasilikogiannaki, I. Titilas, C. Gryparis, A. Louka, I. N. Lykakis, M. Stratakis, *Tetrahedron* **2014**, *70*, 6106-6113.
[47]   a) A. D. Becke, *J. Chem. Phys.* **1993**, *98*, 5648; b) C. Lee, W. Yang, R. G. Parr, *Phys. Rev. B* **1988**, *37*, 785-789; c) S. Grimme, *J. Chem. Phys.* **2006**, *124*, 034108.
[48]   G. W. Spitznagel, T. Clark, J. Chandrasekhar, P. R. Schleyer, *J. Comput. Chem.* **1982**, *3*, 363-371.
[49]   A. V. Marenich, C. J. Cramer, D. G. Truhlar, *J. Phys. Chem. B* **2009**, *113*, 6378.
[50]   Maestro 12.2.012, New York, **2019**.
[51]   a) C. Riplinger, F. Neese, *J. Chem. Phys.* **2013**, *138*, 034106; b) C. Riplinger, B. Sandhoefer, A. Hansen, F. Neese, *J. Chem. Phys.* **2013**, *139*, 134101; c) F. Weigend, R. Ahlrichs, *Phys. Chem. Chem. Phys.* **2005**, *7*, 3297-3305.
[52]   A. Hellweg, C. Hättig, S. Höfener, W. Klopper, *Theor. Chem. Acc.* **2007**, *117*, 587-597.
[53]   M. Marin-Luna, P. Patschinski, H. Zipse, *Chem. Eur. J.* **2018**, *24*, 15052-15058.
[54]   G. W. T. M. J. Frisch, H. B. Schlegel, G. E. Scuseria, M. A. Robb, J. R. Cheeseman, G. Scalmani, V. Barone, B. Mennucci, G. A. Petersson, H. Nakatsuji, M. Caricato, X. Li, H. P. Hratchian, A. F. Izmaylov, J. Bloino, G. Zheng, J. L. Sonnenberg, M. Hada, M. Ehara, K. Toyota, R. Fukuda, J. Hasegawa, M. Ishida, T. Nakajima, Y. Honda, O. Kitao, H. Nakai, T. Vreven, J. A. Montgomery, Jr., J. E. Peralta, F. Ogliaro, M. Bearpark, J. J. Heyd, E. Brothers, K. N. Kudin, V. N. Staroverov, T. Keith, R. Kobayashi, J. Normand, K. Raghavachari, A. Rendell, J. C. Burant, S. S. Iyengar, J. Tomasi, M. Cossi, N. Rega, J. M. Millam, M. Klene, J. E. Knox, J. B. Cross, V. Bakken, C. Adamo, J. Jaramillo, R. Gomperts, R. E. Stratmann, O. Yazyev, A. J. Austin, R. Cammi, C. Pomelli, J. W. Ochterski, R. L. Martin, K. Morokuma, V. G. Zakrzewski, G. A. Voth, P. Salvador, J. J. Dannenberg, S. Dapprich, A. D. Daniels, O. Farkas, J. B. Foresman, J. V. Ortiz, J. Cioslowski, and D. J. Fox,, Gaussian 09, Revision D.01, Wallingford CT, **2010**.
[55]   F. Neese, *Comput. Mol. Sci.* **2012**, *2*, 73-78.

Chapter 3. Size-Dependent Rate Acceleration in the Silylation of Secondary Alcohols: the Bigger the Faster.

Marta Marín-Luna, Benjamin Pölloth, Fabian Zott, and Hendrik Zipse

Author contributions: M.M.-L. and B.P. contributed equally to this work. F.Z. contributed to the project within his "Forschungspraktikum" supervised by MML. The study was designed by M.M.-L., B.P. and H.Z. The experimental study was performed by M.M.-L., B.P. and F.Z. (competition experiments: M.M.-L., B.P. and F.Z.; synthesis of silyl chlorides: B.P.; solvent study: B.P). The computational study was performed by M.M.-L. The manuscript was jointly written by M.M.-L., B.P. and H.Z. Experimental part of the SI was prepared by B.P., computational part was prepared by M.M.-L. and herein adapted by B.P.

Copyright: This research was originally published under a Creative Commons Licence in *Chemical Science* by the Royal Society of Chemistry and can thus be used in other publications provided that the correct acknowledgement is given with the reproduced material and it is not used for commercial purposes.

Additional information: The herein printed Supporting Information (SI) is an altered version of the published SI. Chapter 3.1 contains additional information, while other chapters were shortened. NMR-spectra, integral tables for competition experiments, crystal structures and tables of energies, enthalpies and free energies for all conformers can be accessed online in the original version of the SI free of charge (https://doi.org/10.1039/C8SC01889H). The original SI file can also be found on the electronic attachment of this thesis.

EDGE ARTICLE

Size-dependent rate acceleration in the silylation of secondary alcohols: the bigger the faster†

Marta Marin-Luna, [ID] Benjamin Pölloth, [ID] Fabian Zott [ID] and Hendrik Zipse [ID] *

Relative rates for the reaction of secondary alcohols carrying large aromatic moieties with silyl chlorides carrying equally large substituents have been determined in organic solvents. Introducing thoroughly matching pairs of big dispersion energy donor (DED) groups enhanced rate constants up to four times, notably depending on the hydrogen bond donor ability of the solvent. A linear correlation between computed dispersion energy contributions to the stability of the silyl ether products and experimental relative rate constants was found. These results indicate a cooperation between solvophobic effects and DED-groups in the kinetic control of silylation reactions.

Introduction

Aromatic interactions[1] play a central role in diverse fields such as organic synthesis,[2] supramolecular self-assembly,[3–5] molecular recognition[6] or protein and peptide structures.[7] They mainly result from the sum of three terms:[8,9] (1) an electrostatic component due to the electronic nature of the substituents at the interacting surfaces,[10] (2) London dispersion interaction[11–14] as the attractive component of van der Waals forces, which arise due to interactions between induced dipoles,[15] and (3) the solvophobic or hydrophobic effect, which results from a balance between solvent–solvent and solvent–solute interactions.[16–18] Whereas numerous studies have detailed the nature of the electrostatic component,[19–24] it is still a challenge to quantify individual dispersive and solvophobic effects in solution.[25] Recent studies by Cockroft *et al.*[26–29] and Shimizu *et al.*[30,31] employ torsional molecular balances[32] to measure these effects through the quantification of conformational equilibria. Most of the studies conclude that the dispersive interactions are of minor importance in solution[33] and that the major contribution to the stabilization of the folded state results from the balance of solvent–solvent and solute–solvent interactions. The conceptually similar idea of using sizeable (rigid) dispersion energy donor groups (DED-group) in reagents and/or ligands in the development of stereoselective catalytic processes has also been explored recently,[2,34] where it has been found that the appropriate placement of interacting DED-moieties in a system can lead to higher selectivity. Interactions between DED groups in bimolecular (associative) reactions were recently analysed for

Department of Chemistry, LMU München, Butenandtstrasse 5-13, 81377, München, Germany. E-mail: zipse@cup.uni-muenchen.de

† Electronic supplementary information (ESI) available: Protocol for competition experiments, experimental procedures, characterization data, NMR spectra, computational data. CCDC 1839390 and 1839391. For ESI and crystallographic data in CIF or other electronic format see DOI: 10.1039/c8sc01889h

acylation reactions of alcohols.[34,36] For this latter class of reactions we have found that acylations mediated by TCAP (9-azajulolidine, marked in red in Fig. 1a) are fastest for pyrenyl-substituted secondary alcohols (marked in green Fig. 1) as compared to alcohols carrying smaller aromatic or even aliphatic substituents.[35] In contrast, reaction rates hardly vary for acylation reagents of different size, which can most easily be accommodated in the general transition state structure shown in Fig. 1a. In the following we explore the question whether the silylation of secondary alcohols with silyl chloride reagents can be accelerated in a similarly targeted fashion through the use of sufficiently large DED substituents in the reagents and substrates. The silylation of alcohols is of outstanding importance in protection group strategies for the synthesis of complex molecular targets,[37,38] and any extension of the currently available toolset will obviously be helpful for organic synthesis in general. The base-catalysed silylation of alcohols is commonly assumed to follow a Lewis base- rather than a general base-catalysed mechanism.[39–42] In contrast to acylation reactions,

Fig. 1 Proposed transition structures for catalysed acylation (left) and silylation reaction (right) of 1-(1-pyrenyl)ethanol.

silyl group transfer reactions proceed along an S_N2-like pathway, which implies the relative orientation of catalyst, reagent and substrate shown in the transition state cartoon in Fig. 1b. For this type of transition state structure, stabilizing interactions between appropriately placed DED substituents are expected between the alcohol and the reagent, but not between the alcohol and the catalyst. In order to probe this hypothesis, we have studied the reaction rates for the reaction of secondary alcohols with silyl chloride reagents carrying alkyl and aryl substituents of varying size. In addition, the influence of reaction temperature and solvent on the reaction rate was studied. The thermochemical stability of the products was explored by theoretical methods in an effort to quantify the dispersion energy contribution to the overall reaction driving force.

Results and discussion

Relative rate constants k_{rel} for the Lewis base-catalysed silylation of alcohols **1a–1f** with silyl chlorides **2a–2f** were determined in 1 : 1 competition experiments employing 1-phenylethanol (**1a**) as the reference system (Scheme 1 and Fig. 2). The other substrate alcohols derived from **1a** through annulation of one (as in **1b** and **1c**), two (as in **1d** and **1e**) or three (as in **1f**) benzene rings to its phenyl group. Depending on the particular position of annulation, this generates no additional repulsive 1,5-interaction with the alcohol oxygen atom (as in **1c** and **1e**), one additional 1,5-interaction (as in **1b** and **1f**), or two such interactions in **1d**. The *peri* positions responsible for the repulsive 1,5-interactions are marked by grey circles in Fig. 2. The silyl chloride reagents chosen here grow in size from trimethylsilyl

Scheme 1 Competition experiments between alcohol **1a** and **1b–f** with silyl reagents **2a–f**.
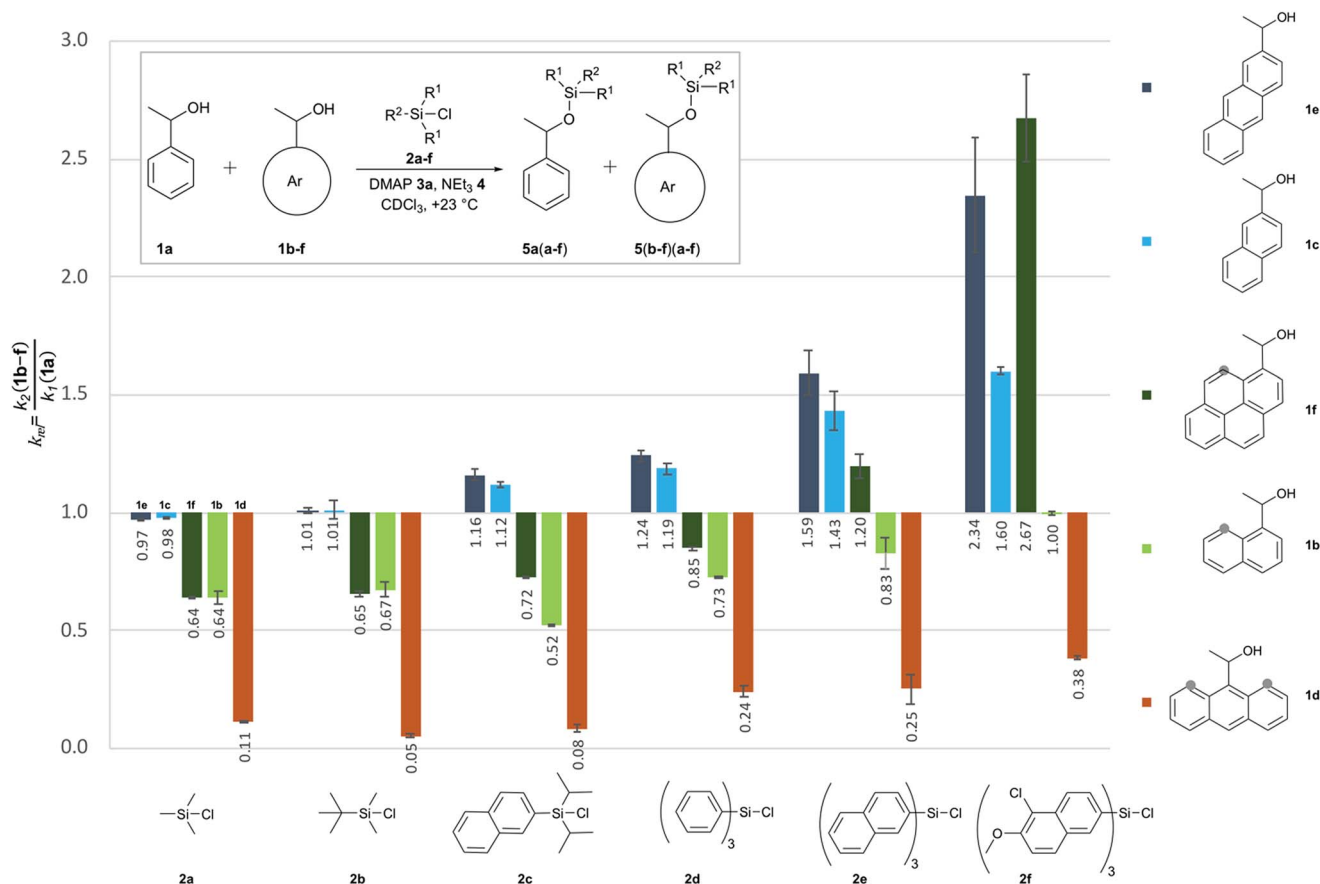
Fig. 2 Relative rate constants (k_{rel}) for competition experiments between reference alcohol **1a** and selected secondary alcohols **1b–1f** with silyl chlorides **2a–f**.
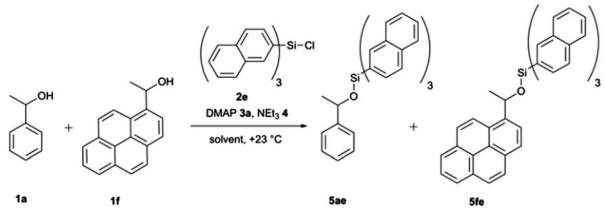
chloride **2a** to substituted trinaphthylsilyl chloride **2f** (see Fig. 2 and S1 of the ESI†). The competition experiments described in Scheme 1 involve equal amounts of reference alcohol **1a** and of one of the substrate alcohols **1b–f**, a quantity of one of the silyl chlorides **2** sufficient enough to obtain between 20–80% turnover of the substrate alcohols **1**, a catalytic amount (0.15 eq. relative to alcohols **1**) of *N,N*-dimethylaminopyridine (**3**, DMAP), and triethylamine (**4**) as the auxiliary base, in deuterated chloroform at a constant temperature of +23 °C. The relative rate constant k_{rel} defined as the ratio of effective rate constants k_2 (**1b–f**) over k_1 (**1a**) was used as main control parameter and obtained from the mole distribution of reactants and products after completion of the reaction as determined by ^{1}H NMR spectroscopy (for full details see ESI†). The resulting rate constant values are shown in Fig. 2 and in Tables S1–S5 of the ESI.†
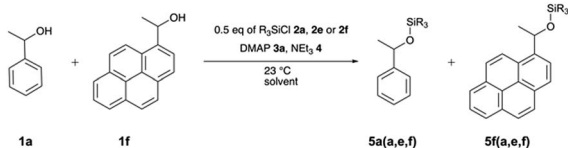
Relative reaction rates for the small trimethylsilyl chloride **2a** (TMSCl) reagent show no response to the size of the alcohol π-systems, but are sensitive to the number of repulsive 1,5-interactions. Reaction rates are therefore quite similar for alcohols **1a**, **1c** and **1e**, then drop notably for alcohols with one 1,5-interaction (**1b** and **1f**), and drop more strongly for the most hindered alcohol **1d**, which reacts nine times slower than **1a**. Moving to *tert*-butyldimethylsilyl chloride **2b** (TBDMSCl) as a sterically more hindered and overall larger reagent we find practically no change in relative rate constants k_{rel}, except for the most hindered alcohol **1d**, whose reactivity drops by another factor of two. With the results for smaller silyl chloride reagents in hand, we next investigated symmetrical silyl reagents **2d–2f** containing sizeable aromatic substituents.

Reactions with triphenylsilyl chloride (**2d**, TPSCl) differ from those with TMSCl in two key aspects. First, all k_{rel} values for silyl chloride **2d** are larger than those for TMSCl (**2a**), the sterically unhindered alcohols **1c** and **1e** now reacting even faster than the reference alcohol **1a**. Second, silyl chloride **2d** differentiates more strongly between alcohols of different size, but identical degree of steric hindrance. Reaction rates for alcohols **1b** and **1f**, for example, are quite similar for TMSCl (**2a**) and also for TBSCl (**2b**), but differ systematically for triphenylsilyl chloride (**2d**) in that the larger alcohol **1f** (k_{rel} = 0.85) reacts faster than alcohol **1b** (k_{rel} = 0.73). Both factors can be seen at work in an enhanced way in reactions of the even larger trinaphthylsilyl chloride **2e**, where the sterically hindered, but pyrenyl-substituted alcohol **1f** now reacts faster than the unhindered reference alcohol **1a** (k_{rel} = 1.20). Polar substituents were then added to the 5,6-positions of the naphthyl groups in silyl chloride **2e** in order to increase its overall polarizability and the contact surface with alcohol reagents. Relative reaction rates for the resulting silyl chloride **2f** (TN*SCl) are all significantly larger than those for trinaphthylsilyl chloride **2e** and appear to be mainly dominated by the size of the alcohol π-system. This makes pyrenyl-substituted alcohol **1f** the most reactive substrate, closely followed by the less hindered anthracenyl-substituted alcohol **1e**. A final test was performed with diisopropylnaphthylsilyl chloride **2c** (DINSCl), which combines a single naphthyl with two α-branched isopropyl substituents. The results obtained for this reagent are basically those for trinaphthylsilyl chloride **2e**, but

Table 1 Relative rate constants (k_{rel}) for competition experiments between alcohol **1a** and **1f** with silyl chloride **2e** in different solvents

Entry	Solvent	k_{rel}
1	Tetrahydrofuran	0.59
2	Carbon disulfide	0.61
3	Dimethylsulfoxide	0.68
4	Dimethoxyethane	0.72
5	Hexafluorobenzene/chloroform-d^a	0.74
6	Trifluorotoluene	0.79
7	Tetrachloromethane	0.84
8	Acetone	1.16
9	Chloroform-d	1.20
10	*t*-Amyl alcohol/chloroform-d^a	1.21
11	Acetonitrile/dichloromethane^a	1.36
12	Dichloromethane	1.38

^{a} Mixture 1 : 1 (v/v).

scaled down towards the results obtained for the trialkylsilyl chlorides **2a** and **2b** (Fig. 2). The spatial disposition of the substituents in the crystal structure of product **5fc** shows no direct interaction between the naphthyl and pyrenyl surfaces (see ESI†). Assuming a similar structure in the transition state, relative rates seem to be influenced by the isopropyl as well as the naphthyl substituents. The results presented in Fig. 2 can also be analysed from the point of view of each reacting alcohol (see Fig. S2†). While the 9-anthracenyl alcohol **1d** containing two *peri* hydrogen atoms is for all silyl chlorides much slower than **1a**, the sterically not hindered alcohols **1c** and **1e** react with all silyl reagents **2** equally fast or faster than **1a**. In the 1-pyrenyl- and 1-naphthyl-substituted alcohols (**1f** and **1b**) the relative rate constants are determined by a balance between interactions of the two aromatic surfaces and repulsive steric effects, the former one being dominant in the case of TN*SCl **2f**. In all of the pairs k_{rel} increases with the growth of the DED-substituent at the silicon centre, which confirms that the size of interacting aromatic surfaces located at the alcohol and silyl substrates determine the chemoselectivity of the silylation reaction.

With the purpose of quantifying the influence of the reaction medium on the relative rate constants, the competition experiment between the reference alcohol **1a** and the biggest alcohol **1f** with TNSCl **2e** was carried out in different solvents. This choice was motivated by two main considerations: (1) both

alcohol **1f** and TNSCl **2e** carry the biggest non-substituted DED-substituents and (2) using alcohol **1f** the balance between attractive aromatic interactions and repulsive steric effects can be studied in different solvents. The k_{rel} values measured in different solvents span a range from 0.59 in tetrahydrofuran to 1.38 in dichloromethane (Table 1, for details see ESI†). Strikingly, relative rates for the reaction of alcohol **1f** with the naphthyl-substituted silyl chloride **2e** were found to be in several solvents (entries 1–3) very similar to k_{rel} of the reaction of this alcohol **1f** in the reference solvent CDCl$_3$ with TMSCl **2a** in which no aromatic interactions between alcohol and silyl moiety occur. Therefore, those solvents seem to cancel aromatic interactions almost completely and repulsive steric effects solely govern the relative rates. In contrast, k_{rel} for the silylation of alcohol **1f** increases up to 2.3 times in other solvents like acetone, chloroform and dichloromethane. In order to prove that those solvent effects are causally related to aromatic interactions, reactions between alcohols **1a** and **1f** with silyl reagents of various sizes were explored by competition experiments in CDCl$_3$ as the reference solvent, and in tetrahydrofuran and dichloromethane as the solvents with the smallest and largest k_{rel} values in Table 1 (Fig. 3). For TMSCl (**2a**) as the smallest reagent, only a negligible solvent sensitivity of k_{rel} was found (Fig. 3), while for the largest reagent TN*SCl **2f** an increase in solvent sensitivity as compared to the relatively smaller TNSCl **2e** is observed. Hence, the observed solvent effects are due to the significant impact of solvents on size-dependent effects, which was also reported in other studies.[26,27,43–46] Distinguishing the different contributions of polarizability (π^* and δ), hydrogen-bond donor (α) and acceptor ability (β) via the linear solvation energy relationship developed by Kamlet and Taft[47,48] revealed that solvent effects are widely independent of the polarizability of the solvent, but correlate strongly with the hydrogen bond donor ability of the solvent (see eqn (S12) of ESI†). This can actually be further condensed to a direct correlation of the experimental k_{rel} values with the general α parameter proposed by Hunter (Fig. 4).[17] Considering that the hydrogen-bond donor ability of aromatic C–H groups is commonly found to be in the range of α = 1.0–1.4 the origin of solvent effects can be clarified. Thus, for solvents with α < 1
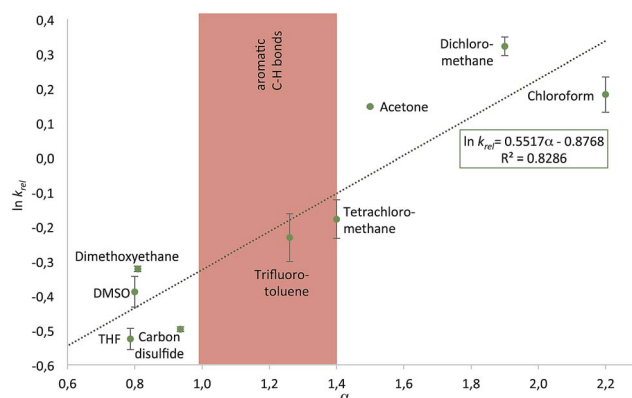
Fig. 4 Plot of experimental ln k_{rel} for the reaction of alcohols **1a** and **1f** with silyl chloride **2e** in different solvents against the solvent hydrogen bond donor parameter α defined by Hunter.[17]

such as THF and CS$_2$ hydrogen bonds of aromatic C–H-bonds with solvent molecules dominate the system whereas interactions of the aromatic surfaces of the alcohol and silyl moieties are minimized. Therefore, reaction rates are barely influenced by the different size of the aromatic systems of the two competing alcohols. As H-bonds between the aromatic C–H-bonds and the solvent get less relevant in solvents with α > 1 such as chloroform and dichloromethane, desolvation of the alcohol and silyl substrates occurs and as a consequence solvent–solvent as well as aromatic solute–solute interactions become more dominant.[17] Both the solvophobic effect of solvent molecules forming additional hydrogen bonds among each other and the attractive dispersion forces between the DED-groups can then enhance the rate of the reaction dependent on the size of the aromatic surfaces.

Differentiating the contributions of the aforementioned two types of effects is one main focus of the ongoing debate on aromatic stacking. The ln k_{rel} determined in different solvents listed in Table 1 were therefore also analysed in terms of the solvent cohesive energy density (ced) as key parameter for the strength of the solvophobic effect of a solvent.[27] Whether a higher ced value leads to an increase or a decrease of relative rates appears to depend on the hydrogen bond donor ability of the solvent (Fig. S14 of ESI†): in solvents with a low α (e.g. THF) higher ced values lead to a reduction in relative rates, possibly through the reinforcement of unfavourable solvent–solute interactions. In contrast, for solvents with a higher H-bond donor ability (e.g. DCM) higher ced values lead to an increase in k_{rel}. Correlations are, however, not very strong in both cases and the ced is thus insufficient to explain the observed differences in k_{rel}. The influence of London dispersion interactions on the experiment shown in Table 1 was subsequently probed through selectivity measurements in CDCl$_3$ at different temperatures, as these interactions are known to be less temperature dependent than dipole-dominated interactions.[11] Measurements in the temperature range from −10 °C to +23 °C lead to similar k_{rel} values for the **1a/1f** substrate pair, but the accuracy of these measurements was not high enough for the reliable extraction of activation parameters (see ESI†).
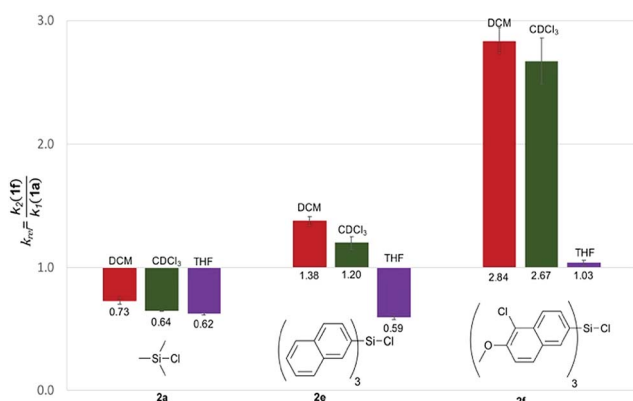
Fig. 3 Relative rate constants k_{rel} for the reaction of alcohols **1a** and **1f** with silyl chlorides **2a**, **2e** and **2f** in different solvents.

In how far the relative reaction rates measured experimentally simply reflect the stability of the silyl ether products formed was explored by the calculation of reaction free energies in chloroform solution. Geometry optimizations were performed at the SMD(CHCl$_3$)/B3LYP-D3/6-311+G(2d)/6-31+G(d)[49–53] level of theory, followed by single point energy calculations at DLPNO-CCSD(T)/def2-TZVPP[54–56] level. Solvation free energies were obtained from single point calculations with the SMD(CHCl$_3$)/B3LYP-D3/6-311+G(2d)/6-31+G(d) model and added to the gas phase results in order to obtain the reaction free energies in solution $\Delta G_{298,sol}$ compiled in Fig. 5 (see ESI† for details). Focusing on the results obtained for pyrenyl-substituted alcohol 1f, we find small and positive reaction energies for the smaller silyl chloride reagents. The positive sign for the reaction energy seen here derives from the fact that the calculated energies exclude the acid/base reaction between HCl and the auxiliary base NEt$_3$. This is in full agreement with experimental results showing basically no turnover between TBDMSCl (2b) and secondary alcohols in the absence of the auxiliary base.[39,40] Reaction energies become more favourable and eventually also negative on increasing the size of the silyl chloride reagent. Interestingly, the tert-butyldimethylsilyl ether 5fb is less stable than the trimethylsilyl ether 5fa, most likely due to repulsive steric interactions between the tert-butyl and the pyrenyl substituents. Although the two interacting aromatic surfaces are the same in the products 5fc and 5fe, the last one is 18.2 kJ mol⁻¹ more stable than 5fc. This energetic difference is possibly associated to the smaller polarizability of the isopropyl substituents than the naphthyl moiety at the Si atom in 5fc. Regarding those results no significant correlations were found between the experimental k_{rel} and the differences between the $\Delta G_{298,sol}$ of the respective silyl ethers (see ESI†), which indicates

that the k_{rel} are purely kinetic phenomena. At this point, we were interested in computing the contribution of the dispersion component to the thermochemical stability of the products. Single point energy calculations were therefore performed at the B3LYP level lacking the D3 dispersion correction over the optimized structures at B3LYP-D3 level (third group, Fig. 5). It was found that $\Delta G_{298,sol}$ decreases dramatically (larger positive values) even indicating that these products would be thermodynamically unstable. The smallest dispersion contributions were found in the silyl ethers 5fa and 5fb with non-polarizable methyl and tert-butyl substituents. However, in the case of silyl ethers carrying bigger aromatic substituents at the Si centre, the dispersion component increases notably up to −85.7 kJ mol⁻¹ (5ff). Conformational analysis of silyl ether 5fe as the silyl ether with the largest unsubstituted aromatic substituents reveals that aromatic surfaces for the best conformers are slightly twisted toward each other so that most non-covalent interactions[57] arise between the interacting π-surfaces with a small contribution of σ–π interactions (see Fig. 5 and ESI† for full details). Interestingly, linear correlations appear to exist between experimental k_{rel} values and differences in dispersion contributions between the respective substrate pairs $\Delta\Delta D_{298,sol}$, grouped by the number of 1,5-interactions at the alcohol substrate (Fig. 6). The similar slope reveals that sizeable DED-groups (higher $\Delta\Delta D_{298,sol}$) increases ln k_{rel} equally in both alcohol groups by 0.2 units per 10 kJ mol⁻¹ of additional dispersion contribution. That the data points for the unhindered alcohols 1c and 1e fall onto the same correlation line implies that it is irrelevant for the increase of k_{rel} whether the increase in $\Delta\Delta D_{298,sol}$ derives from growing the substrate alcohol or the silyl chloride reagent. The presence of one repulsive 1,5-interaction reduces the relative rate by 1.6 times

Fig. 5 Reaction free energies (kJ mol⁻¹) for the reaction of 1f with the silyl reagent 2a–f at different levels of theory. Computed non-covalent interaction surfaces (green) of the silyl ether 5fe.
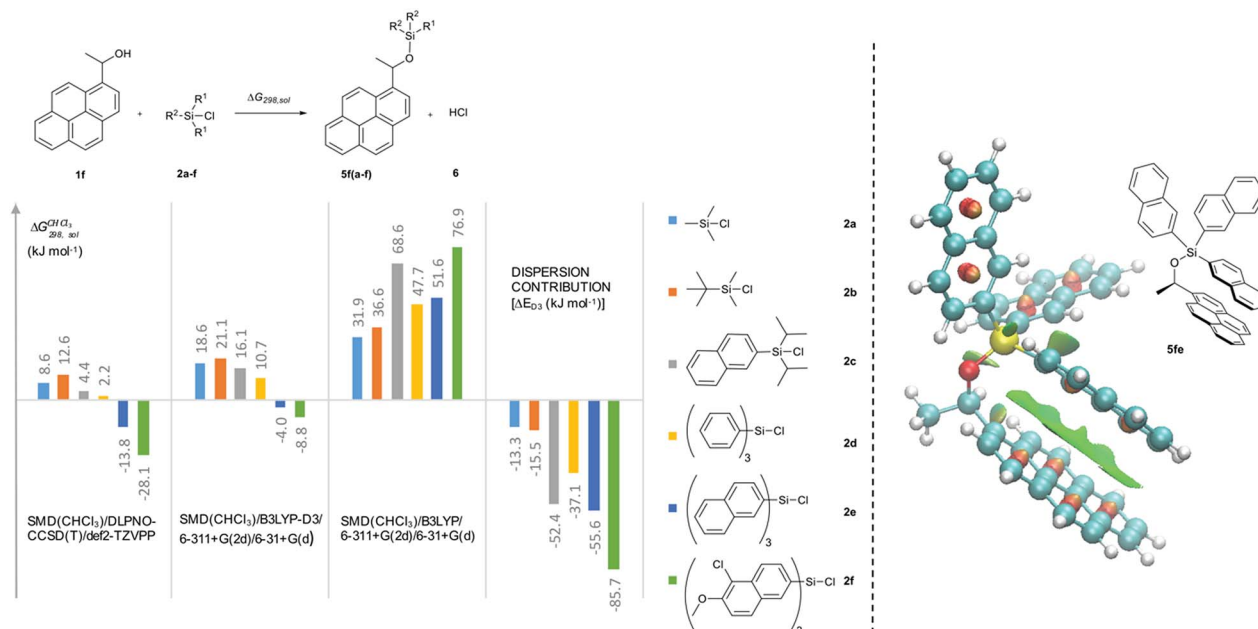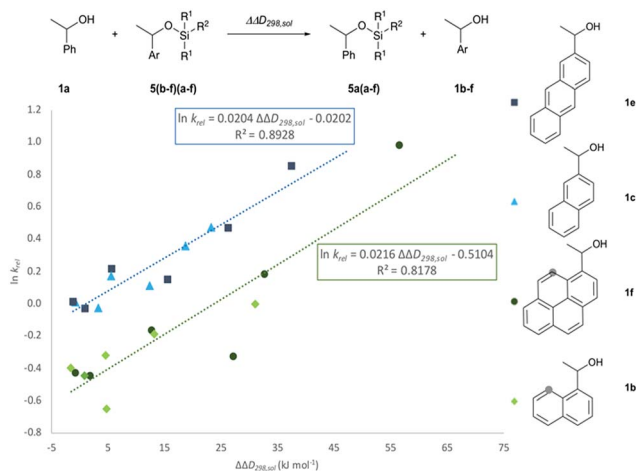
Fig. 6 Correlation of ln k_{rel} with calculated differences in the dispersion energy contributions, $\Delta\Delta D_{298,sol}$.

with respect to the non-hindered alcohols represented by the gap between the two correlation lines in Fig. 6. This analysis demonstrates that the experimentally measured relative rate constants k_{rel} directly relate to the size of the interacting surfaces and to repulsive steric effects in the alcohol substrates, whereby the dispersion energy component increases together with substrate size.

Conclusions

In summary, we have experimentally determined relative rates between two secondary alcohols bearing sizeable aromatic surfaces in silylation experiments designed as 1 : 1 competition experiments. In experiments with the comparatively small silyl chloride reagents TMSCl and TBDMSCl the relative rate constants are exclusively governed by repulsive steric effects provoked by the *peri* hydrogen atoms of the alcohol substrates. However, k_{rel} increases with the size of the DED groups at the silyl reagent, and aromatic interactions eventually dominate the silylation reactions with reagents as large as TN*SCl. No significant impact of the reaction temperature on k_{rel} has been found. In contrast, k_{rel} depends notably on the solvent used in the competition experiments. While size effects of the interacting aromatic surfaces appear to be cancelled in solvents with poor hydrogen bond donor abilities like tetrahydrofuran, they magnify as solvent–solute interactions get less important in halogenated solvents such as chloroform or dichloromethane depending to a notable extent on the higher solvophobic effect. Computed reaction free energies for the formation of silyl ether products predict that the dispersion component plays a key role in their thermochemical stability. Furthermore, linear correlations were found between experimental k_{rel} values and the dispersion contribution to the silyl ether formation energy. Therefore, the interplay of attractive dispersion forces and the solvophobic effect enhances relative rates for the silylation of a secondary alcohol up to 4.5 times. In this sense, the combination of sterically less hindered alcohols, tailor-made silyl

chloride reagents with bigger DED groups and thoroughly chosen solvents could enhance rate constants even further than in the systems presented here.

Conflicts of interest

There are no conflicts to declare.

Acknowledgements

Notes and references

1 C. A. Hunter, K. R. Lawson, J. Perkins and C. J. Urch, *J. Chem. Soc., Perkin Trans. 2*, 2001, **5**, 651–669.
2 E. H. Krenske and K. N. Houk, *Acc. Chem. Res.*, 2013, **46**, 979–989.
3 J. K. Klosterman, Y. Yamauchi and M. Fujita, *Chem. Soc. Rev.*, 2009, **38**, 1714–1725.
4 F. Biedermann and H.-J. Schneider, *Chem. Rev.*, 2016, **116**, 5216–5230.
5 A. Lamouroux, L. Sebaoun, B. Wicher, B. Kauffmann, Y. Ferrand, V. Maurizot and I. Huc, *J. Am. Chem. Soc.*, 2017, **139**, 14668–14675.
6 C. Hunter, *Chem. Soc. Rev.*, 1994, **23**, 101–109.
7 M. L. Waters, *Biopolymers*, 2004, **76**, 435–445.
8 J. W. Hwang, P. Li and K. D. Shimizu, *Org. Biomol. Chem.*, 2017, **15**, 1554–1564.
9 C. R. Martinez and B. L. Iverson, *Chem. Sci.*, 2012, **3**, 2191–2201.
10 S. E. Wheeler, *Acc. Chem. Res.*, 2013, **46**, 1029–1038.
11 J. P. Wagner and P. R. Schreiner, *Angew. Chem., Int. Ed.*, 2015, **54**, 12274–12296.
12 S. Grimme, R. Huenerbein and S. Ehrlich, *ChemPhysChem*, 2011, **12**, 1258–1261.
13 S. Grimme and P. R. Schreiner, *Angew. Chem., Int. Ed.*, 2011, **50**, 12639–12642.
14 S. Rösel, C. Balestrieri and P. R. Schreiner, *Chem. Sci.*, 2017, **8**, 405–410.
15 J. N. Israelachvili, *Contemp. Phys.*, 1974, **15**, 159–178.
16 Y. Zhao and J. S. Moore, in *Foldamers: Structure, Properties, and Applications*, ed. S. Hecht and I. Huc, Wiley-VCH Verlag GmbH & Co. KGaA, 2007, ch. 3, pp. 75–108.
17 C. A. Hunter, *Angew. Chem., Int. Ed.*, 2004, **43**, 5310–5324.
18 S. Otto, *Chem. Sci.*, 2013, **4**, 2953–2959.
19 F. Cozzi, F. Ponzini, R. Annunziata, M. Cinquini and J. S. Siegel, *Angew. Chem., Int. Ed. Engl.*, 1995, **34**, 1019–1020.
20 S. L. Cockroft, C. A. Hunter, K. R. Lawson, J. Perkins and C. J. Urch, *J. Am. Chem. Soc.*, 2005, **127**, 8594–8595.

21 S. L. Cockroft, J. Perkins, C. Zonta, H. Adams, S. E. Spey, C. M. R. Low, J. G. Vinter, K. R. Lawson, C. J. Urch and C. A. Hunter, *Org. Biomol. Chem.*, 2007, **5**, 1062–1080.

22 S. E. Wheeler and K. N. Houk, *J. Am. Chem. Soc.*, 2008, **130**, 10854–10855.

23 J. Hwang, P. Li, W. R. Carroll, M. D. Smith, P. J. Pellechia and K. D. Shimizu, *J. Am. Chem. Soc.*, 2014, **136**, 14060–14067.

24 H. Gardarsson, W. B. Schweizer, N. Trapp and F. Diederich, *Chem.–Eur. J.*, 2014, **20**, 4608–4616.

25 H.-J. Schneider, *Acc. Chem. Res.*, 2015, **48**, 1815–1822.

26 L. Yang, C. Adam, G. S. Nichol and S. L. Cockroft, *Nat. Chem.*, 2013, **5**, 1006–1010.

27 L. Yang, C. Adam and S. L. Cockroft, *J. Am. Chem. Soc.*, 2015, **137**, 10084–10087.

28 C. Adam, L. Yang and S. L. Cockroft, *Angew. Chem., Int. Ed.*, 2015, **54**, 1164–1167.

29 L. Yang, J. B. Brazier, T. A. Hubbard, D. M. Rogers and S. L. Cockroft, *Angew. Chem., Int. Ed.*, 2016, **55**, 912–916.

30 J. Hwang, B. E. Dial, P. Li, M. E. Kozik, M. D. Smith and K. D. Shimizu, *Chem. Sci.*, 2015, **6**, 4358–4364.

31 J. Hwang, P. Li, M. D. Smith and K. D. Shimizu, *Angew. Chem., Int. Ed.*, 2016, **55**, 8086–8089.

32 B. Bhayana and C. S. Wilcox, *Angew. Chem., Int. Ed.*, 2007, **46**, 6833–6836.

33 R. Pollice, M. Bolt, I. J. Kobylianskii, I. Shenderovich and P. Chen, *J. Am. Chem. Soc.*, 2017, **139**, 13126–13140.

34 E. H. Krenske, K. N. Houk and M. Harmata, *Org. Lett.*, 2010, **12**, 444–447.

35 J. Helberg, M. Marin-Luna and H. Zipse, *Synthesis*, 2017, **49**, 3460–3470.

36 E. Procházková, A. Kolmer, J. Ilgen, M. Schwab, L. Kaltschnee, M. Fredersdorf, V. Schmidts, R. C. Wende, P. R. Schreiner and C. M. Thiele, *Angew. Chem., Int. Ed.*, 2016, **55**, 15754–15759.

37 T. W. Green and P. G. M. Wuts, in *Protective Groups in Organic Synthesis*, John Wiley & Sons, Inc, 3rd edn, 2002.

38 P. J. Kocienski, *Protecting Groups*, Thieme, Stuttgart, 3rd edn, 2005.

39 P. Patschinski and H. Zipse, *Org. Lett.*, 2015, **17**, 3318–3321.

40 P. Patschinski, C. Zhang and H. Zipse, *J. Org. Chem.*, 2014, **79**, 8348–8357.

41 M. Marin-Luna, P. Patschinski and H. Zipse, *Chem.–Eur. J.*, 2018, submitted.

42 R. K. Akhani, M. I. Moore, J. G. Pribyl and S. L. Wiskur, *J. Org. Chem.*, 2014, **79**, 2384–2396.

43 M. S. Cubberley and B. L. Iverson, *J. Am. Chem. Soc.*, 2001, **123**, 7560–7563.

44 S. L. Cockroft and C. A. Hunter, *Chem. Commun.*, 2006, **0**, 3806–3808.

45 B. U. Emenike, S. N. Bey, B. C. Bigelow and S. V. S. Chakravartula, *Chem. Sci.*, 2016, **7**, 1401–1407.

46 A. S. Rury, C. Ferry, J. R. Hunt, M. Lee, D. Mondal, S. M. O. O'Connell, E. N. H. Phan, Z. Peng, P. Pokhilko, D. Sylvinson, Y. Zhou and C. H. Mak, *J. Phys. Chem. C*, 2016, **120**, 23858–23869.

47 M. J. Kamlet, J. M. Abboud and R. W. Taft, *J. Am. Chem. Soc.*, 1977, **99**, 6027–6038.

48 M. J. Kamlet, J. M. Abboud, M. H. Abraham and R. W. Taft, *J. Org. Chem.*, 1983, **48**, 2877–2887.

49 S. Y. Park, J.-W. Lee and C. E. Song, *Nat. Commun.*, 2015, **6**, 7512.

50 A. D. Becke, *J. Chem. Phys.*, 1993, **98**, 5648–5652.

51 W. Y. C. Lee and R. G. Parr, *Phys. Rev. B*, 1988, **37**, 785–789.

52 S. Grimme, *J. Chem. Phys.*, 2006, **124**, 034108.

53 A. V. Marenich, C. J. Cramer and D. G. Truhlar, *J. Phys. Chem. B*, 2009, **113**, 6378–6396.

54 C. Riplinger and F. Neese, *J. Chem. Phys.*, 2013, **138**, 034106.

55 C. Riplinger, B. Sandhoefer, A. Hansen and F. Neese, *J. Chem. Phys.*, 2013, **139**, 134101.

56 F. Weigend and R. Ahlrichs, *Phys. Chem. Chem. Phys.*, 2005, **7**, 3297–3305.

57 J. Contreras-Garcia, E. R. Johnson, S. Keinan, R. Chaudret, J.-P. Piquemal, D. N. Beratan and W. Yang, *J. Chem. Theory Comput.*, 2011, **7**, 625–632.
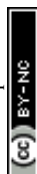
3.1. Supplementary Data of Competition Experiments

3.1.1. Additional Results
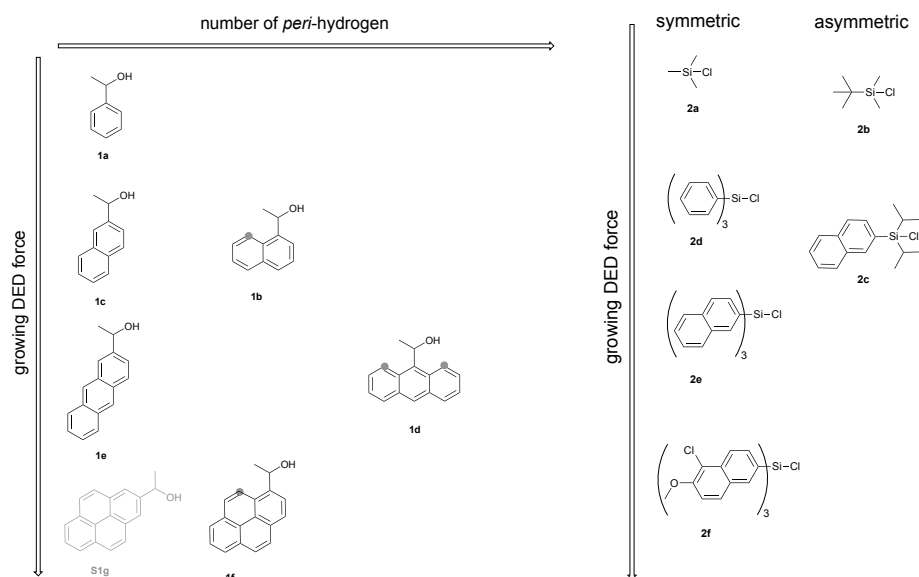
Figure 3.1. Set of investigated alcohols and silyl chlorides shown as a function of their DED force and steric demand. **S1g** was only investigated in these supporting information (SI) but not in the main text of the manuscript and is therefore depicted in grey.

Figure 3.1 shows the set of alcohols and silyl chlorides that was chosen to investigate both the influence of repulsive and attractive steric effects in this study. The goal of this choice is to monitor the interplay of the repulsive and the attractive part of aromatic-aromatic interactions. Mainly looking at symmetric silyl chlorides allows to presume a certain interplay of at least one surface of the silyl chloride with the alcohol. Nevertheless, also two asymmetric silyl chlorides were investigated to see the influence of a mixed set of moieties on the Si-atom. Additionally to the alcohols described in the main text, 1-(2-pyrenyl)ethanol **S1g** was used in competition experiments with **1a** and the most important silyl chlorides **2a**, **2d**, and **2f** (the update version of Figure 2 of the main manuscript is shown in **Figure 3.2**). Indeed, the expected trends are confirmed for **S1g**: In the reaction with small trimethylsilyl chloride TMSCl (**2a**) similar rates are observed for all *peri*-hydrogen free alcohols **1a**, **1c**, **1e**, and **S1g**. Using aromatic silyl chlorides like triphenylsilyl chloride TPSCl (**2d**) a notable size-dependent rate acceleration can be observed depending on the size of the aromatic system. In the case of a 2-pyrenyl-group of **S1g** rates are 1.5 times higher than for phenyl-substituted **1a**. Employing substituted and very bulky silyl chloride **2f** relative rates are even accelerated by a factor of 3 for **S1g**. Thus, for the biggest alcohol system without *peri*-hydrogen the highest relative rates were found. The same data are replotted in **Figure 3.3** sorted by alcohols. Therein, the systematic rate acceleration with increasing aromatic surfaces can be clearly seen for every alcohol. Also the impact of one repulsive 1,5-interactions can be eventually overcome through stabilization by attractive interactions. However, for alcohol **1d** bearing two *peri*-hydrogens those repulsive interactions dominate relative rates in all cases. 9-Anthracenyl is thus not suitable as dispersion

energy donor, as it is also discussed in Chapter 6 for size-accelerated kinetic resolution experiments[1]. The relative rate-constant values and associated standard deviations can be found in **Table 3.1** to **Table 3.5**.
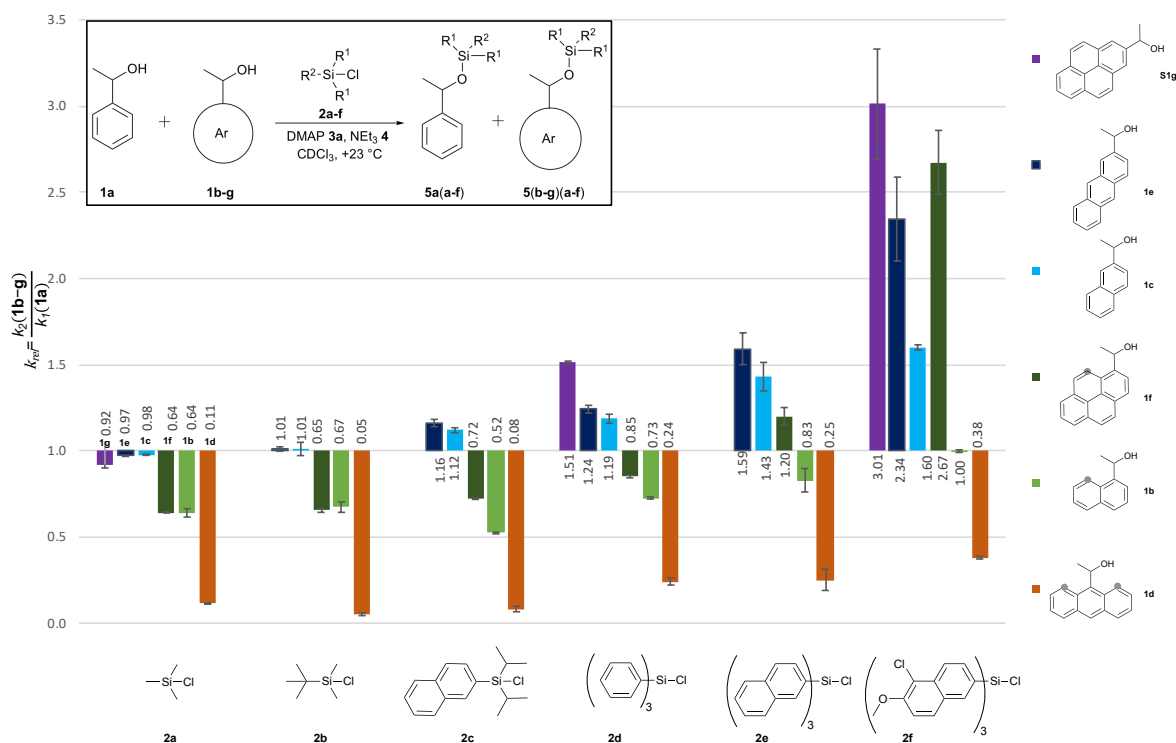
Figure 3.2. Updated Fig. 2 of main text including alcohol **S1g**. Relative rate constants from competition experiments between reference alcohol **1a** and selected secondary alcohols **1b–S1g** with silyl chlorides **2a–f**.
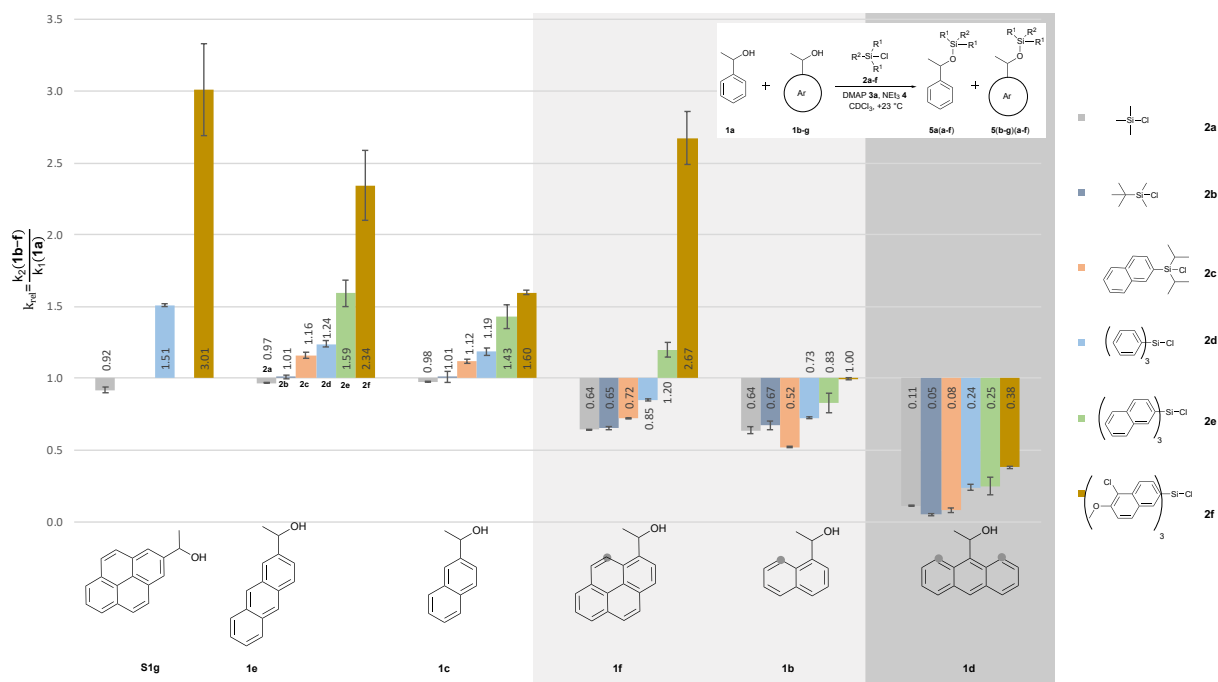
Figure 3.3. Relative rate constants for the silylation of alcohols depending on the size of the silyl chloride. Grey coloured areas indicate the number of *peri*-hydrogens in relevant alcohols.

3.1.2. Table of Competition Experiments Results

Table 3.1. Conversion, corrected chemoselectivity and relative rate constants with standard deviations (derived from five points) calculated from ^{1}H-NMR measurements for competition experiments with alcohol **1a** and **1b**.

Conversion (%)	Chemo-selectivity	Conversion (%)	Chemo-selectivity	Conversion (%)	Chemo-selectivity
	2a		**2b**		**2c**
13.865	-0.175	21.171	-0.159	22.368	-0.277
30.233	-0.191	31.687	-0.170	29.169	-0.272
45.045	-0.166	44.829	-0.155	41.438	-0.242
59.426	-0.145	64.470	-0.125	55.379	-0.206
77.949	-0.096	71.212	-0.085	67.642	-0.169
k_{rel}		k_{rel}		k_{rel}	
0.640±0.024		**0.673**±0.030		**0.523**±0.005	
	2d		**2e**		**2f**
Conversion (%)	Chemo-selectivity	Conversion (%)	Chemo-selectivity	Conversion (%)	Chemo-selectivity
19.894	-0.140	15.553	-0.134	17.325	-0.002
33.497	-0.128	30.387	-0.097	26.192	0.003
46.740	-0.120	44.963	-0.070	39.763	-0.004
61.058	-0.094	58.394	-0.048	52.723	-0.003
75.264	-0.073	74.354	-0.018	66.018	0.001
k_{rel}		k_{rel}		k_{rel}	
0.726±0.006		**0.829**±0.068		**0.998**±0.008	

109

Table 3.2. Conversion, corrected chemoselectivity and relative rate constants with standard deviations (derived from five points) calculated from ^{1}H-NMR measurements for competition experiments with alcohol **1a** and **1c**.

2a		2b		2c	
Conversion (%)	Chemo-selectivity	Conversion (%)	Chemo-selectivity	Conversion (%)	Chemo-selectivity
23.509	-0.009	18.845	0.028	25.520	0.056
32.827	-0.008	31.894	-0.001	29.814	0.044
53.343	-0.008	46.448	-0.010	43.240	0.045
64.271	-0.007	58.237	0.003	56.938	0.033
75.116	-0.007	74.006	0.195	62.470	0.030
k_{rel}		k_{rel}		k_{rel}	
0.977±0.003		**1.010±0.038**		**1.119±0.014**	

2d		2e		2f	
Conversion (%)	Chemo-selectivity	Conversion (%)	Chemo-selectivity	Conversion (%)	Chemo-selectivity
21.114	0.088	21.703	0.120	22.791	0.204
32.374	0.072	23.765	0.145	27.153	0.202
50.573	0.048	36.611	0.137	38.102	0.177
63.154	0.051	51.650	0.134	53.053	0.157
74.976	0.037	64.604	0.120	64.738	0.129
k_{rel}		k_{rel}		k_{rel}	
1.186±0.026		**1.430±0.083**		**1.599±0.015**	

Table 3.3. Conversion, corrected chemoselectivity and relative rate constants with standard deviations (derived from five points) calculated from ¹H-NMR measurements for competition experiments with alcohol **1a** and **1d**.

Conversion (%)	Chemo-selectivity	Conversion (%)	Chemo-selectivity	Conversion (%)	Chemo-selectivity
20.269	-0.750	20.057	-0.860	13.552	-0.789
31.347	-0.724	31.861	-0.863	25.449	-0.809
48.222	-0.658	45.977	-0.834	42.558	-0.762
59.346	-0.573	58.883	-0.713	51.304	-0.734
75.734	-0.338	62.807	-0.624	60.546	-0.652
k_{rel}		k_{rel}		k_{rel}	
0.114±0.004		**0.051**±0.008		**0.082**±0.016	

Conversion (%)	Chemo-selectivity	Conversion (%)	Chemo-selectivity	Conversion (%)	Chemo-selectivity
19.594	-0.528	16.714	-0.645	16.423	-0.410
30.339	-0.571	30.345	-0.594	30.392	-0.388
52.660	-0.446	45.458	-0.478	42.903	-0.358
61.251	-0.402	59.555	-0.363	52.231	-0.309
76.578	-0.261	75.326	-0.228	57.650	-0.296
k_{rel}		k_{rel}		k_{rel}	
0.242±0.021		**0.251**±0.061		**0.380**±0.008	

Table 3.4. Conversion, corrected chemoselectivity and relative rate constants with standard deviations (derived from five points) calculated from ^{1}H-NMR measurements for competition experiments with alcohol **1a** and **1e**.

Conversion (%)	Chemo-selectivity	Conversion (%)	Chemo-selectivity	Conversion (%)	Chemo-selectivity
2a		**2b**		**2c**	
21.353	-0.015	15.479	0.007	12.745	0.061
33.088	-0.011	28.281	0.011	14.871	0.082
49.509	-0.011	40.967	0.000	25.390	0.062
64.805	-0.008	55.161	-0.002	34.317	0.062
79.547	-0.006	66.235	0.004	46.925	0.050
k_{rel}		k_{rel}		k_{rel}	
0.970±0.003		**1.010**±0.013		**1.161**±0.021	
2d		**2e**		**2f**	
Conversion (%)	Chemo-selectivity	Conversion (%)	Chemo-selectivity	Conversion (%)	Chemo-selectivity
28.007	0.099	14.650	0.169	17.612	0.411
33.300	0.096	23.847	0.190	32.237	0.361
48.936	0.072	37.639	0.190	49.407	0.299
61.764	0.061	50.214	0.176	65.953	0.210
75.547	0.045	63.484	0.144	78.651	0.140
k_{rel}		k_{rel}		k_{rel}	
1.241±0.022		**1.592**±0.092		**2.344**±0.243	

Table 3.5. Conversion, corrected chemoselectivity and relative rate constants with standard deviations (derived from five points) calculated from ^{1}H-NMR measurements for competition experiments with alcohol **1a** and **1f**.

Conversion (%)	Chemo-selectivity	Conversion (%)	Chemo-selectivity	Conversion (%)	Chemo-selectivity
	2a		**2b**		**2c**
22.909	-0.191	22.056	-0.177	13.686	-0.145
32.226	-0.183	31.809	-0.172	28.209	-0.136
46.926	-0.157	44.500	-0.153	40.559	-0.125
61.981	-0.130	63.723	-0.122	55.836	-0.103
77.344	-0.094	75.076	-0.103	62.950	-0.096
k_{rel}		k_{rel}		k_{rel}	
0.642±0.003		**0.654**±0.011		**0.722**±0.004	

Conversion (%)	Chemo-selectivity	Conversion (%)	Chemo-selectivity	Conversion (%)	Chemo-selectivity
	2d		**2e**		**2f**
20.342	-0.069	17.691	0.054	14.989	0.451
32.896	-0.069	28.697	0.074	27.020	0.405
48.088	-0.055	45.279	0.066	40.279	0.370
64.070	-0.045	59.617	0.058	53.006	0.319
76.392	-0.039	73.404	0.057	70.551	0.211
k_{rel}		k_{rel}		k_{rel}	
0.850±0.007		**1.199**±0.051		**2.674**±0.184	

Table 3.6. Conversion, corrected chemoselectivity and relative rate constants with standard deviations (derived from five points) calculated from ^{1}H-NMR measurements for competition experiments with alcohol **1a** and **S1g**.

Conversion (%)	Chemo-selectivity	Conversion (%)	Chemo-selectivity	Conversion (%)	Chemo-selectivity
13.99	-0.045	19.05	0.182	7.99	0.535
26.55	-0.032	25.11	0.172	20.53	0.472
60.05	-0.019	36.72	0.162	36.55	0.395
56.21	-0.038	54.40	0.139	53.34	0.306
k_{rel}		k_{rel}		k_{rel}	
0.916±0.019		**1.511±0.013**		**3.005±0.324**	

3.2. Determination of Relative Rate Constants

3.2.1. Experimental Methodology of Competition Experiments

For the competition experiments the stringent adherence to the protocol is vital. All experimental equipment, including calibrated flasks, NMR-tubes, gas chromatography vials (GC-vials), magnetic stir bars, was dried in the oven at 110°C overnight prior to use. All Hamilton syringes were cleaned with acetone, dried under vacuum, and flushed with nitrogen. The GC-vial holder (Shimadzu 221-44998-91) was connected to the circuit of a cryostat maintaining +23 °C (noted temperatures, resp.) constantly and placed on a magnetic stirrer. The speed of stirring was fixed at 750 rpm for all the experiments described in the following. Calibrated flasks of various sizes (1 mL, 2 mL, 5mL, 10 mL and 20 mL) are placed in a Schlenk flask and evacuated and purged with N_2 for three times. The compounds are weighed in and the solvent is applied via Hamilton syringe under N_2-atmosphere in the same Schlenk flask. The stock solutions are kept in a nitrogen-filled desiccator until employed. A guideline for the preparation of the stock solutions is shown for an example reaction below. All percentages and equivalents are regarding the concentration of both alcohols together (0.2 M). Stock A contains the alcohols **1a** and **1f** in a concentration of 0.1 M each. Stock solutions B_1 to B_5 contain the silyl chloride **2e** in different concentrations (20%, 35%, 50%, 65% and 80% of 0.2 M). Stock solution C contains the catalyst **3a** (0.09 M, 15%) and triethyl amine (**4**, 1.17 eq).

Table 3.7. Composition of stock solutions for competition experiments.

name of stock solution	compounds in stock solution
Stock A	1:1 – mixture of alcohol **1a** and competing alcohol
Stock B	silyl chloride (conc. regarding both alcohols in%)
B_1	20%
B_2	35%
B_3	50%
B_4	65%
B_5	80%
Stock C	Catalyst (conc. reg. both alcohols in%) + Et$_3$N (1.15 eq reg. both alcohols)

1a   1f   2e   4   3a
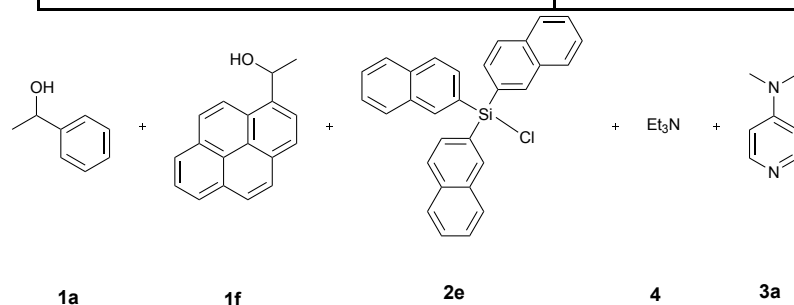
Scheme 3.1. Example of a competition experiment with alcohols **1a** and **1f**, silylation agent **2e**, catalyst DMAP (**3a**) and triethylamine (**4**).

Table 3.8. Preparation of initial stock solutions for competition experiments.

		c [mol/l]	Vol. Flask [mL]	N [mmol]	M.W	m [mg]
Stock A	1a	0.10	10.00	1.00	122.17	122.17
	1f	0.10	10.00	1.00	222.29	222.29
Stock B_1 (20%)	2e	0.04	2.00	0.08	445.03	35.60
Stock B_2 (35%)	2e	0.07	2.00	0.14	445.03	62.30
Stock B_3 (50%)	2e	0.10	2.00	0.20	445.03	89.01
Stock B_4 (65%)	2e	0.13	2.00	0.26	445.03	115.71
Stock B_5 (80%)	2e	0.16	2.00	0.32	445.03	142.41
Stock C	3a	0.23	10.00	2.30	101.19	232.74
	4 (15%)	0.03	10.00	0.30	122.17	36.65

An oven dried empty GC-vial is transferred to a Schlenk flask. The Schlenk flask containing the vial and the cap is three times evacuated and flushed with nitrogen. Now 0.5 mL of the stock solutions are transferred in the GC-vial via a Hammilton-type syringe in the order A (mixture of alcohols), C

(catalyst **3** and triethylamine **4**) and B_x (silyl chloride in the corresponding concentration). Then, the GC-vial is capped under nitrogen and placed quickly in the tempered GC-vial and stirred at 750 rpm for the stated time. The reaction is monitored by ^{1}H-NMR of the sample with the highest concentration of silylation agent. An oven dried NMR tube is evacuated and flushed with N_2 three times. The caped GC-vial containing the reaction mixture is placed in a special Schlenk flask and evacuated and vented three times with N_2. Now, 0.6 mL of the reaction solution is transferred via syringe into the NMR-tube, caped and sealed with Parafilm[©]. The NMR spectrum is measured using a 600 MHz NMR machine.

3.2.2. Analysis of Competition Experiments

^{1}H-NMR spectra are processed using MestReNova[©]. Automated phase correction and a Bernstein polynomial fit with polynomial order 3 are applied, the spectra are referenced by the $CDCl_3$ solvent signal ($\delta = 7.26$ ppm). If possible the α-hydrogen signal of the two alcohols and the two silyl ethers is integrated in each of the spectra. If those signals are overlapping, the corresponding methane-signal is used instead.
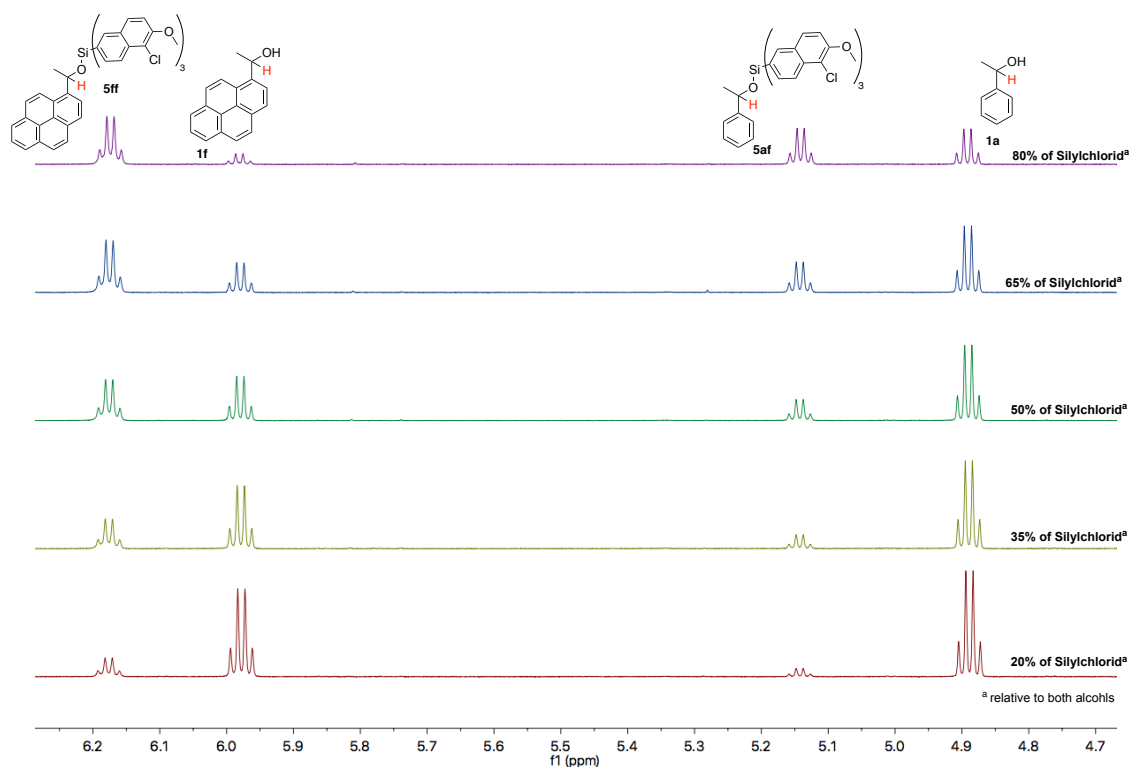
Figure 3.4. Representative example of stacked spectra with the relevant signals.

As we were able to rule out that after the end of the reaction the product ratio is varied through equilibration processes (see Chapter 3.4.3), relative rate constants can be calculated from the product ratios. Relative rate constants (equal to selectivity *s*) are defined for competition experiments described by the general equations shown in **Scheme 3.2** relative to the rate constant for the silylation of 1-phenylethanol (**1a**) (Eq. 3.1).
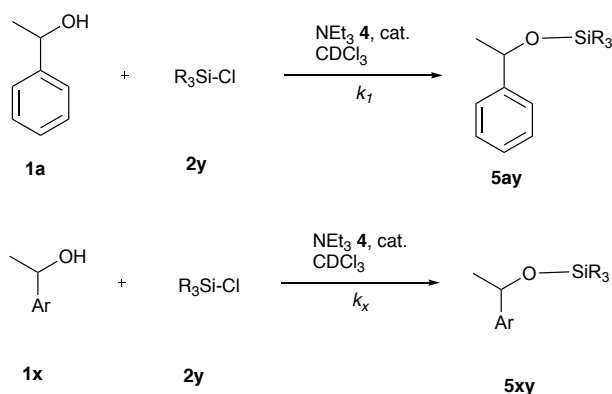
Scheme 3.2. General equation of the competing reactions.

$$s = k_{rel} = \frac{k_x}{k_1} = \frac{k_{(1x+2y)}}{k_{(1a+2y)}}$$

<div align="right">Eq. 3.1</div>

Selectivity can be readily calculated from the chemoselectivity and the conversion. The exact conversion is calculated by Eq. 3.2, whereby the integrals of the ^{1}H-NMR spectra are used to determine concentrations.

$$conversion\ [\%] = \left(\frac{[5ay] + [5xy]}{[1a] + [1x] + [5ay] + [5xy]}\right) \cdot 100$$

<div align="right">Eq. 3.2</div>

Regarding the definition of selectivity in Eq. 3.1, the experimental chemoselectivity C_{exp} is defined by Eq. 3.3.

$$C_{exp} = \frac{[5xy] - [5ay]}{[5xy] + [5ay]}$$

<div align="right">Eq. 3.3</div>

This definition of C_{exp} presumes an exact 1:1 ratio of both reactants **1a** and **1x**. To eliminate errors from small deviations of this ratio due to unavoidable experimental inaccuracies, a correction factor is introduced, that calculates the actual initial ratio of both reactants by Eq. 3.4.

$$f = \frac{[1x]_0}{[1a]_0} = \frac{[1x] + [5xy]}{[1a] + [5ay]}$$

<div align="right">Eq. 3.4</div>

The effective chemoselectivity C can then be calculated as

$$C = \frac{[5xy] - [5ay] \cdot f}{[5xy] + [5ay] \cdot f}$$

<div align="right">Eq. 3.5</div>

In this project, always this effective chemoselectivity C is reported. Having the chemoselectivity C and the conversion in hand, the selectivity s, which corresponds to the relative rate constant, can be calculated by Eq. 3.6.[2] The stated numbers are the average of five experiments with various amounts (20%, 35%, 50%, 65%, 80% of both alcohols) of silyl chlorides.

$$k_{rel} = s = \frac{\ln\left(1 - conv(1 + C)\right)}{\ln\left(1 - conv(1 - C)\right)}$$

<div align="right">Eq. 3.6</div>

3.2.3. Simulation of Competition Experiments

Competition experiments were simulated using CoPaSi[3] as shown in **Scheme 3.3**.

$$[Cat] + [SiCl] \quad \underset{k_{-1}}{\overset{k_1}{\rightleftharpoons}} \quad [Cat\text{-}Si]^+ + [Cl]^-$$

$$[R1\text{-}OH] + [Cat\text{-}Si]^+ \quad \overset{k_{silyl1}}{\longrightarrow} \quad [R1\text{-}OSi] + [Cat\text{-}H]^+$$

$$[R2\text{-}OH] + [Cat\text{-}Si]^+ \quad \overset{k_{silyl2}}{\longrightarrow} \quad [R2\text{-}OSi] + [Cat\text{-}H]^+$$

$$[Cat\text{-}H]^+ + [Et_3N] \quad \overset{k_3}{\longrightarrow} \quad [Cat] + [Et_3N\text{-}H]^+$$
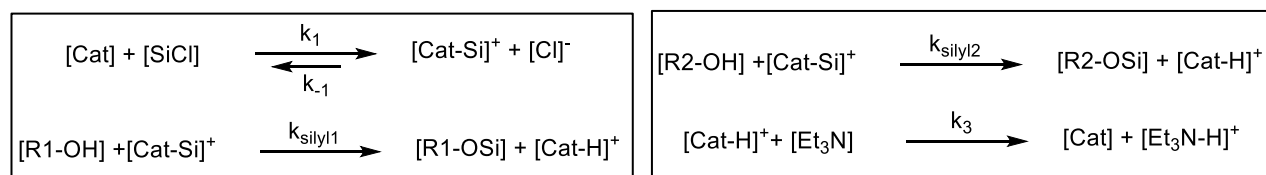
Scheme 3.3. Reaction model for the simulation of selectivity curves.

Presuming that the reaction between the alcohol and the loaded catalyst is the rate limiting step, the values of k_1, k_{-1} and k_3 were fixed for all the simulations to:

$$k_1 = 0.1 \frac{l}{mol\ s}\ ; k_{-1} = 0.001 \frac{l}{mol\ s}; k_3 = 0.1 \frac{l}{mol\ s}.$$

Setting arbitrarily $k_{silyl1} = 0.01 \frac{l}{mol\ s}$, k_{silyl2} can be calculated using the relative rate constant received from Eq. 3.6 by:

$$k_{silyl2} = k_{rel} \cdot k_{silyl1} = k_{rel} \cdot 0.01 \frac{l}{mol \cdot s} \qquad \text{Eq. 3.7}$$

From those rate constants and the experimental starting concentration, the concentrations of all relevant species along the reaction path were simulated by CoPaSi. The resulting time and concentration values were used to calculate the chemoselectivity by Eq. 3.3 and the conversion by Eq. 3.2. Plotting those values using ProFit[4] allowed us to compare experimental results with the simulation and to verify the calculated relative rate constants as shown in in **Figure 3.5** to **Figure 3.9**.
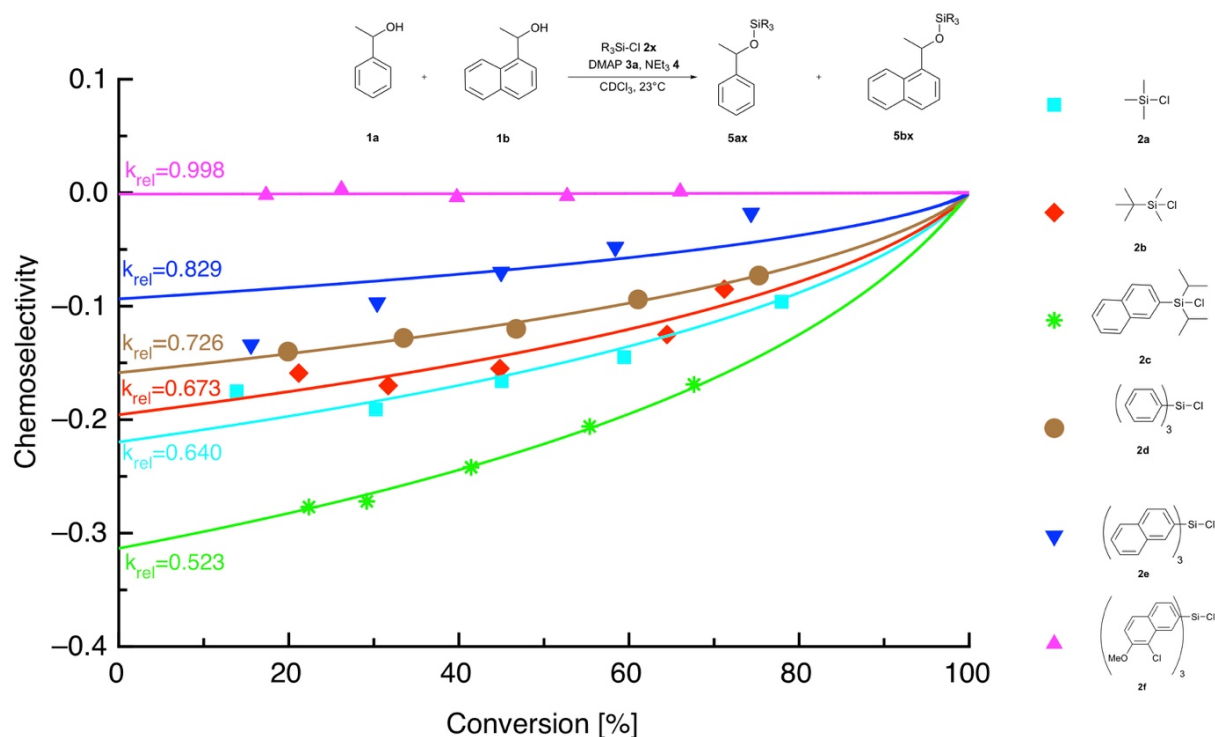
Figure 3.5. Plot of conversion vs. chemoselectivity values for competition experiments of alcohol **1a** and **1b**. The curves for the average relative rate constant were simulated using CoPaSi.
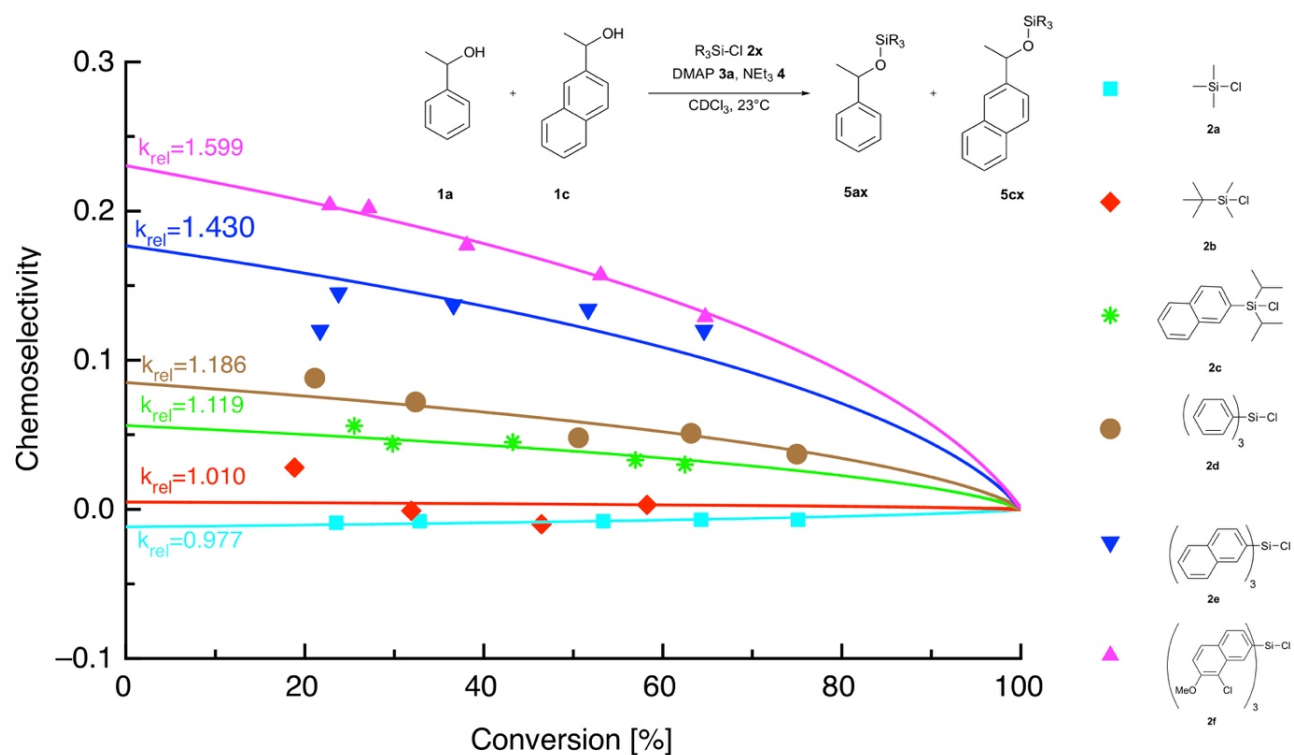
Figure 3.6. Plot of conversion vs. chemoselectivity values for competition experiments of alcohol **1a** and **1c**. The curves for the average relative rate constant were simulated using CoPaSi.
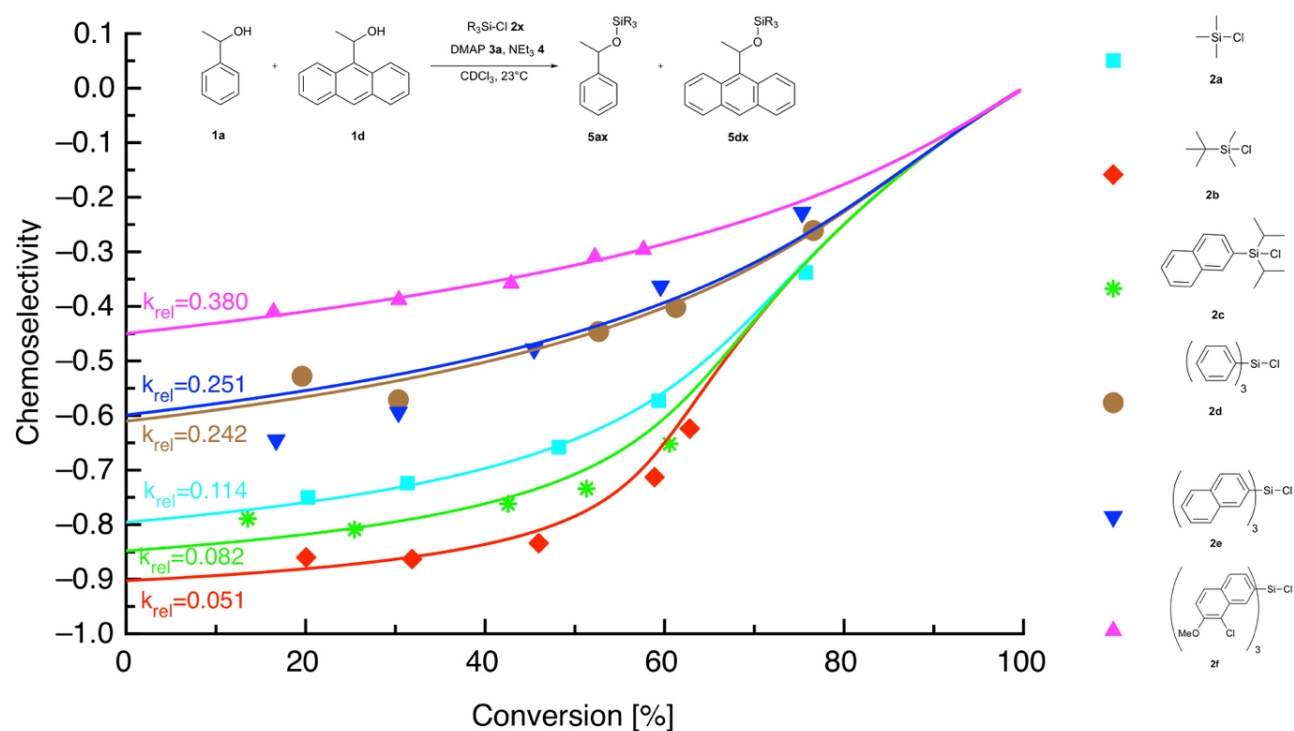
Figure 3.7. Plot of conversion vs. chemoselectivity values for competition experiments of alcohol **1a** and **1d**. The curves for the average relative rate constant were simulated using CoPaSi.
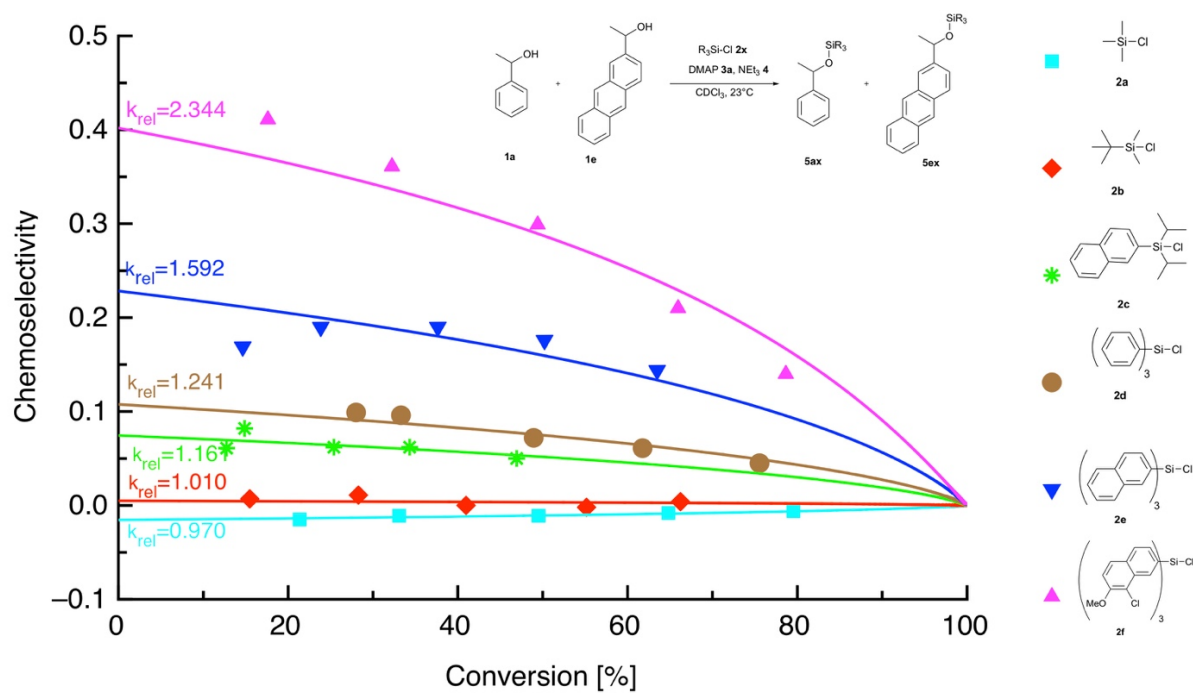
Figure 3.8. Plot of conversion vs. chemoselectivity values for competition experiments of alcohol **1a** and **1e**. The curves for the average relative rate constant were simulated using CoPaSi.
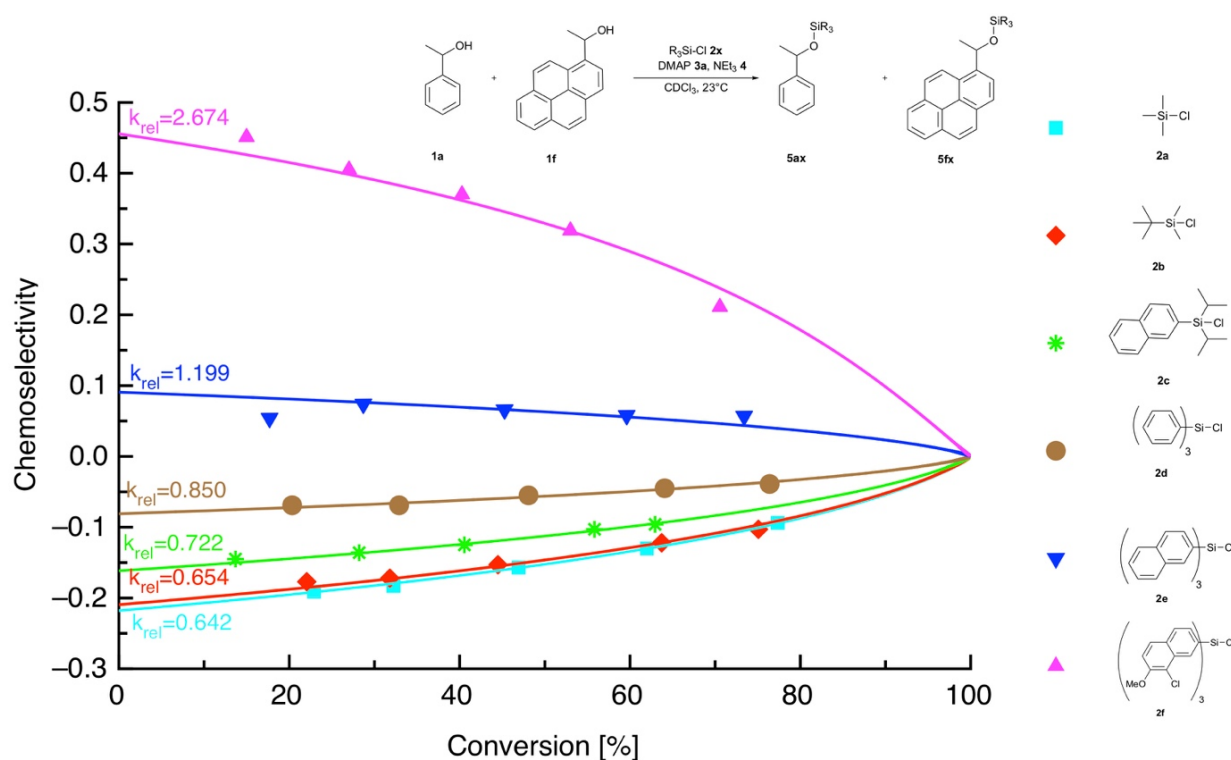
Figure 3.9. Plot of conversion vs. chemoselectivity values for competition experiments of alcohol **1a** and **1f**. The curves for the average relative rate constant were simulated using CoPaSi.

3.3. Investigation of Solvent Effects

3.3.1. Methodology of Solvent Competition Experiments

The influence of various solvents on the relative rate constant was investigated. As a benchmark reaction, the competition experiment between alcohol **1a** and **1f** and silyl chloride **2e** was used (**Scheme 3.4**). Reason for the choice of this reaction were, that 1) we were able to observe small influences of the solvent as rate constants of both alcohols are quite similar (k_{rel} = 1.20 in CDCl$_3$); 2) alcohol **1e** shows as well attractive dispersive forces as repulsive steric effects, so it is possible to examine the whole scope of solvent effects.
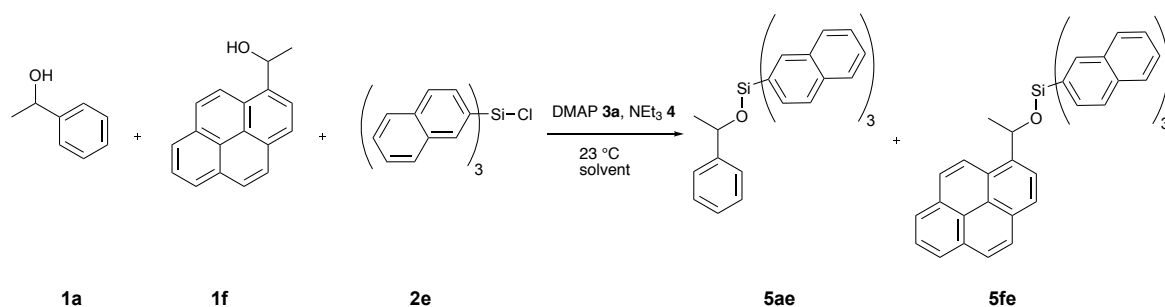
Scheme 3.4. Benchmark reaction used for solvent screening.

The competition experiments were proceeded as similar as possible to the method described in chapter 3.2.1. Instead of measuring five different conversions, the experiment with 50% of silyl chloride relative to both alcohols was repeated three times. All solvents were purchased "extra dry" or were dried following typical procedures (see chapter 3.5.1).[5] To be able to measure ^{1}H-NMR spectra after full conversion, different methods had to be applied:

Method A: As far as possible and reasonable the experiments were done in deuterated solvents (DMSO, Acetone, DCM). With 0.6 mL of the reaction mixture a ^{1}H-NMR spectrum was measured, using the corresponding solvent residual signal as reference.

Method B: If hydrogen-atom-free solvents (CS$_2$, C$_6$F$_6$, CCl$_4$) were used, after full conversion 0.3 mL of the reaction mixture and 0.3 mL of CDCl$_3$ were mixed in the NMR-tube and a ^{1}H-NMR spectrum using the CDCl$_3$-signal as a reference was recorded.

Method C: In all other cases after full conversion the solvent was removed under reduced pressure using a cannula through the septum of the GC-vial. Then the vial was purged with N$_2$ and 1.5 mL of CDCl$_3$ were added in order to resolve the reaction mixture. 0.6 mL of this solution were transferred to a NMR-tube and a ^{1}H-NMR using the CDCl$_3$-signal as a reference was recorded.

To ensure that all methods lead to the same result, some experiments were carried out using different methods as well as different amounts of silyl chloride. As **Table 3.9** shows, the results are reproducible among the different conditions.

Table 3.9: Relative rate constants in different solvents measured using different methods..

Solvent	Method	Amount of silyl chloride	Relative rate constant
DCM	A	20%	1.354±0.025
	C	50%	1.379±0.036
CCl$_4$	B	50%	0.836±0.047
	C	50%	0.868

Several solvents had to be excluded due to bad solubility or unwanted side reactions (compare **Table 3.10**).

Table 3.10. Not suitable solvents for competition experiments of the benchmark reaction following **Scheme 3.4**.

Solvents	Problem
Hexafluoropropanol, Acetonitrile (pure), *tert*-Amylalcohol (pure), Diethyl ether, Triethylamine, Methyl *tert*-Butyl Ether, *N,N*-Diisopropylethylamine	silyl chloride **2e** and **2f** not soluble
Hexafluorobenzene (pure)	Alcohol **1f** not soluble
Dichloromethyl methyl ether	Side reaction with NEt$_3$ and alcohols

If a possibly reactive solvent (acetone, DMSO, *tert*-amylalcohol[6]) was used, a blind probe was performed. Therefore, silyl chloride **2e**, DMAP (**3a**) and triethylamine (**4**) were solved in the corresponding solvent. A ^{1}H-NMR spectrum was recorded to ensure, that no background reaction with the solvent did happen. In the case of DMSO a non-specified background reaction between solvent and silyl chloride occurred in the blind probe, which led to the precipitation of NEt$_3$HCl. This led to a lower conversion rate than expected in the competition experiments.

3.3.2. Results of Solvent Experiments

The results in **Figure 3.10** show the big influence of the solvents on the relative rate constants, as long as the DED **2e** is used as silylation agent. In the case of non-aromatic TMSCl (**2a**) the effect of solvents is minor. Interestingly the relative rate constant with **2e** approach those of the "size-effect-free" reaction with TMSCl (**2a**) for several solvents. This allows to state that for those solvents size effects plays only a minor role in the formation of the silyl ethers, even if the reactants bear two big surfaces. To prove that the differences in rate constants are due to the influence of the solvent on size effects, competition experiments with different systems were carried out in the three solvents THF, CDCl$_3$ and DCM (**Figure 3.11**).
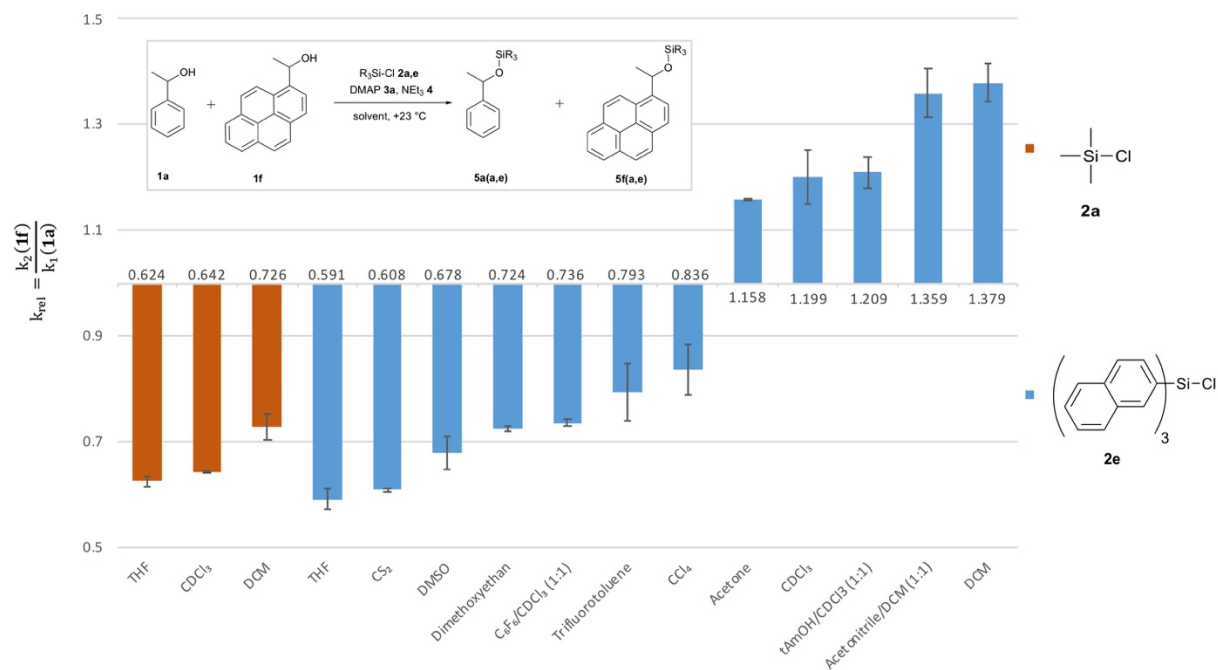
Figure 3.10. Relative rate constants of competition experiment between alcohol **1a** and **1f** with silyl chloride **2a** or **2e** in various solvents.
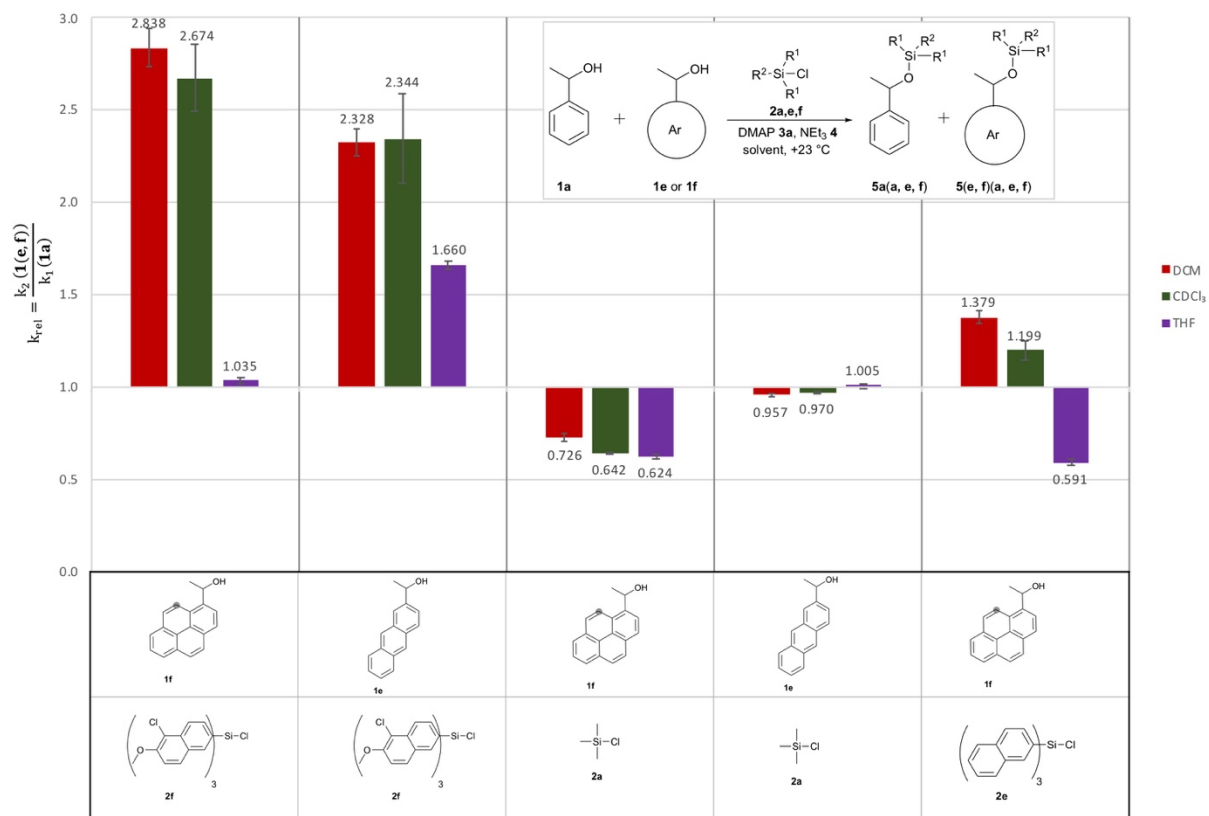
Figure 3.11. Relative rate constants in DCM, CDCl₃ and THF for various alcohols and silyl chlorides.

In these results the following trends can be observed:

1. The observed solvent effects are closely related to size effects. If systems without a high degree of aromatic overlapping like those with TMSCl (**2a**) are investigated, the change of solvent does not affect selectivities.

2. THF seems to lower size effects dramatically compared to CDCl₃ and DCM. Therefore, the influence on dispersive interaction seems to be a solvent property.

3. The rate constants for the investigated alcohol only vary between DCM and CDCl₃ if alcohol **1f** is used. The main difference between **1f** and **1a** is the possibility of 1,5-interactions between the *peri* hydrogen atoms and the hydroxyl reactive site in the case of alcohol **1f**. It is likely that DCM lowers those interactions, while CDCl₃ and THF do not influence on them. This could also explain why alcohol **1f** reacts a little faster with TMSCl (**2e**) in DCM than in CDCl₃ and THF.

3.3.3. Short Overview of Selected Solvent Parameters

In order to find an explanation for the differences in rate constants due to different solvents, herein a short overview of the different used solvent parameters is given.

Kamlet-Taft developed the linear solvation energy relationship which allows to distinguish the different contributions of hydrogen-bond donor (α), hydrogen-bond acceptor (β), polarizability (π^* and δ) to solvation.[7] Abraham eventually refined this scale naming the new hydrogen-bond basicity and acidity parameters β_2^H and α_2^H.[8] One of the major limitations of the both models is, that all less polar hydrogen-bond donor than CCl₄ were assigned due to the experimental determination with $\alpha = 0$ leading to an error for non-polar solvents. The interpretation of all intermolecular interactions except aromatic stacking as interactions between electron-rich and electron-poor regions of a molecule and therewith as a form of hydrogen bonds, Hunter redefined α and β as a function of the maximal and minimal energy of the molecules' electrostatic potential surface.[9] The energy that is needed to break the intermolecular forces between solvent molecules in order to bring them to gas phase can be described by the internal energy of vaporization $\Delta_{vap}U°$. Through norming this value by division through the molar volume of the solvent as shown in Eq. 3.8 the cohesive energy density (*ced*) can be calculated.[10]

$$ced = \frac{\Delta_{vap}U°}{V_m}$$

Eq. 3.8

The Hildebrand parameter δ_H is closely related to the *ced* by Eq. 3.9.[10c]

$$\delta_H = \sqrt{ced} = \left(\frac{\Delta_{vap}U°}{V_m}\right)^{\frac{1}{2}}$$

Eq. 3.9

Therefore, *ced* and δ_H are indicators for the strength of the intermolecular forces between solvent molecules. Hansen expanded Hildebrand's understanding of solubility by accounting for three

different forces that influence the solubility of a compound. These are dispersive forces (δ_d), polar forces (δ_p) and hydrogen bonds (δ_h).[11]

$$\delta_H^2 = \delta_d^2 + \delta_p^2 + \delta_h^2 \qquad\qquad \text{Eq. 3.10}$$

The three Hansen parameters are empirical parameters that are determined experimentally. The compound is therefore solved in a solvent in which it is good soluble. Solvents in which the compound is insoluble are eventually added to determine the mixture at which phase separation takes place. Putting those number in a three-dimensional sphere gives the numbers of interest.[11b] The solvent parameter E_T (30) is built on the solvatochromism of Reichardt's dye 30 to describe the polarity of a solvent. The stronger the polar interactions between the polar dye and the solvent molecules are, the shorter the wavelength of absorbed light gets. The E_T (30) is gained by measuring an UV/Vis-spectrum of the solved dye and putting the resulting maximum of absorption in Eq. 3.11.[12] The E_T (30) value is an indicator for the polarity of a solvent.

$$E_T (30) = hcN_A\tilde{v}_{max} \qquad\qquad \text{Eq. 3.11}$$

Similarly, for Catalán's polarity-polarizability scale (SPP) the UV/vis-spectrum of 2-(dimethylamino)-7-nitrofluorene (DMANF) is investigated. As the solvation of DMANF is driven as well by van der Waals forces as polar intermolecular interactions, this scale measures both polar and nonpolar solvent properties.[13] In contrast for the solvent polarizability scale (SP) a nonpolar dye is used, so that only dispersive interactions are involved in the solvation process and only these interactions will determine the maximum absorption. As dispersive interactions are a function of the polarizability of both compounds, the obtained values can be used to set up a relative scale of polarizabilities of solvents.[14] Presuming that SPP is measuring nonpolar and polar interactions, whereas SP measures only the nonpolar part, it is possible compare those scales, in order to get a scale of the polar interactions. Polar interactions are caused by the permanent dipole moment of a molecule, which allows to derive the solvent dipolarity scale (SdP).[15]

3.3.4. Tables of Relative Rates and Relevant Solvent Parameters

Table 3.11. Relative rate constant for the competition experiment of alcohol **1a** and **1f** with silyl chloride **2e**, Hunter parameter and Kamlet-Taft parameters. These parameters were used to fit parameters and predict ln k_{rel}. [a] Calculated from α_2^H by $\alpha = 4.1(\alpha_2^H + 0.33)$. [9] [b] Geometry of solvents was optimized at B3LYP/6-31G(d) level of theory, maxima and minima of the electrostatic potential surface were calculated by using Multiwfn 3.6 program [16] over the isodensity surface with a radius=0.002 Bohr Å^{-3}. [17] [c] Calculated from β_2^H by $\beta = 10.3(\beta_2^H + 0.06)$. [9]

	k_{rel}	ln(k_{rel})	StDev ln(k_{rel})	α[17]	β[17]	ln (k_{rel}) predicted	$\pi*$[18]	β[18]	α[18]	δ[18]	ln (k_{rel}) predicted
				Hunter hydrogen-bond donor	Hunter hydrogen-bond acceptor	- 1.13 + 0.66 α + 0.032 β	Kamlet-Taft polarization parameter	Kamlet-Taft hydrogen-bond acceptor parameter	Kamlet-Taft hydrogen-bond donor parameter	Kamlet-Taft polarizability correction factor	-0.34 -0.24 $\pi*$ +0.26 β +3.67 α +0.27 δ
THF	0.591±0.018	-0.526	0.031	0.8[b]	5.9	-0.42	0.55	0.55	0.00	0.00	-0.33
CS$_2$	0.608±0.004	-0.498	0.007	0.9[b]	1.3[19],[c]	-0.47	0.51	0.07	0.00	0.00	-0.44
Dimethoxy-ethan	0.724±0.006	-0.322	0.008	0.8[b]	5.3	-0.43	0.53[7]	0.41[7]	0.00[7]	0.00[7]	-0.36
Trifluorotoluene	0.793±0.055	-0.232	0.069	1.3[b]	1.7[b]	-0.25	0.64[20]	0.00[20]	0.00[20]	1.00[20]	-0.22
CCl$_4$	0.836±0.047	-0.179	0.056	1.4	0.6	-0.19	0.21	0.10	0.00	0.50	-0.23
Acetone	1.158±0.002	0.147	0.002	1.5[21],[a]	5.7[21],[c]	0.04	0.62	0.48	0.08	0.00	-0.07
CDCl$_3$	1.199±0.051	0.182	0.051	2.2	0.8	0.34	0.69	0.10	0.20	0.50	0.39
DCM	1.379±0.036	0.321	0.027	1.9	2.0	0.18	0.73	0.10	0.13	0.50	0.13
DMSO	0.678±0.031	-0.389	0.045	0.8[9]	8.9	-0.32	1.00	0.76	0.00	0.00	-0.38

Table 3.12. Compilation of relative rate constants and solvent parameters. Solvent mixtures are reported in v/v. For deuterated solvents the value of the non-deuterated solvents are given. [a]Relative rate constants and standard deviations of the competition experiment shown in **Scheme 3.4**. [b]ced values were calculated from the Hildebrand solubility parameters by ced=δ_H^2. [c]For solvent mixtures a linear relationship between the parameters of pure solvents depending on the v/v%-composition was assumed. As only 1:1-mixtures were used, the given values were calculated as the average of the values of the corresponding solvent. [d]In the case of DMSO a non-specified background reaction between solvent and silyl chloride occurred in the blind probe, which led to the precipitation of NEt$_3$HCl.

	$k_{rel} = \dfrac{k(1f)}{k(1a)}$ [a]	ced[10c, 22] [cal/cm³][b] Intermolecular forces of solvent molecules	$E_T(30)$[12b] [kcal/mol] polarity	SP[14-15] Solvent Polarizability	SdP[15] Solvent Dipolarity	δ_d[23] Hansen dispersion parameter	δ_p[23] Hansen polar parameter	δ_h[23] Hansen Hydrogen-bond parameter
THF	**0.591**±0.018	86.3	37.4	0.7139	0.634	16.8	5.7	8.0
CS$_2$	**0.608**±0.004	99.5	32.8	1.000	0	20.2	0	0.6
DMSO[d]	**0.678**±0.031	169.2	45.1	0.829	1.000	18.4	16.4	10.2
Dimethoxyethan	**0.724**±0.006	78.3	38.2	0.680	0.625	15.4	6.3	6
C$_6$F$_6$/CDCl$_3$ (1:1)	**0.736**±0.008	77.5[c]	36.7[c]	0.7031[c]	0.433[c]	15.8[c]	5.2[c]	3.5[c]
Trifluorotoluene	**0.793**±0.055	68.3	38.7	0.6938	0.663	17.5	8.8	0
CCl$_4$	**0.836**±0.047	74.1	32.4	0.7677	0	17.8	0	0.6
Acetone	**1.158**±0.002	92.8	42.3	0.6510	0.907	15.5	10.4	7.0
CDCl$_3$	**1.199**±0.051	85.4	39.0	0.7833	0.614	17.8	3.1	5.7
tAmOH/CDCl$_3$ (1:1)	**1.209**±0.03	97.7c	40.2 [c]	n.a.	n.a	16.7c	4.7c	9.5[c]
AcCN/DCM (1:1)	**1.359**±0.046	118.9[c]	43.15[c]	0.7030[c]	0.872[c]	16.2[c]	12.5[c]	6.7c
DCM	**1.379**±0.036	98.5	40.7	0.7612	0.769	17	7.3	7.1

3.3.5. Discussion of the Influence of Solvent Properties on the Rate Constant

In order to analysis the influence of solvent properties on the relative rate constant a linear solvation energy relationship was performed, as recent research proved it a suitable way for rationalizing solvent effects in noncovalent interactions.[24] Analysis of experimental k_{rel} with literature parameters (**Table 3.11**) and fitting the parameters for hydrogen-bond donor (α), hydrogen-bond acceptor (β) and polarizability (π^* and δ) with StatPlus[25] led to Eq. 3.12.

$$k_{rel} = -0.34 - 0.24\ \pi^* + 0.26\ \beta + 3.67\ \alpha + 0.27\ \delta \qquad \text{Eq. 3.12}$$

Eq. 3.12 strikingly proves, that solvent effects are widely independently of the polarizability of the solvent but correlate strongly with the hydrogen bond donor ability of the solvent.
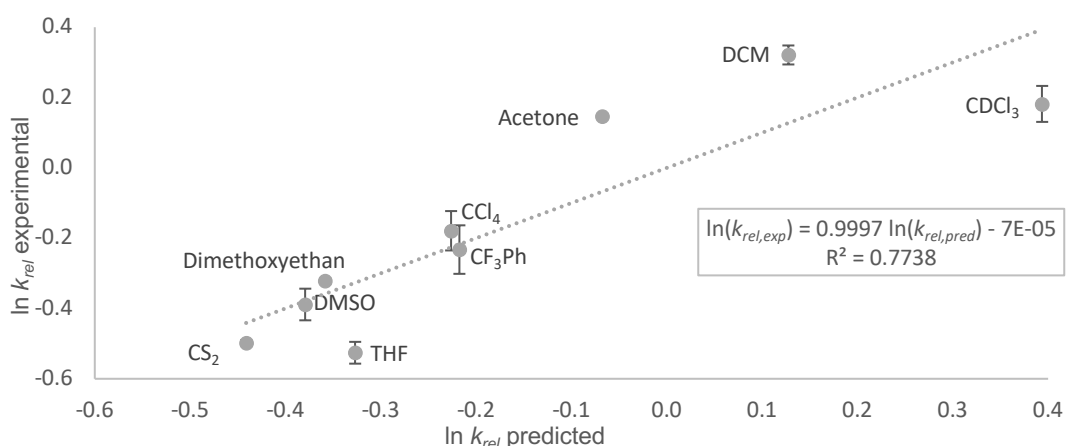
Figure 3.12. Kamlet-Taft-Plot of predicted ln k_{rel} values using Eq. 3.12 against experimental ln k_{rel} values.

The plot of predicted and experimental values in **Figure 3.12** gives a moderate correlation. One of the major limitations of the Kamlet-Taft-model is, that all less polar hydrogen-bond donor than CCl_4 were assigned due to the experimental determination with α=0 leading to an error for non-polar solvents. Indeed, using Hunter's α and β values and fitting parameters led to Eq. 3.13.

$$k_{rel} = -1.13 + 0.66\ \alpha + 0.032\ \beta \qquad \text{Eq. 3.13}$$
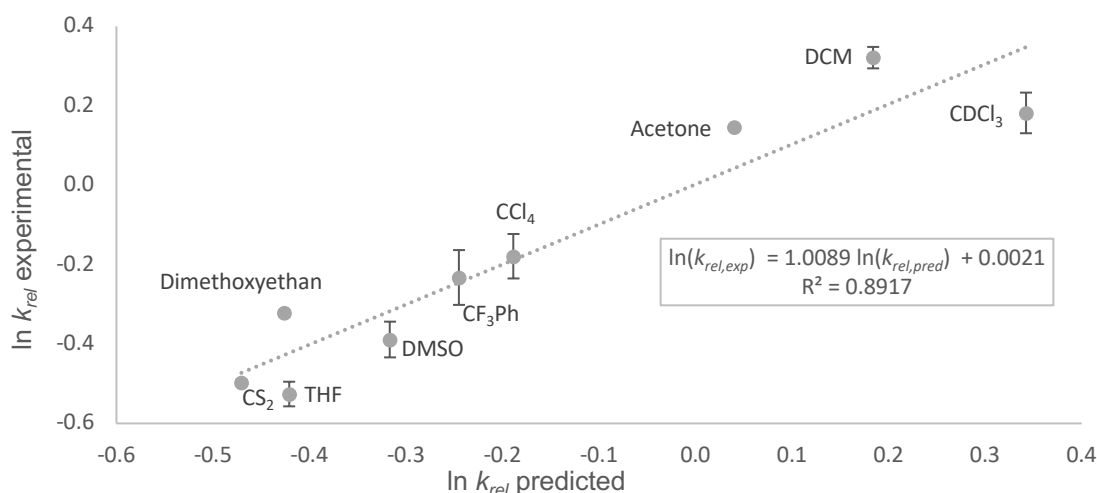
Figure 3.13. Predicted ln k_{rel} values using Hunter's parameter and Eq. 3.13 against experimental ln k_{rel} values

Figure 3.13 shows a good correlation of predicted and experimental ln k_{rel} values. A closer look to Eq. 3.13 reveals that ln k_{rel} is mainly influenced by its α value, simplifying the discussion by using Fig. 4 of the main text.
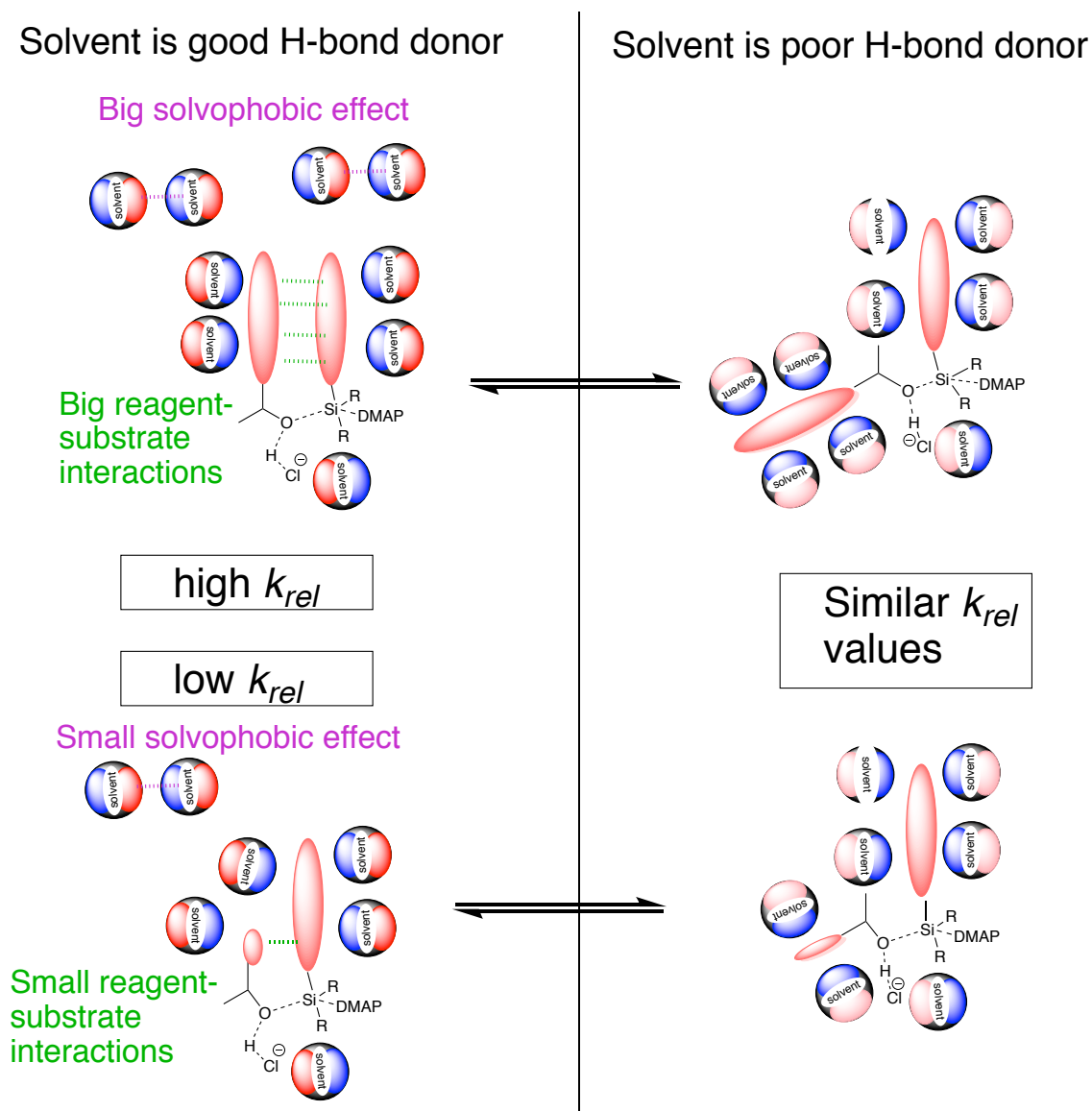
Figure 3.14: Graphical explanation of solvent effects. Right side: reaction in a solvent with an α value smaller than α of C-H-bonds. Solvent molecules accept H-bonds from the aromatic surfaces and in order to maintain these interactions the transition state is more likely in a conformation without aromatic overlapping. Therefore, size effects cannot influence k_{rel}. Left side: the solvent is a good hydrogen bond donor itself and prefers interacting with other solvent molecules. These interactions cause the solvophobic effect but also allows attractive interactions between the aromatic moieties of alcohol and the silyl to take place. Thus, the reaction with the higher degree of aromatic overlapping is enhanced. For solvents with low α a higher *ced* even pushes the equilibrium further on the right side as solvent-solute interactions get stronger, too. Only in solvents with a high α the discussion about the contribution of solvophobic effect vs. dispersive interactions is meaningful. A higher *ced* strengthens the solvophobic effect, dispersive interactions are temperature independent and can be quantified by computational methods. Those studies show that both effects work together in enhancing reaction rates through size effects.

Interestingly, the calculated hydrogen-bond donor ability for aromatic C-H groups was found to be in the range of $\alpha = 1.0$ - 1.4.[9] This could comprise a part of the explanation of solvent effects (see **Figure 3.14**). If solvent molecules are an even worse hydrogen-bond donor than the aromatic CH-bonds of the solute, hydrogen-bonds arise between solvent and these aromatic C-H-bonds. Compared to these solvent-solute interactions the attractive interactions that arise from the aromatic

surfaces of the reactants are minor and their influence on the stability of the transition state is diminished. Particularly the stronger interaction of the naphthyl moiety of **2e** and the pyrenyl moiety of alcohol **1f** as compared to alcohol **1a** cannot significantly enhance the reaction rate of the bigger system. Moving to solvents with a higher H-bond donor ability makes H-bonds in-between the aromatic C-H-bonds and the solvent less likely. The induced desolvation of the solutes strengthens solvent-solvent as well as solute-solute interactions. Both, the solvophobic effect of solvent molecules forming hydrogen bonds among each other and the attractive dispersion forces in-between the solutes can then enhance the rate of the reaction. The size of each of these effects depends on the size of the aromatic moieties.

There is an ongoing discussion if aromatic stacking is caused either mainly by dispersion forces or mainly by solvophobic effects. Solvophobic effects are the generalized idea of hydrophobic effects. If a molecule with a nonpolar surface is solved in a polar solvent, the non-covalent interactions of the solvents are disturbed. Therefore, regaining the energy of those intermolecular forces among solvent molecules could be the driving force behind the stacking of non-polar surfaces. This driving force would also grow with bigger aromatic surfaces, as the distortion of the solvent-solvent-interactions gets higher, too. The solvophobicity is a function of the intermolecular forces among the solvent molecules. Therefore, the *ced* seems to be the best parameter to predict the solvophobic effect of a solvent, as Cockroft showed by comparing different solvent parameters.[26] (for further details see introduction). To see the effect of solvophobic effects in our reaction design ln k_{rel} of alcohol **1f** compared to **1a** using silyl chloride **2e** were plotted against the cohesive energy density (**Figure 3.15**).
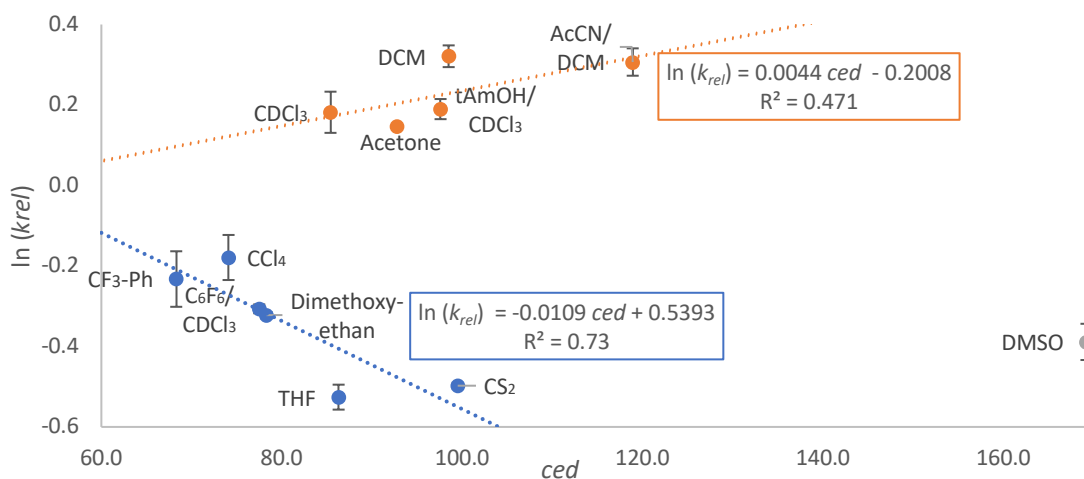
Figure 3.15. Plot of natural logarithm of relative rate constants of alcohol **1f** compared to **1a** for the Silylation reaction using **2e** against the cohesive energy density.

Solvents were grouped with respect to their hydrogen bond donor ability as the α value is critical in promoting solvent-solute interactions (see discussion above). On the one hand, in solvents that mainly promote solvent-solute interactions a higher *ced* is unfavourable for the size-depending rate acceleration, as in a solvent with high *ced* also unfavourable solvent-solute interactions are strong.

For solvents with a higher H-bond donor ability, a positive influence of growing *ced* on k_{rel} can be observed pointing to the relevance of solvophobic effects in enhancing rates for systems with bigger overlapping surfaces. Still, the low correlation coefficient and the very small slope of the correlation line prove that solvophobic effects alone cannot cause the differences in k_{rel}. In order to find other solvent influences also other solvent parameters were investigated, but let to no significant correlation (see **Table 3.12**). Also for other solvent polarity values like $E_T(30)$-value , Catalán's SdP-Parameter and Hansen's polar parameter no correlation could be found (see **Table 3.12**). One problem of measuring dispersion forces in solution is that compared to the gas phase not only dispersion between two reacting molecules is possible but they are competing with solvent-arene dispersion interactions.[27] Those interactions should be stronger in more polarizable solvents that is, for example, described by Catalán's SP-value. However, in **Figure 3.16** no correlation was found. These results are in accordance with the Kamlet-Taft-analysis, as not dispersive interactions but moreover electrostatic interactions between solvent and solute are the counter player to size-depending interactions in this kind of reaction.
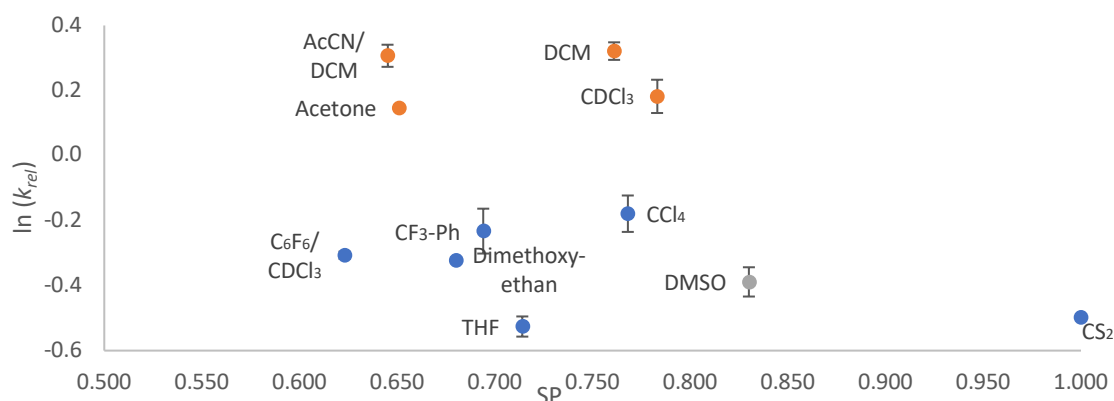
Figure 3.16. Plot of relative rate constants of alcohol **1f** compared to **1a** for the Silylation reaction using **2e** against solvent bulk polarizability.

Recent studies also proposed an influence of size and shape of the solvent on stacking interactions of polyaromatics.[28] In our study we could observe the trend that small and round-sized solvent molecules seem to be favourable, while rigid and planar molecules disturb aromatic interactions. Further research on the origins of this observation has to be carried out.

3.4. Investigation of Other Influences on the Rate Constant

3.4.1. Influence of the Catalyst

In a recent work a size-dependent rate acceleration for the acylation of secondary alcohols due to attractive interactions of catalyst and alcohol was shown.[29] Thus, the impact of the catalyst on the relative rates of silylation reactions was investigated. Therefore, the three Lewis base catalysts DMAP (**3a**), 9-azajulolidine (TCAP, **3b**) and DMAP-N-oxide (**3c**) were investigated.

DMAP **3a**   TCAP **3b**   DMAP-N-Oxide **3c**
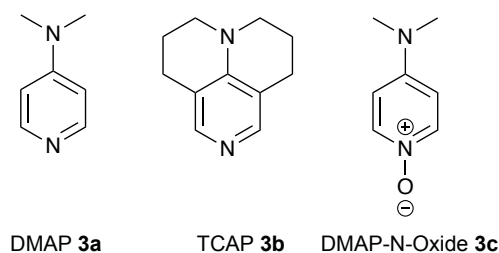
Figure 3.17. Lewis base catalysts used for silylation reactions in this work.

TCAP (**3b**) was used as its surface is extended as compared to DMAP (**3a**). Therefore, any aromatic-aromatic interaction should get more relevant. In the proposed transition state for acylation reactions the surfaces of alcohol and catalyst can interact (see **Figure 3.18**). In contrast, in the proposed transition state for silylation reactions the pyridinium core is oriented vertical to the silyl moieties. Therefore, dispersive interactions of the pyridinium system with other parts of the transition state are unlikely. To diminish this angle and to enable aromatic interactions between silylation agent and catalyst also DMAP-N-oxide (**3c**) was used. Additionally, the uncatalysed reaction was investigated.

TCAP **3b** catalyzed   DMAP **3a** catalyzed   DMAP-N-Oxide **3c** catalyzed
acylation of **1f**   silylation of **1f**   silylation of **1f**
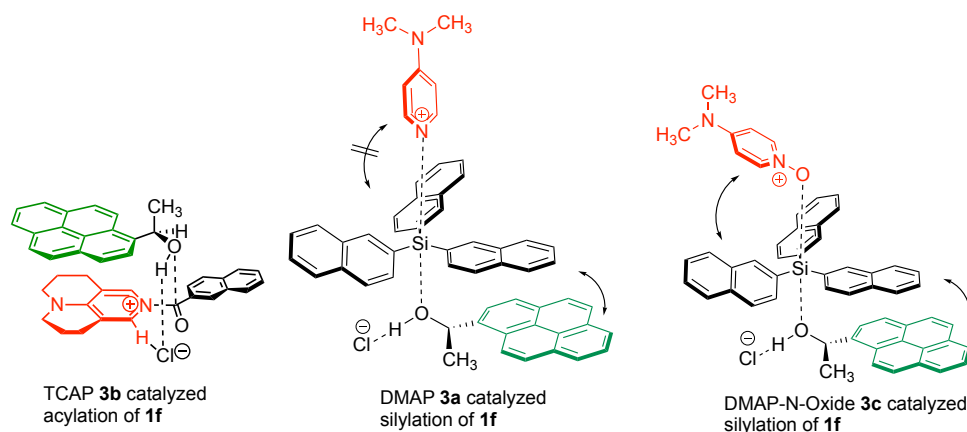
Figure 3.18. Proposed transition state structures for TCAP catalysed acylation, and DMAP or DMAP-N-oxide catalysed silylation of **1f**.

The competition experiments for catalyst screening followed precisely the same procedure as described in chapter 3.2.1. For uncatalysed reactions pure solvent was added instead of catalyst stock solution.
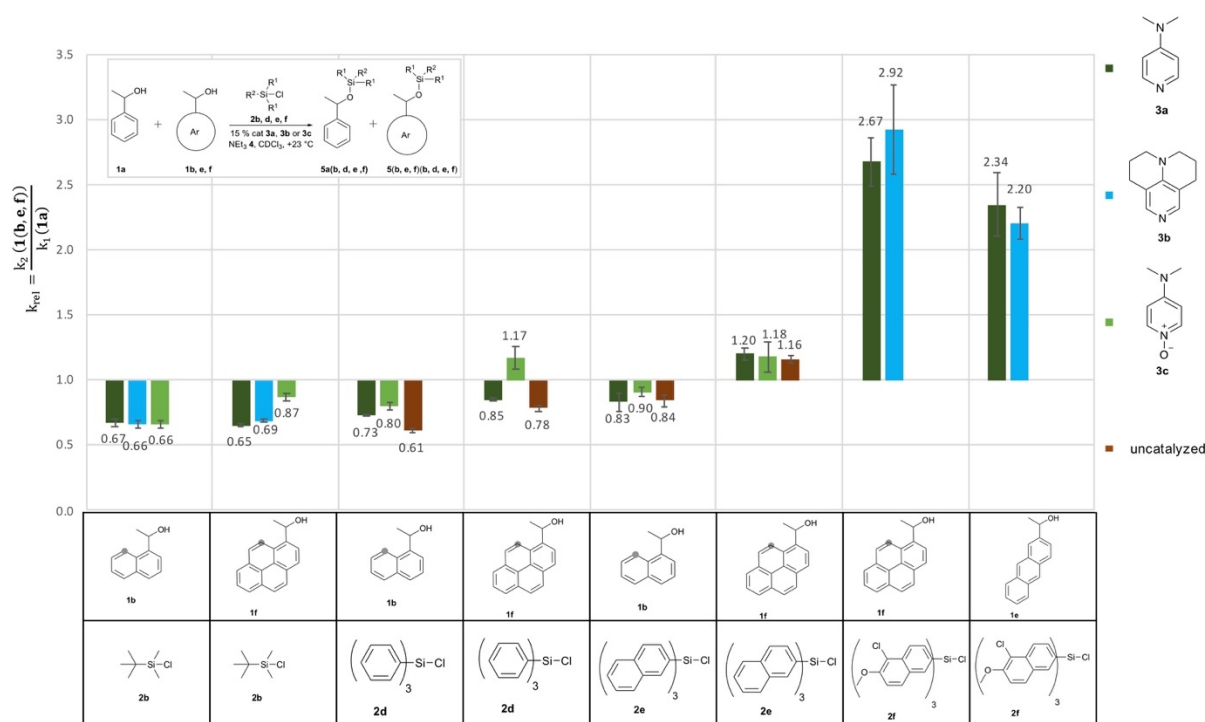
Figure 3.19. Relative rate of silylation reactions using different catalysts, alcohols and silyl chlorides.

The results in **Figure 3.19** support the hypothesis that selectivity values are not affected by variation of the catalyst DMAP (**3a**) or TCAP (**3b**) or in uncatalysed reactions. The minor differences for the biggest silyl chloride **2f** follow no clear trend and lie within the standard deviation. Thus, the selectivity of the investigated systems does not respond to the growth of aromatic system in **3b** nor to the lack of any catalyst. This finding is in agreement with the proposed transition structure shown above, that does not predict interactions between catalyst and silylation agent side chains. On the other hand, for DMAP-N-oxide (**3c**) minor accelerations of the reaction rates can be observed. They are most prominent for the combinations of relatively small silyl chlorides **2b** and **2d** and pyrenyl-substituted alcohol **1f**. Indeed, the changed N-Si-O-angle in the proposed transition state seems to allow a slight interaction of pyridinium core and bulky alcohol moieties. However, all observed differences are very small and far from accelerations that were observed for acylation reactions through attractive interactions of catalyst and alcohol.

3.4.2. Temperature Effects

A decrease in temperature is commonly expected to increase selectivity.[30] In the competition experiments that were carried out here, the variation from +23 °C to -10 °C in the temperature of the competition experiment provides very small changes in k_{rel} (for raw competition data see original SI). This translates to a change in the entropy barrier of 7.7 J/K·mol. In order to clarify this entropy variation, the development of the well-known *Eyring* equation Eq. 3.14 is presented here. As the

differences in k_{rel} are that small that they are within the experimental standard deviation, discussion of the calculated entropy barrier would not be reliable.
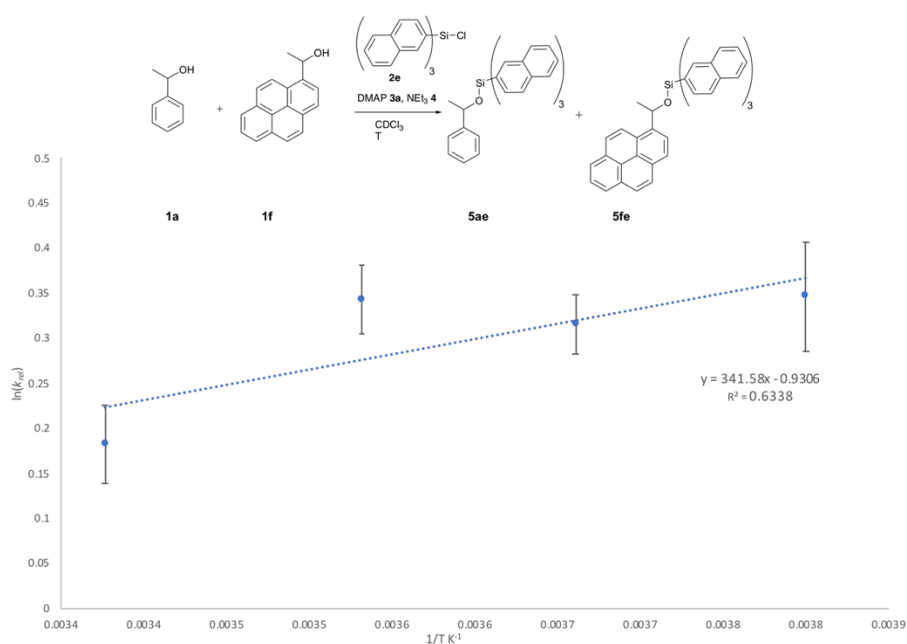
Figure 3.20. Eyring plot of temperature screening competition experiments.

$$\ln\frac{k_2}{k_1} = \frac{\Delta\Delta H^{\neq}}{R \cdot T} - \frac{\Delta\Delta S^{\neq}}{R}$$

Eq. 3.14

Experimental we got:

$$\ln\frac{k_2}{k_1} = \frac{341.58}{T} - 0.9306$$

Eq. 3.15

And taking these terms as:

$$\Delta\Delta H^{\neq} = \Delta\Delta H_2^{\neq} - \Delta\Delta H_1^{\neq}$$

$$\Delta\Delta S^{\neq} = \Delta\Delta S_2^{\neq} - \Delta\Delta S_1^{\neq}$$

$$R = 8.31451 \ J/K \cdot mol$$

Next results were calculated,

$$\Delta\Delta H^{\neq} = \Delta\Delta H_2^{\neq} - \Delta\Delta H_1^{\neq} = 2840.1 \ J/mol = 2.84 \ kJ/mol$$

Eq. 3.16

$$\Delta\Delta S^{\neq} = \Delta\Delta S_2^{\neq} - \Delta\Delta S_1^{\neq} = 7.73 \ J/K \cdot mol$$

Eq. 3.17

The very small temperature effects are in agreement with the temperature independence of dispersion interactions.[31]

3.4.3. Transetherification Experiment

Due to long reaction times for some catalysts and substrates the possibility of transetherification (**Scheme 3.5**) had to be investigated. This unwanted side reaction would alter the values for the chemoselectivity and selectivity.
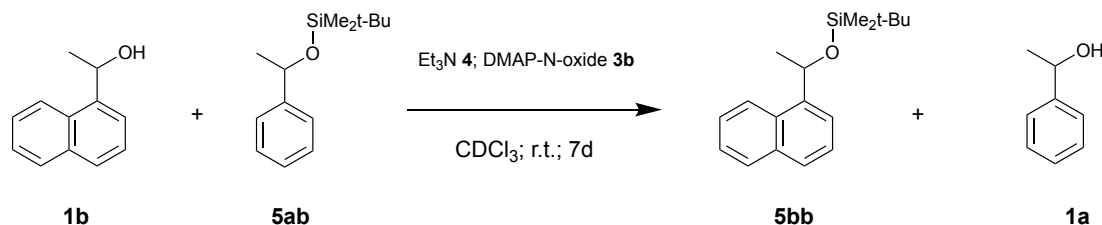
Scheme 3.5. Possible transetherfication reaction between alcohol **1b** and silyl ether **5ab** under competition experiment conditions.

To verify if transetherfication does happen under competition experiment conditions, a control reaction is done (see **Scheme 3.6**). Therefore, 1 eq. of alcohol **1a** and 0.5 eq. of silylation agent TBDMSCl (**2b**) were put to reaction under competition experiment conditions in a GC-vial to form the silylation product **5ab**. After full reaction, a ^{1}H-NMR spectrum was recorded. Now the alcohol **1b** was added to the mixture and after seven days another ^{1}H-NMR spectrum was recorded.
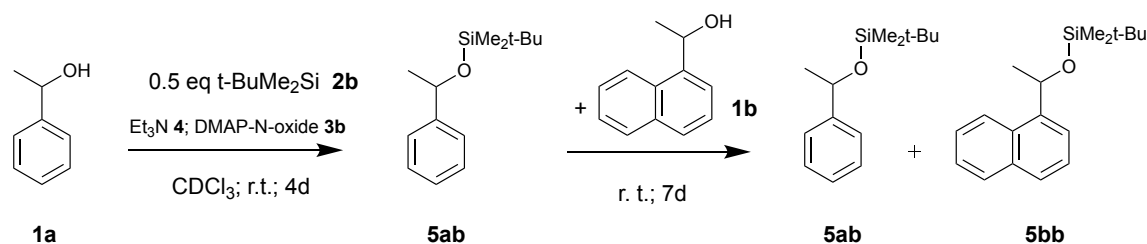
Scheme 3.6. Transetherfication experiment starting by a mixture of alcohol **1a** and silyl ether **5ab** adding alcohol **1b**.

The experiment was repeated in the reversed order, so alcohol **1a** was added to a mixture of **1b** and **5bb** (see **Scheme 3.7**, **Figure 3.22**).
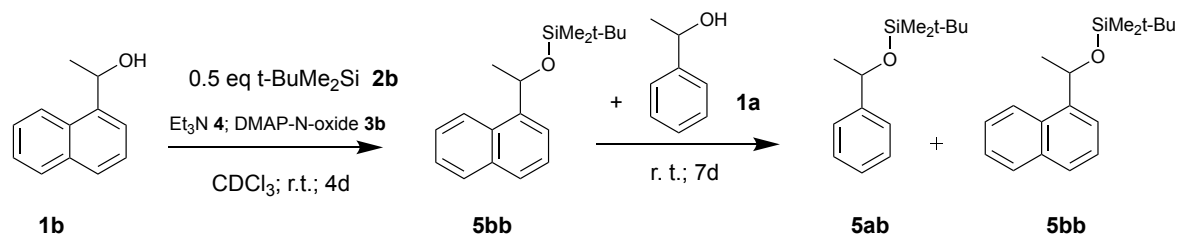
Scheme 3.7. Transetherfication experiment starting by a mixture of alcohol **1b** and silyl ether **5bb** adding alcohol **1a**.

The NMR-spectra (**Figure 3.21** and **Figure 3.22**) show clearly that after addition of the competing alcohol no corresponding silyl ether was formed.
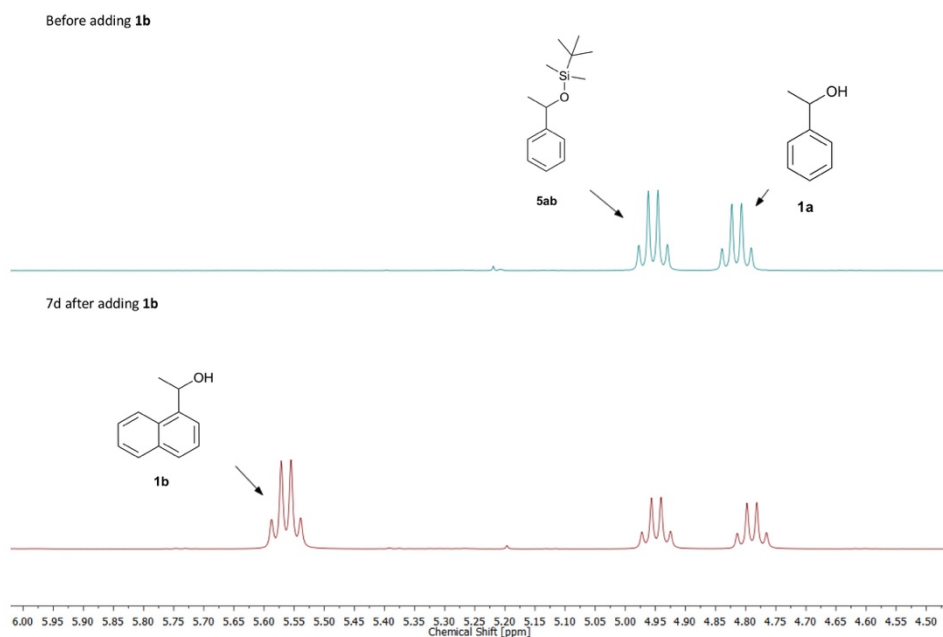
Figure 3.21. NMR spectra of transetherfication experiment shown in **Scheme 3.6**.
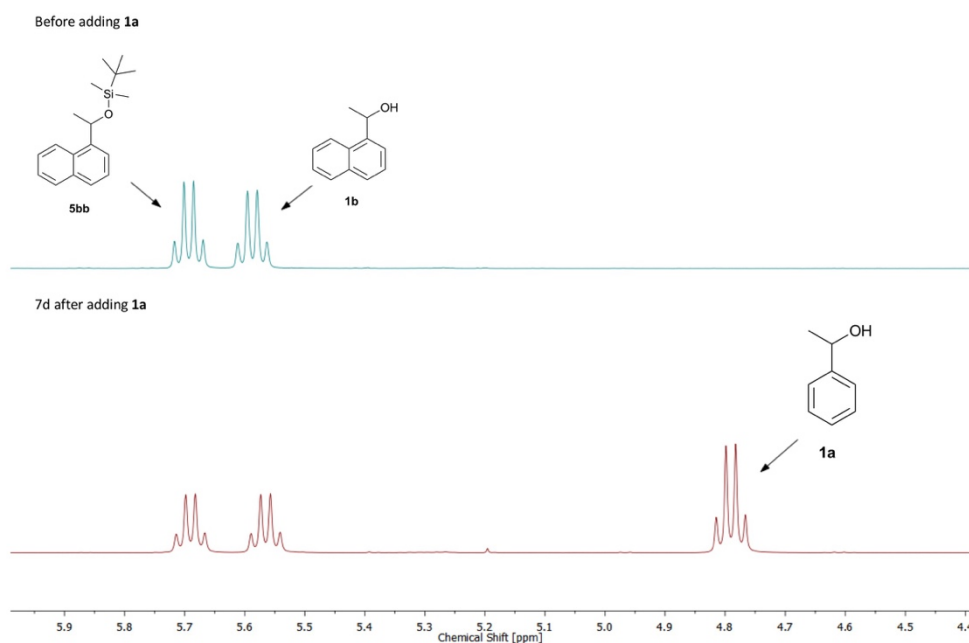
Figure 3.22. NMR spectra of transetherfication experiment shown in **Scheme 3.7**.

With those results in hand, it can be stated that under the conditions of competition experiments no transetherification takes place. Therefore, the selectivity values and relative rate constants are valid and differences in product ratios originate from the kinetics of the investigated reactions.

3.5. Synthetic Data

3.5.1. General Experimental and Analytical Information and Techniques

General Methods: All reactions sensitive to air and moisture were proceeded under a nitrogen atmosphere and the glassware as well as magnetic stir bars were dried overnight in a dry oven at 110°C.

Solvents: If not further specified, solvents were obtained from the companies Acros Organics, Sigma Aldrich, Fluka or Merck and purified by distillation in a rotary evaporator. $CDCl_3$, triethylamine Et_3N **4** and DCM were freshly distilled from calcium hydride (CaH_2) under nitrogen atmosphere. THF, DCM-d_2, DMSO-d_6 and Acetone-d_6 for solvent competition experiments were purchased "extra-dry" and used without further purification. CCl_4 was freshly distilled from molecular sieve (4 Å), CS_2 from $MgSO_4$ and dimethoxyethan from sodium, all of them were stored over molecular sieve (4 Å).

Reagents and Catalysts: All reagents were purchased from the companies TCI, Sigma Aldrich or Acros and used without further purification, if not mentioned otherwise. All air- or water-sensitive reagents were stored under nitrogen.

Chromatography: Silica gel for column chromatography was purchased from Acros Organics (mesh 35-70). Thin-layer chromatograpy was performed by using TLC plates purchased by Merck (silica gel 60 F254, thickness 0.2 mm). Preparative layer chromatography (PLC) was carried out by using Merck TLC glass plates (silica gel 60 F254, thickness 2 mm).

NMR spectroscopy: All ^{1}H-NMR spectra were recorded by Varian INOVA 400 and 600 machines in $CDCl_3$ or DMSO at 400 MHz or 600MHz at 23 °C. All ^{13}C-NMR spectra were recorded respectively at 101 MHz and 151 MHz. The ^{29}Si-NMR spectra were recorded with Bruker 400 TR or JEOL 400 machine at 79 MHz. The chemical shifts are reported in ppm (δ), relative to the chemical shift of tetramethylsilane (TMS). For ^{1}H and ^{13}C spectra the resonance of $CHCl_3$ at δ = 7.26 ppm resp. δ = 77.16 ppm was used as an internal reference. Spectra were imported and processed in the MestreNova 10.0.2 program. Peaks were assigned using HSQC-spectra.

Mass spectrometry: HRMS spectra were obtained by using a Thermo Finnigan LTQ FT machine of the MAT 95 type with a direct exposure probe (DEP) and electron impact ionization (EI, 70 eV).

X-ray crystallography: crystallographic measurements were done using an Oxford Diffraction XCalibur with Saphir CCD-detector and a molybdenum-K_α–source (λ = 0.71073 Å) with concentric circle kappa-device. Structures were resolved using SHELXS or SIR97 and refined with SHELXS.

Melting points: melting point were measure at a Stuart SMP10 and are stated uncorrected.

3.5.2.Synthetic Procedures and Compound Characterization

Synthesis of Silyl Chlorides

General Procedure 1 for the Grignard-synthesis of Silanes (GP1)

In an oven-dried three-neck-flask 2 eq magnesium-turnings and anhydrous LiCl (1.1 eq) were heated to 600 °C under high vacuum for 5 minutes. After flushing with nitrogen and cooling down, magnesium turnings were covered with dry THF. 1 eq of the corresponding bromoarene was dissolved in dry THF and $\frac{1}{10}$ of this solution was added to the flask. After the reaction started, the rest of the solution was slowly dropped in over approx. 30 min. The solution was then stirred for another 30 min at room temperature. The corresponding amount of chlorosilane in dry THF was added slowly under ice-cooling and then refluxed for 3 hours. The reaction mixture was quenched with ice water, then HCl (aq) was added until all $Mg(OH)_2$ was solved. The reaction mixture was extracted with EtOAc (1x 20mL) and with DCM (2x 20mL). The combined organic layers were dried over $MgSO_4$ and the solvent was removed under reduced pressure. The residue was purified through recrystallizations or distillation.

General Procedure for Chlorination of Silanes[32] (GP2)

In an oven dried 50 mL Schlenk-flask the silane was dissolved in dry CCl_4 under nitrogen at room temperature. SO_2Cl_2 was added via syringe and the solution was refluxed. After full conversion (monitored by the disappearance of the silane-H via ^{1}H-NMR) solvent and excess reagents were evaporated under vacuum (extra cooling trap is used). The residue was purified by recrystallization or distillation.

Diisopropyl(naphthalen-2-yl)silane 7c
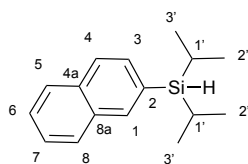
Diisopropyl(naphthalen-2-yl)silane **7c** was synthesized according to GP1 starting from magnesium-turnings (240 mg, 10.0 mmol), LiCl (252 mg, 6.00 mmol) and 2-bromonaphtalene (1.04 g, 5.00 mmol) in 5 mL of THF. Chlorodiisopropylsilane (754 mg, 5.00 mmol) in 2 mL THF was added. Kugelrohr-distillation yielded **7c** (890 mg, 3.68 mmol, 73.5%) as a colorless oil with a boiling point of 156 °C (1 mbar). **^{1}H NMR** (400 MHz, CDCl$_3$) δ 8.27 (1H, s, 1-H), 8.06 – 8.01 (1H, m, 4-H), 7.99 (2H, d, J = 7.2 Hz, 5-H, 8-H), 7.84 – 7.76 (1H, m, 3-H), 7.69 – 7.60 (2H, m, 6-H, 7-H), 4.35 – 4.31 (1H, m, Si-*H*), 1.57 – 1.44 (2H, m, 1'-H), 1.29 (12H, ddt, J = 30.1, 7.3, 1.8 Hz, 2'-H, 3'-H). **^{13}C NMR** (101 MHz, CDCl$_3$) δ 136.60 (C1), 134.01 (s), 133.14 (s), 131.92 (s), 131.67 (C2), 128.20, 127.89, 126.95, 126.46, 125.99, 18.93 (C*H*$_3$), 18.76 (C*H*$_3$), 11.03 (C*H*-CH$_3$). **^{29}Si NMR** (53.7 MHz, CDCl$_3$) δ 7.16. **HRMS** (70 eV, EI) m/z calc. for C$_{16}$H$_{22}$Si [M]$^+$ 242.1485; found 242.1484.

Chlorodiisopropyl(naphthalen-2-yl)silane 2c
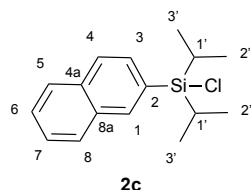
Chlorodiisopropyl(naphthalen-2-yl)silane **2c** was synthesized according to GP2 with 760 mg (3.14 mmol) of diisopropyl(naphthalen-2-yl)silane **7c** and 466 mg (3.45 mmol) of SO_2Cl_2 in 5 mL of CCl_4. Refluxing for 5 hrs and Kugelrohr-distillation yielded 589 mg of **2c** (2.13 mmol, 67.9%) with a boiling point of 169 °C (1mbar). **^{1}H NMR** (400 MHz, CDCl$_3$) δ 8.19 (1H, s, 1-H), 7.96 – 7.86 (3H, m, 4-H, 5-H, 8-H), 7.69 (1H, d, J = 8.2 Hz, 3-H), 7.60 – 7.51 (2H, m, 6-H, 7-H), 1.55 (2H, hept, J = 7.3 Hz, 1'-H), 1.18 (6H, d, J = 7.3 Hz, 2'-H), 1.10 (6H, d, J = 7.4 Hz, 3'-H). **^{13}C NMR** (101 MHz, CDCl$_3$) δ 135.80, 134.25 (s), 132.88 (s), 130.07 (s), 129.87, 128.49, 127.86, 127.24, 127.04, 126.27, 17.24 (CH_3), 16.98 (CH_3), 14.09 (CH-CH$_3$). **^{29}Si NMR** (53.7 MHz, CDCl$_3$) δ 27.88. **HRMS** (70 eV, EI) m/z calc. for C$_{16}$H$_{22}$ClSi [M]$^+$ 276.1095; found 276.1091.

Tri(naphthalen-2-yl)silane 7e
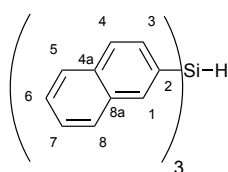
Tri(naphthalen-2-yl)silane **7e** was synthesized according GP1 using magnesium-turnings (2.40 g, 100 mmol), anhydrous LiCl (2.33 g, 55.0 mmol), 2-bromonaphtalene (10.4 g, 50 mmol) in 20 mL of THF and trichlorosilane (2.03 g, 15.0 mmol) in 5 mL of THF.

A white powder was obtained through twice recrystallization from a 4:1-mixture of *iso*-hexane and ethyl acetate (4.90 g, 11.9 mmol, 79.5%), **mp** 144-146 °C. **Elemental analysis:** Found: C, 87.3; H, 5.4. Calc. for C$_{30}$H$_{22}$Si: C, 87.8; H, 5.4%; **^{1}H NMR** (400 MHz; CDCl$_3$) δ 8.24 (3H, s, 1-H), 7.95 – 7.88 (6H, m, 5-H, 8-H), 7.85 (3H, d, J = 7.9 Hz, 4-H), 7.77 (3H, d, J = 8.1 Hz, 3-H), 7.60 – 7.49 (6H, m, 6-H, 7-H), 5.98 – 5.85 (1H, m, Si-H). **^{13}C NMR** (101 MHz, CDCl$_3$) δ 137.43 (C1), 134.28 (s), 133.18 (s), 131.59 (C3), 130.87 (s), 128.40 (C4), 127.94, 127.60, 127.02, 126.26. **^{29}Si NMR** (79 MHz, CDCl$_3$) δ -16.95. **HRMS** (70 eV, EI) m/z calc. for C$_{30}$H$_{22}$Si [M]$^+$ 410.1485; found 410.1482.

Chlorotri(naphthalen-2-yl)silane 2e
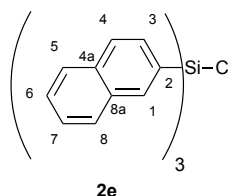
Chlorotri(naphthalen-2-yl)silane **2e** was synthesized following GP2 using tri(naphthalen-2-yl)silane **7e** (2.05 g, 5.00 mmol) in 20 mL of dry CCl_4 and 1.35 g of SO_2Cl_2 (10 mmol). The product was recrystallized from *iso*-Hexane/DCM (11:7) and Schlenk filtrated to yield in chlorotri(naphthalen-2-yl)silane **2e** (1.22 g, 2.70 mmol, 55.0%), **mp** 180 – 182 °C. **^{1}H NMR** (400 MHz, CDCl$_3$) δ 8.23 (3H, s, 1-H), 7.95 – 7.87 (6H, m, 5-H, 8-H), 7.84 (3H, d, J = 8.1 Hz, 4-H), 7.80 (3H, dd, J = 8.2, 1.2 Hz, 3-H), 7.60 – 7.49 (6H, m, 6-H, 7-H). **^{13}C NMR** (101 MHz, CDCl$_3$) δ 137.25, 134.64 (s), 132.91 (s), 130.58, 130.39 (s), 128.75, 127.97, 127.84, 127.60, 126.51. **^{29}Si NMR** (79 MHz, CDCl$_3$) δ +2.76. **HRMS** (70 eV, EI) m/z calc. for C$_{30}$H$_{21}$ClSi [M]$^+$ 444.1096; found 444.1104.

Tris(6-methoxynaphthalen-2-yl)silane 7f
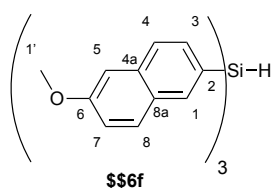
Tris(6-methoxynaphthalen-2-yl)silane **7f** was synthesized according to GP1 using magnesium-turnings (2.40 g, 100 mmol), anhydrous LiCl (2.33 g, 55.0 mmol), 2-bromo-6-methoxynaphtalene (11.9 g, 50.0 mmol) in 35 mL of THF and trichlorosilane (2.03 g, 7.50 mmol) in 5 mL of THF. After quenching, the precipitated product was filtered out, solved in hot $CHCl_3$, hot filtrated to remove remaining magnesium turnings and recrystallized. The filtrate was treated as described in general procedure 1, the crude product was then recrystallized from $CHCl_3$. Combining the purified products led to 7.50 g (14.9 mmol, 99.0%) of **7f** as a white powder, **mp** 132-134 °C. **^{1}H NMR** (400 MHz; $CDCl_3$) δ 8.07 (3H, s, 1-H), 7.76 (3H, d, J = 8.2 Hz, 8-H), 7.72 – 7.68 (3H, m, 4-H), 7.66 (3H, dd, J = 8.2, 1.1 Hz, 3-H), 7.15 (3H, s, 5-H), 7.17 – 7.12 (3H, m, 7-H), 5.79 (1H, s, Si-*H*), 3.93 (9H, s, 1'-H). **^{13}C NMR** (101 MHz, $CDCl_3$) δ 158.52 (s, C6), 137.03 (C1), 135.56 (s), 132.35 (C3), 129.99 (C4), 128.83 (s), 128.38 (s), 126.50 (C8), 119.02 (C7), 105.82 (C5), 55.50 (C1'). **HRMS** (70 eV, EI) m/z calc. for $C_{33}H_{28}O_3Si$ [M]$^+$ 500.1802; found 500.1795.

Chlorotris(7-chloro-6-methoxynaphthalen-2-yl)silane 2f
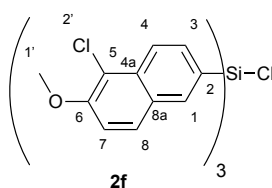
Chlorotris(7-chloro-6-methoxynaphthalen-2-yl)silane **2f** was synthesized following GP2 using Tris(6-methoxynaphthalen-2-yl)silane **7e** (1.40 g, 2.80 mmol) in 15 mL of dry CCl_4 and 1.51 g of SO_2Cl_2 (11.2 mmol). The product was recrystallized from *iso*-Hexane/DCM and Schlenk filtrated to yield in **2f** (1.14 g, 1.79 mmol, 64%), **mp** 175-177 °C. **^{1}H NMR** (400 MHz, $CDCl_3$) δ 8.29 (3H, d, J = 8.6 Hz, 4-H), 8.12 (3H, s, 1-H), 7.84 (3H, dd, J = 8.6, 1.2 Hz, 3-H), 7.77 (3H, d, J = 8.9 Hz, 8-H), 7.33 (3H, d, J = 9.1 Hz, 7-H), 4.06 (9H, s, 1'-H). **^{13}C NMR** (101 MHz, $CDCl_3$) δ 153.91 (s, C6), 137.32 (C1), 133.22 (s), 132.04 (C4), 128.99 (C8), 128.94 (s), 128.26 (s), 123.49 (C4), 116.93 (s, C5), 113.96 (C7), 57.04 (C1'). **^{29}Si NMR** (79 MHz, $CDCl_3$) δ +2.56. **HRMS** (70 eV, EI) m/z calc. for $C_{33}H_{24}Cl_4O_3Si$ [M]$^+$ 636.0242; found 636.0233.

Synthesis of Alcohols

General Procedures for the Preparation of Secondary Alcohols (GP3)

The aryl ketone was solved in 30 mL of methanol and cooled to 0 °C. $NaBH_4$ was added slowly and the reaction mixture was stirred for 3 hours. The solution was extracted with dichloromethane (3 x 15 mL) and washed with brine. Then the product was precipitated through addition of n-hexane.

Alcohol **1d**[33] and **1e**[34] were synthesized following GP3 and characterised by ^{1}H-NMR, ^{13}C-NMR and HRMS in accordance with the literature.

Alcohol **1f** was synthesized from the corresponding aldehyde according to the literature.[29]

Synthesis of catalyst

4-Dimethylaminopyridine-N-oxide 3c
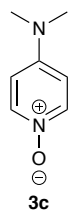
4-Nitropyridine-N-Oxide (3.55 g, 25.4 mmol) was dissolved in acetyl chloride (30 mL) and the resulting reaction mixture was refluxed for 2.5h. After removing excess acetyl chloride at reduced pressure, the crude product was poured into a mixture of ice (50 g) and a saturated aq. solution of $NaHCO_3$. The reaction mixture was extracted with dichloromethane (10 x 30 mL), dried over anhydrous $MgSO_4$ and the solvent was removed under vacuo. Washing with n-hexane yielded 76% of 4-chloropyridine-N-oxide (2.51 g, 18.38 mmol).

The 4-chloropyridine-N-oxide (1.5 g, 11.58 mmol) was then dissolved in dimethylamine (4.5 mL, 40%wt aq. sol.) and radiated in a microwave for 1h at 110 °C. The reaction mixture was conc. in vacuo (toluene used to azeotrope water), dissolved in dichloromethane (10 mL), washed with sat. sodium carbonate (5 mL) and extracted with DCM (10 x 20 mL). The combined organic layers were then dried over anhydrous $MgSO_4$. After the solvent was removed under reduced pressure, the product was washed with n-hexane to afford 98% (1.57 g, 11.35 mmol) of DMAP-N-oxide **3c** as a light brown solid.

DMAP-N-oxide **3c** was characterized according to the literature.[35]

Synthesis of silyl ethers

General procedure for the synthesis of silyl ethers (GP4)

0.15 mmol of the alcohol and 0.023 mmol of DMAP **3a** were solved in 5 mL of anhydrous DCM in an oven-dried flask under N_2. 0.18 mmol of NEt_3 **4** and 0.18 mmol of the corresponding silyl chloride were added, the reaction was stirred and monitored via TLC. After full conversion, the reaction mixture was washed with $NaHCO_3$ (1x 5 mL), the solvent was evaporated under reduced pressure and the crude residue was purified by preparative TLC. Yields were calculated from competition experiment NMRs regarding the silyl chloride conversion.

Trimethyl(1-phenylethoxy)silane 5aa[36]
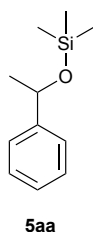
Synthesized according to GP4 using **1a** and **2a** yielding a colourless oil (84%). **¹H NMR** (400 MHz, $CDCl_3$) δ 7.36 – 7.29 (4H, m, Ar-*H*), 7.25 – 7.20 (1H, m, Ar-*H*), 4.86 (1H, q, *J* = 6.4 Hz, O-C*H*-CH₃), 1.44 (3H, d, *J* = 6.4 Hz, O-CH-C*H₃*), 0.08 (9H, s, Si-C*H₃*). **¹³C NMR** (101 MHz, $CDCl_3$) δ ¹³C NMR (101 MHz, $CDCl_3$) δ 146.60 (s), 128.28, 126.98, 125.50, 70.74 (O-*CH*), 27.02 (O-CH-*CH₃*), 0.26 (Si-*CH₃*). **²⁹Si NMR** (79 MHz, $CDCl_3$) δ +17.27. **HRMS** (70 eV, EI) m/z calc. for $C_{11}H_{18}OSi$ [M-H]⁺ 193.1043; found 193.1044; calc. for [M-CH₃]⁺ 179.0886; found 179.0885.

tert-Butyldimethyl(1-phenylethoxy)silane 5ab
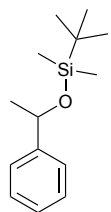
Synthesized according to GP4 using **1a** and **2b** yielding a colourless oil (87%). **^{1}H NMR** (400 MHz, CDCl$_3$) δ 7.39 – 7.30 (4H, m, Ar-*H*), 7.30 – 7.20 (1H, m, Ar-*H*), 4.91 (1H, q, *J* = 6.4 Hz, O-C*H*-CH$_3$), 1.45 (3H, d, *J* = 6.3 Hz, O-CH-C*H*$_3$), 0.94 (9H, s, Si-C-C*H*$_3$), 0.09 (3H, s, Si-C*H*$_3$), 0.01 (3H, s, Si-C*H*$_3$). **^{13}C NMR** (101 MHz, CDCl$_3$) δ 146.94 (s), 128.06, 126.66, 125.18, 70.82 (O-*C*H), 27.29 (O-CH-*C*H$_3$), 25.89 (Si-C-*C*H$_3$), 18.28 (s, Si-*C*-CH$_3$), -4.78 (Si-*C*H$_3$), -4.82 (Si-*C*H$_3$). **^{29}Si NMR** (79 MHz, CDCl$_3$) δ +18.14. **HRMS** (70 eV, EI) m/z calc. for C$_{14}$H$_{24}$OSi [M-CH$_3$]$^+$ 221.1362; found: 221.1349, [M-tBu]$^+$ 179.0886 found; 179.0880.

Diisopropyl(naphtalen-2-yl)(1-phenylethoxy)silane 5ac
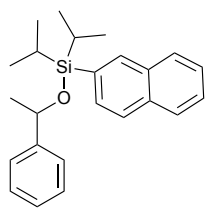
Synthesized according to GP4 using **1a** and **2c** yielding a colourless oil (75%). **R$_f$** 0.67 (*i*Hex:EtOAc=19:1) . **^{1}H NMR** (400 MHz, CDCl$_3$) δ 8.00 (1H, s, Ar-*H*), 7.86 – 7.72 (3H, m, Ar-*H*), 7.59 (1H, d, *J* = 8.1 Hz, Ar-*H*), 7.52 – 7.44 (2H, m, Ar-*H*), 7.42 (2H, d, *J* = 7.5 Hz, Ar-*H*), 7.35 (2H, t, *J* = 7.6 Hz, Ar-*H*), 7.31 – 7.26 (1H, m, Ar-*H*), 5.06 (1H, q, *J* = 6.3 Hz, O-C*H*-CH$_3$), 1.55 (3H, d, *J* = 6.3 Hz, O-CH-C*H*$_3$), 1.37 (2H, hept, *J* = 7.4 Hz, iPr-C*H*), 1.08 – 0.98 (12H, m, iPr-C*H*$_3$). **^{13}C NMR** (101 MHz, CDCl$_3$) δ 147.10 (s), 135.91, 133.96 (s), 132.90 (s), 132.52 (s), 131.05, 128.41, 128.32, 127.78, 127.05, 126.68, 126.47, 125.81, 125.54, 71.90 *(O-C*H), 27.94 (O-CH-*C*H$_3$), 17.65 (iPr-*C*H$_3$), 17.59 (iPr-*C*H$_3$), 17.52 (iPr-*C*H$_3$), 17.42 (iPr-*C*H$_3$), 12.65 (iPr-*C*H), 12.54 (iPr-*C*H). **HRMS** (70 eV, EI) m/z calc. for C$_{24}$H$_{30}$OSi [M]$^+$ 362.2060; found 362.2046.

Triphenyl(1-phenylethoxy)silane 5ad[37]
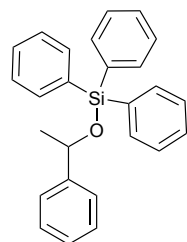
Synthesized according to GP4 using **1a** and **2d** yielding a colourless oil (95%). **^{1}H NMR** (400 MHz, CDCl$_3$) δ 7.71 – 7.64 (6H, m, Ar-*H*), 7.51 – 7.44 (3H, m, Ar-*H*), 7.44 – 7.37 (8H, m, Ar-*H*), 7.37 – 7.31 (2H, m, Ar.*H*), 7.30 – 7.26 (1H, m, Ar-*H*), 5.11 (1H, q, *J* = 6.3 Hz, O-C*H*-CH$_3$), 1.50 (3H, d, *J* = 6.4 Hz, O-CH-C*H*$_3$). **^{13}C NMR** (101 MHz, CDCl$_3$) δ 145.99 (s), 135.51, 134.62 (s), 129.96, 128.16, 127.81, 126.91, 125.51, 72.06 (O-*C*H), 26.96 (O-CH-*C*H$_3$). **^{29}Si NMR** (79 MHz, CDCl$_3$) δ -13.21. **HRMS** (70 eV, EI) m/z calc. for C$_{26}$H$_{24}$OSi [M]$^+$ 380.1590; found 380.1596.

Tri(naphtalen-2-yl)(1-phenylethoxy)silane 5ae
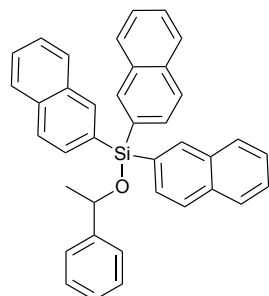
Synthesized according to GP4 using **1a** and **2e** yielding a colourless liquid (88%). **R$_f$** 0.65 (*i*Hex:EtOAc=19:1). **^{1}H NMR** (400 MHz, CDCl$_3$) δ 8.18 (3H, s, Ar-*H*), 7.86 (6H, dd, J = 8.0, 3.9 Hz, Ar-*H*), 7.80 – 7.73 (6H, m, Ar-*H*), 7.57 – 7.45 (6H, m, Ar-*H*), 7.44 – 7.39 (2H, m, Ar-*H*), 7.34 – 7.24 (3H, m, Ar-*H*), 5.19 (1H, q, *J* = 6.3 Hz, O-C*H*-CH$_3$), 1.54 (3H, d, *J* = 6.3 Hz, O-CH-C*H*$_3$). **^{13}C NMR** (101 MHz, CDCl$_3$) δ 146.08 (s), 137.17, 134.36, 132.97, 132.18, 131.26, 128.64, 128.36, 127.88, 127.27, 127.20 (s), 127.02, 126.10, 125.82,

72.57 (O-CH), 27.12 (O-CH-CH_3). **²⁹Si NMR** (79 MHz, CDCl$_3$) δ -12.15. **HRMS** (70 eV, EI) m/z calc. for C$_{38}$H$_{30}$OSi [M]$^+$ 530.2060; found 530.2060.

Tris(5-chloro-6-methoxynaphthalen-2-yl)(1-phenylethoxy)silane 5af

Synthesized according to GP4 using **1a** and **2f** yielding a brown oil (84%). **R$_f$** 0.78 (*i*Hex:EtOAc=1:1). **¹H NMR** (400 MHz, CDCl$_3$) δ 8.18 (3H, d, *J* = 8.5 Hz, Ar-*H*), 8.02 (3H, s, Ar-*H*), 7.77 (3H, dd, *J* = 8.5, 1.1 Hz, Ar-*H*), 7.64 (3H, d, *J* = 9.0 Hz, Ar-*H*), 7.35 (2H, dd, *J* = 8.2, 1.2 Hz, Ar-*H*), 7.29 – 7.19 (6H, m, Ar-*H*), 5.12 (1H, q, *J* = 6.3 Hz, O-C*H*-CH$_3$), 4.00 (9H, s, O-C*H$_3$*), 1.49 (3H, d, *J* = 6.4 Hz, O-CH-C*H$_3$*). **¹³C NMR** (101 MHz, CDCl$_3$) δ 153.51 (s), 145.89 (s), 137.25, 132.90 (s), 132.74, 130.08, 129.09, 128.83, 128.41, 127.31 (s), 125.81, 122.92, 116.88 (s), 113.71, 72.69 (O-C*H*), 57.05 (O-C*H$_3$*), 27.07 (O-CH-*CH$_3$*). **²⁹Si NMR** (79 MHz, CDCl$_3$) δ -12.22. **HRMS** (70 eV, EI) m/z calc. for C$_{41}$H$_{33}$Cl$_3$O$_4$Si [M]$^+$ 722.1208; found 722.1219.

Trimethyl(1-(naphthalen-1-yl)ethoxy)silane 5ba[38]
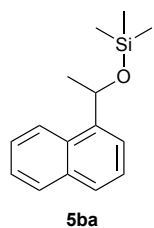
Synthesized according to GP4 using **1b** and **2a** yielding a colourless oil (97%). **¹H NMR** (400 MHz, CDCl$_3$) δ 8.19 (1H, d, *J* = 8.3 Hz, Ar-*H*), 7.93 (1H, d, *J* = 7.9 Hz, Ar-*H*), 7.82 – 7.75 (2H, m, Ar-*H*), 7.59 – 7.49 (3H, m, Ar-*H*), 5.68 (1H, q, *J* = 6.4 Hz, O-C*H*-CH$_3$), 1.77 – 1.57 (3H, m, *J* = 6.3 Hz, O-CH-C*H$_3$*), 0.17 (9H, s, Si-C*H$_3$*). **¹³C NMR** (101 MHz, CDCl$_3$) δ 142.27 (s), 133.80 (s), 129.96 (s), 128.90, 127.36, 125.64, 125.60, 125.24, 123.32, 122.80, 68.18 (O-C*H*), 26.54 (O-CH-*CH$_3$*), 0.16 (Si-*CH$_3$*). **²⁹Si NMR** (79 MHz, CDCl$_3$) δ +17.36. **HRMS** (70 eV, EI) m/z calc. for C$_{15}$H$_{20}$OSi [M]$^+$ 244.1277; found 244.1277.

tert-Butyldimethyl (1-(naphthalen-1-yl)ethoxy)silane 5bb
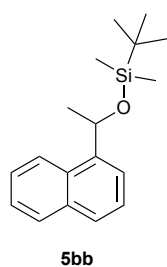
Synthesized according to GP4 using **1b** and **2b** yielding a colourless oil (89%). **¹H NMR** (400 MHz, CDCl$_3$) δ = 8.11 (1H, d, *J* = 8.3 Hz, Ar-*H*), 7.88 (1H, d, *J* = 7.8 Hz, Ar-*H*), 7.75 (1H, d, *J* = 8.2 Hz, Ar-*H*), 7.71 (1H, d, *J* = 7.2 Hz, Ar-*H*), 7.53 – 7.45 (3H, m, Ar-*H*), 5.61 (1H, q, *J* = 6.2 Hz, O-C*H*-CH$_3$), 1.59 (3H, d, *J* = 6.2, O-CH-C*H$_3$*), 0.97 – 0.93 (9H, m, Si-C-C*H$_3$*), 0.09 (3H, d, *J* = 1.7 Hz, Si-C*H$_3$*), -0.02 (3H, d, *J* = 1.7 Hz, Si-C*H$_3$*). **¹³C NMR** (101 MHz, CDCl$_3$) δ 142.69 (s), 133.88 (s), 130.00 (s), 128.99, 127.34, 125.73, 125.69, 125.31, 123.50, 122.83, 68.66 (O-C*H*), 26.79 (O-CH-*CH$_3$*), 26.06 (Si-C-*CH$_3$*), 18.47 (s, Si-*C*-CH$_3$), -4.65 (Si-*CH$_3$*), -4.74 (Si-*CH$_3$*). **²⁹Si NMR** (79 MHz, CDCl$_3$) δ +18.48. **HRMS** (70 eV, EI) m/z calc. for C$_{18}$H$_{28}$OSi, [M-CH$_3$]$^+$ 271.1518 found; 271.1505, [M-tBu]$^+$ 229.1043; found: 229.1033.

Diisopropyl(naphtalen-2-yl)(1-(naphthalen-1-yl)ethoxy)silane 5bc
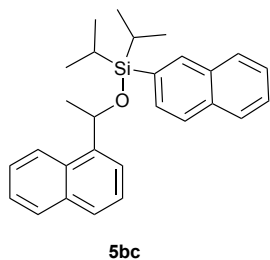
Synthesized according to GP4 using **1b** and **2c** yielding a colourless oil (85%). **R$_f$** 0.64 (*i*Hex:EtOAc=19:1). **^{1}H NMR** (400 MHz, CDCl$_3$) δ 8.10 – 8.04 (1H, m, Ar-*H*), 8.03 (1H, s, Ar-*H*), 7.91 – 7.87 (1H, m, Ar-*H*), 7.86 – 7.75 (4H, m, Ar-*H*), 7.68 (1H, d, *J* = 7.8 Hz, Ar-*H*), 7.61 (1H, dd, *J* = 8.2, 1.0 Hz, Ar-*H*), 7.54 – 7.42 (5H, m, Ar-*H*), 5.80 (1H, q, *J* = 6.3 Hz, O-C*H*-CH$_3$), 1.71 (3H, d, *J* = 6.3 Hz, O-CH-C*H$_3$*), 1.40 (2H, m, Si-C*H*-CH$_3$), 1.09 – 0.97 (12H, m, Si-CH-C*H$_3$*). **^{13}C NMR** (101 MHz, CDCl$_3$) δ 142.70 (s), 135.92, 133.96 (s), 133.90 (s), 132.91 (s), 132.43 (s), 131.00, 129.94 (s), 128.98, 128.38, 127.76, 127.53, 126.74, 126.48, 125.81, 125.79, 125.73, 125.38, 123.52, 123.18, 69.45 (O-*C*H), 27.12(O-CH-*C*H$_3$), 17.66 (iPr-*C*H$_3$), 17.64 (iPr-*C*H$_3$), 17.55 (iPr-*C*H$_3$), 17.46 (iPr-*C*H$_3$), 12.72 (iPr-*C*H), 12.56 (iPr-*C*H). **HRMS** (70 eV, EI) m/z calc. for C$_{28}$H$_{32}$OSi [M]$^+$ 412.2216; found 412.2226.

Triphenyl(1-(naphthalen-1-yl)ethoxy)silane 5bd
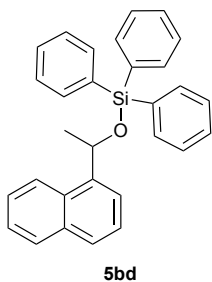
Synthesized according to GP4 using **1b** and **2d** yielding a colourless oil (94%). **^{1}H NMR** (400 MHz, CDCl$_3$) δ 7.92 (1H, d, *J* = 8.1 Hz, Ar-*H*), 7.87 – 7.80 (2H, m, Ar-*H*), 7.74 (1H, d, *J* = 8.2 Hz, Ar-*H*), 7.64 (6H, d, *J* = 7.9 Hz, Ar-*H*), 7.51 – 7.38 (6H, m, Ar-*H*), 7.36 – 7.27 (6H, m, Ar-*H*), 5.80 (1H, q, *J* = 6.3 Hz, O-C*H*-CH$_3$), 1.60 (3H, d, *J* = 6.4 Hz, O-CH-C*H$_3$*). **^{13}C NMR** (101 MHz, CDCl$_3$) δ 141.66 (s), 135.49, 134.50, 133.70 (s), 129.99, 129.80 (s), 128.78, 127.84, 127.42, 125.63, 125.58, 125.21, 123.39, 123.10, 69.61 (O-*C*H), 26.44 (O-CH-*C*H$_3$). **^{29}Si NMR** (79 MHz, CDCl$_3$) δ -13.22. **HRMS** (70 eV, EI) m/z calc. C$_{30}$H$_{26}$OSi for [M]$^+$ 430.1747; found 430.1746.

Tri(naphtalen-2-yl)(1-(naphthalen-1-yl)ethoxy)silane 5be
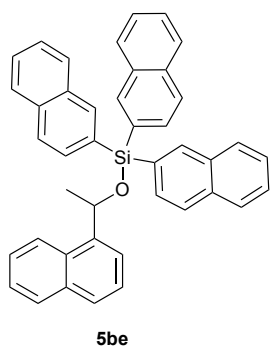
Synthesized according to GP4 using **1b** and **2e** yielding a colourless oil (93%). **R$_f$** 0.60 (*i*Hex:EtOAc=19:1). **^{1}H NMR** (400 MHz, CDCl$_3$) δ 8.20 (3H, s, Ar-*H*), 8.01 (1H, d, *J* = 8.3 Hz, Ar-*H*), 7.92 – 7.81 (8H, m, Ar-*H*), 7.80 – 7.67 (7H, m, Ar-*H*) 7.53 (3H, t, *J* = 7.4 Hz, Ar-*H*), 7.50 – 7.40 (5H, m, Ar-*H*), 7.40 – 7.34 (1H, m, Ar-*H*), 5.95 (1H, q, *J* = 6.3 Hz, O-C*H*-CH$_3$), 1.72 (3H, d, *J* = 6.3, O-CH-C*H$_3$*). **^{13}C NMR** (101 MHz, CDCl$_3$) δ 141.71(s), 137.17, 134.35 (s), 133.89 (s), 132.95 (s), 132.09 (s), 131.22, 130.05 (s), 128.88, 128.61, 127.85, 127.71, 127.29, 127.00, 126.08, 125.74, 125.67, 125.37, 123.64, 123.53, 70.32 (O-*C*H), 26.58 (O-CH-*C*H$_3$). **^{29}Si NMR** (79 MHz, CDCl$_3$) δ -11.71. **HRMS** (70 eV, EI) m/z calc. for C$_{42}$H$_{32}$OSi [M]$^+$ 580.2216; found 580.2225.

Tris(5-chloro-6-methoxynaphthalen-2-yl)(1-(naphthalen-1-yl)ethoxy)silane 5bf

5bf
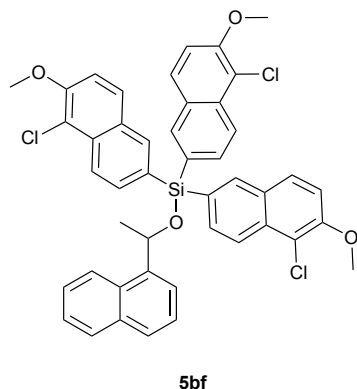
Synthesized according to GP4 using **1b** and **2f** yielding a colourless oil (81%). R_f 0.72 (*i*Hex:EtOAc=1:1). **^{1}H NMR** (400 MHz, CDCl$_3$) δ 8.18 (3H, d, *J* = 8.5 Hz, Ar-*H*), 8.06 (3H, s, Ar-*H*), 7.98 (1H, d, *J* = 8.5 Hz, Ar-*H*), 7.84 – 7.79 (5H, m, Ar-*H*), 7.72 (1H, d, *J* = 8.2 Hz, Ar-*H*), 7.60 (3H, d, J = 9.0 Hz, Ar-*H*), 7.45 – 7.31 (3H, m, Ar-*H*), 7.24 (2H, d, J = 1.9 Hz, Ar-*H*), 5.89 (1H, q, *J* = 6.3 Hz, C*H*-CH$_3$), 4.02 (9H, s, O-C*H*$_3$), 1.71 (3H, d, *J* = 6.4 Hz, CH-C*H*$_3$). **^{13}C NMR** (101 MHz, CDCl$_3$) δ 153.33 (s), 141.36 (s), 137.09, 133.74 (s), 132.72 (s), 132.53, 129.86 (s), 129.81 (s), 128.91 (s), 128.74, 128.65, 127.67, 125.64, 125.47, 125.26, 123.41, 123.39, 122.77, 116.69 (s), 113.52, 70.27 (O-CH), 56.88 (O-CH$_3$), 26.37 (O-CH-CH$_3$). **^{29}Si NMR** (79 MHz, CDCl$_3$) δ -11.82. **HRMS** (70 eV, EI) m/z calc. for C$_{45}$H$_{35}$Cl$_3$O$_4$Si [M]$^+$ 772.1364; found 772.1365.

Trimethyl(1-(naphthalen-2-yl)ethoxy)silane 5ca[38]

5ca

Synthesized according to GP4 using **1c** and **2a** yielding a colourless oil (94%). **^{1}H NMR** (400 MHz, CDCl$_3$) δ 7.88 – 7.80 (3H, m, Ar-*H*), 7.78 (1H, s, Ar-*H*), 7.55 – 7.41 (3H, m, Ar-*H*), 5.05 (1H, q, *J* = 6.4 Hz, O-C*H*-CH$_3$), 1.54 (3H, d, *J* = 6.4 Hz, O-CH-C*H*$_3$), 0.13 (9H, s, Si-C*H*$_3$). **^{13}C NMR** (101 MHz, CDCl$_3$) δ 143.97 (s), 133.33 (s), 132.74 (s), 127.92 (2C), 127.66, 125.93, 125.49, 124.12, 123.64, 70.80 (O-CH), 26.92 (O-CH-CH$_3$), 0.18 (Si-CH$_3$). **^{29}Si NMR** (79 MHz, CDCl$_3$) δ +17.00. **HRMS** (70 eV, EI) m/z calc. for C$_{15}$H$_{20}$OSi [M]$^+$ 244.1277; found 244.1276.

tert-Butyldimethyl (1-(naphthalen-2-yl)ethoxy)silane 5cb

5cb
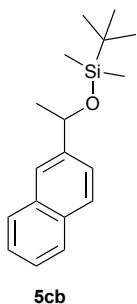
Synthesized according to GP4 using **1c** and **2b** yielding a colourless oil (93%). **^{1}H NMR** (400 MHz, CDCl$_3$) δ 7.95 – 7.82 (3H, m, Ar-*H*), 7.81 (1H, s, Ar-*H*), 7.61 – 7.46 (3H, m, Ar-*H*), 5.08 (1H, q, *J* = 6.4 Hz, O-C*H*-CH$_3$), 1.54 (3H, d, *J* = 6.4 Hz, O-CH-C*H*$_3$), 0.98 (9H, s, Si-C-C*H*$_3$), 0.13 (3H, s, Si-C*H*$_3$), 0.05 (3H, s, Si-C*H*$_3$). **^{13}C NMR** (101 MHz, CDCl$_3$) δ 144.46 (s), 133.37 (s), 132.71 (s), 127.95, 127.86, 127.70, 125.91, 125.43, 124.07, 123.48, 71.05 (O-CH), 27.30 (Si-C-CH$_3$), 25.96 (Si-C-CH$_3$), 18.38 (O-CH-CH$_3$), -4.68 (Si-CH$_3$), -4.74 (Si-CH$_3$). **^{29}Si NMR** (79 MHz, CDCl$_3$) δ +18.98. **HRMS** (70 eV, EI) m/z calc. for C$_{18}$H$_{26}$OSi [M]$^+$ 286.1747; found 286.1745.

Diisopropyl(naphtalen-2-yl)(1-(naphthalen-2-yl)ethoxy)silane 5cc

5cc
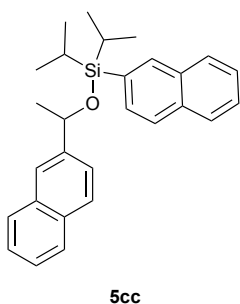
Synthesized according to GP4 using **1c** and **2c** yielding a colourless oil (78%). R_f 0.78 (iHex:EtOAc=19:1). **^{1}H NMR** (400 MHz, CDCl$_3$) δ 8.05 (1H, s, Ar-*H*), 7.90 – 7.79 (6H, m, Ar-*H*), 7.74 (1H, d, J = 7.5 Hz, Ar-*H*), 7.65 – 7.59 (2H, m, Ar-*H*), 7.53 – 7.44 (4H, m, Ar-*H*), 5.24 (1H, q, *J* = 6.3 Hz, O-C*H*-CH$_3$), 1.64 (3H, d, *J* = 6.2 Hz, O-CH-C*H*$_3$), 1.42 (2H, heptd, *J* = 7.4, 1.6 Hz, iPr-C*H*), 1.12 – 1.01 (12H, m, iPr-C*H*$_3$). **^{13}C NMR** (101 MHz, CDCl$_3$) δ 144.53 (s), 135.94, 133.98 (s), 133.47 (s), 132.93 (s), 132.91 (s), 132.43 (s), 131.05, 128.39,

128.13, 128.08, 127.84, 127.78, 126.73, 126.49, 126.05, 125.83, 125.61, 124.22, 123.88, 72.03 (O-CH), 27.87 (O-CH-CH$_3$), 17.66 (iPr-CH$_3$), 17.62 (iPr-CH$_3$), 17.56 (iPr-CH$_3$), 17.47 (iPr-CH$_3$), 12.64 (iPr-CH), 12.55 (iPr-CH). ^{29}Si NMR (79 MHz, CDCl$_3$) δ 6.91. HRMS (70 eV, EI) m/z calc. for C$_{28}$H$_{32}$OSi [M]$^+$ 412.2216; found 412.2197.

Triphenyl(1-(naphthalen-2-yl)ethoxy)silane 5cd[37]
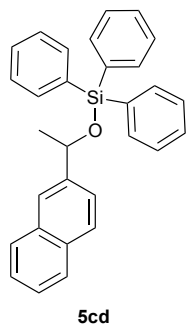
Synthesized according to GP4 using **1c** and **2e** yielding a colourless oil (94%). ^{1}H NMR (400 MHz, CDCl$_3$) δ 7.89 – 7.76 (3H, m, Ar-*H*), 7.74 (1H, s, Ar-*H*), 7.72 – 7.65 (6H, m, Ar-H), 7.57 (1H, dd, *J* = 8.5, 1.7 Hz, Ar-*H*), 7.51 – 7.41 (6H, m, Ar-*H*), 7.41 – 7.34 (6H, m, Ar-*H*), 5.26 (1H, q, *J* = 6.3 Hz, O-C*H*-CH$_3$), 1.56 (d, *J* = 6.4 Hz, O-CH-C*H*$_3$). ^{13}C NMR (101 MHz, CDCl$_3$) δ 143.44 (s), 135.62, 135.12 (s), 134.66 (s), 133.39 (s), 132.85 (s), 130.08, 128.10, 128.03, 127.92, 127.74, 125.96, 125.60, 124.23, 124.11, 72.32 (O-CH), 26.93 (O-CH-CH$_3$). ^{29}Si NMR (79 MHz, CDCl$_3$) δ -12.94. HRMS (70 eV, EI) m/z calc. for C$_{30}$H$_{26}$OSi [M]$^+$ 430.1747; found 430.1748.

Tri(naphtalen-2-yl)(1-(naphthalen-2-yl)ethoxy)silane 5ce
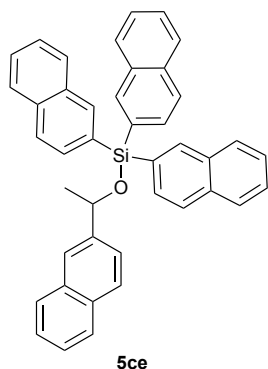
Synthesized according to GP4 using **1c** and **2e** yielding a colourless oil (81%). **R$_f$** 0.63 (iHex:EtOAc=19:1). ^{1}H NMR (400 MHz, CDCl$_3$) δ 8.22 (3H, s, Ar-*H*), 7.88 – 7.81 (8H, m, Ar-*H*), 7.80 – 7.69 (8H, m, Ar-*H*), 7.62 (1H, dd, J = 8.5, 1.7 Hz, Ar-*H*), 7.56 – 7.43 (8H, m, Ar-*H*), 5.37 (1H, q, *J* = 6.3 Hz, O-C*H*-CH$_3$), 1.64 (3H, d, *J* = 6.4 Hz, O-CH-C*H*$_3$). ^{13}C NMR (101 MHz, CDCl$_3$) δ 143.37 (s), 137.19, 134.36 (s), 133.40 (s), 132.97 (s), 132.94 (s), 132.14 (s), 131.25, 128.61, 128.15, 128.08, 127.87, 127.74, 127.30, 127.02, 126.11, 126.03, 125.68, 124.38, 124.35, 72.76 (O-CH), 26.95 (O-CH-CH$_3$). ^{29}Si NMR (79 MHz, CDCl$_3$) δ -11.93. HRMS (70 eV, EI) m/z calc. for C$_{42}$H$_{32}$OSi [M]$^+$ 580.2216; found 580.2222.

Tris(5-chloro-6-methoxynaphthalen-2-yl)(1-(naphthalen-2-yl)ethoxy)silane 5cf
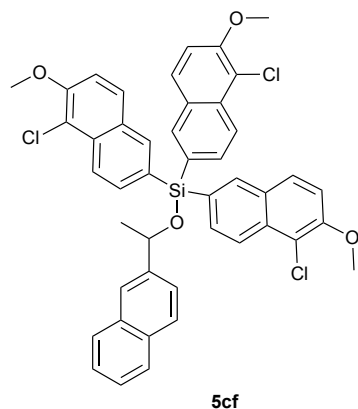
Synthesized according to GP4 using **1c** and **2f** yielding a colourless oil (81%). **R$_f$** 0.72 (iHex:EtOAc=1:1). ^{1}H NMR (400 MHz, CDCl$_3$) δ 8.19 (3H, d, *J* = 8.5 H, Ar-*H*), 8.05 (3H, s, Ar-*H*), 7.86 – 7.75 (6H, m, Ar-*H*), 7.67 – 7.63 (2H, m, Ar-*H*), 7.61 (3H, d, *J* = 9.0 Hz, Ar-*H*), 7.56 (1H, dd, *J* = 8.5, 1.6 Hz, Ar-*H*), 7.46 – 7.38 (2H, m, Ar-*H*), 7.24 (2H, d, *J* = 4.1 Hz, Ar-*H*), 5.29 (1H, q, *J* = 6.3 Hz, C*H*-CH$_3$), 4.02 (9H, s, O-C*H*$_3$), 1.61 (3H, d, *J* = 6.4 Hz, CH-C*H*$_3$). ^{13}C NMR (101 MHz, CDCl$_3$) δ 153.32 (s), 142.94 (s), 137.08, 133.17 (s), 132.78 (s), 132.72 (s), 132.54, 129.86 (s), 128.91 (s), 128.62, 128.05, 127.83, 127.55, 125.91, 125.58, 124.27, 124.08, 122.76, 116.70 (s), 113.53, 72.73 (O-CH), 56.88 (O-CH$_3$), 26.70

(O-CH-CH_3). **^{29}Si NMR** (79 MHz, CDCl$_3$) δ -12.12. **HRMS** (70 eV, EI) m/z calc. for C$_{45}$H$_{35}$Cl$_3$O$_4$Si [M]$^+$ 772.1364; found 772.1365.

(1-(Anthracen-9-yl)ethoxy)trimethylsilane 5da
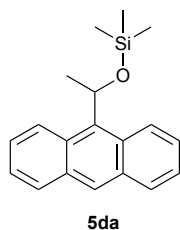
Synthesized according to GP4 using **1d** and **2a** yielding a yellow oil (95%). **^{1}H NMR** (400 MHz, CDCl$_3$) δ 8.80 (2H, br-s, Ar-*H*), 8.42 (1H, s, Ar-*H*), 8.04 (2H, d, *J* = 8.2 Hz, Ar-*H*), 7.58 – 7.47 (4H, m, Ar-*H*), 6.48 (1H, q, *J* = 6.6 Hz, O-C*H*-CH$_3$), 1.95 (3H, d, *J* = 6.7 Hz, O-CH-C*H*$_3$), -0.01 (9H, s, Si-C*H*$_3$). **^{13}C NMR** (101 MHz, CDCl$_3$) δ 136.82 (s), 131.86 (s), 129.37, 127.61 (2C), 125.26 (s), 124.76 (2C), 67.54 (O-*C*H), 25.49 (O-CH-*C*H$_3$), -0.08 (Si-*C*H$_3$). **^{29}Si NMR** (79 MHz, CDCl$_3$) δ +17.50. **HRMS** (70 eV, EI) m/z calc. for C$_{19}$H$_{22}$OSi [M]$^+$ 294.1434; found 294.1434.

(1-(Anthracen-9-yl)ethoxy)tert-butyldimethylsilane 5db
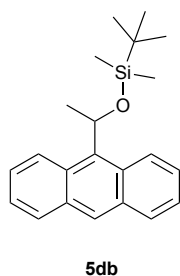
Synthesized according to GP4 using **1d** and **2b** yielding a yellow solid (79%). **mp** 85 – 87 °C. **^{1}H NMR** (400 MHz, CDCl$_3$) δ 9.20 (1H, br-s, Ar-*H*), 8.38 (1H, s, Ar-*H*), 8.25 (1H, br-s, Ar-*H*), 8.00 (2H d, *J* = 9.3 Hz, Ar-*H*), 7.57 – 7.38 (4H, m, Ar-*H*), 6.40 (1H, q, *J* = 6.6 Hz, O-C*H*-CH$_3$), 1.87 (3H, d, *J* = 6.8 Hz, O-CH-C*H*$_3$), 0.87 (9H, s, Si-C-C*H*$_3$), 0.03 (3H, s, Si-C*H*$_3$), -0.36 (3H, s, Si-C*H*$_3$). **^{13}C NMR**[1] (101 MHz, CDCl$_3$) δ 136.97, 129.26, 127.42, 124.69, 67.78 (O-*C*H), 25.96 (Si-C-*C*H$_3$), 25.48 (O-CH-*C*H$_3$), 18.30 (s, Si-*C*-CH$_3$), -4.89 (Si-*C*H$_3$), -4.93 (Si-*C*H$_3$). **^{29}Si NMR** (79 MHz, CDCl$_3$) δ +18.92. **HRMS** (70 eV, EI) m/z calc. for C$_{22}$H$_{28}$OSi [M]$^+$ 336.1903; found 336.1902.

(1-(Anthracen-9-yl)ethoxy)diisopropyl(naphtalen-2-yl)silane 5dc
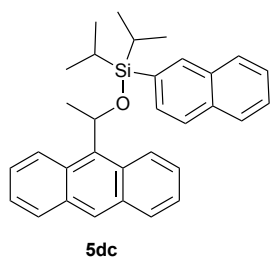
Synthesized according to GP4 using **1d** and **2c** yielding a yellow oil (76%). **R$_f$** 0.71 (*i*Hex:EtOAc=19:1) . **^{1}H NMR** (400 MHz, CDCl$_3$) δ 9.39 (1H, br-s, Ar-*H*), 8.40 (1H, s, Ar-*H*), 8.07 – 7.94 (3H, d, *J* = 6.2 Hz, Ar-*H*), 7.87 (1H, s, Ar-*H*), 7.77 (1H, d, *J* = 8.0 Hz, Ar-*H*), 7.69 (1H, d, *J* = 8.1 Hz, Ar-*H*), 7.55 – 7.34 (8H, m, Ar-*H*), 6.57 (1H, q, *J* = 6.7 Hz, O-C*H*-CH$_3$), 2.01 (3H, d, *J* = 6.7 Hz, O-CH-C*H*$_3$), 1.45 – 1.26 (2H, m, Si-C*H*), 0.98 (6H, t, *J* = 7.6 Hz, Si-CH-C*H*$_3$), 0.86 (6H, dd, *J* = 19.5, 7.4 Hz, Si-CH-C*H*$_3$). **^{13}C NMR**[1] (101 MHz, CDCl$_3$) δ 136.85, 136.04, 134.28 (s), 133.84, 132.79, 132.01, 130.87, 128.72 (s), 128.32, 127.65, 127.63, 127.38 (s), 126.60, 126.40, 126.13 (s), 125.68, 125.48 (s), 125.24 (s), 68.47 (O-*C*H), 25.55 (O-CH-*C*H$_3$), 17.58 (*i*Pr-*C*H$_3$), 17.45 (*i*Pr-*C*H$_3$), 17.25 (*i*Pr-*C*H$_3$), 12.38 (*i*Pr-*C*H). **HRMS** (70 eV, EI) m/z calc. for C$_{32}$H$_{34}$OSi [M]$^+$ 462.2373; found 462.2374.

---

[1] In all of the ^{13}C-NMR spectra of silylethers with alcohol **1d** the resolution of the alcohol carbons was found to be diffuse.

(1-(Anthracen-9-yl)ethoxy)triphenylsilane 5dd
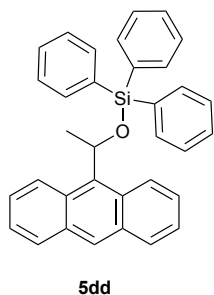
Synthesized according to GP4 using **1d** and **2d** yielding a colourless oil (96%). **¹H NMR** (400 MHz, CDCl₃) δ 9.43 (1H, br-s, Ar-*H*), 8.32 (1H, s, Ar-*H*), 7.96 (2H, d, *J* = 7.8 Hz, Ar-*H*), 7.70 (1H, d, *J* = 6.7 Hz, Ar-*H*), 7.52 (6H, d, *J* = 6.9 Hz, Ar-*H*), 7.45 – 7.37 (3H, m, Ar-*H*), 7.36 – 7.31 (3H, m, Ar-*H*), 7.29 (1H, d, *J* = 7.5 Hz, Ar-*H*), 7.27 – 7.20 (6H, m, Ar-*H*), 6.54 (1H, q, *J* = 6.7 Hz, O-C*H*-CH₃), 1.92 (3H, d, J = 6.7 Hz, O-CH-C*H₃*). **¹³C NMR**[1] (101 MHz, CDCl₃) δ 135.94, 135.59, 135.46, 135.32, 134.32, 129.93, 129.17, 127.84, 127.79, 127.68, 68.81 (O-*C*H), 25.16 (O-CH-*C*H₃). **²⁹Si NMR** (79 MHz, CDCl₃) δ -12.40. **HRMS** (70 eV, EI) m/z calc. for C₃₄H₂₈OSi [M]⁺ 480.1903; found 480.1904.

(1-(Anthracen-9-yl)ethoxy)tri(naphtalen-2-yl)silane 5de
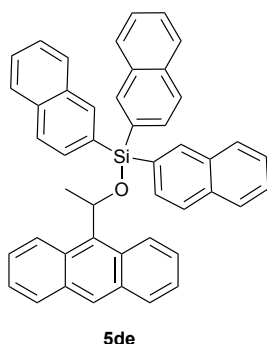
Synthesized according to GP4 using **1d** and **2e** yielding a yellow solid (94%). **mp** 115 °C. **R$_f$** 0.60 (*i*Hex:EtOAc=19:1). **¹H NMR** (400 MHz, CDCl₃) δ 9.58 (1H, br-s, Ar-*H*), 8.27 (1H, s, Ar-*H*), 8.08 (3H, s, Ar-*H*), 7.90 (2H, s, Ar-*H*), 7.79 (3H, d, *J* = 8.1 Hz, Ar-*H*), 7.71 (3H, d, *J* = 8.2 Hz, Ar-*H*), 7.69 – 7.35 (10H, m, Ar-*H*), 7.63 (3H, d, *J* = 8.1 Hz, Ar-*H*), 7.57 (3H, d, *J* = 8.1 Hz, Ar-*H*), 7.01 (1H, br-s, Ar-*H*), 6.69 (1H, q, *J* = 6.7 Hz, O-C*H*-CH₃), 2.03 (3H, d, *J* = 6.7 Hz, O-CH-C*H₃*). **¹³C NMR**[1] (101 MHz, CDCl₃) δ 137.05, 135.87 (s), 134.24 (s), 132.85 (s), 131.78 (s), 130.94, 129.19, 128.56 (s), 127.77, 127.27, 127.15, 127.02, 126.91, 126.06, 125.97, 124.70, 69.10 (O-*C*H), 25.22 (O-CH-*C*H₃). **²⁹Si NMR** (79 MHz, CDCl₃) δ -11.02. **HRMS** (70 eV, EI) m/z calc. for C₄₆H₃₄OSi [M+H]⁺ 631.2451; found 631.2447.

(1-(Anthracen-9-yl)ethoxy)tris(5-chloro-6-methoxynaphthalen-2-yl)silane 5df
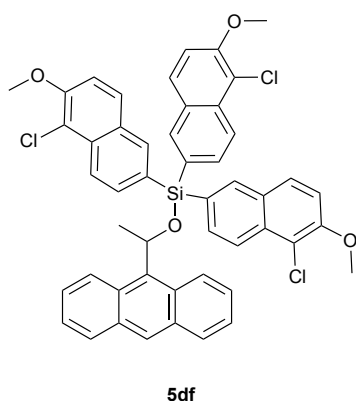
Synthesized according to GP4 using **1d** and **2f** yielding a yellow oil (72%). **¹H NMR** (400 MHz, CDCl₃) δ 9.51 (1H, br-s, Ar-*H*), 8.26 (1H, s, Ar-*H*), 8.24 – 8.14 (1H, br-s, Ar-*H*), 8.09 (3H, d, *J* = 8.5 Hz, Ar-*H*), 7.96 (3H, s, Ar-*H*), 7.95 – 7.71 (4H, m, Ar-*H*), 7.67- 7.31 (4H, m, Ar-*H*), 7.69 (3H, d, *J* = 9.4 Hz, Ar-*H*), 7.50 (3H, d, *J* = 9.0 Hz, Ar-*H*), 7.29 (5H, d, *J* = 4.0 Hz, Ar-*H*), 7.03 (1H, br-s, Ar-*H*), 6.66 (1H, q, *J* = 6.7 Hz, O-C*H*-CH₃), 4.07 (9H, s, O-CH₃), 2.07 (3H, d, *J* = 6.7 Hz, O-CH-C*H₃*). **¹³C NMR**[1] (101 MHz, CDCl₃) δ 153.36, 137.07, 135.62, 134.28, 133.64, 132.73, 132.48, 129.60, 129.20, 128.94, 128.76, 127.83, 127.38, 122.75, 116.69, 113.50, 69.15 (O-*C*H), 57.04 (O-*C*H₃), 29.86 (grease), 25.15 (O-CH-*C*H₃). **²⁹Si NMR** (79 MHz, CDCl₃) δ -11.84. **HRMS** (70 eV, EI) m/z calc. for C₄₉H₃₇Cl₃O₄Si [M]⁺ 822.1521; found 822.1531.

(1-(anthracen-2-yl)ethoxy)trimethylsilane 5ea
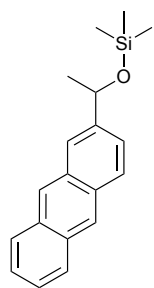
Synthesized according to GP4 using **1e** and **2a** yielding a brown solid (99%). **mp** 123 – 125 °C. **^{1}H NMR** (400 MHz, CDCl$_3$) δ 8.40 (2H, s, Ar-*H*), 8.03 – 7.93 (3H, m, Ar-*H*), 7.91 (1H, s, Ar-*H*), 7.52 – 7.40 (3H, m, Ar-*H*), 5.06 (1H, q, *J* = 6.4 Hz, O-C*H*-CH$_3$), 1.56 (3H, d, *J* = 6.4 Hz, O-CH-C*H*$_3$), 0.13 (9H, s, Si-C*H*$_3$). **^{13}C NMR** (101 MHz, CDCl$_3$) δ 143.16 (s), 131.82 (s), 131.55 (s), 131.52 (s), 131.16 (s), 128.22, 128.12, 128.02, 126.06, 125.92, 125.24, 125.09, 124.09, 123.33, 70.84 (O-CH), 26.44 (O-CH-CH$_3$), 0.15 (Si-CH$_3$). **^{29}Si NMR** (79 MHz, CDCl$_3$) δ +17.59. **HRMS** (70 eV, EI) m/z calc. for C$_{19}$H$_{22}$OSi [M]$^+$ 294.1434; found 294.1436.

5ea

(1-(anthracen-2-yl)ethoxy)tert-butyldimethyl silane 5eb
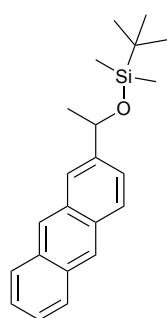
Synthesized according to GP4 using **1e** and **2b** yielding a colourless oil (83%). **^{1}H NMR** (400 MHz, CDCl$_3$) δ 8.45 (1H, s, Ar-*H*), 8.44 (1H, s, Ar-*H*), 8.11 – 8.00 (3H, m, Ar-*H*), 7.52 (1H, s, Ar-*H*), 7.60 – 7.42 (3H, m, Ar-*H*), 5.13 (1H, q, *J* = 6.3 Hz, O-C*H*-CH$_3$), 1.60 (3H, d, *J* = 6.4 Hz, O-CH-C*H*$_3$), 1.04 (9H, s, Si-C-C*H*$_3$), 0.19 (3H, s, Si-C*H*$_3$), 0.10 (3H, s, Si-C*H*$_3$). **^{13}C NMR** (101 MHz, CDCl$_3$) δ 143.72 (s), 131.93 (s), 131.69 (s), 131.60 (s), 131.25 (s), 128.25, 128.24, 128.12, 126.14, 126.05, 125.34, 125.16, 124.17, 123.23, 71.19 (O-CH), 26.93 (O-CH-CH$_3$), 26.03 (Si-C-CH$_3$), 18.44 (s, Si-*C*-CH$_3$), -4.61 (Si-CH$_3$), -4.67 (Si-CH$_3$). **^{29}Si NMR** (79 MHz, CDCl$_3$) δ +19.08. **HRMS** (70 eV, EI) m/z calc. for C$_{22}$H$_{28}$OSi [M]$^+$ 336.1903; found 336.1899.

5eb

(1-(anthracen-2-yl)ethoxy)diisopropyl(naphtalen-2-yl)silane 5ec
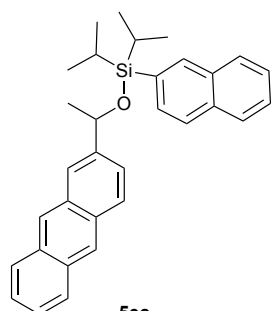
Synthesized according to GP4 using **1e** and **2c** yielding a yellow oil (72%). **R$_f$** 0.63 (*i*Hex:EtOAc=19:1). **^{1}H NMR** (400 MHz, CDCl$_3$) δ 8.45 (1H, s, Ar-*H*), 8.40 (1H, s, Ar-*H*), 8.08 (1H, s, Ar-*H*), 8.07 – 7.99 (3H, m, Ar-*H*), 7.97 (1H, s, Ar-*H*), 7.86 – 7.79 (2H, m, Ar-*H*), 7.74 (1H, d, *J* = 8.0 Hz, Ar-*H*), 7.63 (2H, m, Ar-*H*), 7.52 – 7.43 (4H, m, Ar-*H*), 5.27 (1H, q, *J* = 6.3 Hz, O-C*H*-CH$_3$), 1.68 (3H, d, *J* = 6.3 Hz, O-CH-C*H*$_3$), 1.44 (2H, hept, *J* = 7.4 Hz, iPr-C*H*), 1.09 (12H, m, iPr-C*H*$_3$). **^{13}C NMR** (101 MHz, CDCl$_3$) δ 143.74 (s), 135.94, 133.98 (s), 132.91 (s), 132.43 (s), 132.00 (s), 131.71, 131.40 (s), 131.06, 128.50, 128.39, 128.32, 128.21, 127.77, 126.75, 126.49, 126.26, 126.16, 125.83, 125.43, 125.28, 124.24, 123.66, 72.12 (O-CH), 27.46 (O-CH-CH$_3$), 17.68 (iPr-CH$_3$), 17.63 (iPr-CH$_3$), 17.59 (iPr-CH$_3$), 17.49 (iPr-CH$_3$), 12.67 (iPr-CH), 12.57 (iPr-CH). **^{29}Si NMR** (79 MHz, CDCl$_3$) δ +6.96. **HRMS** (70 eV, EI) m/z calc. for C$_{32}$H$_{34}$OSi [M]$^+$ 462.2373; found 462.2379.

5ec

(1-(anthracen-2-yl)ethoxy)triphenylsilane 5ed
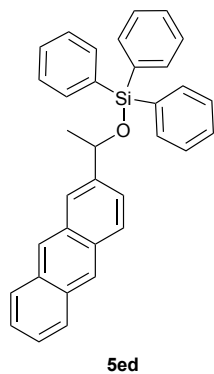
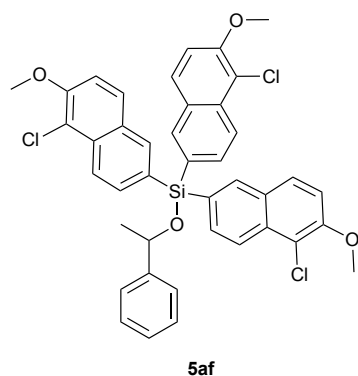Synthesized according to GP4 using **1e** and **2d** yielding a colourless oil (94%). **¹H NMR** (400 MHz, CDCl₃) δ 8.43 (1H, s, Ar-*H*), 8.36 (1H, s, Ar-*H*), 8.08 – 7.96 (3H, m, Ar-*H*), 7.87 (1H, s, Ar-*H*), 7.76 – 7.68 (6H, m, Ar-*H*), 7.57 (1H, dd, *J* = 8.8, 1.6 Hz, Ar-*H*), 7.52 – 7.44 (5H, m, Ar-*H*), 7.42 – 7.37 (6H, m, Ar-*H*), 5.30 (1H, q, *J* = 6.3 Hz, O-C*H*-CH₃), 1.62 (3H, d, *J* = 6.4 Hz, O-CH-C*H₃*). **¹³C NMR** (101 MHz, CDCl₃) δ ¹³C NMR (101 MHz, CDCl₃) δ 142.67 (s), 135.63 , 135.13 (s), 134.66 (s)², 131.93 (s), 131.68 (s), 131.65 (s), 131.32 (s), 130.10, 128.40, 128.30, 128.21, 127.94, 126.33, 126.06, 125.38, 125.27, 124.22, 123.88, 72.42 (O-*C*H), 26.58 (O-CH-*C*H₃). **²⁹Si NMR** (79 MHz, CDCl₃) δ -12.86. **HRMS** (70 eV, EI) m/z calc. for C₃₄H₂₈OSi [M]⁺ 480.1903; found 480.1899.

(1-(anthracen-2-yl)ethoxy)tri(naphtalen-2-yl)silane 5ee
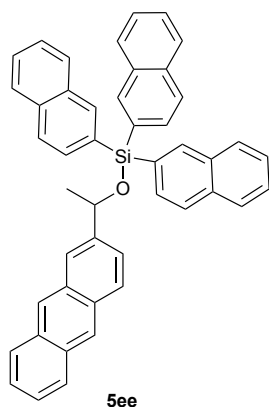
Synthesized according to GP4 using **1e** and **2e** yielding a yellow oil (79%). **R_f** 0.52 (*i*Hex:EtOAc=19:1). **¹H NMR** (400 MHz, CDCl₃) δ 8.39 (1H, s, Ar-*H*), 8.23 (3H, s, Ar-*H*), 8.19 (1H, s, Ar-*H*), 8.03 – 7.92 (3H, m, Ar-*H*), 7.86 – 7.71 (13H, m, Ar-*H*), 7.61 (1H, dd, *J* = 8.8, 1.6 Hz, Ar-*H*), 7.56 – 7.49 (3H, m, Ar-*H*), 7.49 – 7.42 (5H, m, Ar-*H*), 5.38 (1H, q, *J* = 6.3 Hz, O-C*H*-CH₃), 1.67 (3H, d, *J* = 6.4 Hz, O-CH-C*H*). **¹³C NMR** (101 MHz, CDCl₃) δ 142.50 (s), 137.19, 134.37, 132.97, 132.13 (s), 131.93 (s), 131.72 (s), 131.58 (s), 131.34 (s), 131.25, 128.61, 128.51, 128.28, 128.26, 127.86, 127.31, 127.02, 126.36, 126.10, 126.05, 125.34, 125.28, 124.28, 124.25, 72.87 (O-*C*H), 26.55 (O-CH-*C*H₃). **²⁹Si NMR** (79 MHz, CDCl₃) δ -11.96. **HRMS** (70 eV, EI) m/z calc. for C₄₆H₃₄OSi [M]⁺ 630.2373; found 630.2378.

(1-(anthracen-2-yl)ethoxy)tris(5-chloro-6-methoxynaphthalen-2-yl)silane 5ef
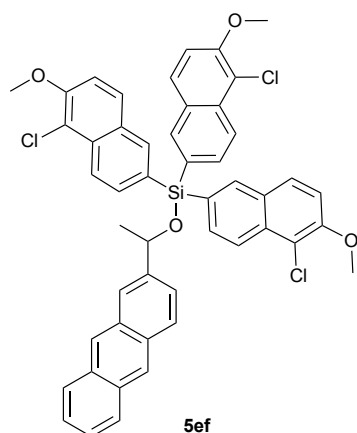
Synthesized according to GP4 using **1e** and **2f** yielding a yellow solid (98%). **mp** 158 °C. **R_f** 0.72 (*i*Hex:EtOAc=1:1) . **¹H NMR** (400 MHz, CDCl₃) δ 8.34 (1H, s, Ar-*H*), 8.23 (3H, d, *J* = 8.5 Hz, Ar-*H*), 8.09 (4H, s, Ar-*H*), 8.00 – 7.90 (3H, m, Ar-*H*), 7.87 (3H, d, *J* = 8.6 Hz, Ar-*H*), 7.64 (1H, s, Ar-*H*), 7.59 (4H, d, *J* = 9.1 Hz, Ar-*H*), 7.49 – 7.42 (2H, m, Ar-*H*), 7.18 (3H, d, *J* = 9.0 Hz, Ar-*H*), 5.34 (1H, q, *J* = 6.3 Hz, C*H*-CH₃), 3.99 (9H, s, O-C*H₃*), 1.70 (3H, d, *J* = 6.4 Hz, CH-C*H₃*). **¹³C NMR** (101 MHz, CDCl₃) δ 153.44, 142.08 (s), 137.25, 132.88, 132.68, 131.90 (s), 131.71 (s), 131.40 (s), 131.26 (s), 129.98 (s), 129.05, 128.75, 128.58 (s), 128.23 (s), 128.22 (s), 126.26 (s), 125.95 (s), 125.32 (s), 125.28 (s), 124.37,

---

² Due to intramolecular interactions the C1-atom of the phenyl rest are not equivalent.

124.08, 122.93, 116.78, 113.58, 73.08 (O-CH), 56.95 (O-CH$_3$), 26.43 (O-CH-CH$_3$). **^{29}Si NMR** (79 MHz, CDCl$_3$) δ -12.29. **HRMS** (70 eV, EI) m/z calc. for C$_{49}$H$_{37}$Cl$_3$O$_4$Si [M]$^+$ 822.1521; found 822.1516.

Trimethyl(1-(pyren-1-yl)ethoxy)silane 5fa
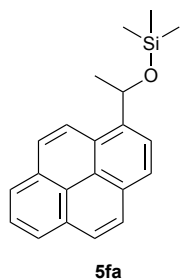
Synthesized according to GP4 using **1f** and **2a** yielding a colourless oil (97%). **^{1}H NMR** (400 MHz, CDCl$_3$) δ 8.45 (1H, d, J = 9.3 Hz, Ar-H), 8.36 (1H, d, J = 8.0 Hz, Ar-H), 8.26 (1H, d, J = 8.0 Hz, Ar-H), 8.23 – 8.19 (2H, m, Ar-H), 8.16 (1H, d, J = 9.3 Hz, Ar-H), 8.12 – 8.00 (3H, m, Ar-H), 6.01 (1H, q, J = 6.4 Hz, O-CH-CH$_3$), 1.82 (3H, d, J = 6.5 Hz, O-CH-CH_3), 0.21 (9H, s, Si-CH_3). **^{13}C NMR** (101 MHz, CDCl$_3$) δ 140.39 (s), 131.50 (s), 130.76 (s), 130.40 (s), 127.63, 127.36, 126.93, 126.74 (s), 125.84, 125.17, 125.15 (s), 125.14, 124.92 (s), 124.89, 123.59, 122.71, 68.39 (O-CH), 27.24 (O-CH-CH$_3$), 0.28 (Si-CH$_3$). **^{29}Si NMR** (79 MHz, CDCl$_3$) δ +17.75. **HRMS** (70 eV, EI) m/z calc. for C$_{21}$H$_{22}$OSi [M]$^+$ 318.1434; found 318.1438.

Tert-butyldimethyl(1-(pyren-1-yl)ethoxy)silane 5fb
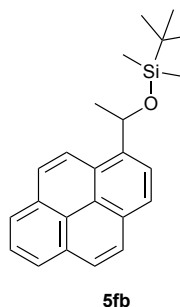
Synthesized according to GP4 using **1f** and **2b** yielding a white solid (94%). **mp** 79-80 °C. **^{1}H NMR** (400 MHz, CDCl$_3$) δ 8.39 (1H, d, J = 9.3 Hz, Ar-H), 8.31 (1H, d, J = 8.0 Hz, Ar-H), 8.26 – 8.17 (3H, m, Ar-H), 8.13 (1H, d, J = 9.3 Hz, Ar-H), 8.11 – 7.98 (3H, m, Ar-H), 5.95 (1H, q, J = 6.3 Hz, O-CH-CH$_3$), 1.73 (3H, d, J = 6.4 Hz, O-CH-CH_3), 0.99 (9H, s, Si-C-CH_3), 0.14 (3H, s, Si-CH_3), 0.01 (3H, s, Si-CH_3). **^{13}C NMR** (101 MHz, CDCl$_3$) δ 140.78 (s), 131.55 (s), 130.81 (s), 130.34 (s), 127.72, 127.34, 126.93, 126.66 (s), 125.90, 125.22, 125.20 (s), 125.16, 124.93 (2C), 123.59, 122.87, 68.82 (O-CH), 27.42 (O-CH-CH$_3$), 26.08 (Si-C-CH$_3$), 18.51 (Si-C-CH$_3$), -4.61 (Si-CH$_3$), -4.69 (Si-CH$_3$). **^{29}Si NMR** (79 MHz, CDCl$_3$) δ +18.97. **HRMS** (70 eV, EI) m/z calc. for C$_{24}$H$_{28}$OSi [M]$^+$ 360.1903; found 360.1904.

Diisopropyl(naphtalen-2-yl)(1-(pyren-1-yl)ethoxy)silane 5fc
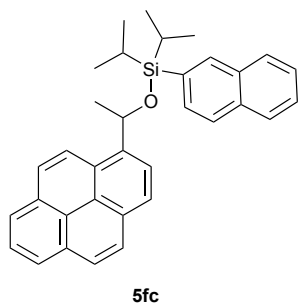
Synthesized according to GP4 using **1f** and **2c** yielding white crystals (79%). **mp** 116 °C. **R$_f$** 0.77 (*i*Hex:EtOAc=19:1). **^{1}H NMR** (400 MHz, CDCl$_3$) δ 8.43 (1H, d, J = 8.0 Hz, Ar-H), 8.31 (1H, d, J = 9.3 Hz, Ar-H), 8.26 (1H, d, J = 8.0 Hz, Ar-H), 8.22 – 8.15 (2H, m, Ar-H), 8.13 – 7.99 (5H, m, Ar-H), 7.84 – 7.76 (2H, m, Ar-H), 7.68 – 7.62 (2H, m, Ar-H), 7.51 – 7.39 (2H, m, Ar-H), 6.12 (1H, q, J = 6.3 Hz, O-CH-CH$_3$), 1.84 (3H, d, J = 6.4 Hz, O-CH-CH_3), 1.45 (2H, heptd, J = 7.5, 1.4 Hz, iPr-CH), 1.11 – 0.99 (12H, m, iPr-CH_3). **^{13}C NMR** (101 MHz, CDCl$_3$) δ 140.64 (s), 135.86, 133.89, 132.84, 132.24 (s), 131.50 (s), 130.93, 130.77 (s), 130.40 (s), 128.27, 127.67, 127.66, 127.34, 126.93, 126.72, 126.61 (s), 126.41, 125.83, 125.73, 125.21, 125.14 (s), 125.10, 124.89 (2C), 123.79 (s), 122.77 (s), 69.43 (O-CH),

27.65 (O-CH-CH_3), 17.59 (iPr-CH_3), 17.56 (iPr-CH_3), 17.50 (iPr-CH_3), 17.39 (iPr-CH_3), 12.63 (iPr-CH), 12.47 (iPr-CH). **^{29}Si NMR** (79 MHz, CDCl$_3$) δ +7.57. **HRMS** (70 eV, EI) m/z calc. for C$_{34}$H$_{34}$OSi [M]$^+$ 486.2373; found 486.2374.

Triphenyl(1-(pyren-1-yl)ethoxy)silane 5fd

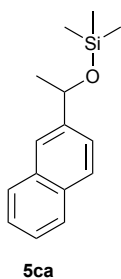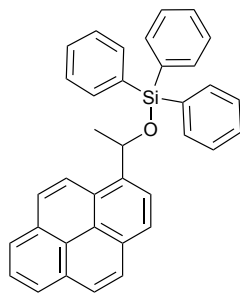Synthesized according to GP4 using **1f** and **2d** yielding a colourless oil (96%). **^{1}H NMR** (400 MHz, CDCl$_3$) δ 8.42 (1h, d, J = 8.0 Hz, Ar-H), 8.17 (4H, dd, J = 19.2, 9.9 Hz, Ar-H), 8.07 (2H, s, Ar-H), 8.01 (2H, d, J = 9.4 Hz, Ar-H), 7.68 (6H, d, J = 6.7 Hz, Ar-H), 7.59 – 7.28 (9H, m, 9H), 6.14 (1H, q, J = 6.4 Hz, O-CH-CH_3), 1.74 (3H, d, J = 6.4 Hz, O-CH-CH_3). **^{13}C NMR** (101 MHz, CDCl$_3$) δ 139.64 (s), 135.43, 134.40, 131.35, 130.62, 130.28, 129.94, 127.80, 127.56, 127.10, 126.84, 126.55, 125.73, 125.12, 125.00, 124.96, 124.78, 124.70, 123.68, 122.69, 69.63 (O-CH), 26.97 (O-CH-CH_3). **^{29}Si NMR** (79 MHz, CDCl$_3$) δ -12.41. **HRMS** (70 eV, EI) m/z calc. for C$_{36}$H$_{28}$OSi [M]$^+$ 504.1903; found 504.1899.

Tri(naphtalen-2-yl)(1-(pyren-1-yl)ethoxy)silane 5fe
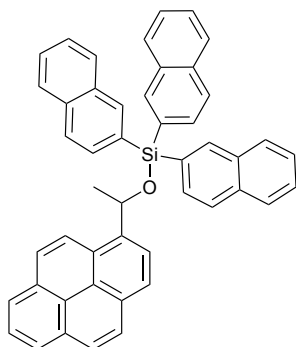
Synthesized according to GP4 using **1f** and **2e** yielding a white solid (79%). **mp** 112 °C. **R$_f$** 0.50(*i*Hex:EtOAc=19:1). **^{1}H NMR** (400 MHz, CDCl$_3$) δ 8.45 (1H, d, J = 8.0 Hz, Ar-H), 8.19 (3H, s, Ar-H), 8.18 – 8.05 (5H, m, Ar-H), 8.03 (2H, s, Ar-H), 7.97 (1H, t, J = 7.6 Hz, Ar-H), 7.87 (1H, d, J = 9.3 Hz, Ar-H), 7.79 (3H, d, J = 8.0 Hz, Ar-H), 7.77 – 7.73 (5H, m, Ar-H), 7.65 (3H, d, J = 8.1 Hz, Ar-H), 7.53 – 7.44 (3H, m, Ar-H), 7.40 (3H, t, J = 8.0 Hz, Ar-H), 6.24 (1H, q, J = 6.3 Hz, O-CH-CH_3), 1.82 (3H, d, J = 6.4 Hz, O-CH-CH_3). **^{13}C NMR** (101 MHz, CDCl$_3$) δ ^{13}C NMR (101 MHz, CDCl$_3$) δ 139.66 (s), 137.13, 134.30, 132.90, 131.99, 131.49 (s), 131.15, 131.02 (s), 130.75 (s), 130.54 (s), 128.55, 127.79, 127.64, 127.30, 127.07, 126.96, 126.88 (s), 126.04, 125.84, 125.24, 125.12, 125.04 (s), 124.96, 124.83 (s), 124.08, 122.82, 70.18 (O-CH), 27.16 (O-CH-CH_3). **^{29}Si NMR** (79 MHz, CDCl$_3$) δ -11.57. **HRMS** (70 eV, EI) m/z calc. for C$_{48}$H$_{234}$OSi [M]$^+$ 654.2373; found 654.2390.

Tris(5-chloro-6-methoxynaphthalen-2-yl)(1-(pyren-1-yl)ethoxy)silane 5ff
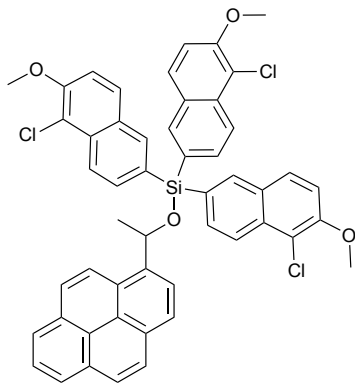
Synthesized according to GP4 using **1f** and **2f** yielding a white solid (88%). **mp** 150 – 153 °C. **R$_f$** 0.70 (*i*Hex:EtOAc=1:1). **1H NMR** (400 MHz, CDCl$_3$) δ 8.37 (1H, d, J = 8.0 Hz, Ar-H), 8.16 – 8.10 (5H, m, Ar-H), 8.07 – 7.99 (7H, m, Ar-H), 7.95 (1H, t, J = 7.6 Hz, Ar-H), 7.85 – 7.80 (4H, m, Ar-H), 7.49 (3H, d, J = 9.0 Hz, Ar-H), 7.13 (3H, d, J = 9.1 Hz, Ar-H), 6.20 (1H, q, J = 6.3 Hz, O-CH), 3.99 (9H, s, O-CH_3), 1.88 (3H, d, J = 6.4 Hz, O-CH-CH_3). **^{13}C NMR** (101 MHz, CDCl$_3$) δ 153.32 (s), 139.36 (s), 137.11, 132.76 (s), 132.56, 131.43 (s), 130.62 (s), 130.52 (s), 129.78, 128.92 (s), 128.64, 127.52, 127.28, 127.11,

126.87 (s), 125.79, 125.18, 125.06, 124.89, 124.87, 124.64 (s), 124.10, 122.88, 122.55, 116.65 (s), 113.44, 70.11 (O-CH), 56.92 (O-CH$_3$), 27.04 (O-CH-CH$_3$). ^{29}**Si NMR** (79 MHz, CDCl$_3$) δ -11.88. **HRMS** (70 eV, EI) m/z calc. for C$_{51}$H$_{37}$Cl$_3$O$_4$Si [M]$^+$ 846.1521; found 846.1526.

Trimethyl(1-(pyren-2-yl)ethoxy)silane 5ga
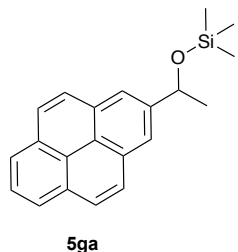
Synthesized according to GP4 using **S1g** and **2a** yielding a colourless oil (56%). ^{1}**H NMR** (400 MHz, CDCl$_3$) δδ 8.21 – 8.16 (4H, m Ar-*H*), 8.08 (4H, s, Ar-*H*), 8.02 – 7.96 (1H, m Ar-*H*), 5.33 (1H, q, J = 6.4 Hz, O-C*H*-CH$_3$), 1.67 (3H, d, J = 6.4 Hz, O-CH-C*H$_3$*), 0.15 (9H, s, Si-C*H$_3$*). ^{13}**C NMR** (101 MHz, CDCl$_3$) δ 144.57 (s), 131.26 (s, 2C), 131.16 (s, 2C), 127.62, 127.56, 125.78, 125.03 (s), 122.16, 71.30 (O-*C*H), 27.87 (O-CH-*C*H$_3$), 0.36 (Si-*C*H$_3$). **HRMS** (70 eV, EI) m/z calc. for C$_{21}$H$_{22}$OSi [M]$^+$ 318.1434; found.

Triphenyl(1-(pyren-2-yl)ethoxy)silane 5gd[39]
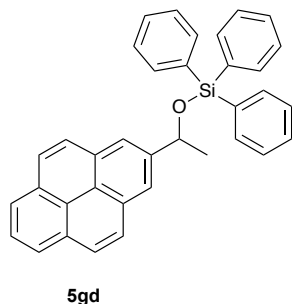
Synthesized according to GP4 using **S1g** and **2d** yielding a shite solid (63%). ^{1}**H NMR** (400 MHz, CDCl$_3$) δ 8.19 (2H, d, J = 7.6 Hz, Ar−*H*), 8.14 (2H, s, Ar−*H*), 8.09 – 7.98 (5H, m, Ar−*H*), 7.67 (6H, dd, J = 7.9, 1.3 Hz, Ar−*H*), 7.45 – 7.40 (3H, m, Ar−*H*), 7.35 (6H, t, J = 7.2 Hz, Ar−*H*), 5.51 (1H, q, J = 6.3 Hz, O−C*H*−CH$_3$), 1.67 (3H, d, J = 6.4 Hz, O−CH−C*H$_3$*). ^{13}**C NMR** (101 MHz, CDCl$_3$) δ 143.78, 135.55, 134.51, 131.08, 131.06, 130.03, 127.86, 127.58, 127.38, 125.70, 124.91, 124.66, 123.96, 122.29, 72.58, 27.62. ^{29}**Si NMR** (79 MHz, CDCl$_3$) δ -13.29. **HRMS** (70 eV, EI) m/z calc. for C$_{36}$H$_{28}$OSi [M]$^+$ 504.1903; found 504.1897.

Tris(5-chloro-6-methoxynaphthalen-2-yl)(1-(pyren-2-yl)ethoxy)silane 5gf[39]
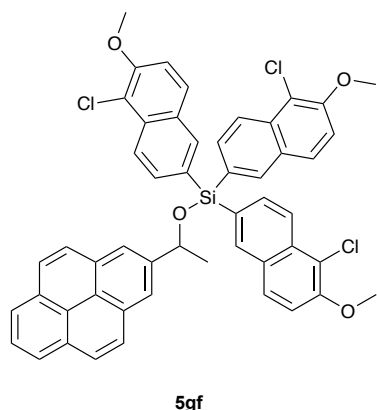
Synthesized according to GP4 using **S1g** and **2f** yielding a yellow oil (60%). ^{1}**H NMR** (400 MHz, CDCl$_3$) δ 8.20 – 8.11 (5H, m, Ar−*H*), 8.08 – 7.95 (8H, m, Ar−*H*), 7.92 – 7.79 (5H, m, Ar−*H*), 7.51 (3H, d, J = 9.0 Hz, Ar−*H*), 7.14 (3H, d, J = 9.1 Hz, Ar−*H*), 5.58 (1H, q, J = 6.2 Hz, O−C*H*−CH$_3$), 3.99 (9H, s, Ar−O−C*H$_3$*), 1.80 (3H, d, J = 6.3 Hz, O−CH−C*H$_3$*). ^{13}**C NMR** (101 MHz, CDCl$_3$) δ 153.34, 143.29, 137.21, 132.78, 132.64, 131.15, 131.12, 129.86, 128.95, 128.66, 127.50, 127.44, 125.77, 124.95, 124.58, 124.04, 122.89, 122.59, 116.65, 113.44, 73.40, 56.94, 27.55. ^{29}**Si NMR** (79 MHz, CDCl$_3$) δ -12.41. **HRMS** (70 eV, EI) m/z calc. for C$_{51}$H$_{37}$Cl$_3$O$_4$Si [M]$^+$ 846.1521; found 846.1512.

3.5.3. X-Ray Crystal Structure Data
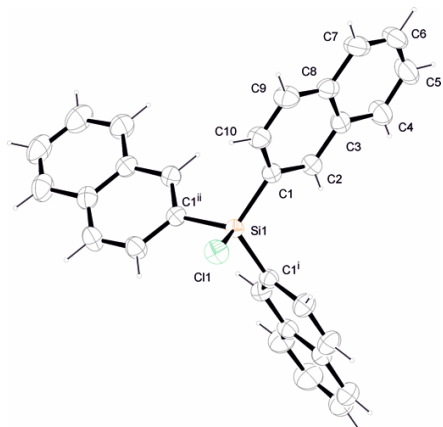
Figure 3.23. Crystal structure of silyl chloride **2e**.

Table 3.13. Crystallographic data for silyl chloride **2e**. A small amount of water was found in the crystal that is not shown in the structure. Symmetric codes: i = 1-x+y, 1-x, z; ii = 1-y, x-y, z.

net formula	$C_{30}H_{21.45}ClO_{0.22}Si$	transmission factor range	0.90–0.99
Mr/g mol^{-1}	449.06	refls. measured	8776
crystal size/mm	0.050 × 0.040 × 0.030	Rint	0.0453
T/K	103.(2)	mean σ(I)/I	0.0367
radiation	MoKα	θ range	3.215–26.371
diffractometer	'Bruker D8 Venture TXS'	observed refls.	1263
crystal system	trigonal	x, y (weighting scheme)	0.0543, 8.1057
space group	'R -3'	hydrogen refinement	constr
a/Å	17.2923(11)	refls in refinement	1649
b/Å	17.2923(11)	parameters	102
c/Å	13.9863(10)	restraints	0
α/°	90	R(F$_{obs}$)	0.0481
β/°	90	R$_w$(F^2)	0.1288
γ/°	120	S	1.026
V/Å^3	3621.9(5)	shift/error$_{max}$	0.001
Z	6	max electron density/ e Å^{-3}	0.433
calc. density/g cm^{-3}	1.235	min electron density/ e Å^{-3}	−0.242
μ/mm^{-1}	0.224		
absorption correction	Multi-Scan		
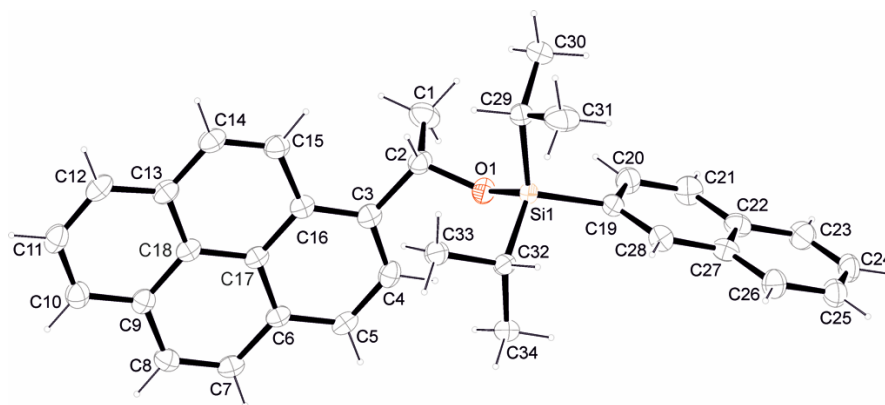
Figure 3.24. Crystal structure of silyl ether **5fc**

Table 3.14. Crystallographic data for silyl ether **5fc**.

net formula	$C_{34}H_{34}OSi$	transmission factor range	0.96–0.99
M_r/g mol^{-1}	486.70	refls. measured	27642
crystal size/mm	0.090 × 0.060 × 0.040	R_{int}	0.0447
T/K	103.(2)	mean $\sigma(I)/I$	0.0332
radiation	MoKα	θ range	3.270–26.372
diffractometer	'Bruker D8 Venture TXS'	observed refls.	4681
crystal system	monoclinic	x, y (weighting scheme)	0.0488, 2.9375
space group	'P 1 21/c 1'	hydrogen refinement	constr
a/Å	10.8826(4)	refls in refinement	5445
b/Å	34.7232(14)	parameters	330
c/Å	7.2800(3)	restraints	0
α/°	90	$R(F_{obs})$	0.0551
β/°	104.291(2)	$R_w(F^2)$	0.1373
γ/°	90	S	1.078
V/Å^3	2665.83(18)	shift/error$_{max}$	0.001
Z	4	max electron density/ e Å^{-3}	0.772
calc. density/g cm^{-3}	1.213	min electron density/ e Å^{-3}	−0.277
μ/mm^{-1}	0.113		
absorption correction	Multi-Scan		

3.6. Computational Methods & Data

3.6.1. Computational Methods

All geometry optimizations and vibrational frequency calculations have been performed using the B3LYP-D3 hybrid functional[40] in combination with the 6-31+G(d) (for H, C, O and N atoms) and 6-311+G(2d) basis set (for Si and Cl atoms).[41] Solvent effects for chloroform have been calculated with the SMD continuum solvation model.[42] Thermochemical corrections to 298.15 K have been calculated for all minima from unscaled vibrational frequencies obtained at this same level.

Initial search of conformational space of every compound has been done with Maestro program. Next, all predicted conformers were optimized and "double-counts" conformers were eliminated, that is, conformers with identical energy or similar geometry to another one. In the case of the silyl ethers **5(a-f)f**, the conformers were generated by taking the three-four best conformers of the analogous silyl ether **5(a-f)e** and adding both methoxy group and chlorine atom. In case of best conformer: the thermochemical corrections have been combined with single point energies calculated at the DLPNO-CCSD(T)/def2-TZVPP//SMD(CHCl$_3$)/B3LYP-D3/6-311+G(2d)/6-31+G(d) level[43]. Solvation factors have been obtained as the difference between the energies computed at B3LYP-D3/6-311+G(2d)/6-31+G(d) in solution and in gas phase. This factor has been added to the energy computed at DLPNO-CCSD(T)/def2-TZVPP//SMD(CHCl$_3$)/B3LYP-D3/6-311+G(2d)/6-31+G(d) to yield free energies G_{298} at 298.15 K. Single point energies at the SMD(CHCl$_3$)/B3LYP/6-31+G(d)/6-311+G(2d) of the optimized geometries were performed to analyse the effect of the dispersion component (D3) on the energies. Free energies in solution have been corrected to a reference state of 1 mol/l at 298.15 K through addition of RTln(24.46) = +7.925 kJ mol^{-1} to the gas phase (1 atm) free energies. All calculations have been performed with Gaussian 09[44] and ORCA version 4.0.[45] The picture in Figure 4 of the manuscript has been plotted with the VMD program.[46]

3.6.2. Geometrical Analysis of Conformers

In order to distinguish π-π stacking and σ-π interactions in the system a geometrical analysis of the conformers for the example of silyl ether **5fe** was performed. One investigated parameter was the distance d between the two aromatic surfaces, measured at the C-atom connected to the bridge. To display the angle α between the aromatic surfaces, the cutting angle of the two planes spanned by three points of each aromatic system was calculated. (see Figure 3.25).
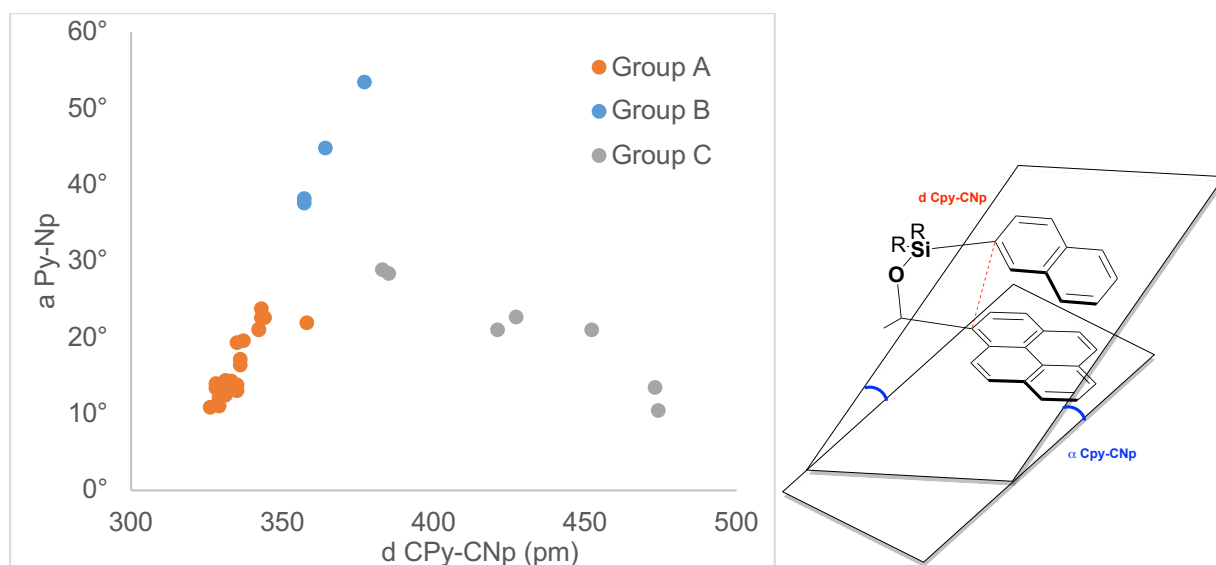
Figure 3.25. left side: Scatter of the found conformers for silyl ether **5fe** depending on the minimal distance between the two aromatic surfaces and the associated angle between the spanned plates. Groups are defined in **Figure 3.26**. Right side: Illustration of the used parameters d and α.
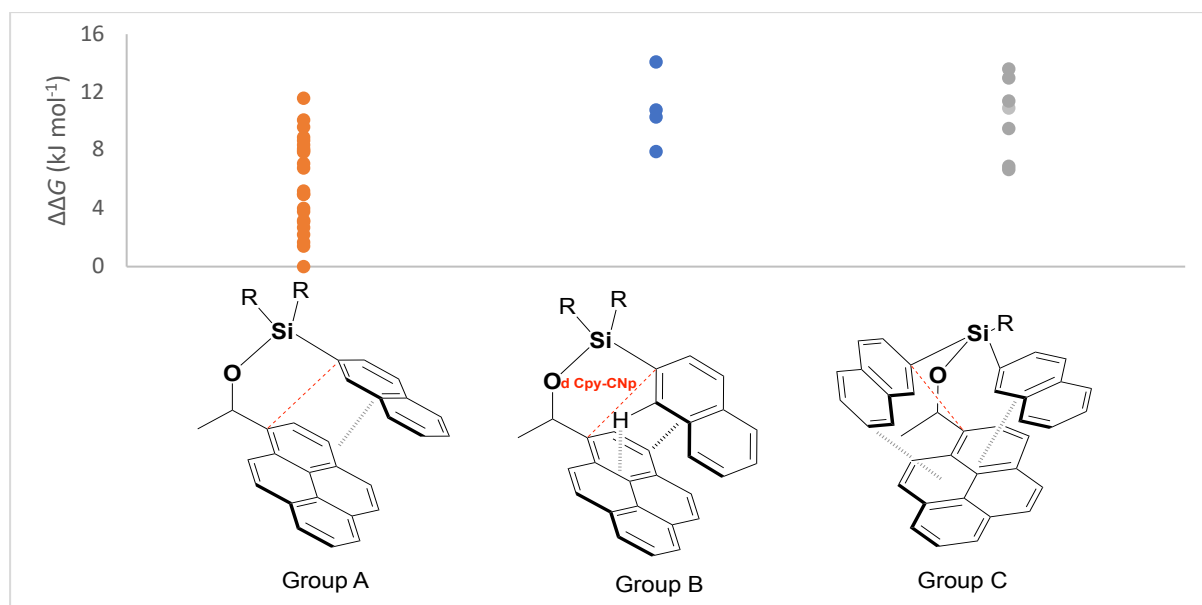
Figure 3.26. Conformers of silyl ether **5fe** grouped by different aromatic-aromatic interactions and relative free energy of conformers in these groups.

The analysis shows that the interacting aromatic surfaces in all conformers are twisted towards each other for at least 10°. Taking the differential angles and distances into account three groups of conformers can be formed (Figure 3.26):

Group A (orange in Figure 3.25), parallel displaced π - π-stacking: The two interacting surfaces are twisted 10°-25° towards each other and the distance of bridge heads is less than 3.6 Å. One aromatic group is slightly parallel displaced with respect to the other group. In those conformers mainly π - π interactions occur. (Number of conformers in this group: 23, among them the 12 most stable conformers)

Group B (blue in Figure 3.25), tilted aromatic stacking: The two big surfaces are twisted more than 35° against each other, the distance of the bridgeheads is in between 3.5 Å and 3.8 Å. The surfaces interact through a combination of π-π stacking and σ - π interaction, the latter one occurs between an aromatic hydrogen of the naphthyl surface and the pyrenyl surface. (Number of conformers in this group: 4, best conformer in this group with $\Delta\Delta G_{298}$ = +7.9 kJ mol^{-1})

Group C (grey in Figure 3.25), double parallel displaced π - π-stacking: The last group samples conformers in which the pyrenyl surface is located in between two different oriented naphthyl surfaces, minimum distance of bridgehead is 3.8 Å. In this case, the two naphthyl surfaces interact with the pyrenyl surface through a combination of σ-π interactions and π-π stacking. (Number of conformers in this group: 7; best conformer in this group with $\Delta\Delta G_{298}$ = +6.7 kJ mol^{-1})

The analysis reveals that conformations with parallel displaced π - π-stacking of one naphthyl group with the pyrenyl group are most stable, while a small twist around 20° of the two interacting moieties also seems to be favourable.
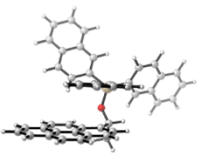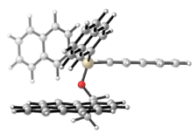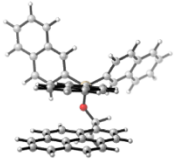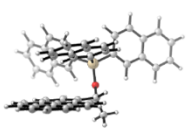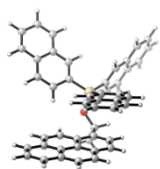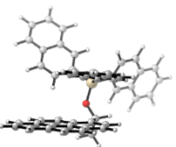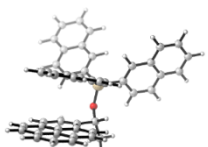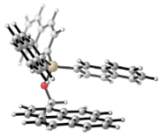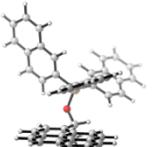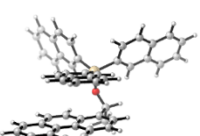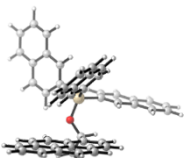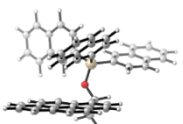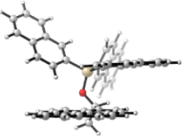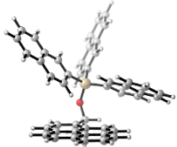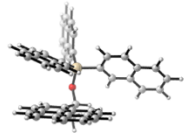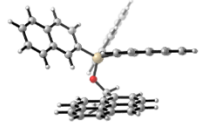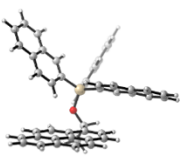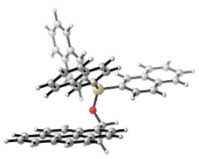
Table 3.15. Geometrical parameters for conformers of silyl ether **5fe** in order of decreasing $G_{298,sol}$. A, B and C refers to the geometrical groups depicted above.

Name of conformer	$G_{298,sol}$ SMD/B3LYP-D3/ 6-311+G(2d)/6-31+G(d)	Group	ΔG_{298}	d CPy-CNp	α CPy-CNp
Np4_1_17	-2214.0629075	A	0.0	3.43	22.6
Np4_1_9	-2214.0623835	A	1.4	3.43	23.8
Np4_1_14	-2214.0622725	A	1.7	3.35	19.4
Np4_1_19	-2214.0620655	A	2.2	3.44	22.6
Np4_1_35	-2214.0618895	A	2.7	3.26	10.9
Np4_1_13	-2214.0617355	A	3.1	3.35	13.8
Np4_1_41	-2214.0617015	A	3.2	3.31	12.5
Np4_1_38	-2214.0614745	A	3.8	3.3	13.4
Np4_1_34	-2214.0613985	A	4.0	3.35	13.1
Np4_1_39	-2214.0610115	A	5.0	3.28	13.4
Np4_1_15	-2214.0609905	A	5.0	3.37	19.6
Np4_1_37	-2214.0609085	A	5.2	3.29	11.1
Np4_1_1	-2214.0603685	C	6.7	4.21	21.0
Np4_1_32	-2214.0603165	A	6.8	3.36	17.2
Np4_1_2	-2214.0602815	C	6.9	4.27	22.7
Np4_1_51	-2214.0601965	A	7.1	3.28	14.0
Np4_1_25	-2214.0599145	A	7.9	3.29	12.1
Np4_1_20	-2214.0598965	B	7.9	3.77	53.5
Np4_1_28	-2214.0598795	A	8.0	3.33	14.3
Np4_1_8	-2214.0598325	A	8.1	3.42	21.1
Np4_1_22	-2214.0597065	A	8.4	3.29	12.2
Np4_1_26	-2214.0595905	A	8.7	3.31	14.4

Np4_1_43	-2214.0595185	A	8.9	3.36	16.4
Np4_1_4	-2214.0592745	C	9.5	3.85	28.4
Np4_1_48	-2214.0592465	A	9.6	3.58	22.0
Np4_1_33	-2214.0590695	A	10.1	3.34	13.7
Np4_1_21	-2214.0589755	B	10.3	3.64	44.8
Np4_1_23	-2214.0588045	B	10.8	3.57	38.2
Np4_1_45	-2214.0587485	C	10.9	4.74	10.5
Np4_1_29	-2214.0585595	C	11.4	3.83	28.9
Np4_1_12	-2214.0585015	A	11.6	3.42	21.0
Np4_1_5	-2214.0579535	C	13.0	4.73	13.5
Np4_1_36	-2214.0577185	C	13.6	4.52	21.0
Np4_1_24	-2214.0575485	B	14.1	3.57	37.6

Table 3.16. Visualisation of conformers for silyl ether **5fe** in order of decreasing $G_{298,sol}$. A, B and C monitors the group the conformer was put in as described above.

Np4_1_25 **A**	Np4_1_20 **B**	Np4_1_28 **A**	Np4_1_8 **A**
Np4_1_22 **A**	Np4_1_26 **A**	Np4_1_43 **A**	Np4_1_4 **C**
Np4_1_48 **A**	Np4_1_33 **A**	Np4_1_21 **B**	Np4_1_23 **B**
Np4_1_45 **C**	Np4_1_29 **C**	Np4_1_12 **A**	Np4_1_5 **C**
Np4_1_36 **C**	Np4_1_24 **B**		

3.6.3. Overview of Reaction Free Energies
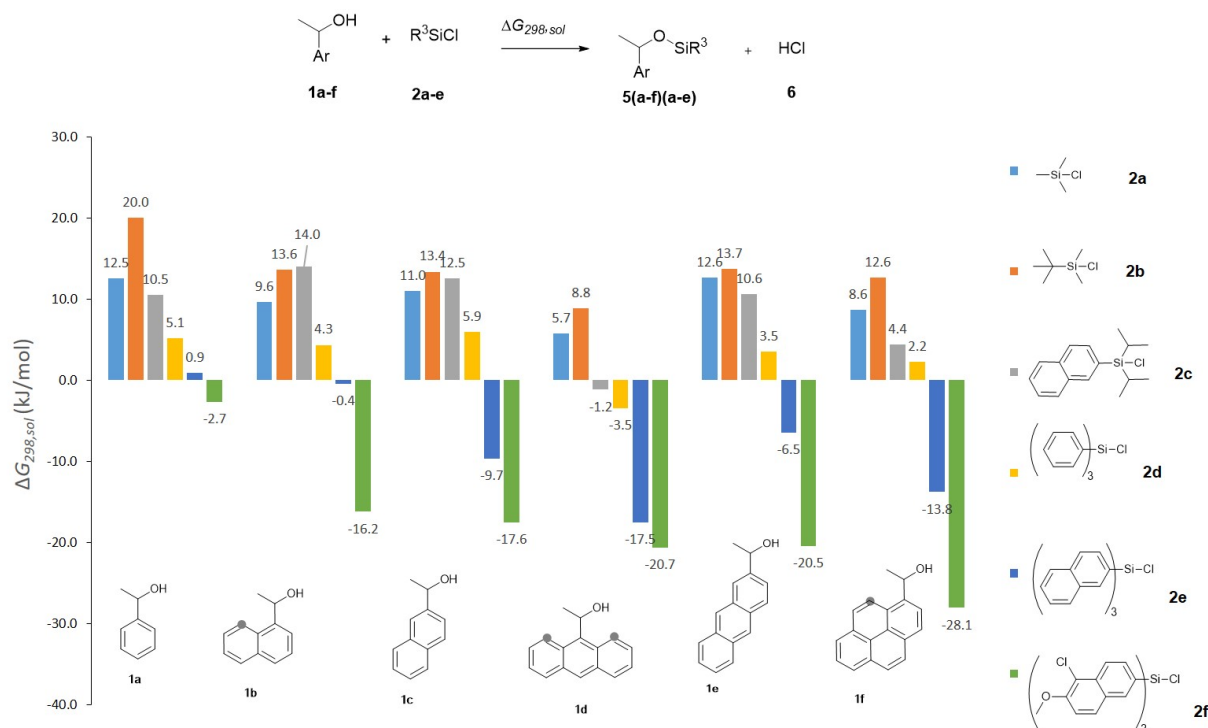
Figure 3.27. Reaction free energies, $\Delta G_{298,sol}$, computed at SMD(CHCl$_3$)/DLPNO-CCSD(T)/def2-TZVPP//SMD(CHCl$_3$)/B3LYP-D3/6-311+G(2d)/6-31+G(d) theoretical level.
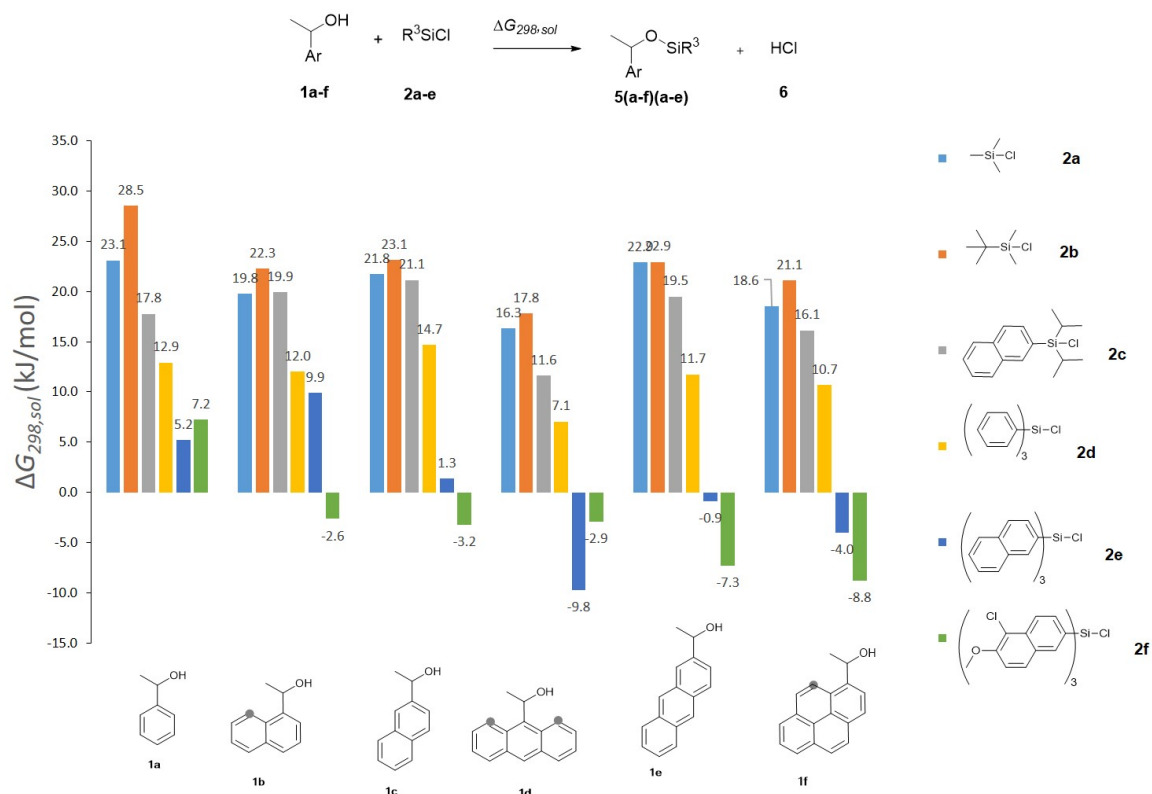
Figure 3.28. Reaction free energies, $\Delta G_{298,sol}$, computed at SMD(CHCl3)/B3LYP-D3/6-311+G(2d)/6-31+G(d) theoretical level.
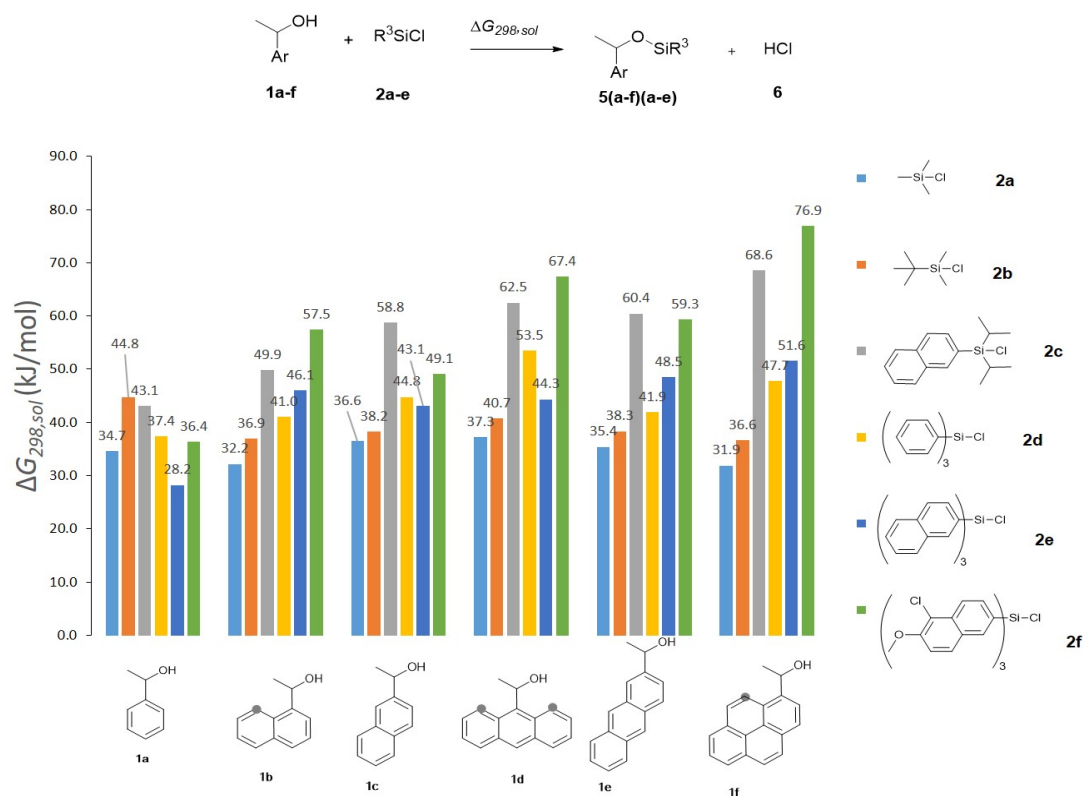
Figure 3.29. Reaction free energies, $\Delta G_{298,sol}$, computed at SMD(CHCl3)/B3LYP /6-311+G(2d)/6-31+G(d)//SMD(CHCl3)/B3LYP-D3/6-311+G(2d)/6-31+G(d) theoretical level.
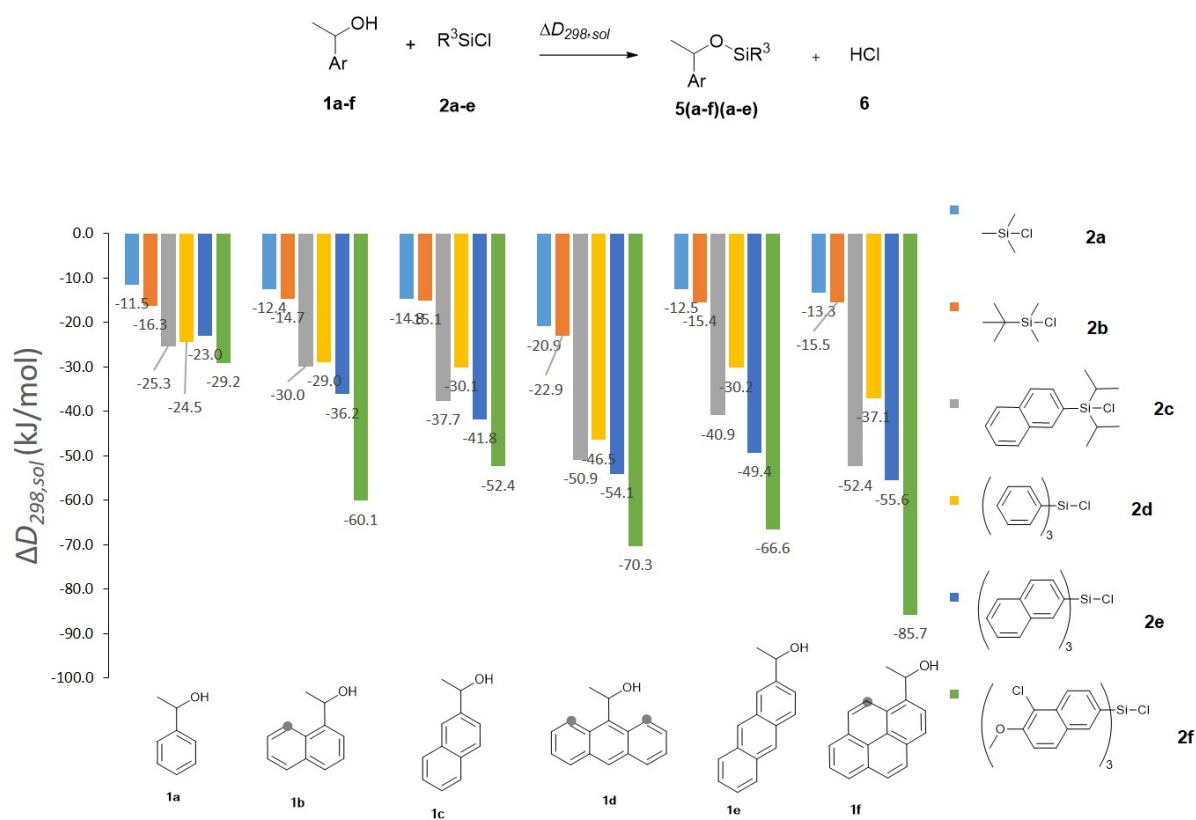
Figure 3.30. Dispersion contribution, $\Delta D_{298,sol}$.

3.6.4. Correlation of Experimental and Computational Results

The Bell-Evans-Polanyi equation describes a linear proportionality of the difference in activation energy between two reactions of the same family and their reaction enthalpy (Eq. 3.18).

$$E_a = E_0 + \alpha \Delta H$$

Eq. 3.18

In this equation E_a is the activation energy of an individual reaction, E_0 is the activation energy of a reference reaction of the same family of reactions and ΔH is the enthalpy of the reaction yielding the product of that individual reaction. Unfortunately, the activation energy is often not directly accessible. The Marcus equation thus proposes a relationship of reaction free energy and the free energy barrier of the reaction $\Delta G^{\ddagger}$ (Eq. 3.19) with $\widetilde{G}$ the intrinsic barrier and ΔG^0 the reaction free energy.[47]

$$\Delta G^{\ddagger} = \tilde{G}\left(1 + \left(\frac{\Delta G^0}{4\tilde{G}}\right)\right)^2$$

Eq. 3.19

For a series of similar reactions – like the silylation reactions in this study – it can be thus expected that reaction free energy and $\Delta G^{\ddagger}$ correlate with each other. With the Eyring equation Eq. 3.20 we can rewrite k_{rel} as Eq. 3.21:

$$k = \frac{k_B T}{h} \cdot e^{-\frac{\Delta G^{\ddagger}}{RT}}$$

Eq. 3.20

$$\ln(k_{rel}) = \ln\left(\frac{k_1}{k_2}\right) = \ln\left(\frac{\frac{k_B T}{h} \cdot e^{-\frac{\Delta G_1^{\ddagger}}{RT}}}{\frac{k_B T}{h} \cdot e^{-\frac{\Delta G_2^{\ddagger}}{RT}}}\right) = \frac{\Delta G_2^{\ddagger} - \Delta G_1^{\ddagger}}{RT}$$

Eq. 3.21

$$\ln(k_{rel}) = \frac{\Delta\Delta G^{\ddagger}}{RT}$$

Eq. 3.22

If we assume a correlation as described by the Marcus equation we get:

$$\ln(k_{rel}) \sim \Delta\Delta G^0$$

Eq. 3.23

Accordingly, in **Figure 3.31** experimental $\ln(k_{rel})$ was plotted against calculated differences in reaction free energy. Linear regressions with good to acceptable correlation factor R^2 were found for the following silyl reagents: TMSCl (**2a**), TBDMSCl (**2b**) and TPSCl (**2d**). However, that quality drops notably for silyl reagents carrying bigger DED: DINSCl (**2c**), TNSCl (**2e**) and TN*SCl (**2f**). From the Marcus equation it can be thus assumed, that intrinsic barriers for these reactions differ among each other and that the observed differences in k_{rel} are a kinetic phenomenon. Interestingly, **Figure 3.32** shows a much better correlation between k_{rel} and the differences in the dispersion contributions. As discussed in the main text it is thus likely that the stabilization of the transition state by attractive dispersion forces governs selectivity.
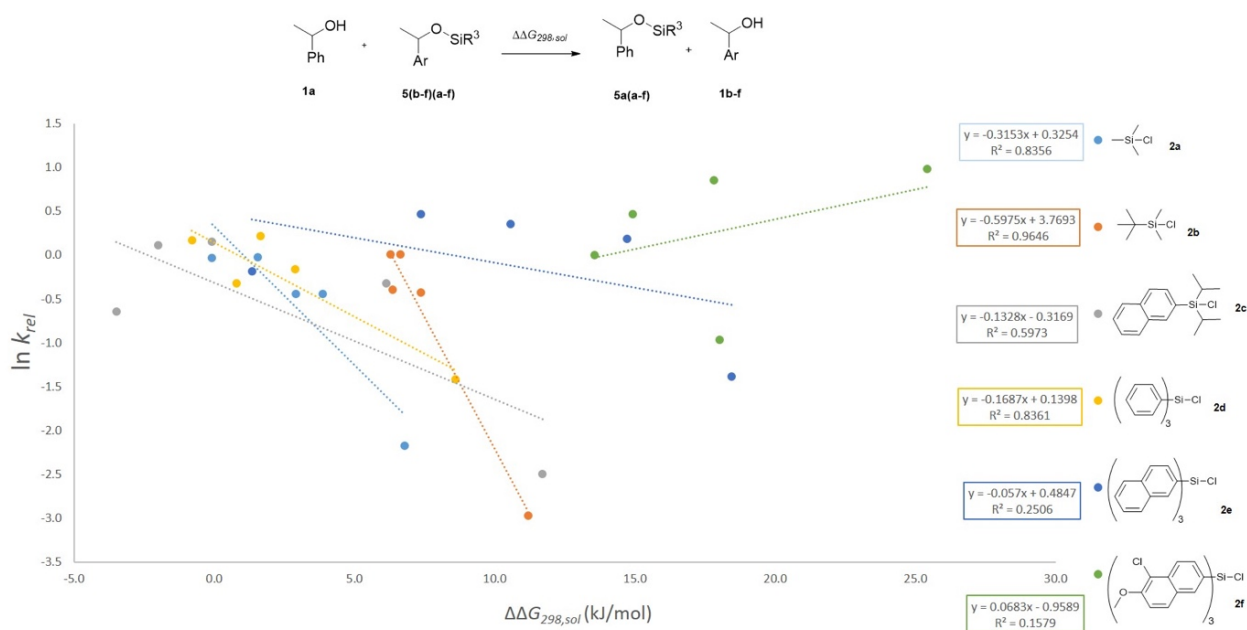
Figure 3.31. Experimental ln (k_{rel}) vs $\Delta\Delta G_{298,sol}$, computed at SMD(CHCl3)/DLPNO-CCSD(T)/def2-TZVPP//SMD(CHCl3)/B3LYP-D3/6-311+G(2d)/6-31+G(d) theoretical level.
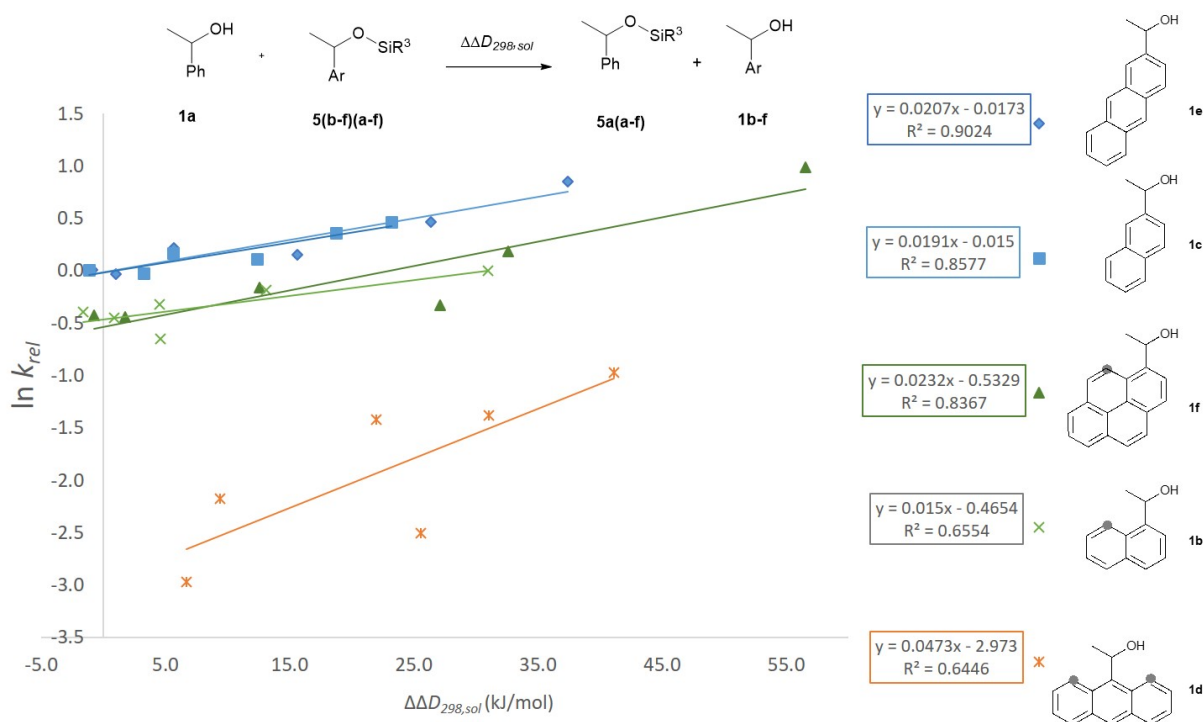
Figure 3.32. Experimental ln (k_{rel}) vs $\Delta\Delta D_{298,sol}$. $\Delta D_{298,sol}$ was calculated as the difference between $\Delta G_{298,sol}$ computed at SMD(CHCl$_3$)/B3LYP-D3/6-311+G(2d)/6-31+G(d) and those computed at SMD(CHCl$_3$)/B3LYP/6-311+G(2d)/6-31+G(d)//SMD(CHCl$_3$)/B3LYP-D3/6-311+G(2d)/6-31+G(d) theoretical level.

3.6.5. Calculation of Reaction Free Energies and Dispersion Contribution

Table 3.17. Total energies and free energies for best conformer of alcohols **1**, silyl reagents **2** and products **5** (in Hartree). Molar free energies in solution at 298.15 K ($G_{298,sol}$) have been calculated at the SMD(CHCl$_3$)/DLPNO-CCSD(T)/def2-TZVPP// SMD(CHCl$_3$)/B3LYP-D3/6-311+G(2d)/6-31+G(d) level and corrected for a solution standard state of 1 M through addition of +7.925 kJ mol^{-1} (0.00301848 Hartree). The SMD(CHCl$_3$)/B3LYP-D3/6-311+G(2d)/6-31+G(d) level of theory has been used to optimize the geometries and calculate solute thermal corrections and solvation factor. Note that the filenames are used in our calculations and do not follow any guide.

	Filename	E_{tot} SMD/B3LYP-D3/ 6-311+G(2d)/6-31+G(d) [a]	E_{tot} SMD/B3LYP/ 6-311+G(2d) /6-31+G(d) [a]	G_{298} SMD/B3LYP-D3/ 6-311+G(2d)/6-31+G(d)	$G_{298,sol}$ SMD/B3LYP-D3/ 6-311+G(2d)/6-31+G(d)	E_{tot} SMD/DLPNO-CCSD(T)/def2-TZVPP [b]	$G_{298,sol}$ SMD/DLPNO-CCSD(T)/def2-TZVPP	Solvation Factor
1a	roh1_1	-386.1285457	-386.1149812	-386.0006440	-385.9976255	-385.4196861	-385.3024998	-0.0137339
1b	roh2_1_1	-539.7816611	-539.7604473	-539.6090270	-539.6060085	-538.7709992	-538.6133748	-0.0180281
1c	roh2_2_2	-539.7847329	-539.7649283	-539.6132800	-539.6102615	-538.7728081	-538.6164995	-0.0181628
1d	roh3_9_1	-693.4236962	-693.3948650	-693.2078480	-693.2048295	-692.1109742	-691.9136651	-0.0215576
1e	roh3_2_2	-693.4345314	-693.4083506	-693.2193170	-693.2162985	-692.1192876	-691.9236697	-0.0226150
1f	roh4_1_1	-769.6780488	-769.6469639	-769.4497090	-769.4466905	-768.2160648	-768.0085874	-0.0238808
2a	TMSCl	-869.6013765	-869.5929900	-869.5210940	-869.5180755	-868.3934327	-868.3171674	-0.0070358
2b	TBSCl_1	-987.5495242	-987.5273332	-987.3893590	-987.3863405	-986.1114994	-985.9572336	-0.0089180
2c	DPNpSiCl_1	-1372.2683456	-1372.2264517	-1371.9882150	-1371.9851965	-1370.0723368	-1369.8088113	-0.0196236
2d	ph3sicl_04	-1444.8488463	-1444.8136734	-1444.6243200	-1444.6213015	-1442.5112315	-1442.3075940	-0.0239073
2e	NpSiCl_6	-1905.8181159	-1905.7630765	-1905.4602600	-1905.4572415	-1902.5720454	-1902.2482170	-0.0370460
2f	NpOMeSiCl_8	-3628.2847123	-3628.2084773	-3627.8742980	-3627.8712795	-3623.0124930	-3622.6432020	-0.0441417
5aa	TMS1__1	-794.8873872	-794.8610407	-794.6673630	-794.6643445	-793.4808859	-793.2705780	-0.0127348
5ab	TBS1_3	-912.8352609	-912.7933123	-912.5335650	-912.5305465	-911.1982956	-910.9077925	-0.0142112
5ac	DiNp1_1	-1297.5573313	-1297.4922339	-1297.1365120	-1297.1334935	-1295.1619109	-1294.7629810	-0.0249078
5ad	Ph1_3	-1370.1406613	-1370.0826056	-1369.7744740	-1369.7714555	-1367.6029972	-1367.2638218	-0.0300304
5ae	Np1_9	-1831.1102695	-1831.0329051	-1830.6133450	-1830.6103265	-1827.6632706	-1827.2060497	-0.0427221
5af	NpOMe1_42	-3553.5779082	-3553.4770053	-3553.0266220	-3553.0236035	-3548.1059294	-3547.6023931	-0.0507684

	Filename	E_{tot} SMD/B3LYP-D3/ 6-311+G(2d)/6-31+G(d) [a]	E_{tot} SMD/B3LYP/ 6-311+G(2d) /6-31+G(d) [a]	G_{298} SMD/B3LYP-D3/ 6-311+G(2d)/6-31+G(d)	$G_{298,sol}$ SMD/B3LYP-D3/ 6-311+G(2d)/6-31+G(d)	E_{tot} SMD/DLPNO-CCSD(T)/def2-TZVPP [b]	$G_{298,sol}$ SMD/DLPNO-CCSD(T)/def2-TZVPP	Solvation Factor
5ba	TMS2_1_1	-948.5409852	-948.5066496	-948.2770250	-948.2740065	-946.8326363	-946.5825621	-0.0169045
5bb	TBS2_1_8	-1066.4893794	-1066.4403939	-1066.1443310	-1066.1413125	-1064.5503938	-1064.2210913	-0.0187644
5bc	DiNp2_1_2	-1451.2119687	-1451.1374544	-1450.7440810	-1450.7410625	-1448.5142636	-1448.0725265	-0.0291691
5bd	Ph2_1_1	-1523.7955173	-1523.7280915	-1523.3831940	-1523.3801755	-1520.9565647	-1520.5750005	-0.0337775
5be	Np2_1_46	-1984.7659439	-1984.6773311	-1984.2241900	-1984.2211715	-1981.0187123	-1980.5205634	-0.0466235
5bf	NpOMe2_1_17	-3707.2352467	-3707.1149023	-3706.6387610	-3706.6357425	-3701.4663062	-3700.9184357	-0.0516337
5ca	TMS2_2_2	-948.5442240	-948.5104011	-948.2805140	-948.2774955	-946.8348894	-946.5851686	-0.0170077
5cb	TBS2_2_4	-1066.4922930	-1066.4445469	-1066.1482600	-1066.1452415	-1064.5523618	-1064.2243232	-0.0190128
5cc	DiNp2_2_12	-1451.2127233	-1451.1366788	-1450.7478700	-1450.7448515	-1448.5153255	-1448.0762163	-0.0287626
5cd	Ph2_2_10	-1523.7980693	-1523.7316379	-1523.3864340	-1523.3834155	-1520.9579262	-1520.5775173	-0.0342447
5ce	Np2_2_38	-1984.7691648	-1984.6784212	-1984.2274580	-1984.2244395	-1981.0228172	-1980.5240753	-0.0459834
5cf	NpOMe2_2_38	-3707.2374636	-3707.1214818	-3706.6432380	-3706.6402195	-3701.4661763	-3700.9220732	-0.0531410
5da	TMS3_9_3	-1102.1852162	-1102.1400278	-1101.8771510	-1101.8741325	-1100.1754559	-1099.8843276	-0.0199553
5db	TBS3_9_2	-1220.1337755	-1220.0740150	-1219.7448550	-1219.7418365	-1217.8932528	-1217.5232200	-0.0219062
5dc	DiNp3_9_26	-1604.8558713	-1604.7657737	-1604.3460630	-1604.3430445	-1601.8597281	-1601.3786060	-0.0317047
5dd	Ph3_9_5	-1677.4402401	-1677.3585337	-1676.9839090	-1676.9808905	-1674.3014524	-1673.8782597	-0.0361568
5de	Np3_9_3	-2138.4115823	-2138.3071103	-2137.8262520	-2137.8232335	-2134.3644870	-2133.8242424	-0.0481043
5df	NpOMe3_9_9	-3860.8783581	-3860.7465177	-3860.2376840	-3860.2346655	-3854.8094477	-3854.2204217	-0.0546666
5ea	TMS_3_2_1	-1102.1932852	-1102.1539443	-1101.8861200	-1101.8831015	-1100.1800958	-1099.8917170	-0.0218050
5eb	TBS3_2_1	-1220.1416168	-1220.0873806	-1219.7543650	-1219.7513465	-1217.8981474	-1217.5313576	-0.0234805
5ec	DiNp3_2_1	-1604.8658113	-1604.7821484	-1604.3545340	-1604.3515155	-1601.8655763	-1601.3841183	-0.0328377
5ed	Ph3_2_3	-1677.4483943	-1677.3755433	-1676.9935910	-1676.9905725	-1674.3048833	-1673.8856213	-0.0385597

	Filename	E_{tot} SMD/B3LYP-D3/ 6-311+G(2d)/6-31+G(d) [a]	E_{tot} SMD/B3LYP/ 6-311+G(2d) /6-31+G(d) [a	G_{298} SMD/B3LYP-D3/ 6-311+G(2d)/6-31+G(d)	$G_{298,sol}$ SMD/B3LYP-D3/ 6-311+G(2d)/6-31+G(d)	E_{tot} SMD/DLPNO-CCSD(T)/def2-TZVPP [b]	$G_{298,sol}$ SMD/DLPNO-CCSD(T)/def2-TZVPP	Solvation Factor
5ee	Np3_2_1	-2138.4202918	-2138.3202677	-2137.8343340	-2137.8313155	-2134.3694687	-2133.8300313	-0.0495388
5ef	NpOMe3_2_12	-3860.8916408	-3860.7638606	-3860.2508240	-3860.2478055	-3854.8187247	-3854.2303504	-0.0554609
5fa	TMS4_1_2	-1178.4377323	-1178.3931826	-1178.1181640	-1178.1151455	-1176.2779169	-1175.9781423	-0.0228122
5fb	TBS4_1_2	-1296.3860085	-1296.3268300	-1295.9854580	-1295.9824395	-1293.9956373	-1293.6166883	-0.0246200
5fc	DiNp4_1_2	-1681.1109569	-1681.0180149	-1680.5862030	-1680.5831845	-1677.9656278	-1677.4714091	-0.0335537
5fd	Ph4_1_3	-1753.6924697	-1753.6120968	-1753.2243870	-1753.2213685	-1750.4031535	-1749.9710061	-0.0389538
5fe	Np4_1_17	-2214.6653811	-2214.5580860	-2214.0659260	-2214.0629075	-2210.4698483	-2209.9177402	-0.0503655
5ff	NpOMe4_1_13	-3937.1365877	-3936.9966171	-3936.4817920	-3936.4787735	-3930.9206560	-3930.3181673	-0.0553255
HCl	hcl_1	-460.8341522	-460.8341495	-460.8455730	-460.8425545	-460.3307889	-460.3443202	-0.0051289

[a] C, H, O : 6-31+G(d) Si, Cl : 6-311+G(d) [b] Solv Factor added

Table 3.18. ln(k_{rel}) and reaction free energies $\Delta G_{298,sol}$ of the formation of the products **5(a-f)(a-e)**, computed at different levels of theory (kJ mol^{-1}). Dispersion contribution ($\Delta D_{298,sol}$) calculated as the difference of the $\Delta G_{298,sol}$ computed at B3LYP-D3 and B3LYP level, respectively, is shown at the end of the table.

	1a-f	2a-e		5(a-f)(a-e)	6

ln(k_{rel})					
	1a	**1b**	**1c**	**1d**	**1e**	**1f**
2a	0.000	-0.447	-0.024	-2.173	-0.031	-0.443
2b	0.000	-0.396	0.010	-2.973	0.010	-0.425
2c	0.000	-0.649	0.113	-2.501	0.149	-0.326
2d	0.000	-0.320	0.170	-1.419	0.216	-0.162
2e	0.000	-0.188	0.357	-1.383	0.465	0.182
2f	0.000	-0.002	0.469	-0.968	0.852	0.984

SMD(CHCl$_3$)/DLPNO-CCSD(T)/def2-TZVPP//SMD(CHCl$_3$)/B3LYP-D3/6-311+G(2d)/6-31+G(d)[a,b]					
	1a	**1b**	**1c**	**1d**	**1e**	**1f**
2a	12.5	9.6	11.0	5.7	12.6	8.6
2b	20.0	13.6	13.4	8.8	13.7	12.6
2c	10.5	14.0	12.5	-1.2	10.6	4.4
2d	5.1	4.3	5.9	-3.5	3.5	2.2
2e	0.9	-0.4	-9.7	-17.5	-6.5	-13.8
2f	-2.7	-16.2	-17.6	-20.7	-20.5	-28.1

SMD(CHCl$_3$)/B3LYP-D3/6-311+G(2d)/6-31+G(d)[a]					
	1a	**1b**	**1c**	**1d**	**1e**	**1f**
2a	23.1	19.8	21.8	16.3	22.9	18.6
2b	28.5	22.3	23.1	17.8	22.9	21.1
2c	17.8	19.9	21.1	11.6	19.5	16.1
2d	12.9	12.0	14.7	7.1	11.7	10.7
2e	5.2	9.9	1.3	-9.8	-0.9	-4.0
2f	7.2	-2.6	-3.2	-2.9	-7.3	-8.8

SMD(CHCl$_3$)/B3LYP/6-311+G(2d)/6-31+G(d)//SMD(CHCl$_3$)/B3LYP-D3/6-311+G(2d)/6-31+G(d)[a]					
	1a	**1b**	**1c**	**1d**	**1e**	**1f**
2a	34.7	32.2	36.6	37.3	35.4	31.9
2b	44.8	36.9	38.2	40.7	38.3	36.6
2c	43.1	49.9	58.8	62.5	60.4	68.6
2d	37.4	41.0	44.8	53.5	41.9	47.7
2e	28.2	46.1	43.1	44.3	48.5	51.6
2f	36.4	57.5	49.1	67.4	59.3	76.9

DISPERSION CONTRIBUTION [$\Delta D_{298,sol} = \Delta G_{298,sol}$(B3LYP) - $\Delta G_{298,sol}$(B3LYP-D3)]					

	1a	1b	1c	1d	1e	1f
2a	-11.5	-12.4	-14.8	-20.9	-12.5	-13.3
2b	-16.3	-14.7	-15.1	-22.9	-15.4	-15.5
2c	-25.3	-30.0	-37.7	-50.9	-40.9	-52.4
2d	-24.5	-29.0	-30.1	-46.5	-30.2	-37.1
2e	-23.0	-36.2	-41.8	-54.1	-49.4	-55.6
2f	-29.2	-60.1	-52.4	-70.3	-66.6	-85.7

[a] C, H, O : 6-31+G(d) Si, Cl : 6-311+G(d) [b] Solv Factor at B3LYP-D3 added to the E(SCF) at DLPNO-CCSD(T)/def2-TZVPP

Table 3.19. ln(k_{rel}), reaction free energy differences $\Delta\Delta G_{298,sol}$ computed at SMD(CHCl3)/DLPNO-CCSD(T)/def2-TZVPP//SMD(CHCl3)/B3LYP-D3/6-311+G(2d)/6-31+G(d)[a,b], and differences in the dispersion contribution ($\Delta\Delta D_{298,sol}$) (kJ mol^{-1}) for the transformation shown in the scheme at the top of the table.

| 1a | 5(b-f)(a-f) | 5a(a-f) | 1b-f |

ln(k_{rel})						
	1a	1b	1c	1d	1e	1f
2a	0.000	-0.447	-0.024	-2.173	-0.031	-0.443
2b	0.000	-0.396	0.010	-2.973	0.010	-0.425
2c	0.000	-0.649	0.113	-2.501	0.149	-0.326
2d	0.000	-0.320	0.170	-1.419	0.216	-0.162
2e	0.000	-0.188	0.357	-1.383	0.465	0.182
2f	0.000	-0.002	0.469	-0.968	0.852	0.984

$\Delta\Delta G_{298,sol}$						
	1a	1b	1c	1d	1e	1f
2a	0.0	2.9	1.6	6.8	-0.1	3.9
2b	0.0	6.4	6.6	11.2	6.3	7.4
2c	0.0	-3.5	-2.0	11.7	-0.1	6.1
2d	0.0	0.8	-0.8	8.6	1.7	2.9
2e	0.0	1.3	10.6	18.5	7.4	14.7
2f	0.0	13.6	14.9	18.0	17.8	25.4

$\Delta\Delta D_{298,sol}$						
	1a	1b	1c	1d	1e	1f
2a	0.0	0.9	3.2	9.4	1.0	1.8
2b	0.0	-1.6	-1.2	6.7	-0.9	-0.8
2c	0.0	4.6	12.4	25.6	15.6	27.1
2d	0.0	4.5	5.6	22.0	5.7	12.6
2e	0.0	13.1	18.7	31.1	26.4	32.6
2f	0.0	31.0	23.2	41.1	37.4	56.6

[a] C, H, O : 6-31+G(d) Si, Cl : 6-311+G(d) [b] Solv Factor at B3LYP-D3 added to the E(SCF) at DLPNO-CCSD(T)/def2-TZVPP

3.7. Supplementary References

[1]   G. Ma, J. Deng, M. P. Sibi, *Angew. Chem. Int. Ed.* **2014**, *53*, 11818-11821.
[2]   H. B. Kagan, J. C. Fiaud, *Top. Stereochem.* **1988**, *18*, 249-300.
[3]   S. Hoops, S. Sahle, R. Gauges, C. Lee, J. Pahle, N. Simus, M. Singhal, L. Xu, P. Mendes, U. Kummer, *Bioinformatics* **2006**, *22*, 3067-3074.
[4]   proFit 7.0.11, Uetikon am See, **2016**.
[5]   W. L. F. Armarego, C. L. L. Chai, *Purification of laboratory chemicals*, 6 ed., Elsevier Inc., Amsterdam, **2009**.
[6]   G. C. Fu, *Acc. Chem. Res.* **2000**, *33*, 412-420.
[7]   M. J. Kamlet, J. M. Abboud, M. H. Abraham, R. W. Taft, *J. Org. Chem.* **1983**, *48*, 2877-2887.
[8]   a) M. H. Abraham, P. L. Grellier, D. V. Prior, P. P. Duce, *J. Chem. Soc. Perkin Trans. II* **1989**, 699-711; b) M. H. Abraham, P. L. Grellier, D. V. Prior, J. J. Morris, P. J. Taylor, *J. Chem. Soc. Perkin Trans II* **1990**, 521-529.
[9]   C. A. Hunter, *Angew. Chem. Int. Ed.* **2004**, *43*, 5310-5324.
[10]   a) J. H. Hildebrand, *J. Am. Chem. Soc.* **1929**, *51*, 66-80; b) J. H. Hildebrand, *Science* **1965**, *150*, 441-450; c) J.-L. M. Abbud, R. Notario, *Pure Appl. Chem.* **1999**, *71*, 645-781.
[11]   a) C. M. Hansen, *The three dimensional solubility parameter and solvent diffusion coefficient*, Technical University of Denmark (Copenhagen), **1967**; b) H. W. Milliman, D. Boris, D. A. Schiraldi, *Macromolecules* **2012**, *45*, 1931-1936.
[12]   a) K. Dimroth, C. Reichardt, T. Siepmann, F. Bohlmann, *Liebigs Ann.* **1963**, *661*, 1-37; b) J. P. Cerón-Carrasco, D. Jacquemin, C. Laurence, A. Planchat, C. Reichardt, K. Sraïdi, *J. Phys. Org. Chem.* **2014**, *27*, 512-518.
[13]   J. Catalán, V. López, P. Pérez, R. Martin-Villamil, J.-G. Rodríguez, *Liebigs Ann.* **1995**, 241-252.
[14]   J. Catalán, H. Hopf, *Eur. J. Org. Chem.* **2004**, 4694-4702.
[15]   J. Catalán, *J. Phys. Chem. B* **2009**, *113*, 5951-5960.
[16]   T. Lu, F. Chen, *J. Comput. Chem.* **2012**, *33*, 580-592.
[17]   C. S. Calero, J. Farwer, E. J. Gardiner, C. A. Hunter, M. Mackey, S. Scuderi, S. Thompson, J. G. Vinter, *Phys. Chem. Chem. Phys.* **2013**, *15*, 18262-18273.
[18]   C. Reichardt, *Solvents and Solvent Effects in Organic Chemistry*, WILEY-VCH, Weinheim, **2003**.
[19]   M. H. Abraham, H. S. Chadha, G. S. Whiting, R. C. Mitchell, *J. Pharm. Sci.* **1994**, *83*, 1085-1100.
[20]   W. K. Stephenson, R. Fuchs, *Can. J. Chem.* **1985**, *63*, 2535-2539.
[21]   F. Besseau, M. Lucon, C. Laurence, M. Berthelot, *J. Chem. Soc. Perkin Trans II* **1998**, 101-107.
[22]   M. Chastrette, M. Rajzmann, M. Chanon, K. F. Purcell, *J. Am. Chem. Soc.* **1985**, *107*, 1-11.
[23]   S. Abbott, "HSP Basics", https://www.stevenabbott.co.uk/practical-solubility/hsp-basics.php, accessed at 13.02.2018, **2013**.
[24]   B. U. Emenike, S. N. Bey, B. C. Bigelow, S. V. S. Chakravartula, *Chem. Sci.* **2016**, *7*, 1401-1407.
[25]   AnalystSoft, StatPlus:mac LE, **2019**.
[26]   L. Yang, C. Adam, S. L. Cockroft, *J. Am. Chem. Soc.* **2015**, *137*, 10084-10087.
[27]   a) R. Pollice, M. Bot, I. J. Kobylianskii, I. Shenderovich, P. Chen, *J. Am. Chem. Soc.* **2017**, *139*, 13126-13140; b) J. W. Hwang, P. Li, K. D. Shimizu, *Org. Biomol. Chem.* **2017**, *15*, 1554-1564; c) C. Adam, L. Yang, S. L. Cockroft, *Angew. Chem. Int. Ed.* **2015**, *54*, 1164-1167; d) L. Yang, C. Adam, G. S. Nichol, S. L. Cockroft, *Nat. Chem.* **2013**, *5*, 1006-1010.
[28]   A. S. Rury, C. Ferry, J. R. Hunt, M. Lee, D. Mondal, S. M. O. O'Connell, E. N. H. Phan, Z. Peng, P. Pokhilko, D. Sylvinson, Y. Zhou, C. H. Mak, *J. Phys. Chem. C* **2016**, *120*, 23858-23869.
[29]   J. Helberg, M. Marin-Luna, H. Zipse, *Synthesis* **2017**, *49*, 3460-3470.
[30]   B. Giese, *Angew. Chem. Int. Ed.* **1977**, *16*, 125-136.
[31]   J. P. Wagner, P. R. Schreiner, *Angew. Chem. Int. Ed.* **2015**, *54*, 12274-12296.
[32]   R. K. Akhani, M. I. Moore, J. G. Pribyl, S. L. Wiskur, *J. Org. Chem.* **2014**, *79*, 2384-2396.
[33]   J. C. Christian Atherton, S. Jones, *J. Chem. Soc., Perkin Trans. 1* **2002**, 2166-2173.
[34]   Y. Li, S. Yu, X. Wu, J. Xiao, W. Shen, Z. Dong, J. Gao, *J. Am. Chem. Soc.* **2014**, *136*, 4031-4039.
[35]   K. Kamieńska-Trela, L. Kania, P. Bernatowicz, M. Bechcicka, Ł. Kaczmarek, J. Wójcik, *Spectrochim. Acta A* **2000**, *56*, 2079-2090.
[36]   R. Mir, T. Dudding, *J. Org. Chem.* **2017**, *82*, 709-714.
[37]   L. C. Wilkins, J. L. Howard, S. Burger, L. Frentzel-Beyme, D. L. Browne, R. L. Melen, *Adv. Synth. Catal.* **2017**, *359*, 2580-2584.
[38]   S. Y. Park, J. W. Lee, C. E. Song, *Nat. Commun.* **2015**, *6*, 7512.
[39]   C. Gross, *Aromatic interactions and size effects in the hydrosilylation reaction of ketones*, Master thesis, LMU München (Munich), **2019**.
[40]   a) A. D. Becke, *J. Chem. Phys.* **1993**, *98*, 5648; b) C. Lee, W. Yang, R. G. Parr, *Phys. Rev. B* **1988**, *37*, 785-789; c) S. Grimme, *J. Chem. Phys.* **2006**, *124*, 034108.
[41]   G. W. Spitznagel, T. Clark, J. Chandrasekhar, P. R. Schleyer, *J. Comput. Chem.* **1982**, *3*, 363-371.
[42]   A. V. Marenich, C. J. Cramer, D. G. Truhlar, *J. Phys. Chem. B* **2009**, *113*, 6378.
[43]   a) C. Riplinger, F. Neese, *J. Chem. Phys.* **2013**, *138*, 034106; b) C. Riplinger, B. Sandhoefer, A. Hansen, F. Neese, *J. Chem. Phys.* **2013**, *139*, 134101; c) F. Weigend, R. Ahlrichs, *Phys. Chem. Chem. Phys.* **2005**, *7*, 3297-3305.
[44]   G. W. T. M. J. Frisch, H. B. Schlegel, G. E. Scuseria, M. A. Robb, J. R. Cheeseman, G. Scalmani, V. Barone, B. Mennucci, G. A. Petersson, H. Nakatsuji, M. Caricato, X. Li, H. P. Hratchian, A. F. Izmaylov, J. Bloino, G. Zheng, J. L. Sonnenberg, M. Hada, M. Ehara, K. Toyota, R. Fukuda, J. Hasegawa, M. Ishida, T. Nakajima, Y. Honda, O. Kitao, H. Nakai, T. Vreven, J. A. Montgomery, Jr., J. E. Peralta, F. Ogliaro, M. Bearpark, J. J. Heyd, E. Brothers, K. N. Kudin, V. N. Staroverov, T. Keith, R. Kobayashi, J. Normand, K. Raghavachari, A. Rendell, J. C. Burant, S. S. Iyengar, J. Tomasi, M. Cossi, N. Rega, J. M. Millam, M. Klene, J. E. Knox, J. B. Cross, V. Bakken, C. Adamo, J. Jaramillo, R. Gomperts, R. E. Stratmann, O. Yazyev, A. J. Austin, R. Cammi, C. Pomelli, J. W. Ochterski, R. L. Martin, K. Morokuma, V. G. Zakrzewski, G. A. Voth, P. Salvador, J. J. Dannenberg, S. Dapprich, A. D. Daniels, O. Farkas, J. B. Foresman, J. V. Ortiz, J. Cioslowski, and D. J. Fox,, Gaussian 09, Revision D.01, Wallingford CT, **2010**.
[45]   F. Neese, *Comput. Mol. Sci.* **2012**, *2*, 73-78.
[46]   W. Humphrey, A. Dalke, K. Schulten, *J. Molec. Graphics* **1996**, *14*, 33-38.
[47]   F. A. Carey, R. J. Sundberg, *Advanced Organic Chemistry, Part A: Structure and Mechanisms*, Springer, New York, **2007**.

Chapter 4. Rate Accelerations in the Lewis Acid-Catalysed Hydrosilylation of Ketones.

Benjamin Pölloth, Christoph Gross, Hendrik Zipse

Unpublished results. Manuscript under preparation.

Parts of the results were already reported by Christoph Gross in "*Aromatic interactions and size effects in the hydrosilylation reaction of ketones*", Master thesis, LMU München (Munich), **2019**. Therein he declares that data from his work can be reused and published by his supervisors (B.P. and H.Z.) if C.G. is mentioned as co-author.

Author contributions: The study was conceived by B.P. and H.Z. Competition experiments were performed by C.G. under the supervision of B.P. in his master project. Syntheses were performed by C.G. and B.P. Analysis of experiments was performed by C.G. and B.P. The computational study was performed by B.P. The manuscript and the supporting information were written by B.P.

Additional information: NMR-spectra, integral tables for competition experiments, and further details on the investigation of side-reactions are available in the master thesis of C.G.

4.1. Introduction

In the previous chapters we showed a notable size-dependent rate acceleration for the silylation of primary and secondary alcohols. While all of those reactions were Lewis base-catalysed or uncatalysed, silyl ethers can also be synthesized from other reactants as shown in **Scheme 4.1**.
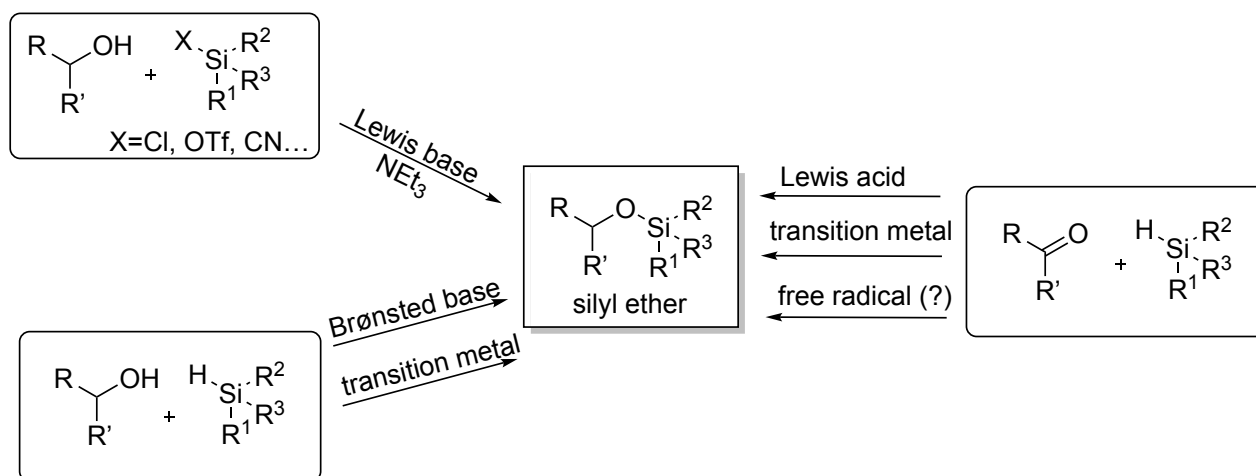
Scheme 4.1. Different approaches for the synthesis of silyl ethers.

Most commonly, for the silylation of alcohols silyl reagents bearing an anionic leaving group are used in Lewis base-catalysed reactions. The nature of the leaving group leads to large differences in reaction rates and also affects the selectivity for primary versus secondary alcohols.[1] Very good leaving groups like triflate react readily in the presence of a simple amine base.[2] Silyl ethers can be synthesized directly from hydrosilanes, for example, through Brønsted base catalysis with *t*BuOK[3] or through transition metal catalysis[4] (for examples for asymmetric catalysis see Chapter 5). However, silyl ethers can also be prepared from the corresponding ketone or aldehyde by reductive hydrosilylation reactions. For this latter transformation a multitude of methods is known. Transition metal catalysts with rhodium,[5] zinc[6] or copper[7] give high yields and offer various possibilities for asymmetric hydrosilylation reactions.[8] Already in the 1950s Gilman and Wittenberg[9] reported a catalyst-free hydrosilylation of benzophenone with various aryl silanes at 250 °C. In 1967, Kumada *et al.*[10] found evidences for the existence of free alkyl silane radicals at 140 °C. In the 1980s the behaviour of silyl radicals was intensely studied by electron paramagnetic resonance spectroscopy.[11] Additionally, rate constants for the addition of triethylsilyl radicals to ketones are reported.[12] However, reports of the synthetic use of free radical hydrosilylation of ketones are rare[13] and usually comprise specific additives like thiols as polarity reversal catalyst.[14] A notable exception is tris(trimethylsilyl)silane that can be used as radical reagent in a variety of reactions.[15] Finally, Chatgilialoglu stated 2008 on free radical hydrosilylation reactions: "Trialkylsilanes are not capable of donating their hydrogen atom at a sufficient rate to propagate the chain. (…) Phenyl or mixed alkyl/phenyl-substituted silicon hydrides show similar reactivities to trialkylsilanes".[15b] Recently, photocatalytic hydrosilylation reactions of alkenes and alkynes were reported.[16] From the class of organocatalysts especially the Lewis acid $B(C_6F_5)_3$ was found as very efficient catalyst for the hydrosilylation reaction of ketones. It was first introduced 1964 by Massey

and Park[17]. Parks and Piers[18] found it an efficient catalyst for the hydrosilylation reaction of aldehydes, ketones and esters. Two different catalytic pathways are possible, involving either silane or ketone activation by the Lewis acid (see **Scheme 4.2**).
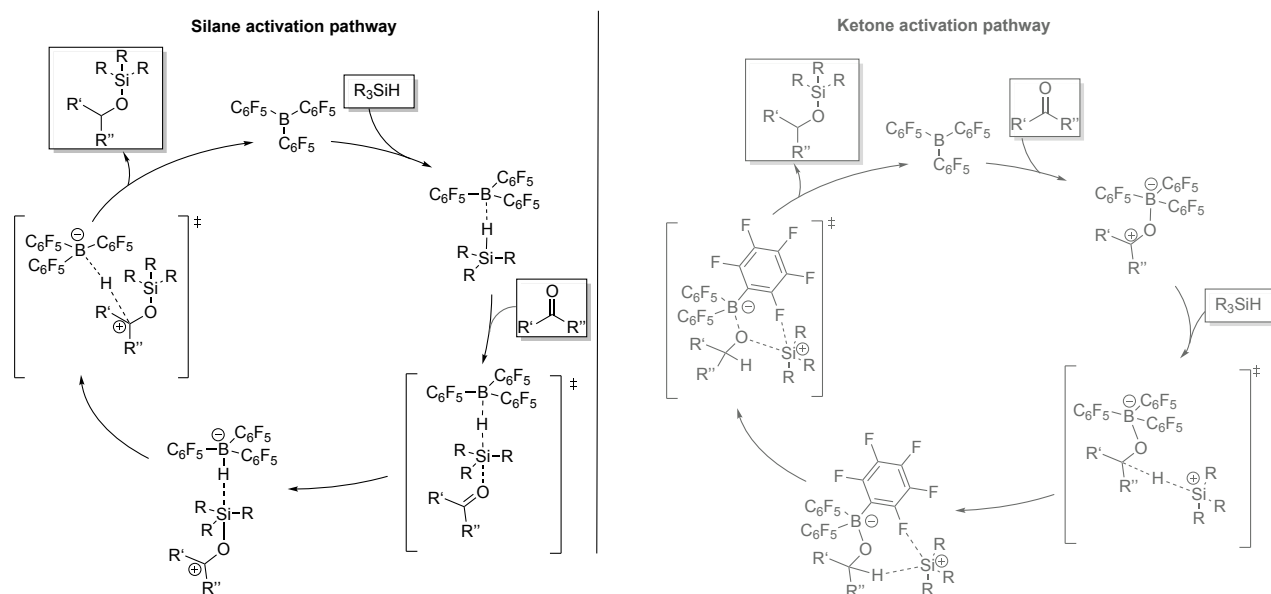
Scheme 4.2. Silane activation pathway (left side) and ketone activation pathway (right side) for the hydrosilylation of ketones catalysed by B(C$_6$F$_5$)$_3$.[19]

In the ketone activation pathway reactivity should be increased by the Lewis basicity of the carbonyl group. In contradiction, Piers *et al.*[19a] found that less Lewis basic substrates (e.g. ester, ketones with electron-withdrawing groups) react much faster than more Lewis basic ketones or even aldehydes in the B(C$_6$F$_5$)$_3$ catalysed hydrosilylation. Moreover, the reaction rate depends *inversely* proportional on the acetophenone concentration. While carbonyl-B(C$_6$F$_5$)$_3$ adducts are known to be stable and can be detected by spectrometric methods, they are accordingly not involved in the hydrosilylation reaction but rather counterplayers of the reaction by blocking catalyst molecules. Thus, the mode of catalysis proceeds most likely via silane activation.[20] Oestreich *et al.*[19b] found in 2008 that the absolute configuration of chiral silanes is inverted in hydrosilylation reactions of acetophenone catalysed by B(C$_6$F$_5$)$_3$. Hence, no free silylium ions are present in the course of the reaction and it rather occurs via a S$_N$2Si mechanism. A computational study by Sakata *et al.*[19c] for a small model system (acetone and trimethyl silane) indicates that the silane pathway is energetically favourable by more than 87 kJ mol^{-1} as compared to the ketone activation pathway and proceeds via a very flat potential energy surface. Therefore, experimental and computational studies clearly indicate a S$_N$2Si transition state that resembles the transition state for the Lewis base-catalysed silylation of alcohols. For our purpose it is thus an ideal model reaction: We have two pathways including different compound classes (alcohols vs. ketones; silyl chlorides vs. silanes; Lewis base vs. Lewis acid) leading via a geometrically similar transition state to similar products. This allows to evaluate in how far the differences in relative rates are influenced by functional groups or if they are a general parameter for differently sized aromatic moieties.

4.2. Results and Discussion

4.2.1. Investigation of Different Reaction Conditions

Before analysing the effects of increased aromatic moieties on relative rates in hydrosilylation reactions general investigations of suitable conditions for the reactions shown in **Scheme 4.3** were necessary.
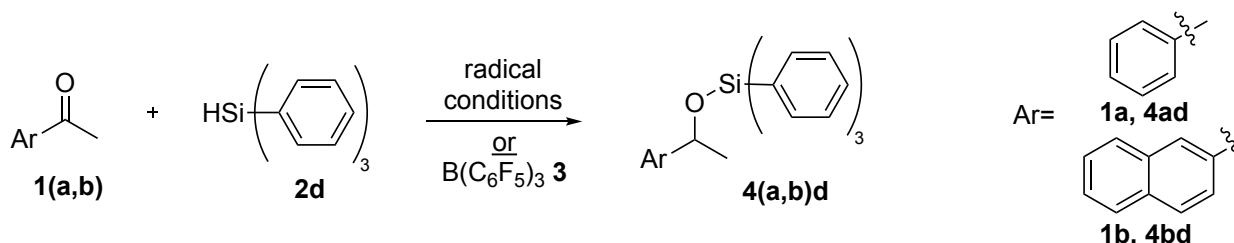
Scheme 4.3. General reaction scheme for the hydrosilylation of aromatic ketones with triphenyl silane (**2d**).

Free-Radical Hydrosilylation

Due to the somehow contradictory literature reports, we decided to investigate a set of typical radical conditions for the hydrosilylation of ketone **1b** with hydrosilane **2d**. As radical starter we used *tert*-butylhyponitrite (TBHN), azobis(isobutyronitril) (AIBN) or di-*tert*-butyl peroxide in different concentrations (2 – 100 mol%) in a broad range of temperatures (20 °C – 80 °C) and degassed solvents (1,2-dichloroethane, benzene, hexane). However, under all of these conditions not even traces of product **4bd** were observed in the quenched reaction mixture via GC-analysis. Neither radiation by a white LED, UV (365 nm) LED or by a Xenon lamp nor addition of polarity reversal catalyst *tert*-dodecylmercaptan[14a, 21] enabled the reaction. Thus, no adequate reaction conditions for the realization of a catalyst- and transition metal-free hydrosilylation of ketones with aryl silanes were found.

Lewis Acid Catalysis

During preliminary studies of the hydrosilylation of ketones catalysed by $B(C_6F_5)_3$ (**3**), we noticed the formation of additional products besides silyl ethers. The amount of side-products prevented a reliable analysis of competition experiments. Further investigation showed that formation of side-product was favoured by water residues in solvent or reagents but was also observed with rigorously dried solvents and reagents. ¹H-NMR analysis of commercially available catalyst showed that even freshly opened samples contained a notable amount of water. It is well-known that catalyst $B(C_6F_5)_3$ (**3**) tends to form the trihydrate **5** acting as a strong Brønsted acid with a pK_a comparable to hydrogen chloride.[22] However, strong acids are commonly used for the cleavage of silyl ethers[2] and also catalyse the condensation of two alcohols to form an ether. For the reaction of acetonaphthone (**1b**) and triphenyl silane (TPS, **2d**) catalysed by partially hydrolysed catalyst **3** several side products could be identified by ¹H-NMR analysis and mass spectrometry (see **Scheme 4.4**): Presumably, 1-(2-naphthyl)ethanol (**7**), formed by the acid-mediated cleavage of the silyl ether **4bd**; ether **8**, formed by an acid-catalysed condensation reaction of **7**; and 2-ethylnaphthalin (**9**),

formed by a reduction with hydrosilane **2d** catalysed by **3**. The latter side product was only observed, when an excess of silane was present in the reaction mixture. The reduction of carbonyl groups by hydrosilanes in the presence of **3** has already been reported in the literature.[23]
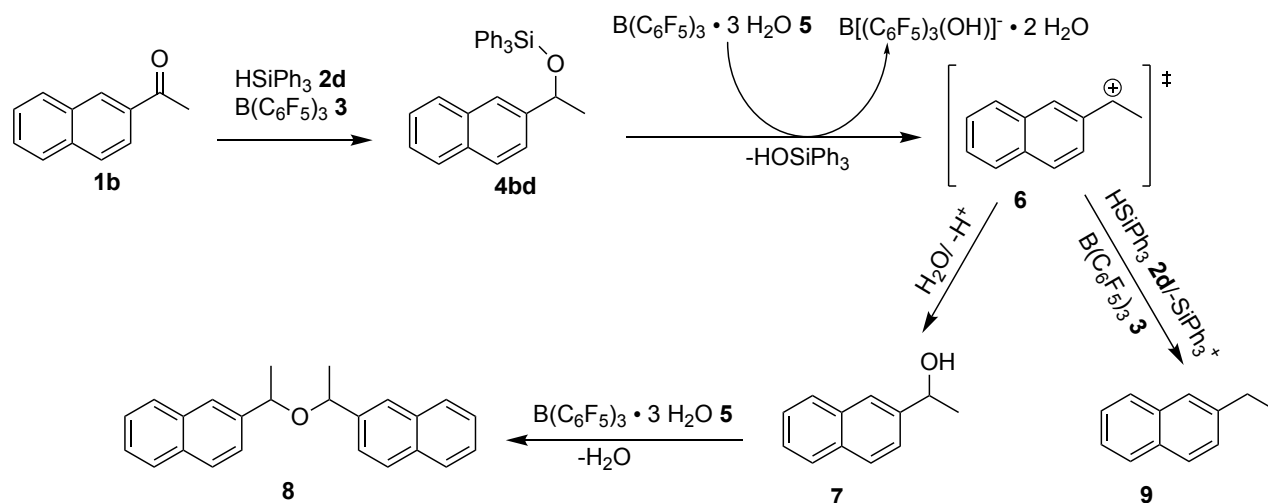
Scheme 4.4. Reaction scheme for the formation of side products in the reaction of **1b** with **2d** in the presence of catalyst **3** and its trihydrate **5**.

Interestingly, in competition experiments of acetonaphthone (**1b**) and acetophenone (**1a**) mainly naphthyl product **4bd** was cleaved while **4ad** was found to be much more stable. The same effect is found if a mixture of **4bd** and **4ad** is reacted with a solution of HCl. Hence, these effects cannot be explained by NCIs. In fact, the proposed cationic intermediate **6** is much better stabilized by mesomeric effects the bigger the π-system is. The observed stability differences therefore indicate an S_N1 mechanism rather than an S_N2Si mechanism as proposed in the literature for the cleavage of silyl ethers.[24] Further details on the investigations of the side reaction are reported by C. Gross.[25] To avoid these kind of side reactions, all competition experiments were performed under argon in a glovebox under strict exclusion of moisture. It should be noted that neither commercially available Lewis acid **3** nor commercially purchased dry solvents were of sufficient quality for a proper investigation of this reaction. A newly synthesized hydrate-free catalyst **3** kindly provided by Robert Mayer of the Ofial group was used and all solvents were dried over molecular sieves for at least 48 hours.

4.2.2. Size Effects

For the determination of relative rates, 1 : 1 competition experiments of ketones were performed. To exclude any moisture, these experiments were performed under argon atmosphere in a glove box. Selectivity *s* is defined relative to acetophenone (**1a**) and is used herein synonymous to k_{rel} (Eq. 4.1). Further experimental details are provided in Chapter 4.4.1.

$$k_{rel} = \frac{k(1(b-f))}{k(1a)} \qquad \text{Eq. 4.1}$$
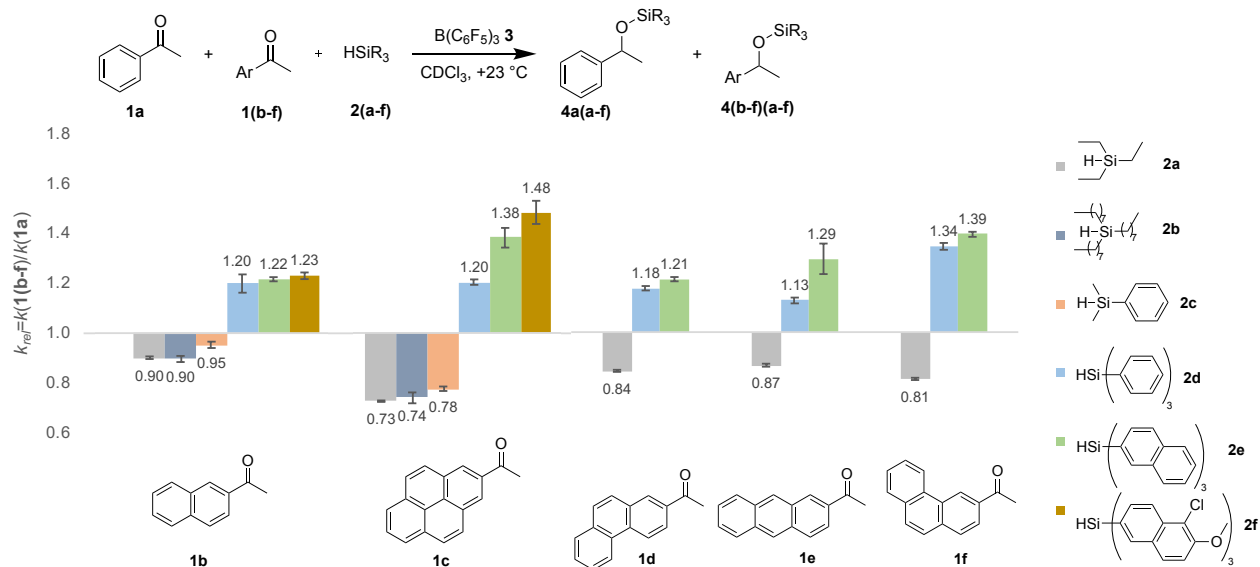
Figure 4.1. Relative rates for the hydrosilylation of ketones **1b** - **1f** with silanes **2a** - **2f** catalysed by **3** relative to ketone **1a**.[25]

As discussed before, size effects on relative rates can be investigated with an appropriate set of reagents with systematically increasing surfaces. For the silylation of alcohols,[26] we found that repulsive interactions with *peri*-hydrogens influence relative rates of a system and make it harder to distinguish repulsive and attractive size-effect. Thus, herein only ketones without *peri*-hydrogens are used. The aromatic surface of the ketones is increased from phenyl (**1a**) to 2-napthyl (**1b**) and finally to 2-pyrenyl (**1c**). Additionally, the different aromatic-substituted ketones with three cycles but without *peri*-hydrogen are utilized: 2-acetylanthracene (**1e**), 2-acetylphenantrene (**1d**) and 3-acetylphenantrene (**1f**). Competition experiments with small triethylsilane (TES, **2a**) allow to evaluate in how far relative rates for those ketones are comparable if size-effects are not possible. (Note that the smaller trimethylsilane is gaseous at +23 °C and thus not suitable for competition experiments.) For this reaction we found a decrease of relative rates by a factor of approximately 1.1 per additional ring on the ketone. To investigate if this decrease could be induced by repulsive steric effects of alkyl and aryl moiety we extended the length of the alkyl chain to tri-*n*-octyl for silane **2b**. However, relative rates are similar for the hydrosilylation of **1b** and **1c** with **2a**. We also tried to use tris(trimethylsilyl)silane but unfortunately no conversion was observed under our reaction conditions. Additionally, the use of dimethylphenyl silane (**2c**) affects relative rates only slightly. It is thus most likely, that the reactivity of the carbonyl group is affected by its number of aromatic rings. This could be explained, for example, by changed electronic properties through the inductive

effect of the increase aromatic systems. These deviations are small enough to still allow the system to be used as model system for measuring size-effects. However, net rate accelerations are somehow distorted due to size-independent rate differences within the ketone reagent set. To investigate the actual rate acceleration by size-effects we thus calculated k_{acc} relative to the reaction with TES (**2a**) as a reference (see Eq. 4.2 and **Figure 4.2**).

$$k_{acc} = \frac{k_{rel}(\mathbf{1(b-f)} + \mathbf{2(e,d)})}{k_{rel}(\mathbf{1(b-f)} + \mathbf{2a})} \qquad \text{Eq. 4.2}$$
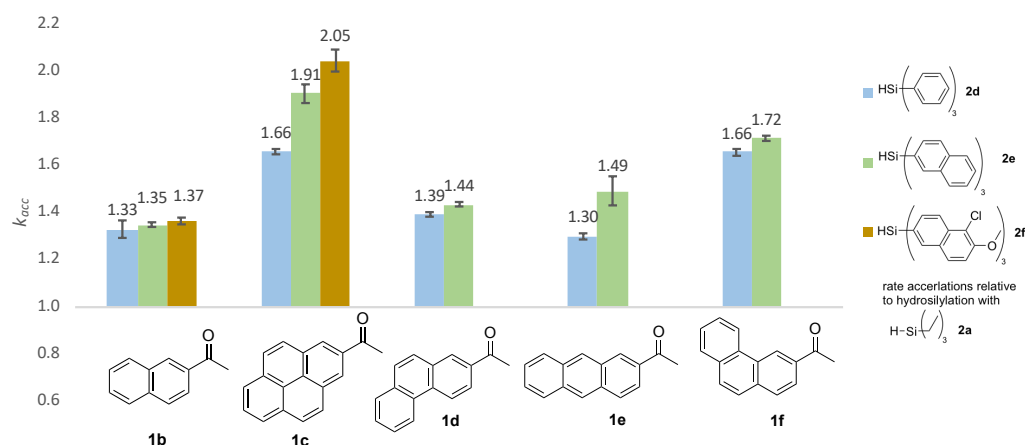
Figure 4.2. Net rate acceleration in the hydrosilylation of ketones **1b** - **1f** with silanes **2d** and **2e** catalysed by **3** relative to the reaction with TES (**2a**). Standard deviation SD was calculated by the law of error propagation as $SD = \sqrt{(SD_1^2 + SD_2^2)}$

Figure 4.2 shows that acetonaphthone (**1b**) reacts notably faster than acetophenone (**1a**) if triple-aryl substituted silanes are used. However, increasing aromatic surfaces of TPS (**2d**) to **2e** and **2f** does not further accelerate rates. For the pyrenyl-substituted ketone **1c**, a systematic size-dependent rate acceleration is observed with growing aromatic surfaces from **2d** to **2f**. However, in contrast to results for the Lewis base-catalysed silylation of alcohols (see Chapter 3) the rate increase by the use of silane **2f** is minor as compared to silane **2e**. Additionally silane **2f** is poorly soluble and even after decreasing the overall concentrations in competition experiments with **2f** solubility problems occurred. Thus, silane **2f** was not further investigated herein. Big differences were found for the rate accelerations of the different ketones with a three-cycled aromatic moiety: The hydrosilylation of 2-acetylanthracene (**1e**) is accelerated systematically with growing aromatic surface of the silane. Relative rates for 2-acetylphenanthrene (**1d**) are, in contrast, comparable to those of acetonaphthone (**1b**) and do not further respond to an increase of silane surface from phenyl in **2d** to naphthyl **2e**. 3-acetylphenanthrene **1f** also gave no notable rate change when reacted with silanes **2d** and **2e**. However, rates of ketone **1f** are accelerated to almost double of the extent as the same-sized ketone **1d**. Indeed, with TPS (**2d**) ketone **1f** was accelerated similarly to bigger ketone **1c**. For naphthyl-, pyrenyl- and anthracenyl-substituted ketones rate accelerations were also reported for the Lewis base-catalysed silylation of alcohols yielding the same products (see Fig. 3.3).[26] Indeed, the observed rate accelerations are comparable for both reaction paths.

4.2.3.Solvent Effects

As in the previous study rate accelerations showed a very strong dependence on the solvent (see Chapter 3), also herein solvent effects were investigated. Especially we wondered, how far the surprising rate acceleration of **1f** with common and rather small triphenyl silane **2d** would respond to a change of solvent. Unfortunately, for the standard analysis by ^{1}H-NMR all non-deuterated solvents have to be evaporated and replaced by $CDCl_3$. Due to the high volatility **1a** is not a suitable reference in solvent experiments analysed in this manner. Thus, **1b** was chosen as reference for the model system shown in **Scheme 4.5**.
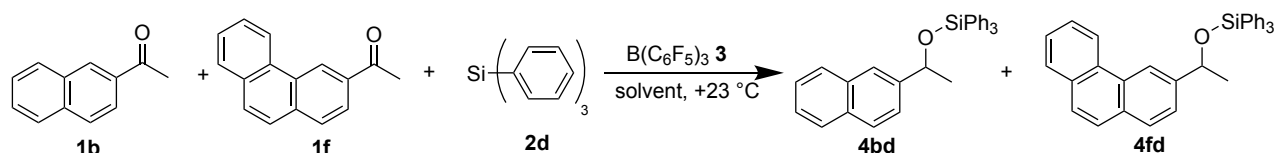
Scheme 4.5. Competition experiments for the investigation of solvent effects. 1.0 eq of **1b**, **1f** and **2c** were used, all experiments were repeated three times.

Table 4.1. Selectivity for the hydrosilylation of **1f** relative to **1b** with silane **2c** in different solvents. For details on experimental rate determination see Chapter 4.4.2.

solvent	$s = \dfrac{k(\mathbf{1f})}{k(\mathbf{1b})}$
1,4-Dioxane	**1.06**±0.01
Benzene	**1.10**±0.02
$CDCl_3$	**1.13**±0.01
Toluene	**1.22**±0.01
DCM	**1.52**±0.01
Hexafluorobenzene	**1.55**±0.01
α,α,α-Trifluorotoluene	**1.59**±0.02

Table 4.1 displays a notable solvent effect on the size-dependent rate acceleration. In 1,4-dioxane almost similar rates are observed for **1f** and **1b**, while accelerations in benzene, chloroform and toluene are comparable. Surprisingly, in DCM and in fluorinated solvents size effects are magnified. These solvents magnified size-dependent rate-accelerations also in other reactions: In the silylation reaction effects were biggest in DCM (but minimized in CF_3Ph),[26] for acylation reactions CF_3Ph gave highest selectivity values.[27] To control the reliability of the results on solvents effects herein another experimental approach was used. As outlined above **1a** is too volatile to be stable under evaporation of the solvent. Competition experiments were thus performed in CF_3Ph and a ^{1}H-NMR spectrum was measured without evaporation of the solvent. Through suppression of low-field signals (>5 ppm) and addition of a capillary filled with deuterated solvent the relevant methyl proton signals of ketones and silyl ethers can be analysed in the original reaction mixture. Results for these experiments are reported in **Table 4.2**. To verify the reliability of this method we calculated the selectivity value for **1f** relative to **1a** which was found to be in perfect agreement with the directly measured selectivity value for this reaction. Surprisingly, the observed selectivity of **1f** with relatively

small TPS (**2d**) is about the same magnitude as the highest selectivity values observed in the Lewis base-catalysed silylation of alcohols. In contrast, in CDCl$_3$ size-effects in the Lewis acid-catalysed hydrosilylation seems to be diminished.

Table 4.2. Competition experiments for the further investigation of selectivities in trifluorotoluene.

$s_{Np} = \dfrac{k(\mathbf{1b})}{k(\mathbf{1a})}$	$s_{3Phen} = \dfrac{k(\mathbf{1f})}{k(\mathbf{1a})}$	$s = \dfrac{s_{3Phen}}{s_{Np}} = \dfrac{k(\mathbf{1f})}{k(\mathbf{1b})}$
2.59±0.07	**4.15**±0.29	*1.60*[a]

[a]calculated from the two former experimental determined values for comparison with **Table 4.1**.

The solvent effects reported in **Table 4.1** do not follow the trends observed in the Lewis base-catalysed silylation of alcohols (see Chapter 3 of this thesis). To elucidate the origin of this solvent-effect different solvent parameters were compared. For an introduction into the used solvent parameters see Chapter 3. No reasonable correlation with a single solvent parameter was found (for all correlation factors see supporting information **Table 4.7** and **Table 4.8**). However, as a general trend it can be seen that polarizable solvents are unfavourable. For further investigation a multi-parameter linear regression analysis of ln(s) and common multidimensional solvent scales were performed. The Kamlet-Taft[28] linear regression analysis gives a moderate correlation, but a closer look reveals that this mainly caused by a single outlier (1,4-dioxane). Accordingly, for the improved parameters by Abraham[29] and Hunter[30] no significant correlation was found. This implies that in contrast to the Lewis base silylation of alcohols the hydrogen bond donor ability of the solvent is not the determining factor for solvent-solute interactions. Unfortunately, in Kamlet-Taft as well as in Abraham scales dipolarity and polarizability are merged into one parameter. However, both solvents with the highest selectivity values, CF$_3$Ph and C$_6$F$_6$, differ dramatically in these parameters: While both have a reduced polarizability due to the electron-withdrawing fluorine substituents, CF$_3$Ph is a dipole molecule but C$_6$F$_6$ has no dipole moment. Catalán[31] proposed two different parameters for dipolarity and polarizability. Indeed, with these parameters a better correlation was found with a significant influence of the polarizability (see **Table 4.3**). Finally, linear regression analysis with the empirical Hansen parameter[32] gave a very good correlation. These correlations clearly reflect the crucial role of solvent polarizability on relative rates. In polarizable solvents dispersive interactions with polarizable (e.g. big aromatic systems) solutes are strong. Thus, the net energetic gain through non-covalent interactions in the transition state of a reaction is reduced as the newly formed NCIs come at the cost of lost solvent-solute interactions. In less polarizable solvents eventually dispersive solute-solute interactions become more prominent and the rates are increased for bigger substrates. It is thus symptomatic, that the two best solvents are fluorinated solvents. Dispersion forces with fluorocarbons are diminished due to their reduced polarizability[33] and are therefore even used as dispersion-reduced control substances in molecular balances.[33b]

However, the need of multi parameter regression analysis shows that solvent-solute interactions are diverse and cannot be readily described by a single parameter or property. For example, also 1,4-dioxane is poorly polarizable but rate accelerations are diminished, most likely due to strong hydrogen bonding interactions. The hard-predictable influence of solvents remains the biggest challenge in the targeted use of dispersive interactions in synthesis.

Table 4.3. Correlations of solvent parameters with ln(*s*) as reported in **Table 4.1**. Multi parameter linear regression is reported and was performed with StatPlus[34]. For full details see **Table 4.7**. **Right side**: Predicted vs experimental ln(k_{rel}) values for the multi parameter linear regression with Hansen parameter shown on the left side (Eq. 4.13). Full details for correlations are provided in Chapter 4.4.5.

Scale	Parameter	meaning	R^2
Catalán[31]	**SP**	*polarizability*	**0.44**
	Sdp	*dipolarity*	0.19
	SA	*acidity*	0.02
	SB	*basicity*	0.18
ln(k_{rel}) = 1.40 - 1.80 SP + 0.73 Sdp - 4.73 SA - 0.45 SB			**0.87**
Hansen solubility parameter[32]	**δD**	*dispersion*	**0.47**
	δP	*polar interactions*	0.33
	δH	*hydrogen bonding*	0.23
ln(k_{rel}) = 2.63 - 0.137 δD + 0.030 δP - 0.023 δH			**0.96**
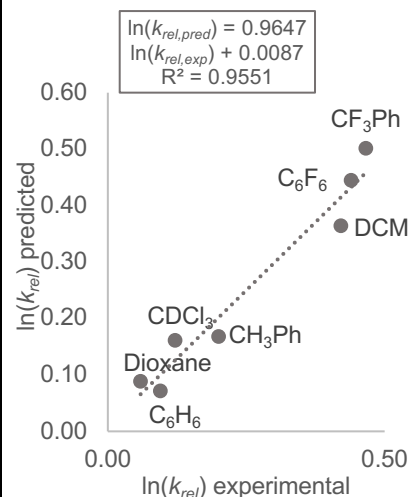
4.2.4. Computational Study

In a computational study all reactants and products with silane **2d** and **2f** were optimized at SMD($CHCl_3$)/B3LYP-D3/6-311+G(2d)/6-31+G(d) level of theory. For the best 3 to 5 conformers single point calculations were performed at the DLPNO-CCSD(T)/def2-TZVPP level (for details see SI). Reaction free energies show that all reactions are clearly exergonic (see **Table 4.4**).

Table 4.4. Reaction free energies at different level of theories for the depicted reactions in kJ mol^{-1}.

	B3LYP-D3[a]	Single point[b]		B3LYP-D3[a]	Single point[b]
Reaction	ΔG_{298} (Boltzmann averaged)	ΔG_{298} (best conformer)	Reaction	ΔG_{298} (Boltzmann averaged)	ΔG_{298} (best conformer)
1a + 2d → 4ad	-72.8	-92.1	**1a + 2e → 4ae**	-81.4	-100.2
1b + 2d → 4bd	-77.5	-97.3	**1b + 2e → 4be**	-84.1	-102.0
1c + 2d → 4cd	-79.7	-100.8	**1c + 2e → 4ce**	-85.5	-107.7
1d + 2d → 4dd	-70.0	-90.4	**1d + 2e → 4de**	-81.4	-103.7
1e + 2d → 4ed	-73.6	-93.5	**1e + 2e → 4ee**	-83.2	-104.2
1f + 2d → 4fd	-75.1	-96.9	**1f + 2e → 4fe**	-87.0	-107.9

[a]SMD($CHCl_3$)/B3LYP-D3/6-311+G(2d)/6-31+G(d) (C,H,O. 6-31+G(d); Si,Cl: 6-311+G(2d))
[b]DLPNO-CCSD(T)/def2-TZVPP (SMD($CHCl_3$) solvation energy added)

Basically no correlation was found for ln(s) with the differences of reaction free energies for the formation of products (see **Figure 4.3**). While a low correlation can be found for products with **2e** (R^2 = 0.65), especially reaction free energies with silane **2d** do not correlate with reaction rates at all.
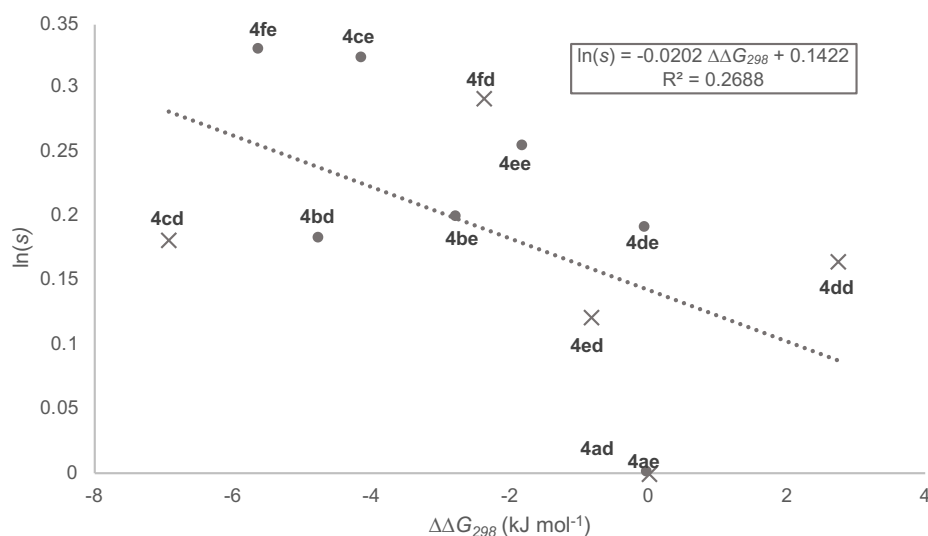
Figure 4.3. Correlation of ln(S) and reaction free energies $\Delta\Delta G_{298}$ at DLPNO-CCSD(T)/def2-TZVPP//SMD(CHCl$_3$)/B3LYP-D3/6-311+G(2d)/6-31+G(d) level of theory.

As already in the silylation of alcohols (Chapter 3) we found good correlations of Grimme-D3 dispersion energy contribution and relative rates this relation was additionally analysed. Indeed, the differences in dispersion contribution to product stabilities (Eq. 4.3) correlate good with the experimental selectivity values ln(s) (see **Figure 4.5**). As discussed above, relative rates in this study do not solely reflect size-effects but also internal reactivity differences between the ketones as displayed by rates with small TES (**2a**). Accordingly, the net rate acceleration k_{acc} (defined above by Eq. 4.2, see **Figure 4.5**) correlate even better with the differences in dispersion energy.

$$\Delta E_{disp} = E_{disp}\big(4(\mathbf{b\text{-}f})(\mathbf{d}, \mathbf{e})\big) - E_{disp}\big(4\mathbf{a}(\mathbf{d}, \mathbf{e})\big) \qquad \text{Eq. 4.3}$$
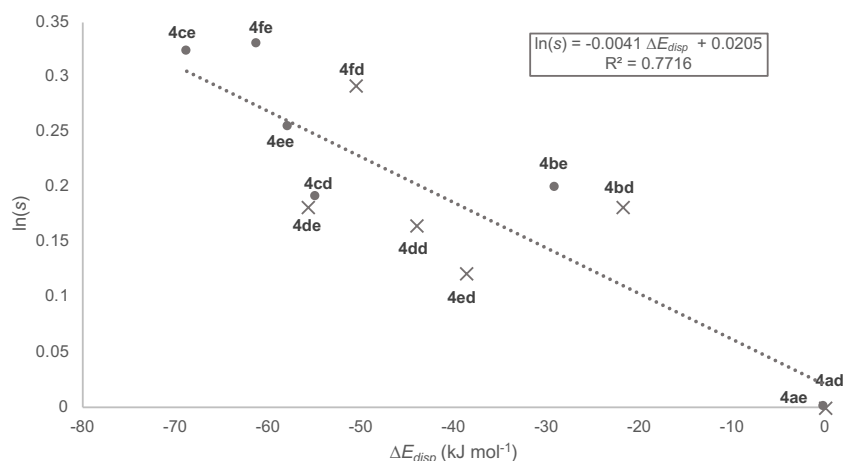
Figure 4.4. Correlation of ln(s) and differences in Grimme-D3 dispersion energy as defined by Eq. 4.3.
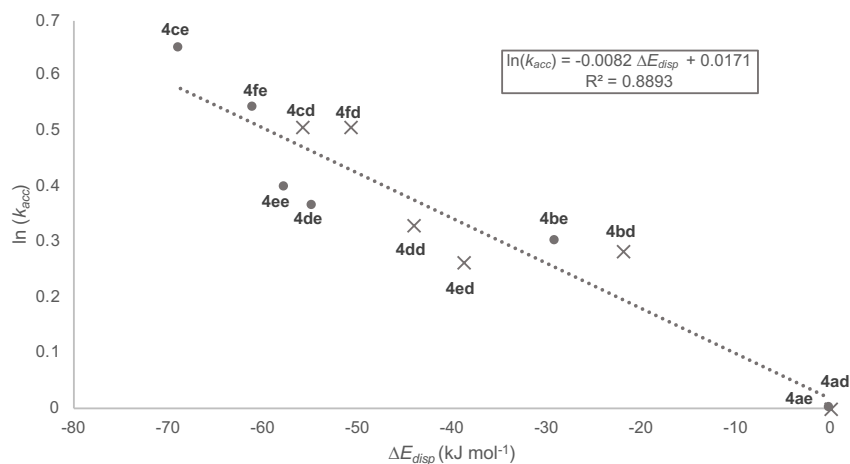
Figure 4.5. Correlation of ln(k_{acc}) and differences in Grimme-D3 dispersion energy as defined by Eq. 4.3.

Based on the proposed silane activation transition state as shown in **Scheme 4.2** it is reasonable to assume that the trends for the dispersion energies in the products reflect dispersion energy trends in the corresponding transition states. Hence, the correlations support the hypothesis that the observed rate accelerations in hydrosilylation reactions root in a stabilization of the transition state through attractive dispersive interactions. It should be, however, pronounced that the dispersion energy differences of several kJ mol^{-1} are not at all reflected by the extent of experimental selectivity values. To illustrate the origin of the differences in dispersion energies NCIplots[35] were generated for the best conformers of all silyl ethers with silane **1d** and **1f** (**Table 4.5**). For the silyl ethers of ketone **1b**, **1c**, and **1e** the growth of attractive interactions (green surfaces) going from **2d** to **2e** can be clearly seen. Furthermore, a notably bigger overlapping of aromatic surfaces can be observed for 3-phenanthryl derivative **1f** as compared to 2-phenanthryl silyl ether **1d**.

Table 4.5. NCiplots for the best conformers of silyl ethers from silane **2d** and **2e**.[35] Green surfaces reflect attractive interactions, red surfaces repulsive ones. Images were generated with VMD.[36]

ketone	Triphenylsilane **2d**	Tris(2-naphthyl)silane **2e**
1a		
1b		

1c		
1d		
1e		
1f		
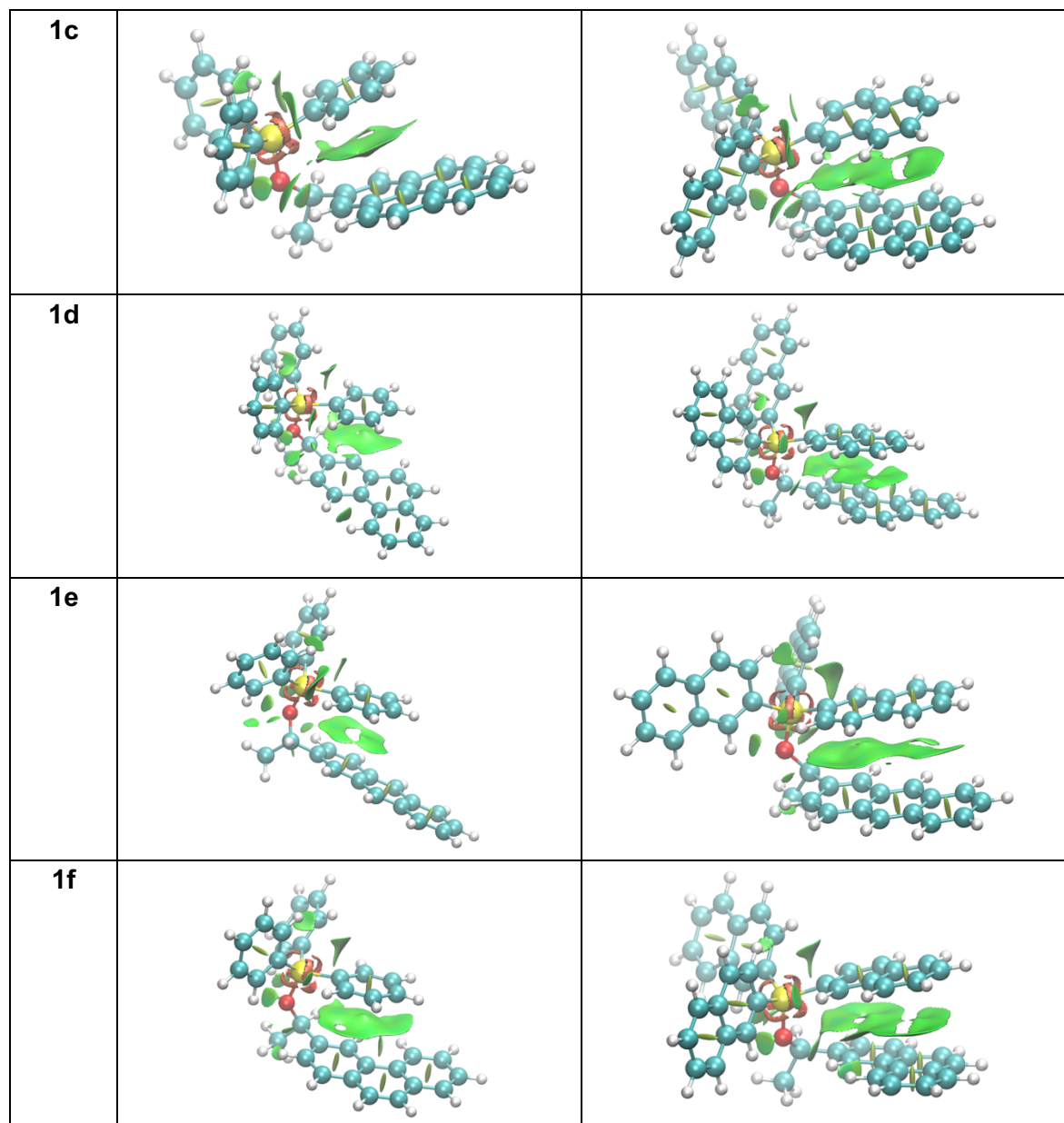
4.3. Conclusion

Relative rates were measured for the hydrosilylation reactions of aromatic ketones with hydrosilanes catalysed by Lewis acid $B(C_6F_5)_3$. Through systematic increase of the aromatic moieties at ketone and triaryl silanes relative rates were increased by a factor of two in $CDCl_3$. Besides the size of the aromatic moieties also their geometry was found to be critical: Size accelerations with 3-acetylphenanthrene were almost double as prominent as for 2-acetylphenanthrene. The choice of solvent is crucial for these size-induced rate accelerations, as size-effects are almost cancelled in very polarizable or strong hydrogen bond acceptor solvents. For a suitable solvent like, for example, trifluorotoluene even with relatively small triphenyl silane rates were increased more than four times. A computational study showed a clear correlation of relative Grimme-D3 dispersion energies and experimental determined relative rates.

While the trends in relative rates are comparable to the Lewis base catalysed silylation of alcohols yielding the same products, the solvent effects and critical solvent parameter are very different. In

the silylation reaction the hydrogen bond donor quality of the solvent influenced selectivities to the highest extent, but herein solvent polarizability plays a crucial role. As the choice of the solvent impacts relative rates even to a stronger extent than the further increase of interacting surfaces the central problem in making dispersion interactions synthetically more useful is the still not predictable influence of solvents.

4.4. Experimental Methods and Data

4.4.1. Experimental Details for Competition Experiments
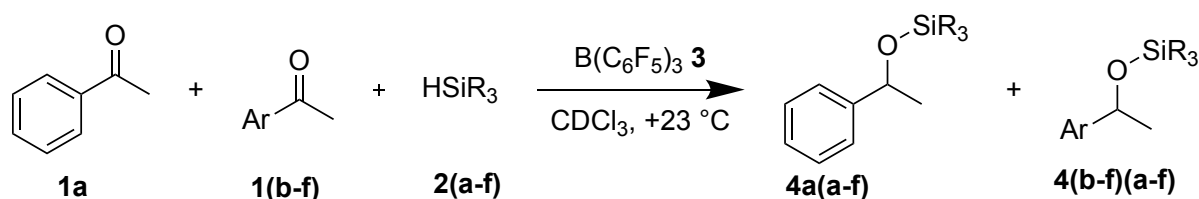
Scheme 4.6. Experimental setup of competition experiments.

Competition experiments were performed and analysed strictly following the protocol described in Chapter 3 with the following changes: Preparation of all stock solutions and reaction mixtures was performed under argon atmosphere in a glovebox. Ketones and silanes were dried azeotropic. We thank the Ofial group for providing synthesized catalyst $B(C_6F_5)_3$ (**3**) that was stored under argon at < 0 °C. The following stock solutions were prepared: A (1 : 1 mixture of ketones, 0.09 M each), B1-B5 (20, 30, 40, 50, 60 mol% relative to total of ketones of silane) and C (5 mol% catalyst **3**). The ketone concentration of 0.03 mol/L in the reaction mixture was reduced to 0.01 mol/L for all competition experiments with ketone **2f** due to its very low solubility. For ^{1}H-NMR analysis the methyl group protons of ketones and silyl ether were integrated.

Selectivity values in this project are defined relative to the rate of ketone **1a** as shown in Eq. 4.4.

$$s = \frac{k(1(b-f))}{k(1a)} \qquad \text{Eq. 4.4}$$

Chemoselectivity *C* of silyl ether products is defined analogous to enantiomeric excess by Eq. 4.6. Correction factor, product chemoselectivity values, conversion and selectivity is calculated by Eq. 4.5 to Eq. 4.8[37] as outlined in Chapter 3.

$$f = \frac{[1(b-f)] + [4(b-f)x]}{[1a] + [4ax]} \qquad \text{Eq. 4.5}$$

$$C_{ethers} = \frac{[4(b-f)x] - [4ax] \cdot f}{[4(b-f)x] + [4ax] \cdot f} \qquad \text{Eq. 4.6}$$

$$conv = \left(\frac{[4ax] + [4(b-f)x]}{[1a] + [1(b-f)] + [4ax] + [4(b-f)x]} \right) \qquad \text{Eq. 4.7}$$

$$s = \frac{ln(1 - conv(1 + C_{ethers}))}{ln(1 - conv(1 - C_{ethers}))} \qquad \text{Eq. 4.8}$$

4.4.2. Competition Experiments for Solvent Evaluation

For the evaluation of solvent effects on selectivity was slightly adopted. Only three points at a silane concentration of 50% were measured instead of five points at different concentrations. After full conversion the (non-deuterated) solvent was evaporated under reduced pressure and the reaction mixture was resolved in $CDCl_3$. In the case of hexafluorobenzene the NMR spectrum was recorded without evaporation of the solvent but after addition of a capillary filled with DCM-d_2 into the NMR tube. Due to its high volatility acetophenone (**1a**) is not a suitable standard if the solvent is removed under reduced pressure. Thus, solid acetonaphthone (**1b**) was employed as reference. To verify comparability this approach was also performed for $CDCl_3$ as solvent yielding the same selectivity values as the standard approach described above.

To enable competition experiments with acetophenone (**1a**) in trifluorotoluene reactions were performed by the standard procedure described in Chapter 4.4.1. For measuring the ^{1}H-NMR spectrum a capillary filled with DCM-d_2 was added. The ^{1}H-NMR was only recorded in the area of 0 to 6 ppm to suppress aromatic solvent signals. For a decent quality of the spectra 16 scans were recorded and the relaxation delay was set to 5 seconds. For processing the NMR spectra instead of automated phase correction and baseline correction by Bernstein polynomial fit a manual polynomial (order 1) multipoint baseline correction was performed.

4.4.3. Synthetic Procedures and Compound Characterizations

General methods: All reactions sensitive to air and moisture were proceeded under a nitrogen or argon atmosphere and the glassware as well as magnetic stir bars were dried overnight in a dry oven at 110°C.

Solvents, reagents, and catalysts: All reagents and solvents were purchased from the companies TCI, Sigma Aldrich or Fisher Scientific. $CDCl_3$ was freshly distilled from calcium hydride (CaH_2) under nitrogen atmosphere. Solvents were dried over appropriate activated molecular sieves for at least 48 hours prior to use in competition experiments. All reagents were used without further purification, if not mentioned otherwise. All air- or water-sensitive reagents were stored under nitrogen or argon.

Chromatography, NMR spectroscopy, mass spectrometry: see Chapter 3.

Syntheses and analytical data for silanes, ketones and all not herein reported silyl ethers is either described in Chapter 3 or in the master thesis of C. Gross.[25]

GP1: Hydrosilylation of ketones

Under argon atmosphere the corresponding silane (0.9 eq) are added to a solution of the relevant ketone (1 eq) and 5 mol% of $B(C_6F_5)_3$ in 5 ml of anhydrous toluene. After 24 hours, 5 mL of water are added and the solution is extracted with DCM (2 x 5 mL), dried over $MgSO_4$, filtered and the solvent is evaporated under reduced pressure. The crude residue is purified by preparative TLC (silica, hexanes/EtOAc=9/1).

(1-Phenylethoxy)trioctylsilane 4ab
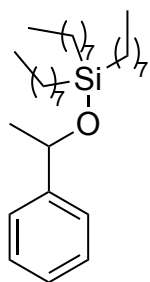
4ab is synthesized following **GP1** with ketone **1a** (11 mg, 0.10 mmol) and silane **2b** (41 mg, 0.11 mmol) and yields 34 mg (0.070 mmol, 70%) of colourless oil.

^{1}H NMR (400 MHz, CDCl$_3$) δ 7.42 – 7.13 (m, 5H), 4.84 (q, J = 6.3 Hz, 1H), 1.41 (d, J = 6.4 Hz, 3H), 1.28 – 1.19 (m, 36H), 0.89 (t, J = 6.9 Hz, 9H), 0.58 – 0.48 (m, 6H) ppm. **^{13}C NMR** (101 MHz, CDCl$_3$) 147.0, 128.2, 126.9, 125.4, 70.8, 33.8, 32.1, 29.4, 27.4, 23.3, 22.9, 15.9, 14.3 ppm. **EI-HRMS** m/z calc. for C$_{32}$H$_{60}$OSi [M]$^+$ 488.4408; found 448.4420.

(1-(2-Naphthyl)ethoxy)trioctylsilane 4bb
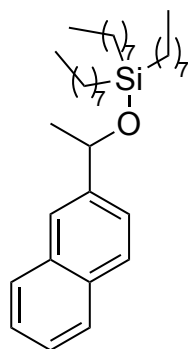
4bb is synthesized following **GP1** with ketone **1b** (17 mg, 0.10 mmol) and silane **2b** (41 mg, 0.11 mmol) and yields 46 mg (0.085 mmol, 85%) of colourless oil.

^{1}H NMR (400 MHz, CDCl$_3$) δ 7.87 – 7.74 (m, 4H), 7.52 – 7.40 (m, 3H), 5.02 (q, J = 6.3 Hz, 1H), 1.50 (d, J = 6.4 Hz, 3H), 1.32 – 1.17 (m, 36H), 0.88 (t, J = 6.9 Hz, 9H), 0.66 – 0.45 (m, 6H) ppm. **^{13}C NMR** (101 MHz, CDCl$_3$) 144.5, 133.4, 132.8, 128.0, 127.9, 127.8, 126.0, 125.5, 124.2, 123.7, 70.9, 33.8, 32.1, 29.4, 27.4, 23.4, 22.8, 14.3, 14.2 ppm. **^{29}Si NMR** (54 MHz, CDCl$_3$) δ 16.74 ppm. **EI-HRMS** m/z calc. for C$_{36}$H$_{62}$OSi [M]$^+$ 538.4564; found 538.4563.

(1-(2-Pyrenyl)ethoxy)trioctylsilane 4cb
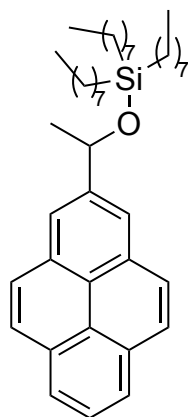
4cb is synthesized following **GP1** with ketone **1c** (24 mg, 0.10 mmol) and silane **2b** (41 mg, 0.11 mmol) and yields 40 mg (0.065 mmol, 65%) of colourless oil.

^{1}H NMR (400 MHz, CDCl$_3$) δ 8.19 – 8.04 (m, 8H), 8.01 – 7.95 (m, 1H), 5.30 (q, J = 6.3 Hz, 1H), 1.63 (d, J = 6.4 Hz, 3H), 1.39 – 1.08 (m, 36H), 0.83 (t, J = 7.0 Hz, 9H), 0.71 – 0.52 (m, 6H) ppm. **^{13}C NMR** (101 MHz, CDCl$_3$) 145.0, 131.2, 131.2, 127.6, 127.5, 125.7, 125.0, 124.9, 124.1, 122.2, 71.3, 33.9, 32.2, 29.5, 28.2, 23.5, 22.9, 16.0, 14.3 ppm. **EI-HRMS** m/z calc. for C$_{42}$H$_{64}$OSi [M]$^+$ 612.4721; found 612.4724.

4.4.4. Tables of Competition Experiment Results

Experimental data for all competition experiments not described herein can be found in the master thesis of C. Gross.[25]

Table 4.6. ^{1}H-NMR data for competition experiments for the hydrosilylation of ketones with specified silanes as outlined above. Raw absolute integrals are reported, analysis is performed as described above. The last row reports mean of selectivity over all measurement points and standard deviation.

conditions					absolute integrals ^{1}H-NMR methyl group				*conv*	chemo-selectivity *C*	selectivity *S*	arithmetic mean	standard deviation
ketone 1	ketone 2 (reference)	silane	solvent	% silane[a]	**4(b,f)x**	**4ax**	**1(b,f)**	**1a**					
1b	**1a**	**2b**	CDCl$_3$	20%	190838	187511	48535	53245	21.20%	-0.0463	0.91	0.90	0.01
				30%	135713	132247	56628	64924	31.21%	-0.0683	0.87		
				40%	106646	103695	67252	74484	40.26%	-0.0510	0.90		
				50%	80415	78066	73425	83243	49.71%	-0.0627	0.89		
				60%	50822	48979	70502	79237	60.01%	-0.0583	0.90		
1f	**1a**	**2b**	CDCl$_3$	20%	157949	154901	36118	50921	21.77%	-0.1701	0.72	0.74	0.03
				30%	124756	119963	45876	65939	31.36%	-0.1794	0.71		
				40%	96925	91710	55267	76123	41.06%	-0.1587	0.75		
				60%	47496	42849	59312	79502	60.58%	-0.1454	0.77		
1b	**1a**	**2d**	PhCF$_3$	20%	7568	9723	2901	1317	19.61%	0.3755	2.55	2.59	0.07
				30%	5312	8318	3583	1845	28.48%	0.3203	2.56		
				50%	3337	7234	6572	3561	48.94%	0.2972	2.70		
				60%	2364	6569	7736	4964	58.71%	0.2183	2.54		
1f	**1a**	**2d**	PhCF$_3$	20%	7309	10033	3496	1108	20.98%	0.5185	3.72	4.15	0.29
				40%	4748	9720	6389	2145	37.10%	0.4973	4.24		
				50%	3374	8918	7714	2840	46.20%	0.4618	4.26		
				60%	2053	7917	8659	3542	55.03%	0.4194	4.38		

[a]relative to overall concentration of ketones

	conditions				absolute integrals ^{1}H-NMR methyl group				conv	chemo-selectivity C	selectivity S	arithmetic mean	standard deviation
ketone 1	ketone 2 (reference)	silane	solvent	% silane[a]	**4fd**	**4bd**	**1f**	**1b**					
1f	**1b**	**2d**	CDCl$_3$	50%	95449	102928	113944	103936	52.34%	0.0459	1.13	1.13	0.01
				50%	93743	102881	113348	103068	52.40%	0.0475	1.14		
				50%	92991	101349	113969	105580	53.05%	0.0382	1.12		
1f	**1b**	**2d**	DCM	50%	74943	96098	97401	69314	49.36%	0.1685	1.53	1.52	0.01
				50%	80573	102595	97758	70264	47.84%	0.1636	1.52		
				50%	76318	98865	93504	69009	48.12%	0.1507	1.51		
1f	**1b**	**2d**	C$_6$H$_6$	50%	80033	85189	89683	85618	51.48%	0.0232	1.08	1.10	0.02
				50%	71359	76382	83526	76543	52.00%	0.0436	1.12		
				50%	68050	72617	81441	75818	52.78%	0.0358	1.10		
1f	**1b**	**2d**	PhCF$_3$	50%	73512	104571	94688	72548	48.43%	0.1324	1.57	1.59	0.02
				50%	74883	107060	91538	68726	46.83%	0.1423	1.61		
				50%	78398	111165	98973	73755	47.68%	0.1460	1.60		
1f	**1b**	**2d**	C$_6$F$_6$	50%	64692	91534	93651	70710	51.27%	0.1396	1.56	1.55	0.01
				50%	55184	80700	83048	65650	52.25%	0.1170	1.54		
				50%	51373	75245	73786	58122	51.02%	0.1188	1.55		

[a]relative to overall concentration of ketones

4.4.5. Compilation of Critical Solvent Parameters

To analyse the origin of solvent effects, Pearson correlation factors and R-squared values were calculated for different sets of solvent descriptor parameters. Furthermore, linear regression analysis was performed.

Table 4.7. Compilation of experimental selectivity values as described in **Table 4.6** and critical solvent parameters together with Pearson correlation factor and R-squared value with ln(s). In the last row the results of linear regression analysis for multi-parameter scales is reported.

solvent	s	ln(s)	Reichardt[38] $E_T(30)$	Kamlet-taft solvent parameter[28] $\pi*$	β	α	δ	Eq. 4.9	Abraham solvent parameter[29] π_2^H	β_2^H	α_2^H	V_x	Eq. 4.10
			polarity	dipolarity/ polariza-bility	hydrogen bond donor	hydrogen bond acceptor	polariza-bility correction factor		dipolarity/ polariza-bility	hydrogen bond donor	hydrogen bond acceptor	solvent volume	
1,4-Dioxane	1.06±0.01	0.06	36.0	0.49	0.37	0.00	0.00	0.07	0.75	0.64	0.00	0.681	0.03
Benzene	1.1±0.02	0.09	34.3	0.45	0.10	0.00	1.00	0.16	0.52	0.14	0.00	0.7164	0.30
CDCl$_3$	1.13±0.01	0.12	39.0	0.69	0.10	0.20	0.50	0.17	0.49	0.02	0.15	0.62	0.22
Toluene	1.22±0.01	0.20	33.9	0.49	0.11	0.00	1.00	0.13	0.52	0.14	0.00	0.86	0.28
DCM	1.52±0.01	0.42	40.7	0.73	0.10	0.13	0.50	0.35	0.47	0.05	0.10	0.49	0.27
C$_6$F$_6$	1.55±0.01	0.44	34.2	0.27	0.02	0.00	1.00	0.40	0.66	0.00	0.00	0.8226	0.40
CF$_3$Ph	1.59±0.02	0.47	38.7	0.50	0.00	0.00	1.00	0.53	0.48	0.10	0.00	0.91	0.30
Pearson correlation			0.34	-0.12	-0.69	-0.07	0.44	0.94	-0.28	-0.56	-0.06	0.23	0.63
R^2			0.11	0.01	0.48	0.00	0.19	0.89	0.08	0.31	0.00	0.05	0.40

	Hunter solvent parameter[26, 30]			Catalán[31]					Hansen solubility parameter[32]			
solvent	α	β	*Eq. 4.11*	*SP*	*Sdp*	*SA*	*SB*	*Eq. 4.12*	δD	δP	δH	*Eq. 4.13*
	hydrogen bond donor	*hydrogen bond acceptor*		*polarizability*	*dipolarity*	*acidity*	*basicity*		*dispersion*	*polar interactions*	*hydrogen bonding*	
1,4-Dioxane		4.7		0.737	0.312	0.000	0.444	0.10	17.5	1.8	9.0	0.09
Benzene	0.9	2.1	0.24	0.793	0.270	0.000	0.124	0.11	18.4	0.0	2.0	0.07
CDCl$_3$	2.2	0.8	0.20	0.783	0.614	0.047	0.071	0.18	17.8	3.1	5.7	0.16
Toluene	0.8	2.1	0.22	0.782	0.284	0.000	0.128	0.14	18.0	1.4	2.0	0.17
DCM	1.9	2.0	0.42	0.761	0.769	0.040	0.178	0.32	17.0	7.3	7.1	0.36
C$_6$F$_6$				0.623	0.252	0.000	0.119	0.41	16.0	0.0	0.0	0.45
CF$_3$Ph	*1.3*	*1.7*	0.22	0.694	0.662	0.014	0.073	0.54	17.5	8.8	0.0	0.50
Pearson r	0.14	-0.36	0.50	-0.67	0.44	0.14	-0.43	0.93	-0.69	0.58	-0.48	0.98
R^2 value	0.02	0.13	0.25	0.44	0.19	0.02	0.18	0.87	0.47	0.33	0.23	0.96

Table 4.8. Results of linear regression analysis performed with StatPlus[34] of ln(S) and multi parameter solvent scales.

Solvent parameter	R^2	linear regression equation	
Kamlet-Taft[28]	0.89	ln(s) = 1.27934 + 0.27207 π* - 3.62284 β - 2.48658 α - 0.88428 δ	Eq. 4.9
Abraham[29]	0.40	ln(s) = 0.36311 + 0.19425 $\pi_2{}^H$ - 0.62934 $\beta_2{}^H$ - 1.03987 $\alpha_2{}^H$ - 0.10813 V_x	Eq. 4.10
Hunter[26, 30]	0.25	ln(s) = - 0.45324 + 0.20708 α + 0.24091 β	Eq. 4.11
Catalán[31]	0.87	ln(s) = 1.40141 - 1.8039 *SP* + 0.73349 *Sdp* - 4.73918 *SA* - 0.45704 *SB*	Eq. 4.12
Hansen[32]	0.96	ln(s) = 2.63388 - 0.1368 δD + 0.02967 δP - 0.02268 δH	Eq. 4.13

4.5. Computational Methods and Data

4.5.1. Theoretical Methods

Geometry optimizations and vibrational frequency calculations were performed with the B3LYP-D3 hybrid functional[39] in combination with the 6-31+G(d) (for H, C, and O atoms) and 6-311+G(2d) basis set (for Si atoms).[40] Solvent effects for chloroform have been calculated with the SMD continuum solvation model.[41] Thermochemical corrections to 298.15 K have been calculated for all minima from unscaled vibrational frequencies obtained at this same level. Initial search of conformational space of every compound was performed with Maestro.[42] If the number of conformers was too high in regard to computational costs redundant conformers were eliminated (maximum atom deviation 0.5 Å) with Maestro. All conformers were then optimized and frequency analysis was performed to control that no imaginary frequencies are present. For the best three to five conformers single point energies were calculated at the DLPNO-CCSD(T)/def2-TZVPP//SMD(CHCl$_3$)/B3LYP-D3/6-311+G(2d)/6-31+G(d) level[43] level with auxiliary basis set def2-TZVPP/C.[44] This combination was found in previous studies to perform well for this kind of systems.[26, 45]. G_{298} is calculated through addition of thermal correction and solvation factors obtained as the difference between the energies computed at B3LYP-D3/6-311+G(2d)/6-31+G(d) in solution and in gas phase. Silyl ethers **4ad**, **4ae**, **4bd**, **4be**, **4cd**, and **4ce** the best conformers were taken from Chapter 3 and additional single points were calculated. All calculations have been performed with Gaussian 09[46] and ORCA version 4.0.[47]

4.5.2. Tables of Energies, Enthalpies and Free Energies.

Table 4.9. Energies, enthalpies, free energies and Grimme-D3 correction (in Hartree) for all conformers at SMD(CHCl$_3$)/B3LYP-D3/6-311+G(2d)/6-31+G(d) level of theory. Single point calculations energies for all the best conformers on different levels of theory (in Hartree).

		SMD(CHCl$_3$)/B3LYP-D3/6-311+G(2d)/6-31+G(d)				SP calculations	
	filename	E_{tot}	H_{298}	G_{298}	$E_{Grimme-D3}$	$E_{gas,B3LYP-D3}{}^a$	$E_{DLPNO-CCSD(T)}{}^b$
1a	2phenCO_1	-692.244210	-691.998200	-692.052994	-0.024310	-692.221633	-690.925512
1a	2phenCO_2	-692.243817	-691.997648	-692.051841	-0.024283	-692.221229	-690.924918
1a	2phenCO_3	-692.241995	-691.997796	-692.049078	-0.023985		
4de	2phenTNpS_23	-2138.428032	-2137.728287	-2137.843282	-0.100044	-2138.378385	-2134.380793
4de	2phenTNpS_20	-2138.428092	-2137.728024	-2137.841821	-0.102211	-2138.379292	-2134.381504
4de	2phenTNpS_25	-2138.428557	-2137.728795	-2137.841921	-0.099758	-2138.378069	-2134.379994
4de	2phenTNpS_22	-2138.428170	-2137.728317	-2137.841494	-0.099976	-2138.378422	-2134.380694
4de	2phenTNpS_18	-2138.427961	-2137.729321	-2137.839780	-0.099926	-2138.378220	-2134.380821
4de	2phenTNpS_19	-2138.426845	-2137.726739	-2137.841390	-0.098928	-2138.376993	-2134.377378
4de	2phenTNpS_16	-2138.427339	-2137.727516	-2137.840757	-0.099016		
4de	2phenTNpS_10	-2138.426841	-2137.726844	-2137.840747	-0.101160		
4de	2phenTNpS_14	-2138.427837	-2137.727838	-2137.840735	-0.100642		
4de	2phenTNpS_12	-2138.424057	-2137.724134	-2137.840143	-0.089615		
4de	2phenTNpS_13	-2138.424065	-2137.724120	-2137.840019	-0.089564		
4de	2phenTNpS_11	-2138.427585	-2137.727462	-2137.839320	-0.099549		
4de	2phenTNpS_15	-2138.425832	-2137.727324	-2137.835339	-0.103106		
4de	2phenTNpS_21	-2138.424718	-2137.726591	-2137.835293	-0.095270		
4de	2phenTNpS_24	-2138.420403	-2137.721071	-2137.827166	-0.109704		
4de	2phenTNpS_1	-2138.416007	-2137.719727	-2137.818285	-0.098905		
4de	2phenTNpS_17	-2138.412989	-2137.718116	-2137.814671	-0.092013		
4dd	2phenTPS_5	-1677.456359	-1676.905016	-1677.001392	-0.074894	-1677.418635	-1674.315601
4dd	2phenTPS_14	-1677.457147	-1676.905530	-1677.001340	-0.075737	-1677.419576	-1674.316453
4dd	2phenTPS_9	-1677.456652	-1676.905374	-1677.001559	-0.073189	-1677.418107	-1674.314533
4dd	2phenTPS_7	-1677.456127	-1676.904363	-1677.001291	-0.075590	-1677.418825	-1674.315328
4dd	2phenTPS_10	-1677.455785	-1676.904329	-1677.001591	-0.074138	-1677.418183	-1674.314222
4dd	2phenTPS_3	-1677.456580	-1676.905216	-1677.001273	-0.075502		
4dd	2phenTPS_15	-1677.456516	-1676.905151	-1677.000909	-0.073590		
4dd	2phenTPS_16	-1677.455657	-1676.904364	-1677.000699	-0.074584		
4dd	2phenTPS_17	-1677.456753	-1676.905283	-1677.000491	-0.073671		
4dd	2phenTPS_4	-1677.456312	-1676.904872	-1677.000457	-0.073042		
4dd	2phenTPS_2	-1677.455309	-1676.903724	-1677.000108	-0.073551		
4dd	2phenTPS_6	-1677.455854	-1676.904501	-1677.000068	-0.074620		
4dd	2phenTPS_11	-1677.455958	-1676.904300	-1676.999834	-0.074408		
4dd	2phenTPS_12	-1677.455863	-1676.904118	-1676.999834	-0.070747		
4dd	2phenTPS_8	-1677.457155	-1676.905439	-1676.999777	-0.075998		

		SMD(CHCl₃)/B3LYP-D3/6-311+G(2d)/6-31+G(d)				SP calculations	
	filename	E_{tot}	H_{298}	G_{298}	$E_{Grimme-D3}$	$E_{gas,B3LYP-D3}$[a]	$E_{DLPNO-CCSD(T)}$[b]
4dd	2phenTPS_1	-1677.455914	-1676.905122	-1676.998048	-0.073995		
1f	3phenCO_1	-692.244294	-691.998150	-692.051957	-0.024490	-692.221657	-690.925585
1f	3phenCO_2	-692.244112	-691.997816	-692.051326	-0.024371	-692.221677	-690.925287
4fe	3phenTNoS_13	-2138.429529	-2137.729843	-2137.843517	-0.102438	-2138.380131	-2134.382910
4fe	3phenTNoS_11	-2138.429449	-2137.729779	-2137.843034	-0.102316	-2138.380408	-2134.383386
4fe	3phenTNoS_2	-2138.430837	-2137.730779	-2137.844361	-0.102297	-2138.381050	-2134.381558
4fe	3phenTNoS_3	-2138.430634	-2137.730691	-2137.843515	-0.102253	-2138.380999	-2134.381184
4fe	3phenTNoS_8	-2138.430640	-2137.730685	-2137.843271	-0.102279	-2138.380999	-2134.381213
4fe	3phenTNoS_10	-2138.430115	-2137.730095	-2137.843031	-0.104045		
4fe	3phenTNoS_4	-2138.428179	-2137.728156	-2137.842845	-0.099091		
4fe	3phenTNoS_1	-2138.429928	-2137.729497	-2137.842809	-0.102894		
4fe	3phenTNoS_5	-2138.429049	-2137.728623	-2137.841384	-0.104683		
4fe	3phenTNoS_7	-2138.428293	-2137.728306	-2137.841250	-0.101660		
4fe	3phenTNoS_12	-2138.429409	-2137.729422	-2137.841094	-0.101748		
4fe	3phenTNoS_9	-2138.424664	-2137.724582	-2137.840809	-0.090513		
4fe	3phenTNoS_6	-2138.428237	-2137.727934	-2137.840791	-0.100901		
4fe	3phenTNoS_14	-2138.427704	-2137.727198	-2137.839757	-0.101427		
4fd	3phenTPS_13	-1677.457463	-1676.906088	-1677.002525	-0.077388	-1677.420391	-1674.317710
4fd	3phenTPS_9	-1677.457650	-1676.906403	-1677.002580	-0.075971	-1677.419987	-1674.316716
4fd	3phenTPS_11	-1677.457454	-1676.906078	-1677.001941	-0.077212	-1677.420346	-1674.317313
4fd	3phenTPS_6	-1677.457946	-1676.906479	-1677.002736	-0.077240	-1677.420850	-1674.316640
4fd	3phenTPS_1	-1677.455510	-1676.903999	-1677.001768	-0.069948	-1677.416876	-1674.312275
4fd	3phenTPS_5	-1677.456701	-1676.905115	-1677.001043	-0.075232		
4fd	3phenTPS_8	-1677.456701	-1676.905115	-1677.001040	-0.075230		
4fd	3phenTPS_4	-1677.458092	-1676.906315	-1677.000974	-0.077018		
4fd	3phenTPS_7	-1677.456735	-1676.905113	-1677.000708	-0.076705		
4fd	3phenTPS_2	-1677.457487	-1676.905886	-1677.000590	-0.075609		
4fd	3phenTPS_10	-1677.457048	-1676.905354	-1677.000103	-0.075660		
4fd	3phenTPS_3	-1677.456706	-1676.905025	-1677.000017	-0.077406		
4fd	3phenTPS_12	-1677.456706	-1676.905025	-1677.000010	-0.077403		
1e	AntCO_1	-692.236362	-691.990509	-692.044373	-0.023924	-692.213587	-690.915711
1e	AntCO_2	-692.235378	-691.989515	-692.043310	-0.023900	-692.212630	-690.914379
1e	AntCO_3	-692.234315	-691.989290	-692.041944	-0.023602		
4af	Np1_22	-1831.110573	-1830.510227	-1830.614850	-0.079201	-1831.067811	-1827.664892
4af	Np1_29	-1831.111030	-1830.510559	-1830.613529	-0.079177	-1831.068103	-1827.665193
4af	Np1_18	-1831.110617	-1830.510201	-1830.613657	-0.079880	-1831.067992	-1827.664934
4af	Np1_9	-1831.110144	-1830.509444	-1830.613768	-0.077364	-1831.067723	-1827.663555
4af	Np1_10	-1831.110573	-1830.509971	-1830.612912	-0.080567		

	filename	SMD(CHCl₃)/B3LYP-D3/6-311+G(2d)/6-31+G(d)				SP calculations	
		E_{tot}	H_{298}	G_{298}	$E_{Grimme-D3}$	$E_{gas,B3LYP-D3}$[a]	$E_{DLPNO-CCSD(T)}$[b]
4af	Np1_14	-1831.110573	-1830.509971	-1830.612901	-0.080567		
4af	Np1_42	-1831.110834	-1830.510165	-1830.611702	-0.079231		
4af	Np1_3	-1831.111040	-1830.511605	-1830.611677	-0.079742		
4bf	Np2_2_5	-1984.769120	-1984.119285	-1984.227853	-0.090256	-1984.722783	-1981.021670
4bf	Np2_2_38	-1984.768967	-1984.119942	-1984.225325	-0.090744	-1984.723181	-1981.023261
4bf	Np2_2_19	-1984.768189	-1984.117994	-1984.227325	-0.088480	-1984.722063	-1981.020098
4bf	Np2_2_18	-1984.768327	-1984.118032	-1984.226645	-0.088624	-1984.722190	-1981.020030
4ef	Np3_2_31	-2138.420656	-2137.721256	-2137.834098	-0.101175	-2138.371247	-2134.372630
4ef	Np3_2_1	-2138.420037	-2137.720161	-2137.834535	-0.100024	-2138.370753	-2134.369712
4ef	Np3_2_23	-2138.420388	-2137.722103	-2137.832055	-0.100590	-2138.370943	-2134.372153
1b	NpCO_1	-538.586369	-538.389852	-538.437213	-0.017555	-538.568051	-537.569437
1b	NpCO_2	-538.585656	-538.390274	-538.435581	-0.017527	-538.567431	-537.568372
1b	NpCO_3	-538.584218	-538.388647	-538.435348	-0.017232		
4ad	Ph1_3	-1370.140686	-1369.688732	-1369.774046	-0.058089	-1370.110848	-1367.603391
4ad	Ph1_5	-1370.140573	-1369.688603	-1369.773885	-0.058310	-1370.110898	-1367.603265
4ad	Ph1_9	-1370.140385	-1369.688211	-1369.774605	-0.055644	-1370.110809	-1367.602349
4ad	Ph1_4	-1370.140545	-1369.688532	-1369.773462	-0.058453		
4ad	Ph1_8	-1370.140545	-1369.688530	-1369.773439	-0.058452		
4ad	Ph1_7	-1370.140695	-1369.688633	-1369.773221	-0.058192		
4ad	Ph1_6	-1370.140695	-1369.688633	-1369.773213	-0.058195		
4ad	Ph1_2	-1370.140229	-1369.688145	-1369.773113	-0.058105		
4bd	Ph2_2_10	-1523.797796	-1523.296307	-1523.388671	-0.066431	-1523.763825	-1520.957872
4bd	Ph2_2_4	-1523.797384	-1523.295943	-1523.387625	-0.066037	-1523.763439	-1520.957205
4bd	Ph2_2_1	-1523.797334	-1523.295702	-1523.387600	-0.066610	-1523.764084	-1520.957610
4bd	Ph2_2_7	-1523.798151	-1523.296727	-1523.387042	-0.065953	-1523.764022	-1520.958101
4bd	Ph2_2_6	-1523.798058	-1523.296438	-1523.386801	-0.066557	-1523.764360	-1520.958177
4ed	Ph3_2_3	-1677.448265	-1676.897433	-1676.994002	-0.072845	-1677.409835	-1674.305002
4ed	Ph3_2_4	-1677.448160	-1676.897255	-1676.993708	-0.073088	-1677.410192	-1674.304820
4ed	Ph3_2_13	-1677.447674	-1676.896624	-1676.993820	-0.071910	-1677.409492	-1674.303817
4ed	Ph3_2_16	-1677.448443	-1676.897313	-1676.992427	-0.074588	-1677.410889	-1674.306318
1a	PhCO_1	-384.929994	-384.783007	-384.824532	-0.011239	-384.916144	-384.216054
1a	PhCO_2	-384.927567	-384.782537	-384.820690	-0.010916		
1c	PyrCO_1	-768.482139	-768.222692	-768.277794	-0.027514	-768.458095	-767.014320
1c	PyrCO_2	-768.479705	-768.222098	-768.273588	-0.027182	-768.455763	-767.011600
4cf	PyrTNpS_10	-2214.667904	-2213.954701	-2214.070032	-0.105368	-2214.616908	-2210.471243
4cf	PyrTNpS_12	-2214.667625	-2213.954520	-2214.069243	-0.104558	-2214.616605	-2210.471306
4cf	PyrTNpS_4	-2214.668352	-2213.955081	-2214.068348	-0.106846	-2214.618080	-2210.473196
4cf	PyrTNpS_11	-2214.667270	-2213.954197	-2214.069005	-0.104423	-2214.616228	-2210.470609

	filename	SMD(CHCl$_3$)/B3LYP-D3/6-311+G(2d)/6-31+G(d)				SP calculations	
		E_{tot}	H_{298}	G_{298}	$E_{Grimme-D3}$	$E_{gas,B3LYP-D3}$[a]	$E_{DLPNO-CCSD(T)}$[b]
4cf	PyrTNpS_14	-2214.667110	-2213.953557	-2214.068853	-0.104816	-2214.616078	-2210.468618
4cf	PyrTNpS_25	-2214.667613	-2213.954307	-2214.068780	-0.104039		
4cf	PyrTNpS_27	-2214.667741	-2213.954531	-2214.068592	-0.103979		
4cf	PyrTNpS_16	-2214.666920	-2213.953870	-2214.068397	-0.104464		
4cf	PyrTNpS_3	-2214.667923	-2213.954610	-2214.068257	-0.107047		
4cf	PyrTNpS_32	-2214.667121	-2213.954029	-2214.067884	-0.107179		
4cf	PyrTNpS_31	-2214.666904	-2213.953691	-2214.067825	-0.105320		
4cf	PyrTNpS_18	-2214.667344	-2213.954130	-2214.067819	-0.104418		
4cf	PyrTNpS_21	-2214.666967	-2213.953737	-2214.067763	-0.104967		
4cf	PyrTNpS_24	-2214.666713	-2213.953279	-2214.067685	-0.103379		
4cf	PyrTNpS_2	-2214.668167	-2213.954342	-2214.067535	-0.107358		
4cf	PyrTNpS_1	-2214.667933	-2213.954003	-2214.067159	-0.106690		
4cf	PyrTNpS_19	-2214.666884	-2213.953661	-2214.067062	-0.104862		
4cf	PyrTNpS_26	-2214.666846	-2213.953172	-2214.066726	-0.104032		
4cf	PyrTNpS_20	-2214.666786	-2213.953184	-2214.066589	-0.104288		
4cf	PyrTNpS_23	-2214.664782	-2213.951648	-2214.064060	-0.100909		
4cd	PyrTPS_5	-1753.695168	-1753.130568	-1753.230298	-0.079330	-1753.656363	-1750.405537
4cd	PyrTPS_4	-1753.695168	-1753.130568	-1753.230334	-0.079330	-1753.656363	-1750.405396
4cd	PyrTPS_2	-1753.695345	-1753.130800	-1753.228588	-0.079956	-1753.656518	-1750.406156
4cd	PyrTPS_11	-1753.695362	-1753.130831	-1753.228882	-0.077206	-1753.655583	-1750.404321
4cd	PyrTPS_9	-1753.695914	-1753.131132	-1753.227736	-0.080139	-1753.657220	-1750.406629
4cd	PyrTPS_10	-1753.695182	-1753.130615	-1753.227966	-0.079375		
4cd	PyrTPS_3	-1753.695182	-1753.130616	-1753.227959	-0.079367		
4cd	PyrTPS_6	-1753.694939	-1753.129751	-1753.226348	-0.079577		
4cd	PyrTPS_1	-1753.694928	-1753.129809	-1753.225931	-0.080023		
4cd	PyrTPS_7	-1753.695230	-1753.129822	-1753.225648	-0.080595		
2f	TNpSH_7	-1446.122879	-1445.675204	-1445.759125	-0.049847	-1446.088534	-1443.378719
2f	TNpSH_6	-1446.122379	-1445.674748	-1445.757362	-0.049595	-1446.087905	-1443.378080
2f	TNpSH_14	-1446.122342	-1445.674540	-1445.757215	-0.049669		
2f	TNpSH_11	-1446.122076	-1445.674297	-1445.757064	-0.049889		
2e	TPSH_10	-985.153660	-984.854507	-984.921163	-0.030077	-985.132473	-983.318377
2e	TPSH_3	-985.153676	-984.854563	-984.922292	-0.029979	-985.132451	-983.316880
2e	TPSH_2	-985.153678	-984.854561	-984.921277	-0.029997	-985.132467	-983.317086
2e	TPSH_9	-985.153676	-984.855474	-984.918116	-0.030006	-985.132468	-983.318312

[a]B3LYP-D3/6-311+G(2d)/6-31+G(d), [b]DLPNO-CCSD(T)/def2-TZVPP//SP

Table 4.10. Relative dispersion energy contribution to product stabilities as compared to the silyl ether of **1a** and the adequate silane. Boltzmann averaged free energy, reaction free energy, reaction dispersion energy and relative reaction dispersion energy at SMD(CHCl$_3$)/B3LYP-D3/6-311+G(2d)/6-31+G(d) level of theory. Reaction free energy and relative reaction free energy at DLPNO-CCSD(T)/def2-TZVPP level for the best conformers. Free energy at single point level of theory was obtained through addition of solvation energy and thermal corrections from SMD(CHCl$_3$)/B3LYP-D3/6-311+G(2d)/6-31+G(d) level frequency calculation. All energies are reported in Hartree.

compound	SMD(CHCl$_3$)/B3LYP-D3/6-311+G(2d)/6-31+G(d)			DLPNO-CCSD(T)/def2-TZVPP//SP	
	G_{298} (Boltzmann averaged) [Hartree]	$\Delta E_{disp} = E_{disp}$(**4yx**) - E_{disp}(**4ax**) [kJ mol^{-1}]	ΔG_{298} reaction free energy [kJ mol^{-1}]	ΔG_{298} reaction free energy (best conformer) [kJ mol^{-1}]	$\Delta\Delta G_{298}$ [kJ mol^{-1}]
1a	-384.824468				
1b	-538.436797				
1c	-768.277746				
1d	-692.052688				
1e	-692.043995				
1f	-692.051743				
2d	-984.921734				
2f	-1445.758584				
4ad	-1369.773912	0.0	-72.8	-92.1	0.0
4ae	-1830.614056	0.0	-81.4	-100.2	0.0
4bd	-1523.388042	-21.9	-77.5	-97.3	-4.7
4be	-1984.227430	-29.0	-84.1	-102.0	-2.7
4cd	-1753.229831	-55.8	-79.7	-100.8	-6.9
4ce	-2214.068904	-68.7	-85.5	-107.7	-4.1
4dd	-1677.001089	-44.1	-70.0	-90.4	2.7
4de	-2137.842286	-54.7	-81.4	-103.7	0.0
4ed	-1676.993761	-38.7	-73.6	-93.5	-0.8
4ee	-2137.834268	-57.7	-83.2	-104.2	-1.8
4fd	-1677.002099	-50.7	-75.1	-96.9	-2.4
4fe	-2137.843471	-61.0	-87.0	-107.9	-5.6

4.5.3. NMR Spectra of Products
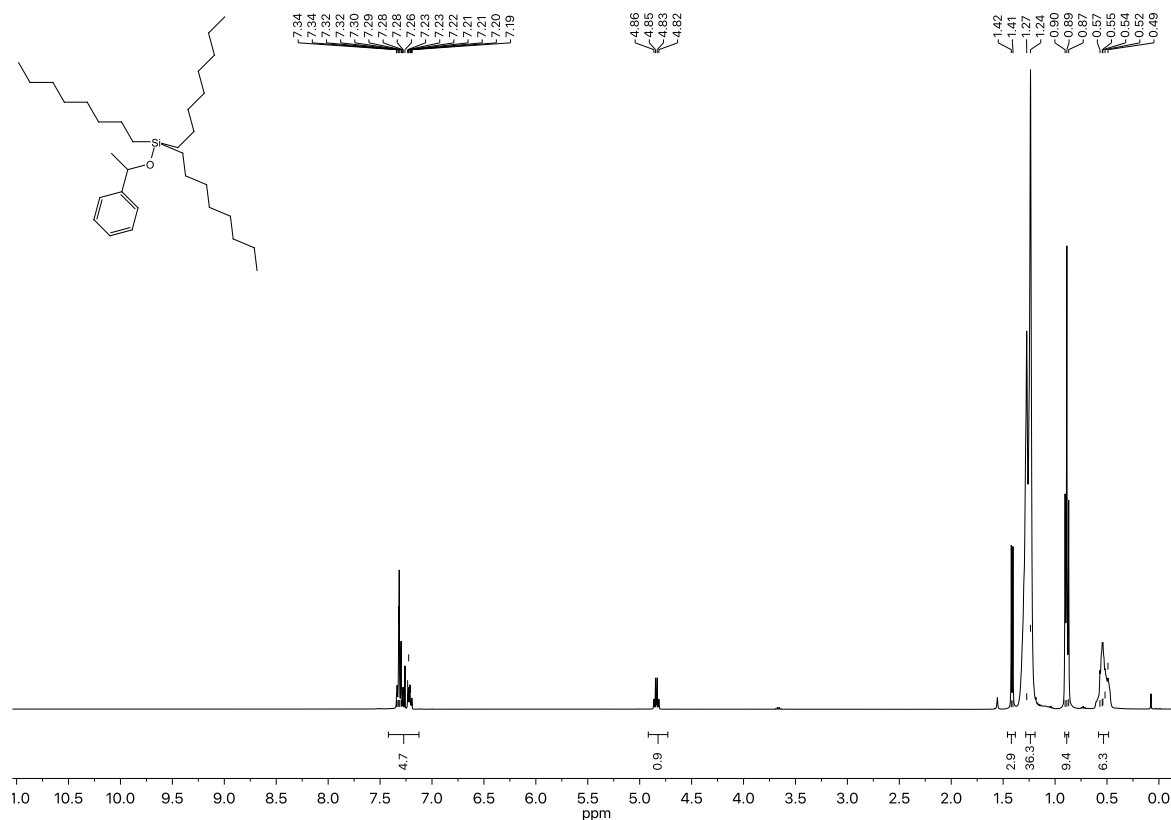
Figure 4.6. ^{1}H-NMR spectrum of silyl ether **4ab**.
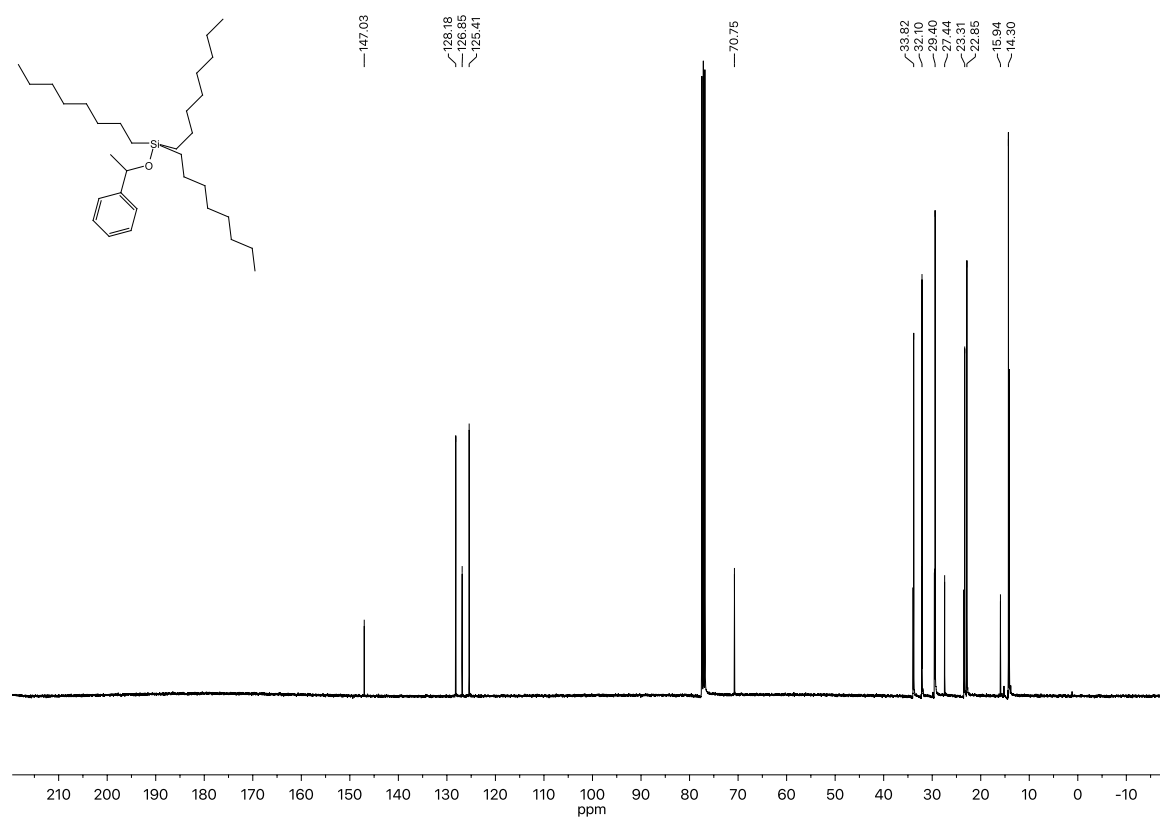
Figure 4.7. ^{13}C-NMR spectrum of silyl ether **4ab**.
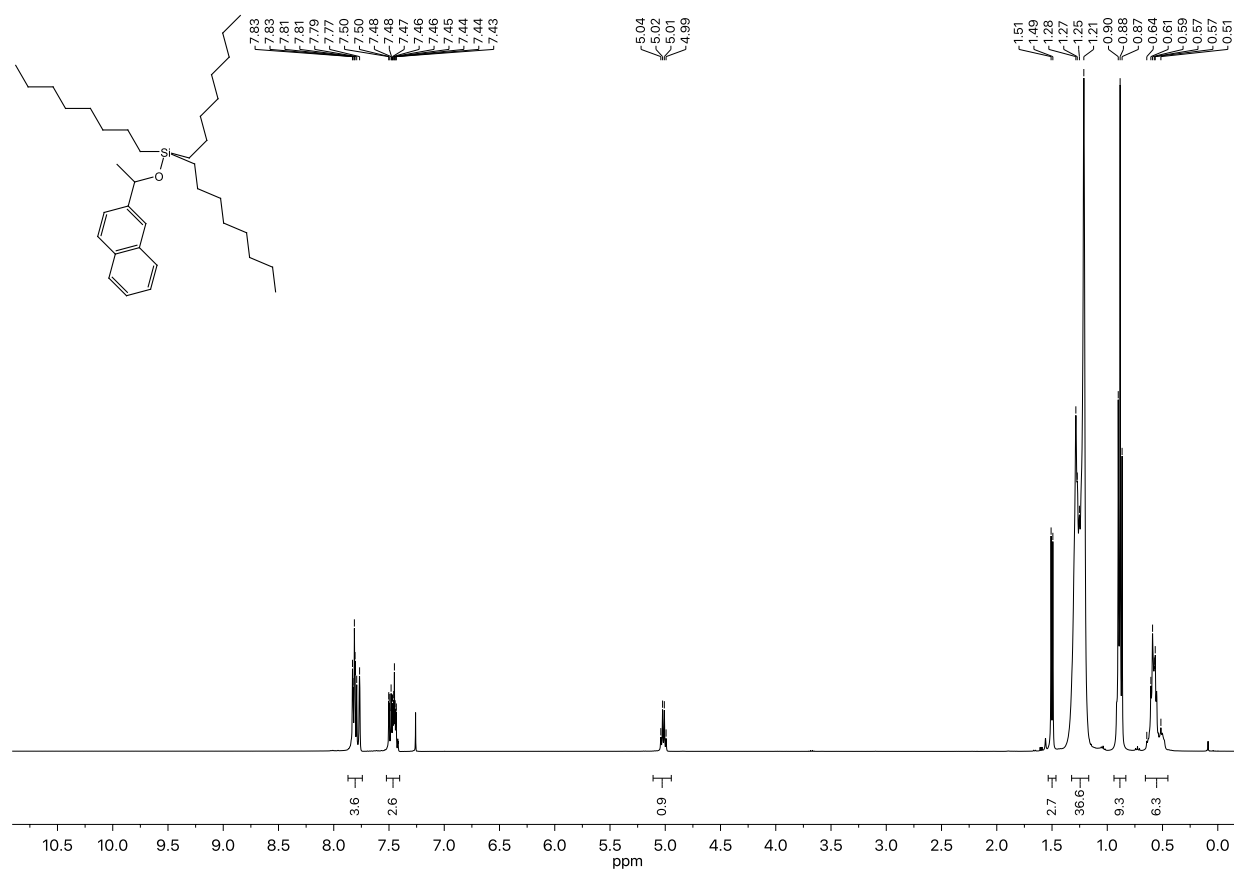
Figure 4.8. ^{1}H-NMR spectrum of silyl ether **4bb**.
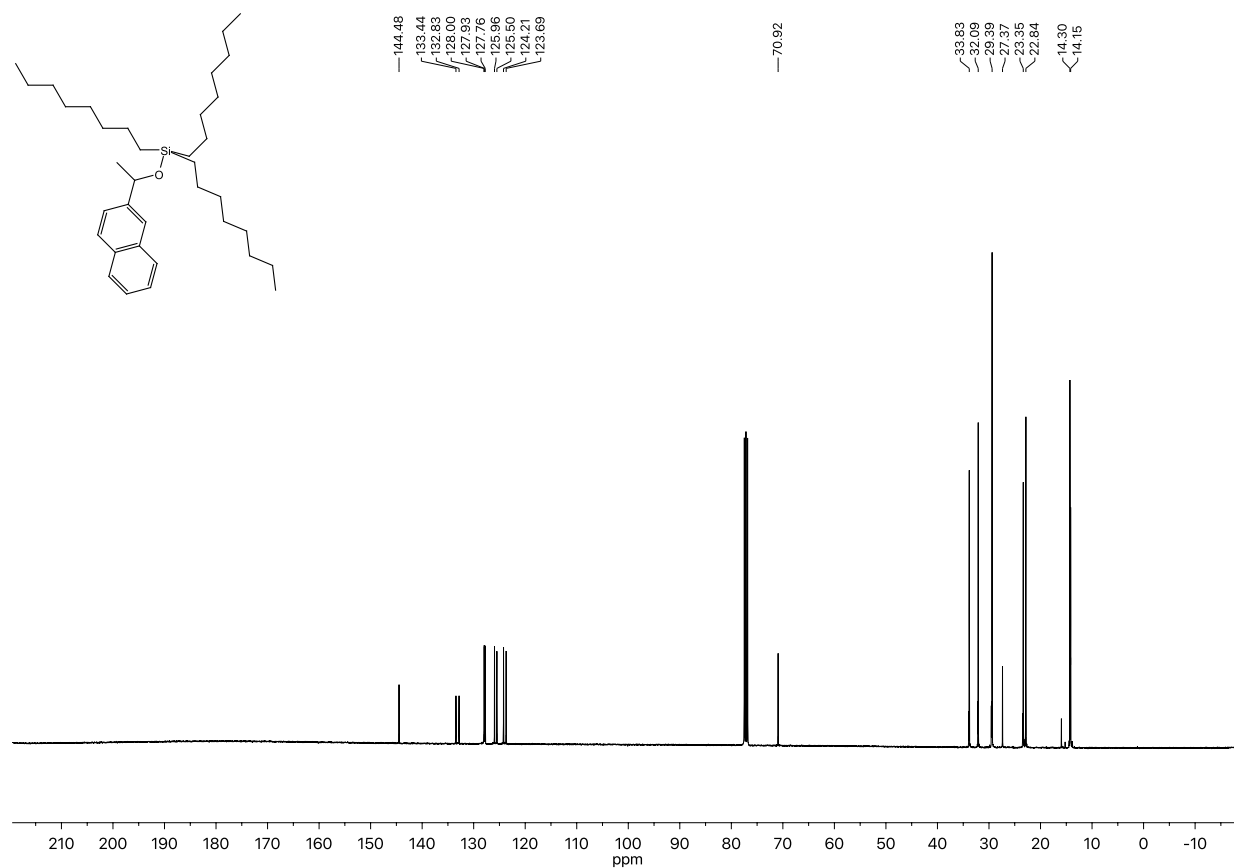
Figure 4.9. ^{13}C-NMR spectrum of silyl ether **4bb**.

—16.74
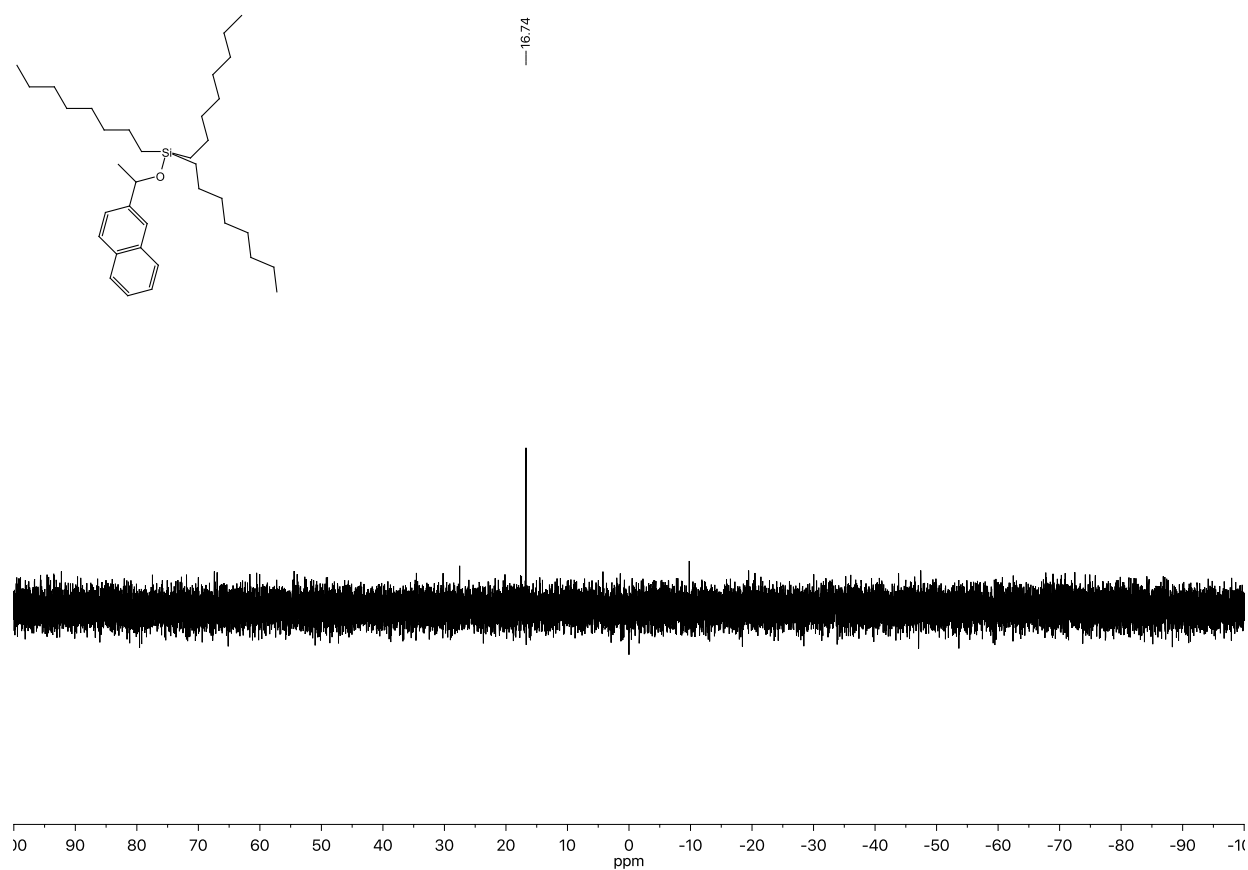
Figure 4.10. ²⁹Si-NMR spectrum of silyl ether **4bb**.
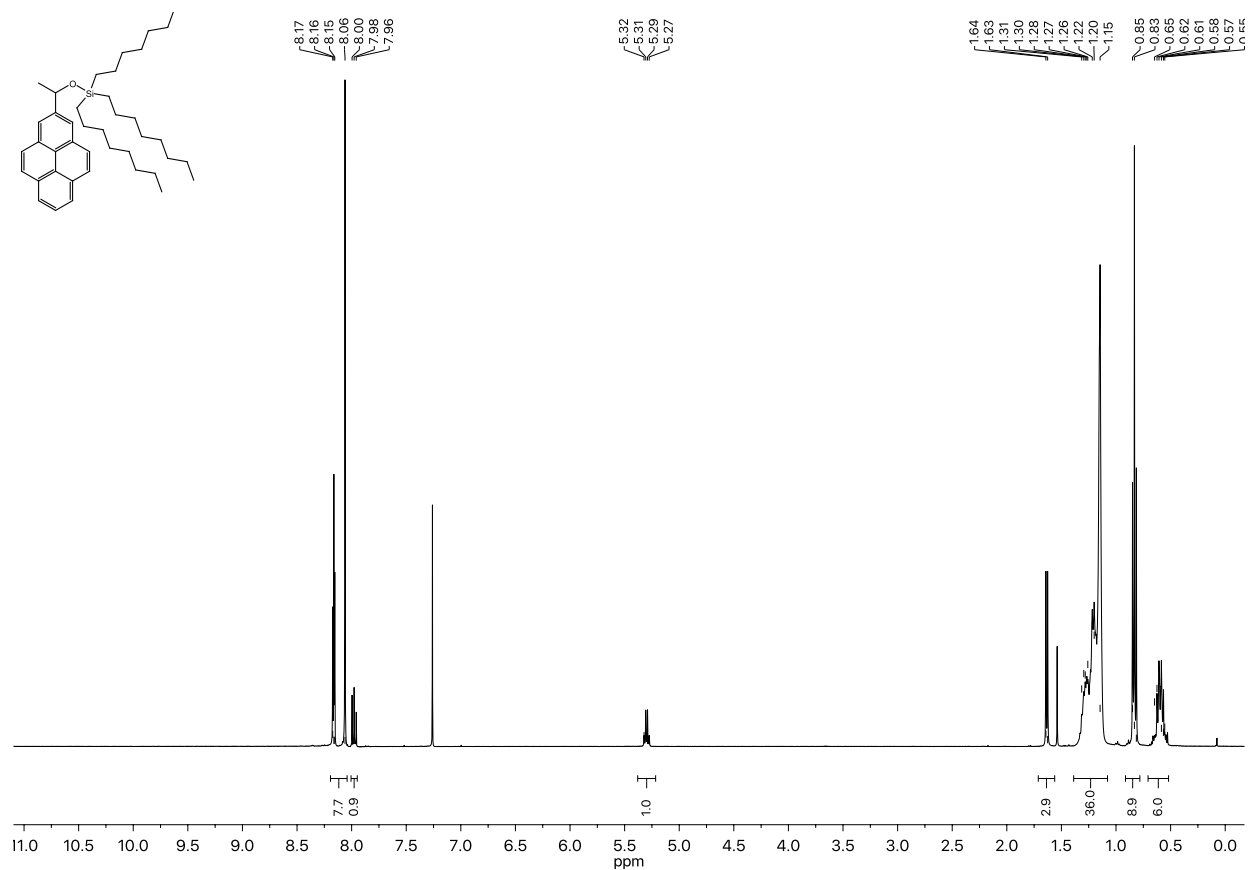
Figure 4.11. ¹H-NMR spectrum of silyl ether **4cb**.
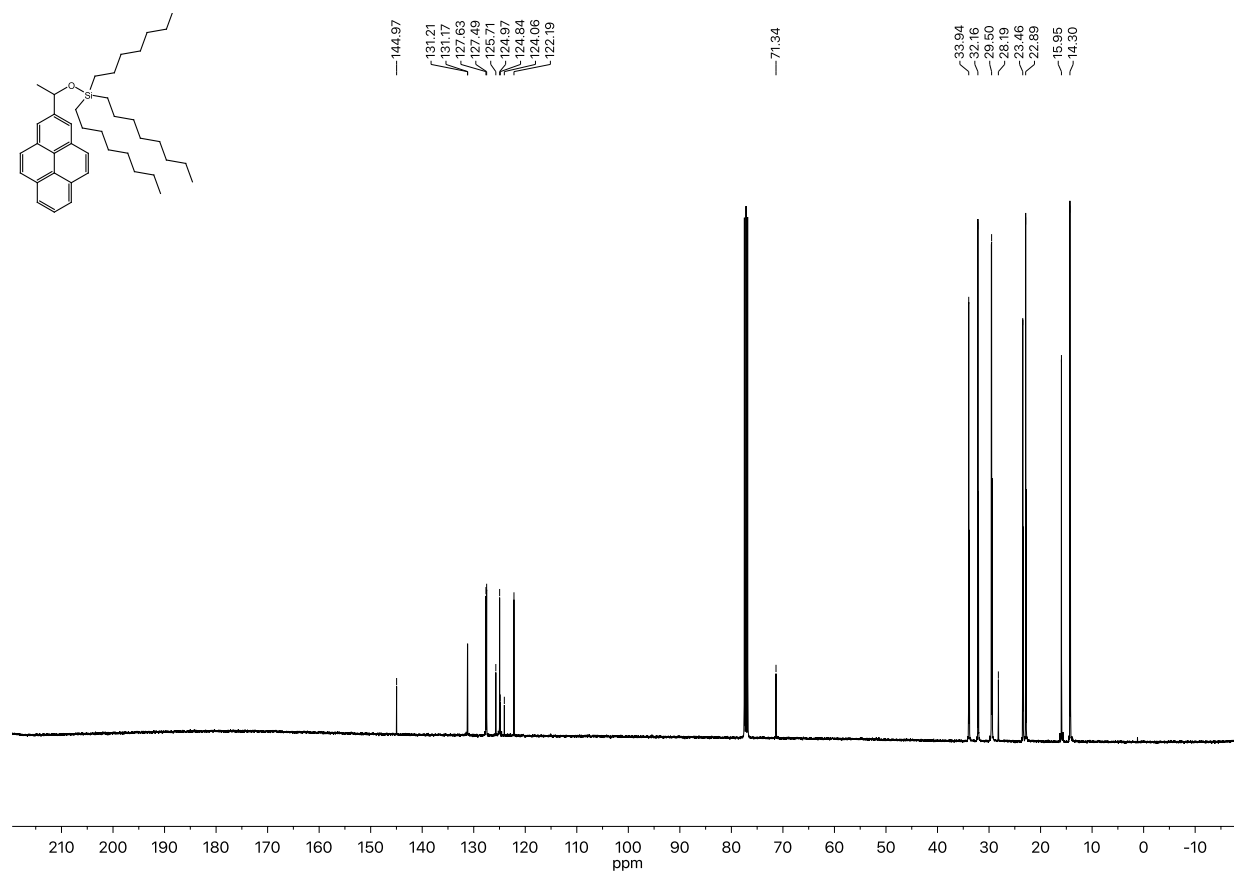
Figure 4.12. ^{13}C-NMR spectrum of silyl ether **4cb**.

4.6. References

[1]   P. Patschinski, H. Zipse, *Org. Lett.* **2015**, *17*, 3318-3321.
[2]   P. G. M. Wuts, T. W. Greene, *Greene's Protective Groups in Organic Synthesis*, John Wiley & Sons, Hoboken, **2006**.
[3]   A. Weickgenannt, M. Oestreich, *Chem. Asian J.* **2009**, *4*, 406-410.
[4]   X. Dong, A. Weickgenannt, M. Oestreich, *Nat. Commun.* **2017**, *8*, 15547.
[5]   I. Ojima, T. Kogure, M. Nihonyanagi, Y. Nagai, *Bull. Chem. Soc. Jpn.* **1972**, *45*, 3506-3506.
[6]   S. Liu, J. Peng, H. Yang, Y. Bai, J. Li, G. Lai, *Tetrahedron* **2012**, *68*, 1371-1375.
[7]   B. H. Lipshutz, W. Chrisman, K. Noson, *J. Organomet. Chem.* **2001**, *624*, 367-371.
[8]   a) M. Hechavarría Fonseca, B. König, *Adv. Synth. Catal.* **2003**, *345*, 1173-1185; b) C. Arena, *Mini-Rev. Org. Chem.* **2009**, *6*, 159-167.
[9]   H. Gilman, D. Wittenberg, *J. Org. Chem.* **1958**, *23*, 501-502.
[10]   H. Sakurai, A. Hosomi, M. Kumada, *Bull. Chem. Soc. Jpn.* **1967**, *40*, 1551-1551.
[11]   C. Chatgilialoglu, *Chem. Rev.* **1995**, *95*, 1229-1251.
[12]   a) C. Chatgilialoglu, K. U. Ingold, J. C. Scaiano, *J. Am. Chem. Soc.* **1982**, *104*, 5119-5123; b) A. Alberti, C. Chatgilialoglu, G. F. Pedulli, P. Zanirato, *J. Am. Chem. Soc.* **1986**, *108*, 4993-4998; c) J. Cooper, A. Hudson, R. A. Jackson, *Perkin Trans. 2* **1973**, 1933-1937.
[13]   A. K. Roy, *Adv. Organomet. Chem.* **2007**, *55*, 1-59.
[14]   a) M. B. Haque, B. P. Roberts, D. A. Tocher, *J. Chem. Soc., Perkin Trans. 1* **1998**, 2881-2890; b) Y. Cai, B. P. Roberts, *Tetrahedron Lett.* **2001**, *42*, 8235-8238.
[15]   a) M. Ballestri, C. Chatgilialoglu, K. B. Clark, D. Griller, B. Giese, B. Kopping, *J. Org. Chem.* **1991**, *56*, 678-683; b) C. Chatgilialoglu, V. Timokhin, *Adv. Organomet. Chem.* **2008**, *57*, 117-181.
[16]   a) J.-S. Li, J. Wu, *ChemPhotoChem* **2018**, *2*, 839-846; b) J. Zhu, W. C. Cui, S. Wang, Z. J. Yao, *Org. Lett.* **2018**, *20*, 3174-3178.
[17]   A. G. Massey, A. J. Park, *J. Organomet. Chem.* **1964**, *2*, 245-250.
[18]   D. J. Parks, W. E. Piers, *J. Am. Chem. Soc.* **1996**, *118*, 9440-9441.
[19]   a) D. J. Parks, J. M. Blackwell, W. E. Piers, *J. Org. Chem.* **2000**, *65*, 3090-3098; b) S. Rendler, M. Oestreich, *Angew. Chem. Int. Ed.* **2008**, *47*, 5997-6000; c) K. Sakata, H. Fujimoto, *J. Org. Chem.* **2013**, *78*, 12505-12512.
[20]   W. E. Piers, A. J. Marwitz, L. G. Mercier, *Inorg. Chem.* **2011**, *50*, 12252-12262.
[21]   R. P. Allen, B. P. Roberts, C. R. Willis, *J. Chem. Soc., Chem. Commun.* **1989**, 1387-1388.
[22]   C. Bergquist, B. M. Bridgewater, C. J. Harlan, J. R. Norton, R. A. Friesner, G. Parkin, *J. Am. Chem. Soc.* **2000**, *122*, 10581-10590.
[23]   a) V. Gevorgyan, M. Rubin, J. X. Liu, Y. Yamamoto, *J. Org. Chem.* **2001**, *66*, 1672-1675; b) K. M. Lucas, A. F. Kleman, L. R. Sadergaski, C. L. Jolly, B. S. Bollinger, B. L. Mackesey, N. A. McGrath, *Org. Biomol. Chem.* **2016**, *14*, 5774-5778.
[24]   P. E. Dietze, *J. Org. Chem.* **1993**, *58*, 5653-5662.
[25]   C. Gross, *Aromatic interactions and size effects in the hydrosilylation reaction of ketones*, Master thesis, LMU München (Munich), **2019**.
[26]   M. Marin-Luna, B. Pölloth, F. Zott, H. Zipse, *Chem. Sci.* **2018**, *9*, 6509-6515.
[27]   J. Helberg, M. Marin-Luna, H. Zipse, *Synthesis* **2017**, *49*, 3460-3470.
[28]   a) M. J. Kamlet, J. M. Abboud, M. H. Abraham, R. W. Taft, *J. Org. Chem.* **1983**, *48*, 2877-2887; b) W. K. Stephenson, R. Fuchs, *Can. J. Chem.* **1985**, *63*, 2535-2539; c) C. Laurence, P. Nicolet, M. T. Dalati, J.-L. M. Abboud, R. Notario, *J. Phys. Chem.* **1994**, *98*, 5807-5816.
[29]   a) M. H. Abraham, H. S. Chadha, G. S. Whiting, R. C. Mitchell, *J. Pharm. Sci.* **1994**, *83*, 1085-1100; b) M. H. Abraham, F. Martins, R. C. Mitchell, C. J. Salter, *J. Pharm. Sci.* **1999**, *88*, 241-247.
[30]   C. A. Hunter, *Angew. Chem. Int. Ed.* **2004**, *43*, 5310-5324.
[31]   J. Catalán, *J. Phys. Chem. B* **2009**, *113*, 5951-5960.
[32]   a) C. M. Hansen, *The three dimensional solubility parameter and solvent diffusion coefficient*, Technical University of Denmark (Copenhagen), **1967**; b) S. Abbott, "HSP Basics", https://www.stevenabbott.co.uk/practical-solubility/hsp-basics.php, accessed at 13.02.2018, **2013**.
[33]   a) J. N. Israelachvili, *Intermolecular and Surface Forces*, 3 ed., Elsevier, Burlington, **2011**; b) C. Adam, L. Yang, S. L. Cockroft, *Angew. Chem. Int. Ed.* **2015**, *54*, 1164-1167.
[34]   AnalystSoft, StatPlus:mac LE, **2019**.
[35]   J. Contreras-Garcia, E. R. Johnson, S. Keinan, R. Chaudret, J. P. Piquemal, D. N. Beratan, W. Yang, *J. Chem. Theory Comput.* **2011**, *7*, 625-632.
[36]   W. Humphrey, A. Dalke, K. Schulten, *J. Mol. Graphics* **1996**, *14*, 33-38.
[37]   H. B. Kagan, J. C. Fiaud, *Top. Stereochem.* **1988**, *18*, 249-300.
[38]   C. Reichardt, *Solvents and Solvent Effects in Organic Chemistry*, WILEY-VCH, Weinheim, **2003**.
[39]   a) A. D. Becke, *J. Chem. Phys.* **1993**, *98*, 5648; b) C. Lee, W. Yang, R. G. Parr, *Phys. Rev. B* **1988**, *37*, 785-789; c) S. Grimme, *J. Chem. Phys.* **2006**, *124*, 034108.
[40]   G. W. Spitznagel, T. Clark, J. Chandrasekhar, P. R. Schleyer, *J. Comput. Chem.* **1982**, *3*, 363-371.
[41]   A. V. Marenich, C. J. Cramer, D. G. Truhlar, *J. Phys. Chem. B* **2009**, *113*, 6378-6396.
[42]   Maestro 12.2.012, New York, **2019**.
[43]   a) C. Riplinger, F. Neese, *J. Chem. Phys.* **2013**, *138*, 034106; b) C. Riplinger, B. Sandhoefer, A. Hansen, F. Neese, *J. Chem. Phys.* **2013**, *139*, 134101; c) F. Weigend, R. Ahlrichs, *Phys. Chem. Chem. Phys.* **2005**, *7*, 3297-3305.
[44]   A. Hellweg, C. Hättig, S. Höfener, W. Klopper, *Theor. Chem. Acc.* **2007**, *117*, 587-597.
[45]   M. Marin-Luna, P. Patschinski, H. Zipse, *Chem. Eur. J.* **2018**, *24*, 15052-15058.
[46]   G. W. T. M. J. Frisch, H. B. Schlegel, G. E. Scuseria, M. A. Robb, J. R. Cheeseman, G. Scalmani, V. Barone, B. Mennucci, G. A. Petersson, H. Nakatsuji, M. Caricato, X. Li, H. P. Hratchian, A. F. Izmaylov, J. Bloino, G. Zheng, J. L. Sonnenberg, M. Hada, M. Ehara, K. Toyota, R. Fukuda, J. Hasegawa, M. Ishida, T. Nakajima, Y. Honda, O. Kitao, H. Nakai, T. Vreven, J. A. Montgomery, Jr., J. E. Peralta, F. Ogliaro, M. Bearpark, J. J. Heyd, E. Brothers, K. N. Kudin, V. N. Staroverov, T. Keith, R. Kobayashi, J. Normand, K. Raghavachari, A. Rendell, J. C. Burant, S. S. Iyengar, J. Tomasi, M. Cossi, N. Rega, J. M. Millam, M. Klene, J. E. Knox, J. B. Cross, V. Bakken, C. Adamo, J. Jaramillo, R. Gomperts, R. E. Stratmann, O. Yazyev, A. J. Austin, R. Cammi, C. Pomelli, J. W. Ochterski, R. L. Martin, K. Morokuma, V. G. Zakrzewski, G. A. Voth, P. Salvador, J. J. Dannenberg, S. Dapprich, A. D. Daniels, O. Farkas, J. B. Foresman, J. V. Ortiz, J. Cioslowski, and D. J. Fox,, Gaussian 09, Revision D.01, Wallingford CT, **2010**.
[47]   F. Neese, *Comput. Mol. Sci.* **2012**, *2*, 73-78.

Chapter 5. Size-Effects in the Silylation-Based Kinetic Resolution of Secondary Alcohols.

Benjamin Pölloth, Hendrik Zipse

Unpublished results

Author contribution: The project was conceived by B.P. and H.Z. The experimental study was performed by B.P. The manuscript was written by B.P.

5.1. Introduction

A broad variety of organocatalysts for acylation reactions is known,[1] that were already briefly discussed in the introduction. In contrast, the number of asymmetric catalysts for the silylation of alcohols are rare. Enantioselectivity was mainly achieved in the silylation of diols or polyols by using bifunctional catalysts.[2] For example, Klare and Oestreich[3] developed transition metal-catalysed dehydrogenative couplings of alcohols with hydrosilanes yielding remarkably high selectivity values. However, this approach is restricted to very specific alcohols with neighbouring donor groups.[2] Ishikawa[4] was the first to report a kinetic resolution reaction of monofunctional alcohols with guanidine derivatives, but the obtained enantioselectivity values were rather small.
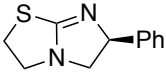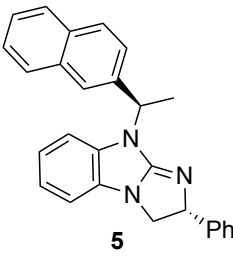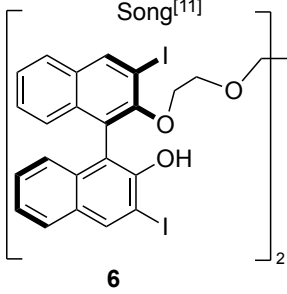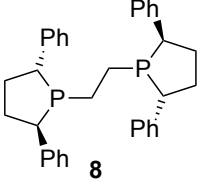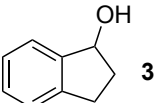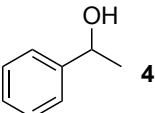
Figure 5.1. Catalyst systems for the silylative kinetic resolution of alcohols. The values in the dashed box refer to enantioselectivity values obtained from acylation reactions under similar conditions and are given for reference.

In 2011, Wiskur et al.[5] reported the kinetic resolution of simple monofunctional alcohols with triphenylsilyl chloride (TPSCl, **1**) catalysed by isothiourea-based deworming agent (-)-tetramisole (**2**). While decent selectivity values were found for bicyclic alcohols like indanol **3**[6], α-hydroxy lactones and lactames[7], and 2-arylcyclohexanols[8], simple aryl alcohols like 1-phenylethanol (**4**) were only poorly resolved (s < 2.8).[5] The selectivity values for indanol derivatives were improved by the chiral guanidine **5** developed by Nakata et al.[9] Nevertheless, the reported scope of this reactions seems to be limited to bicyclic alcohols.[10] To the best of our knowledge no enantioselectivity values for simple alcohols like 1-phenylethanol (**4**) have been reported. In 2015 Song et al.[11] developed the BINOL (1,1'-bi-2-naphtol) derivative **6**, which gave good selectivity values for the kinetic resolution of simple aromatic alcohols with ppm catalyst loadings only. This reaction is based on the Brønsted acid activation of hexamethyldisilazane (**7**). 2017 the Oestreich group[12] reported the kinetic resolution of simple aryl alcohols by copper-catalysed dehydrogenative

couplings with chiral ligand **8** and tri-*n*-butyl hydrosilane (**9**). Despite these advances with alternative reagents, to date no reasonable catalyst for the kinetic resolution of simple aromatic alcohols like **4** based on silylation reactions with silyl chlorides is known.[13] This is, however, surprising as the Lewis base-catalysed silylation of alcohols by silyl chlorides is the commonly employed standard procedure for the synthesis of silyl ethers.[14]

Proposed TS Birman[15]   Proposed TS Wiskur[6]

s = 31 *(S)*   s = 2.8 *(R)*
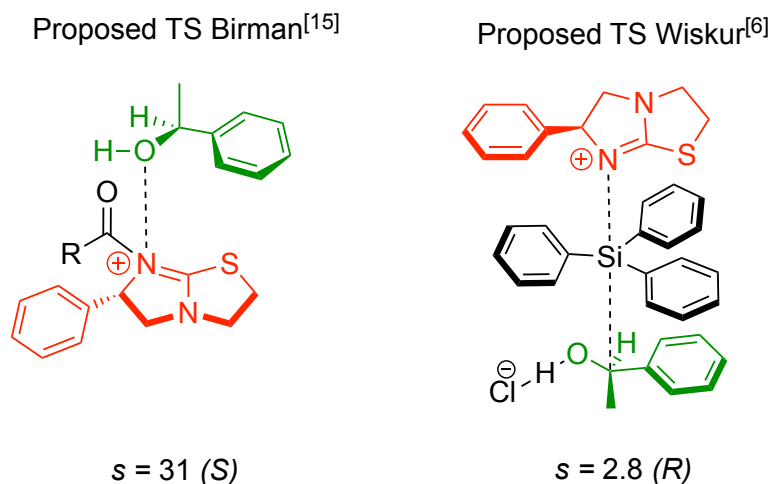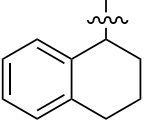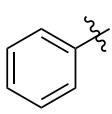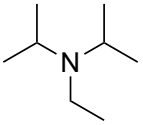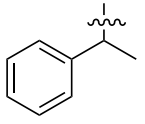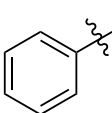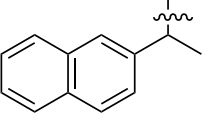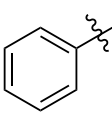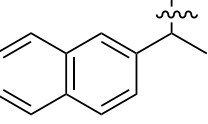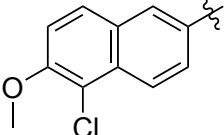
Figure 5.2. Proposed transition states for the kinetic resolution with (-)-tetramisole **2** in acylation reactions (right)[15] and in silylation reactions (right).[6]

Both catalysts **2** and **5** were originally employed as asymmetric catalyst for acylation reactions.[15-16] However, the selectivity values reported for the acylation of alcohol **4** are much higher than in comparable silylation reactions (see **Figure 5.1**). Additionally, in both cases the opposite enantiomer with respect to the silylation reaction is preferred. These differences can be rationalized by the different structure of transition states as proposed for acylation reactions by Birman *et al.*[15] and for silylation reactions by Wiskur *et al.*[6] (see **Figure 5.2**). However, especially the mechanism of the asymmetric silylation reaction is not fully elucidated. Based on preferred atropisomers of the *(R)*- and *(S)*-silyl ether products Wiskur *et al.*[17] proposed that the chiral information from the catalyst is transferred via a helical chirality of the silyl chloride onto the alcohol. We thus wondered in how far bigger alcohols and silyl chlorides would affect the enantioselectivity. If (helical) chirality was transferred via attractive aromatic-aromatic interactions increasing those interactions could also improve the selectivity.

5.2. Results and Discussion

Enantioselectivity values were determined by kinetic resolution experiments of the racemic alcohol and relevant silyl chloride (0.6 equivalents) in the presence of 25 mol% catalyst **2** and an amine as auxiliary base. Further details are provided in Chapter 0.

Table 5.1. Results of kinetic resolution experiments using (-)-tetramisole **2**.

R¹	R²	amine	solvent	T	c	s
10	**1**	Hünig's base **12**	THF	-78 °C	42%	10.6
			THF	23 °C	53%	4.1
			CHCl₃	23 °C	55%	3.7
			DCM	-78 °C	51%	6.7
4	**1**	NEt₃ **13**	THF	-78 °C	55%	1.8
14	**1**	Hünig's base **12**	THF	-78 °C	51%	1.5
		NEt₃ **13**	THF	-78 °C	54%	1.4
			DCM	-78 °C	49%ᵃ	1.1
14	**16**	NEt₃ **13**	THF	-78 °C	no conv.	-
			DCM	-78 °C	32%ᵃ	1.0

ᵃdetermined by ¹H-NMR analysis (due to very small *ee* values)

In a first step we reproduced the reported selectivity value (*s* = 11) for alcohol **10**.[6] Note that a dependence of the selectivity values on the used amine is reported: *N,N*-diisopropyl-3-pentylamine (**11**) gave slightly higher selectivity values,[5] yet in the preceding publication always the sterically less hindered Hünig's base (**12**) was used.[6] In our studies we did not find notable differences for the use of Hünig's base (**12**) as compared to (even less hindered) triethylamine (**13**). Changes in temperature or solvent decreased selectivity significantly. Moreover, changing **10** to 1-phenylethanol (**4**) led to a significant decrease in enantioselectivity, as reported by Wiskur *et al.*[6] (the above mentioned *s* = 2.8 was obtained with amine **11**). We thus hoped that an increase in size of the aromatic moiety at the alcohol by using 1-(2-naphthyl)ethanol (**14**) would improve selectivity.

In contrast to our expectations, enantioselectivity was even further lowered. Since we found for the achiral silylation of secondary alcohols with DMAP (**15**) that attractive interactions were cancelled in THF due to its strong hydrogen bond donor ability (see Chapter 3) we tried to use DCM as the solvent with highest relative rates for bigger alcohols in the previous study. Unfortunately, the selectivity was lowered further for 1-(2-naphthylethanol) (**14**) as well as for **10**. As increasing the surface of the alcohol did not result in the expected changes, we used the best and largest silyl chloride **16** from the previous study. No conversion was obtained in THF at -78 °C most likely caused by the low solubility of silyl chloride **16**. While in DCM the reaction proceeded, no enantioselectivity could be observed for this reaction at all.

5.3. Conclusion

Enantioselectivity values for the kinetic resolution of secondary alcohol by (-)-tetramisole (**2**) were diminished for bigger alcohols and silyl chlorides. Thus, enantioselectivity for this type of reaction does not appear to be caused by rate accelerations through attractive interactions of alcohol and silyl chloride moiety. In contrast, rate acceleration even seems to lower the selectivity for these reactions. A similar observation was reported by Wiskur *et al.*[6] as the rate acceleration through the introduction of electron-donating groups on the silyl groups also lowers enantioselectivities. However, further work is necessary to fully elucidate the cause of the observed enantioselectivity and the mechanism of this reaction.

As the goal of this work was to investigate size-effects on kinetic resolution experiments we decided, that silylation reactions are not a suitable model system for our purpose. This can be explained referring to the proposed transition state in **Figure 5.2**: The geometry does not allow a direct interaction of moieties of catalyst and alcohol reagents. Additionally, also in the achiral silylation no rate effects through an increase of catalyst surfaces was found (see Chapter 3). In contrast, for acylation reactions rate accelerations through attractive interaction of catalyst and alcohol moieties are possible and were reported before.[18] Accordingly, we decided to use an acylation reaction as model system for further studies on size-effects in asymmetric organocatalysis as described in the next chapter.

5.4. Supporting Information

General procedures and details on analytic hardware are similar to those reported in Chapter 6.3.

5.4.1. Experimental Determination of Enantioselectivity Values
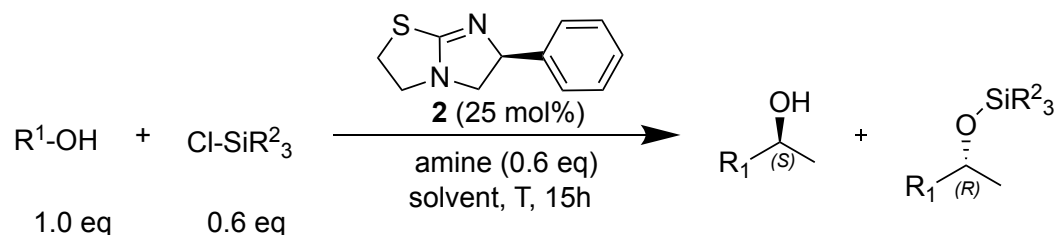
Scheme 5.1. Kinetic resolution experiment for the determination of enantioselectivity.

General procedure for kinetic resolution experiments: 0.24 mmol (1.0 eq) of the racemic alcohol is weighed into a Schlenk flask with stirring bar, evacuated and flushed three times with nitrogen. 1.6 mL of a stock solution containing 0.14 mmol (0.60 eq) of amine and 0.06 mmol (0.25 eq) of catalyst are added. After the mixture is cooled to reaction temperature, 0.8 mL of the pre-cooled silyl chloride stock solution (0.14 mmol, 0.60 eq) is added. The reaction is stirred for 15 hours at appropriate temperature. The mixture is quenched through addition of 250 μl Methanol and 1.5 mL saturated NH_4Cl-solution, extracted with DCM (3 x 10 mL), dried, filtered and evaporated. A ^{1}H-NMR (400 MHz) in $CDCl_3$ is measured. Reactants and products are separated by column chromatography (10 g silica, 100 mL hexanes/DCM = 1/1 → 100 mL DCM/MeOH = 98/2). The products are dissolved in 3 mL THF and stirred with 1 mL of 1M tetrabutyl ammonium fluorid (TBAF) solution for 8 hours. The reaction is quenched through addition of brine, extracted with DCM (3x10 mL), dried over $MgSO_4$, filtered and concentrated in vacuum. Deprotected products are purified by column chromatography (10 g silica, 50 mL DCM → 100 mL DCM/MeOH = 98:2). HPLC spectra (Daicel IB-N5, hexanes/*iso*propanol = 96/4, 0.5 mL/min, T = +25 °C) are recorded for non-reacted reactants and deprotected products.

Enantiomeric excess *ee*, conversion *c* and selectivity value *s* were calculated by Eq. 5.1 - Eq. 5.3.[19]

$$ee = \frac{[major\ enantiomer] - [minor\ enantiomer]}{[major\ enantiomer] + [minor\ enantiomer]} \qquad \text{Eq. 5.1}$$

$$c = \frac{ee_{substrate}}{ee_{substrate} + ee_{product}} \qquad \text{Eq. 5.2}$$

$$s = \frac{ln\big(1 - c(1 + ee_{product})\big)}{ln\big(1 - c(1 - ee_{product})\big)} \qquad \text{Eq. 5.3}$$

5.4.2. Data Tables for Kinetic Resolution Experiments

Table 5.2. HPLC absorption for kinetic resolution experiments as described above.

alcohol	silyl chloride	solvent	T] [°C]	amine		(S)	(R)	e.e.	conversion	s
10	1	THF	-78	12	reactants	1321	414	0.5227	41.82%	10.6
					products	147	928	0.7271		
10	1	THF	23	12	reactants	17937	6054	0.50	53.08%	4.1
					products	458	1172	0.44		
10	1	CHCl3	23	12	reactants	626	214	0.49	55.00%	3.7
					products	882	2065	0.40		
10	1	DCM	-78	12	reactants	1563	394	0.60	50.26%	7.0
					products	1504	5848	0.59		
4l	1	THF	-78	13	reactants	901	1440	0.230	54.84%	1.8
					products	2373	1616	0.190		
14	1	THF	-78	12	reactants	9338	6981	0.144	50.81%	1.5
					products	4056	5375	0.140		
14	1	THF	-78	13	reactants	1701	1292	0.137	53.70%	1.4
					products	9595	12157	0.118		
14	1	DCM	-78	13	reactants	3901	3570	0.044	48.50%[a]	1.1
					products	6977	7013	0.003		
14	T6	DCM	-78	13	reactants	5313	5259	0.005	31.80%[a]	1.0
					products	6517	6788	0.020		

[a]determined by ^{1}H-NMR

5.5. References

[1]   a) C. E. Muller, P. R. Schreiner, *Angew. Chem. Int. Ed.* **2011**, *50*, 6012-6042; b) H. Mandai, K. Fujii, S. Suga, *Tetrahedron Lett.* **2018**, *59*, 1787-1803.
[2]   L. W. Xu, Y. Chen, Y. Lu, *Angew. Chem. Int. Ed.* **2015**, *54*, 9456-9466.
[3]   H. F. Klare, M. Oestreich, *Angew. Chem. Int. Ed.* **2007**, *46*, 9335-9338.
[4]   T. Isobe, K. Fukuda, Y. Araki, T. Ishikawa, *Chem. Commun.* **2001**, 243-244.
[5]   C. I. Sheppard, J. L. Taylor, S. L. Wiskur, *Org. Lett.* **2011**, *13*, 3794-3797.
[6]   R. K. Akhani, M. I. Moore, J. G. Pribyl, S. L. Wiskur, *J. Org. Chem.* **2014**, *79*, 2384-2396.
[7]   R. W. Clark, T. M. Deaton, Y. Zhang, M. I. Moore, S. L. Wiskur, *Org. Lett.* **2013**, *15*, 6132-6135.
[8]   L. Wang, R. K. Akhani, S. L. Wiskur, *Org. Lett.* **2015**, *17*, 2408-2411.
[9]   S. Yoshimatsu, A. Yamada, K. Nakata, *J. Org. Chem.* **2018**, *83*, 452-458.
[10]   S. Yoshimatsu, K. Nakata, *Adv. Synth. Catal.* **2019**, *361*, 4679-4684.
[11]   S. Y. Park, J. W. Lee, C. E. Song, *Nat. Commun.* **2015**, *6*, 7512.
[12]   X. Dong, A. Weickgenannt, M. Oestreich, *Nat. Commun.* **2017**, *8*, 15547.
[13]   J. Seliger, M. Oestreich, *Chem. Eur. J.* **2019**, *25*, 9358-9365.
[14]   P. G. M. Wuts, T. W. Greene, *Greene's Protective Groups in Organic Synthesis*, John Wiley & Sons, Hoboken, **2006**.
[15]   V. B. Birman, X. Li, *Org. Lett.* **2006**, *8*, 1351-1354.
[16]   K. Nakata, I. Shiina, *Org. Biomol. Chem.* **2011**, *9*, 7092-7096.
[17]   L. Wang, T. Zhang, B. K. Redden, C. I. Sheppard, R. W. Clark, M. D. Smith, S. L. Wiskur, *J. Org. Chem.* **2016**, *81*, 8187-8193.
[18]   J. Helberg, M. Marin-Luna, H. Zipse, *Synthesis* **2017**, *49*, 3460-3470.
[19]   H. B. Kagan, J. C. Fiaud, *Top. Stereochem.* **1988**, *18*, 249-300.

Chapter 6. The Size-Accelerated Kinetic Resolution of Secondary Alcohols.

Benjamin Pölloth, Mukund P. Sibi, and Hendrik Zipse*

Angewandte Chemie International Edition, **2020**, *in review. Manuscript ID: 202011687.*

Author contributions: The project was conceived by B.P. and H.Z. Experimental and computational studies were performed by B.P. The manuscript was jointly written by B.P. and H.Z. The supporting information was prepared by B.P. Discussion, manuscript approval and catalyst samples for initial screening were provided by M.S.

Copyright: The manuscript was submitted to *Angewandte Chemie International Edition* on 26th of August 2020 and assigned the manuscript ID 202011687 (© 2020 Wiley VCH). The manuscript was at the time of print under review.

Additional information: The herein printed Supporting Information (SI) is similar to the SI submitted to *Angewandte Chemie* except for NMR spectra and HPLC traces that can be found in the original electronic SI file. The original SI file can also be found on the electronic attachment of this thesis.

The Size-Accelerated Kinetic Resolution of Secondary Alcohols

Benjamin Pölloth,[a] Mukund P. Sibi,[b] and Hendrik Zipse*[a]

[a] B. Pölloth, Prof. Dr. H. Zipse
Department of Chemistry
LMU München
Butenandtstr. 5-13, 81377, Munich (Germany)
E-mail: zipse@cup.uni-muenchen.de

[b] Prof. Dr. M. P. Sibi
Department of Chemistry and Biochemistry
North Dakota State University
Fargo, ND 58108 (USA)

Supporting information for this article is given via a link at the end of the document.
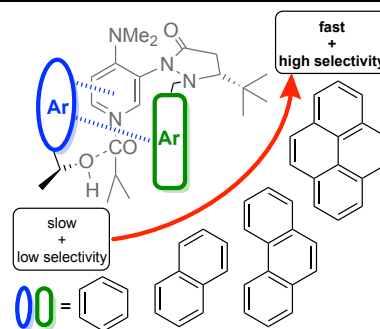
Abstract: The factors responsible for the kinetic resolution of alcohols by chiral pyridine derivatives have been elucidated by measurements of relative rates for a set of substrates of systematically increasing size using accurate competitive linear regression analysis. Increasing the side chain size from phenyl to pyrenyl results in a rate acceleration of more than 40 for the major enantiomer. Based on this observation a new catalyst with increased steric bulk has been designed that gives enantioselectivity values of up to $s = 250$. Extensive conformational analysis of the relevant transition states indicates that alcohol attack to the more crowded side of the acyl-catalyst intermediate is favoured due to stabilizing CH-π-stacking interactions. Experimental and theoretical results imply that enantioselectivity enhancements result from accelerating the transformation of the major enantiomer through attractive non-covalent interactions (NCIs) rather than retarding the transformation of the minor isomer through repulsive steric forces.

Introduction

Enzymes catalyse a wide variety of reactions with near perfect enantioselectivity as the results of a precisely tuned network of attractive non-covalent interactions (NCI) between the substrate and the enzyme binding pocket.[1] Thus, selectivity is mainly achieved by selective rate acceleration of the desired enantiomer whereas the role of repulsive steric interactions to retard transformation of the minor enantiomer is negligible.[2] In contrast, steric repulsion traditionally served as a key guiding principle in the design of asymmetric catalysts,[3] e.g. by using large "blocking groups".[4] This does not necessarily exclude the simultaneous influence of attractive interactions as recently highlighted in studies by, for example, Hawkins,[5] Corey,[6] Noyori,[7] Sharpless,[8] or Fuji.[9] Thus, small-molecule catalysts can induce enantioselectivity through a combination of several weakly attractive NCIs[3a, 10] such as aromatic interactions.[11] Accordingly it was found that the role of attractive London dispersion forces[12] on chemical reactivity, catalysis and stability was traditionally underestimated.[13] These analyses were helped by the development of dispersion-corrected DFT[14] and linear scaling coupled cluster theories,[15] both of which facilitate the quantification of NCIs in extended molecular systems.[16] Most of this progress in elucidating the role of NCIs in asymmetric catalysis is based on theoretical studies,[17] either alone or in combination with NMR- or X-ray- based structure analyses.[18] While the influence of NCIs on ground state properties has recently been studied thoroughly,[19] most experimental studies

on enantioselective catalysis restrict themselves to the determination of the stereoselectivity factor s. This latter quantity is defined as the ratio of rate constants for conversion of the faster and slower reacting isomer, respectively ($s = k_{major}/k_{minor}$). However, the s values themselves cannot answer the question whether selectivity results from the acceleration of the major enantiomer through attractive NCIs or a deceleration of the minor enantiomer through repulsive steric interactions. Surprisingly, kinetic studies on this question are very rare.[20] This may result from the fact, that acceleration or deceleration can only be made with reference to a system with "zero" steric repulsion or attraction. Elimination of groups that induce steric hindrance and attraction is, unfortunately, linked to possible changes of electronic, kinetic and thermodynamic properties. Herein we present a different approach where the aromatic side chains of alcohol substrates are increased systematically such that no additional degrees of freedom are introduced.[21] From the rate data measured for these reactions we can infer how increasing substrate size impacts k_{major} and k_{minor}. This novel approach allows us to elucidate the origin of enantioselectivity through direct kinetic measurements. Initial acylation experiments were performed with fluxionally chiral *N,N*-dimethylaminopyridine (DMAP) derivative **3** developed by Sibi *et al.*[22] This catalyst displays moderate selectivity for the acylation of 1-phenylethanol **1a** ($s = 6$) with isobutyric anhydride (**2**), while a much larger selectivity was found for the larger substrate 1-(2-naphthyl)ethanol (**1b**) with $s = 37$.

Results and Discussion

Experimental studies

In order to precisely determine relative rates and ensure absolutely comparable reaction conditions competition experiments for the acylation of 1 : 1 mixtures of racemic **1b** as reference and racemic **1a,c,d** (see **Fig. 1**) were performed and monitored by chiral HPLC. Enantioselectivity values s of (pseudo)-first order kinetic resolution experiments are commonly calculated by Kagan's formulas[23] from the enantiomeric excess (*ee*) of products and reactants at a single conversion point. It should be emphasized, that the reliability of this approach is very limited for higher s values and neither the internal consistency nor the preconditions for the Kagan equation can be controlled by a single measurements (for a detailed analysis see Supporting Information (SI)).[24]
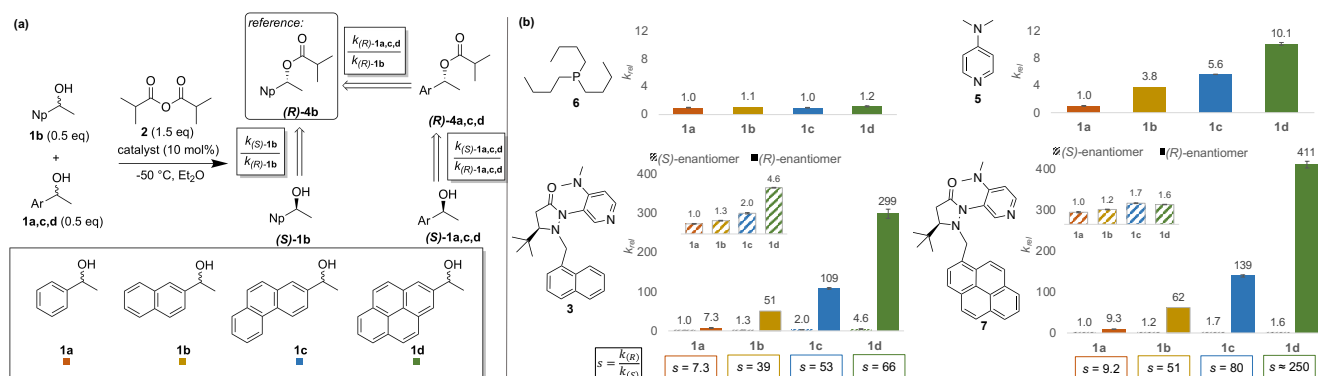
Figure 1. (a) Setup of competitive kinetic resolution experiments: 0.01 mmol of catalyst, 0.05 mmol of *(rac)*-**1b** and *(rac)*-**1a,c,d** were solved in 2 mL diethyl ether. At -50 °C 0.15 mmol of **2** were added. After defined periods of time 0.05 mL of the reaction mixture was quenched and analysed by chiral HPLC. Relative rates were then determined by linear regression analysis and chemoselectivity calculation (for more details see SI). **(b)** Relative rates for the acylation of alcohols **1a-1d** with catalyst **3** and **5-7**. Values are averaged over two independent runs. Experimental reference was *(R)*-**1b**, rates are displayed relative to *(S)*-**1a** for ease of discussion. HPLC traces, linear regression analysis, simulations and reliability analysis are provided in the SI.

Thus, herein all enantioselectivity values were determined by the more accurate linear regression analysis method[25] (see **Fig. 2**). Through simultaneous determination of chemoselectivity values for the two *(R)*-enantiomers relative rates for all four alcohols are obtained as shown **Fig. 1a**. The reliability of this approach was validated by reproducibility measurements and by comparison to literature data.[22a] In an appropriate model system for measuring the size-dependence of reaction rates aromatic side chains should be increased systematically without adding unfavourable interactions (e.g. 1,5-interactions).[21, 26] That alcohols **1a-d** represent a suitable series for such a purpose is supported by the following characteristics: a) The calculated reaction free energies for the acylation with anhydride **2** was found to be almost identical for all four alcohols **1a-d**. b) The same calculations indicate that the partial charge on the alcohol oxygen atom and the acidity of the hydroxyl group is very similar for all four systems. c) Reaction rates for the acylation of alcohols **1a-d** with anhydride **2** are almost identical when using tri-(*n*-butyl)phosphane (NBP, **6**) as the catalyst (**Fig. 1b**). This may be due to the large conformational flexibility of this catalyst, which is incapable of differentiating the substrate alcohols on the basis of size (or any other intrinsic property). In sharp contrast, reaction rates between the largest alcohol **1d** and the smallest alcohol **1a** differ by a factor of 10.1 when using DMAP (**5**) as the acylation catalyst. These reactivity differences are likely due to cation-π interactions in the respective transition states.[26-27]

These measurements have been repeated for different DMAP concentrations in order to verify that there is basically no uncatalyzed background reactivity of the respective substrates. With these results in hand, relative rate constants k_{rel} for the acylation of **1a-d** with anhydride **2** catalysed by chiral DMAP derivative **3** were evaluated. Enantioselectivity values for this reaction increase by a factor of 9 from $s = 7$ for 1-phenylethanol (**1a**) to 66 for 1-(2-pyrenyl)ethanol (**1d**). Relative rates in **Fig. 1** using alcohol *(S)*-**1a** as the reference show that the reaction of both *(S)*- and *(R)*-enantiomers is notably accelerated with the growing aromatic side chain. However, while the rate constant for *(S)*-**1d** is increased by a factor of 4.6 relative to *(S)*-**1a**, alcohol *(R)*-**1d** reacts 40 times faster than *(R)*-**1a**! The size-induced rate acceleration is thus significantly larger for the (R)- than for the (S)-alcohols and is also about four times larger for chiral catalyst **3** as compared to DMAP (**5**). Based on these findings we explored, whether suitably modified catalysts can further increase the selectivities obtained with catalyst **3**. Sibi *et al.* have already reported that enantioselectivity decreases if the naphthyl moiety in **3** ($s = 23$ at 0 °C) is replaced by both phenyl ($s = 15$) or 9-anthracenyl ($s = 14$).[22a] The first result is in agreement with the above-mentioned mechanism for size selection. The comparatively low selectivity for the 9-anthracenyl substituent is likely due to unfavourable 1,5-interactions that have already burdened other systematic studies of size effects.[21] We therefore synthesized 1-pyrenyl-substituted DMAP derivative **7** as a possibly even more size-selective catalyst (see SI). Repeating the acylation reactions of alcohols **1a-d** with anhydride **2** and catalyst **7** under otherwise identical conditions we find generally increased selectivities for all substrates, the largest selectivity for alcohol **1d** now amounting to approx. $s = 250$ (**Fig. 1**). For a quantitative analysis the size of the alcohol reagents was calculated as the volume of the van der Waals cavity used in the SMD solvation model at the B3LYP-D3/6-31+G(d) level of theory. As shown in **Fig. 3** the molecular volume strongly correlates with $\ln(k_{rel})$ for the acylation of *(R)*-alcohols with catalysts **3**, **7**, and DMAP (**5**). The slope of the correlations is notably higher for the chiral catalysts **3** and **7** than in the case of DMAP (**5**). Thus, the bulky substituents in **3** and **7** further increase the size-acceleration of the reaction rates.
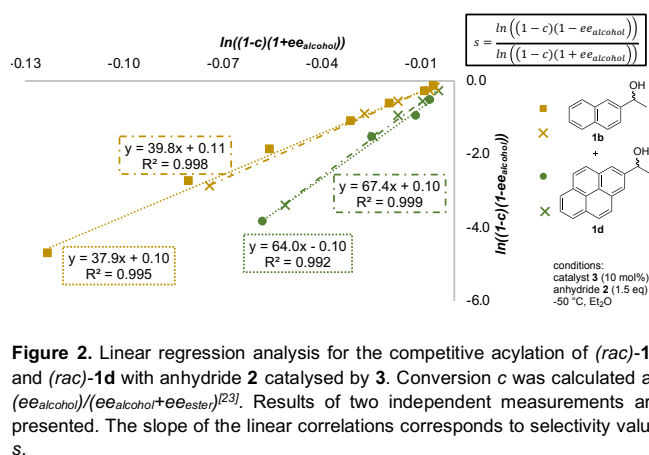
Figure 2. Linear regression analysis for the competitive acylation of *(rac)*-**1b** and *(rac)*-**1d** with anhydride **2** catalysed by **3**. Conversion *c* was calculated as $(ee_{alcohol})/(ee_{alcohol}+ee_{ester})$[23]. Results of two independent measurements are presented. The slope of the linear correlations corresponds to selectivity value *s*.
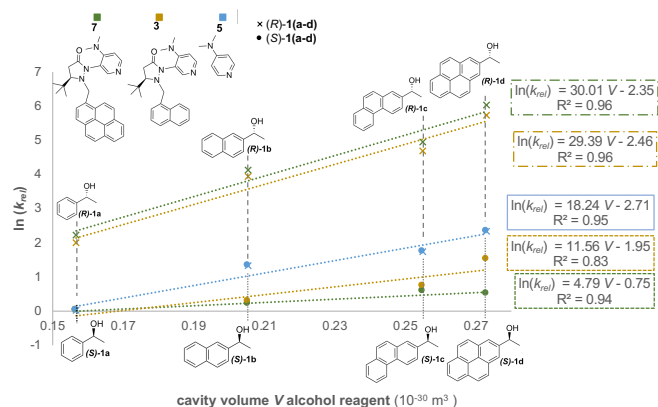
Figure 3. Correlation of ln(k_{rel}) for the different catalysts and alcohols with the molecular volume of the reagents calculated at the B3LYP-D3/6-31+G(d) level of theory.

Furthermore, also ln(k_{rel}) of the (S)-alcohols correlates positively with the reagent volume, which is contradictory to a possible steric hindrance argument for the minor enantiomer! However, the correlation slope is significantly smaller than in the case of DMAP (**5**) and is further flattened for catalyst **7**. Alternative correlations with similar trends for the calculated polarizability of the reagents (see SI) highlight the crucial role of dispersion forces. It can thus be concluded that enantioselectivity improvements result from a rate acceleration of the major enantiomer through reinforced dispersion interactions, if simultaneously the structure of the loaded catalyst minimizes the rate accelerations for the minor enantiomer.

Computational studies

The acylation of **1b** with anhydride **2** catalysed by DMAP-derivative **3** was investigated computationally. Geometry optimizations and frequency analyses were performed at SMD(Et$_2$O)/B3LYP-D3/6-31+G(d)[28] level of theory, followed by single point calculations at the DLPNO-CCSD(T)/def2-TZVPP level[15, 29]. In accordance with recent results of Wheeler et al.[30]
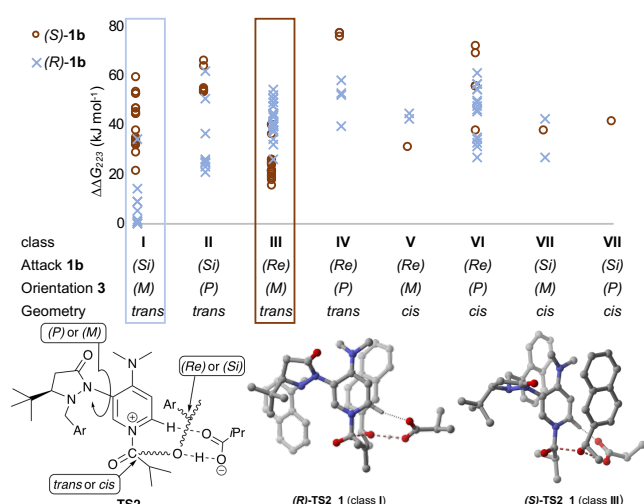
Figure 4. Relative free energies at the SMD(Et$_2$O)/B3LYP-D3/6-31+G(d) level of theory for **TS2** of (S)-**1b** (red circles) and (R)-**1b** (blue crosses). TS conformers are categorized by Re/Si face attack of **1b**, pyrazolidinone side chain orientation and relative position of the isobutyryl group (see bottom left). Structures of the best conformers for (R)- and (S)-**1b** are presented (for others see SI).

the energy profile of the reaction (see SI) shows that loading of the catalyst **3** through a first transition state **TS1** is rate limiting, followed by the selectivity-determining acylation of alcohol **1b** through transition state **TS2**. To ensure a comprehensive and systematic conformational search for **TS2**, the conformational space was partitioned into eight geometrical classes as a function of three criteria (**Fig. 4**): The Re or Si face attack of the alcohol substrate; orientation of the pyrazolidinone side chain; and the relative orientation of the isobutyryl group.

Due to its absolute configuration alcohol (R)-**1b** attacks the acyl-catalyst intermediate preferentially from the (Si) face, while alcohol (S)-**1b** shows the opposite preference. For both alcohols we find a preference for a trans-conformation of isobutyryl and pyrazolidinone side chain. Thus, all conformations populated by more than 1% are either in class **I** ((R)-**1b**) or in class **III** ((S)-**1b**). Conformations for (S)-**TS2** are best described as "triple-sandwich" structures of the aromatic alcohol side chain, catalyst pyridinium core, and catalyst sidechain. Wheeler et al. found geometrically similar conformations governing the kinetic resolution of biaryl substrates by catalyst **3**.[30] In the best (R)-**TS2**, in contrast, attack occurs from the crowded side of the catalyst resulting in a cage structure of the three aromatic rings. A similar structure for (S)-**1b** is strongly disfavoured by the absolute configuration of the tert-butyl group of **3**. The difference in free energy ($\Delta\Delta G^{\ddagger}_{223}$ = +8.6 kJ mol^{-1}) on single point level for the energetically best conformers of each enantiomer (R)-**TS2_1** and (S)-**TS2_1** is in good accordance with the experimental enantioselectivity value. In order to identify the origin of this selectivity the respective free energy difference $\Delta\Delta G^{\ddagger}_{223}$ (black bar in **Fig. 5**) was decomposed into its contributors. Surprisingly, the solvation energy (blue bar in **Fig. 5**) stabilizes all of the relevant (S) conformers relative to (R)-**TS2_1**. Thus, solvation is a counterplayer of enantioselectivity. Hence, we also found a very good negative correlation of experimental ln(s) values and solvent polarity parameter $E_T(30)$[31] (see SI). To further distinguish the impact of NCIs involving the aromatic moiety of the alcohol, relative single point energies were calculated for **TS2_HC** structures, wherein the naphthyl moiety of **1b** was replaced by a hydrogen atom (see **Fig. 5**).[17c, 32] While almost no energy difference is found for the H-capped structures **TS2_HC** (green bars in **Fig. 5**), the NCI energy contribution (yellow bar in **Fig. 5**) is very significant at -10.9 kJ mol^{-1} and thus the dominant component for the preference of the (R)-**TS2_1**. Similar trends were found for all of the other relevant conformers (see SI).
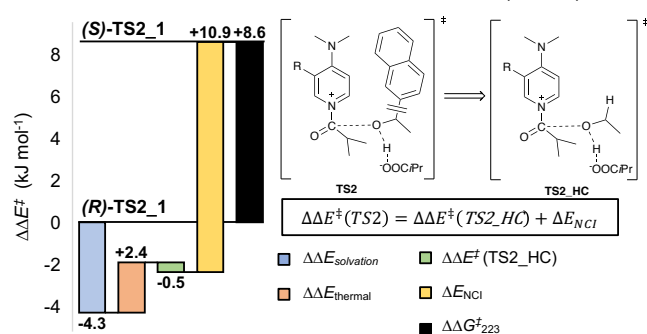
Figure 5. Energy decomposition scheme for (S)-**TS2_1** relative to (R)-**TS2_1**. Solvation energies and thermal corrections were calculated at the SMD(Et$_2$O)/B3LYP-D3/6-31+G(d) level of theory. The differences between DLPNO-CCSD(T)/def2-TZVPP single point energies for **TS2** and **TS2_HC** yield NCI energies.

3

A local energy decomposition analysis[33] confirmed that the intermolecular dispersion energy of alcohol (**R**)-**TS2_1** and loaded catalyst is -6.7 kJ mol^{-1} more stabilizing as compared to (**S**)-**TS2_1**. Thus, stronger dispersive interactions of catalyst and alcohol are indeed the crucial factors in determining the enantioselectivity for this system. A qualitative NCI analysis by the Atoms In Molecules (AIM)[34] method as well as NCI plots[35] indicate that for both **TS2** structures pyridinium-naphthyl stacking orientations are present. However, (**R**)-**TS2_1** is further stabilized by additional CH-π- and tilted π- π-stacking interactions (see **Fig. 6**) of catalyst sidechain and alcohol moiety.

(R)-TS2_1

(S)-TS2_1 (ΔE_{NCi}=+10.9 kJ mol^{-1})
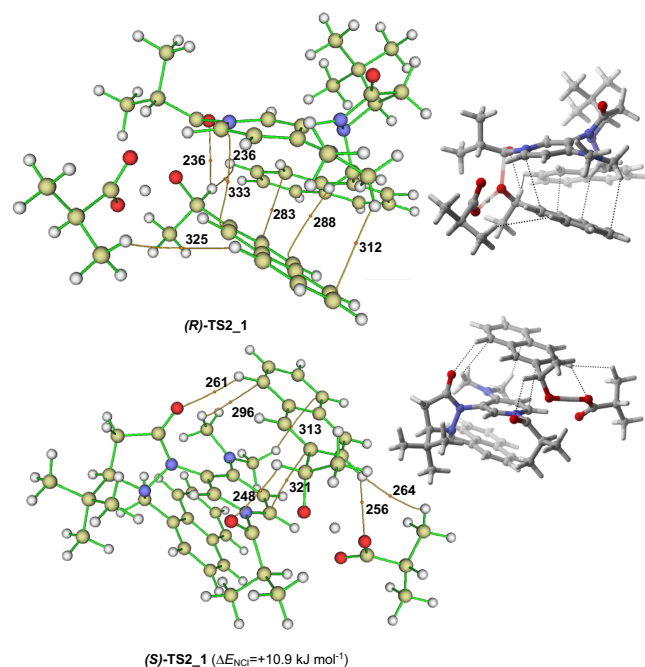
Figure 6. Non-covalent bond paths between alcohol **1b** and loaded catalyst analysed by AIM analysis[36] with relevant distances in pm. Right hand structures are printed for orientation only. For full results see SI.

Conclusion

The enantioselectivity of acylation reactions catalysed by chiral DMAP derivates increases systematically with increasing steric bulk of the alcohol substrates. Rate measurements for alcohols with different-sized aromatic side chains reveal that reaction rates for the major enantiomer are increased more than 40 times by substitution of phenyl by pyrenyl. These rate acceleration correlate with the polarizability and volume of the reagents. When also increasing the size of the catalyst side chain in a similar manner enantioselectivity values of up to *s* = 250 have been obtained. Computational studies show that alcohol attack from the more crowded side of the loaded catalyst is most favourable and stabilized by CH-π-stacking interactions. In combination with the results of kinetic measurements this implies that the selectivity values obtained result from a targeted rate acceleration of the transformation of the major enantiomer through dispersive interactions and not from steric hindrance of the minor enantiomer. The approach for elucidating the origins of enantioselectivity described in this study should also be useful

for the analysis and systematic improvement of catalyst performance in other cases.

[1]   S. J. Benkovic, S. Hammes-Schiffer, *Science* **2003**, *301*, 1196-1202.

[2]   A. Warshel, P. K. Sharma, M. Kato, Y. Xiang, H. Liu, M. H. Olsson, *Chem. Rev.* **2006**, *106*, 3210-3235.

[3]   a) R. R. Knowles, E. N. Jacobsen, *Proc. Natl. Acad. Sci. USA* **2010**, *107*, 20678-20685; b) H. J. Davis, R. J. Phipps, *Chem. Sci.* **2017**, *8*, 864-877; c) M. S. Sigman, J. J. Miller, *J. Org. Chem.* **2009**, *74*, 7633-7643.

[4]   a) G. C. Fu, *Acc. Chem. Res.* **2000**, *33*, 412-420; b) S. Yamada, K. Yamashita, *Tetrahedron Lett.* **2008**, *49*, 32-35.

[5]   J. M. Hawkins, S. Loren, *J. Am. Chem. Soc.* **1991**, *113*, 7794-7795.

[6]   a) E. J. Corey, T. P. Loh, *J. Am. Chem. Soc.* **1991**, *113*, 8966-8967; b) E. J. Corey, J. J. Rohde, *Tetrahedron Lett.* **1997**, *38*, 37-40.

[7]   M. Yamakawa, I. Yamada, R. Noyori, *Angew. Chem. Int. Ed.* **2001**, *40*, 2818-2821.

[8]   H. C. Kolb, P. G. Andersson, K. B. Sharpless, *J. Am. Chem. Soc.* **1994**, *116*, 1278-1291.

[9]   T. Kawabata, M. Nagato, K. Takasu, K. Fuji, *J. Am. Chem. Soc.* **1997**, *119*, 3169-3170.

[10]   S. J. Zuend, E. N. Jacobsen, *J. Am. Chem. Soc.* **2009**, *131*, 15358-15374.

[11]   a) E. H. Krenske, K. N. Houk, *Acc. Chem. Res.* **2013**, *46*, 979-989; b) A. J. Neel, M. J. Hilton, M. S. Sigman, F. D. Toste, *Nature* **2017**, *543*, 637-646.

[12]   F. London, *Trans. Faraday Soc.* **1937**, *33*, 8-26.

[13]   a) J. P. Wagner, P. R. Schreiner, *Angew. Chem. Int. Ed.* **2015**, *54*, 12274-12296; b) S. Grimme, P. R. Schreiner, *Angew. Chem. Int. Ed.* **2011**, *50*, 12639-12642; c) M. Raynal, P. Ballester, A. Vidal-Ferran, P. W. van Leeuwen, *Chem. Soc. Rev.* **2014**, *43*, 1660-1733; d) F. D. Toste, M. S. Sigman, S. J. Miller, *Acc. Chem. Res.* **2017**, *50*, 609-615.

[14]   S. Grimme, J. Antony, S. Ehrlich, H. Krieg, *J. Chem. Phys.* **2010**, *132*, 154104.

[15]   C. Riplinger, B. Sandhoefer, A. Hansen, F. Neese, *J. Chem. Phys.* **2013**, *139*, 134101.

[16]   S. E. Wheeler, T. J. Seguin, Y. Guan, A. C. Doney, *Acc. Chem. Res.* **2016**, *49*, 1061-1069.

[17]   a) E. K. Kemppainen, G. Sahoo, A. Piisola, A. Hamza, B. Kotai, I. Papai, P. M. Pihko, *Chem. Eur. J.* **2014**, *20*, 5983-5993; b) R.-Z. Liao, S. Santoro, M. Gotsev, T. Marcelli, F. Himo, *ACS Catalysis* **2016**, *6*, 1165-1171; c) T. J. Seguin, T. Lu, S. E. Wheeler, *Org. Lett.* **2015**, *17*, 3066-3069; d) D. Yepes, F. Neese, B. List, G. Bistoni, *J. Am. Chem. Soc.* **2020**, *142*, 3613-3625.

[18] a) A. J. Metrano, N. C. Abascal, B. Q. Mercado, E. K. Paulson, A. E. Hurtley, S. J. Miller, *J. Am. Chem. Soc.* **2017**, *139*, 492-516; b) J. M. Crawford, M. S. Sigman, *Synthesis* **2019**, *51*, 1021-1036.

[19] a) L. Yang, J. B. Brazier, T. A. Hubbard, D. M. Rogers, S. L. Cockroft, *Angew. Chem. Int. Ed.* **2016**, *55*, 912-916; b) J. Hwang, B. E. Dial, P. Li, M. E. Kozik, M. D. Smith, K. D. Shimizu, *Chem. Sci.* **2015**, *6*, 4358-4364; c) H.-J. Schneider, *New J. Chem.* **2019**, *43*, 15498-15512.

[20] S. Lin, E. N. Jacobsen, *Nat. Chem.* **2012**, *4*, 817-824.

[21] M. Marin-Luna, B. Pölloth, F. Zott, H. Zipse, *Chem. Sci.* **2018**, *9*, 6509-6515.

[22] a) G. Ma, J. Deng, M. P. Sibi, *Angew. Chem. Int. Ed.* **2014**, *53*, 11818-11821; b) G. Ma, M. P. Sibi, *Org. Chem. Front.* **2014**, *1*, 1152-1156; c) G. Ma, C. Deng, J. Deng, M. P. Sibi, *Org. Biomol. Chem.* **2018**, *16*, 3121-3126.

[23] H. B. Kagan, J. C. Fiaud, *Top. Stereochem.* **1988**, *18*, 249-300.

[24] M. D. Greenhalgh, J. E. Taylor, A. D. Smith, *Tetrahedron* **2018**, *74*, 5554-5560.

[25] a) S. F. Musolino, O. S. Ojo, N. J. Westwood, J. E. Taylor, A. D. Smith, *Chem. Eur. J.* **2016**, *22*, 18916-18922; b) H. F. Klare, M. Oestreich, *Angew. Chem. Int. Ed.* **2007**, *46*, 9335-9338.

[26] J. Helberg, M. Marin-Luna, H. Zipse, *Synthesis* **2017**, *49*, 3460-3470.

[27] a) S. Xu, I. Held, B. Kempf, H. Mayr, W. Steglich, H. Zipse, *Chem. Eur. J.* **2005**, *11*, 4751-4757; b) E. Larionov, M. Mahesh, A. C. Spivey, Y. Wei, H. Zipse, *J. Am. Chem. Soc.* **2012**, *134*, 9390-9399.

[28] a) A. D. Becke, *J. Chem. Phys.* **1993**, *98*, 1372 -1377; b) C. Lee, W. Yang, R. G. Parr, *Phys. Rev. B* **1988**, *37*, 785-789; c) S. Grimme, *J. Chem. Phys.* **2006**, *124*, 034108.

[29] a) C. Riplinger, F. Neese, *J. Chem. Phys.* **2013**, *138*, 034106; b) F. Weigend, R. Ahlrichs, *Phys. Chem. Chem. Phys.* **2005**, *7*, 3297-3305.

[30] R. Maji, H. Ugale, S. E. Wheeler, *Chem. Eur. J.* **2019**, *25*, 4452-4459.

[31] C. Reichardt, *Solvents and Solvent Effects in Organic Chemistry*, WILEY-VCH, Weinheim, **2003**.

[32] S. Malakar, S. V. Shree Sowndarya, R. B. Sunoj, *Org. Biomol. Chem.* **2018**, *16*, 5643-5652.

[33] W. B. Schneider, G. Bistoni, M. Sparta, M. Saitow, C. Riplinger, A. A. Auer, F. Neese, *J. Chem. Theory Comput.* **2016**, *12*, 4778-4792.

[34] R. F. W. Bader, *Acc. Chem. Res.* **1985**, *18*, 9-15.

[35] J. Contreras-Garcia, E. R. Johnson, S. Keinan, R. Chaudret, J. P. Piquemal, D. N. Beratan, W. Yang, *J. Chem. Theory Comput.* **2011**, *7*, 625-632.

[36] T. Lu, F. Chen, *J. Comput. Chem.* **2012**, *33*, 580-592.

6.1. Method Evaluation for Selectivity Determination in Kinetic Resolution Reactions

In order to answer the research question in this project properly, quite accurate measurements of relative rates for highly selective kinetic resolution reactions are needed. Therefore, in this chapter different approaches to determine the selectivity of kinetic resolution reactions are discussed and evaluated.

6.1.1. Definition of Enantioselectivity

The central descriptor for enantiomeric purity of a sample is the enantiomeric excess (*ee*) defined by Eq. 6.1.

$$ee = \frac{[major\ enantiomer] - [minor\ enantiomer]}{[major\ enantiomer] + [minor\ enantiomer]}$$

Eq. 6.1

Ee values are conversion-dependent and therefore at least two values have to be reported (e.g. *ee* of substrate and *ee* of product or *ee* of product/substrate and conversion) which makes it inconvenient to compare different *ee* values. Thus, it is established to report the selectivity value *s* which is defined as the relative rate constant of the faster enantiomer to the slower one (Eq. 6.2).

$$s = \frac{k_{fast}}{k_{slow}}$$

Eq. 6.2

6.1.2. Absolute Rate Measurements

Selectivity values *s* can be measured directly through determination of absolute rates of each of the two enantiomers. However, in practice this approach is chosen very rarely due to the following experimental problems:

1. Usually the enantiopure substrates are not easily accessible.
2. For the reliable determination of absolute rate constants the reaction should be followed to almost full conversion. In highly selective reactions the minor enantiomer reacts very slowly. Reaction times of several weeks especially at very low temperatures lead to inaccuracies due to factors like evaporation of solvent, precipitation of substrates or products or hydrolysis. To avoid those problems, in this study no data of kinetic resolution experiments running longer than approx. four days are used to ensure experimental reliability.
3. The reliability of direct kinetic measurements is limited due to differences in the experimental environment of two independent reactions. However, even minor differences in temperature, catalyst or reagent concentration impacts absolute rates significantly. This is especially true in kinetic resolution reactions, where mostly very low absolute quantities are used and thus the impact of relatively small experimental errors (e.g. weighing in of the catalyst) becomes crucial. In general, it is recommendable to work with stock solutions which allows to weigh

in larger quantities. However, availability and solubility of chiral catalysts often limits possibilities for stock solutions.

Thus, comparison of independently measured rate constants bears very often internal errors. In this project direct kinetic measurements were only used to measure background reaction with 4-dimethylaminopyridine (DMAP, **5**) (see Chapter 6.2.8).

6.1.3.Derivation of Kagan's formulas

To avoid the mentioned problems of absolute rate measurements most commonly competition experiments with the racemic substrate are performed. This guarantees exactly comparable reaction conditions and allows analysis with chiral high performance liquid chromatography (HPLC) or chiral gas chromatography (GC). Moreover, reactions ideally run only to 50% total conversion *c* resulting in much shorter reaction times, as they are mainly dominated by the absolute rate of the fast reacting enantiomer. As mentioned above *ee* values are conversion dependent and thus reporting the selectivity value *s* is preferable as *s* values can be directly compared. Kagan and Fiaud[1] developed fundamental equations to experimentally determine *s* values. In the following the derivation of these central equations is described. Therefore, we assume a racemic mixture of two enantiomers R and S with a total starting concentration of 1 (unit). Furthermore, we assume that R and S react with B in an irreversible (pseudo-)first order reaction to products P and Q.

$$R + B \xrightarrow{k_R} P \qquad\qquad\qquad \text{Eq. 6.3}$$

$$S + B \xrightarrow{k_S} Q \qquad\qquad\qquad \text{Eq. 6.4}$$

The first-order rate law (Eq. 6.5) can be integrated by separation of the variable and gives Eq. 6.9. Similar operations can be performed for the reaction of S.

$$\frac{d[R]}{dt} = -k_R[R] \qquad\qquad\qquad \text{Eq. 6.5}$$

$$\frac{d[R]}{[R]} = -k_R dt \qquad\qquad\qquad \text{Eq. 6.6}$$

$$\int_{[R]_0}^{[R]} \frac{1}{[R]} d[R] = \int_0^t -k_R dt \qquad\qquad\qquad \text{Eq. 6.7}$$

$$\ln[R] - \ln[R]_0 = -k_R t \quad (\text{for } t \neq 0) \qquad\qquad\qquad \text{Eq. 6.8}$$

$$k_R = \ln\left(\frac{[R]}{[R]_0}\right)\left(-\frac{1}{t}\right) \quad (\text{for } t \neq 0) \qquad\qquad\qquad \text{Eq. 6.9}$$

If we assume that $k_R > k_S$ (as herein), selectivity *s* is defined by Eq. 6.10. Together with Eq. 6.9 and the assumed starting concentrations of 0.5 (units) for both enantiomers, *s* can be expressed by Eq. 6.13.

$$s = \frac{k_R}{k_S} \qquad\qquad\qquad \text{Eq. 6.10}$$

$$s = \frac{\ln\left(\frac{[R]}{[R]_0}\right)}{\ln\left(\frac{[S]}{[S]_0}\right)} \qquad \text{Eq. 6.11}$$

$$[R]_0 = [S]_0 = 0.5 \qquad \text{Eq. 6.12}$$

$$s = \frac{ln(2[R])}{ln(2[S])} \qquad \text{Eq. 6.13}$$

The conversion c (Eq. 6.14) can be described relative to the substrate concentrations by Eq. 6.16. Combining the conversion with the definition of *ee* in Eq. 6.19 gives Eq. 6.23 and similarly Eq. 6.24 for [S].

$$c = \frac{[P] + [Q]}{[R]_0 + [S]_0} \qquad \text{Eq. 6.14}$$

$$[P] = [R]_0 - [R] \quad \text{and} \quad [Q] = [S]_0 - [S] \qquad \text{Eq. 6.15}$$

$$1 - c = \frac{[R] + [S]}{[R]_0 + [S]_0} \quad (\text{with } [R]_0 + [S]_0 = 1) \qquad \text{Eq. 6.16}$$

$$1 - c = [R] + [S] \qquad \text{Eq. 6.17}$$

$$[S] = 1 - c - [R] \qquad \text{Eq. 6.18}$$

$$ee_{substrate} = \frac{[S] - [R]}{[S] + [R]} \qquad \text{Eq. 6.19}$$

$$ee_{substrate} = \frac{[S] - [R]}{1 - c} \qquad \text{Eq. 6.20}$$

$$ee_{substrate} = \frac{(1 - c - [R]) - [R]}{1 - c} \qquad \text{Eq. 6.21}$$

$$2[R] = -ee_{substrate}(1 - c) + (1 - c) \qquad \text{Eq. 6.22}$$

$$2[R] = (1 - c)(1 - ee_{substrate}) \qquad \text{Eq. 6.23}$$

$$2[S] = (1 - c)(1 + ee_{substrate}) \qquad \text{Eq. 6.24}$$

Inserting Eq. 6.23 and Eq. 6.24 into Eq. 6.13 yields Kagan's central formula Eq. 6.25.

$$s = \frac{ln((1 - c)(1 - ee_{substrate}))}{ln((1 - c)(1 + ee_{substrate}))} \qquad \text{Eq. 6.25}$$

Similar mathematical operations on *ee*$_{product}$ (Eq. 6.26) with Eq. 6.17 and Eq. 6.15 for irreversible reactions yields the second formulation of Kagan's formulas Eq. 6.28.

$$ee_{product} = \frac{[Q] - [P]}{[Q] + [P]} \qquad \text{Eq. 6.26}$$

$$ee_{product} = \frac{[S] - [R]}{c} \qquad \text{Eq. 6.27}$$

$$s = \frac{ln\left(1 - c(1 + ee_{product})\right)}{ln\left(1 - c(1 - ee_{product})\right)} \qquad \text{Eq. 6.28}$$

The conversion c can be determined by directly measured concentrations (e.g. by NMR, GC, HPLC) using Eq. 6.29. If the conversion is known exactly, only the *ee* of either the substrates or the products are needed. However, *ee* values can be determined experimentally more exactly than

conversion values.[2] The division of Eq. 6.27 by Eq. 6.20 gives Eq. 6.32 and makes it thus possible to calculate conversion and *s* directly from the *ee* values of substrate and product.

$$c_{direct} = \frac{[P] + [Q]}{[P] + [Q] + [R] + [S]}$$

Eq. 6.29

$$\frac{ee_{product}}{ee_{substrate}} = \frac{\frac{[S] - [R]}{c}}{\frac{[S] - [R]}{1 - c}}$$

Eq. 6.30

$$\frac{ee_{product}}{ee_{substrate}} = \frac{1 - c}{c}$$

Eq. 6.31

$$c_{ee} = \frac{ee_{substrate}}{ee_{substrate} + ee_{product}}$$

Eq. 6.32

6.1.4. Kinetic Resolution Experiments

As a benchmark experiment the kinetic resolution of 1-(2-naphthyl)ethanol (**1b**) with catalyst **3** as presented in **Scheme 6.1** is used. Sibi *et al.*[3] reported an enantioselectivity of *s* = 37 for this reaction under the stated conditions.
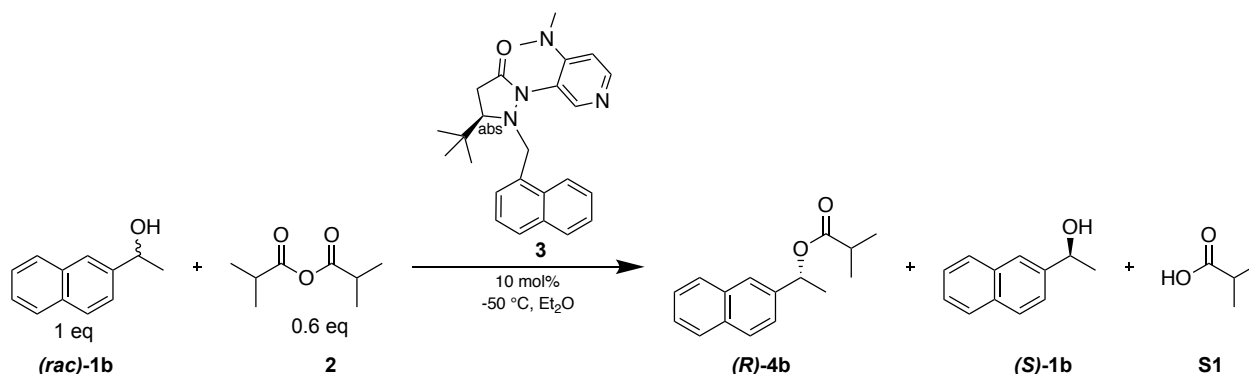
Scheme 6.1. Kinetic resolution of 1-(2-naphthyl)ethanol (**1b**) with catalyst **3**.

Experimental procedure for kinetic resolution experiments:

1 eq of alcohol **1b** and 10 mol% of catalyst **3** are weighed into a Schlenk flask, dissolved under N_2 in 1.8 mL of dry diethyl ether and cooled to -50 °C. 0.2 mL of a stock solution of freshly distilled isobutyric anhydride (**2**, 0.6 eq) in dry diethyl ether is added. After 48 hours the reaction is quenched through addition of 1 mL of methanol. Substrates and products are separated by column chromatography (hexanes/EtOAc = 9/1). Enantiomeric excess is determined by chiral HPLC chromatography (Chiracel IB-N5, flow 0.5 mL/min, T = 10 °C, λ = 289 nm, *n*Hex/*i*Prop = 90/10 (substrate), *n*Hex/*i*Prop = 98/2 (product)). HPLC traces are presented in **Figure 6.1**, calculation of *s* value in Table 6.1.
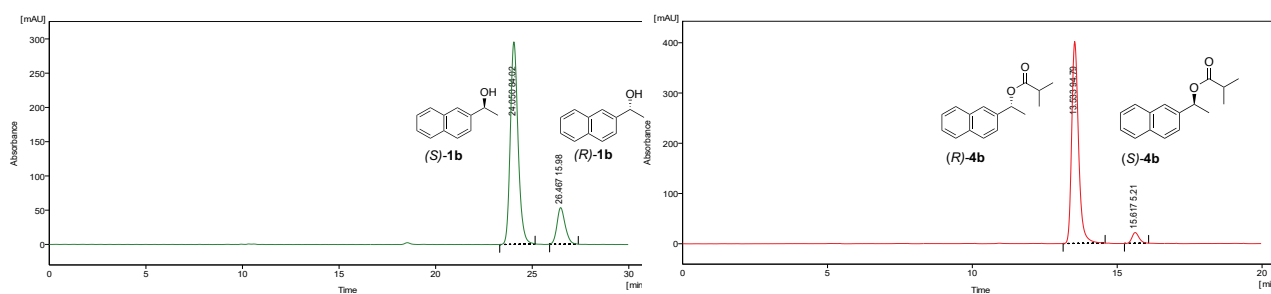
Figure 6.1. HPLC traces of substrates (left) and products (right) for the kinetic resolution experiment shown in **Scheme 6.1**.

Table 6.1. Calculation of conversion, *ee* values and enantioselectivity value *s* for the reaction shown in **Scheme 6.1**.

	UV-Absorbance HPLC (λ = 285 nm), raw data [mAUs]		Enantiomeric excess (Eq. 6.1)	Conversion (Eq. 6.32)	Selectivity (Eq. 6.25)
	(S)-enantiomer	*(R)*-enantiomer			
1-(2-naphthyl)ethanol (**1b**)	8247	1569	0.680	43.2%	37.0
1-(2-naphthyl)ethyl isobutyrate (**4b**)	363	6600	0.896		

Due to the high suitability and practicability kinetic resolution experiments are almost exclusively analysed in this manner. However, the reliability of single point kinetic resolution experiments is questionable especially for *s* values larger than 50.[2, 4] This is mainly caused by the logarithmic nature of the equations magnifying experimental inaccuracies in determining *ee* and conversion values, which will be investigated in the next chapter.

6.1.5. Error Estimation of Single Point Kinetic Resolution Experiments

In order to gain a better understanding of error influences on selectivity values we simulated kinetic resolution (KR) experiments with a hypothetical selectivity value of *s* = 80 and *s* = 200 using CoPaSi[5]. These exactly calculated intermediate concentrations were altered by a randomized error of -0.5% to +0.5%, which is in the range of typical errors in kinetic resolution experiments analysed by chiral HPLC[4b]. From 1 000 randomly distorted intermediate concentrations selectivity values were calculate by:

(1) Kagan's equation for products Eq. 6.28 with conversion calculated from Eq. 6.29

(2) Kagan's equation for substrates Eq. 6.25 with conversion calculated from Eq. 6.29 and

(3) Kagan's equation Eq. 6.28 with conversion calculated from Eq. 6.32 (which is equivalent to use Eq. 6.25 and conversions from Eq. 6.32).

Table 6.2. Error estimates for the evaluation of single point kinetic resolution experiments with implemented randomized relative errors. Data was gained from 1000 runs.

	Reaction with s = 80 Randomized relative error of +/-0.5%			Reaction with s = 200 Randomized relative error of +/-0.5%		
Selectivity values calculated by	Eq. 6.28 with Eq. 6.29 (ee product, direct conversion)	Eq. 6.28 with Eq. 6.25 (ee substrate, direct conversion)	Eq. 6.28 with Eq. 6.32 (conversion from both ee values)	Eq. 6.28 with Eq. 6.29 (ee product, direct conversion)	Eq. 6.28 with Eq. 6.25 (ee substrate, direct conversion)	Eq. 6.28 with Eq. 6.32 (conversion from both ee values)
Average	80.1	81.0	80.0	201.4	209.0	200.0
Standard Deviation	2.8	8.5	0.7	11.3	48.4	1.7
Mean absolute error	2.3	6.9	0.6	9.1	37.3	1.4

Table 6.2 demonstrates that calculating s values from direct conversions results in high standard deviations. However, it seems that using the conversion calculated by Eq. 6.32 gives very reliable results even for high selectivity values. Nonetheless, relative errors do not properly describe experimental realities as especially small numbers are less accurate to measure and several disruptive factors (e.g. baseline inaccuracies) add rather absolute than relative errors to measured data. Therefore, in another experiment a randomized absolute error in the range of +/- 0.25% of absolute starting concentrations was added to each compound and evaluated in the same ways as described above.

Table 6.3. Error estimation for the evaluation of single point kinetic resolution experiments with implemented randomized absolute errors. Data was gained from 1000 runs.

	Reaction with s = 80 Randomized absolute error of +/-0.25% of start concentration			Reaction with s = 200 Randomized absolute error of +/-0.25% of start concentration		
Selectivity values calculated by[a]	Eq. 6.28 with Eq. 6.29 (ee product, direct conversion)	Eq. 6.28 with Eq. 6.25 (ee substrate, direct conversion)	Eq. 6.28 with Eq. 6.32 (conversion from both ee values)	Eq. 6.28 with Eq. 6.29 (ee product, direct conversion)	Eq. 6.28 with Eq. 6.25 (ee substrate, direct conversion)	Eq. 6.28 with Eq. 6.32 (conversion from both ee values)
Average	80.2	80.2	80.2	201.1	201.1	200.9
Standard Deviation	3.4	3.4	3.0	17.3	17.7	15.5
Mean absolute error	2.9	2.8	2.6	14.9	14.1	13.3
Smallest obtained s	73.4	71.5	74.4	170.0	159.0	172.9
Biggest obtained s	87.8	91.8	87.0	241.9	265.6	235.4

First of all, deviation and mean absolute errors in **Table 6.3** show, in agreement with **Table 6.2**, that it is most convenient to calculate conversion by Eq. 6.32, even if differences between the methods are much smaller than above. Only in cases with extremely high enantioselectivity values it may be necessary to use directly calculated conversion as analysis of *ee* of the products is out of experimental possibilities.[4a] Moreover, the obtained standard deviations in **Table 6.3** demonstrate that selectivity values around 80 can still be reported with acceptable reliability, while selectivity values of around 200 cannot be properly determined using single point kinetic resolution experiments. In those cases, maximal and minimal selectivity values from the simulation differ by 70 or more. Thus, several authors propose to rely on *s* values higher than 50 only to the closest ten and to not report higher *s* values than 200.[2, 4b]. To illustrate the problem of measuring high *s* values, in **Figure 6.2** the *ee* values of the products for simulated reactions with defined enantioselectivity values are plotted against conversion values. It becomes obvious, that while *ee* differences are prominent for *s* values smaller than around 30, for higher *s* values the curves are lying together closely. However, most prominent differences can be found in the region of 40 – 52% conversion, so that most kinetic resolution reactions aim to target into that region. For *s* > 200 the differences become too small to be measured accurately in experiments.
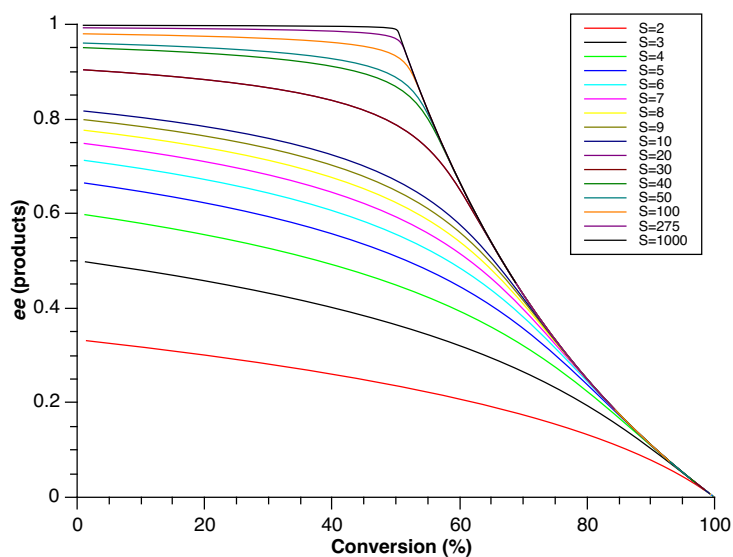
Figure 6.2. Plot of *ee* values of products against conversion values for reactions with different selectivity values. Intermediate concentrations of substrates and products were determined by simulation with CoPaSi[5] and plotted with QTIplot[6].

6.1.6. Linear Regression

Additional to the evaluated inaccuracies of single point kinetic resolution measurements there are two conceptional problems related to the use of Kagan's formulas at a single concentration:

1) Relying on a single measured point is in most cases inappropriate as internal consistency cannot be controlled if only one value is obtained as the result.

2) As outlined above the KR formulas only apply to (pseudo) first order reaction that are not reversible and without any further reaction or decomposition of products.[1, 4b] However, using a single point measurement does not allow to control these conditions.

A more elaborate way to measure enantioselectivity values is therefore the use of a linear regression analysis. Intermediate concentrations of product and substrate are measured at different conversion points. Thus, $ee_{products}$ and $ee_{substrates}$ can be calculated. Eq. 6.32 allows to determine the intermediate conversion. As outlined in Chapter 6.1.3 s can be expressed by Eq. 6.25. Plotting the numerator $ln(1-c)(1-ee_{substrate})$ against the denominator $ln(1-c)(1+ee_{substrate})$ for different conversion points should thus give a straight line through the origin with its slope being the selectivity value.[4, 7] Statistical analysis of the correlation allows to control internal consistency of the measurements. The R^2 value describes the goodness of fit and displays if the conditions for the use of Kagan's formula are fulfilled.[4b] The deviation of intercept from zero mainly reflects experimental and analytical inaccuracies of measurements.

Experimental procedure for kinetic resolution experiments analysed by linear regression:

10 mol% of catalyst are weighed into a Schlenk flask, evacuated and filled with N$_2$. 1.8 mL of a stock solution of racemic alcohol (1 eq) in dry diethyl ether are added and cooled to -50 °C. 0.2 mL of a stock solution of freshly distilled isobutyric anhydride (0.6 eq) in dry diethyl ether is added. After defined periods of time probes of 0.05 mL of the reaction mixture are taken by syringe and quenched in 0.1 mL of methanol in a HPLC vial. 1 mL of *n*-hexane is added and a chiral HPLC spectrum is recorded (Chiracel IB-N5, flow 0.5 mL/min, T = 10°C, λ = 285 nm, *n*Hex/*i*Pr = 90/10).
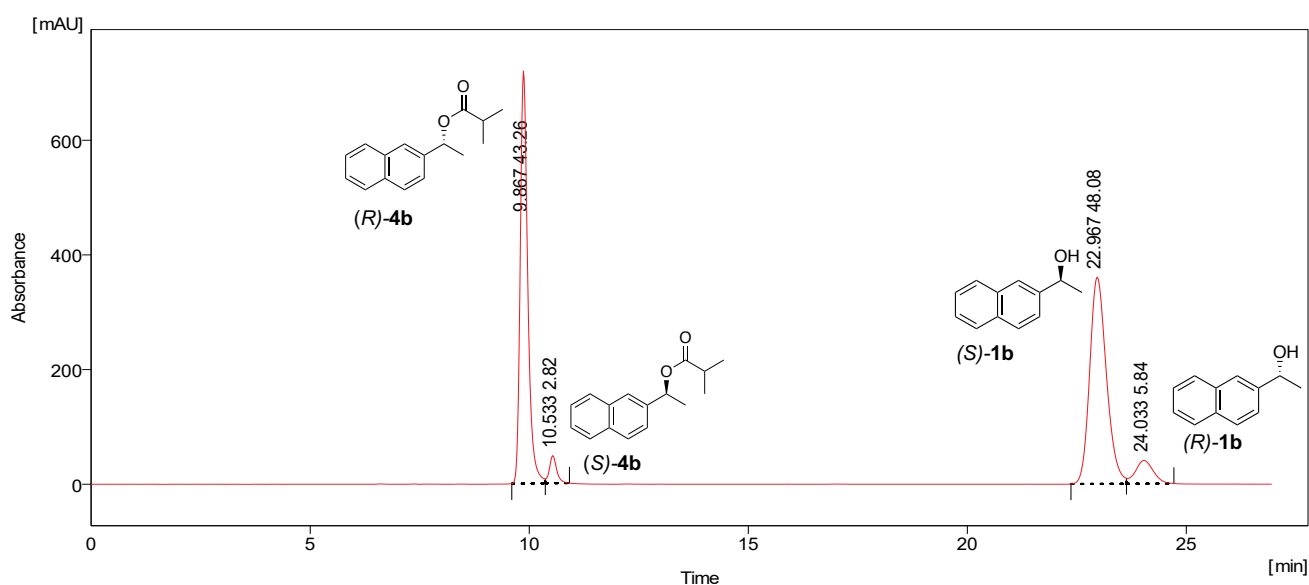
As an example, for a linear regression analysis experimental data for the experiment shown in **Scheme 6.1** are outlined. Choosing an appropriate HPLC methods as shown in **Figure 6.3** allows to quantify substrate and product concentrations at the same time and makes a manual separation by column chromatography redundant. This allows to investigate numerous experiments in this manner. In both independent runs of the experiment the points fit the line in **Figure 6.4** excellent with negligible intercept. The slope of this line reflects the selectivity value of s = 38.5 ± 1.25 in good agreement with the previous obtained value. Every measured point is the equivalent of a kinetic resolution as reported above. Major deviations of the selectivity values can be observed, however, if they are calculated from a single conversion point as shown in column 9 of **Table 6.4**. Thus, even for medium enantioselectivity values results of linear regression are more reliable than single point kinetic resolution measurements. This trend gets even more important as selectivity values increase.

Table 6.4. Raw data for two independent runs of linear regression shown in **Scheme 6.1**.

run	time [min]	R-NpEtOiPr *(R)*-**4b**	S-NpEtOiPr *(S)*-**4b**	S-NpEtOH *(R)*-**1b**	R-NpEtOH *(S)*-**1b**	Ester **4b**	Alcohol **1b**	conversion c (Eq. 6.32)	s (Eq. 6.25)	$\ln((1-c)(1+ee_{alc}))$	$\ln((1-c)(1-ee_{alc}))$
1	91	819.1	26.6	7099.8	6561.5	0.9370	0.0394	4.035%	32.0	-0.00254	-0.08139
1	424	1556.4	56.9	4073.3	2677.7	0.9294	0.2067	18.20%	33.5	-0.01293	-0.43241
1	1314	5187.3	251.6	7332.4	2481.0	0.9075	0.4944	35.27%	33.7	-0.03317	-1.11680
1	1982	4534.7	230.3	5420.5	1145.9	0.9033	0.6510	41.88%	38.6	-0.04132	-1.59534
1	2696	6954.8	433.0	7663.3	1110.2	0.8828	0.7469	45.83%	36.0	-0.05522	-1.98713
1	3138	8919.7	575.9	9585.4	1174.3	0.8787	0.7817	47.08%	36.7	-0.05880	-2.15833
2	31	153.9	6.0	3954.8	3809.2	0.9245	0.0187	1.988%	26.0	-0.001503	-0.039006
2	94	333.1	11.4	3464.1	3123.6	0.9336	0.0517	5.247%	30.6	-0.003492	-0.106971
2	180	631.4	22.0	3878.4	3257.1	0.9326	0.0871	8.539%	31.2	-0.005774	-0.180361
2	976	5175.1	192.4	10376.0	5096.5	0.9283	0.3412	26.88%	37.5	-0.019453	-0.730403
2	1272	6422.9	262.3	11431.7	4700.1	0.9215	0.4173	31.17%	36.9	-0.024762	-0.913567
2	1525	6690.6	287.2	11004.7	4014.8	0.9177	0.4654	33.65%	36.9	-0.028085	-1.036429
2	2945	6309.7	324.8	7914.9	1516.0	0.9021	0.6785	42.93%	39.5	-0.042946	-1.695612
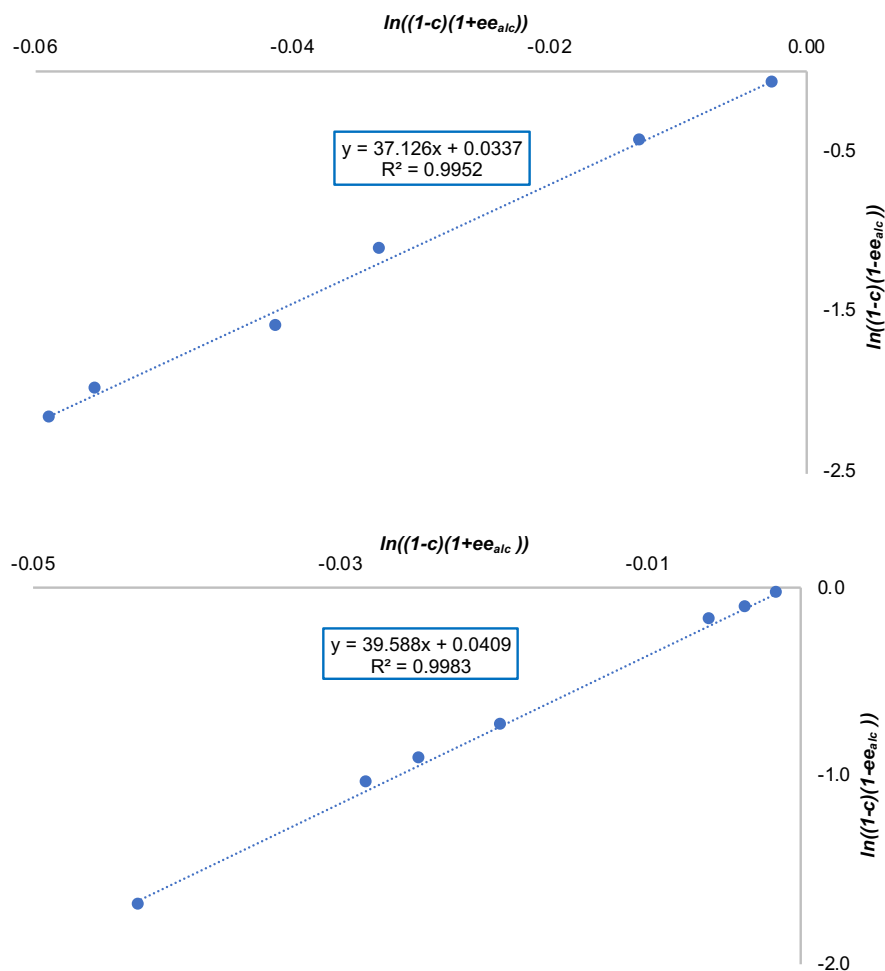
Figure 6.4. Linear regression analysis of data shown in **Table 6.4** (upper graph: run 1, lower graph: run 2).

6.1.7. Simulation of Effective Rate Constants

Another possibility especially for cases that do not follow pseudo-first order kinetics is the simulation of reaction curves. In linear regression experiments several intermediate concentrations of a reaction are measured. Those values together with the reaction times as reported in **Table 6.4** allow to plot time-turnover curves and to calculate effective rate constants (for technical details see Chapter 6.2.3).
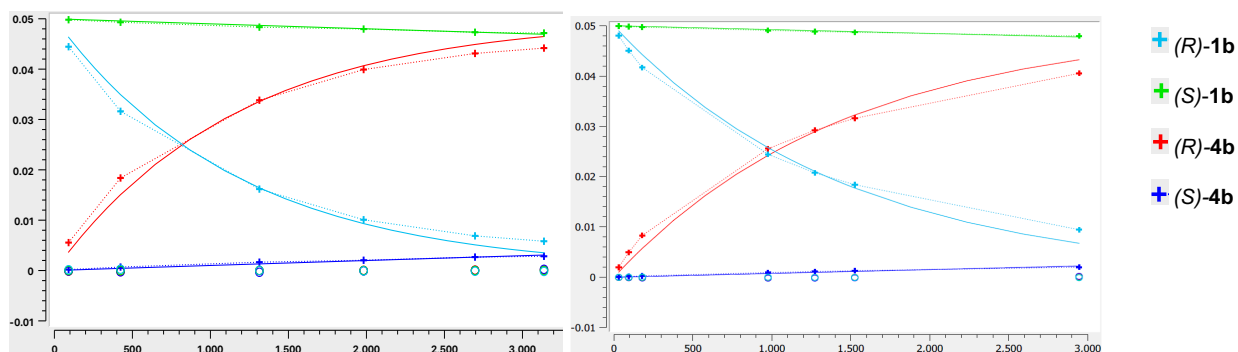
Figure 6.5. Fitted time [min] (x-axis) vs. intermediate concentration [mol L^{-1}] (y-axis) curve of data shown in **Table 6.4** (left: run 1, right: run 2). Hollow circles show weighted errors.

Table 6.5. Results of Copasi parameter estimation for linear regression shown in **Scheme 6.1**.

	Run 1			Run 2		
	Estimated effective rate constant	Standard Deviation of Parameter Estimation	$s = \dfrac{k_{(R)}}{k_{(S)}}$	Estimated effective rate constant	Standard Deviation of Parameter Estimation	$s = \dfrac{k_{(R)}}{k_{(S)}}$
$k_{(S)\text{-}\mathbf{1b}}$	0.002045	3.09E-04	41.8	0.001562	3.77E-05	43.5
$k_{(R)\text{-}\mathbf{1b}}$	0.085408	0.0126		0.067928	0.0027	

As **Figure 6.5** shows the fitting of the concentration of the faster alcohol (red line) is satisfying. For the slower alcohol (dark-blue line) conversion is very low and therefore the fitted relative rate value is rather unreliable. As discussed in Chapter 6.1.2 absolute rate constants carry a major deviation. Despite those limitations the enantioselectivity value of 42.6±0.84 is still quite close to the expected value of 39.

Regarding reliable simulations, the conversion of each substrate should be higher (ideally close to 100%) and more points should be measured. In kinetic resolution experiments with high enantioselectivities this poses again the problem that the reaction of the slower enantiomer exceeds in general well-controllable reaction times. Hence, the same problems as described for absolute rate measurements occur.

6.1.8. Chemoselectivity

Additional to relative rates of two enantiomers also relative rates of two different aromatic alcohols have to be investigated as shown in **Scheme 6.2**. This chemoselectivity can be defined in perfect analogy to enantioselectivity. In this report *(R)*-1-(2-naphthyl)ethanol (**1b**) is always used as the reference for relative rates if not stated otherwise (Eq. 6.33). Instead of starting the reaction with a racemic mixture a 1 : 1 mixture of two competing substrates is reacted and relative concentrations of substrates and products at different conversion values are analysed. In practice, either several independent reactions with a varying under-stochiometric concentration of substrate can be run or one reaction can be quenched at different times. The chemoselectivity *C* for the products (Eq. 6.34) is calculated (equivalent to *ee* values) and the selectivity can be obtained via formula Eq. 6.35 with conversion values *c* calculated by Eq. 6.36.
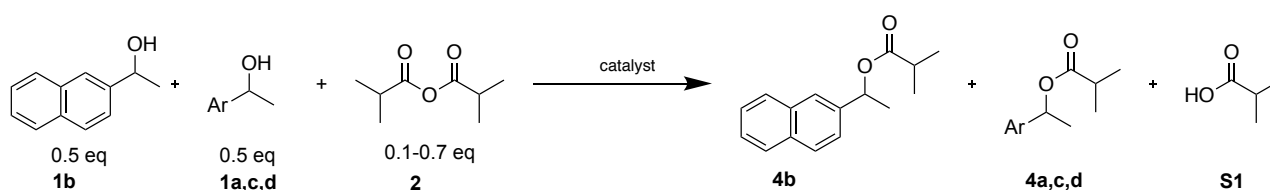
Scheme 6.2. Competition experiment of 1-(2-naphthylethanol) (**1b**) and an aromatic alcohol.

$$s = \frac{k\,(\mathbf{1a,c,d})}{k\,(\mathbf{1b})} \qquad \text{Eq. 6.33}$$

$$C = \frac{[\mathbf{4a,c,d}] - [\mathbf{4b}]}{[\mathbf{4a,c,d}] + [\mathbf{4b}]} \qquad \text{Eq. 6.34}$$

$$s = \frac{ln(1 - c(1 + C)}{ln(1 - c(1 - C)} \qquad \text{Eq. 6.35}$$

$$c = \frac{[\mathbf{4a,c,d}] + [\mathbf{4b}]}{[\mathbf{4a,c,d}] + [\mathbf{4b}] + [\mathbf{1a,c,d}] + [\mathbf{1b}]} \qquad \text{Eq. 6.36}$$

Intermediate concentrations of substrates and products as needed in Eq. 6.34 can be obtained for example via NMR, GC or HPLC. While NMR integrals of appropriate protons can be directly used to determine the intermediate concentrations, GC or HPLC signal intensities have to be normalized using a calibration curve. In HPLC analysis with a UV detector the absorbance mainly depends on the size of the chromophore system. The alcohols in this project bear by design very differently sized aromatic moieties. While UV absorbance of alcohol substrates and ester products are very similar as the chromophore system does not grow significantly, differences magnify for the different aromatic systems (see **Scheme 6.3**). For 1-phenylethanol (**1a**) a smaller wavelength must be used than for the big aromatic systems. For the other alcohols too high UV absorbance values at low wavelengths have to be avoided, as the linear dependence on the concentration is only true for UV absorbances up to 1.5 AU.
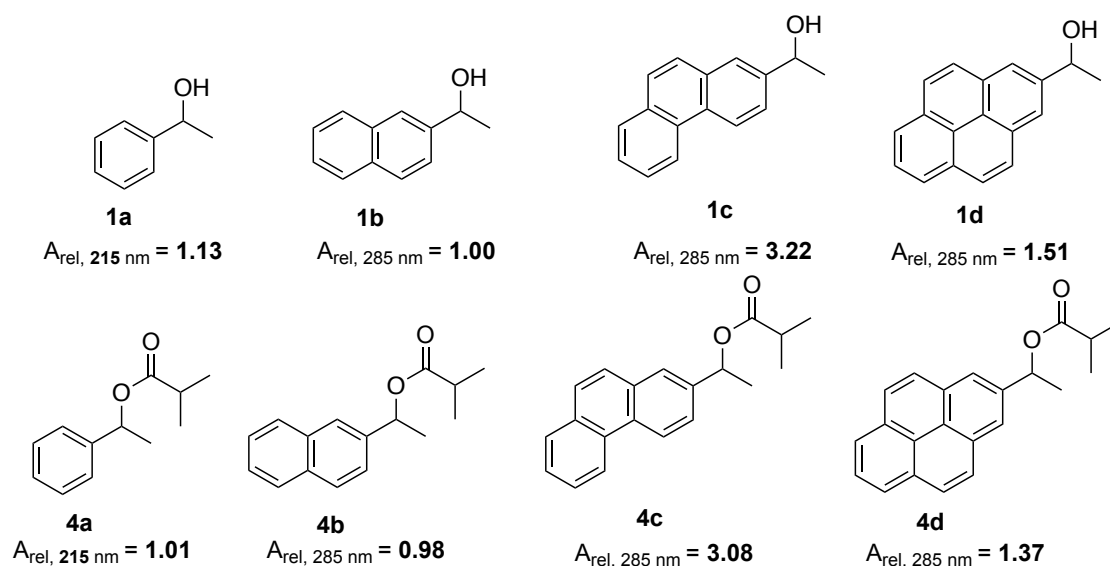
Scheme 6.3. UV absorbance values A$_{rel}$ relative to 1-(2-naphthyl)ethanol (**1b**) determined by calibration curves.

To avoid major deviations of results through calibration errors only similarly absorbing species should be compared. Therefore, conversion values c are calculated for each substrate separately (Eq. 6.37 and Eq. 6.38). Thus, Eq. 6.39 is used instead of Eq. 6.34 for the calculation of chemoselectivity values C as in reaction mixtures starting from a 1 : 1 ratio of two substrates Eq. 6.40 becomes valid. Moreover, a correction factor from minor deviations of the 1 : 1 starting conditions[8] becomes redundant.

$$c_{Np} = \frac{[\mathbf{4b}]}{[\mathbf{4b}] + [\mathbf{1b}]}$$
Eq. 6.37

$$c_{Ar} = \frac{[\mathbf{4a,c,d}]}{[\mathbf{4a,c,d}] + [\mathbf{1a,c,d}]}$$
Eq. 6.38

$$C = \frac{c_{Ar} - c_{Np}}{c_{Ar} + c_{Np}}$$
Eq. 6.39

$$[\mathbf{4b}] + [\mathbf{1b}] = [\mathbf{4a,c,d}] + [\mathbf{1a,c,d}]$$
Eq. 6.40

6.1.9.Methodological Conclusion

Answering the research question of this projects needs reliable measurements of relative rates for different alcohols in kinetic resolution experiments. Regarding the outlined methods above it should be guaranteed, that:

1) Rather than single point kinetic resolution experiments linear regression experiments are performed.

2) Conversion values are not directly measured but calculated from *ee* of product and *ee* of substrate by Eq. 6.32.

3) While those methods seem robust for selectivity values up to 80, selectivity values greater than 200 should be investigated carefully.

4) Instead of absolute rates relative rates should be measured to guarantee similar reaction conditions and to avoid reaction times that are out of experimental accuracy.

Thus, a protocol for "competitive linear regression for kinetic resolution" was developed. Racemic 1-(2-naphthyl)ethanol (**1b**) was chosen as the reference system allowing the determination of relative rates for *(R)* and *(S)* enantiomers of more selective reagents. To guarantee faster reactions and higher conversion rates of the slower enantiomer 1.5 eq of anhydride **2** were used.

6.2. Determination of Relative Rates

6.2.1. Experimental Protocol for Competitive Linear Regression Experiments
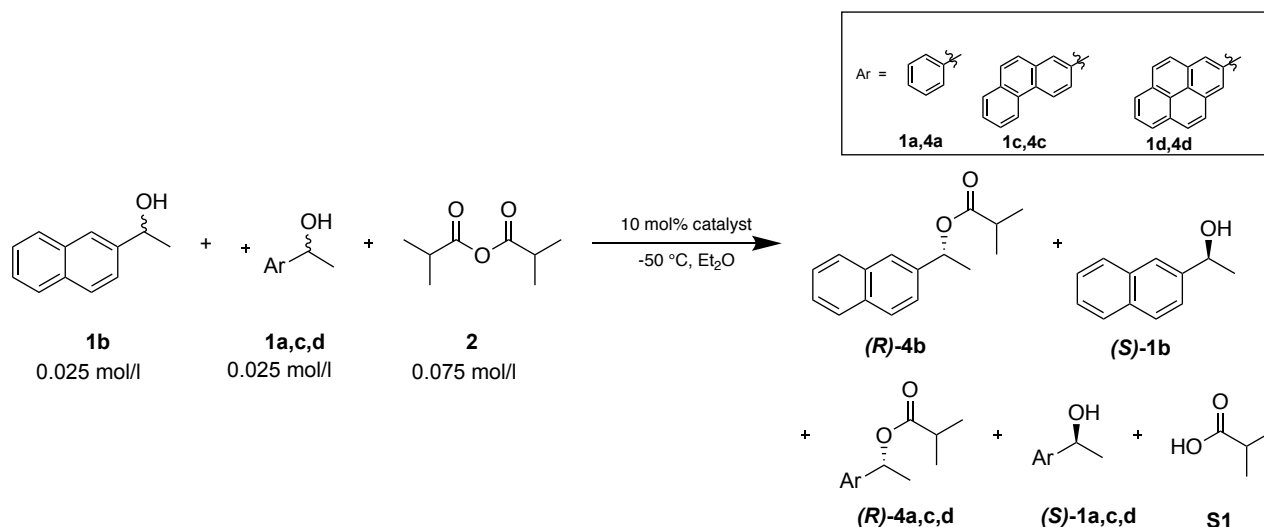
Scheme 6.4. Competitive linear regression for the kinetic resolution of 1-(2-naphthyl)ethanol (**1b**) and alcohols **1a-4a**.

0.01 mmol (10%) of catalyst are weighed into an oven dried Schlenk flask with magnetic stir bar, evacuated and filled with N$_2$. 1.8 mL of a 1 : 1 molar stock solution of the two racemic alcohols (0.05 mmol of each) in dry diethyl ether are added. After cooling the solution to -50 °C 0.2 mL of a stock solution of freshly distilled isobutyric anhydride (0.15 mmol, 1.5 eq) in dry diethyl ether is added and stirred at -50 °C under N$_2$. After defined periods of time probes of 0.05 mL of the reaction mixture are gathered by syringe and quenched in 0.1 mL of methanol in an HPLC vial. 1 mL of *n*-hexanes is added and a chiral HPLC spectrum of the reaction mixture is recorded (Chiracel IB-N5, flow 0.5 mL/min, T = 10 °C, λ = 285 nm or λ = 215 nm, gradients of *n*-hexanes and *iso*-propanol). All measurements were repeated independently and analysed in three different ways as discussed below.

6.2.2. Determination of Absolute Configurations

Absolute configurations for *(R)*- and *(S)*-1-(2-naphthyl)ethanol (**1b**) and *(R)*- and *(S)*-1-phenyl-ethanol (**1a**) were determined through comparison of HPLC retention times with original samples of commercial available enantiopure alcohols. For 1-(2-phenanthryl)ethanol (**1c**) and 1-(2-pyrenyl)ethanol (**1d**) remaining alcohol after a kinetic resolution experiment with catalyst **3** and isobutyric anhydride (**2**, 0.6 eq) was isolated by column chromatography. The slow-reacting enantiomer of 1-(2-phenanthryl)ethanol **1c** could be identified as (-)-*(S)*-enantiomer through comparison of its optical rotation ($[\alpha]_{25}^{D}$ = -48.4°, 0.41 g/L, CHCl$_3$) with literature values[9]. The slow-reacting enantiomer of 1-(2-pyrenyl)ethanol (**1d**) was esterified by a Steglich reaction with N-(*tert*-butoxycarbonyl)-L-phenylalanine (**S2**) (**Scheme 6.5**). The configuration of diastereomeric **S3** was

determined by X-ray crystal structure analysis. Absolute configuration of *(S)*-**1d** could then be determined relative to the known absolute configuration of **S2**.
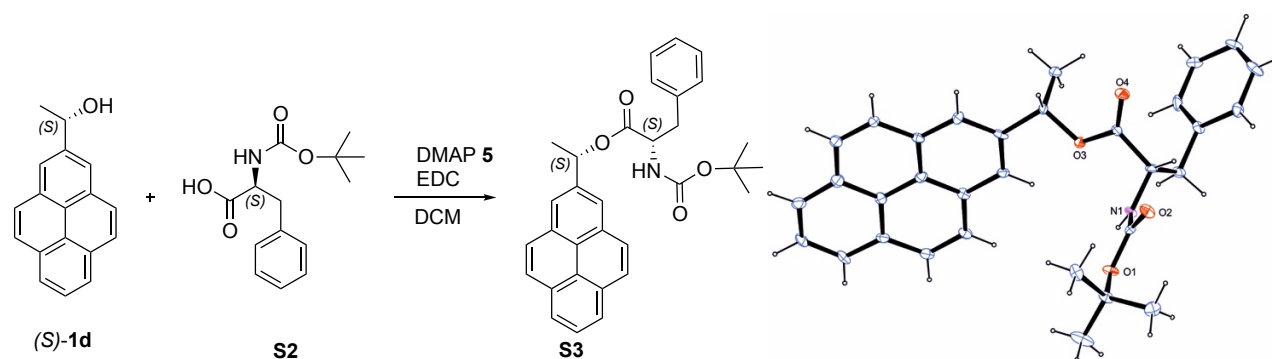
Scheme 6.5. Esterfication of *(S)*-1-(2-pyrenyl)ethanol (**1d**) with N-(*tert*-butoxycarbonyl)-L-phenylalanine **S2**. Right side: Single crystal X-ray crystal structure of **S3** with stereochemistry resolved relative to *(S)*-BOC-phenylalanine **S2**. For full details see Chapter 6.3.5.

The absolute configuration of ester products **4a** - **4d** was determined through deprotection and comparison of retention times with known alcohols.

6.2.3. Analysis of Experiments

The UV absorbance of all species in the HPLC spectra from competitive linear regression experiments as described in Chapter 6.2.1 were integrated. If intermediate concentrations in the UV-Vis spectrum were too small to be integrated reliably, intermediate concentrations were not determined (n.d.). Integrals were calibrated and corrected by the ratio of the enantiomers from the stock solution. All calculations were performed with Microsoft Excel if not stated differently.

Enantiomeric excess was calculated by Eq. 6.1, conversion (*c*) from *ee* of substrates and products by Eq. 6.32 and selectivity values by Eq. 6.25. Linear regression was performed with Microsoft Excel, graphs with linear fit and mean square error are given below.

Chemoselectivity values were calculated for the two fast reacting enantiomers and respectively for the two slow reacting enantiomers as discussed in Chapter 6.1.8. Only data points with a minimal conversion of 4% and a maximal conversion of 96% for both substrates are considered to avoid errors from too small absolute intermediate concentrations. On the one hand this is due to the higher relative analytical error in integrating very small values, on the other hand this can be rationalized when considering the conversion-chemoselectivity-relation as shown in **Figure 6.2**. As (chemo)selectivity values are always below 10 in this project, error estimation as discussed in Chapter 6.1.5 becomes not significant and numbers from Kagan's formulas are reliable.

Intermediate concentrations for each enantiomer *[x]* at a time *t* were calculated from the calibrated UV absorption of each compound in the HPLC spectra by Eq. 6.41.

$$[x]_t = \frac{[product]}{[product] + [substrate]} \cdot [x]_0 \qquad \text{Eq. 6.41}$$

Reactions were simulated with CoPaSi[5] using the kinetic model shown in **Table 6.6**. Parameter estimation for those reactions was done by "Differential Evolution" algorithm (Number of generations: 2000, population size: 10).

Table 6.6. Kinetic model for the simulation of reaction course with CoPaSi.

Name	Reaction	Rate Law
cat loading	cat + anhydride -> cat-complex	Mass action (irreversible)
R-Alc1	R-Alc1 + cat-complex -> R-Est1 + cat + acid	Mass action (irreversible)
S-Alc1	S-Alc1 + cat-complex -> S-Est1 + cat + acid	Mass action (irreversible)
R-Alc2	R-Alc2 + cat-complex -> R-Est2 + cat + acid	Mass action (irreversible)
S-Alc2	S-Alc2 + cat-complex -> S-Est2 + cat + acid	Mass action (irreversible)

6.2.4. Results with Chiral Catalysts
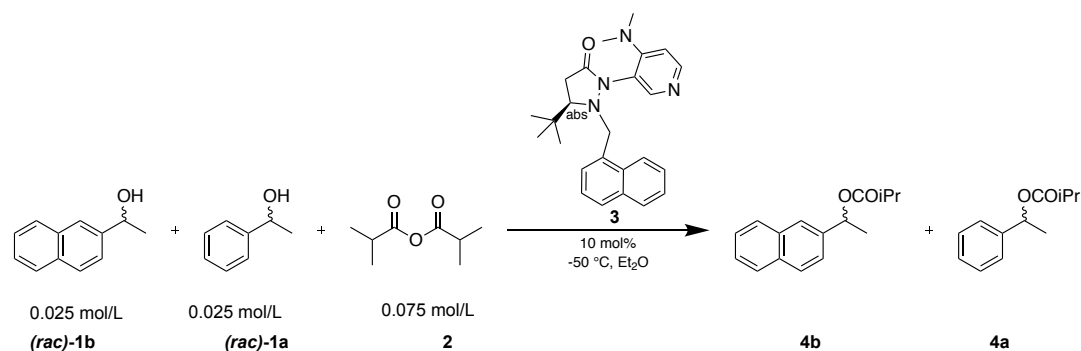
Scheme 6.6. Competitive linear regression of (*rac*)-1-(2-naphthyl)ethanol (**1b**) (NpEtOH) and (*rac*)-1-phenylethanol (**1a**) (PhEtOH) yielding **4b** (NpEtOiPr) and **4a** (PhEtOiPr) with catalyst **3**.

Table 6.7. Raw HPLC absorbance data for competitive linear regression shown in **Scheme 6.6**. Data were calibrated and normalized from the stock solution before analysis. Concentrations too small to be integrated reliably were not determined (n.d.). Enantiomeric excess was calculated by Eq. 6.1, conversion (*c*) by Eq. 6.32 and Selectivity by Eq. 6.25.

Run	time [min]	UV-Absorbance HPLC (λ = 285 nm (naphthyl), (λ = 215 nm (phenyl)), raw data [mAUs]								Enantioselectivity PhEtOH 1a				Enantioselectivity NpEtOH 1b			
		R-PhEtOiPr (R)-**4a**	S-PhEtOiPr (S)-**4a**	R-NpEtOiPr (R)-**4b**	S-NpEtOiPr (S)-**4b**	R-PhEtOH (R)-**1a**	S-PhEtOH (S)-**1a**	S-NpEtOH (S)-**1b**	R-NpEtOH (R)-**1b**	$ee_{product}$	$ee_{substrate}$	c	s	$ee_{product}$	$ee_{substrate}$	c	s
1	0	-	-	-	-	7327.0	7508.6	7359.2	7427.4	-	-	-	-	-	-	-	-
1	94	n.d.	n.d.	2860.6	n.d.	8069.0	8535.2	8584.8	6130.0	n.d.	0.016	n.d.	n.d.	n.d.	0.171	n.d.	n.d.
1	321	1082.1	97.0	4696.6	238.8	6370.9	7166.6	6840.8	2097.4	0.839	0.047	5.3%	12.0	0.902	0.534	37.2%	33.2
1	421	1161.2	90.5	4418.1	256.4	5035.3	5863.0	5277.7	1049.2	0.859	0.064	6.9%	14.0	0.889	0.671	43.0%	34.3
1	566	2042.0	238.5	6321.3	455.8	6247.1	7557.0	6991.5	770.1	0.795	0.083	9.4%	9.5	0.864	0.803	48.2%	33.8
1	1259	3802.1	604.6	7446.3	1067.1	4897.2	7485.7	6952.6	66.5	0.731	0.197	21.2%	7.8	0.747	0.990	57.0%	35.2
1	1806	5290.4	934.6	7894.6	1510.3	4308.7	7876.3	6978.3	n.d.	0.706	0.282	28.5%	7.6	0.676	n.d.	n.d.	n.d.
1	3282	5898.1	1309.5	6472.3	1922.8	1936.0	6134.1	4873.9	n.d.	0.644	0.511	44.3%	7.6	0.539	n.d.	n.d.	n.d.
2	0	-	-	-	-	4652.7	4733.3	4102.3	4123.1	-	-	-	-	-	-	-	-

Run	time [min]	UV-Absorbance HPLC (λ = 285 nm (naphthyl), (λ = 215 nm (phenyl)), raw data [mAUs]								Enantioselectivity PhEtOH 1a				Enantioselectivity NpEtOH 1b			
		R-PhEtOiPr (R)-4a	S-PhEtOiPr (S)-4a	R-NpEtOiPr (R)-4b	S-NpEtOiPr (S)-4b	R-PhEtOH (R)-1a	S-PhEtOH (S)-1a	S-NpEtOH (S)-1b	R-NpEtOH (R)-1b	$ee_{product}$	$ee_{substrate}$	c	s	$ee_{product}$	$ee_{substrate}$	c	s
2	182	1173.8	185.9	6028.3	283.8	10189.7	11018.2	11816.7	6215.0	0.731	0.030	4.0%	6.6	0.910	0.313	25.6%	28.7
2	564	2310.1	287.1	7089.9	446.9	7103.7	8633.1	8504.2	1163.7	0.782	0.089	10.2%	8.9	0.881	0.760	46.3%	36.1
2	842	3021.4	414.3	7108.9	652.9	6111.4	8097.1	7711.2	391.9	0.762	0.131	14.7%	8.4	0.831	0.904	52.1%	33.4
2	1176	3657.5	554.6	7156.1	840.5	5188.0	7652.9	6850.6	69.1	0.741	0.184	19.9%	8.0	0.789	0.980	55.4%	38.0
2	1794	5843.4	890.8	8000.4	1533.6	5025.7	8926.9	7774.5	n.d.	0.739	0.272	26.9%	8.7	0.677	n.d.	n.d.	n.d.
2	3197	4760.0	1076.8	4998.7	1497.3	1628.0	5196.8	3951.2	n.d.	0.636	0.517	44.8%	7.4	0.537	n.d.	n.d.	n.d.

Table 6.8. Chemoselectivity values for the two fast reacting and the two slow reacting enantiomers for the competition experiment shown in **Scheme 6.6**. To minimize influence of analytical errors, only data points with at minimum 4% and maximal 96% conversion (*c*) for both substrates are analysed. Selectivity was derived as described in Chapter 6.1.8.

Run	time [min]	c (R)-1b	c (R)-1d	total c	Chemosel	Select	StDev	Run	time [min]	c (S)-1b	c (S)-1d	total c	Chemosel	Select	StDev
1	321	69.8%	15.9%	42.8%	-0.629	0.145		1	1259	13.7%	8.2%	11.0%	-0.247	0.586	
1	421	81.3%	20.4%	50.8%	-0.599	0.136		1	1806	18.2%	11.7%	15.0%	-0.220	0.616	
1	566	89.4%	26.7%	58.0%	-0.541	0.138		1	3282	28.9%	19.2%	24.0%	-0.202	0.624	
2	564	86.3%	26.6%	56.4%	-0.529	0.156		2	842	8.0%	5.4%	6.7%	-0.197	0.661	
2	842	94.9%	35.5%	65.2%	-0.456	0.147		2	1176	11.2%	7.5%	9.3%	-0.202	0.651	
-								2	1794	16.9%	10.0%	13.4%	-0.257	0.569	
-								2	3197	28.1%	18.7%	23.4%	-0.200	0.629	
					average	0.144	0.007						average	0.619	0.031

Figure 6.6. Linear regression analysis of two independent runs of competition experiment shown in **Scheme 6.6**.

Run 1	Estimated rate constant $\left[\frac{ml}{mmol \cdot min}\right]$	Standard Deviation	k_{rel} to (R)-**1b**
(R)-**1b**	0.7842	0.0113	1.000
(R)-**1a**	0.0972	0.0015	0.124
(R)-**4b**			
(R)-**4a**			
(S)-**1b**	0.0216	0.0003	0.028
(S)-**1a**	0.0131	0.0002	0.017
(S)-**4b**			
(S)-**4a**			

Run 2	Estimated rate constant $\left[\frac{ml}{mmol \cdot min}\right]$	Standard Deviation	k_{rel} to (R)-**1b**
(R)-**1b**	0.7373	0.0092	1.000
(R)-**1a**	0.0972	0.0012	0.132
(R)-**4b**			
(R)-**4a**			
(S)-**1b**	0.0205	0.0002	0.028
(S)-**1a**	0.0128	0.0001	0.017
(S)-**4b**			
(S)-**4a**			

Figure 6.7. Parameter estimation for competition experiment shown in **Scheme 6.6**. Estimation was performed with CoPaSi[5], x-axis shows time in min, y-axis intermediate concentration in mol/L of each species. Estimated rate constants with standard deviation for each alcohol are shown right hand.
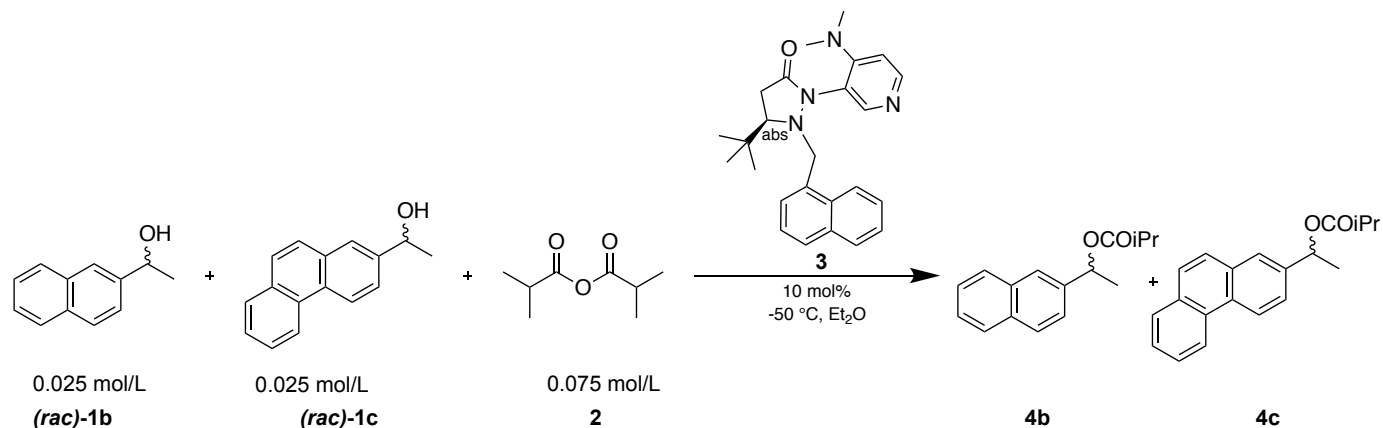
Scheme 6.7. Competitive linear regression of (*rac*)-1-(2-naphthyl)ethanol (**1b**) (NpEtOH) and (*rac*)-1-(2-phenanthryl)ethanol (**1c**) (PhantEtOH) yielding **4b** (NpEtOiPr) and **4c** (PhantEtOiPr) with catalyst **3**.

Table 6.9. Raw HPLC absorbance data for competitive linear regression shown in **Scheme 6.7**. Data were calibrated and normalized from the stock solution before analysis. Concentrations too small to be integrated reliably were not determined (n.d.). Enantiomeric excess was calculated by Eq. 6.1, conversion (*c*) by Eq. 6.32 and Selectivity by Eq. 6.25.

Run	time [min]	UV-Absorbance HPLC (λ = 285 nm), raw data [mAUs]								Enantioselectivity NpEtOH 1b				Enantioselectivity PhantEtOH 1c			
		R-NpEtOiPr (*R*)-**4b**	S-NpEtOiPr (*S*)-**4b**	R-Phant-EtOiPr (*R*)-**4c**	S-Phant-EtOiPr (*S*)-**4c**	S-NpEtOH (*S*)-**1b**	R-NpEtOH (*R*)-**1b**	S-Phant-EtOH (*S*)-**1c**	R-Phant-EtOH (*R*)-**1c**	$ee_{product}$	$ee_{substrate}$	*c*	*s*	$ee_{product}$	$ee_{substrate}$	*c*	*s*
1	0	-	-	-	-	2845.0	2842.9	8719.0	8705.4	-	-	-	-	-	-	-	-
1	28	252.3	n.d.	1556.9	n.d.	3589.1	3360.7	11078.5	9564.4	n.d.	0.032	n.d.	n.d.	n.d.	0.073	n.d.	n.d.
1	66	389.6	n.d.	2311.1	48.8	2689.3	2322.2	8299.8	6005.7	n.d.	0.073	n.d.	n.d.	0.959	0.160	14.3%	55.5
1	182	1063.5	37.7	5523.4	137.5	3190.4	2133.9	9977.0	4274.6	0.932	0.198	17.5%	34.3	0.951	0.399	29.6%	59.6
1	362	1235.4	54.3	5471.1	255.5	2207.2	1005.3	6744.7	1211.0	0.916	0.374	29.0%	32.8	0.911	0.695	43.3%	44.6
1	558	1252.6	60.5	4811.3	277.2	1704.1	487.3	5153.1	339.6	0.908	0.555	37.9%	36.2	0.891	0.876	49.6%	50.0
1	859	2185.0	150.6	7342.7	631.9	2375.9	298.9	7015.7	75.8	0.871	0.776	47.1%	34.1	0.842	0.979	53.8%	51.9
1	1166	1275.2	108.6	3904.7	500.6	1249.9	56.0	3713.0	n.d.	0.843	0.914	52.0%	37.5	0.773	n.d.	n.d.	n.d.
1	1791	2369.0	323.0	6832.0	1299.7	2089.4	n.d.	6027.3	n.d.	0.760	n.d.	n.d.	n.d.	0.681	n.d.	n.d.	n.d.
1	3199	2719.1	644.4	7519.4	2256.7	2162.3	n.d.	5922.5	n.d.	0.617	n.d.	n.d.	n.d.	0.539	n.d.	n.d.	n.d.

		UV-Absorbance HPLC (λ = 285 nm), raw data [mAUs]								Enantioselectivity NpEtOH 1b				Enantioselectivity PhantEtOH 1c			
Run	time [min]	R-NpEtOiPr (R)-4b	S-NpEtOiPr (S)-4b	R-Phant-EtOiPr (R)-4c	S-Phant-EtOiPr (S)-4c	S-NpEtOH (S)-1b	R-NpEtOH (R)-1b	S-Phant-EtOH (S)-1c	R-Phant-EtOH (R)-1c	$ee_{product}$	$ee_{substrate}$	c	s	$ee_{product}$	$ee_{substrate}$	c	s
2	0	-	-	-	-	4674.7	4808.4	14867.1	14587.7	-	-	-	-	-	-	-	-
2	35	277.0	n.d.	1681.9	n.d.	3163.4	3314.4	10577.0	8796.4	n.d.	n.d.	n.d.	n.d.	n.d.	0.082	n.d.	n.d.
2	75	437.1	10.3	2559.8	66.4	2694.0	2365.0	8597.2	5963.9	0.953	0.079	7.7%	44.8	0.950	0.172	15.3%	46.5
2	199	1096.5	31.5	5832.5	168.5	3202.7	2232.4	10167.9	4255.6	0.943	0.192	16.9%	40.8	0.945	0.402	29.8%	52.3
2	359	2357.3	82.6	10813.6	416.1	4434.0	2209.2	13860.8	2860.5	0.930	0.347	27.2%	38.9	0.927	0.652	41.3%	52.1
2	511	1958.6	74.3	7937.6	375.1	2843.4	1029.7	8882.9	885.4	0.925	0.479	34.1%	41.2	0.911	0.816	47.2%	54.5
2	1237	3254.9	229.3	10350.6	1066.6	3305.8	182.6	9986.2	n.d.	0.865	0.898	50.9%	42.0	0.816	n.d.	n.d.	n.d.
2	2980	3030.3	448.2	9273.0	2020.8	2680.6	n.d.	7840.4	n.d.	0.736	n.d.	n.d.	n.d.	0.648	n.d.	n.d.	n.d.

Table 6.10. Chemoselectivity values for the two fast reacting and the two slow reacting enantiomers for the competition experiment shown in **Scheme 6.7**. To minimize influence of analytical errors, only data points with at minimum 4% and maximal 96% conversion (c) for both substrates are analysed. Selectivity was derived as described in Chapter 6.1.8.

Run	time [min]	c (R)-1b	c (R)-1c	total c	Chemosel	Select	StDev	Run	time [min]	c (S)-1b	c (S)-1c	total c	Chemosel	Select	StDev
1	28	7.2%	14.5%	10.9%	0.339	2.1		1	859	6.1%	8.6%	7.4%	0.168	1.4	
1	66	14.7%	28.7%	21.7%	0.321	2.1		1	1166	8.2%	12.3%	10.3%	0.201	1.5	
1	182	33.9%	57.4%	45.7%	0.257	2.1		1	1791	13.7%	18.4%	16.1%	0.145	1.4	
1	362	55.9%	82.5%	69.2%	0.193	2.1		1	3199	23.5%	28.5%	26.0%	0.096	1.3	
1	558	72.6%	93.7%	83.1%	0.127	2.1		2	1237	6.7%	10.0%	8.4%	0.202	1.5	
2	35	7.9%	16.6%	12.3%	0.355	2.2		2	2980	14.7%	21.2%	17.9%	0.181	1.5	
2	75	16.0%	30.9%	23.5%	0.319	2.1		-							
2	199	33.6%	58.9%	46.2%	0.273	2.2		-							
2	359	52.4%	79.8%	66.1%	0.208	2.2		-							
2	511	66.2%	90.3%	78.3%	0.154	2.2		-							
					average	2.1	0.039						average	1.4	0.111
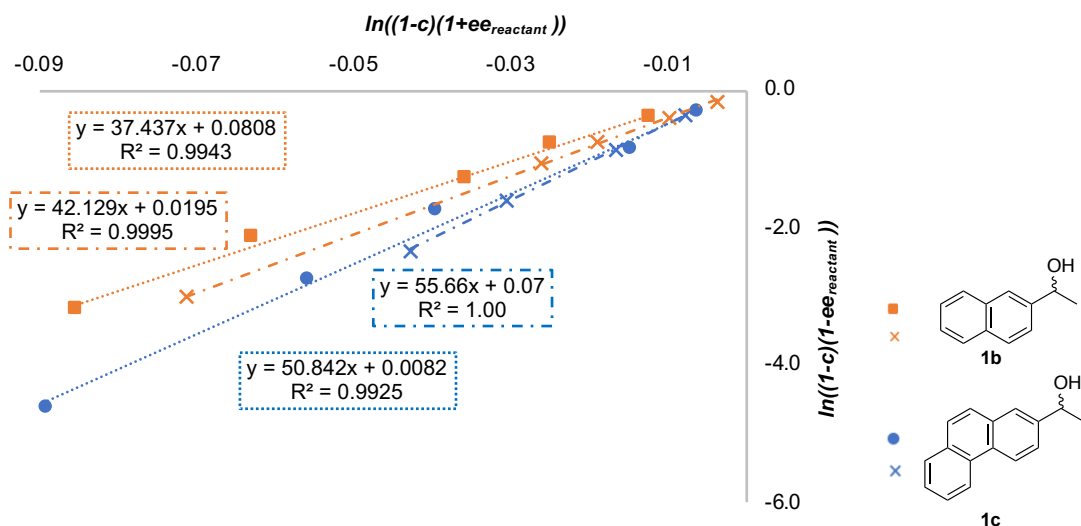
Figure 6.8. Linear regression analysis of two independent runs of competition experiment shown in **Scheme 6.7**.

Run 1	Estimated rate constant $\left[\frac{ml}{mmol \cdot min}\right]$	Standard Deviation	k_{rel} to (R)-**1b**
(R)-**1b**	0.4797	0.0093	1.000
(R)-**1c**	1.0036	0.0264	2.092
(R)-**4b**			
(R)-**4c**			
(S)-**1b**	0.0163	0.0001	0.034
(S)-**1c**	0.0216	0.0002	0.045
(S)-**4b**			
(S)-**4c**			

Run 2	Estimated rate constant $\left[\frac{ml}{mmol \cdot min}\right]$	Standard Deviation	k_{rel} to (R)-**1b**
(R)-**1b**	0.4250	0.0061	1.000
(R)-**1c**	0.9179	0.0159	2.160
(R)-**4b**			
(R)-**4c**			
(S)-**1b**	0.0107	0.0001	0.025
(S)-**1c**	0.0162	0.0001	0.038
(S)-**4b**			
(S)-**4c**			

Figure 6.9. Parameter estimation for competition experiment shown in **Scheme 6.7** (run 1). Estimation was performed with CoPaSi[5], x-axis shows time in min, y-axis intermediate concentration in mol/L of each species. Estimated rate constants with standard deviation for each alcohol are shown right hand.
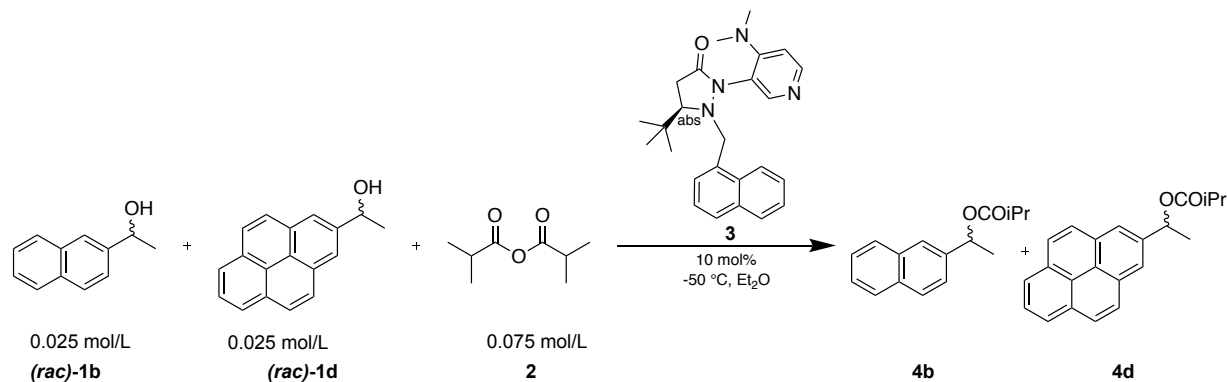
Scheme 6.8. Competitive linear regression of (*rac*)-1-(2-naphthyl)ethanol (**1b**) (NpEtOH) and (*rac*)-1-(2-pyrenyl)ethanol (**1d**) (PyrEtOH) yielding **4b** (NpEtOiPr) and **4a** (PyrEtOiPr) with catalyst **3**.

Table 6.11. Raw HPLC absorbance data for competitive linear regression shown in **Scheme 6.8**. Data were calibrated and normalized from the stock solution before analysis. Concentrations too small to be integrated reliably were not determined (n.d.). Enantiomeric excess was calculated by Eq. 6.1, conversion (*c*) by Eq. 6.32 and Selectivity by Eq. 6.25.

Run	time [min]	UV-Absorbance HPLC (λ = 285 nm), raw data [mAUs]								Enantioselectivity NpEtOH 1b				Enantioselectivity PyrEtOH 1d			
		R-NpEtOiPr (R)-**4b**	S-NpEtOiPr (S)-**4b**	R-PyrEtOiPr (R)-**4d**	S-PyrEtOiPr (S)-**4d**	S-NpEtOH (S)-**1b**	R-NpEtOH (R)-**1b**	S-PyrEtOH (S)-**1d**	R-PyrEtOH (R)-**1d**	$ee_{product}$	$ee_{substrate}$	*c*	*s*	$ee_{product}$	$ee_{substrate}$	*c*	*s*
1	0	-	-	-	-	5978.9	5985.5	7365.4	7703.8	-	-	-	-	-	-	-	-
1	25	132.2	n.d.	887.3	n.d.	3245.5	3122.6	4156.5	3451.3	n.d.	0.020	n.d.	n.d.	n.d.	0.115	10.3%	n.d.
1	62	258.6	n.d.	1579.6	25.6	3065.5	2813.9	3979.0	2500.4	n.d.	0.043	n.d.	n.d.	0.967	0.249	20.5%	75.4
1	117	450.0	16.2	2249.1	38.6	2967.4	2533.2	3833.9	1566.2	0.931	0.079	7.9%	30.1	0.965	0.438	31.2%	85.8
1	176	704.2	24.5	2864.4	85.6	3079.3	2346.9	3882.3	926.3	0.933	0.136	12.7%	32.7	0.939	0.629	40.1%	61.0
1	360	1541.3	62.4	3725.6	203.5	3319.8	1814.9	4116.3	99.5	0.922	0.294	24.2%	32.8	0.892	0.955	51.7%	66.5
1	563	1806.3	81.3	3134.5	281.2	2668.4	903.9	3326.3	n.d.	0.914	0.494	35.1%	36.3	0.828	n.d.	n.d.	n.d.
1	854	2586.0	164.2	3546.2	522.7	2983.2	479.7	3572.4	n.d.	0.880	0.723	45.1%	34.0	0.733	n.d.	n.d.	n.d.
1	1174	4188.7	344.0	5072.2	1037.5	4309.0	299.3	4828.2	n.d.	0.848	0.870	50.6%	34.3	0.648	n.d.	n.d.	n.d.
1	1789	3354.4	389.5	3937.3	1192.7	3109.6	31.9	3412.7	n.d.	0.792	0.980	55.3%	38.4	0.519	n.d.	n.d.	n.d.
1	4688	2514.6	668.7	2981.2	1747.6	1921.7	n.d.	1581.7	n.d.	0.579	n.d.	n.d.	n.d.	0.240	n.d.	n.d.	n.d.

		UV-Absorbance HPLC (λ = 285 nm), raw data [mAUs]								Enantioselectivity NpEtOH 1b				Enantioselectivity PyrEtOH 1d			
Run	time [min]	R-NpEtOiPr (R)-4b	S-NpEtOiPr (S)-4b	R-PyrEtOiPr (R)-4d	S-PyrEtOiPr (S)-4d	S-NpEtOH (S)-1b	R-NpEtOH (R)-1b	S-PyrEtOH (S)-1d	R-PyrEtOH (R)-1d	$ee_{product}$	$ee_{substrate}$	c	s	$ee_{product}$	$ee_{substrate}$	c	s
2	0	-	-	-	-	3622.7	3810.1	5121.0	5283.3	-	-	-	-	-	-	-	-
2	28	132.7	n.d.	1025.2	19.4	3308.1	3415.0	4735.6	3792.2	n.d.	0.009	n.d.	n.d.	0.962	0.126	11.6%	58.0
2	73	220.2	n.d.	1469.7	30.9	2458.8	2397.3	3622.4	2164.8	n.d.	0.038	n.d.	n.d.	0.957	0.266	21.8%	59.7
2	122	569.9	22.8	3125.3	83.6	3924.1	3586.6	5494.5	2312.3	0.919	0.070	7.1%	25.5	0.946	0.421	30.8%	54.8
2	195	717.9	23.7	3234.9	96.8	3125.9	2610.6	4486.4	1037.4	0.933	0.115	11.0%	32.2	0.940	0.634	40.3%	62.2
2	358	1850.4	70.1	5168.2	258.7	4319.4	2653.7	5898.1	218.5	0.923	0.263	22.1%	32.4	0.902	0.931	50.8%	66.0
2	510	2233.8	96.4	4627.6	333.9	3693.6	1626.1	5047.0	n.d.	0.913	0.410	31.0%	32.9	0.861	n.d.	n.d.	n.d.
2	1245	3421.5	245.5	4583.0	811.1	3466.6	224.2	4430.3	n.d.	0.860	0.884	50.7%	38.8	0.691	n.d.	n.d.	n.d.
2	2982	2160.9	333.6	2818.5	1058.4	1872.5	n.d.	2170.1	n.d.	0.721	n.d.	n.d.	n.d.	0.442	n.d.	n.d.	n.d.

Table 6.12. Chemoselectivity values for the two fast reacting and the two slow reacting enantiomers for the competition experiment shown in **Scheme 6.8**. To minimize influence of analytical errors, only data points with at minimum 4% and maximal 96% conversion (c) for both substrates are analysed. Selectivity was derived as described in Chapter 6.1.8.

Run	time [min]	c (R)-1b	c (R)-1d	total c	Chemosel	Select	StDev	Run	time [min]	c (S)-1b	c (S)-1d	total c	Chemosel	Select	StDev
1	62	8.6%	41.2%	24.9%	0.654	5.9		1	1174	7.6%	19.2%	13.4%	0.435	2.7	
1	117	15.4%	61.4%	38.4%	0.599	5.7		1	1789	11.4%	27.9%	19.6%	0.421	2.7	
1	176	23.5%	77.4%	50.5%	0.534	5.5		1	4688	26.3%	55.0%	40.7%	0.353	2.6	
2	73	8.6%	42.9%	25.8%	0.666	6.2		2	1245	6.8%	16.9%	11.8%	0.427	2.6	
2	122	14.0%	59.9%	37.0%	0.621	6.1		2	2982	15.4%	35.1%	25.3%	0.389	2.6	
2	195	22.0%	77.5%	49.8%	0.558	6.0		-							
					average	5.9	0.231						average	2.7	0.054
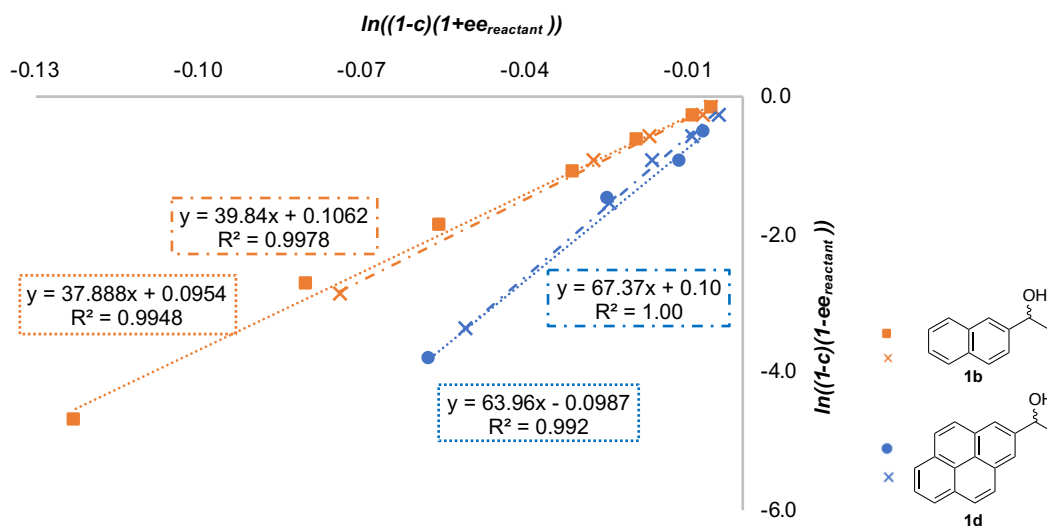
Figure 6.10. Linear regression analysis of two independent runs of competition experiment shown in **Scheme 6.8**.

Run 1	Estimated rate constant $\left[\frac{ml}{mmol\cdot min}\right]$	Standard Deviation	k_{rel} to (R)-**1b**
(R)-**1b**	0.3956	0.0080	1.000
(R)-**1d**	1.8721	0.0603	4.733
(R)-**4b**			
(R)-**4d**			
(S)-**1b**	0.0132	0.0001	0.033
(S)-**1d**	0.0352	0.0004	0.089
(S)-**4b**			
(S)-**4d**			

Run 2	Estimated rate constant $\left[\frac{ml}{mmol\cdot min}\right]$	Standard Deviation	k_{rel} to (R)-**1b**
(R)-**1b**	0.3438	0.0090	1.000
(R)-**1d**	1.7629	0.0670	5.127
(R)-**4b**			
(R)-**4d**			
(S)-**1b**	0.0114	0.0001	0.033
(S)-**1d**	0.0295	0.0004	0.086
(S)-**4b**			
(S)-**4d**			

Figure 6.11. Parameter estimation for competition experiment shown in **Scheme 6.8**. Estimation was performed with CoPaSi[5], x-axis shows time in min, y-axis intermediate concentration in mol/L of each species. Estimated rate constants with standard deviation for each alcohol are shown right hand.
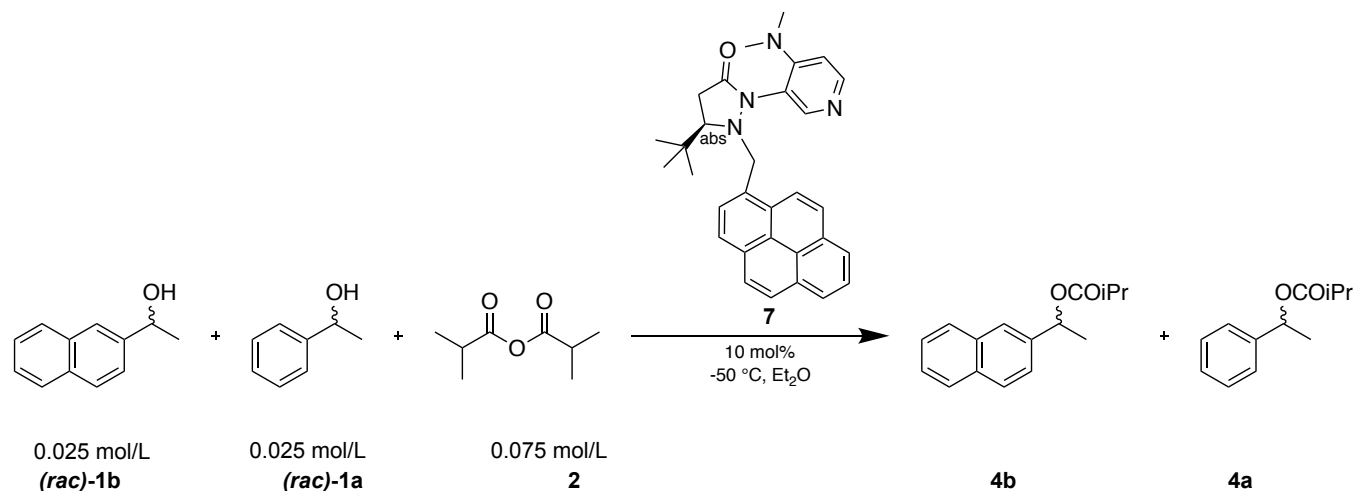
Scheme 6.9. Competitive linear regression of (*rac*)-1-(2-naphthyl)ethanol (**1b**) (NpEtOH) and (*rac*)-1-phenylethanol (**1a**) (PhEtOH) yielding **4b** (NpEtOiPr) and **4a** (PhEtOiPr) with catalyst **7**.

Table 6.13. Raw HPLC absorbance data for competitive linear regression shown in **Scheme 6.9**. Data were calibrated and normalized from the stock solution before analysis. Concentrations too small to be integrated reliably were not determined (n.d.). Enantiomeric excess was calculated by Eq. 6.1, conversion (*c*) by Eq. 6.32 and Selectivity by Eq. 6.25.

Run	time [min]	UV-Absorbance HPLC (λ = 285 nm (naphthyl), (λ = 215 nm (phenyl)), raw data [mAUs]								Enantioselectivity PhEtOH 1a				Enantioselectivity NpEtOH 1b			
		R-PhEtOiPr (R)-**4a**	S-PhEtOiPr (S)-**4a**	R-NpEtOiPr (R)-**4b**	S-NpEtOiPr (S)-**4b**	R-PhEtOH (R)-**1a**	S-PhEtOH (S)-**1a**	S-NpEtOH (S)-**1b**	R-NpEtOH (R)-**1b**	$ee_{product}$	$ee_{substrate}$	c	s	$ee_{product}$	$ee_{substrate}$	c	s
1	0	-	-	-	-	7327.0	7508.6	7359.2	7427.4	-	-	-	-	-	-	-	-
1	92	144.0	n.d.	920.4	25.4	7935.7	8171.6	8226.8	7376.6	n.d.	n.d.	n.d.	n.d.	0.946	0.059	5.9%	38.0
1	201	220.1	n.d.	1246.4	38.2	5917.8	6138.4	5740.1	4510.9	n.d.	0.006	n.d.	n.d.	0.940	0.124	11.7%	36.5
1	321	403.9	n.d.	2271.7	75.3	6558.8	6905.7	6657.4	4433.6	n.d.	0.014	n.d.	n.d.	0.935	0.205	18.0%	36.5
1	421	534.4	n.d.	2720.1	98.0	6295.3	6746.5	6249.6	3598.1	n.d.	0.022	n.d.	n.d.	0.930	0.274	22.7%	35.9
1	566	903.4	129.7	4366.2	170.4	7296.5	7990.1	7688.8	3413.6	0.754	0.033	4.2%	7.4	0.924	0.389	29.6%	37.2
1	1259	2157.5	220.5	6588.3	362.8	6349.4	7734.7	7483.8	821.4	0.819	0.086	9.5%	10.9	0.895	0.804	47.3%	44.4
1	1806	3030.9	359.0	6730.7	496.8	5406.9	7363.5	6993.6	179.9	0.793	0.141	15.1%	9.9	0.861	0.950	52.5%	49.6
1	3282	5138.3	799.4	6757.6	986.6	3348.3	6978.1	6299.0	n.d.	0.736	0.341	31.6%	9.2	0.743			

Run	time [min]	UV-Absorbance HPLC (λ = 285 nm (naphthyl), (λ = 215 nm (phenyl)), raw data [mAUs]								Enantioselectivity PhEtOH 1a				Enantioselectivity NpEtOH 1b			
		R-PhEtOiPr (R)-4a	S-PhEtOiPr (S)-4a	R-NpEtOiPr (R)-4b	S-NpEtOiPr (S)-4b	R-PhEtOH (R)-1a	S-PhEtOH (S)-1a	S-NpEtOH (S)-1b	R-NpEtOH (R)-1b	$ee_{product}$	$ee_{substrate}$	c	s	$ee_{product}$	$ee_{substrate}$	c	s
2	0	-	-	-	-	4652.7	4733.3	4102.3	4123.1	-	-	-	-	-	-	-	-
2	74	260.6	n.d.	1327.9	52.7	10433.5	10854.9	11743.9	10507.2	n.d.	0.011	n.d.	n.d.	0.923	0.058	5.9%	26.6
2	188	444.6	n.d.	2890.1	84.8	8264.7	8761.5	8807.7	6174.6	n.d.	0.021	n.d.	n.d.	0.943	0.178	15.9%	40.4
2	571	968.1	n.d.	4092.2	164.8	5799.3	6586.7	6096.1	1914.6	n.d.	0.055	n.d.	n.d.	0.922	0.524	36.2%	41.7
2	846	1632.6	201.3	5294.4	263.7	5860.8	7037.3	6482.9	1042.9	0.784	0.083	9.5%	9.0	0.905	0.724	44.5%	43.3
2	1180	3316.7	371.2	8206.8	530.1	7239.3	9263.3	9151.0	481.0	0.802	0.114	12.5%	10.2	0.878	0.901	50.6%	47.3
2	1798	4876.3	569.7	9436.3	871.1	6224.9	9187.3	8969.2	61.6	0.794	0.184	18.8%	10.4	0.830	0.986	54.3%	52.5
2	3201	4874.9	762.8	6198.9	971.1	2657.9	6191.7	5329.3	n.d.	0.733	0.392	34.8%	9.5	0.728	n.d.	n.d.	n.d.

Table 6.14. Chemoselectivity values for the two fast reacting and the two slow reacting enantiomers for the competition experiment shown in **Scheme 6.9**. To minimize influence of analytical errors, only data points with at minimum 4% and maximal 96% conversion (c) for both substrates are analysed. Selectivity was derived as described in Chapter 6.1.8.

Run	time [min]	c (R)-1b	c (R)-1d	total c	Chemosel	Select	StDev	Run	time [min]	c (S)-1b	c (S)-1d	total c	Chemosel	Select	StDev
1	201	22.2%	4.0%	13.1%	-0.696	0.162		1	1259	4.8%	3.1%	3.9%	-0.215	0.640	
1	321	34.6%	6.4%	20.5%	-0.687	0.156		1	1806	6.8%	5.1%	6.0%	-0.140	0.747	
1	421	43.8%	8.6%	26.2%	-0.671	0.157		1	3282	13.9%	11.3%	12.6%	-0.103	0.801	
1	566	56.9%	12.1%	34.5%	-0.649	0.153		2	1798	9.1%	6.5%	7.8%	-0.170	0.699	
1	1259	89.2%	27.4%	58.3%	-0.530	0.144		2	3201	15.8%	12.1%	13.9%	-0.135	0.746	
2	188	32.5%	5.6%	19.1%	-0.704	0.148		-							
2	571	68.8%	15.7%	42.2%	-0.629	0.146		-							
2	846	84.0%	23.7%	53.8%	-0.560	0.147		-							
2	1180	94.6%	33.8%	64.2%	-0.474	0.141		-							
					average	0.149	0.005						average	0.748	0.036
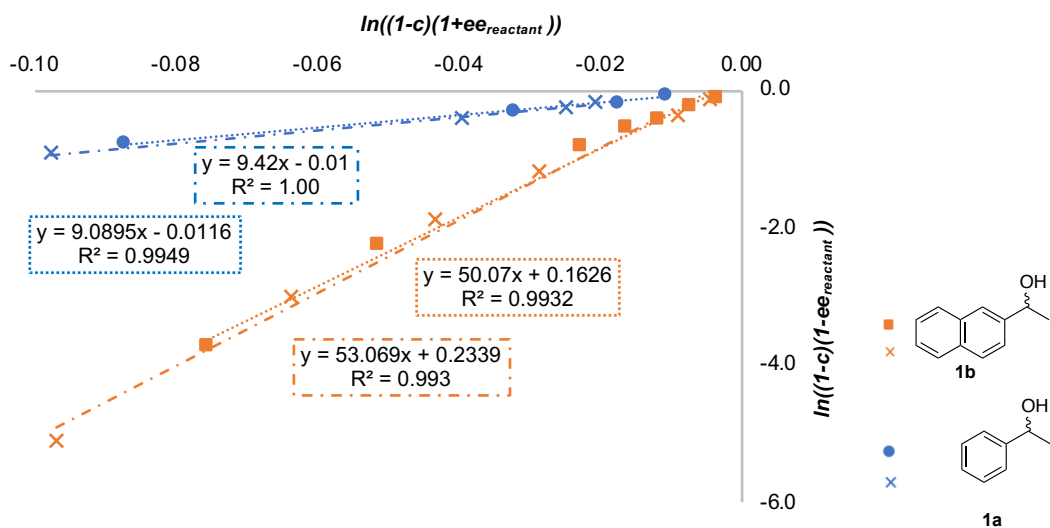
Figure 6.12. Linear regression analysis of two independent runs of competition experiment shown in **Scheme 6.9**.

Run 1	Estimated rate constant $[\frac{ml}{mmol \cdot min}]$	Standard Deviation	k_{rel} to (R)-**1b**
(R)-**1b**	0.6001	0.0326	1.000
(R)-**1a**	0.0810	0.0027	0.135
(R)-**4b**			
(R)-**4a**			
(S)-**1b**	0.0120	0.0003	0.020
(S)-**1a**	0.0092	0.0003	0.015
(S)-**4b**			
(S)-**4a**			

Run 2	Estimated rate constant $[\frac{ml}{mmol \cdot min}]$	Standard Deviation	k_{rel} to (R)-**1b**
(R)-**1b**	0.5615	0.0305	1.000
(R)-**1a**	0.0788	0.0025	0.140
(R)-**4b**			
(R)-**4a**			
(S)-**1b**	0.0119	0.0003	0.021
(S)-**1a**	0.0086	0.0002	0.015
(S)-**4b**			
(S)-**4a**			
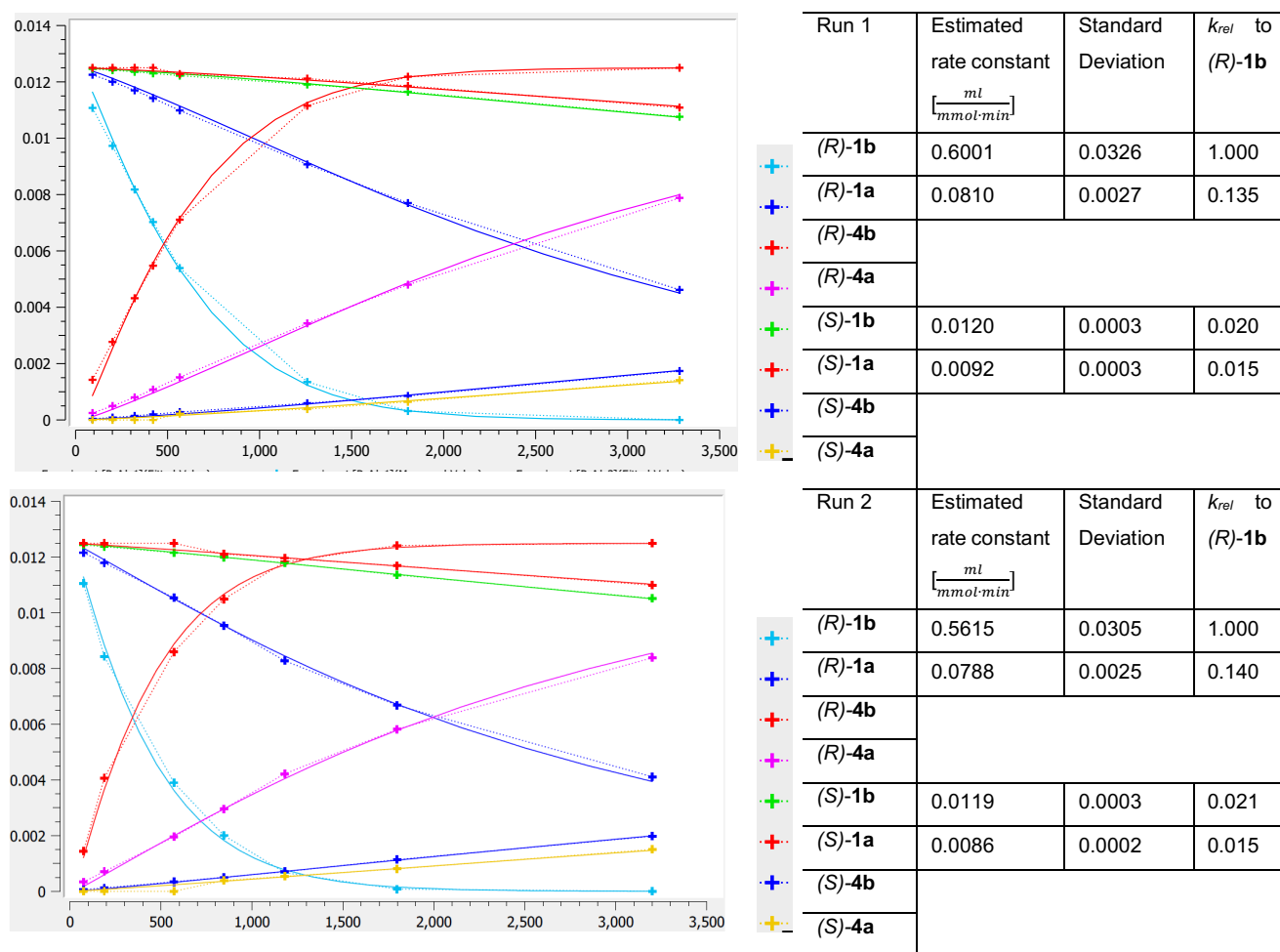
Figure 6.13. Parameter estimation for competition experiment shown in **Scheme 6.9**. Estimation was performed with CoPaSi[5], x-axis shows time in min, y-axis intermediate concentration in mol/L of each species. Estimated rate constants with standard deviation for each alcohol are shown right hand.
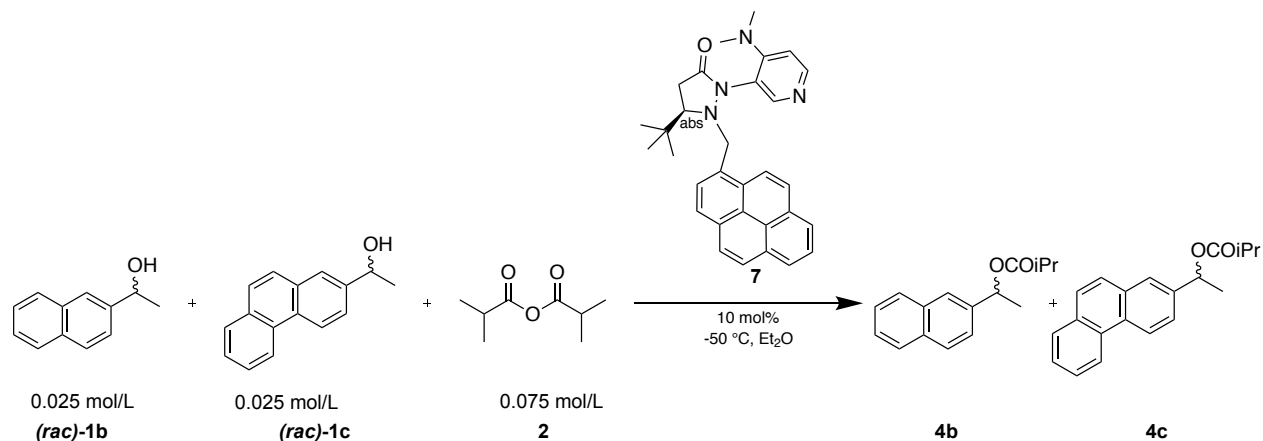
Scheme 6.10. Competitive linear regression of (*rac*)-1-(2-naphthyl)ethanol (**1b**) (NpEtOH) and (*rac*)-1-(2-phenanthryl)ethanol (**1c**) (PhantEtOH) yielding **4b** (NpEtOiPr) and **4c** (PhantEtOiPr) with catalyst **7**.

Table 6.15. Raw HPLC absorbance data for competitive linear regression shown in **Scheme 6.10**. Data were calibrated and normalized from the stock solution before analysis. Concentrations too small to be integrated reliably were not determined (n.d.). Enantiomeric excess was calculated by Eq. 6.1, conversion (*c*) by Eq. 6.32 and Selectivity by Eq. 6.25.

Run	time [min]	UV-Absorbance HPLC (λ = 285 nm), raw data [mAUs]								Enantioselectivity NpEtOH 1b				Enantioselectivity PhantEtOH 1c			
		R-NpEtOiPr (R)-**4b**	S-NpEtOiPr (S)-**4b**	R-Phant-EtOiPr (R)-**4c**	S-Phant-EtOiPr (S)-**4c**	S-NpEtOH (S)-**1b**	R-NpEtOH (R)-**1b**	S-Phant-EtOH (S)-**1c**	R-Phant-EtOH (R)-**1c**	$ee_{product}$	$ee_{substrate}$	*c*	*s*	$ee_{product}$	$ee_{substrate}$	*c*	*s*
1	0	-	-	-	-	2845.0	2842.9	8719.0	8705.4	-	-	-	-	-	-	-	-
1	28	146.1	n.d.	997.7	n.d.	4112.9	4037.7	12545.1	11757.1	n.d.	0.009	n.d.	n.d.	n.d.	0.032	n.d.	n.d.
1	66	279.6	10.4	1913.5	64.2	4803.1	4586.6	14785.1	12938.7	0.928	0.023	2.4%	27.4	0.935	0.066	6.6%	31.9
1	182	634.6	21.3	3904.8	97.8	4144.8	3554.1	13085.0	9342.6	0.935	0.076	7.5%	32.1	0.951	0.166	14.9%	47.0
1	362	561.9	14.9	3283.4	64.4	2197.6	1655.9	6806.8	3468.3	0.948	0.140	12.9%	43.3	0.962	0.324	25.2%	70.1
1	558	1336.8	36.2	6884.4	177.1	3435.6	2156.5	10566.0	3556.0	0.947	0.228	19.4%	46.1	0.950	0.496	34.3%	63.8
1	859	1600.1	43.8	7176.4	213.9	2862.1	1299.1	8759.1	1431.6	0.947	0.375	28.4%	52.9	0.942	0.719	43.3%	72.4
1	1166	2061.8	73.4	8211.9	332.1	2944.2	881.3	8968.0	602.1	0.931	0.539	36.7%	48.3	0.922	0.874	48.7%	71.1
1	1791	2635.9	128.2	8786.0	541.6	2939.5	341.2	8915.5	66.5	0.907	0.792	46.6%	49.8	0.884	0.985	52.7%	78.6
1	3199	2273.9	187.7	6784.2	783.8	2179.6	n.d.	6525.6	n.d.	0.848	n.d.	n.d.	n.d.	0.793	n.d.	n.d.	n.d.

		UV-Absorbance HPLC (λ = 285 nm), raw data [mAUs]								Enantioselectivity NpEtOH 1b				Enantioselectivity PhantEtOH 1c			
Run	time [min]	R-NpEtOiPr (R)-4b	S-NpEtOiPr (S)-4b	R-Phant-EtOiPr (R)-4c	S-Phant-EtOiPr (S)-4c	S-NpEtOH (S)-1b	R-NpEtOH (R)-1b	S-Phant-EtOH (S)-1c	R-Phant-EtOH (R)-1c	$ee_{product}$	$ee_{substrate}$	c	s	$ee_{product}$	$ee_{substrate}$	c	s
2	0	-	-	-	-	4674.7	4808.4	14867.1	14587.7	-	-	-	-	-	-	-	-
2	35	125.7	n.d.	828.7	n.d.	2642.8	2594.4	8359.4	7487.4	n.d.	0.023	n.d.	n.d.	n.d.	0.046	n.d.	n.d.
2	74	206.8	n.d.	1343.0	n.d.	2261.1	2114.0	7072.3	5777.0	n.d.	0.048	n.d.	n.d.	n.d.	0.091	n.d.	n.d.
2	198	711.6	14.1	4295.3	66.2	3521.4	2903.1	11103.3	6698.0	0.960	0.110	10.3%	54.7	0.970	0.239	19.7%	83.5
2	360	1090.2	22.2	5983.2	100.1	3331.1	2318.6	10405.0	4306.3	0.959	0.193	16.7%	57.5	0.968	0.407	29.6%	90.9
2	510	1529.6	38.0	7750.4	170.6	3518.1	2078.5	11073.9	3073.0	0.950	0.270	22.1%	51.0	0.958	0.559	36.9%	81.4
2	2982	2828.8	207.8	8661.2	831.6	2738.0	n.d.	8402.6	n.d.	0.859	n.d.	n.d.	n.d.	0.828	n.d.	n.d.	n.d.

Table 6.16. Chemoselectivity values for the two fast reacting and the two slow reacting enantiomers for the competition experiment shown in **Scheme 6.10**. To minimize influence of analytical errors, only data points with at minimum 4% and maximal 96% conversion (*c*) for both substrates are analysed. Selectivity was derived as described in Chapter 6.1.8.

Run	time [min]	c (R)-1b	c (R)-1c	total c	Chemosel	Select	StDev	Run	time [min]	c (S)-1b	c (S)-1c	total c	Chemosel	Select	StDev
1	66	5.9%	13.4%	9.6%	0.387	2.4		1	1791	4.3%	6.0%	5.1%	0.162	1.4	
1	182	15.5%	30.4%	23.0%	0.323	2.1		1	3199	8.1%	11.1%	9.6%	0.155	1.4	
1	362	25.9%	49.7%	37.8%	0.315	2.3		2	2982	7.3%	9.4%	8.3%	0.127	1.3	
1	558	39.0%	66.9%	52.9%	0.264	2.2		-							
1	859	55.9%	84.0%	69.9%	0.200	2.2		-							
1	1166	70.7%	93.4%	82.1%	0.139	2.2		-							
2	74	9.2%	19.5%	14.3%	0.362	2.3		-							
2	198	20.2%	40.1%	30.1%	0.331	2.3		-							
2	360	32.6%	59.2%	45.9%	0.289	2.3		-							
					average	2.2	0.043						average	1.3	0.042
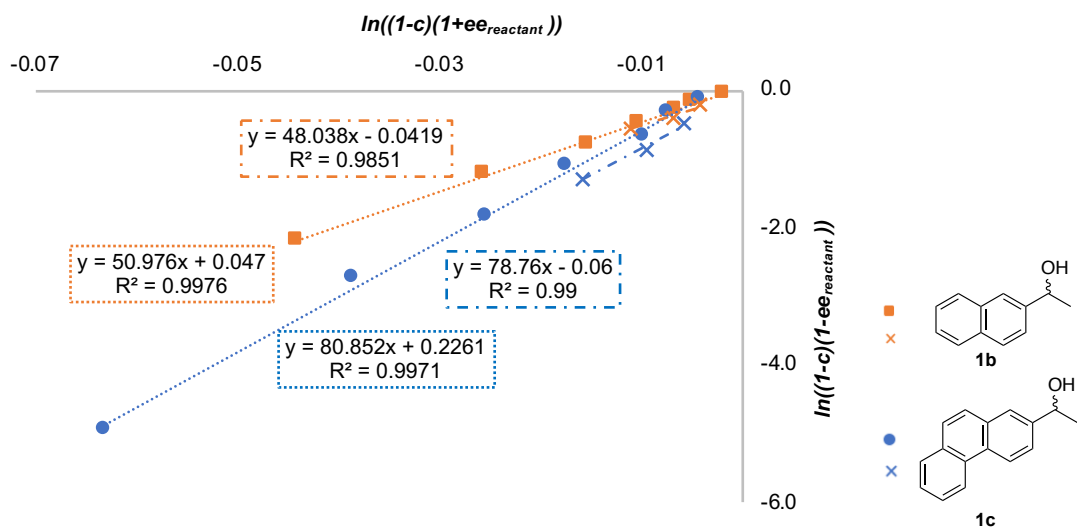
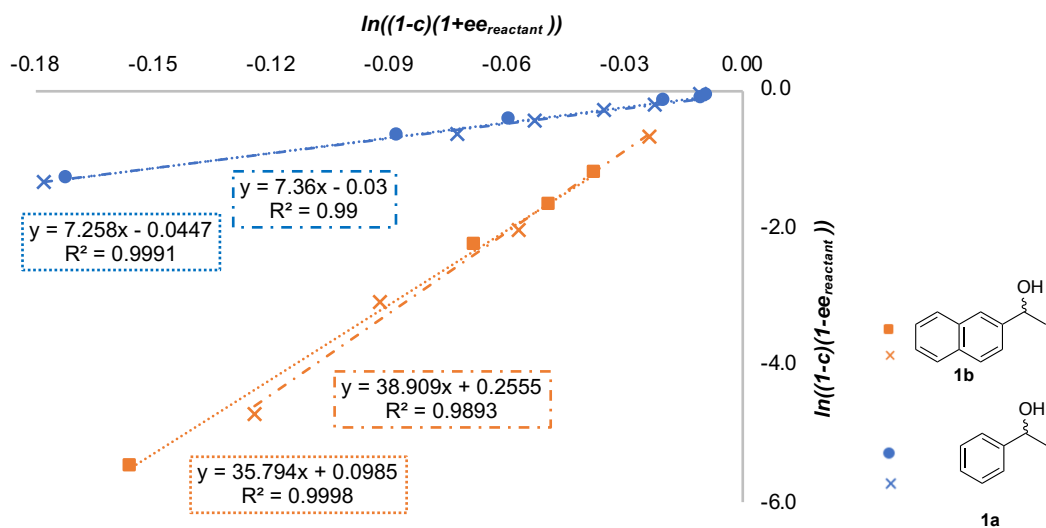**Figure 6.14**. Linear regression analysis of two independent runs of competition experiment shown in **Scheme 6.10**.
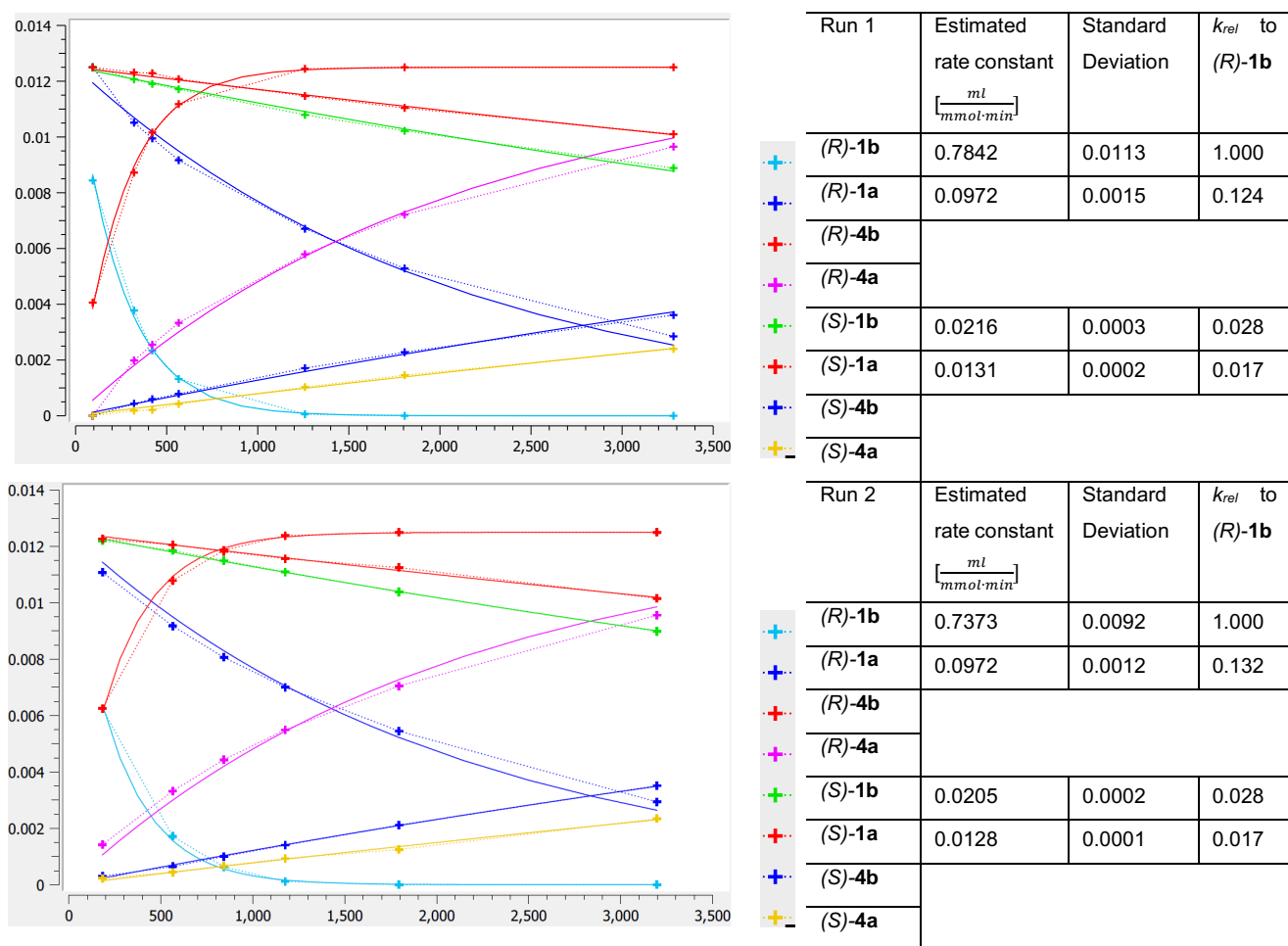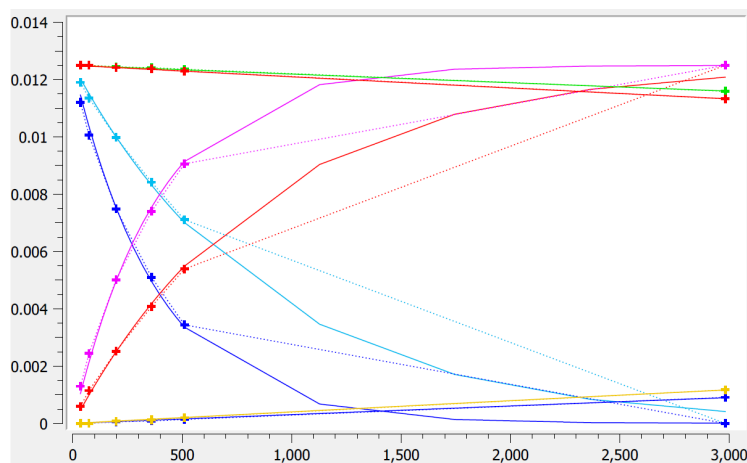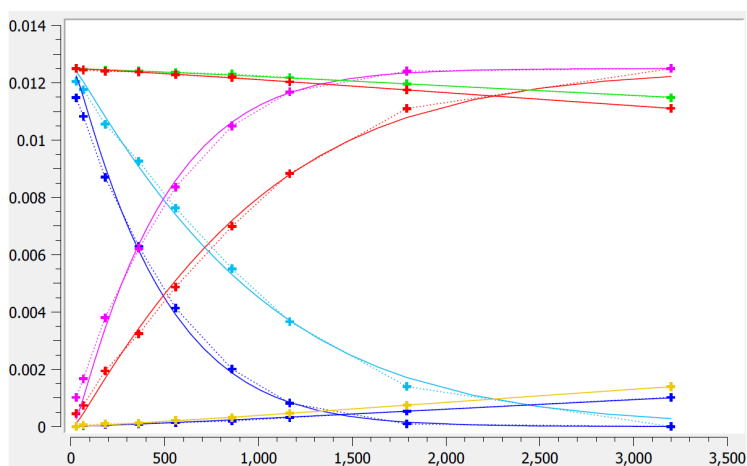

Run 1	Estimated rate constant $\left[\frac{ml}{mmol \cdot min}\right]$	Standard Deviation	k_{rel} to (R)-**1b**
(R)-**1b**	0.2651	0.0080	1.000
(R)-**1c**	0.5878	0.0212	2.217
(R)-**4b**			
(R)-**4c**			
(S)-**1b**	0.0058	0.0001	0.022
(S)-**1c**	0.0082	0.0001	0.031
(S)-**4b**			
(S)-**4c**			

Run 2	Estimated rate constant $\left[\frac{ml}{mmol \cdot min}\right]$	Standard Deviation	k_{rel} to (R)-**1b**
(R)-**1b**	0.2293	0.0060	1.000
(R)-**1c**	0.5210	0.0141	2.272
(R)-**4b**			
(R)-**4c**			
(S)-**1b**	0.0050	0.0001	0.022
(S)-**1c**	0.0066	0.0001	0.029
(S)-**4b**			
(S)-**4c**			

Figure 6.15. Parameter estimation for competition experiment shown in **Scheme 6.10**. Estimation was performed with CoPaSi[5], x-axis shows time in min, y-axis intermediate concentration in mol/L of each species. Estimated rate constants with standard deviation for each alcohol are shown right hand.
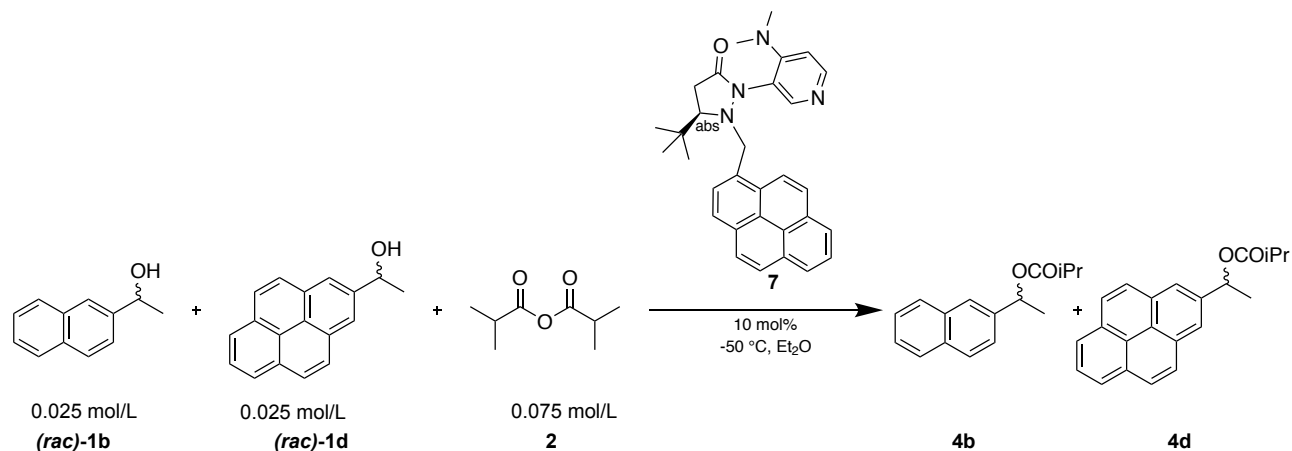
Scheme 6.11. Competitive linear regression of (*rac*)-1-(2-naphthyl)ethanol (**1b**) (NpEtOH) and (*rac*)-1-(2-pyrenyl)ethanol (**1d**) (PyrEtOH) yielding **4b** (NpEtOiPr) and **4a** (PyrEtOiPr) with catalyst **7**.

Table 6.17. Raw HPLC absorbance data for competitive linear regression shown in **Scheme 6.11**. Data were calibrated and normalized from the stock solution before analysis. Concentrations too small to be integrated reliably were not determined (n.d.). Enantiomeric excess was calculated by Eq. 6.1, conversion (*c*) by Eq. 6.32 and Selectivity by Eq. 6.25.

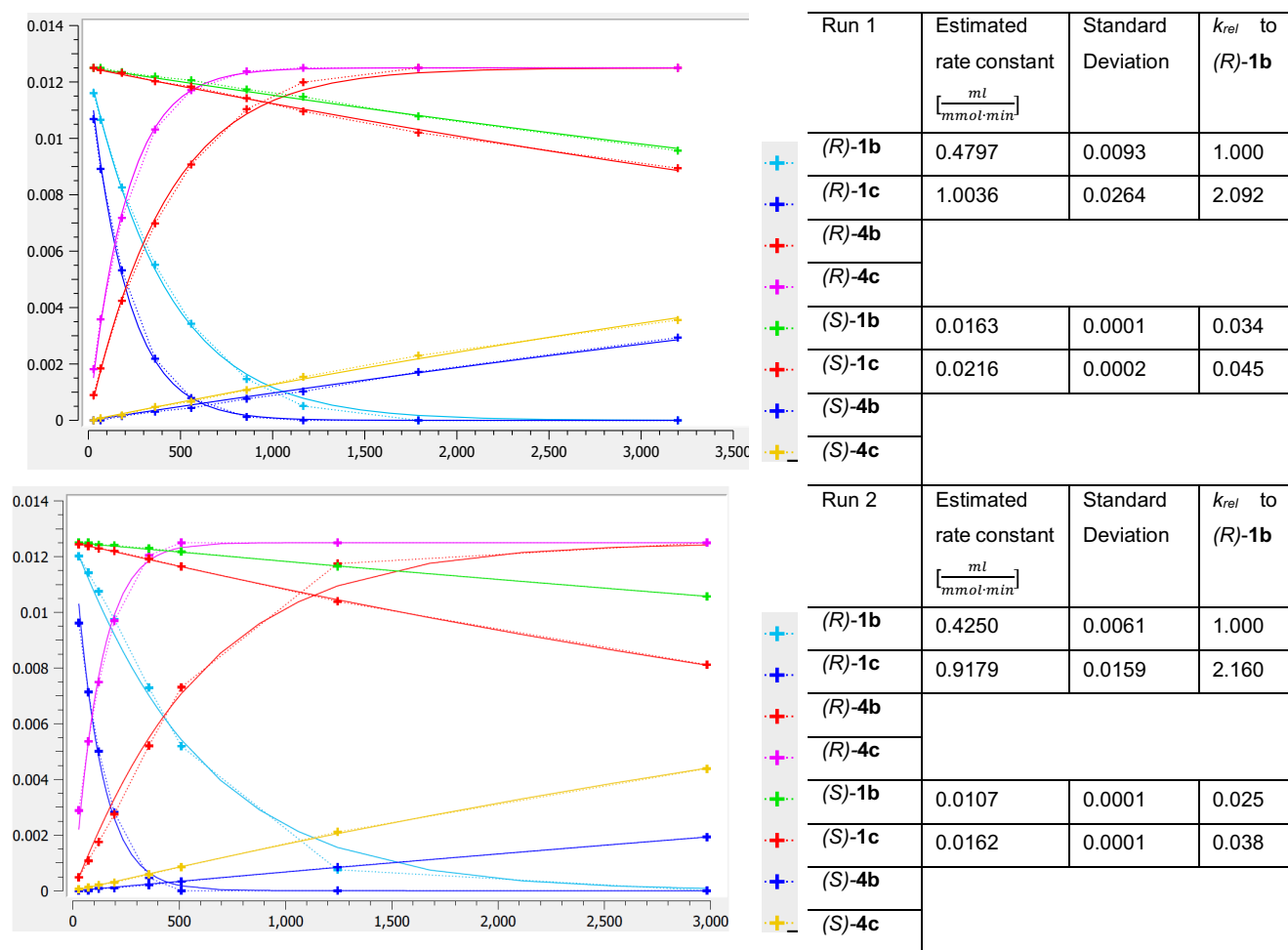| Run	time [min]	UV-Absorbance HPLC (λ = 285 nm), raw data [mAUs]								Enantioselectivity NpEtOH 1b				Enantioselectivity PyrEtOH 1d			
		R-NpEtOiPr (R)-**4b**	S-NpEtOiPr (S)-**4b**	R-PyrEtOiPr (R)-**4d**	S-PyrEtOiPr (S)-**4d**	S-NpEtOH (S)-**1b**	R-NpEtOH (R)-**1b**	S-PyrEtOH (S)-**1d**	R-PyrEtOH (R)-**1d**	$ee_{product}$	$ee_{substrate}$	*c*	S	$ee_{product}$	$ee_{substrate}$	*c*	S
1	0	-	-	-	-	5978.9	5985.5	7365.4	7703.8	-	-	-	-	-	-	-	-
1	25	69.6	n.d.	536.5	n.d.	3555.5	3485.0	4569.7	4229.6	n.d.	0.011	n.d.	n.d.	n.d.	0.061	n.d.	n.d.
1	64	79.7	n.d.	575.2	n.d.	2183.1	2109.0	2933.4	2432.3	n.d.	0.018	n.d.	n.d.	n.d.	0.116	n.d.	n.d.
1	119	219.7	7.4	1576.7	16.8	3679.0	3458.1	4713.4	3321.3	0.935	0.032	3.3%	30.5	0.978	0.195	16.6%	108.6
1	178	242.4	7.3	1535.1	18.0	2664.1	2428.9	3511.7	1993.8	0.942	0.047	4.7%	34.9	0.976	0.296	23.3%	109.2
1	366	614.3	19.2	2841.8	30.8	3089.6	2516.0	3995.4	962.7	0.939	0.103	9.9%	35.3	0.978	0.626	39.0%	168.1
1	566	1118.2	26.2	3529.8	55.1	3217.2	2135.1	4154.8	239.8	0.954	0.203	17.5%	51.9	0.968	0.895	48.1%	187.2
1	854	1692.6	47.3	3454.6	82.1	3001.9	1317.3	3877.5	13.5	0.946	0.390	29.2%	52.4	0.951	0.993	51.1%	228.5
1	1174	2357.8	73.0	3657.2	145.4	3170.2	810.2	4046.2	n.d.	0.940	0.593	38.7%	59.0	0.920	n.d.	n.d.	n.d.

		UV-Absorbance HPLC (λ = 285 nm), raw data [mAUs]								Enantioselectivity NpEtOH 1b				Enantioselectivity PyrEtOH 1d			
Run	time [min]	R-NpEtOiPr *(R)*-**4b**	S-NpEtOiPr *(S)*-**4b**	R-PyrEtOiPr *(R)*-**4d**	S-PyrEtOiPr *(S)*-**4d**	S-NpEtOH *(S)*-**1b**	R-NpEtOH *(R)*-**1b**	S-PyrEtOH *(S)*-**1d**	R-PyrEtOH *(R)*-**1d**	$ee_{product}$	$ee_{substrate}$	*c*	S	$ee_{product}$	$ee_{substrate}$	*c*	S
1	1789	3451.3	151.2	4256.9	313.4	3655.0	258.4	4573.6	n.d.	0.916	0.868	48.7%	64.5	0.857	n.d.	n.d.	n.d.
1	4688	3178.5	401.8	3700.9	774.0	2907.0		3511.1	n.d.	0.775	n.d.	n.d.	n.d.	0.641	n.d.	n.d.	n.d.
2	0	-	-	-	-	3622.7	3810.1	5121.0	5283.3	-	-	-	-	-	-	-	-
2	28	64.5	n.d.	522.0	n.d.	2500.2	2570.4	3645.3	3184.9	n.d.	0.011	n.d.	n.d.	n.d.	0.083	n.d.	n.d.
2	72	113.4	n.d.	880.9	n.d.	1988.6	2006.6	2970.1	2132.3	n.d.	0.021	n.d.	n.d.	n.d.	0.179	n.d.	n.d.
2	124	178.1	4.9	1270.6	16.8	1860.5	1788.9	2771.1	1525.8	0.944	0.045	4.5%	36.1	0.973	0.304	23.8%	98.5
2	197	262.1	5.2	1641.8	18.4	1952.0	1803.6	2911.1	1211.2	0.959	0.065	6.3%	51.0	0.977	0.425	30.3%	131.5
2	358	382.0	7.3	1765.1	25.4	1524.9	1204.6	2302.9	342.5	0.961	0.142	12.9%	57.5	0.971	0.748	43.5%	152.4
2	509	1253.9	29.2	4148.7	64.1	3385.2	2318.2	4781.9	224.0	0.952	0.211	18.2%	50.2	0.969	0.913	48.5%	202.5
2	1247	2890.6	86.2	4439.2	201.3	3570.8	756.1	4871.5	n.d.	0.939	0.665	41.4%	63.8	0.911	n.d.	n.d.	n.d.
2	2980	2743.6	181.4	3569.0	390.3	2649.9	n.d.	3647.1	n.d.	0.870	n.d.	n.d.	n.d.	0.797	n.d.	n.d.	n.d.

Table 6.18. Chemoselectivity values for the two fast reacting and the two slow reacting enantiomers for the competition experiment shown in **Scheme 6.11**. To minimize influence of analytical errors, only data points with at minimum 4% and maximal 96% conversion (*c*) for both substrates are analysed. Selectivity was derived as described in Chapter 6.1.8.

| Run	time [min]	*c (R)*-**1b**	*c (R)*-**1d**	total *c*	Chemosel	Select	StDev	Run	time [min]	*c (S)*-**1b**	*c (S)*-**1d**	total *c*	Chemosel	Select	StDev
1	119	6.1%	34.5%	20.3%	0.699	6.7		1	1789	4.1%	7.1%	5.6%	0.268	1.8	
1	178	9.3%	46.0%	27.6%	0.664	6.3		1	4688	12.4%	19.6%	16.0%	0.225	1.6	
1	366	20.0%	76.6%	48.3%	0.586	6.5		2	2980	6.6%	10.6%	8.6%	0.235	1.7	
1	566	34.9%	94.2%	64.6%	0.459	6.6		-							
2	72	5.5%	31.4%	18.4%	0.703	6.7		-							
2	124	9.3%	48.0%	28.6%	0.676	6.7		-							
2	197	13.0%	60.0%	36.5%	0.645	6.6		-							
2	358	24.5%	85.1%	54.8%	0.552	6.8		-							
				average	6.6	0.133						**average**	1.7	0.053	
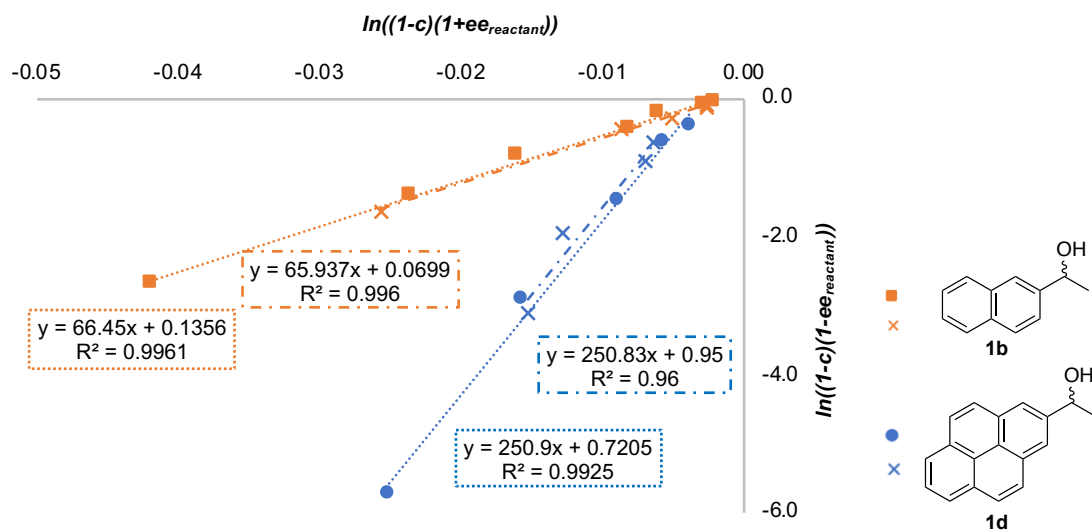
Figure 6.16. Linear regression analysis of two independent runs of competition experiment shown in **Scheme 6.11**.
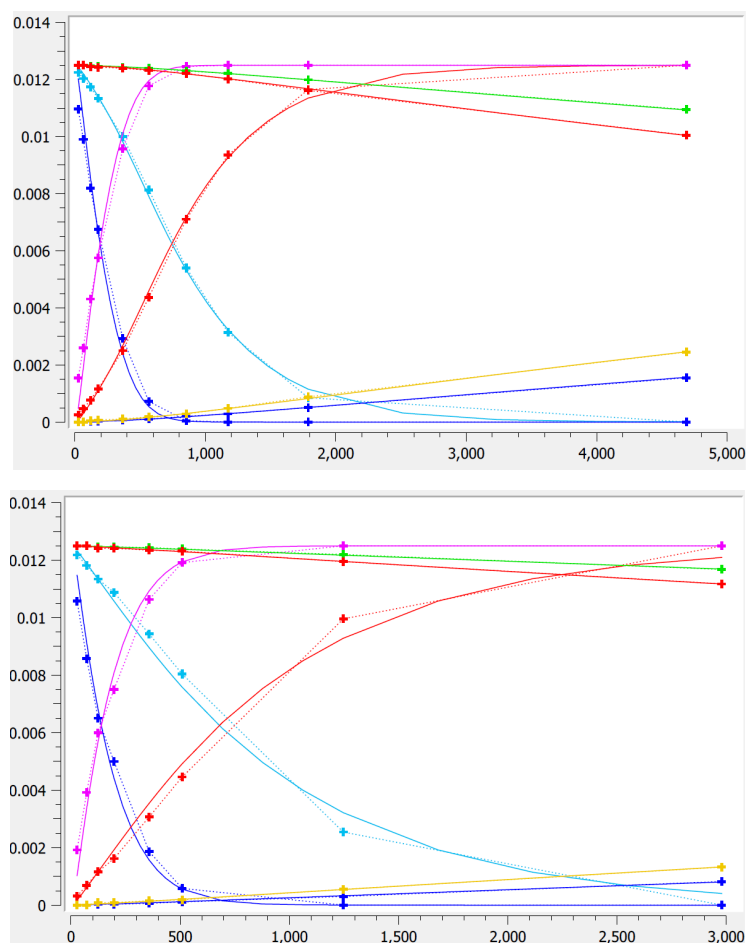
Run 1	Estimated rate constant $[\frac{ml}{mmol \cdot min}]$	Standard Deviation	k_{rel} to (R)-**1b**
(R)-**1b**	0.3780	0.0127	1.000
(R)-**1d**	2.5936	0.1390	6.860
(R)-**4b**			
(R)-**4d**			
(S)-**1b**	0.0066	0.0001	0.017
(S)-**1d**	0.0108	0.0001	0.029
(S)-**4b**			
(S)-**4d**			

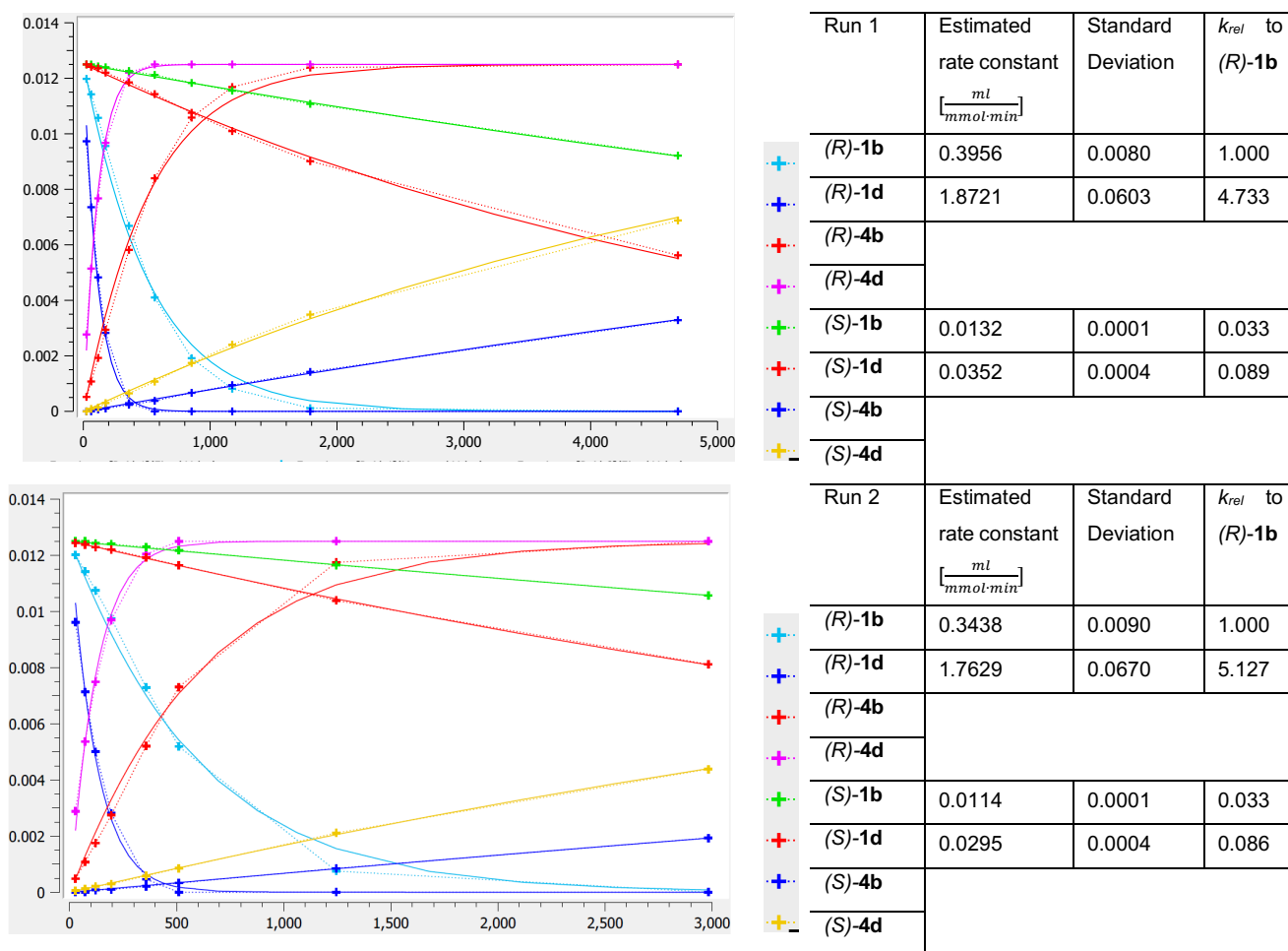| Run 2	Estimated rate constant $[\frac{ml}{mmol \cdot min}]$	Standard Deviation	k_{rel} to (R)-**1b**
(R)-**1b**	0.2433	0.0093	1.000
(R)-**1d**	1.5163	0.0898	6.232
(R)-**4b**			
(R)-**4d**			
(S)-**1b**	0.0047	0.0001	0.019
(S)-**1d**	0.0080	0.0001	0.033
(S)-**4b**			
(S)-**4d**			

Figure 6.17. Parameter estimation for competition experiment shown in **Scheme 6.11**. Estimation was performed with CoPaSi[5], x-axis shows time in min, y-axis intermediate concentration in mol/L of each species. Estimated rate constants with standard deviation for each alcohol are shown right hand.

6.2.5. From Experimental Data to Relative Rates

Through experiments and chiral HPLC analysis described in Chapter 6.2.1 intermediate concentrations of eight species can be followed over the course of a reaction. **Scheme 6.12** gives an overview of those species and the possible selectivity values that can be gathered.
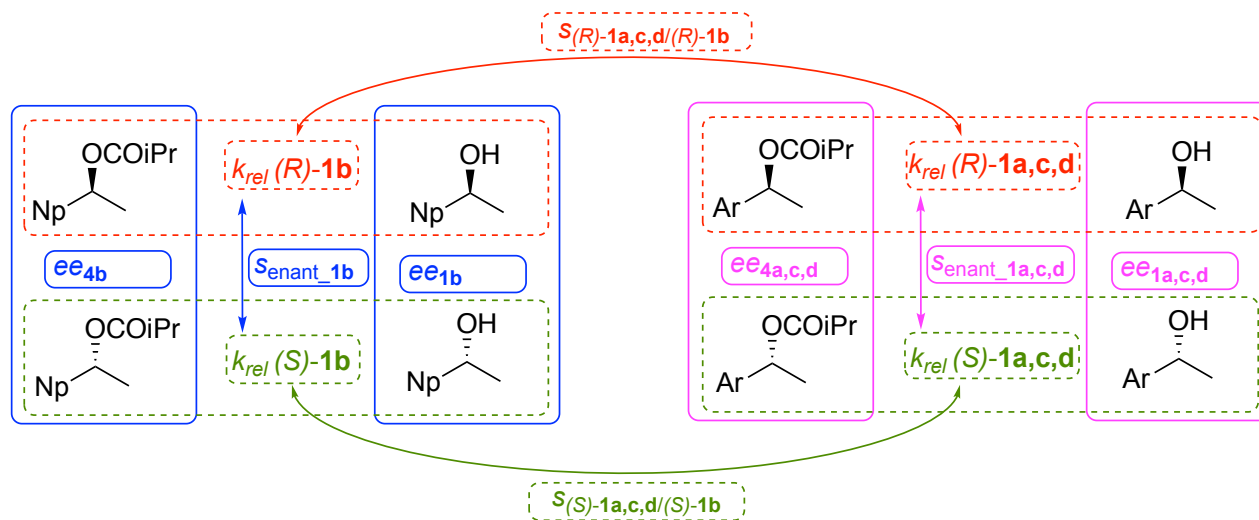
Scheme 6.12. Overview of different approaches to analyse reaction mixtures gained by competitive linear regression experiments as described in Chapter 6.2.1.

1. **Enantioselectivity:** (blue and pink boxes in **Scheme 6.12**): Enantioselectivity values for each alcohol can be calculated by linear regression (see Chapter 6.1.6) from *ee* values of substrates and products. This gives the enantioselectivity of 1-(2-naphthyl)ethanol **1b** (s_{enant_1b}, blue lines in **Scheme 6.12**) and for the competing alcohol ($s_{enant\_1a,c,d}$, pink lines in **Scheme 6.12**). As several conversion points are used in linear regression, gained enantioselectivity values are more reliable than those of single point kinetic resolution measurements.

2. **Chemoselectivity:** Chemoselectivity of two different alcohols can be gained as outlined in Chapter 6.1.8 from individual conversion values of enantiopure alcohols. This value is gathered at different total conversions and averaged. In principle chemoselectivity could be obtained for each pair of enantiopure alcohols in the system. However, relative rates are most reliable for reactions that occur with comparable rates (the same error considerations as outlined for kinetic resolution in Chapter 6.1.5 become significant for cases if reaction rates differ too much). Thus, reliable chemoselectivity values can be gained for the two fast reacting enantiomers in relation to each other ($s_{(R)-1a,c,d/(R)-1b}$, red lines in **Scheme 6.12**) and for the two slow reacting enantiomers vice versa ($s_{(S)-1a,c,d/((S)-1b}$, green lines in **Scheme 6.12**). However, for the slow enantiomers experimental data are less reliable as reactions cannot be followed to full conversion without significant experimental errors due to the slow absolute reaction rates (as outlined in Chapter 6.1.2).

Combining the different selectivity values as shown in Eq. 6.42 - Eq. 6.46 leads to comparable relative rate values for all species:

$$k_{rel}\big((R)\text{-}\mathbf{1b}\big) = 1 \qquad\qquad \text{Eq. 6.42}$$

$$k_{rel}\big((S)\text{-}\mathbf{1b}\big) = \frac{1}{s_{enant\_\mathbf{1b}}} \qquad\qquad \text{Eq. 6.43}$$

$$k_{rel}\big((R)\text{-}\mathbf{1a,c,d}\big) = s_{(R)-\mathbf{1a,c,d}/(R)-\mathbf{1b}} \qquad\qquad \text{Eq. 6.44}$$

$$k_{rel}\big((S)\text{-}\mathbf{1a,c,d}\big) = \frac{k_{rel}\big((R)\text{-}\mathbf{1a,c,d}\big)}{s_{enant\_\mathbf{1a,c,d}}} \qquad\qquad \text{Eq. 6.45}$$

$$k_{rel}\big((S)\text{-}\mathbf{1a,c,d}\big) = k_{rel}\big((S)\text{-}\mathbf{1b}\big) \cdot s_{(S)-\mathbf{1a,c,d}/(S)-\mathbf{1b}} \qquad\qquad \text{Eq. 6.46}$$

As a reference the rate for *(R)*-**1b** is set to 1. The relative rate for *(S)*-**1b** can be directly calculated by the enantioselectivity value by Eq. 6.43 (blue line in **Scheme 6.12**). As this enantioselectivity value was obtained by repeated independent methods (see Chapter 1) it is reliable. The chemoselectivity for the two fast reacting enantiomers (red line in **Scheme 6.12**) can also be measured reliably and the relative rate of the fast reacting enantiomer of the second alcohol can thus be calculated by Eq. 6.44. This gives two possibilities to calculate relative rates for the slow enantiomer of the competing alcohol: It can either be calculated by the enantioselectivity with Eq. 6.45 from the relative rate of the corresponding fast enantiomer (red line and then pink line in **Scheme 6.12**) or by the chemoselectivity relative to *(S)*-**1b** by Eq. 6.46 (blue line and then green line in **Scheme 6.12**). Those two pathways are largely independent as enantioselectivity values by linear regression are mainly calculated from conversion values smaller than 52 %, while for the chemoselectivity of the slower enantiomers measuring points with more than 50% conversion are needed.

A third method of analysis is a simulation of the reaction curse giving directly all relative rates as described in Chapter 6.1.7.

All three analysis methods were performed with all experiments as shown in Chapter 6.2.4. All results and the resulting selectivity values are compiled on the following pages and discussed below.
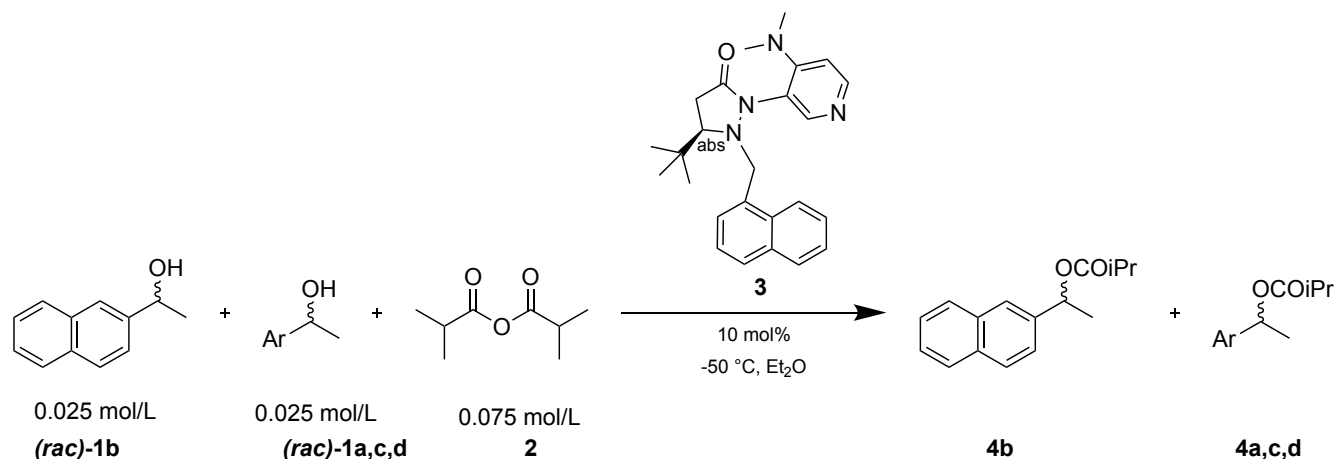
Scheme 6.13. Competitive linear regression of (*rac*)-1-(2-naphthyl)ethanol (**1b**) with aromatic alcohol **1a** - **1d** with catalyst **3**.

Table 6.19. Rates for the reaction shown in **Scheme 6.13** relative to *(R)*-1-(2-naphthyl)ethanol (**1b**) calculated by different pathways with colour code as defined in **Scheme 6.12**. Standard deviations are derived from two independent runs.

Pathway	Rates relative to (R)-NpEtOH (R)-1b								Enantioselectivity			
	(S)-PhEtOH (S)-1a	(S)-NpEtOH (S)-1b	(S)-PhantEtOH (S)-1c	(S)-Pyr EtOH (S)-1d	(R)-PhEtOH (R)-1a	(R)-Np EtOH (R)-1b	(R)-Phant EtOH (R)-1c	(R)-Pyr EtOH (R)-1d	Ph EtOH 1a	Np EtOH 1b	PhantEtOH 1c	PyrEtOH 1d
1 via $S_{enant\text{-}1b}$ (blue[a]), $S_{R\text{-}1a,c,d/R\text{-}1b}$(red[a]), $S_{S\text{-}1ac,d/S\text{-}1b}$ (green[a])	0.0166 ±0.0004 (Eq. 6.46)	0.0259 ±0.0007 (Eq. 6.43)	0.0356 ±0.0006 (Eq. 6.46)	0.0682 ±0.0027 (Eq. 6.46)	0.1443 ±0.0069 (Eq. 6.44)	1	2.1421 ±0.0387 (Eq. 6.44)	5.9068 ±0.2308 (Eq. 6.44)	8.8 ±0.58	38.6 ±1.00	58.3 ±1.73	87.0 ±6.33
2 via $S_{enant\text{-}1b}$ (blue[a]), $S_{R\text{-}1ac,d/R\text{-}1b}$(red[a]), $S_{enant\_1a,c,d}$(pink[a])	**0.0197 ±0.0007 (Eq. 6.45)**	**0.0259 ±0.0007 (Eq. 6.43)**	**0.0402 ±0.0013 (Eq. 6.45)**	**0.0900 ±0.0007 (Eq. 6.45)**	**0.1443 ±0.0069 (Eq. 6.44)**	**1**	**2.1421 ±0.0387 (Eq. 6.44)**	**5.9068 ±0.2308 (Eq. 6.44)**	**7.3 ±0.05**	**38.6 ±1.00**	**53.3 ±2.40**	**65.7 ±1.70**
S CoPaSi simulation	0.0170 ±0.0003	0.0302 ±0.0034	0.0416 ±0.0034	0.0874 ±0.0016	0.1279 ±0.0040	1	2.1261 ±0.0338	4.9300 ±0.1971	7.5 ±0.10	33.6 ±3.89	51.1 ±5.03	56.4 ±3.28

[a]colours refer to the pathways depicted in **Scheme 6.12**.
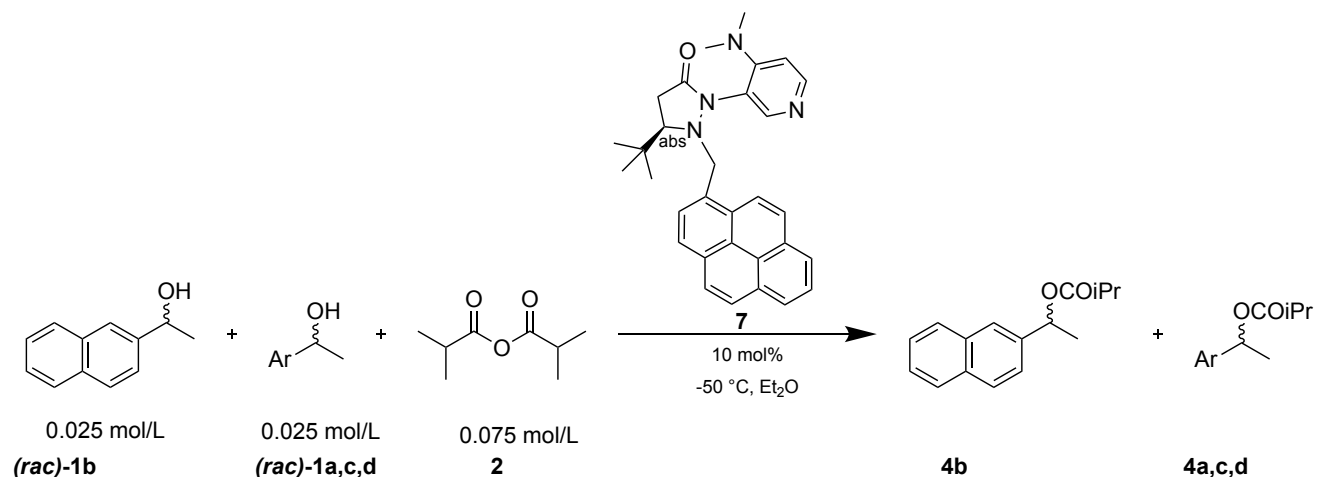
Scheme 6.14. Competitive linear regression of (*rac*)-1-(2-naphthyl)ethanol (**1b**) with aromatic alcohol **1a** - **1d** with catalyst **7**.

Table 6.20. Rates for the reaction shown in **Scheme 6.14** relative to *(R)*-1-(2-naphthyl)ethanol (**1b**) calculated by different pathways as shown in **Scheme 6.12**. Standard deviations are derived from two independent runs.

| Pathway | Rates relative to *(R)*-NpEtOH *(R)*-**1b** | | | | | | | | Enantioselectivity | | | |
	(S)-PhEtOH (S)-**1a**	(S)-NpEtOH (S)-**1b**	(S)-PhantEtOH (S)-**1c**	(S)-PyrEtOH (S)-**1d**	(R)-PhEtOH (R)-**1a**	(R)-NpEtOH (R)-**1b**	(R)-PhantEtOH (R)-**1c**	(R)-PyrEtOH (R)-**1d**	PhEtOH **1a**	NpEtOH **1b**	PhantEtOH **1c**	PyrEtOH **1d**
1 via $S_{enant-1b}$ (blue[a]), $S_{R-1a,c,d/R-1b}$(red[a]), $S_{S-1ac,d/S-1b}$ (green[a])	0.0145 ±0.0005 (Eq. 6.46)	0.0198[b] ±0.0004 (Eq. 6.43)	0.0272 ±0.0001 (Eq. 6.46)	0.0255 ±0.0003 (Eq. 6.46)	0.1491 ±0.0054 (Eq. 6.44)	1	2.2430 ±0.0433 (Eq. 6.44)	6.6180 ±0.1325 (Eq. 6.44)	10.6 ±0.04	50.5[b] ±1.03	82.8 ±0.66	261.1 ±6.20
2 via $S_{enant-1b}$ (blue[a]), $S_{R-1ac,d/R-1b}$(red[a]), $S_{enant\_1a,c,d}$(pink[a])	**0.0161 ±0.0008 (Eq. 6.45)**	**0.0198[b] ±0.0022 (Eq. 6.43)**	**0.0281 ±0.0005 (Eq. 6.45)**	**0.0264 ±0.0003 (Eq. 6.45)**	**0.1491 ±0.0054 (Eq. 6.44)**	**1**	**2.2430 ±0.0433 (Eq. 6.44)**	**6.6180 ±0.1325 (Eq. 6.44)**	**9.3 ±0.17**	**50.5[b] ±1.03**	**79.8 ±1.05**	**250.9 ±0.04**
S CoPaSi simulation	0.0153 ±0.0000	0.0203 ±0.0016	0.0299 ±0.0011	0.0306 ±0.0021	0.1377 ±0.0027	1	2.2447 ±0.0275	6.5464 ±0.3141	9.0 ±0.20	49.6 ±4.09	75.3 ±3.77	215.4 ±24.8

[a]colours refer to the pathways depicted in **Scheme 6.12**. [b]without value (s = 66) from competition experiment with PyrEtOH **1d** (Table 6.17) as discussed below.
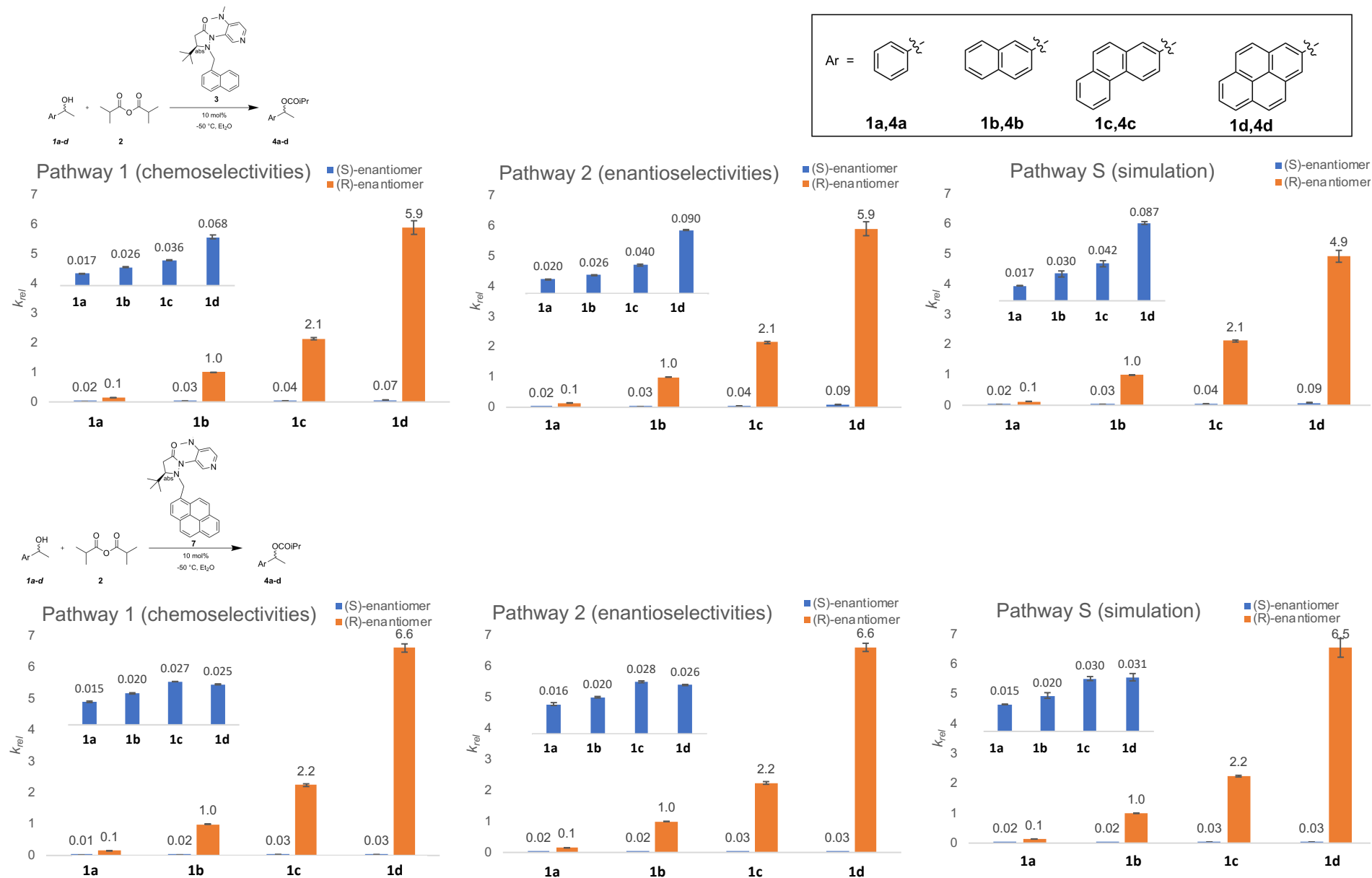
Figure 6.18. Overview of resulting relative rate constants for the different alcohols via different pathways of analysis as described in **Table 6.19** and **Table 6.20**.

6.2.6.Reliability estimation of relative rates

The gathered data allow now to validate the different methods to determine relative rates and enantioselectivity values:

- Single point kinetic resolution: Enantioselectivity values obtained by the Kagan formulas for a single point (reported in **Table 6.7** to **Table 6.18**) are – as expected – very dependent on the conversion especially for high selectivity values. As an example, in **Table 6.17** enantioselectivity values vary from s = 109 (conversion 16.6%) to s = 229 (conversion 51.5%). However, values obtained close to 50% conversion are at least comparable with values obtained from linear regression experiments.

- Linear regression: Root mean square values (0.985 – 0.999) as well as small intercepts from 0 indicate in all experiments with a selectivity value < 100 a very good linear fit. Even for selectivity values > 200 (see **Figure 6.16**) good root mean square values (0.960 - 0.993) and acceptable intercepts were found. Reproducibility of slopes (=selectivity values) in independent experiments is good. Relative standard deviations for the two independent runs are in the range of 0.1% to 3.0% except for the experiment shown in **Figure 6.8** (relative standard deviation of 5.9%). As all discussed differences in this project are far above those deviations linear regression values can be used as valid descriptors.

- Competitive linear regression: It must be excluded, that the changed experimental environment through the addition of a second alcohol to the reaction mixture in linear regression experiments impacts the selectivity of the reaction. As a measure of quality the selectivity values for the acylation of 1-(2-naphthyl)ethanol **1b** with catalyst **3** can be used. The literature value for kinetic resolution (s = 37)[3], standard kinetic resolution experiments (s = 37.0, see Chapter 6.1.3), the result of independent single-alcohol linear regression (s = 38.5 ± 1.25, see Chapter 6.1.6) and values reported for the different competitive linear regression experiments above (s = 38.9 ± 0.98 in competition with PyrEtOH **1d**, s = 39.8 ± 2.41 in competition with PhantEtOH **1c**, s = 37.4 ± 1.56 in competition with PhEtOH **1a**) are in good agreement. Similarly, selectivity values for 1-(2-naphthyl)ethanol (**1b**) with catalyst **7** are in good agreement for the competition experiments with PhEtOH (**1a**) (s = 51.6 ± 1.50) and PhantEtOH (**1c**) (s = 49.5 ± 1.47). However, in the highly selective competitive linear regression experiment with PyrEtOH (**1d**) a slightly higher selectivity value of s = 66.2 ± 0.26 was measured. As those values were reproducible in independent experiments, it is likely that the changed reaction environment influences the selectivity for **1b** slightly, which could be explained by the changed polarity of the solvent-substrate mixture (see Chapter 6.4.6). Thus, that value was dismissed for the enantioselectivity of **1b** with catalyst **7** to guarantee comparable reaction conditions in all cases.

- There are two pathways to determine relative rates for the slower *(S)*-enantiomer as shown in **Scheme 6.12**. For all experiments calculation of relative rates by the chemoselectivity of

the slower enantiomer relative to *(S)*-NpEtOH (**1b**) (first row in **Table 6.19** and **Table 6.20**) gives comparable, but slightly higher enantioselectivities than by direct linear regression (second row in **Table 6.19** and **Table 6.20**). Most chemoselectivity values for the slower enantiomer could only be measured for conversion values smaller than 30%. Thus, the relative standard deviation of chemoselectivities for the slow reacting enantiomer is up to 7.9% and the use of linear regression analysis is more reliable. However, general trends are well confirmed by those independent chemoselectivity values.

- Simulation of relative rates with CoPaSi[5]: As outlined above the determination of absolute rates especially at -50 °C and with low concentrations has a significant error margin. Hence, the absolute rates of two independent measurements have relative standard deviations of up to 26.2% even for the fast reacting enantiomer and are therefore not reliable. In contrast, relative standard deviation of relative rates is smaller than 4.8% for the fast reacting enantiomer and for the slow reacting enantiomer smaller than 8.4%. Thus, the enantioselectivity values obtained by simulations have higher standard deviations compared to linear regression methods and differ also from reported values. Despite some deviations, trends for relative rates and enantioselectivity values obtained from simulations are in general also in agreement with the other methods.

In conclusion, data analysis by three different and partially independent methods and independent repetition of experiments proves the reliability of the reported data. Values determined by linear regression (for conversion values smaller than 52%) are in satisfactory agreement with those depicted by chemoselectivity of fast and slow reacting enantiomer with the reference system. Also, simulation of reactions leads to comparable results. The compilation of different data above also indicates that enantioselectivity values of up to 80 can be measured reliably by linear regression in the range of ±5%. For *s* > 200 reliability estimation is not possible in this project as only one system is in that range. However, the values obtained from different analytical methods and two independent runs allow to report values to the nearest 50.

For all cases, standard deviations for independent experiments are by far the lowest by using linear regression analysis. Thus, all numbers discussed in the main text are gathered from those experiments, if not stated differently.

6.2.7. Results with achiral catalysts

As benchmark experiments for the reactivity of the alcohols, relative rates for the acylation were also measured with achiral catalysts DMAP (**5**) and tri(*n*-butyl)phosphane PBu$_3$ (**6**). The reaction setup, data collection (by chiral HPLC analysis) and – as far as meaningful – data analysis was performed as described in the chapters above for chiral catalysts in order to ensure full comparability. **Figure 6.19** gives an overview of results, the tables below report full data of measurements. Reactions catalysed by achiral amine Lewis bases diazabicycloundecene (DBU, **S4**) and diazabicyclooctane (DABCO, **S5**) did not give any conversion. As also reactions with PBu$_3$ (**6**) were found to be very slow, catalyst concentration was increased to 40%. Control measurements at low conversion values with 10% PBu$_3$ (**6**) confirmed that increased catalyst loading does not affect relative rates.
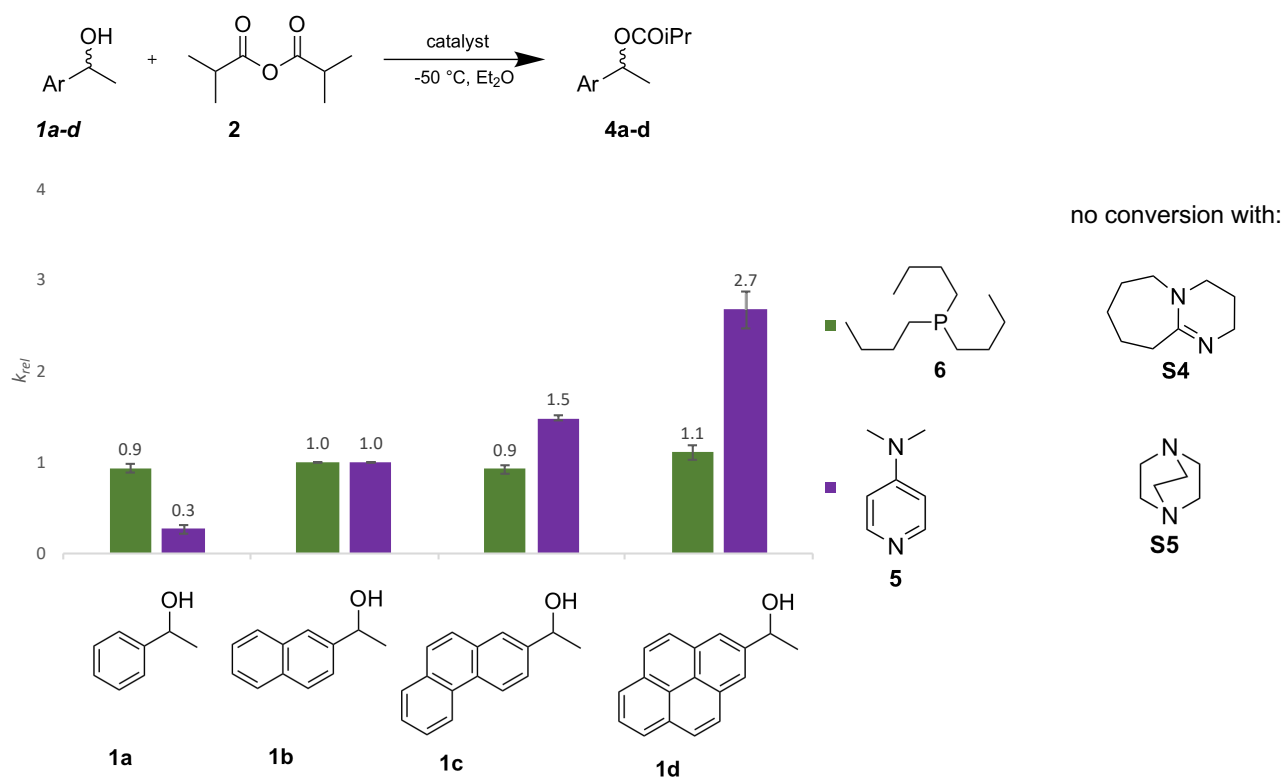
Figure 6.19. Overview of relative rate constants for the acylation of different alcohols with achiral catalysts as described in the tables below.
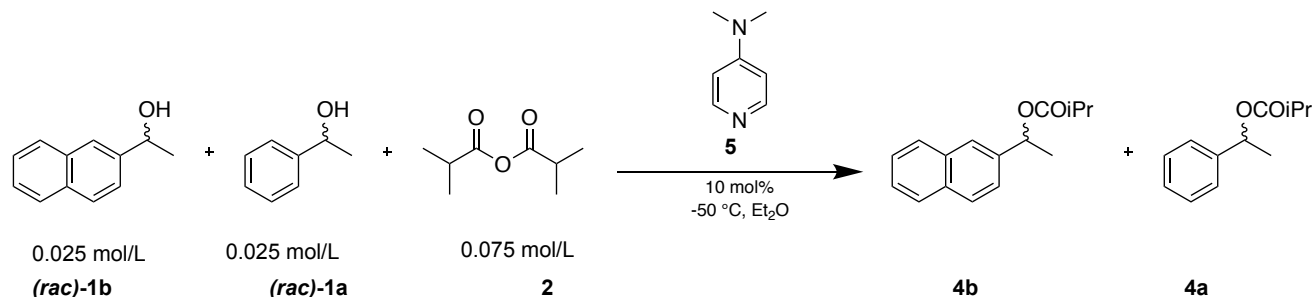
Scheme 6.15. Competition experiment of (*rac*)-1-(2-naphthyl)ethanol (**1b**) and (*rac*)-1-phenylethanol (**1a**) with DMAP (**5**).

Table 6.21. Raw HPLC absorbance data for competitive linear regression shown in **Scheme 6.15**. Data were calibrated and normalized from the stock solution before analysis. To minimize influence of analytical errors selectivities were not determined (n.d.) for points with a conversion lower than 4% or higher than 96% for one substrate. Selectivity was derived as described in Chapter 6.1.8.

Run	time [min]	UV-Absorbance HPLC (λ = 285 nm (naphthyl), (λ = 215 nm (phenyl)), raw data [mAUs]								Chemoselectivity					StDev
		R-PhEtOiPr (*R*)-**4a**	S-PhEtOiPr (*S*)-**4a**	R-NpEtOiPr (*R*)-**4b**	S-NpEtOiPr (*S*)-**4b**	R-PhEtOH (*R*)-**1a**	S-PhEtOH (*S*)-**1a**	S-NpEtOH (*S*)-**1b**	R-NpEtOH (*R*)-**1b**	*c* **1a**	*c* **1b**	total *c*	Chemo-selectivity	*s*	
1	17	635.1	546.6	2048.8	2021.1	6701.5	6804.8	4803.7	4808.6	8.9%	30.4%	19.6%	-0.548	0.26	
1	28	1087.5	1044.6	3384.0	3339.7	7375.9	7508.0	4948.8	4952.6	13.7%	41.2%	27.5%	-0.499	0.28	
1	49	1573.1	1521.9	4427.7	4428.0	7181.5	7279.4	3773.3	3774.6	19.2%	54.7%	37.0%	-0.480	0.27	
1	83	2130.8	2041.5	5238.8	5264.4	6485.9	6591.3	2621.4	2624.6	26.2%	67.4%	46.8%	-0.440	0.27	
1	180	2757.4	2803.0	5458.0	5495.9	4826.7	4859.2	971.6	949.5	39.0%	85.5%	62.2%	-0.374	0.26	
1	304	4127.2	4170.9	7313.5	7289.1	4881.8	4941.6	532.3	525.8	48.4%	93.4%	70.9%	-0.317	0.24	
1	549	3610.0	3672.6	5122.3	5217.5	2601.6	2601.9	97.3	92.1	n.d.	n.d.	n.d.	n.d.	n.d.	
2	0	-	-	-	-	7327.0	7508.6	7359.2	7427.4	-	-	-	-	-	
2	9	588.6	584.7	1995.6	1975.0	7816.2	7974.9	6498.5	6575.2	7.6%	23.8%	15.7%	-0.515	0.29	
2	20	688.6	661.2	2276.6	2220.7	5751.2	5829.1	3770.6	3798.4	11.5%	38.0%	24.7%	-0.536	0.26	
2	31	1274.2	1200.2	3756.4	3769.3	7044.9	7178.9	4276.2	4307.9	16.2%	47.5%	31.8%	-0.491	0.27	
2	66	1748.8	1702.0	4605.6	4651.1	6088.8	6163.8	2632.5	2653.2	23.9%	64.4%	44.1%	-0.459	0.26	
2	127	2210.2	2263.3	5008.6	5042.4	5107.0	5141.4	1420.8	1419.3	32.7%	78.5%	55.6%	-0.412	0.26	

Run	time [min]	UV-Absorbance HPLC (λ = 285 nm (naphthyl), (λ = 215 nm (phenyl)), raw data [mAUs]								Chemoselectivity					
		R-PhEtOiPr (R)-**4a**	S-PhEtOiPr (S)-**4a**	R-NpEtOiPr (R)-**4b**	S-NpEtOiPr (S)-**4b**	R-PhEtOH (R)-**1a**	S-PhEtOH (S)-**1a**	S-NpEtOH (S)-**1b**	R-NpEtOH (R)-**1b**	c **1a**	c **1b**	total c	Chemo-selectivity	s	StDev
2	240	3335.1	3366.2	6279.7	6311.0	4792.5	4827.8	730.8	734.5	43.7%	89.9%	66.8%	-0.346	0.25	
2	467	4014.8	3979.6	5876.3	5996.1	3276.2	3286.3	169.3	163.8	n.d.	n.d.	n.d.	n.d.	n.d.	
													average	0.26	0.013
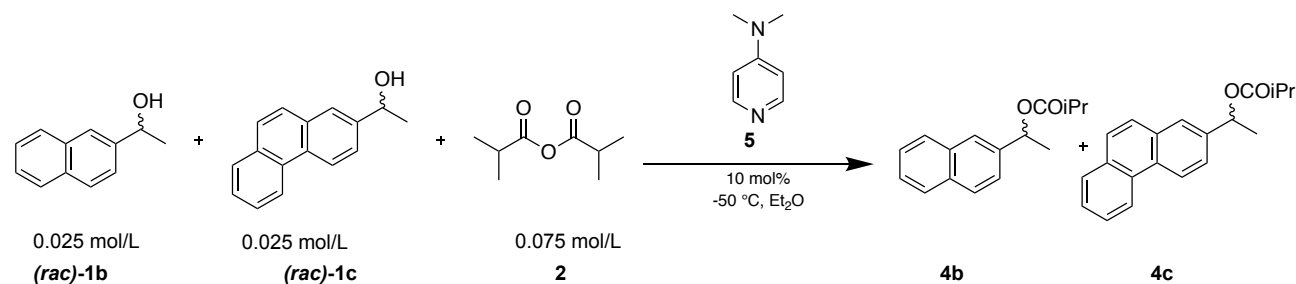
Scheme 6.16. Competition experiment of (*rac*)-1-(2-naphthyl)ethanol (**1b**) and (*rac*)-1-(2-phenanthryl)ethanol (**1c**) with DMAP (**5**).

Table 6.22. Raw HPLC absorbance data for competitive linear regression shown in **Scheme 6.16**. Data were calibrated and normalized from the stock solution before analysis. To minimize influence of analytical errors selectivities were not determined (n.d.) for points with a conversion lower than 4% or higher than 96% for one substrate. Selectivity was derived as described in Chapter 6.1.8.

Run	time [min]	UV-Absorbance HPLC (λ = 285 nm), raw data [mAUs]								Chemoselectivity					
		R-NpEtOiPr (R)-**4b**	S-NpEtOiPr (S)-**4b**	R-Phant-EtOiPr (R)-**4c**	S-Phant-EtOiPr (S)-**4c**	S-NpEtOH (S)-**1b**	R-NpEtOH (R)-**1b**	S-Phant-EtOH (S)-**1c**	R-Phant-EtOH (R)-**1c**	c **1b**	c **1c**	total c	Chemo-selectivity	s	StDev
1	0	-	-	-	-	2845.0	2842.9	8719.0	8705.4	-	-	-	-	-	
1	6	506.3	501.9	2265.9	2240.4	3913.9	3915.1	11432.3	11405.5	11.7%	17.1%	14.4%	0.187	1.50	
1	11	964.1	954.5	4117.8	4154.8	4839.6	4860.3	13753.2	13724.8	16.9%	23.9%	20.4%	0.171	1.47	
1	30	980.4	971.6	4156.1	4149.7	2089.4	2093.8	5487.8	5493.4	32.5%	44.1%	38.3%	0.152	1.48	
1	65	2269.4	2255.3	9177.2	9244.2	3247.1	3257.4	7798.6	7779.7	41.7%	55.3%	48.5%	0.139	1.49	
1	223	1395.3	1397.2	5173.4	5136.1	618.2	622.8	1091.2	1096.0	69.9%	83.1%	76.5%	0.087	1.48	

		UV-Absorbance HPLC (λ = 285 nm), raw data [mAUs]								Chemoselectivity					
Run	time [min]	R-NpEtOiPr (R)-**4b**	S-NpEtOiPr (S)-**4b**	R-Phant-EtOiPr (R)-**4c**	S-Phant-EtOiPr (S)-**4c**	S-NpEtOH (S)-**1b**	R-NpEtOH (R)-**1b**	S-Phant-EtOH (S)-**1c**	R-Phant-EtOH (R)-**1c**	c **1b**	c **1c**	total c	Chemo-selectivity	s	StDev
1	1195	1615.5	1639.6	4958.8	4868.6	18.9	22.9	16.7	15.4	n.d.	n.d.	n.d.	n.d.	n.d.	
2	0	-	-	-	-	2542.1	2545.5	8037.2	8022.9	-	-	-	-	-	
2	6	298.4	297.3	1457.6	1427.1	2135.6	2123.2	6741.1	6733.0	12.6%	18.3%	15.4%	0.184	1.50	
2	13	532.4	531.7	2560.3	2515.6	2595.6	2586.5	8005.2	7991.7	17.5%	24.9%	21.2%	0.175	1.49	
2	24	616.6	616.6	2892.9	2839.5	1978.6	1968.7	5840.5	5833.1	24.3%	33.9%	29.1%	0.164	1.48	
2	45	1015.5	1017.0	4606.4	4627.6	1991.8	1983.1	5481.7	5458.7	34.5%	46.8%	40.7%	0.152	1.49	
2	80	1495.5	1498.0	6482.9	6539.0	1842.5	1836.1	4639.2	4641.7	45.6%	59.4%	52.5%	0.132	1.48	
2	180	1414.9	1407.4	5758.1	5804.3	836.3	839.8	1741.9	1734.5	63.4%	77.6%	70.5%	0.101	1.49	
2	304	2151.0	2137.0	8287.9	8429.7	749.0	745.8	1291.2	1294.3	74.7%	87.1%	80.9%	0.077	1.49	
2	549	2463.4	2438.9	8884.4	8956.4	382.2	381.6	475.5	477.8	86.9%	95.1%	91.0%	0.045	1.49	
													average	1.49	0.007
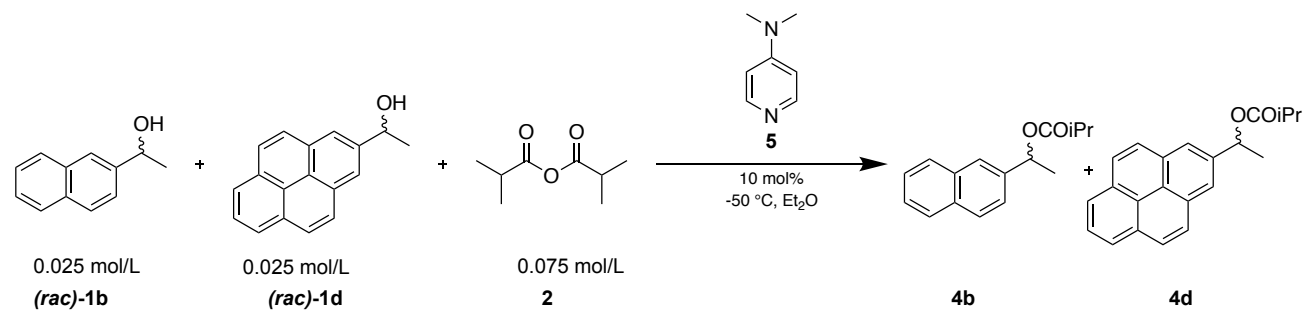
Scheme 6.17. Competition experiment of (*rac*)-1-(2-naphthyl)ethanol (**1b**) and (*rac*)-1-(2-pyrenyl)ethanol (**1d**) with DMAP (**5**).

Table 6.23. Raw HPLC absorbance data for competitive linear regression shown in **Scheme 6.17**. Data were calibrated and normalized from the stock solution before analysis. To minimize influence of analytical errors selectivities were not determined (n.d.) for points with a conversion lower than 4% or higher than 96% for one substrate. Selectivity was derived as described in Chapter 6.1.8.

Run	time [min]	UV-Absorbance HPLC (λ = 285 nm), raw data [mAUs]								Chemoselectivity					
		R-NpEtOiPr (R)-**4b**	S-NpEtOiPr (S)-**4b**	R-PyrEtOiPr (R)-**4d**	S-PyrEtOiPr (S)-**4d**	S-NpEtOH (S)-**1b**	R-NpEtOH (R)-**1b**	S-PyrEtOH (S)-**1d**	R-PyrEtOH (R)-**1d**	*c* **1d**	*c* **1b**	total *c*	Chemo-selectivity	*s*	StDev
1	0	-	-	-	-	5978.9	5985.5	7365.4	7703.8	-	-	-	-	-	
1	7	292.7	299.7	912.7	927.4	3007.5	3016.0	3322.0	3453.1	9.2%	23.1%	16.1%	0.433	2.74	
1	12	531.1	528.2	1574.9	1593.3	3614.3	3631.0	3667.6	3813.2	13.0%	31.9%	22.5%	0.420	2.76	
1	31	914.5	913.0	2450.5	2448.9	3235.7	3248.4	2750.3	2847.5	22.4%	49.2%	35.8%	0.374	2.67	
1	66	1628.0	1670.1	3775.8	3892.6	3192.8	3588.7	2259.5	2313.6	33.3%	65.0%	49.1%	0.323	2.60	
1	225	1549.5	1562.1	2878.9	2971.9	1169.2	1176.5	368.4	375.2	57.6%	89.7%	73.7%	0.218	2.65	
1	1194	2916.6	2913.4	3450.5	3541.0	55.1	57.7	11.1	10.7	n.d.	n.d.	n.d.	n.d.	n.d.	
2	0	-	-	-	-	2889.2	2899.9	2347.0	2405.6	-	-	-	-	-	
2	9	255.0	250.8	797.7	805.8	2358.8	2352.2	2626.4	2726.0	9.9%	24.9%	17.4%	0.431	2.75	
2	15	397.8	392.6	1179.2	1192.8	2492.1	2489.8	2574.6	2669.8	14.0%	33.4%	23.7%	0.409	2.69	
2	26	647.9	646.9	1820.0	1816.0	2623.5	2621.9	2400.5	2486.2	20.2%	45.2%	32.7%	0.382	2.66	
2	47	897.8	902.9	2271.3	2276.8	2194.8	2190.6	1657.2	1708.3	29.6%	59.9%	44.8%	0.338	2.60	
2	81	1236.7	1248.5	2770.5	2852.4	1888.1	1881.0	1083.1	1109.1	40.4%	74.0%	57.2%	0.294	2.60	
2	180	1826.4	1824.3	3318.7	3409.7	1286.9	1287.3	378.8	382.0	59.3%	90.7%	75.0%	0.210	2.65	
2	304	2369.1	2372.7	3688.9	3808.3	916.2	912.5	128.8	129.2	72.7%	97.0%	84.8%	0.143	2.70	
2	549	2810.8	2828.0	3776.8	3866.2	436.8	439.4	18.0	18.8	n.d.	n.d.	n.d.	n.d.	n.d.	
													average	2.67	0.054
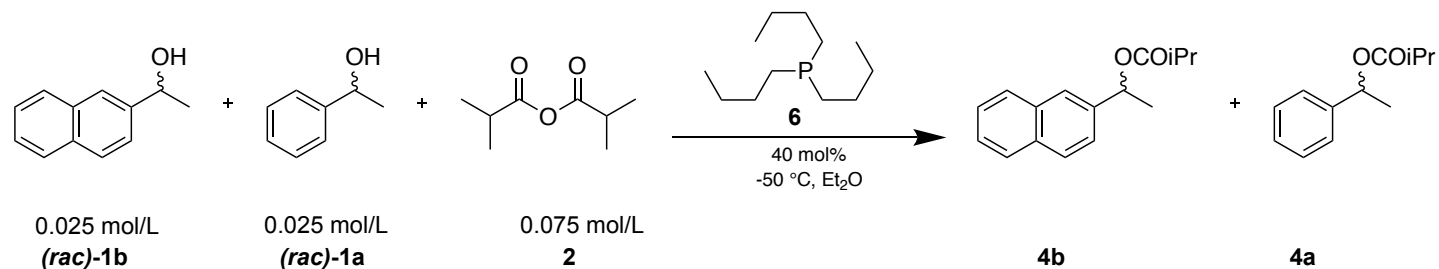
Scheme 6.18. Competition experiment of (*rac*)-1-(2-naphthyl)ethanol (**1b**) and (*rac*)-1-phenylethanol (**1a**) with tri-*n*-butyl phosphane (**5**).

Table 6.24. Raw HPLC absorbance data for competitive linear regression shown in **Scheme 6.18**. Data were calibrated and normalized from the stock solution before analysis. To minimize influence of analytical errors selectivities were not determined (n.d.) for points with a conversion lower than 4% or higher than 96% for one substrate. Selectivity was derived as described in Chapter 6.1.8.

Run	time [min]	UV-Absorbance HPLC (λ = 285 nm (naphthyl), (λ = 215 nm (phenyl)), raw data [mAUs]								Chemoselectivity					
		R-PhEtOiPr (*R*)-**4a**	S-PhEtOiPr (*S*)-**4a**	R-NpEtOiPr (*R*)-**4b**	S-NpEtOiPr (*S*)-**4b**	R-PhEtOH (*R*)-**1a**	S-PhEtOH (*S*)-**1a**	S-NpEtOH (*S*)-**1b**	R-NpEtOH (*R*)-**1b**	*c* **1a**	*c* **1b**	total *c*	Chemo-selectivity	*s*	StDev
1	1754	833.5	831.8	871.8	825.6	5245.2	5224.5	4633.4	4656.7	15.0%	15.8%	15.4%	-0.026	0.94	
1	7090	1931.2	1967.8	1899.4	1914.0	5073.8	5082.2	4335.6	4347.2	29.9%	31.2%	30.5%	-0.020	0.95	
1	10130	3303.0	3345.3	3278.5	3235.4	4774.8	4871.0	3952.4	3974.1	43.4%	45.9%	44.6%	-0.028	0.93	
1	12914	4015.2	4092.2	3839.7	3833.2	3845.2	3928.7	3019.9	3023.7	53.7%	56.7%	55.2%	-0.027	0.92	
													average	**0.94**	**0.013**
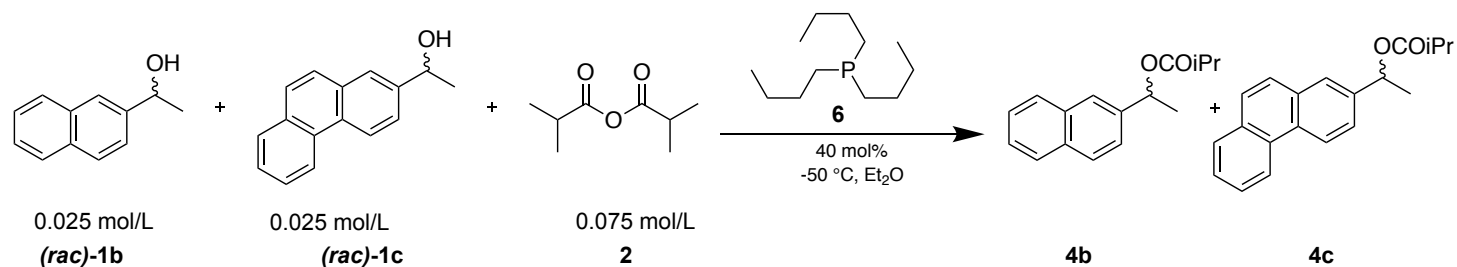
Scheme 6.19. Competition experiment of (*rac*)-1-(2-naphthyl)ethanol (**1b**) and (*rac*)-1-(2-phenanthryl)ethanol (**1c**) with tri-*n*-butyl phosphane (**5**).

Table 6.25. Raw HPLC absorbance data for competitive linear regression shown in **Scheme 6.19**. Data were calibrated and normalized from the stock solution before analysis. To minimize influence of analytical errors selectivities were not determined (n.d.) for points with a conversion lower than 4% or higher than 96% for one substrate. Selectivity was derived as described in Chapter 6.1.8.

Run	time [min]	UV-Absorbance HPLC (λ = 285 nm), raw data [mAUs]								Chemoselectivity					
		R-NpEtOiPr (*R*)-**4b**	S-NpEtOiPr (*S*)-**4b**	R-Phant-EtOiPr (*R*)-**4c**	S-Phant-EtOiPr (*S*)-**4c**	S-NpEtOH (*S*)-**1b**	R-NpEtOH (*R*)-**1b**	S-Phant-EtOH (*S*)-**1c**	R-Phant-EtOH (*R*)-**1c**	*c* **1b**	*c* **1c**	total *c*	Chemo-selectivity	*s*	StDev
1	1754	243.1	243.2	653.8	600.9	1497.5	1506.3	4219.2	4217.2	14.3%	13.4%	13.9%	-0.031	0.94	
1	7090	897.9	892.1	2215.2	2216.0	2374.8	2391.5	6716.7	6700.0	27.9%	25.6%	26.8%	-0.042	0.91	
1	10130	886.6	877.9	2253.3	2212.6	1376.4	1371.3	3952.8	3955.8	39.8%	37.1%	38.5%	-0.035	0.91	
1	12914	1801.5	1792.0	4603.5	4618.8	1873.7	1890.2	5398.1	5401.2	49.6%	47.1%	48.4%	-0.025	0.93	
													average	0.92	0.012
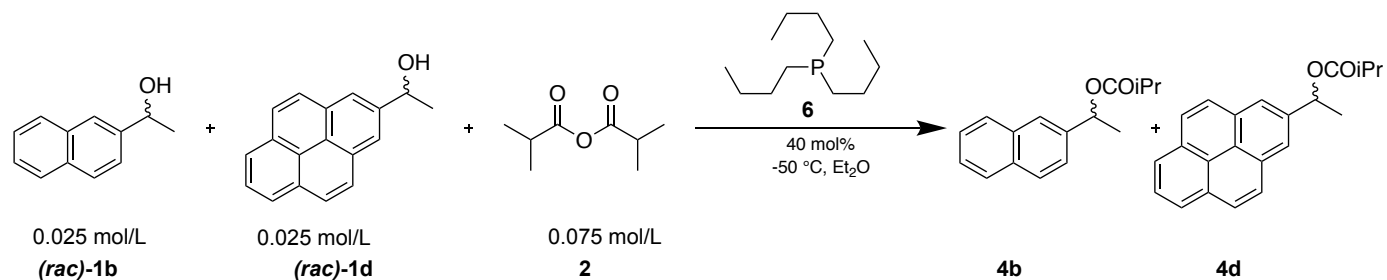
Scheme 6.20. Competition experiment of (*rac*)-1-(2-naphthyl)ethanol (**1b**) and (*rac*)-1-(2-pyrenyl)ethanol (**1d**) with tri-*n*-butyl phosphane (**5**).

Table 6.26. Raw HPLC absorbance data for competitive linear regression shown in **Scheme 6.20**. Data were calibrated and normalized from the stock solution before analysis. To minimize influence of analytical errors selectivities were not determined (n.d.) for points with a conversion lower than 4% or higher than 96% for one substrate. Selectivity was derived as described in Chapter 6.1.8.

Run	time [min]	UV-Absorbance HPLC (λ = 285 nm), raw data [mAUs]								Chemoselectivity					
		R-NpEtOiPr (R)-**4b**	S-NpEtOiPr (S)-**4b**	R-PyrEtOiPr (R)-**4d**	S-PyrEtOiPr (S)-**4d**	S-NpEtOH (S)-**1b**	R-NpEtOH (R)-**1b**	S-PyrEtOH (S)-**1d**	R-PyrEtOH (R)-**1d**	*c* **1d**	*c* **1b**	total *c*	Chemo-selectivity	*s*	StDev
1	1754	234.5	228.0	340.5	348.0	1385.2	1389.6	1917.3	1980.9	14.6%	16.4%	15.5%	0.057	1.13	
1	7090	1152.7	1185.6	1606.2	1639.0	2760.5	2765.3	3527.2	3676.6	30.2%	33.3%	31.8%	0.048	1.12	
1	10130	1301.3	1303.5	1771.7	1814.8	1600.8	1606.1	2080.8	2155.6	45.4%	48.4%	46.9%	0.032	1.09	
1	12914	2077.4	2064.3	2746.6	2759.6	1607.3	1612.2	2034.2	2101.8	56.7%	59.6%	58.1%	0.025	1.08	
													average	**1.11**	**0.021**

6.2.8.Background Measurements

In order to estimate the rates of the uncatalysed background reaction for the acylation of alcohols **1a** and **1b** with isobutyric anhydride (**2**) in this project, absolute rate measurements with different concentrations of DMAP (**5**) were performed. For practical reasons these measurements were performed at +4 °C.

General procedure

Stock solutions for alcohol (c = 0.03 mol/L), catalyst (c = 0.003 mol/L) and freshly distilled isobutyric anhydride (c = 0.06 mol/L) in dry diethyl ether are prepared. After cooling 0.8 mL stock solution alcohol and 0.8 mL stock solution catalyst in a 20 mL flask to 4 °C (N$_2$, stirring), 0.8 mL of pre-cooled stock solution anhydride is added. A 0.5 mL sample of the reaction mixture is then transferred into a nitrogen-flushed HPLC flask (4 vials in total), closed with a screw septum cap and kept at +4 °C. A sample of 1 μl (4 μl in the case of 1-phenylethanol) of the reaction mixture is taken by the HPLC autosampler after a defined time and a HPLC spectrum (Vertex Eurospher II, 1.5 mL/min, *n*Hexan/*i*Propanol = 100/0→93/7, T = 10 °C, t = 3 min, λ = 275 nm [NpEtOH]/ λ = 210 nm [PhEtOH]) is measured (max. 4 times per vial). The substrate/product ratio is calculated using calibration curves of optical absorbance and concentration. Simulation of the reaction with CoPaSi leads to the effective rate constants *k*. **Figure 6.20** demonstrates that for both alcohols no significant background reaction occurs at +4 °C. Raw data can be found below.
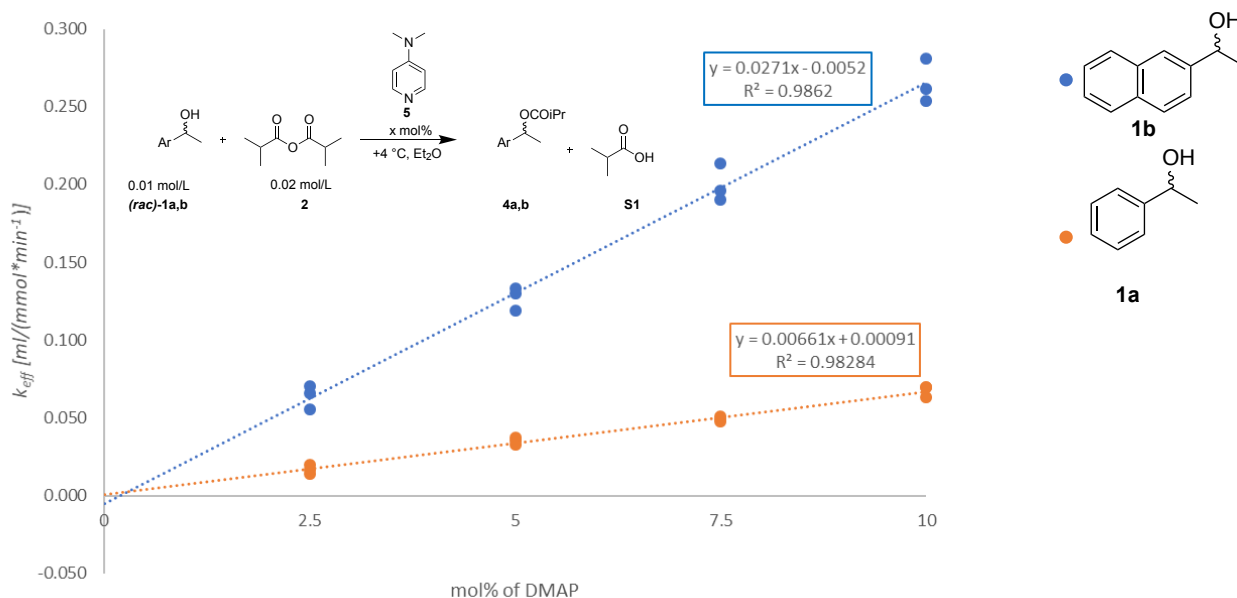
Figure 6.20. Plots of effective rate constants shown in **Table 6.27** and **Table 6.28** to determine rate constant and background reaction.

Table 6.27. Effective rate constants for the acetylation of 1-(2-naphthyl)ethanol (**1b**) with isobutyric anhydride (**2**, 2 eq) catalysed by DMAP (**5**). The results of three independent runs of each experiment are presented. A representative CoPaSi simulation for one run is shown, x-axis gives time [min], y-axis intermediate concentration [mol/L] for substrate (red) and product (blue).
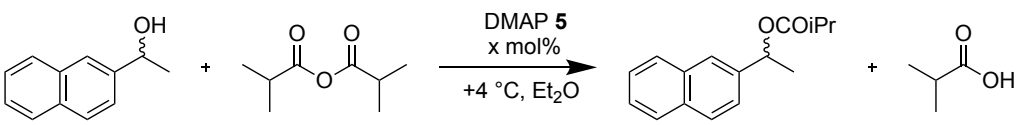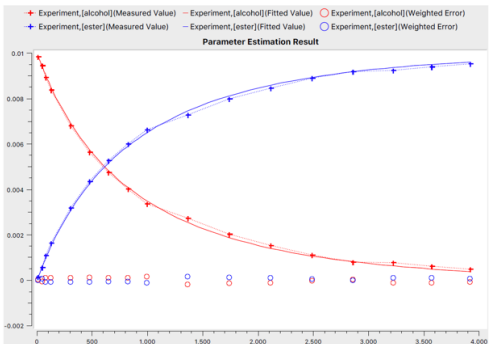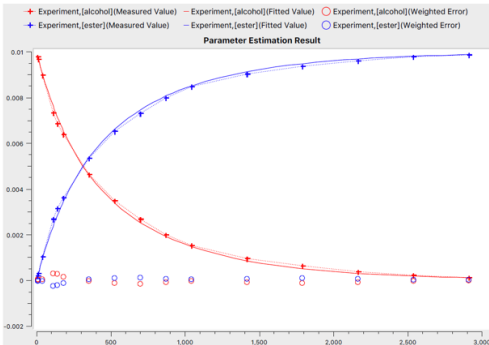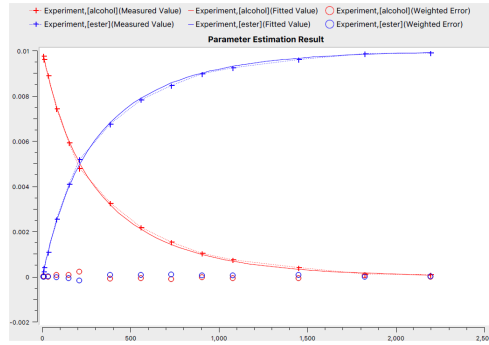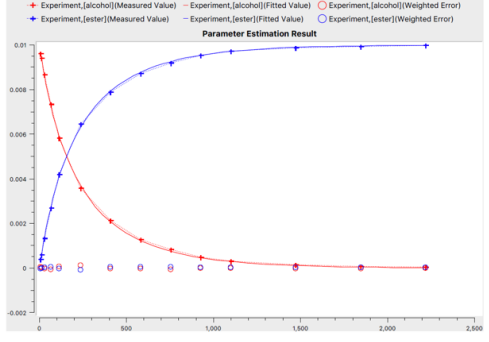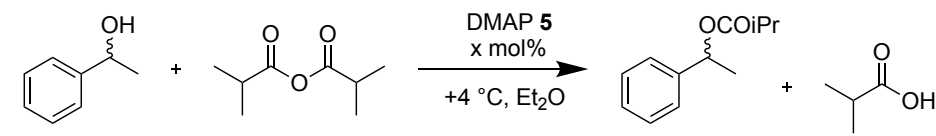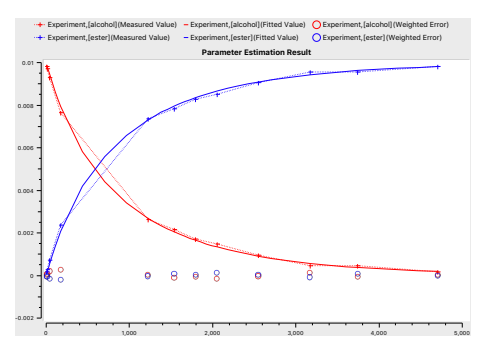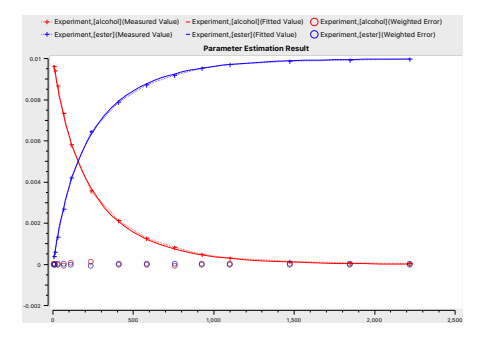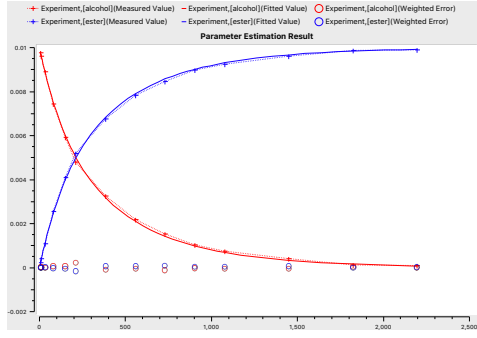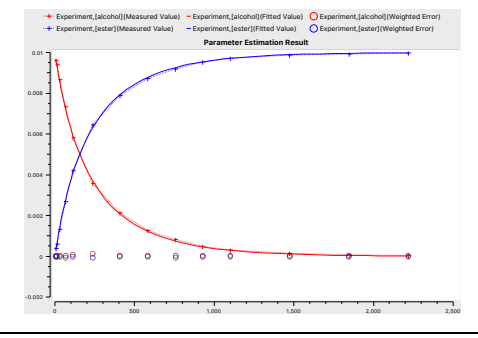
Catalyst [mol%]	Representative CoPaSi simulation	k_{eff} [ml/(mmol*min^{-1}]	Averaged k_{eff}	St.Dev.
2.5		0.066	0.064	0.008
		0.055		
		0.070		
5.0		0.130	0.127	0.008
		0.119		
		0.134		
7.5		0.190	0.200	0.012
		0.213		
		0.196		
10.0		0.262	0.266	0.014
		0.254		
		0.281		

Table 6.28. Effective rate constants for the acetylation of 1-phenylethanol (**1a**) with isobutyric anhydride (**2**, 2 eq) catalysed by DMAP (**5**). The results of three independent runs of each experiment are presented. A representative CoPaSi simulation for one run is shown, x-axis gives time [min], y-axis intermediate concentration [mol/L] for substrate (red) and product (blue).

Catalyst [mol%]	Representative CoPaSi simulation	k_{eff} [ml/(mmol*min^{-1})]	Averaged k_{eff}	St.Dev.
2.5		0.017	0.017	0.003
		0.020		
		0.014		
5.0		0.033	0.035	0.002
		0.036		
		0.037		
7.5		0.049	0.049	0.002
		0.047		
		0.051		
10.0		0.063	0.067	0.004
		0.070		
		0.069		

6.3. Experimental Procedures

6.3.1. General Procedures

General methods: All reactions sensitive to air and moisture were proceeded under a nitrogen atmosphere and the glassware as well as magnetic stir bars were dried overnight in a dry oven at 110°C.

Solvents, reagents, and catalysts: All reagents and solvents were purchased from the companies TCI, Sigma Aldrich or Fisher Scientific. Diethyl ether was purchased "extra-dry over molecular sieves" from Sigma-Aldrich. $CDCl_3$ was freshly distilled from calcium hydride (CaH_2) under nitrogen atmosphere. 1-Phenylethanol (**1a**) was purified by flash chromatography prior to use. Isobutyric anhydride (**2**) and PBu_3 (**6**) were freshly purified by Kugelrohr-distillation under N_2 before every use. All other reagents were used without further purification, if not mentioned otherwise. All air- or water-sensitive reagents were stored under nitrogen.

HPLC analysis: All HPLC spectra were measured on a Knauer Azura machine with normal-phase optimized pump P6.1L, autosampler AS6.1, column thermostat CT2.1 and diode array detector DAD2.1L. Chiralpak IB-N5 250 x 4.6 mm 5 mic and Vertex Eurospher II 50 x 4.6 mm columns were utilized. Data analysis was performed with ClarityChrom 7.4.1.

Cryostat: For reactions at +4 °C the thermostat of the HPLC autosampler AS6.1 was used. For reactions at -50 °C an isopropanol bath cooled by the immersion cooler of a Huber TC100E cryostat was used.

Chromatography: Silica gel for column chromatography was purchased from Acros Organics (mesh 35-70). Thin-layer chromatography was performed by using TLC plates purchased by Merck (silica gel 60 F254, thickness 0.2 mm).

NMR spectroscopy: All ^{1}H-NMR spectra were recorded by Varian INOVA 400 or a Bruker BioSpin NanoBay 400 machine in $CDCl_3$ at 400 MHz at 23 °C. All ^{13}C-NMR spectra were recorded respectively at 101 MHz. The chemical shifts for ^{1}H and ^{13}C-NMR spectra are reported in ppm (δ), relative to the chemical shift of tetramethylsilane (TMS) and the resonance of $CHCl_3$ at δ = 7.26 ppm resp. δ = 77.16 ppm was used as an internal reference. Spectra were imported and processed in the MestreNova 12.0.4 program. For ^{1}H-NMR spectra multiplicity (d = doublet, t = triplet, q = quartet, hept = heptet, dd = doublet of doublets, m = multiplet), coupling constants J, number or protons and assignment to the structure are reported. In ^{13}C-NMR spectra singular carbons are marked with (s).

Mass spectrometry: Electron ionization (EI) HRMS spectra were recorded on a Thermo Finnigan LTQ FT machine of the MAT 95 type with a direct exposure probe (DEP) and electron impact ionization (EI, 70 eV). For electrospray ionization (ESI) spectra a Thermo Finnigan LTQ FT Ultra Fourier Transform Ion Cyclotron Resonance Mass Spectrometer was utilized.

X-ray crystallography: Crystallographic measurements were done using an Oxford Diffraction XCalibur with Saphir CCD-detector and a molybdenum-K_α–source (λ = 0.71073 Å) with concentric circle kappa-device. Structures were resolved using SHELXS or SIR97 and refined with SHELXS.

Optical rotation: Optical rotation were measured at a Krüss P8000 machine.

Infrared spectroscopy: Infrared (IR) spectra were measured at FT-IR Perkin Elmer Spectrum BXII/1000 with Smiths ATR.

Melting points: Melting point were measure at a Büchi M560 and are stated uncorrected.

6.3.2. Synthesis of Catalysts

Catalyst **7** was synthesized following an adapted protocol reported by Sibi *et al.*[3, 10] as shown in **Scheme 6.21**.
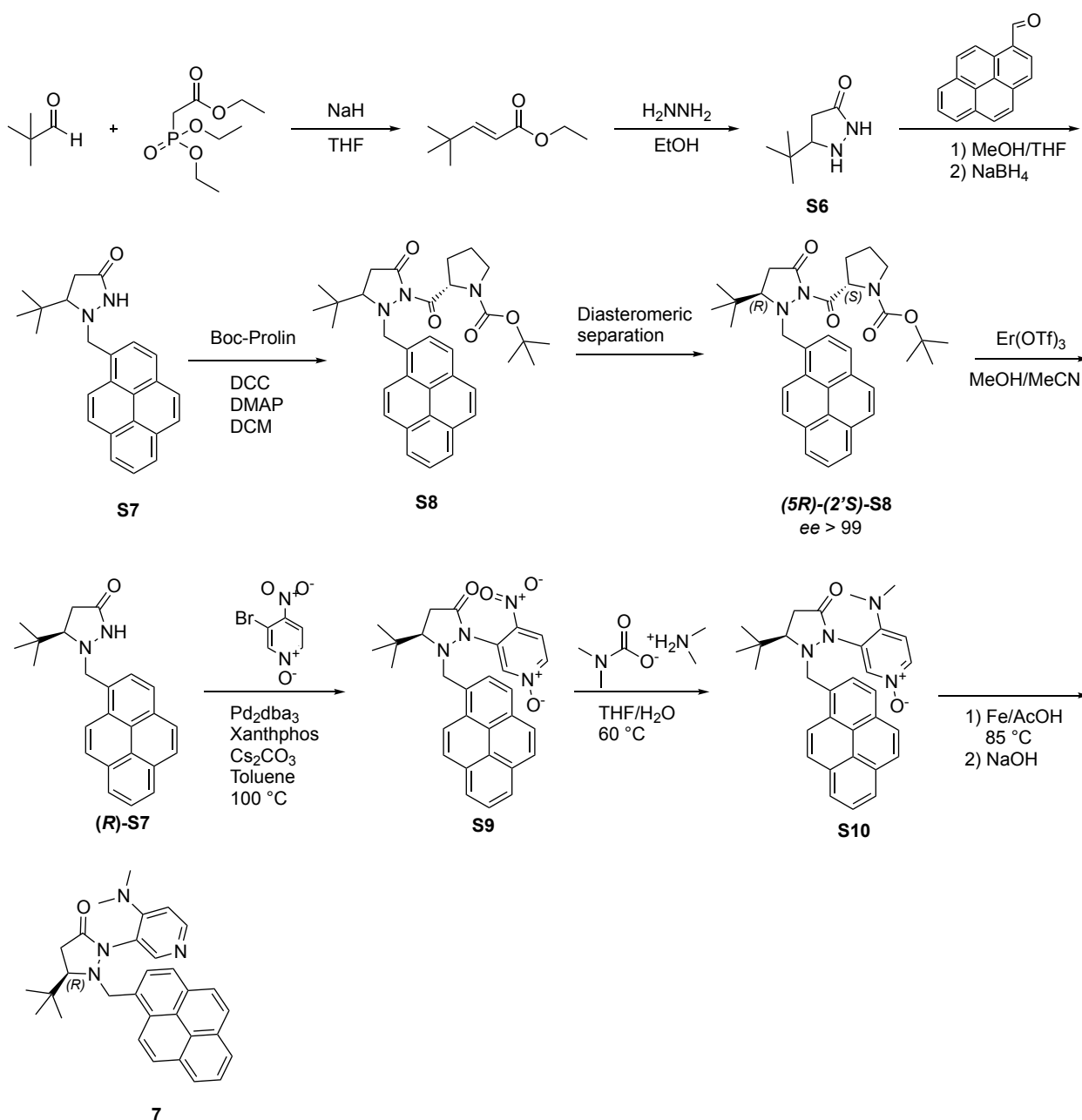
Scheme 6.21. Synthesis of catalyst **7**.[3, 10]

5-(*Tert*-butyl)pyrazolidin-3-one (S6)
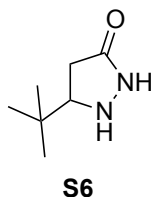
Pivaldehyd (2.15 g, 25.0 mmol, 1.00 eq) is suspended in 30 mL dry THF under N_2 atmosphere, cooled to 0 °C and triethyl phosphonoacetate (6.16 g, 27.5 mmol, 1.10 eq) is added dropwise. After stirring for 15 min sodium hydride (660 mg, 27.5 mmol, 1.10 eq) is carefully added. The mixture is stirred overnight, quenched through addition of 30 mL water, stirred for another 15 min and extracted with diethyl ether (3 x 20 mL), dried over magnesium sulphate, filtered and the solvent was removed under reduced pressure. The solution is used without further purification in the next step.

To the crude solution 50 mL of Ethanol and 2.02 mL of hydrazine monohydrate (1.25 g, 25 mmol, 1.00 eq of hydrazine) is added and heated to reflux for 20 hours. Excess of reagents and solvent is removed under reduced pressure and the residue is used directly without further purification in the next step.

5-(*Tert*-butyl)-1-(1-pyrenylmethyl)pyrazolidin-3-one (S7)
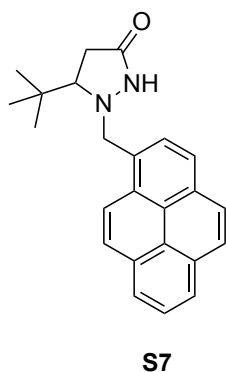
Crude **S6** (3.55 g, 25.0 mmol, 1.00 eq) is dissolved in 120 mL of MeOH/THF (1 : 1) and cooled to 0 °C. Pyren-1-carbaldehyde (5.47 g, 23.8 mmol, 0.95 eq) is added and stirred overnight at rt. The solution is cooled to 0 °C and NaBH$_4$ (898 mg, 23.8 mmol, 0.95 eq) is slowly added. After stirring for 10 min at 0 °C and 30 °min at rt a saturated solution of NaHCO$_3$ and water is added. The dispersion is filtered, the filtrate extracted with DCM (3 x 20 mL), washed with brine, dried over MgSO$_4$ and the solvent is removed under reduced pressure. After column chromatography (silica gel, *i*Hex/EtOAc = 1/1 – 0/1) 3.78 g of **S7** (10.6 mmol, 45% over three steps) is obtained as a yellow powder.

mp +178.2 °C. **R$_f$** 0.21 (*i*Hex:EtOAc = 1:1). **^{1}H NMR** (400 MHz, CDCl$_3$) δ 8.48 (d, *J* = 9.3 Hz, 1H, Ar-*H*), 8.22 (dd, *J* = 7.6, 2.6 Hz, 2H, Ar-*H*), 8.19 – 8.12 (m, 2H, Ar-*H*), 8.12 – 8.00 (m, 3H, Ar-*H*), 7.95 (d, *J* = 7.8 Hz, 1H, Ar-*H*), 6.65 (s, 1H, N*H*), 4.63 (d, *J* = 12.1 Hz, 1H, NC*H$_2$*), 4.52 (d, *J* = 12.1 Hz, 1H, NC*H$_2$*)), 3.23 (dd, *J* = 9.6, 2.1 Hz, 1H, COC*H$_2$*), 3.03 (dd, *J* = 17.4, 9.6 Hz, 1H, C*H*tBu), 2.32 (dd, *J* = 17.4, 2.1 Hz, 1H, COC*H$_2$*), 0.88 (s, 9H, *t*Bu*H*) ppm. **^{13}C NMR** (101 MHz, CDCl$_3$) δ = 174.6 (C=O), 131.6 (s), 131.4 (s), 130.9 (s), 130.1 (s), 129.6, 129.2, 128.0, 127.8, 127.5, 126.2, 125.6, 125.5, 125.1 (s), 124.8 (s), 124.7, 123.8, 71.8, 63.9, 35.1, 30.2, 25.8 ppm. **ESI-HRMS** m/z calc. for C$_{24}$H$_{24}$N$_2$O [M+H]$^+$ 357.1967; found 357.19658; [M-H]$^-$ 355.1816; found 355.18167. **IR** ν = 3033 (w, =C-H), 2948 (w, -C-H), 1694 (vs, C=O), 1348 (m), 839 (s), 711 (m) cm^{-1}.

2-(*L*-Boc-prolyl)-5-(*R*)-(*tert*-butyl)-1-(1-pyrenylmethyl)pyrazolidin-3-one (S8)

(5R)-(2'S)-S8
ee > 99
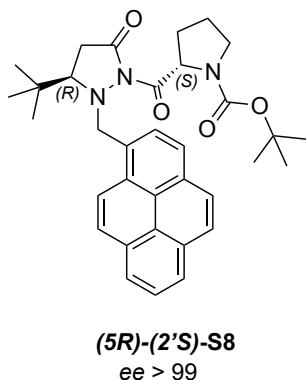
A flask with **S7** (3.78 g, 10.6 mmol, 1.00 eq), *N,N'*-dicyclohexyl carbodiimide (2.28 g, 10.6 mmol, 1.00 eq), and DMAP (258 mg, 2.12 mmol, 0.20 eq) is evacuated, purged with N_2 and 110 mL dry DCM is added. After addition of 3.78 g *L*-Boc-prolin (10.6 mmol, 1.00 eq) the mixture is stirred for 48 h. The mixture is filtered and the solvent is evaporated under reduced pressure. After column chromatography (silica, *i*Hex/Acetone = 4/1) 4.85 g (8.76 mmol, 83%) of diastereomeric **S8** is obtained. (5*R*)-(2'*S*)-**S8** (1.87 g, 3.38 mmol, 63% of (*R*)-substrate) was isolated by repeated column chromatography (silica gel, *i*Hex/Acetone = 9/1, later diastereomer) followed by repeated recrystallization from *i*Hex/Acetone = 9/1 with diastereomeric excess > 99.5 analysed by NMR and HPLC as a white powder.

mp +212.2°C. R_f 0.23 (*i*Hex/Acetone = 9/1). $[\alpha]_{25}^D$ = -81.7° (c 0.50, CHCl₃). **¹H NMR** (400 MHz, CDCl₃) δ 9.24 (dd, *J* = 9.2, 5.4 Hz, 1H, Ar-*H*), 8.33 – 8.17 (m, 3H, Ar-*H*), 8.16 – 7.98 (m, 4H, Ar-*H*), 7.93 – 7.85 (m, 1H, Ar-*H*), 5.38 (dd, *J* = 9.0, 2.3 Hz, 1H, NC*H*CO), 5.08 (dd, *J* = 11.4, 8.3 Hz, 1H, NC*H₂*Pyr), 4.18 (dd, *J* = 16.4, 11.5 Hz, 1H, NC*H₂*Pyr), 3.71 (tt, *J* = 13.4, 5.8 Hz, 1H), 3.63 – 3.42 (m, 1H), 3.31 – 2.99 (m, 2H), 2.58 (d, *J* = 18.1 Hz, 1H), 2.52 – 2.29 (m, 1H), 2.04 – 1.75 (m, 3H), 1.48 (d, *J* = 32.7 Hz, 9H, O*t*Bu*H*), 0.43 (d, *J* = 13.3 Hz, 9H, *t*Bu*H*) ppm. **¹³C NMR** (101 MHz, CDCl₃) δ = 174.6 (d, C=O), 169.4 (d, C=O), 154.3 (C=O), 131.8 (d), 131.5, 131.3, 131.2, 129.5, 129.0, 128.2 (d), 128.0 (d), 127.3, 126.2 (d), 125.8 (d), 125.6 (d), 125.2 (d), 125.0, 124.6, 124.2, 79.8 (d), 64.0 (d), 60.6, 59.8, 47.0 (d), 34.5 (d), 32.0, 31.6, 28.6 (d, 3C, *t*Bu), 25.6 (3C, *t*Bu), 22.6 ppm. **ESI-HRMS** m/z calc. for $C_{34}H_{39}N_3O_4$ [M+H]⁺ 554.30133; found 554.30239; [M-H]⁻ 552.28678; found 552.28726. **IR** ν = 2928 (w, -C-H), 1734 (s, C=O ester), 1713 (vs, C=O), 1685 (vs, C=O), 1415 (s), 1249 (s), 1199 (s), 1154 (s), 853 (vs) cm⁻¹.

(*R*)-5-(*Tert*-butyl)-1-(1-pyrenylmethyl)pyrazolidin-3-one (S7)

(R)-S7
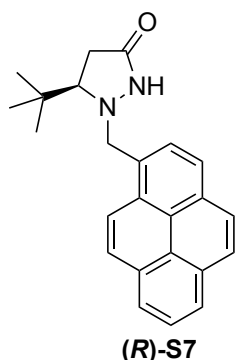
S8 (1.75 g, 3.16 mmol, 1.00 eq) and Er(OTf)₃ (388 mg, 0.64 mmol, 0.20 eq) is dissolved in 45 mL of MeOH/MeCN (3 : 2) and stirred at rt for two weeks. Solvent is removed under reduced pressure and purification by column chromatography (silica gel, *i*Hex/EtOAc = 1:1) gives 490 mg enantiopure *(R)*-**S7** (1.38 mmol, 44%) as a yellow powder.

$[\alpha]_{25}^D$ = +99.0° (c 0.51, CHCl₃). Other analytical data are in accordance with *(rac)*-**S7**.

(R)-3-(3-(tert-butyl)-5-oxo-2-(1-pyrenylmethyl)pyrazolidin-1-yl)-4-nitropyridine N-oxide (S9)
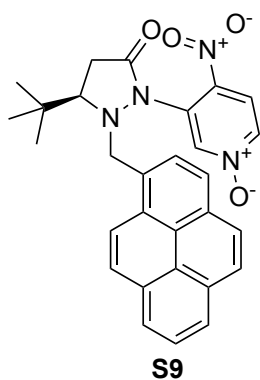
A flask with *(R)*-**S7** (151 mg, 0.42 mmol, 1.0 eq), 3-bromo-4-nitropyridine N-oxide (93 mg, 0.42 mmol, 1.0 eq), Pd_2dba_3 (19 mg, 0.021 mmol, 0.050 eq), Xantphos (12 mg, 0.021 mmol, 0.050 eq), and Cs_2CO_3 (239 mg, 0.51 mmol, 1.20 eq) is evacuated, purged with N_2 (3x) and 30 mL dry toluene is added. The mixture is degassed and stirred for 19 h at 100 °C. After cooling and filtration, the solvent is evaporated under reduced pressure. Column chromatography (silica gel, *i*Hex/EtOAc = 1/1) gives 130 mg (0.263 mmol, 62%) of **S9** as a white solid.

mp +153°C. R_f 0.23 (*i*Hex/EtOAc = 1/1). $[\alpha]_{25}^D$ = -309.7 ° (c 0.51, CHCl₃). **¹H NMR** (400 MHz, CDCl₃) δ 8.50 (s, 1H, Ar-*H*), 8.40 (d, *J* = 9.2 Hz, 1H, Ar-*H*), 8.33 – 8.16 (m, 3H, Ar-*H*), 8.12 – 7.90 (m, 5H, Ar-*H*), 7.54 (s, 2H, Ar-*H*), 4.86 (s, 2H, NC*H₂*), 3.39 – 3.25 (m, 2H, COC*H₂*), 2.61 – 2.46 (m, 1H, C*H*tBu), 0.76 (s, 9H, *t*Bu*H*) ppm. **¹³C NMR** (101 MHz, CDCl₃) δ 171.1 (C=O), 136.7 (s), 135.7, 134.5, 131.9 (s), 131.2 (s), 130.7 (s), 130.2 (s), 130.0, 129.4 (s), 129.2, 128.3, 127.6 (s), 127.2, 126.5, 126.0 (2C), 124.7 (s), 124.7 (s), 124.3, 122.5, 121.6, 68.9, 62.1, 35.0, 31.0, 25.8 (3C) ppm. **ESI-HRMS** m/z calc. for $C_{29}H_{26}N_4O_4$ [M+H]⁺ 495.20268; found 495.20215; [M-H]⁻ 493.18813; found 493.18817. **IR** ν = 2960 (w, -C-H), 1722 (vs, C=O), 1465 (s), 1268 (s), 847 (s), 748 (s) cm⁻¹.

(R)-3-(3-(tert-butyl)-5-oxo-2-(1-pyrenylmethyl)pyrazolidin-1-yl)-DMAP N-oxide (S10)
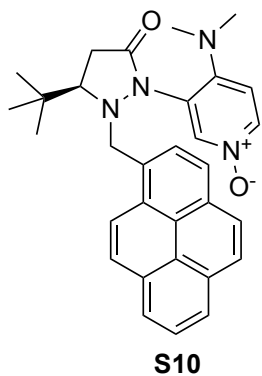
S9 (202 mg, 0.408 mmol, 1.00 eq) and dimethylammonium dimethylcarbamate (Dimcarb, 1.44 mL, 1.52 g, 20.0 eq) are stirred in 10 mL THF/H₂O (9/1) at 85 °C for 10 days. The solvent is evaporated under reduced pressure. Column chromatography (silica gel, EtOAc/MeOH = 9/1 → EtOAc/MeOH/NEt₃= 85/10/5) yields 163 mg (0.33 mmol, 81%) of **S10** as orange powder. The product still contained hardly removable traces of a triethylammonium salt and was used without further purification in the next step.

mp +177°C. R_f 0.16 (EtOAc/MeOH = 9/1). $[\alpha]_{25}^D$ = -110.2 ° (c 0.51, CHCl₃). **¹H NMR** (400 MHz, CDCl₃) δ 8.82 (d, *J* = 2.1 Hz, 1H, Ar-*H*), 8.29 (d, *J* = 9.3 Hz, 1H, Ar-*H*), 8.25 – 8.18 (m, 3H, Ar-*H*), 8.17 – 7.99 (m, 5H, Ar-*H*), 7.95 (d, *J* = 7.8 Hz, 1H, Ar-*H*), 6.73 (d, *J* = 7.4 Hz, 1H, Ar-*H*), 5.07 (d, *J* = 11.6 Hz, 1H, NC*H₂*), 4.54 (d, *J* = 11.7 Hz, 1H, NC*H₂*), 3.50 – 3.40 (m, impurities of HNEt₃⁺), 3.33 – 3.19 (m, 2H, COC*H₂*, C*H*tBu), 3.04 (s, 6H, NEt₂), 2.54 (d, *J* = 17.1 Hz, 1H, COC*H₂*), 1.97 (s, impurities of HNEt₃⁺), 1.41 – 1.13 (t, impurities of HNEt₃⁺),), 0.41 (s, 9H, *t*Bu*H*) ppm. **¹³C NMR** (101 MHz, CDCl₃) δ 169.5 (C=O), 145.9 (s), 137.7, 137.0, 131.8 (s), 131.3 (s), 130.8 (s), 130.5 (s), 129.4, 129.0, 128.2, 128.1, 127.4, 126.4, 125.9, 125.8, 124.9 (s), 124.7 (s), 124.4, 123.1 (s), 122.8, 113.9, 66.2, 59.6, 41.3 (2C), 34.5, 31.1, 25.6 (3C) ppm. **ESI-HRMS** m/z calc. for $C_{31}H_{32}N_4O_2$ [M+H]⁺ 493.25980; found 493.25906. **IR** ν = 2956 (w, -C-H), 1698 (vs, C=O), 1424 (s), 1241 (s), 844 (s), 716 (vs) cm⁻¹.

(R)-3-(3-(*tert*-butyl)-5-oxo-2-(1-pyrenylmethyl)pyrazolidin-1-yl)-DMAP (7)
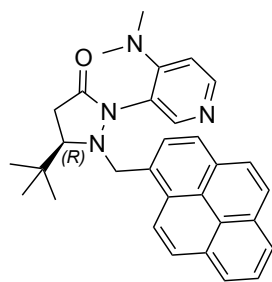
7

S10 (164 mg, 0.333 mmol, 1.00 eq) and iron powder (93 mg, 1.66 mmol, 5.00 eq) are suspended in 8 mL of glacial acetic acid and heated to 85 °C for 21 h. Crushed ice is added and the mixture is basified trough addition of 32% NaOH. 10 mL of EtOAc are added and stirred heavily for 1 hour. After filtration the aqueous phase is extracted with EtOAc (3 x 15 mL). The combined organic layers are dried over MgSO$_4$ and the solvent is evaporated under reduced pressure. Column chromatography (silica gel, EtOAc/MeOH = 98/2) yields 65 mg (0.14 mmol, 41%) of **7** as brown needles.

mp +234°C (decomposition). R_f 0.29 (EtOAc/MeOH = 98/2). $[\alpha]_{25}^D$ = +38.9 ° (c 0.48, CHCl$_3$). **^{1}H NMR** (400 MHz, CDCl$_3$) δ 8.99 (s, 1H, Ar-*H*), 8.28 (d, *J* = 5.9 Hz, 1H, Ar-*H*), 8.19 (d, *J* = 7.6 Hz, 2H, Ar-*H*), 8.16 – 7.98 (m, 6H, Ar-*H*), 7.91 (d, *J* = 7.7 Hz, 1H, Ar-*H*), 6.74 (d, *J* = 5.9 Hz, 1H, Ar-*H*), 5.16 (d, *J* = 11.8 Hz, 1H, NC*H$_2$*), 4.46 (d, *J* = 11.7 Hz, 1H, NC*H$_2$*), 3.44 (dd, *J* = 16.9, 9.7 Hz, 1H, C*Ht*Bu), 3.24 (d, *J* = 9.6 Hz, 1H, COC*H$_2$*), 3.08 (s, 6H, NEt$_2$), 2.56 (d, *J* = 16.9 Hz, 1H, COC*H$_2$*), 0.42 (s, 9H, *t*Bu*H*) ppm. **^{13}C NMR** (101 MHz, CDCl$_3$) δ = 169.7 (C=O), 152.7 (s), 149.4 (s), 148.7 (s), 131.6 (s), 131.3 (s), 130.9 (s), 130.6 (s), 129.2, 129.1, 128.2, 127.9, 127.4, 126.2, 125.7, 125.5, 124.9 (s), 124.7 (s), 124.3, 123.5, 121.4, 111.6, 66.3, 59.5, 41.2 (2C), 34.6, 31.5, 25.6 (3C) ppm. **ESI-HRMS** m/z calc. for C$_{31}$H$_{32}$N$_4$O [M+H]$^+$ 477.26489; found 477.26468. **EA** calc. for C$_{31}$H$_{32}$N$_4$O N 11.76, C 78.12, H 6.77, O 3.36; found N 11.62, C 77.34, H 7.01. **IR** ν = 2947 (w, -C-H), 1700 (vs, C=O), 1592 (s), 1382 (m), 854 (vs) cm^{-1}. **Crystal structure** see Chapter 6.3.5.

Catalyst **3** was freshly synthesized following the protocol described by Sibi *et al.*[3, 10] described above.

2-*L*-Boc-prolin-5-(R)-(*tert*-butyl)-1-(1-naphthylmethyl)pyrazolidin-3-one (S12)
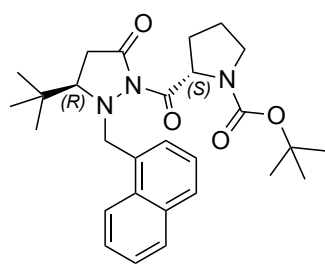
(R)-S12
ee > 99

Following literature procedure[3] with 2.51 g (8.9 mmol) racemic 5-(*tert*-butyl)-1-(1-naphthylmethyl)pyrazolidin-3-one **S11** yields 1.05 g of (*R*)-**S12** (2.18 mmol, 49%) as colourless crystals. Diastereomeric separation was performed by repeated column chromatography (silica gel, *i*Hex/Acetone = 9/1, later diastereomer) followed by repeated recrystallization from *i*Hex/Acetone = 9/1 yielding a diastereomeric excess > 99.5 analysed by NMR and HPLC. Absolute configuration was confirmed by single crystal X-ray analysis. Analytical data are in accordance with literature values.[3]

$[\alpha]_{25}^D$ = -32.8° (c 0.50, CHCl$_3$). **^{1}H NMR** (400 MHz, CDCl$_3$) δ 9.03 (t, *J* = 7.6, 7.6 Hz, 1H), 7.83 (t, *J* = 7.0 Hz, 2H), 7.65 (q, *J* = 6.8, 6.8, 5.5 Hz, 1H), 7.51 (t, *J* = 7.0 Hz, 1H), 7.37 (dt, *J* = 14.4, 6.9 Hz, 2H), 5.34 (d, *J* = 8.9 Hz, 1H), 4.82 (t, *J* = 10.3 Hz, 1H), 3.97 – 3.82 (m, 1H), 3.76 – 3.62 (m, 1H), 3.62 – 3.42 (m, 1H), 3.23 – 2.94 (m, 2H), 2.54 (d, *J* = 18.1 Hz, 1H), 2.50 – 2.34 (m, 1H), 1.99 – 1.72 (m, 3H), 1.45 (d, *J* = 32.1 Hz, 9H), 0.47 (d, *J* = 10.9 Hz, 9H) ppm. **^{13}C NMR** (101 MHz, CDCl$_3$) δ

174.6 (d), 169.3 (d), 154.3 (d), 133.8, 133.3, 132.2 (d), 129.6, 129.4 (d), 128.0 (d), 126.8, 126.8 (d), 126.3 (d), 124.7 (d), 79.7 (d), 63.9 (d), 60.5, 59.8 (d), 47.0 (d), 34.4 (d), 31.9, 31.0 (d), 28.6 (d), 25.7, 23.3 (d) ppm. **ESI-HRMS** m/z calc. for $C_{28}H_{37}N_3O_4$ [M+H]$^+$ 480.28568; found 480.28627; [M-H]$^-$ 478.27113; found 478.27142. **Crystal structure** see Chapter 6.3.5.

(R)-5-(Tert-butyl)-1-(1-naphthylmethyl)pyrazolidin-3-one ((R)-S11)
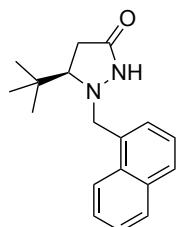
(R)-S11

Following literature procedure[3] with 1.04 g (2.2 mmol) (R)-**S12** yields 850 mg (1.77 mmol, 84%) of (R)-**S11** as yellow solid. Analytical data are in accordance with literature values.[3]

$[\alpha]_{25}^D$ = -158.5° (c 0.42, CHCl$_3$). **^{1}H NMR** (400 MHz, CDCl$_3$) δ 8.26 (d, J = 8.3 Hz, 1H), 7.93 – 7.77 (m, 2H), 7.60 – 7.47 (m, 2H), 7.47 – 7.37 (m, 2H), 6.78 (s, br, 1H), 4.39 (d, J = 12.1 Hz, 1H), 4.23 (d, J = 12.1 Hz, 1H), 3.14 (dd, J = 9.6, 2.0 Hz, 1H),

2.99 (dd, J = 17.4, 9.6 Hz, 1H), 2.30 (d, J = 19.4 Hz, 1H), 0.88 (s, 9H) ppm. **^{13}C NMR** (101 MHz, CDCl$_3$) 174.5, 134.0, 132.2, 132.2, 129.2, 129.0, 128.8, 126.4, 126.0, 125.3, 124.6, 71.8, 64.0, 35.1, 30.1, 25.8 ppm. **ESI-HRMS** m/z calc. for $C_{18}H_{22}N_2O$ [M+H]$^+$ 283.1810; found 283.1808; [M-H]$^-$ 281.1659; found 281.1658.

(R)-3-(3-(tert-butyl)-5-oxo-2-(1-naphthylmethyl)pyrazolidin-1-yl)-4-nitropyridine N-oxide

S13
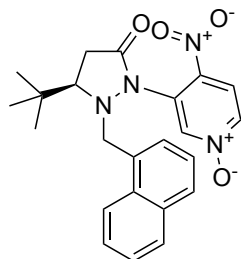
(S13)

Following literature procedure[3] with 419 mg (1.49 mmol) (R)-**S12** yields 474 mg (1.13 mmol, 76%) of (R)-**S11** as reddish solid. Analytical data are in accordance with literature values.[3]

$[\alpha]_{25}^D$ = -559.4° (c 0.51, CHCl$_3$). **^{1}H NMR** (400 MHz, CDCl$_3$) δ 8.22 (d, J = 8.5 Hz, 1H), 8.09 (s, 1H), 7.83 (dd, J = 8.3, 1.2 Hz, 1H), 7.75 – 7.63 (m, 2H), 7.63 – 7.48 (m, 4H), 7.24 – 7.13 (m, 1H), 4.67 (d, J = 12.1 Hz, 1H), 4.55 (d, J = 12.1 Hz, 1H), 3.42 – 3.27 (m, 2H), 2.53 (d, J = 16.0 Hz, 1H), 0.89 (s, 9H) ppm. **^{13}C NMR** (101 MHz, CDCl$_3$) δ 171.0, 136.1, 135.5, 134.3, 133.4, 132.0, 130.4, 130.3, 129.9, 129.5, 129.1, 127.5, 126.5, 124.8, 123.3, 121.4, 70.1, 63.1, 35.2, 31.0, 25.9 ppm. **ESI-HRMS** m/z calc. for $C_{23}H_{24}N_4O_4$ [M+H]$^+$ 421.1876; found 421.1877; [M-H]$^-$ 419.1725; found 419.1728.

(R)-3-(3-(tert-butyl)-5-oxo-2-(1-naphthylmethyl)pyrazolidin-1-yl)-DMAP N-oxide (S14)
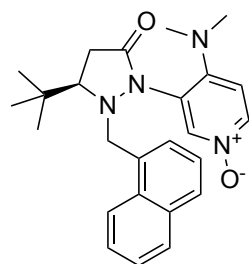
S14

Following literature procedure[3] with 463 mg (1.10 mmol) **S13** yields 323 mg (0.84 mmol, 77%) of **S14** as yellow solid. Analytical data are in accordance with literature values.[3]

$[\alpha]_{25}^D$ = -166° (c 0.49, CHCl$_3$). **^{1}H NMR** (400 MHz, CDCl$_3$) δ 8.66 (d, J = 2.2 Hz, 1H), 8.07 – 7.91 (m, 2H), 7.91 – 7.78 (m, 2H), 7.71 – 7.60 (m, 1H), 7.50 (t, J = 7.5, 7.5 Hz, 1H), 7.46 – 7.34 (m, 2H), 6.71 (d, J = 7.4 Hz, 1H), 4.84 (d, J = 11.6 Hz, 1H), 4.23 (d, J = 11.6 Hz, 1H), 3.35 (dd, J = 17.1, 9.8 Hz, 1H),

3.16 (d, *J* = 10.9 Hz, 1H), 3.01 (s, 6H), 2.49 (d, *J* = 18.3 Hz, 1H), 0.47 (s, 9H) ppm. **^{13}C NMR** (101 MHz, CDCl$_3$) *δ* 169.6, 146.0, 137.7, 137.1, 133.7, 132.5, 131.1, 129.6, 129.4, 128.8, 127.4, 126.4, 124.8, 123.6, 123.1, 113.7, 66.3, 59.8, 41.3, 34.5, 31.0, 25.6 ppm. **ESI-HRMS** m/z calc. for C$_{25}$H$_{30}$N$_4$O$_2$ [M+H]$^+$ 419.2447; found 419.2452; [M-H]$^-$ 417.2296; found 417.2303.

(R)-3-(3-(*tert*-butyl)-5-oxo-2-(1-naphthylmethyl)pyrazolidin-1-yl)-DMAP (3)
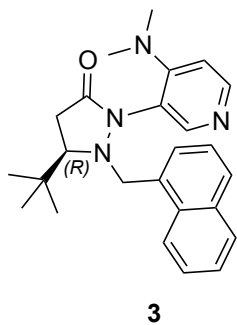
Following literature procedure[3] with 200 mg (0.48 mmol) **S14** yields 102 mg (0.25 mmol, 53%) of **S14** as colourless crystals. Analytical data are in accordance with literature values.[3]

[*α*]$_{25}^D$ = -130.1 ° (c 0.54, CHCl$_3$). **^{1}H NMR** (400 MHz, CDCl$_3$) *δ* 8.83 (s, 1H, Ar-*H*), 8.23 (d, *J* = 5.9 Hz, 1H, Ar-*H*), 7.90 – 7.74 (m, 3H, Ar-*H*), 7.51 – 7.32 (m, 4H, Ar-*H*), 6.70 (d, *J* = 5.9 Hz, 1H, Ar-*H*), 4.92 (d, *J* = 11.7 Hz, 1H, NC*H$_2$*), 4.15 (d, *J* = 11.7 Hz, 1H, NC*H$_2$*), 3.34 (dd, *J* = 17.0, 9.9 Hz, 1H, C*H*tBu), 3.15 (d, *J* = 9.7 Hz, 1H, COC*H$_2$*), 3.03 (s, 6H, NEt$_2$), 2.51 (d, *J* = 18.2 Hz, 1H, COC*H$_2$*), 0.48 (s, 9H, tBu*H*) ppm. **^{13}C NMR** (101 MHz, CDCl$_3$) *δ* 169.8 (C=O), 152.9 (s), 149.6, 148.7, 133.7 (s), 132.6 (s), 131.9 (s), 129.3, 129.0, 128.5, 126.6, 126.1, 124.8, 124.2, 121.3 (s), 111.5, 66.2, 59.6, 41.2 (2C), 34.5, 31.4, 25.6 (3C) ppm. **ESI-HRMS** m/z calc. for C$_{25}$H$_{30}$N$_4$O [M+H]$^+$ 403.24924; found 403.24855; [M+Cl]$^-$ 437.21137; found 437.2114.

6.3.3. Synthesis of Alcohols

1-(2-Phenanthryl)ethanol (1c)
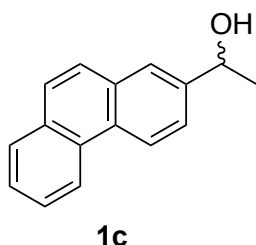
A solution of 2-acetylphenanthren (300 mg, 1.36 mmol, 1.00 eq) in dry THF (10 mL) is dropped into a suspension of LiAlH$_4$ (77 mg, 2.03 mmol, 1.50 eq) in 5 ml of dry THF at 0 °C. After heating to reflux for 2 h the reaction mixture is cooled to 0 °C and 5 mL of water is added. The mixture is stirred for 15 min at rt and HCl (2M) is added. The mixture is extracted with DCM (3 x 10 mL), the organic phase washed with brine (10 mL), dried over MgSO$_4$ and the solvent is evaporated under reduced pressure. Recrystallization from *i*Hex/EtOAc (9/1) yields 210 mg (0.95 mmol, 70%) **1c** as white needles. Analytical data were found to be in accordance with literature values.[11]

mp +126°C. **^{1}H NMR** (400 MHz, CDCl$_3$) *δ* 8.68 (d, *J* = 8.5 Hz, 2H, Ar-*H*), 7.96 – 7.85 (m, 2H, Ar-*H*), 7.75 (d, *J* = 1.5 Hz, 2H, Ar-*H*), 7.71 – 7.54 (m, 3H, Ar-*H*), 5.14 (qd, *J* = 6.4, 2.9 Hz, 1H, C*H*OH), 1.95 (d, *J* = 3.1 Hz, 1H, O*H*), 1.63 (d, *J* = 6.5 Hz, 3H, C*H$_3$*CHOH) ppm. **EI-HRMS** m/z calc. for C$_{16}$H$_{14}$O [M]$^+$ 222.1039; found 222.1039. **HPLC** (Chiralpak IB-N5, 0.5 mL/min, *i*Hex/*i*Prop = 98/2 (13 min) → 91/9 (39 min) → 70/30, *T* = +10, *λ* = 285 nm) t$_1$ *(S)* = 49.7 min, t$_2$ *(R)* = 51.9 min.
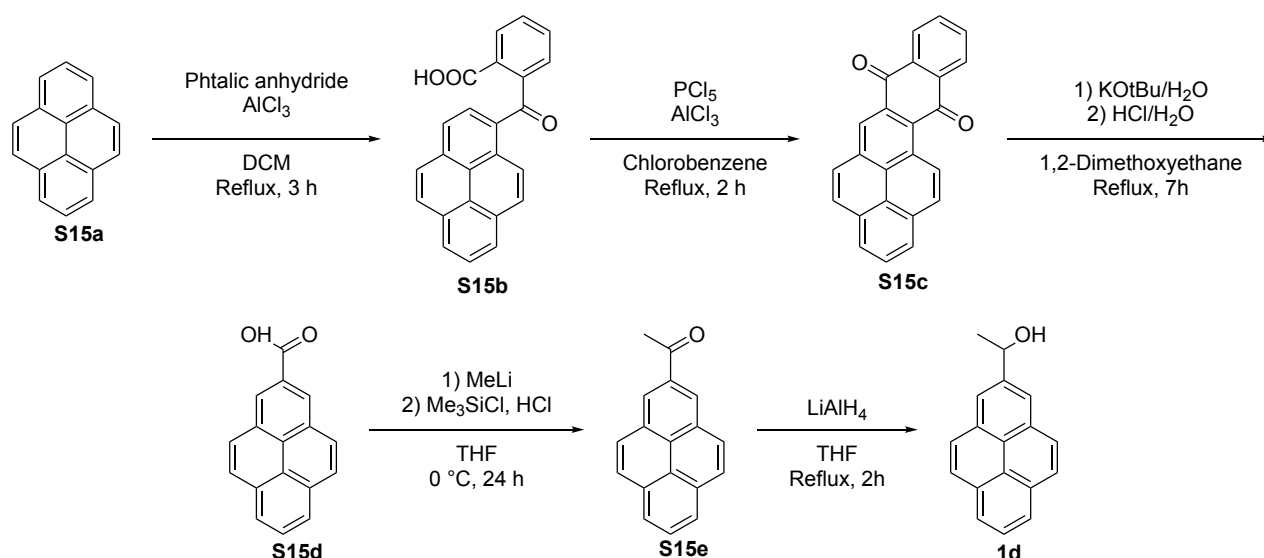
Scheme 6.22. Synthesis of 1-(2-pyrenyl)ethanol (**1d**). The first three steps to **S15d** follow a procedure described in the literature.[12] Synthesis of **1d** was adapted from literature.[13]

2-Acetylpyren (S15e)
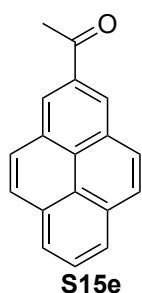
2-Pyrenyl carboxylic acid **S15d** was synthesized following the literature procedure[12] shown in **Scheme 6.22** starting from 5.0 g of pyrene **S15a** (24.7 mmol, 1.0 eq). Crude intermediates NMR data were in accordance with literature values. Crude 2-pyrenyl carboxylic acid **S15d** (4.50 g, 18.2 mmol, 1.0 eq) was solved in 80 mL of dry THF under N_2 atmosphere and cooled to 0 °C. A 1.6 M solution of methyl lithium in diethyl ether (28.5 mL, 45 mmol, 2.5 eq) is dropped slowly into the solution under ice cooling. The reaction mixture is stirred for 24 h and quenched with trimethyl silyl chloride (12.7 mL, 100 mmol). After addition of 50 mL of HCl (aq) the reaction mixture is extracted with EtOAc (3 x 20 mL), dried over $MgSO_4$, filtered and the solvent is evaporated. Column chromatography (silica, *i*Hex/EtOAc = 9/1) gives 1.93 g of **1de** (7.9 mmol, 32% over 4 steps) as brown solid. **mp** +145°C. **^{1}H NMR** (400 MHz, CDCl$_3$) δ 8.64 (s, 2H, Ar-*H*), 8.16 (d, *J* = 7.5 Hz, 2H, Ar-*H*), 8.11 – 7.97 (m, 5H, Ar-*H*), 2.87 (s, 3H, COC*H$_3$*) ppm. **^{13}C NMR** (101 MHz, CDCl$_3$) δ 198.8 (C=O), 134.1 (s), 131.8 (s), 131.0 (s), 128.3, 127.9, 127.2 (s), 127.0 (s), 125.5, 124.5, 124.2 (s), 27.2 ppm. **EI-HRMS** m/z calc. for $C_{18}H_{12}O$ [M]$^+$ 244.0888; found 244.0890. **IR** ν = 3039 (w, =C-H), 1674 (vs, C=O), 1292.7 (s), 1205.8 (s), 873.7 (s), 843.8 (s), 838.7 (s), 704.6 (vs) cm^{-1}.

1-(2-Pyrenyl)ethanol (1d)
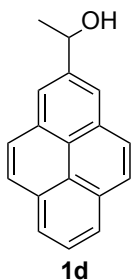
A solution of 2-acetylpyren **S15e** (1.9 g, 7.8 mmol, 1.0 eq) in dry THF (50 mL) is dropped to a dispersion of 444 mg of LiAlH₄ (11.7 mmol, 1.5 eq) in 10 ml of dry THF at 0 °C. After heating to reflux for 2 h the reaction mixture is cooled to 0 °C and 10 mL of water is added. The mixture is stirred for 15 min at rt and HCl (*2M*) is added. The mixture is extracted with DCM (3 x 10 mL), the organic phase washed with brine (10 mL), dried over MgSO₄, filtered and the solvent is evaporated under reduced pressure. Column chromatography (silica, *i*Hex/EtOAc = 4/1 → 2/1) followed by repeated recrystallization from *i*Hex/EtOAc (9/1) yields 1.8 g (7.32 mmol, 94%) **1d** as brown needles. Synthetic data are in accordance with literature data.[14]

mp +136°C. **¹H NMR** (400 MHz, CDCl₃) δ 8.18 (t, *J* = 3.8, 4H, Ar-*H*), 8.13 – 8.03 (m, 4H, Ar-*H*), 8.00 (t, *J* = 7.6, 7.6 Hz, 1H, Ar-*H*), 5.47 – 5.24 (m, 1H, C*H*OH), 2.12 (d, *J* = 2.4 Hz, 1H, O*H*), 1.73 (d, *J* = 6.5 Hz, 3H, C*H₃*CHOH) ppm. **¹³C NMR** (101 MHz, CDCl₃) δ 143.7 (s), 131.4 (s), 131.1 (s), 127.8, 127.5, 125.9 (s), 125.2, 124.7 (s), 124.3 (s), 122.0, 71.1, 26.1 ppm. **EI-HRMS** m/z calc. for C₁₈H₁₄O [M]⁺ 246.1039; found 246.1040. **EA** calc. for C₁₈H₁₄O C 87.78, H 5.73; found C 87.88, H 5.78. **IR** ν = 3279 (br, O-H), 2961 (w, -C-H), 1474 (m), 1099 (m), 880 (s), 712 (vs) cm⁻¹. **Crystal structure** see Chapter 6.3.5. **HPLC** (Chiralpak IB-N5, 0.5 mL/min, *i*Hex/*i*Prop = 98/2 (19 min) → 87/13 (38 min) → 70/30, *T* = +10, λ = 285 nm) t₁ *(S)* = 46.8 min, t₂ *(R)* = 51.0 min.

6.3.4. Synthesis of Esters

(*S*)-1-(pyren-2-yl)ethyl (tert-butoxycarbonyl)-L-phenylalaninate (S3)
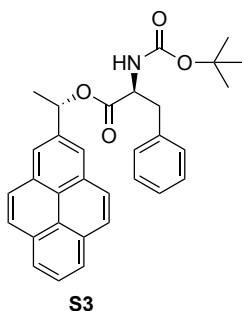
In a kinetic resolution experiment alcohol **1d** (98.4 mg, 0.40 mmol, 1.0 eq) and catalyst **3** (16 mg, 0.04 mmol, 0.10 eq) are solved in 8 mL of dry diethyl ether and cooled to -50 °C. Isobutyric anhydride (37.8 mg, 0.24 mmol, 0.60 eq) in 1 mL of diethyl ether is added and stirred for 48 h at -50 °C. The reaction mixture is quenched through addition of methanol and the solvent is removed under reduced pressure. Unreacted alcohol *(S)*-**1d** is isolated from the reaction mixture by column chromatography (silica, *i*Hex/EtOAc = 9/1). 36 mg of enantiopure *(S)*-**1d** (0.15 mmol, 1.0 eq), 34 mg of EDC (1-ethyl-3-(3-dimethylaminopropyl)carbodiimide, 0.22 mmol, 1.5 eq), 3.6 mg DMAP (0.03 mmol, 0.2 eq) and 46 mg (0.18 mmol, 1.2 eq) of N-(*tert*-butoxycarbonyl)-L-phenylalanine **S2** are solved under N₂ atmosphere in dry DCM and stirred at rt for 24 hours. The reaction mixture is washed with water and brine, dried over MgSO₄, filtered and the solvent is removed under reduced pressure. Column chromatography (silica, *i*Hex/EtOAc = 6/1) followed by recrystallization from diethyl ether yields 66 mg (0.13 mmol, 84% over two steps) of **S3** as white crystals.

mp +148°C. **¹H NMR** (400 MHz, CDCl₃) δ 8.24 – 7.98 (m, 9H, Pyr-*H*), 7.07 – 6.77 (m, 5H, Ph-*H*), 6.37 (q, J = 6.6 Hz, 1H, PyrC*H*OR), 4.97 (d, J = 8.2 Hz, 1H, N*H*), 4.68 (q, J = 6.0 Hz, 1H, C*H*NH),

3.12 – 2.94 (m, 2H, PhCH$_2$), 1.79 (d, J = 6.6 Hz, 3H, CH$_3$), 1.41 (s, 9H, tBu-H) ppm. **^{13}C NMR** (101 MHz, CDCl$_3$) δ 171.5 (s), 155.3 (s), 138.5 (s), 135.7, 131.4 (s), 131.3 (s), 129.4, 128.4, 128.0, 127.5, 126.9 (s), 126.2, 125.3, 124.6 (s, 2C), 123.1, 80.0 (s), 74.2, 54.5, 38.2, 28.5, 22.6 ppm. **EI-HRMS** m/z calc. for C$_{32}$H$_{31}$NO$_4$ [M]$^+$ 493.2248; found 493.2249. **IR** ν = 3377 (m, N-H), 2930 (w, -C-H), 1737 (s, C=O), 1685 (s, C=O), 1515 (s), 1246 (vs), 710 (vs) cm^{-1}. **Crystal structure** see Chapter 6.3.5.

GP1: Esterification of alcohols

A dry Schlenk flask with 1.0 eq of the corresponding alcohol and 0.1 eq of DMAP is evaporated and purged with N$_2$. After addition of 1.1 eq of isobutyric anhydride the mixture is solved in dry THF and stirred at rt under N$_2$ atmosphere overnight. The reaction is quenched through addition of water, extracted with DCM (3x), dried over MgSO$_4$, filtered and the solvent is evaporated. The crude product is purified by column chromatography (iHex/EtOAc = 9/1).
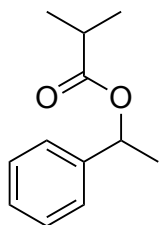
1-Phenylethyl isobutyrate (4a)

4a is synthesized following **GP1** with **1c** (1.22 g, 10.0 mmol) and yields 1.40 g (7.29 mmol, 73%) of colorless liquid. ^{1}H-NMR data were found to be in accordance with literature values.[15]

^{1}**H NMR** (400 MHz, CDCl$_3$) δ 7.39 – 7.27 (m, 5H, Ar-H), 5.87 (q, J = 6.6 Hz, 1H), 2.57 (hept, J = 7.0 Hz, 1H, CH(CH$_3$)$_2$), 1.53 (d, J = 6.6 Hz, 3H, CH$_3$CHO), 1.18 (d, J = 7.0 Hz, 3H, CH(CH$_3$)$_2$), 1.16 (d, J = 7.0 Hz, 3H, CH(CH$_3$)$_2$) ppm. **EI-HRMS** m/z calc. for C$_{12}$H$_{16}$O$_2$ [M]$^+$ 192.1145; found 192.1141. **HPLC** (Chiralpak IB-N5 250 x 4.6 mm, 0.5 mL/min, iHex/iProp = 100/0 (10 min) → 98/2, T = +10, λ = 215 nm) t$_1$ (R) = 18.1 min, t$_2$ (S) = 20.9 min.
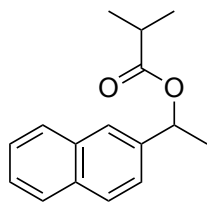
1-(2-Naphthyl)ethyl isobutyrate (4b)

4b is synthesized following **GP1** with **1b** (320 mg, 1.9 mmol) and yields 310 mg (1.28 mmol, 67%) of colourless liquid. ^{1}H-NMR data were found to be in accordance with literature values.[16]

^{1}**H NMR** (400 MHz, CDCl$_3$) δ 7.90 – 7.73 (m, 4H, Ar-H), 7.48 (dd, J = 6.7, 2.9 Hz, 3H, Ar-H), 6.05 (q, J = 6.6 Hz, 1H, CHOCOiPr), 2.60 (hept, J = 7.0 Hz, 1H, CH(CH$_3$)$_2$), 1.62 (d, J = 6.6 Hz, 3H, CH$_3$CHO), , 1.20 (d, J = 7.0 Hz, 3H, CH(CH$_3$)$_2$), 1.17 (d, J = 7.0 Hz, 3H, CH(CH$_3$)$_2$) ppm. **EI-HRMS** m/z calc. for C$_{16}$H$_{18}$O$_2$ [M]$^+$ 242.1301; found 242.1302. **HPLC** (Chiralpak IB-N5, 0.5 mL/min, iHex/iProp = 98/2, T = +10, λ = 285 nm) t$_1$ (R) = 11.8 min, t$_2$ (S) = 13.8 min.

1-(2-Phenanthryl)ethyl isobutyrate (4c)
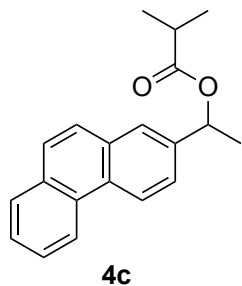
4c is synthesized following **GP1** from **1c** (50 mg, 0.23 mmol) and yields 62 mg (0.21 mmol, 94%) as white fluffy solid.

mp +73.5°C. ^{1}**H NMR** (400 MHz, CDCl$_3$) δ 8.67 (dd, J = 8.3, 2.5 Hz, 2H, Ar-*H*), 7.92 – 7.84 (m, 2H, Ar-*H*), 7.79 – 7.70 (m, 2H, Ar-*H*), 7.66 (t, J = 7.1 Hz, 2H, Ar-*H*), 7.60 (t, J = 7.3 Hz, 1H, Ar-*H*), 6.10 (q, J = 6.6 Hz, 1H, C*H*OCOiPr), 2.62 (hept, J = 6.7 Hz, 1H, C*H*(CH$_3$)$_2$), 1.65 (d, J = 6.6 Hz, 3H, C*H*$_3$CHO), 1.22 (d, J = 7.0 Hz, 3H, CH(C*H*$_3$)$_2$), 1.19 (d, J = 7.0 Hz, 3H, CH(C*H*$_3$)$_2$) ppm. ^{13}**C NMR** (101 MHz, CDCl$_3$) δ 176.5 (C=O), 140.3 (s), 132.2 (s), 132.1 (s), 130.3 (s), 130.0 (s), 128.7, 127.4, 127.0, 126.8, 126.7, 125.9, 124.7, 123.2, 122.8, 72.0, 34.3, 22.5, 19.1 (2C) ppm. **EI-HRMS** m/z calc. for C$_{20}$H$_{20}$O$_2$ [M]$^+$ 292.1458; found 292.1457. **IR** ν = 2974 (w, -C-H), 1726 (vs, C=O), 1196 (s), 1061 (s), 815 (s), 749 (vs), 717 (s) cm^{-1}. **HPLC** (Chiralpak IB-N5, 0.5 mL/min, *i*Hex/*i*Prop = 98/2 (13 min) → 91/9, T = +10, λ = 285 nm) t$_1$ *(R)* = 19.5 min, t$_2$ *(S)* = 31.5 min (br).

1-(2-Pyrenyl)ethyl isobutyrate (4d)
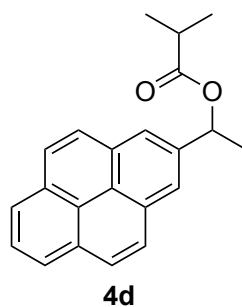
4d is synthesized following **GP1** from **1d** (60 mg, 0.24 mmol) and yields 69 mg (0.22 mmol, 91%) of white powder.

mp +59.6°C. ^{1}**H NMR** (400 MHz, CDCl$_3$) δ 8.18 (m, 4H, Ar-*H*), 8.08 (m, 4H, Ar-*H*), 8.04 – 7.97 (m, 1H) , Ar-*H*, 6.33 (q, J = 6.6 Hz, 1H, C*H*OCOiPr), 2.66 (hept, J = 7.0 Hz, 1H, C*H*(CH$_3$)$_2$), 1.76 (d, J = 6.6 Hz, 3H, C*H*$_3$CHO), 1.24 (d, J = 7.0 Hz, 3H, CH(C*H*$_3$)$_2$), 1.20 (d, J = 7.0 Hz, 3H, CH(C*H*$_3$)$_2$) ppm. ^{13}**C NMR** (101 MHz, CDCl$_3$) δ 176.6 (C=O), 139.8 (s), 131.4 (s, 2C), 131.2 (s, 2C), 127.9 *(S,* 2C*)*, 127.5 *(S,* 2C*)*, 126.1, 125.2 (2C), 124.6 (s), 124.4 (s), 122.6 (2C), 72.6, 34.4, 23.1, 19.2, 19.1 (2C) ppm. **EI-HRMS** m/z calc. for C$_{22}$H$_{20}$O$_2$ [M]$^+$ 316.1458; found 316.1460. **IR** ν = 2970 (w, -C-H), 1719 (vs, C=O), 1196 (s), 1060 (s), 816 (s), 712 (s) cm^{-1}. **HPLC** (Chiralpak IB-N5, 0.5 mL/min, *i*Hex/*i*Prop = 98/2 (19 min) → 87/13, T = +10, λ = 285 nm) t$_1$ *(R)* = 18.9 min, t$_2$ *(S)* = 22.4 min.

6.3.5. X-Ray Crystal Structure Data

Catalyst 7
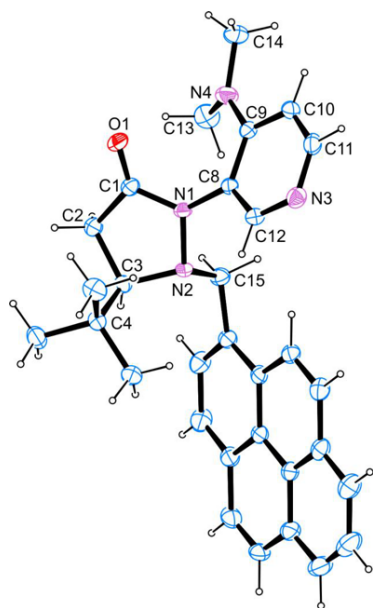
Figure 6.21. X-ray crystal structure of catalyst **7**. The crystal structure can be retrieved from the Cambridge Crystallographic Data Centre (CCDC) with deposition number 2008575.

Table 6.29. Crystallographic data for catalyst **7**.

net formula	$C_{31}H_{32}N_4O$	transmission factor range	0.85–1.00
Mr/g mol^{-1}	476.60	refls. measured	15007
crystal size/mm	0.100 × 0.070 × 0.050	R_{int}	0.0410
T/K	102.(2)	mean σ(I)/I	0.0498
radiation	MoKα	θ range	3.154–27.478
diffractometer	'Bruker D8 Venture TXS'	observed refls.	5528
crystal system	monoclinic	x, y (weighting scheme)	0.0365, 0.3227
space group	'P 1 21 1'	hydrogen refinement	constr
a/Å	9.5123(4)	Flack parameter	−0.2(7)
b/Å	12.9168(6)	refls in refinement	5913
c/Å	11.0888(5)	parameters	330
α/°	90	restraints	1
β/°	106.633(2)	R(F_{obs})	0.0399
γ/°	90	$R_w(F^2)$	0.1011
V/Å^3	1305.46(10)	S	1.070
Z	2	shift/error$_{max}$	0.001
calc. density/g cm^{-3}	1.212	max electron density/e Å^{-3}	0.222
μ/mm^{-1}	0.075	min electron density/e Å^{-3}	−0.179
absorption correction	Multi-Scan		

2-L-Boc-prolin-5-(R)-(tert-butyl)-1-(1-naphthylmethyl)pyrazolidin-3-one (S12)

Figure 6.22. X-ray crystal structure of precursor **S12** for determination of absolute configuration for catalyst **3**. The crystal structure can be retrieved from Cambridge Crystallographic Data Centre (CCDC) with deposition number 2008577.

Table 6.30. Crystallographic data for precursor **S12**.

net formula	$C_{28}H_{37}N_3O_4$	transmission factor range	0.82–1.00
Mr/g mol^{-1}	479.60	refls. measured	5448
crystal size/mm	0.100 × 0.070 × 0.020	R_{int}	0.0815
T/K	102.(2)	mean σ(I)/I	0.0472
radiation	MoKα	θ range	2.456–26.371
diffractometer	'Bruker D8 Venture TXS'	observed refls.	5050
crystal system	monoclinic	x, y (weighting scheme)	0.0368, 2.0438
space group	'P 1 21 1'	hydrogen refinement	constr
a/Å	8.9974(5)	Flack parameter	0.2(16)
b/Å	11.9330(4)	refls in refinement	5448
c/Å	25.1442(11)	parameters	644
α/°	90	restraints	1
β/°	98.388(2)	R(F_{obs})	0.0497
γ/°	90	R_w(F^2)	0.1140
V/Å^3	2670.8(2)	S	1.098
Z	4	shift/error$_{max}$	0.001
calc. density/g cm^{-3}	1.193	max electron density/e Å^{-3}	0.212
μ/mm^{-1}	0.080	min electron density/e Å^{-3}	−0.227
absorption correction	Multi-Scan		

1-(2-Pyrenyl)ethanol (1d)
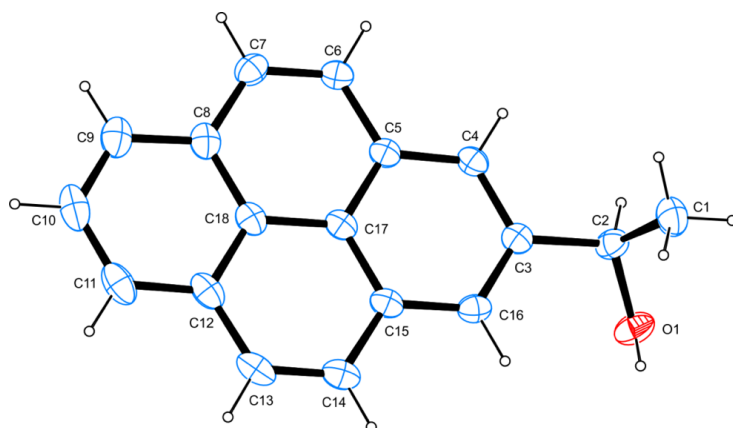
Figure 6.23. X-ray crystal structure of 1-(2-pyrenyl)ethanol (**1d**). The crystal structure can be retrieved from the Cambridge Crystallographic Data Centre (CCDC) with deposition number 2008574.

Table 6.31. Crystallographic data for 1-(2-pyrenyl)ethanol **1d**.

net formula	$C_{18}H_{14}O$	transmission factor range	0.86–1.00
Mr/g mol^{-1}	246.29	refls. measured	12646
crystal size/mm	0.100 × 0.070 × 0.050	R_{int}	0.0370
T/K	102.(2)	mean σ(I)/I	0.0296
radiation	MoKα	θ range	3.210–26.372
diffractometer	'Bruker D8 Venture TXS'	observed refls.	2066
crystal system	monoclinic	x, y (weighting scheme)	0.0614, 0.3144
space group	'P 1 21/c 1'	hydrogen refinement	H(C) constr, H(O) refall
a/Å	20.3785(19)	refls in refinement	2513
b/Å	4.8023(4)	parameters	177
c/Å	13.0679(12)	restraints	0
α/°	90	R(F_{obs})	0.0416
β/°	103.761(3)	R_w(F^2)	0.1230
γ/°	90	S	1.090
V/Å^3	1242.16(19)	shift/error$_{max}$	0.001
Z	4	max electron density/e Å^{-3}	0.172
calc. density/g cm^{-3}	1.317	min electron density/e Å^{-3}	−0.180
μ/mm^{-1}	0.080		
absorption correction	Multi-Scan		

(S)-1-(2-Pyrenyl)ethyl BOC-L-phenylalaninate (S3)

Figure 6.24. X-ray crystal structure of *(S)*-1-(2-pyrenyl)ethyl BOC-L-phenylalaninate (**S3**). The crystal structure can be retrieved from at the Cambridge Crystallographic Data Centre (CCDC) with deposition number 2008576.

Table 6.32. Crystallographic data for *(S)*-1-(2-pyrenyl)ethyl BOC-L-phenylalaninate (**S3**).

net formula	$C_{32}H_{31}NO_4$	transmission factor range	0.78–1.00
$Mr/g\ mol^{-1}$	493.58	refls. measured	19775
crystal size/mm	0.100 × 0.030 × 0.020	R_{int}	0.0459
T/K	102.(2)	mean $\sigma(I)/I$	0.0794
radiation	MoKα	θ range	2.277–25.345
diffractometer	Bruker D8 Venture TXS'	observed refls.	7205
crystal system	monoclinic	x, y (weighting scheme)	0.0408, 0.5045
space group	'P 1 21 1'	hydrogen refinement	constr
a/Å	5.2875(3)	Flack parameter	0.6(7)
b/Å	39.464(2)	refls in refinement	8548
c/Å	12.1953(7)	parameters	676
α/°	90	restraints	1
β/°	90.0081(18)	$R(F_{obs})$	0.0519
γ/°	90	$R_w(F^2)$	0.1086
V/Å^3	2544.7(2)	S	1.043
Z	4	shift/error$_{max}$	0.001
calc. density/g cm^{-3}	1.288	max electron density/e Å^{-3}	0.244
μ/mm^{-1}	0.084	min electron density/e Å^{-3}	−0.212
absorption correction	Multi-Scan		

6.4. Computational Study

6.4.1. Computational Methods

All stationary points (substrate, product and transition state structures) were optimized with the B3LYP-D3 hybrid functional[17] with the 6-31+G(d) basis set. Solvent effects for diethyl ether have been calculated with the SMD continuum solvation model.[18] Frequency and gas phase single point calculations were performed at the same level of theory. As in big systems ubiquitous low-lying frequencies tend to impact entropy and enthalpy in an unpredictable manner a free-rotor approximation for entropy as proposed by Grimme[19] and a quasi-harmonic treatment for enthalpy as proposed by Head-Gordon[20] was applied together with a correction for a concentration of 0.05 mol/L with GoodVibes[21]. All thermochemical properties reported at 298.15 K and 223.15 K were corrected in this manner using (unscaled) frequency calculations at the B3LYP-D3/6-31+G(d) level of theory. Thermochemical corrections as well as solvation energies obtained from the difference of gas and solution phase B3LYP-D3/6-31+G(d) calculations were added to the single point energies calculated at DLPNO-CCSD(T)/def2-TZVPP//SMD(Et$_2$O)/B3LYP-D3/6-31+G(d)[22] level with auxiliary basis set def2-TZVPP/C[23]. This combination was found in previous studies to perform well for this kind of systems.[8, 24] All calculations have been performed with Gaussian 09[25] and ORCA version 4.0.[26] Input structures for reactants and products were generated by a conformational search using Maestro[27] with the OPLS3e force field. Input structures for transition states (TS) were adapted and modified from the literature[28] (for details see Chapter 6.4.5). The conformational space of TS structures was explored with frozen reaction center atoms using Maestro[27] with the OPLS3e force field. Structures were preoptimized with frozen reaction center atoms at the SMD(Et$_2$O)/B3LYP-D3/6-31g(d) level of theory with a convergence criterion of 10^{-5} Hartree before full optimization at SMD(Et$_2$O)/B3LYP-D3/6-31+G(d) level. Transition state structures were confirmed as correct structures through mode analysis of a single negative frequency. For the best 2-3 conformers of each group (see Chapter 6.4.5) intrinsic reaction coordinate (IRC) calculations were performed and the final structures optimized to the respective minima at the SMD(Et$_2$O)/B3LYP-D3/6-31+G(d) level of theory.

AIM analysis was performed with Multiwfn[29]. Plots of non-covalent interaction areas were created using NCIplot[30] and the VMD program.[31] NBO version 3.1[32] was used for analysis of natural charges. Pictures of structures were created with GaussView 5[33] or by CYLview[34]. If not stated otherwise, the following atom colour code was applied: hydrogen (white), carbon (grey), nitrogen (blue), oxygen (red).

6.4.2. Energy Profile of the Reaction

The reaction shown in **Scheme 6.23** was used as a model reaction to determine the origins of stereoselectivity in the computational study.
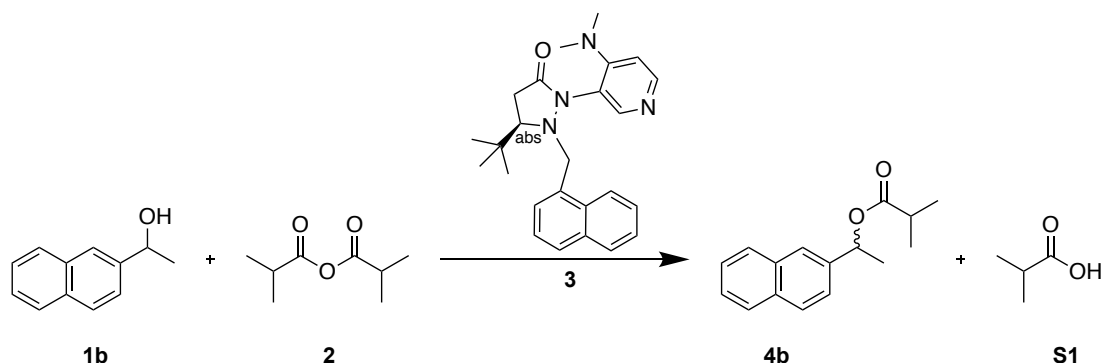
Scheme 6.23. Model reaction for the computational study.
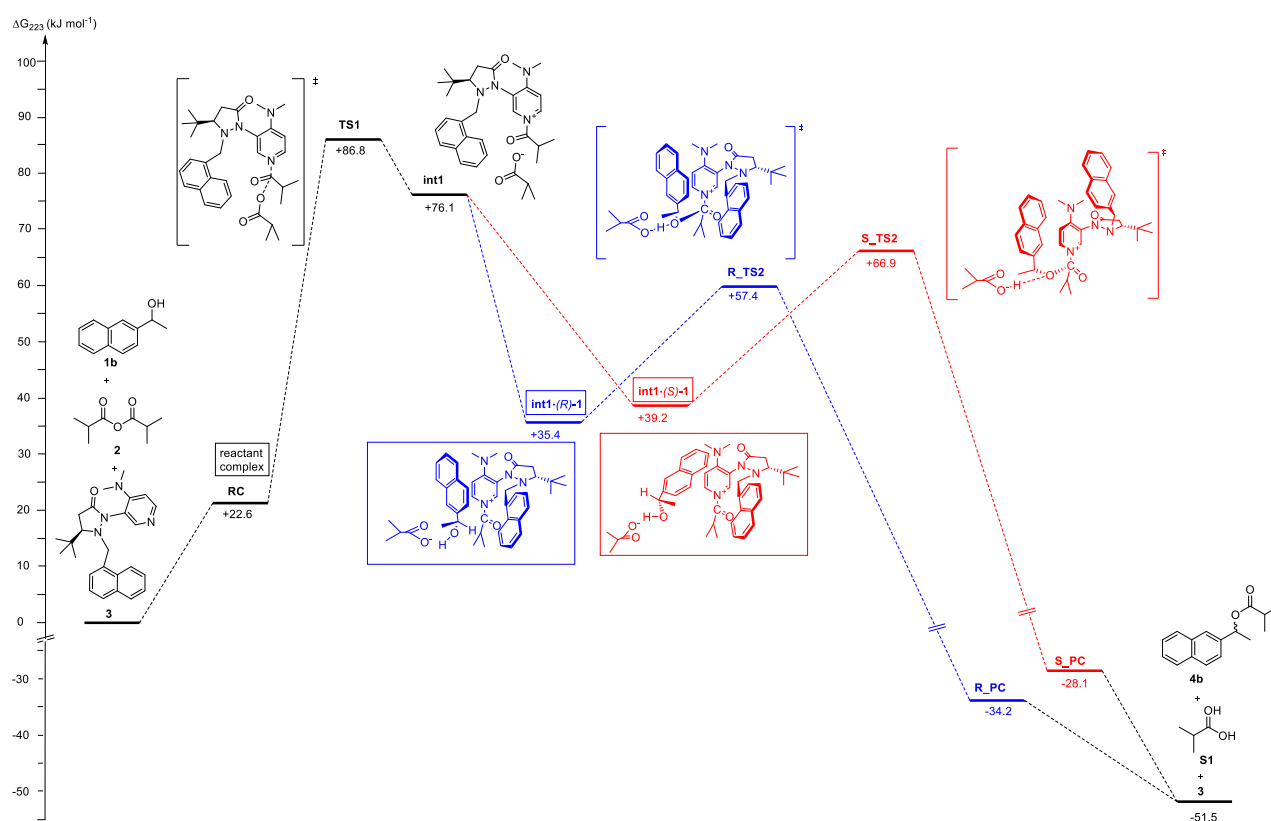
Figure 6.25. Free energy profile for the model reaction as presented in **Scheme 6.23** calculated at DLPNO-CCSD(T)/def2-TZVPP//SMD(Et$_2$O)/B3LYP-D3/6-31+G(d) level of theory. All free energies are Boltzmann averaged and given in kJ mol^{-1} relative to the free energy of the reactants. The depicted structures reflect the best conformation.

Several computational studies on the energy profile for the DMAP-(derivative) catalysed acylation of alcohols were already performed.[28, 35] All studies found that pathways with DMAP acting as a Lewis base and not as a general base are energetically preferable. Accordingly, in this study only the nucleophilic pathway was investigated. The free energy reaction profile (see **Figure 6.25**) implies that loading of the catalyst with isobutyric anhydride in **TS1** is the rate-limiting step. Similar

results were found by Wheeler *et al.*[28b] In contrast, for DMAP and Spivey's chiral DMAP catalysts the acyl transfer was found to be rate limiting.[28a, 35] In all of the mentioned studies the addition of alcohol substrate to **TS1** to form a ternary complex for the acylation of the catalyst was found to be energetically unfavourable. As all kinetic resolution experiments are competition experiments, relative rates are in any case determined in **TS2**. In agreement with the other studies complexing **int1** with the alcohol leads to a major stabilization of the intermediate. This can be mainly attributed to a stabilizing effect on the zwitterionic intermediate through hydrogen bonding and other non-covalent interactions between substrate and loaded catalyst. Interestingly, adduct **int1·***(R)*-**1b** is more stable by about -4 kJ mol^{-1} as compared to **int1·***(S)*-**1b**. In all cases, the isobutyrate moiety is hydrogen bonded to the DMAP pyridinium core. Finally, in **TS2** (see **Scheme 6.24**) the alcohol oxygen atom attacks at the isobutyryl pyridinium cation. In a concerted manner a new C-O-bond is formed and the hydroxyl hydrogen atom is transferred to the isobutyrate moiety. As this step is selectivity determining, the focus of this study lies on **TS2**. Finally, cleavage of the complex leads via product complexes **R_PC** and **S_PC** to ester product **4b**, isobutyric acid **S1** and the recovered catalyst **3**.
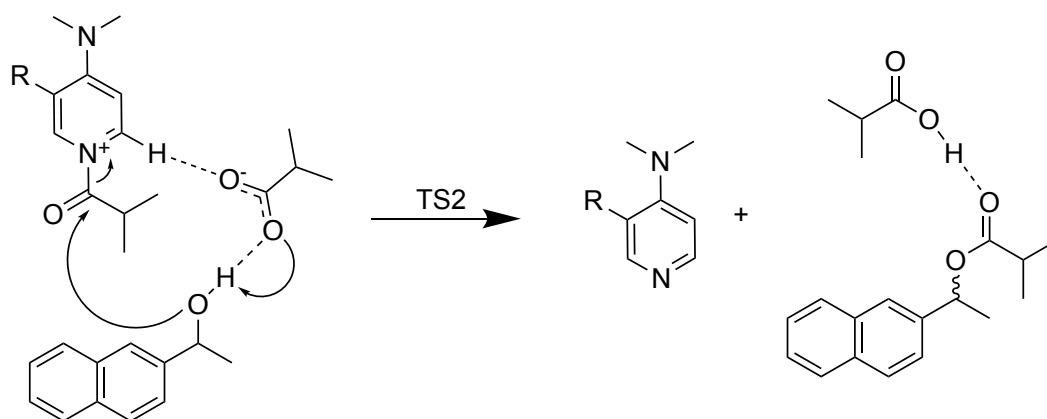
Scheme 6.24. Reaction occurring via the selectivity-determining step **TS2**.

6.4.3. Correlation of Enantioselectivity and Computational Results

The Eyring equation for a (pseudo-)first order reaction Eq. 6.47 allows to correlate experimental selectivity values with differences in activation free energy for the selectivity-determining step **TS2** (Eq. 6.48 with Boltzmann's constant k_B, Planck's constant h, temperature T, gas constant R). The computed difference in Gibb's free energy between the relevant transition states for the *(R)*- and the *(S)*- enantiomers can be correlated with experimental selectivity values according to Eq. 6.49.[36]

$$k = \frac{k_B T}{h} \cdot e^{-\frac{\Delta G^{\ddagger}}{RT}}$$ Eq. 6.47

$$\ln s = \ln\left(\frac{k_R}{k_S}\right) = \ln\left(\frac{\frac{k_B T}{h} \cdot e^{-\frac{\Delta G_R^{\ddagger}}{RT}}}{\frac{k_B T}{h} \cdot e^{-\frac{\Delta G_S^{\ddagger}}{RT}}}\right) = \frac{\Delta G_S^{\ddagger} - \Delta G_R^{\ddagger}}{RT}$$ Eq. 6.48

$$s = e^{\frac{\Delta\Delta G^{\ddagger}}{RT}}$$ Eq. 6.49

Table 6.33. Gibbs's free energies for selectivity-determining transition states **TS2** for *(R)*- and *(S)*-**1b** (see **Scheme 6.23**). Row 2: expected difference in free energy form experimental enantioselectivity value. Row 3 and 4: Results of optimization and thermochemical corrections at B3LYP-D3/6-31+G(d) level of theory. Row 5 and 6: Results for optimized structures without Grimme-D3 dispersion correction. Row 5 and 6 give final values after single point calculations.

method	G_{223} (S)-**TS2** [Hartree]	G_{223} (R)-**TS2** [Hartree]	$\Delta\Delta G^{\ddagger}_{223}$ [kJ mol^{-1}]	G_{298} (S)-**TS2** [Hartree]	G_{298} (R)-**TS2** [Hartree]	$\Delta\Delta G^{\ddagger}_{298}$ [kJ mol^{-1}]
experimental (s = 39)			**6.8**			
SMD(Et2O)/B3LYP-D3/6-31+G(d) Best conformer	-2343.061688	-2343.067300	14.7	-2342.952125	-2342.957966	15.3
SMD(Et2O)/B3LYP-D3/6-31+G(d) Boltzmann average	-2343.061329	-2343.067533	16.3	-2343.091056	-2343.097035	15.7
SMD(Et2O)/B3LYP/6-31+G(d)^a Best conformer	-2342.897980	-2342.898248	0.7			
SMD(Et2O)/B3LYP/6-31+G(d)^a Boltzmann average	-2342.897660	-2342.897892	0.6			
DLPNO-CCSD(T)/def2-TZVPP//SP Best conformer	-2338.801645	-2338.804904	**8.6**	-2338.831417	-2338.83451	8.1
DLPNO-CCSD(T)/def2-TZVPP//SP Boltzmann average	-2338.800977	-2338.804587	**9.5**	-2338.830618	-2338.834046	9.0

^{a}without D3-Dispersion correction

In **Table 6.33** computational and experimental results are compared. SMD(Et2O)/B3LYP-D3 calculations (row 3 and 4) predict the correct trends for enantioselectivity, but overestimate the differences in free energy. When Grimme-D3 dispersion corrections are not included (row 5 and 6), the SMD(Et2O)/B3LYP/6-31+G(d) free energies are almost identical for the different enantiomers and do not reflect the experimentally found enantioselectivities. These findings point to the significant influence of dispersion interactions in governing the enantioselectivity of this reaction.

Finally, single point calculations (row 7 and 8) predict experimental selectivity properly within the reliability of computational methods. Interestingly, the predictions based on free energies of the best conformer are slightly closer to actual values than Boltzmann averaged free energies at 223.15 K. The deviation of 2-3 kJ mol^{-1} from the experimental value is within chemical accuracy (defined as 4 kJ mol^{-1})[37].

6.4.4. Benchmarking of Single Point Calculations

The DLPNO-CCSD(T)/def2-TZVPP//SMD(Et2O)B3LYP-D3/6-31+G(d) combination was already successfully used to describe other Lewis base-catalysed reactions.[8, 24] To verify that this level of theory was chosen properly, single point calculations at different levels of theory for the best three conformers of both enantiomers (based on $G_{223.15}$ after optimization at SMD(Et2O)/B3LYP-D3/6-31+G(d) level) were performed. The respective theoretical methods were chosen based on reports for similar systems.[28] The experimental enantioselectivity of the model reaction (**Scheme 6.23**, s = 39 at 223.15 K) was used as a reference.

Table 6.34. Boltzmann-averaged Gibbs's free energy for selectivity-determining transition state **TS2** on different levels of theory. Single point calculations (SP) were performed for the best three conformers after optimization at SMD(Et2O)/B3LYP-D3/6-31+G(d) level of theory. Thermochemical corrections were added from frequency calculations at optimization level of theory.

	$G_{223.15}$ (S)-**TS2** [Hartree]	$G_{223.15}$ (R)-**TS2** [Hartree]	$\Delta\Delta G^{\ddagger}_{223.15}$ [kJ mol^{-1}]
experimental			6.8
SMD(Et2O)/B3LYP-D3/6-31+G(d) (best 3 conformers)	-2343.937191	-2343.943485	16.5
DLPNO-CCSD(T)/def2-TZVPP//SP (best 3 conformers)	**-2338.801413**	**-2338.804734**	**8.7**
B3LYP-D3/6-311+G(d,p)//SP	-2346.900817	-2346.907257	16.9
M06-2x/6-311+G(d,p)//SP	-2343.532817	-2343.538922	16.0
wB97XD/6-311+G(d,p)//SP	-2342.429061	-2342.434589	14.5

Increasing the basis set for B3LYP-D3 level or use of the M06-2X[38] functional has only minor consequences for the calculated free energy differences (see **Table 6.34**). Results for the long-range corrected method wB97XD[39], that was created to properly describe non-covalent interactions, are much closer to experimental values. However, the use of the coupled cluster method DLPNO-CCSD(T) clearly gives most exact results. CCSD(T)/CBS is known as "golden standard" for calculating noncovalent interactions[40] and close to chemical accuracy. However, calculations are too expensive to be performed with big systems. Neese *et al.*[37] developed the domain based local pair natural orbital DLPNO-CCSD(T) method that can achieve 99.9% of coupled cluster accuracy. Thus the supremacy of this method as shown above is not surprising.

6.4.5. Geometrical Analysis of Conformational Space for TS2

In a big and flexible system like the present one, a systematic strategy is required to address the large conformational space of the transition states in an appropriate manner. We therefore define eight conformational subclasses following the criteria defined below.
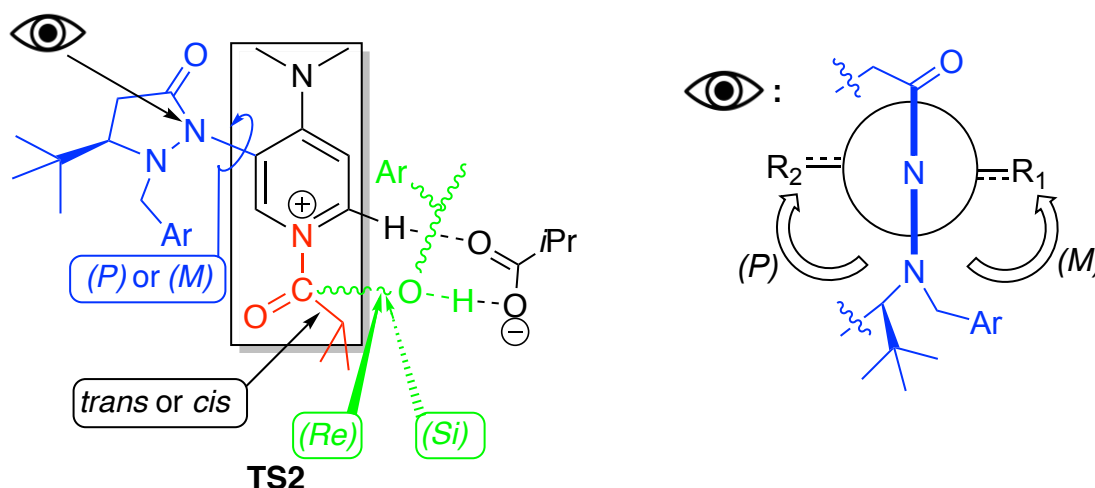
Figure 6.26. Overview of descriptors for the conformation of **TS2** structures based on substituents at the prochiral carbon atom ordered in clockwise decreasing priority. On the right hand the Newman-projection along the atropisomeric C-N-bond is shown. If priority of $R_1 > R_2$ the isomer is denoted *(M)*, if $R_2 > R_1$ it is called *(P)*.

In the loaded catalyst the pyridinium ring and the bonded carbonyl group lie in one plane (see **Figure 6.26**). If the substituents at the prochiral carbonyl C-atom are arranged in clockwise decreasing Cahn-Ingold-Prelog (CIP) priorities, *(Re)* and *(Si)* nomenclature can be applied. The attack of the oxygen atom on the carbonyl carbon (**Figure 6.26**, red part) demands an approximately tetrahedral O-C-O angle. Thus, the oxygen atom of the alcohol (**Figure 6.26**, green part) has to attack the carbon from the "right" side in the so-oriented structure either from *(Re)* or *(Si)*. The position of the isobutyrate is predetermined by the hydrogen-bond to a pyridinium H and by the O-H bond, which is to be formed. Rotation of the pyridinium-N-isobutyryl-C-bond leads to *cis* or *trans* conformations of the pyrazolidinone side-chain of the catalyst (**Figure 6.27**, blue part) relative to the isobutyryl group. Furthermore, atropisomers based on the rotation of the pyrazolidinone ring relative to the pyridinium ring can be distinguished. In the Newman-projection along the pyridinium-C to pyrazolidinone-N-bond CIP (see **Figure 6.26** right side) priorities are assigned to the *ortho* substituents. Note, that in the DMAP core ghost atoms have to be included. If the shortest connection of the atoms with highest priorities on each side of the atropisomeric bond is clockwise, the conformation is denoted *(P)* (plus); a counter clockwise conformation is called *(M)* (minus).[41] All in all, there are eight categories as shown in **Figure 6.27** that adequately partition the conformational space of **TS2**.
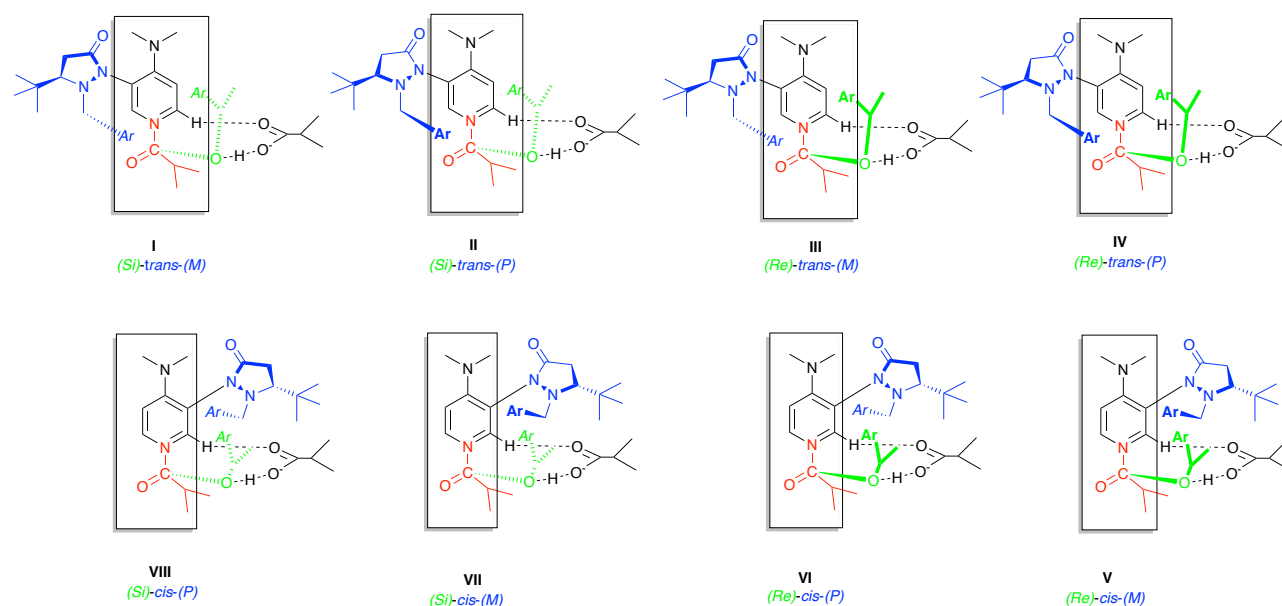
Figure 6.27. Categories defining the conformational space for **TS2**.

Comparable categories were also used before to describe transition states of acylation reactions for other chiral DMAP derivatives.[28] However, previous reports only needed four categories: The chiral DMAP catalyst investigated by Zipse *et al.*[28a] is less flexible and thus no atropisomers were reported. From each of those four categories of both enantiomers the best three transition state conformations (as far as available) were chosen and adapted through substitution of the catalyst side-chain and the alcohol moiety describing the herein investigated system. For the biaryl systems with catalyst **3** investigated by Wheeler *et al.*[28b] no conformers are reported where the alcohol attacks from the more crowded side of the catalyst. This can be rationalized by the much bigger steric demands of a biaryl alcohol compared to the herein investigated secondary alcohols. The reported transition state structures from this study were also adapted to fit the model system. All of these structures were used as starting points for a conformational search with Maestro with frozen reaction centre atoms.

After full optimization of the transition states, the resulting geometries were categorized according to **Figure 6.27**. If for a category no adequate transition state structure existed, new input structures were generated manually either from relevant structures of the other enantiomer or from related categories of the same enantiomer. Also, the best conformers of both enantiomers were cross changed to create new input structures. Overall almost 200 different structures per enantiomer were submitted to transition state optimization after pre-optimization with frozen reaction centres. **Figure 6.28** represents the total energies for all transition state optimizations. All green lines converged to the actual transition states while the negative frequency of red dotted conformers does not fit the investigated reaction (and usually represent e.g. a methyl rotation). Grey marks did not converge to any stationary point. **Figure 6.28** visualizes that a transition state search was performed unbiased and the conformational space is covered in an appropriate manner.
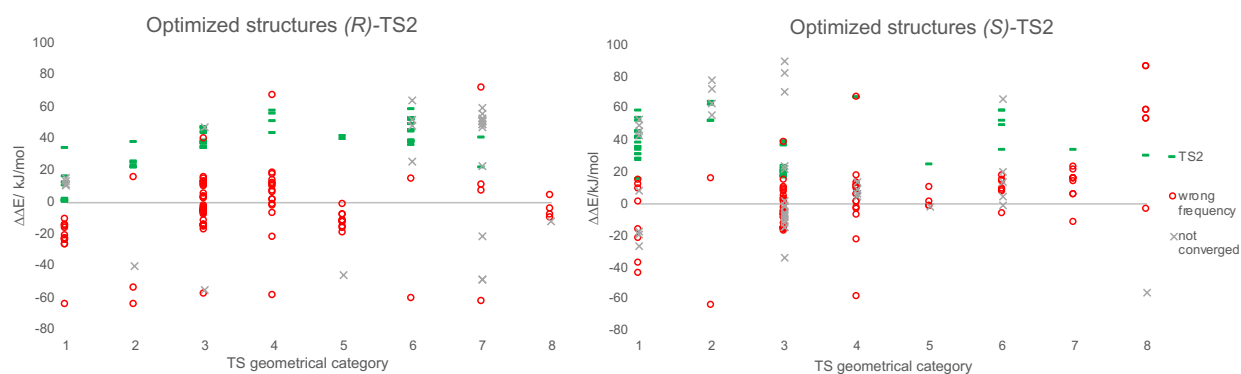
Figure 6.28. Relative energies (in kJ mol^{-1} relative to **R_TS2_1)** at SMD(Et$_2$O)/B3LYP-D3/6-31+G(d) level of theory of all conformers optimized for **TS2** sorted by geometry categories. Green lines represent optimizations that led to the correct transition state, for structures with red signs the negative frequency does not represent the searched transition state. Grey crossed structures did not converge to a stationary point.

As an overview of actual transition state structures **Figure 6.29** show Gibb's free energies at optimization level of theory for all structures that converged into the search transition state relative to best conformer **R_TS2_1.** The structure for the best conformer of each category with relative single point free energy is finally displayed in **Figure 6.30** and **Figure 6.31**.
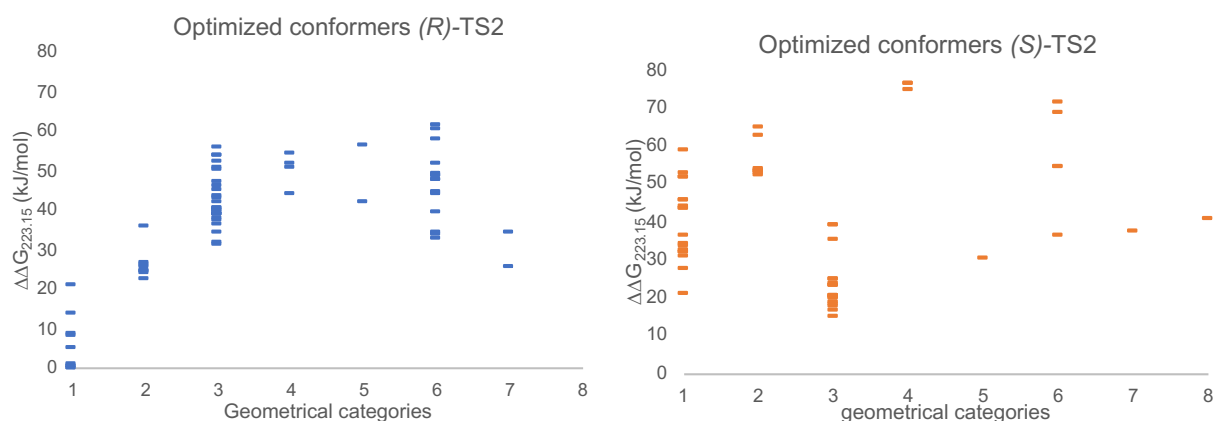
Figure 6.29. Gibb's free energy for optimized conformers for **TS2** (in kJ mol^{-1} relative to **R_TS2_1)** at SMD(Et$_2$O)/B3LYP-D3/6-31+G(d) level of theory sorted by geometrical categories. Transition states were confirmed by mode analysis of the negative frequency and by intrinsic reaction coordinates (IRC) analysis for the best conformers.

Those categories allow a discussion of factors influencing the stability of the transition states. One general trend within the categories is that *(Si)* attack is preferable for the *(R)*-alcohol, while reaction for *(S)*-**1b** proceeds best via a *(Re)*-attack. This can be rationalized by the position of the alcohol methyl group. Moreover, conformations with *trans*-orientation of catalyst side-chain and alcohol are in general more favourable.

Alcohol attack from the more crowded side (category I, IV, V, VIII): For this classes the energetically most preferable conformation may best be described as "cage" structure. *(Si)*-attack of *(R)*-**1b** on *trans-(M)*-oriented catalyst (e.g. **R_TS2_1)** is energetically most favourable. In this class the aromatic side chains of alcohol and catalyst are on the same side of the DMAP core and can interact with each other. In contrast, for the *(S)*-alcohol this perfect geometry interferes with the position of

the methyl group of the alcohol. Thus, it should be expected that a *(Re)*-attack of the *(S)*-alcohol could give a similarly good geometry if the catalyst sidechain is also positioned *(Re)* (cat. IV, V). However, for those positions repulsive interactions of the aromatic rings with the chiral *tert*-butyl group avoids formation of cage structures and significantly higher energies were found. Indeed, the categories with alcohol, catalyst sidechain and *tert*-butyl group together either *(Re)* (cat. IV) or *(Si)* (cat VIII) are most destabilized. Especially for category VIII creation of input structures without overlapping atoms proved to be difficult; for the *(R)*-enantiomer no conformer converged into the correct transition state.

Alcohol attack from the less crowded side (category II, III, VI, VII): In those structures "triple sandwich structures" of catalyst sidechain, pyridinium DMAP core and aromatic alcohol are energetically most favourable. Due to the different orientations of the methyl group in the alcohol enantiomers, those structures are found for *(S)*-**1b** by a *(Re)*-attack (cat. III) and for *(R)*-**1b** by a *(Si)*-attack (cat II). In analogous *cis*-structure (VI and VII) the orientation of chiral *tert*-butyl group of the catalyst disturbs the formation of a triple sandwich to some extent.

As analysis of free energies and calculation of Boltzmann population showed that for *(R)*-**TS2** only category I conformers and for *(S)*-**TS2** only category III conformers are populated by more than 1% those categories are discussed below in detail.
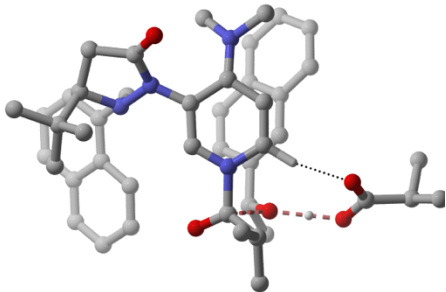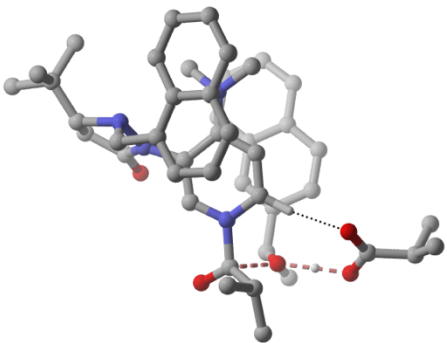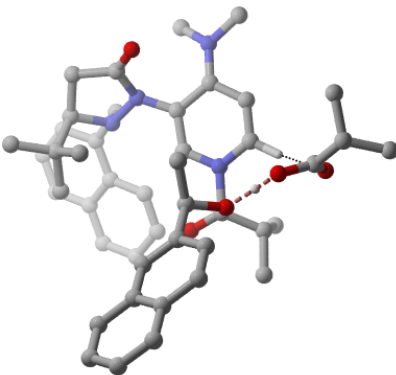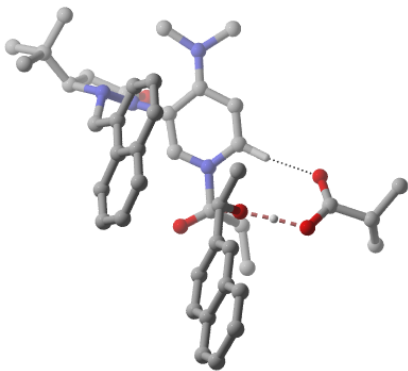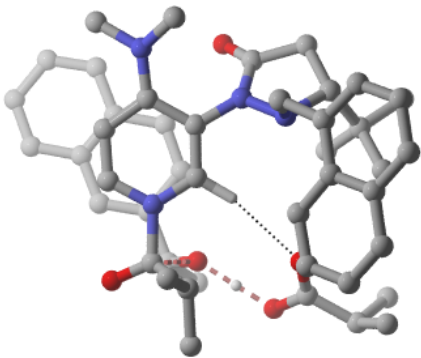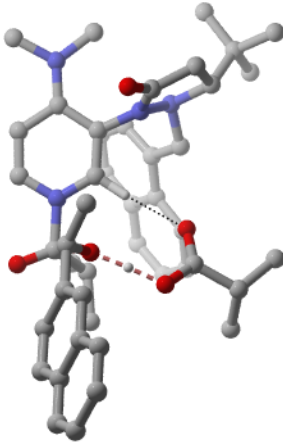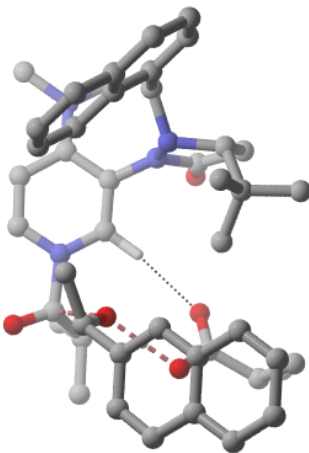
category	I	II	III	IV
geometry				
name	**R_TS2_1**	**R_TS2_10**	**R_TS2_16**	**R_TS2_33**
$\Delta\Delta G^{\ddagger}$	**+0.0**	**+15.3**	**+31.9**	**+40.3**
category	VIII	VII	VI	V
geometry	*No conformer found*			
name		**R_TS2_15**	**R_TS2_18**	**R_TS2_39**
$\Delta\Delta G^{\ddagger}$		**+23.3**	**+32.4**	**+43.3**

Figure 6.30. Structures for the best conformers for each geometrical group for *(R)*-1-(2-naphthyl)ethanol (**1b**). Hydrogens not involved in the reaction are hidden for visual clarity. Differences of free reaction energy of **TS2** relative to best conformer **R_TS2_1** are given in kJ mol^{-1} as calculated on DLPNO-CCSD(T)/def-TZVPP//SMD(Et$_2$O)/B3LYP-D3/6-31+G(d) level of theory.
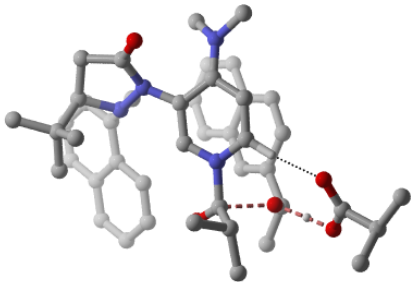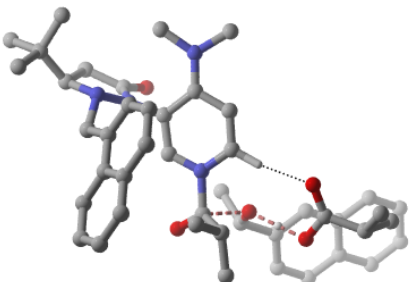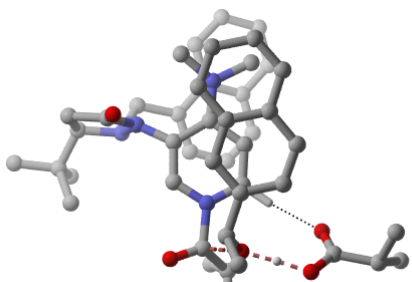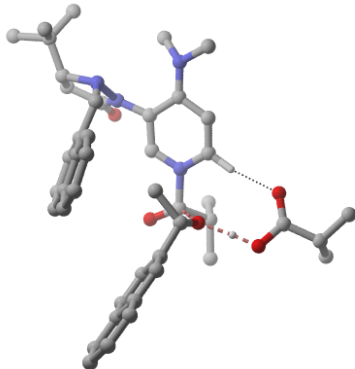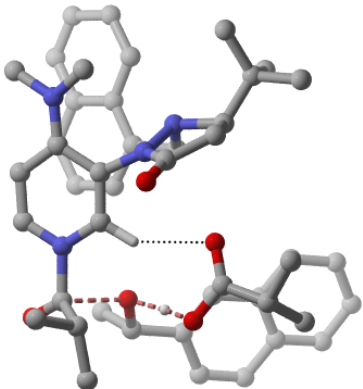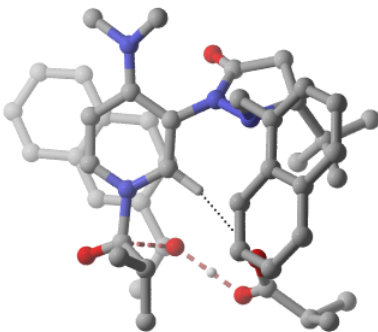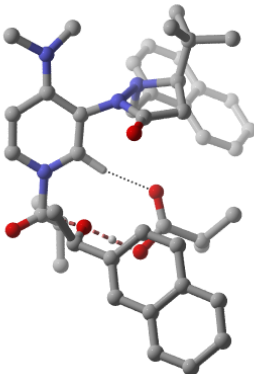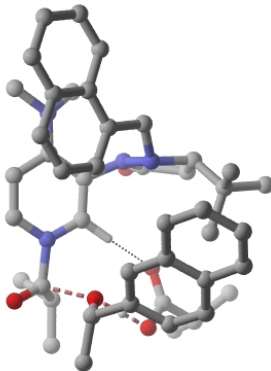
category	I	II	III	IV
geometry				
name	**S_TS2_13**	**S_TS2_29**	**S_TS2_1**	**S_TS2_34**
ΔΔG‡	**+15.7**	**+48.4**	**+8.6**	**+75.3**
category	VIII	VII	VI	V
geometry				
name	**S_TS2_27**	**S_TS2_25**	**S_TS2_24**	**S_TS2_18**
ΔΔG‡	**+39.6**	**+34.71**	**+34.18**	**+27.75**

Figure 6.31. Structures of the best conformers for each geometrical group for *(S)*-1-(2-naphthyl)ethanol (**1b**). Hydrogens not involved in the reaction are hidden for visual clarity. Differences of free reaction energy of **TS2** relative to best conformer **R_TS2_1** are given in kJ mol^{-1} as calculated on DLPNO-CCSD(T)/def-TZVPP//SMD(Et$_2$O)/B3LYP-D3/6-31+G(d) level of theory.

6.4.6. Energetical Analysis of Selectivity-Determining Transition State Structures

The final free energy is composed of gas-phase single-point energies at DLPNO-CCSD(T)/def2-TZVPP level of theory, thermal corrections for free energy and solvation corrections calculated by SMD (Et$_2$O). In order to analyse which of those contributions is mainly responsible for the selectivity-determining differences in Gibbs free energy, individual differences for each of those terms relative to those of the best conformer **R_TS2_1** are presented in **Figure 6.32**.
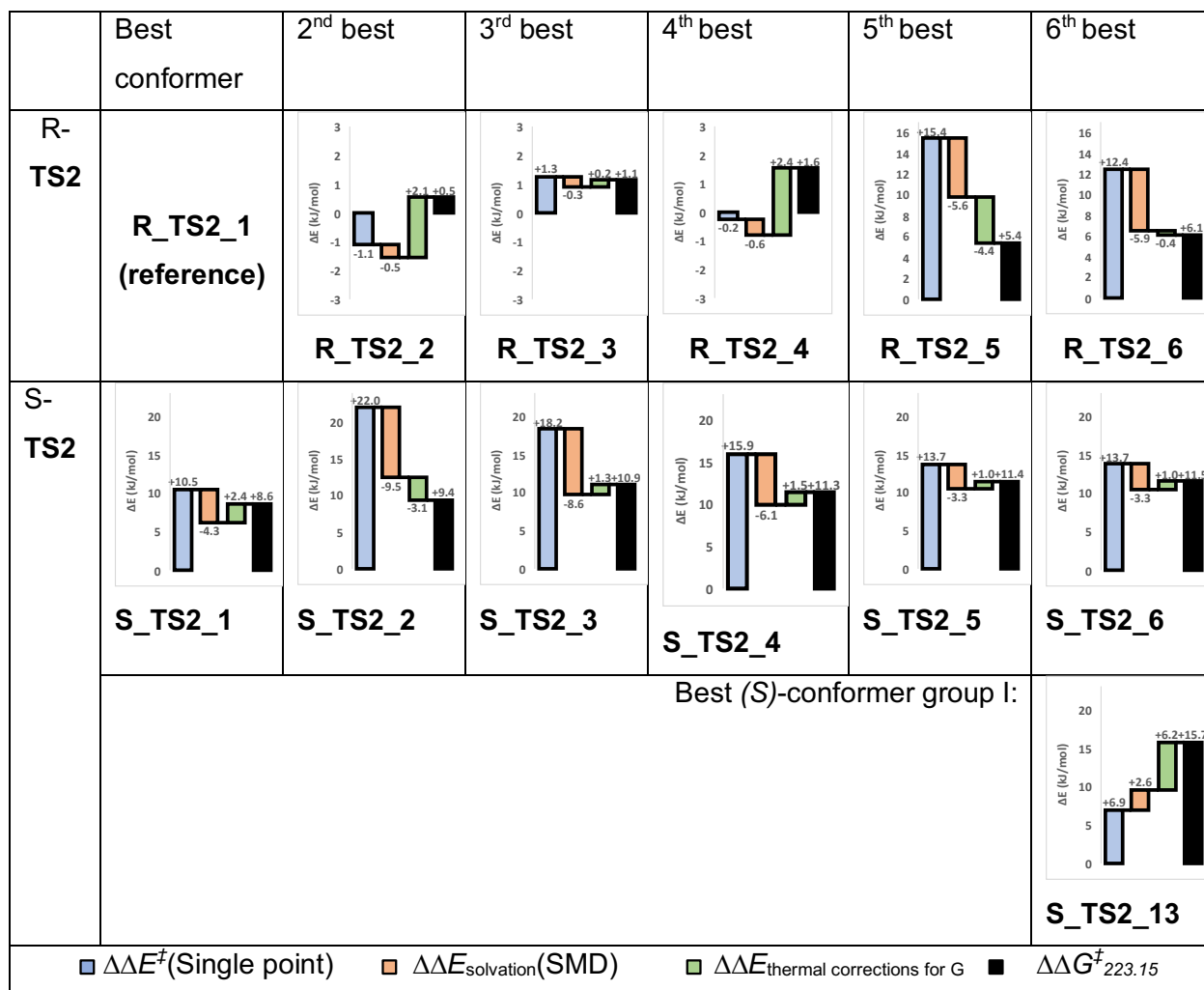
Figure 6.32. Analysis of contributions to Gibbs free energy of the best six conformers for **TS2** of both enantiomers. All energies are given relative to the best conformer for R-**TS2** in kJ mol^{-1}. Blue bars give single point energies at DLPNO-CCSD(T)/def2-TZVPP level of theory, red bars solvation energy from SMD (Et$_2$O) at B3LYP-D3/6-31+G(d) level, green bars thermal correction calculated for the quasi-harmonic rotator Gibbs free energy at 223.15 K and a concentration of 0.05 mol/L, black bars sum of the three former differences resulting in total difference in free energy of conformers.

Best Conformers of (R)-TS2

Within the four best conformers of R-**TS2** only negligible differences are found. Despite the fact that **R_TS2_5** and **R_TS2_6** are also in geometrical class I their single point energy is much higher compared to the other conformers, while solvation and thermal correction have both more negative contribution and are thus more stabilizing. Interestingly, such different patterns in energies reflect a specific difference in geometries in all cases: in **R_TS2_1** to **R_TS2_4** the naphthyl moiety of the catalyst sidechain is oriented towards the hydrophobic pocket formed by pyridine and naphthyl of the alcohol (see **Figure 6.33** left side). In contrast, for **R_TS2_5** and **R_TS2_6** the bigger part of the naphthyl moiety of the sidechain is oriented away from this pocket (see **Figure 6.33** right side). Thus, for those two conformer subgroups the attractive interaction of catalyst side chain with the other aromatic groups in the systems can be estimated. Single point energies (blue bars in **Figure 6.32**) are favoured by around 11 – 16 kJ mol^{-1} through the additional dispersive interactions at DLPNO-CCSD(T) level of theory, which is also reflected by the Grimme D3-dispersion correction for B3LYP-D3/6-31+G(d) calculations, which is in **R_TS2_5** +12.8 kJ mol^{-1} (resp. +8.7 kJ mol^{-1} for **R_TS2_6)** less stabilizing than for **R_TS2_1.** However, those conformations gain stabilizing solvation energy (red bars in **Figure 6.32**). These energetic differences agree with experimental results of Sibi *et al.*[3] that found for catalyst **3** at 0 °C a enantioselectivity of *s = 23* while the analogues catalyst bearing a phenyl instead of a naphthyl moiety (in which only interactions as found in **R_TS2_5** are possible) only gave *s = 15.*

R_TS2_1   **R_TS2_5**

$\triangle\triangle G^{\ddagger}_{223.15}$ = 5.4 kJ mol^{-1}
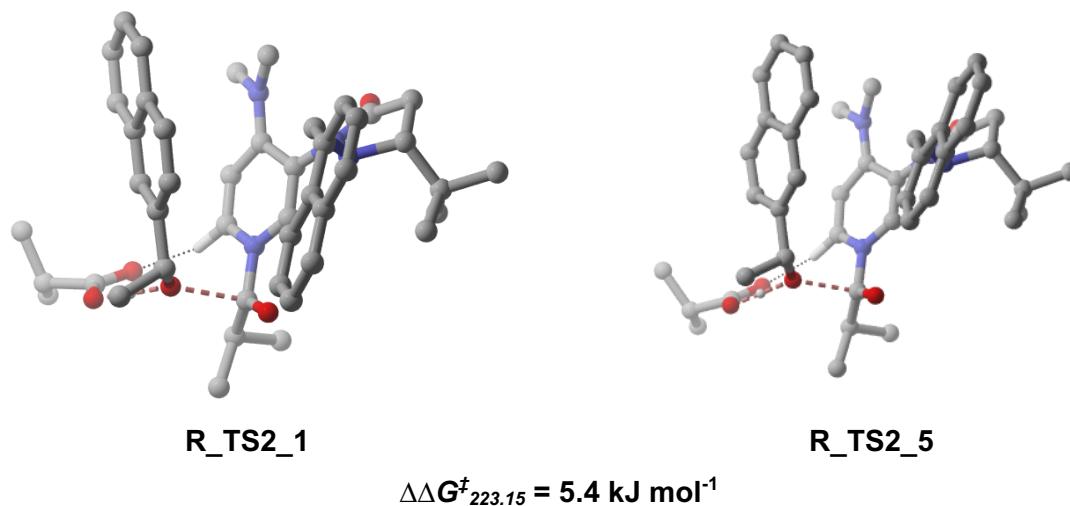
Figure 6.33. Conformation of optimized structures **R_TS2_1** and **R_TS2_5**. The main difference between those two structures is orientation of naphthyl moiety at the catalyst that is either oriented towards or away from hydrophobic pocket.

Best Conformers of (S)-TS2

Regarding the differences in between the best six conformers for *(S)*-**TS2** there are also two distinguished subgroups. **S_TS2_2** and **S_TS2_3** have a much higher single point energy compared to other conformers but they are better stabilized by solvation energy. Basically, **S_TS2_2** and **S_TS2_3** show an edge-to-face aromatic stacking of catalyst naphthyl chain and pyridine moiety, while the other conformers have a triple sandwich structure with face-to-face aromatic stacking (**Figure 6.34**). This is also reflected in Grimme D3-dispersion correction for B3LYP-D3/6-31+G(d) calculations, that is around 15 kJ mol^{-1} less stabilizing for **S_TS2_2** and **S_TS2_3** compared to triple sandwich structure **S_TS2_1**. Parts of this energy difference is equalized by a better stabilization through solvation for **S_TS2_2** and **S_TS2_3.** This result is in agreement with studies indicating that face-to-face and edge-to-face aromatic stacking are energetically comparable.[42]

S_TS2_1   **S_TS2_2**

$\triangle\triangle G^{\ddagger}_{223.15}$ = 0.8 kJ mol^{-1}
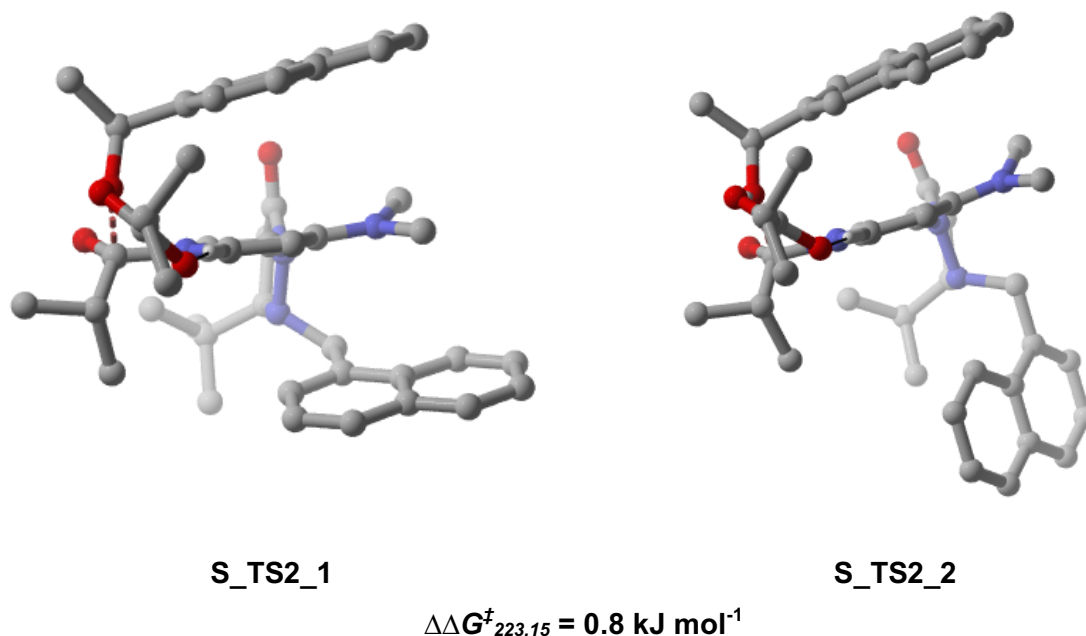
Figure 6.34. Conformation of optimized structures **S_TS2_1** and **S_TS2_2**. The main difference between those two structures is orientation of naphthyl moiety at the catalyst that is either parallel or vertical to the pyridine ring.

Influence of Thermal Correction and Solvation Energy

R_TS2_1   **S_TS2_13**

$\Delta\Delta G^{\ddagger}_{223.15}$ = +15.7 kJ mol^{-1}
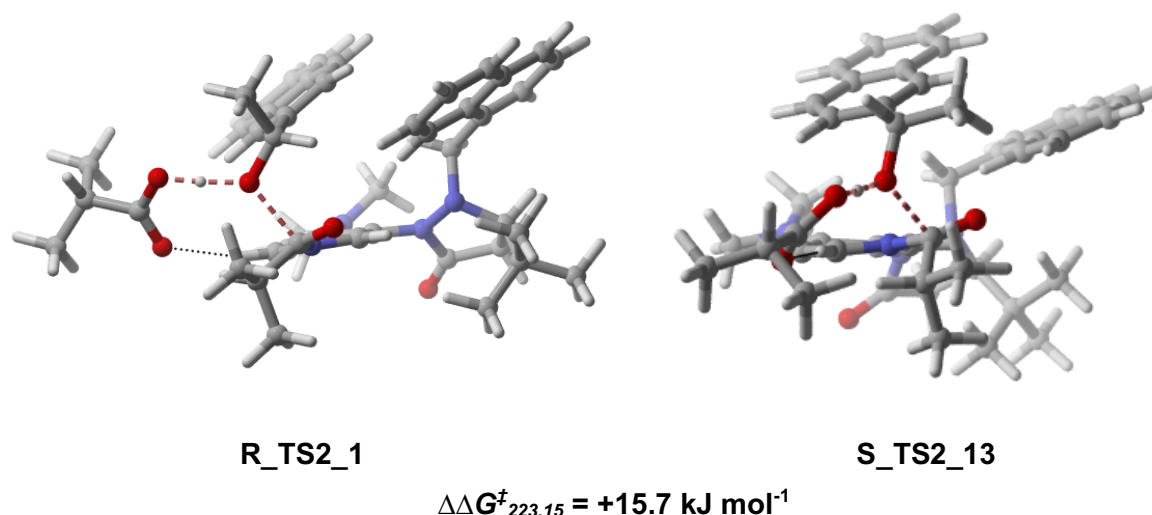
Figure 6.35. Conformation of optimized structures for the best structures in category I for *(R)*- and *(S)*-enantiomer **R_TS2_1** and **S_TS2_13**.

The best *(S)*-conformer in category I **S_TS2_13** has a very similar structure to **R_TS2_1** (see **Figure 6.35**). Interestingly, the single point gas phase energy for **S_TS2_13** is the lowest of all *(S)*-enantiomers, but still disfavoured by +6.9 kJ mol^{-1} relative to **R_TS2_1.** Additionally, the solvation energy of **S_TS2_13** is the least stabilizing of all **TS2** conformers and thermal corrections are energetically unfavourable by +6.2 kJ mol^{-1} relative to **R_TS2_1** (see **Figure 6.32**). The main reason for this difference is the vibrational energy that has a clearly higher impact on thermal corrections for **S_TS2_13** than in **R_TS2_1.** Accordingly, the calculated IR spectrum for **S_TS2_13** shows a very intense scissoring vibration of the alcohol methyl group at 1517 cm^{-1} that does not appear prominently for **R_TS2_1.** The changed position of the methyl group for the *(S)*-enantiomer is thus also thermochemically unfavourable.

However, one should keep in mind that all of the more than 1% populated *(R)*-**TS2** conformers are in category I, while all relevant *(S)*-**TS2**-conformers are in category III. For discussing selectivity determining differences in Gibbs free energy between those *(R)*- and *(S)*-conformers thermal corrections play in general a minor role and do not follow a clear trend.

Solvation energies (red bars in **Figure 6.32**) are more stabilizing for all *(S)*-conformers compared to the best *(R)*-conformers. Strikingly, solvation energy for best conformer **R_TS2_1** is among the least stabilizing of all found **TS2** conformers. Solvation is therefore a counterplayer of the desired enantioselectivity. This is also reflected by a strong solvent-dependence of enantioselectivity values as observed in the original study by Sibi *et al.*[3]. The more detailed analysis of those experimentally reported selectivity values in **Table 6.35** reveals a surprisingly good inverse correlation of ln*(S)* with solvent polarity as described by Reichardt's solvent parameter $E_T(30)$[43]. In more polar solvents stronger solvent-solute interactions appear and energetical contribution of solvation energy grows. Thus, better solved transition state structures are further stabilized by more polar solvents, while this effect is much smaller for complexes with low solvation energy like **R_TS2_1**. This growth in

solvation energy diminishes $\Delta\Delta G^{\ddagger}$ yielding a lower enantioselectivity. From another point of view enantioselectivity is also driven by solvophobic effects that are most prominent in less polar solvents. As the system is already at solvation limit in diethyl ether, it is not possible to increase that effect experimentally by using even less polar solvents.

Table 6.35. Solvent effects on the kinetic resolution of **1b** with **3** at room temperature. Experimental data are reported following Sibi *et al.*[3]. A very good correlation with Reichardt's solvent parameter $E_T(30)$[43] was found.

	s[3]	$\ln(s)$	$E_T(30)$[43]	
THF	9	2.20	37.4	
Et$_2$O	12	2.48	34.5	
Toluene	11	2.40	33.9	
CH$_3$CN	4	1.39	45.6	
CH$_2$Cl$_2$	6	1.79	40.7	

$y = -10.466x + 59.893$
$R^2 = 0.9821$
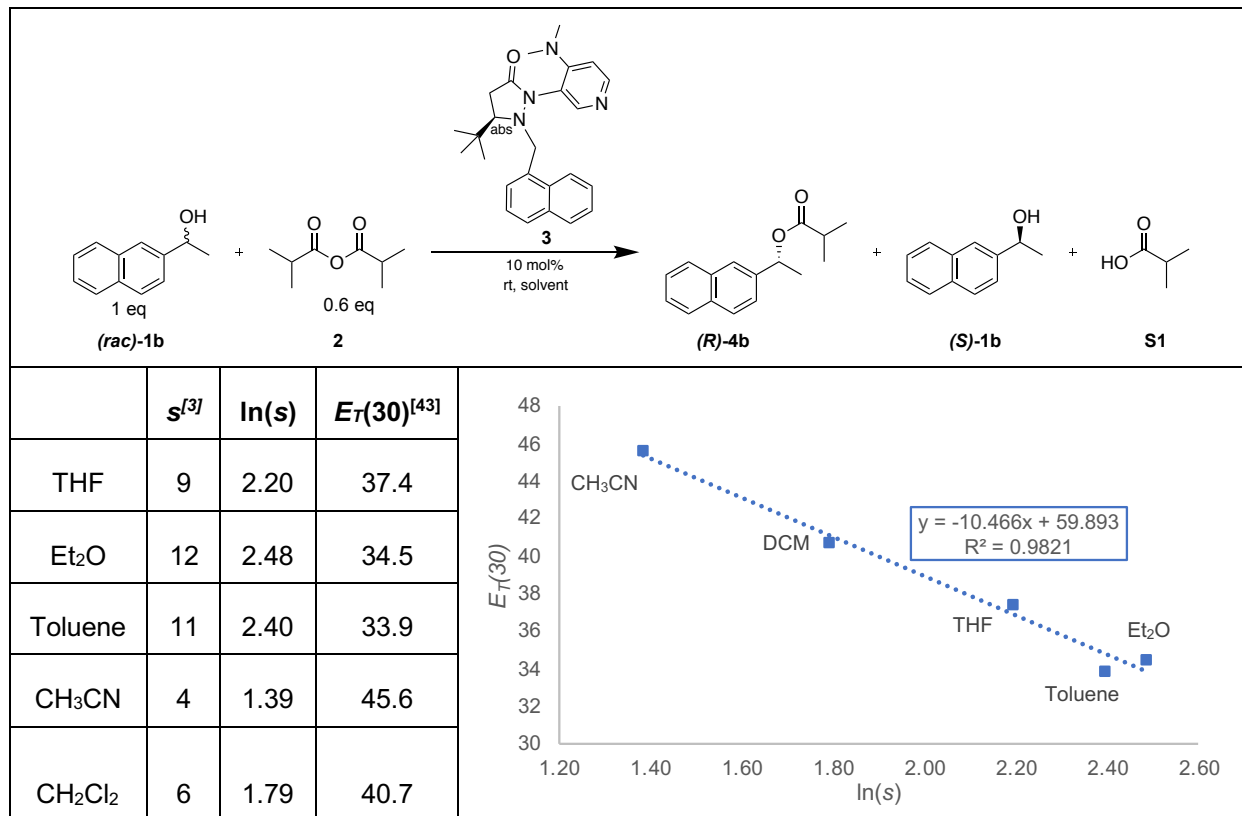
Nonetheless, selectivity-determining differences in Gibbs free energy between the best *(R)*- and *(S)*- conformations are mainly governed by the differences in gas phase single point energies (blue bars in **Figure 6.32**). The following chapter investigates the question in how far those energy differences can be attributed to non-covalent interactions.

6.4.7. Quantification of Intramolecular Non-Covalent Interactions

One way to quantify the strength of non-covalent interactions is to compare Grimme D3-dispersion corrections terms for different systems.[19, 44] As shown in Chapter 6.4.3 ignoring D3-dispersion corrections yields similar free energies for *(R)*- and *(S)*-**TS2**. However, this approach is only partially meaningful. First of all, free energies at B3LYP-D3 level of theory do not reproduce experimental results quantitatively. Deviations for dispersion-corrected DFT methods from high accuracy coupled-cluster methods like DLPNO-CCSD(T) are still in the range of 5%-10%[45]. For coupled-cluster methods no dispersion correction is needed. Secondly, the D3 correction is not designed to quantify the total of non-covalent interactions in a system, but to correct the shortage of DFT methods in describing medium- to long-range dispersion interactions.[46] Thus, especially short-

distance dispersion energies are not reflected by this term. Finally, the D3-dispersion reflects dispersion distributions of inter- and intramolecular non-covalent interactions. While also notable intramolecular dispersion interactions are present in the catalyst, only intermolecular interactions influence the relative rates of the enantiomers in the enantioselectivity determining step **TS2**. Thus, an appropriate method should quantify solely intermolecular dispersion interactions between the alcohol and the loaded catalyst in **TS2** on the coupled-cluster level. One possible strategy is to separate the transition state structure into two or more parts and to calculate single point energies for each of the structures.[44, 47] Energy differences between the separated parts in relation to the full structure reflect then the non-covalent interactions between those two parts. Separation should not be performed at atoms directly involved in the reaction centre as there are presumably very strong intermolecular interactions. Thus, the bond of alcohol and aromatic moiety in **TS2** was cleaved homolytically. The open shell was capped by a H-atom[44, 48] leading to hypothetical structure **TS2**-**HC** and a naphthyl radical (**Scheme 6.25**). This computational approach is in line with the experimental approach of constantly increasing aromatic surfaces.
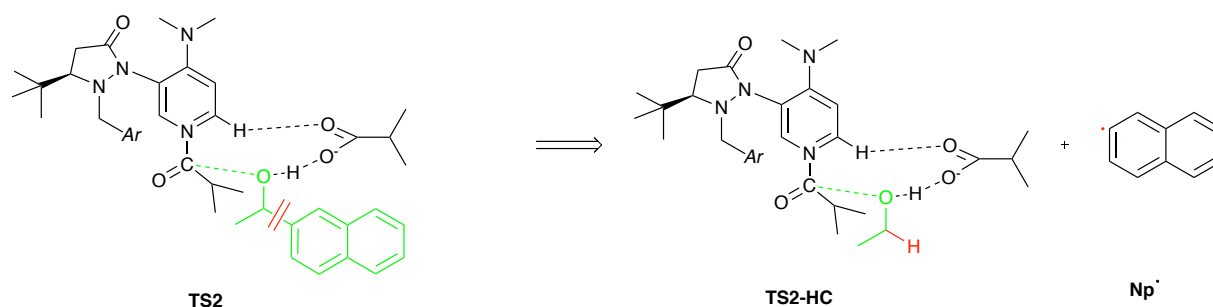
Scheme 6.25. Hypothetical cleavage of **TS2** into H-capped **TS2-HC** and a naphthyl radical.

The energy of any conformer of **TS2** can then be separated into the energy of the H-capped residue **TS2_HC**, the energy of the naphthyl radical, the energy differences of a C-C-bond relative to the new C-H bond and finally the non-covalent interaction energy between the naphthyl moiety and the rest of the catalyst (Eq. 6.50). As for all conformers an identical naphthyl radical results from the cleavage, a similar C-C-bond is cleaved and the same C-H bond is formed additionally, those terms disappear in Eq. 6.51 for the energy difference to a reference system (herein best conformer **R_TS2_1** is used as reference). The basis set superposition error (BSSE) is supposed to be negligible as a big basis set is used. Moreover, a hypothetical BSSE would be cancelled as only differences of energy differences of similar systems are investigated. Relative interaction energies between the naphthyl moiety and the rest of the structure in **TS2** can then be calculated by Eq. 6.52.

$$E^{\ddagger}(\textbf{TS2}) = E^{\ddagger}(\textbf{TS2\_HC}) + E(Np\cdot) + E(\text{C-C}) - E(\text{C-H}) + E_{NCI} \qquad \text{Eq. 6.50}$$

$$\Delta\Delta E^{\ddagger}(\textbf{TS2}) = \Delta\Delta E^{\ddagger}(\textbf{TS2\_HC}) + \Delta E_{NCI} \qquad \text{Eq. 6.51}$$

$$\Delta E_{NCI} = \Delta\Delta E^{\ddagger}(\textbf{TS2}) - \Delta\Delta E^{\ddagger}(\textbf{TS2\_HC}) \qquad \text{Eq. 6.52}$$

	Best conformer	2nd best	3rd best	4th best	5th best	6th best
R-TS2	**R_TS2_1 (reference)**	R_TS2_2	R_TS2_3	R_TS2_4	R_TS2_5	R_TS2_6
S-TS2	S_TS2_1	S_TS2_2	S_TS2_3	S_TS2_4	S_TS2_5	S_TS2_6
				S_TS2_7	S_TS2_8	S_TS2_13 (cat I)

□ $\Delta\Delta E^{\ddagger}$(Full **TS2**)   □ $\Delta\Delta E^{\ddagger}$(H-capped **TS2-HC**)   ■ $\Delta\Delta E_{\text{non-covalent interactions}}$
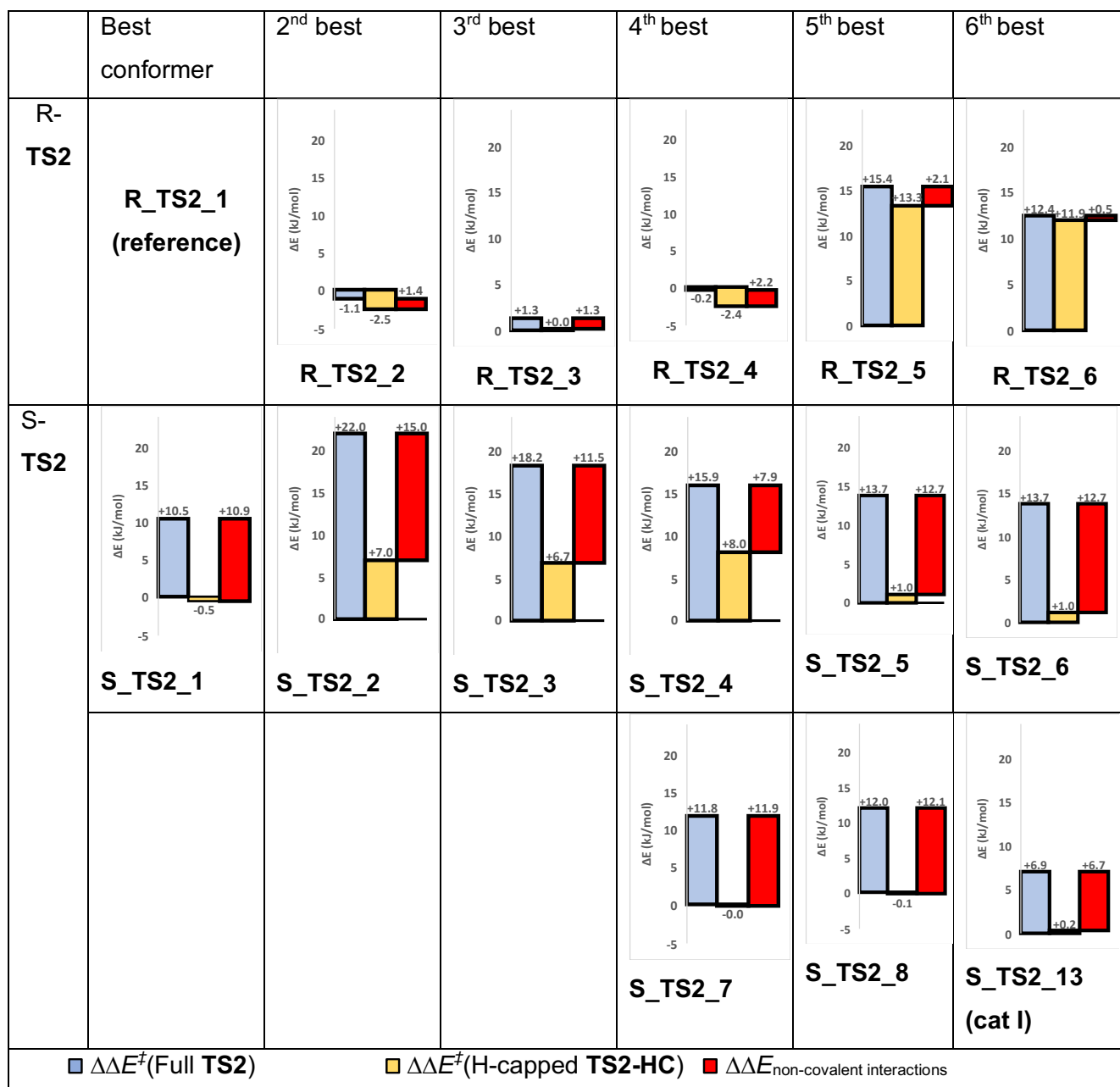
Figure 6.36. Relative single point energies for **TS2** structures (blue bars) compared to relative energy of H-capped structures **TS2**-HC (yellow bars) as shown in **Scheme 6.25** for all conformers populated to more than 5% and the best category-I-*(S)*-conformer. The difference of those terms gives the difference non-covalent interaction energy (red bars) between naphthyl moiety of the alcohol and the rest of transition state structure. All energies are given relative to the best conformer for R-**TS2** in kJ mol^{-1} and energies were obtained at DLPNO-CCSD(T)/def2-TZVPP level of theory.

Interestingly, single point energies for the H-capped structure of **TS2** without aromatic moiety are almost identical for the best *(R)*- and *(S)*-**TS2** conformers (yellow bars in **Figure 6.36**). Moreover, this is also true for most of the other conformers that are populated by more than 5% according to the Boltzmann distribution. Exceptions are the above discussed subgroups **S_TS2_2** – **S_TS2_4** with T-stacking of the naphthyl system and pyridinium ring and **S_TS2_5** and **S_TS2_6**. However, those differences are readily compensated by the increase in solvation energies as shown in **Figure 6.32**, leaving non-covalent interactions as the free-energy determining factors.

As only the naphthyl group was cleaved, relative H-capped energies (yellow bars in **Figure 6.36**) comprise energy differences due to the structure of the loaded catalyst, interactions of the alcohol-methyl group with the rest of the system and the reacting atoms themselves. Interestingly, none of those factors determines the energy differences between the most important *(R)-* and *(S)-* conformers. Indeed, energy differences mainly result from interactions between the naphthyl ring with the rest of the system. Quantification of these interactions by Eq. 6.52 results in relative non-covalent interaction energies symbolized by the red bars in **Figure 6.36**. The non-covalent interaction energy is around +7.9 kJ mol^{-1} to +15.0 kJ mol^{-1} less stabilizing for all of the more than 5% populated *(S)*-conformers compared to the best *(R)*-enantiomer. Also for the best category-I-*(S)*-conformer **S_TS2_13** almost all of the energy difference to **R_TS2_1** can be attributed to non-covalent interactions.

Non-covalent interactions always include a repulsive and an attractive term. However, it is very unlikely that in triple-sandwich structures like **S_TS2_1** steric repulsion is higher than in crowded cage structures as found in category I. Thus, differences in non-covalent interaction energies can be mainly attributed to non-covalent attractive interactions between alcohol and loaded catalyst. To support this hypothesis, a qualitative analysis of these interactions has been performed.

6.4.8. Qualitative Investigation of Non-Covalent Interactions

AIM Analysis

Different methods for qualifying non-covalent interactions are found in the literature. The straightforward analysis of pairwise distances can be readily applied for distinct and relatively strong non-covalent interactions like hydrogen bonding.[49] However, if a multitude of rather weak and diffuse interactions between several atoms is present in a big system, this approach does not allow a complete analysis of non-covalent interactions. Bader[50] approached this question with the hypothesis that all atom-atom interactions – covalent as well as non-covalent – root on molecular level in an accumulation of electron density between the nuclei. Thus the atoms in molecules (AIM)[51] theory proposes to analyse critical points of electron density ρ (with $\nabla\rho(r) = 0$) on the bond paths between two atoms. If analysis of the curvature indicates the critical point to be a maximum it is classified as a (3, -1) bond critical point (bcp). The line following the maximal increase in ρ in both directions connects two nuclei and is called bond path.[50] The value of electron density at the bond critical point ρ_{bcp} allows to distinguish different types of bonding: hydrogen bonds are characterized by an approximately 10 times smaller value of ρ_{bcp} compared to covalent bonds, while ρ_{bcp} for van-der-Waals interactions is around 100 times smaller.[52] For several cases like hydrogen bonding a correlation between density parameters and the strengths of the interactions were found.[53] However, no clear correlation of the strength of van-der-Waals interactions with density interaction parameter is known.[52] Thus, AIM analysis is a very common tool in the qualitative analysis of non-covalent interactions.[28b, 47, 54]

AIM analysis was performed for the best conformers of both enantiomers using Multiwfn[29] restricted to (3,-1) bcp in a density region of 0.0 – 0.1 *au* for interactions between alcohol substrate and the rest of the transition state structure. Results are presented in **Figure 6.37** and **Figure 6.38**. Reported descriptors of those interactions in **Table 6.36** and **Table 6.37** comprise distance of the two nuclei *d*, electron density at the bcp ρ_{bcp}, Laplacian of electron density $\nabla^2\rho$, potential electron density *V(R)* and Hamilton kinetic energy *K(R)*. Additionally, the type of non-covalent interaction is described. Note, that the term π-π may be misleading as it implicates an interaction of the two delocalized π-electron systems, while most of aromatic-aromatic interactions are caused by the polarizability of the aromatic system.[42a, 42b] In that sense π refers here always to the total of the aromatic system. AIM analysis shows that aromatic face-to-face stacking of alcohol and DMAP core is comparable for **R_TS2_1** and **S_TS2_1** (*bcp* **1** in **Figure 6.37** and **Figure 6.38**). In **R_TS2_1** one CH-π interaction (*bcp* **2** in **Figure 6.37**) between the aromatic system of the alcohol and the methyl groups of the DMAP-core is found while two of them are present in **S_TS2_1** (*bcp* **2a,b** in **Figure 6.38**). The most important differences regarding non-covalent interactions is the additional tilted aromatic stacking (*bcp* **3a** in **Figure 6.37**) and a CH-π interaction (*bcp* **3b** in **Figure 6.37**) between the aromatic system of the alcohol and the sidechain of the catalyst. Those interactions are not possible in triple-sandwich-structures like **S_TS2_1.** In **S_TS2_1** an additional interaction between the carbonyl unit of the catalyst with the aromatic system of the alcohol can be seen (*bcp* **3** in **Figure 6.38**). Further interactions comprise CH-π interaction (*bcp* **4**) of the aromatic system with the isobutyrate and interactions of the CH-group of the alcohol with C=O group of the loaded catalyst (*bcp* **4**) and catalyst sidechain in **R_TS2_1** (*bcp* **6** in **Figure 6.37**) resp. with the carbonyl group of the free isobutyrate for **S_TS2_1** (*bcp* **3** in **Figure 6.38**).
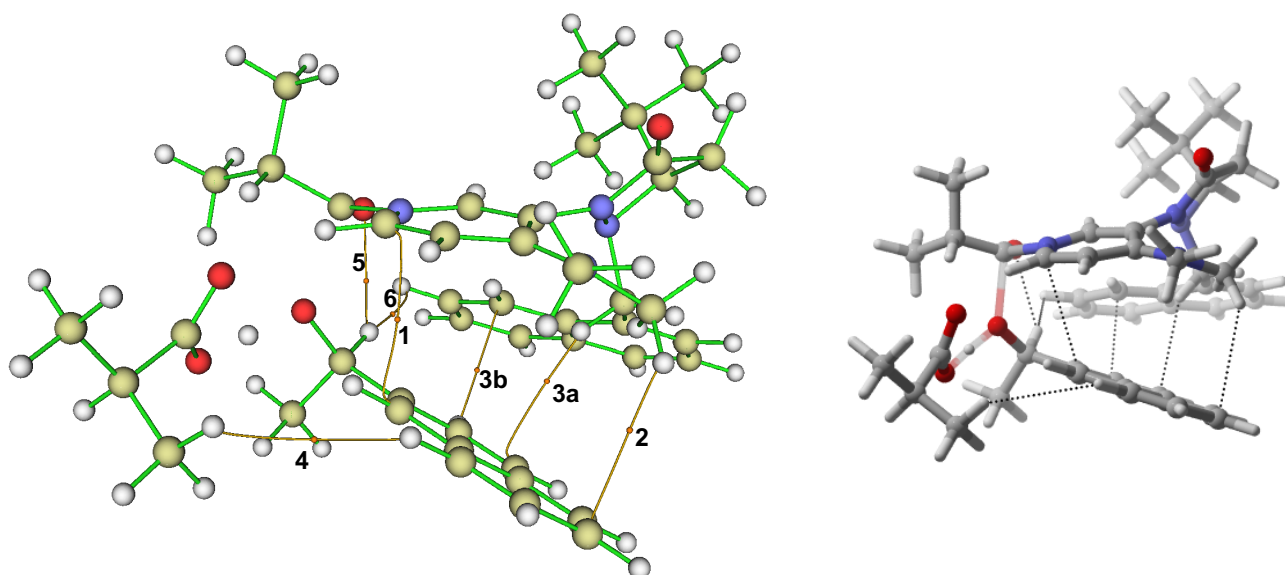
Figure 6.37. AIM analysis of **R_TS2_1.** Yellow dots symbolize bond critical points, yellow lines bond paths. Analysis and left picture was performed using Multiwfn[29] (yellow: carbon), the picture on the right hand is plotted for better visualization with CYLview[34].

Table 6.36. Parameters of AIM analysis describing non-covalent interactions between alcohol and the rest of the transition state structure for **R_TS2_1.**

bcp	type	description	Distance nuclei [pm]	electron density ρ_{bcp} [10^{-2} au]	Laplacian of electron density $\nabla^2\rho$ [10^{-2} au]	potential electron density $V(R)$ [10^{-2} au]	Hamilton kinetic energy $K(R)$ [10^{-2} au]
1	$\pi-\pi^+$ face-to-face stacking	π(alcohol) to π(DMAP)	333	0.6567	1.9862	-0.2856	-0.1055
2	CH-π	π(alcohol) to CH_3(DMAP)	312	0.3791	1.1124	-0.1551	-0.0615
3a	Tilted aromatic stacking	π(alcohol) to π(catalyst sidechain)	288	0.5813	1.7011	-0.2419	-0.0917
3b	CH-π	π(alcohol) to CH(catalyst sidechain)	283	0.6163	1.9716	-0.2699	-0.1115
4	CH-π	π(alcohol) to CH(isobutyrate)	325	0.0906	0.2801	-0.0323	-0.0188
5	CH-O	CH(alcohol) to C=O(loaded isobutyrate)	236	1.3332	4.7732	-0.9642	-0.1145
6	CH-π	CH(alcohol) to π(catalyst sidechain)	236	0.5407	1.9962	-0.2385	-0.1303
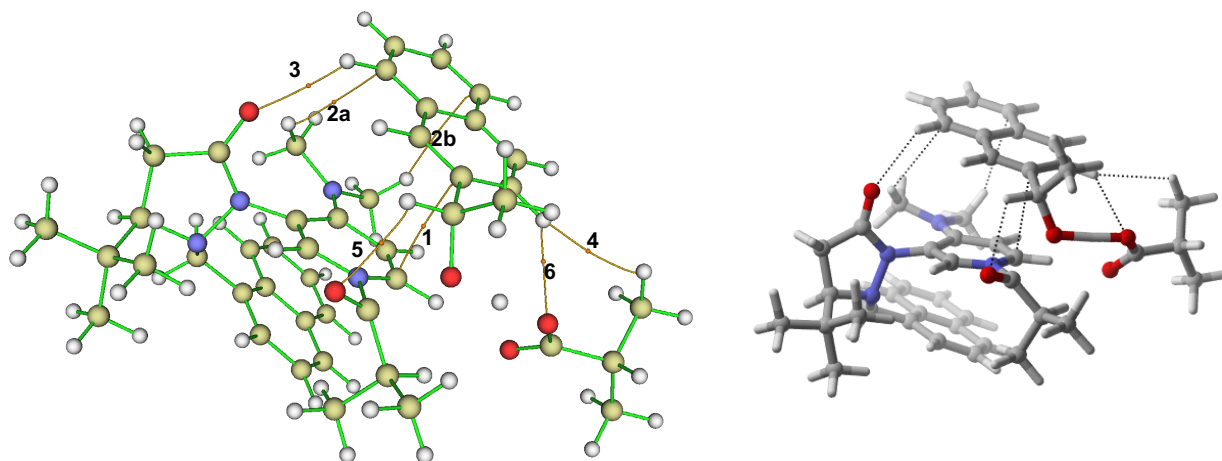
Figure 6.38. AIM analysis of **S_TS2_1.** Yellow dots symbolize bond critical points, yellow lines bond paths. Analysis and left picture was performed using Multiwfn[29] (yellow: carbon), the picture on the right hand is plotted for better visualization with CYLview[34].

Table 6.37. Parameters of AIM analysis describing non-covalent interactions between alcohol and the rest of the transition state structure for **S_TS2_1.**

bcp	type	description	Distance nuclei [pm]	electron density ρ_{bcp} [10^{-2} au]	Laplacian of electron density $\nabla^2\rho$ [10^{-2} au]	potential electron density $V(R)$ [10^{-2} au]	Hamilton kinetic energy $K(R)$ [10^{-2} au]
1	$\pi-\pi^+$ face-to-face stacking	π(alcohol) to π(DMAP)	321	0.6963	2.2440	-0.3466	-0.1072
2a	CH-π	π(alcohol) to CH$_3$(DMAP)	296	0.4970	0.3067	-0.2205	-0.0862
2b	CH-π	π(alcohol) to CH$_3$(DMAP)	313	0.3568	1.0386	-0.1414	-0.0591
3	O-π	π(alcohol) to C=O(catalyst sidechain)	261	0.6760	2.5653	-0.4333	-0.1040
4	CH-π	π(alcohol) to CH(isobutyrate)	264	0.2944	1.0606	-0.1186	-0.0733
5	CH-O	CH(alcohol) to C=O(loaded isobutyrate)	248	1.0967	4.5172	-0.8160	-0.1567
6	CH-O	CH(alcohol) to C=O(isobutyrate)	256	0.9332	3.2569	-0.6392	-0.0875

NCI Plots

Another approach is the analysis of the reduced density gradient (RDG). While covalent bonds are characterized by saddle points of the electron density, non-covalent bonds lead to steep troughs of the RDG in the low density region.[55] Those patterns in the RDG are comparable for repulsive and attractive interactions. However, analysis of the second eigenvalue of the electron-density Hessian sign(λ_2) allows to analyse the variation of electron density ρ along internuclear connections.[30] Van-der-Waals interactions are characterized by a second eigenvalue of the Hessian close to zero in an area of small energy density ρ. Thus, it is possible to only plot van-der-Waals interactions if an appropriately small cut-off value (here 0.03 au) for the density is chosen.

Both NCIplots for the best conformers **R_TS2_1** and **S_TS2_1** show big areas of non-covalent interactions between the alcohol and the pyridinium ring (**Figure 6.39**, first line). In agreement with the AIM analysis performed above for **R_TS2_1** an additional area of non-covalent interactions is found between the aromatic moiety of the alcohol and the aromatic sidechain of the catalyst which corresponds to a tilted aromatic stacking interaction. In contrast, in **S_TS2_1** a big area of aromatic stacking between this aromatic moiety and the pyridinium is found. However, this interaction does not involve the alcohol and does thus not impact enantioselectivity.

Second best conformers (**Figure 6.39**, second line) show similar trends. In **S_TS2_2** the smaller interaction between pyridinium and vertical oriented catalyst sidechain interaction explains the lower single point energy of **S_TS2_2** compared to **S_TS2_1.** As seen above, parts of this energy are compensated by an increased solvation energy.

The third line in **Figure 6.39** shows some special cases for category I structures. **R_TS2_5** has a lower non-covalent interaction surface compared to **R_TS2_1** due to the different orientation of the napththyl group as discussed in **Figure 6.33**.

The structure of the best *(S)*-conformer in category I (**S_TS_13**) is quite similar to **R_TS2_1.** However, the alcohol-methyl group forces the alcohol to orient differently yielding a smaller aromatic interaction surface between the alcohol, pyridinium and catalyst sidechain. Consequently, in **S_TS_13** non-covalent interaction energy is lowered compared to **R_TS2_1.**

Aromatic face-to-face stacking alcohol - pyridinium

Tilted aromatic stacking alcohol – catalyst sidechain

Aromatic face-to-face stacking pyridinium – catalyst sidechain

R_TS2_1

S_TS2_1

R_TS2_2

S_TS2_2

R_TS2_5

Reduced stacking alcohol – catalyst sidechain

S_TS2_13
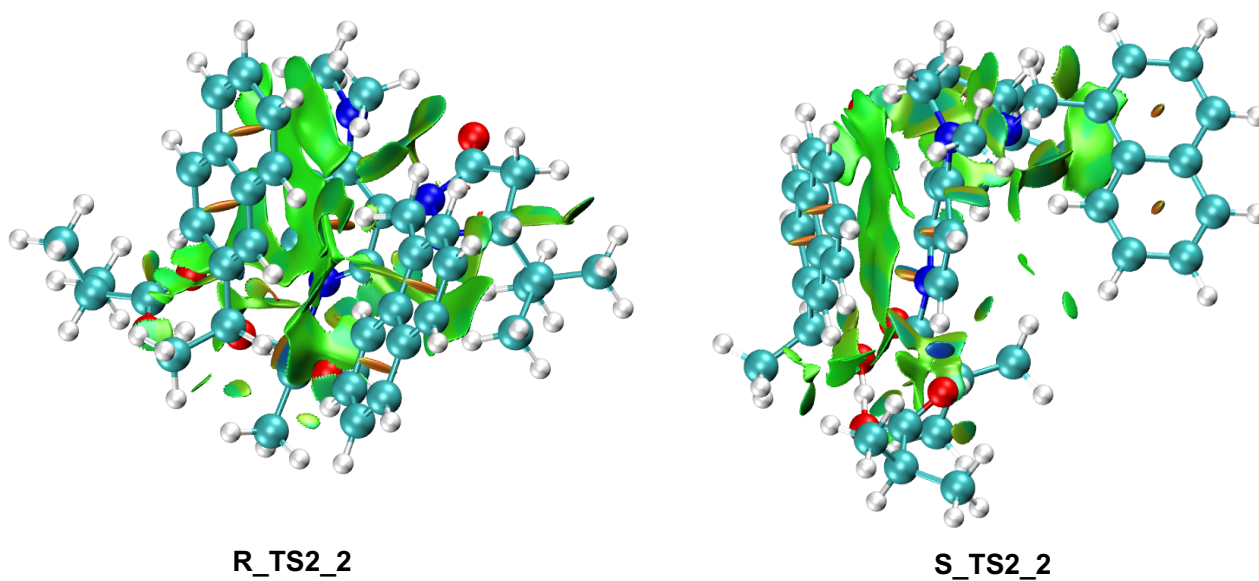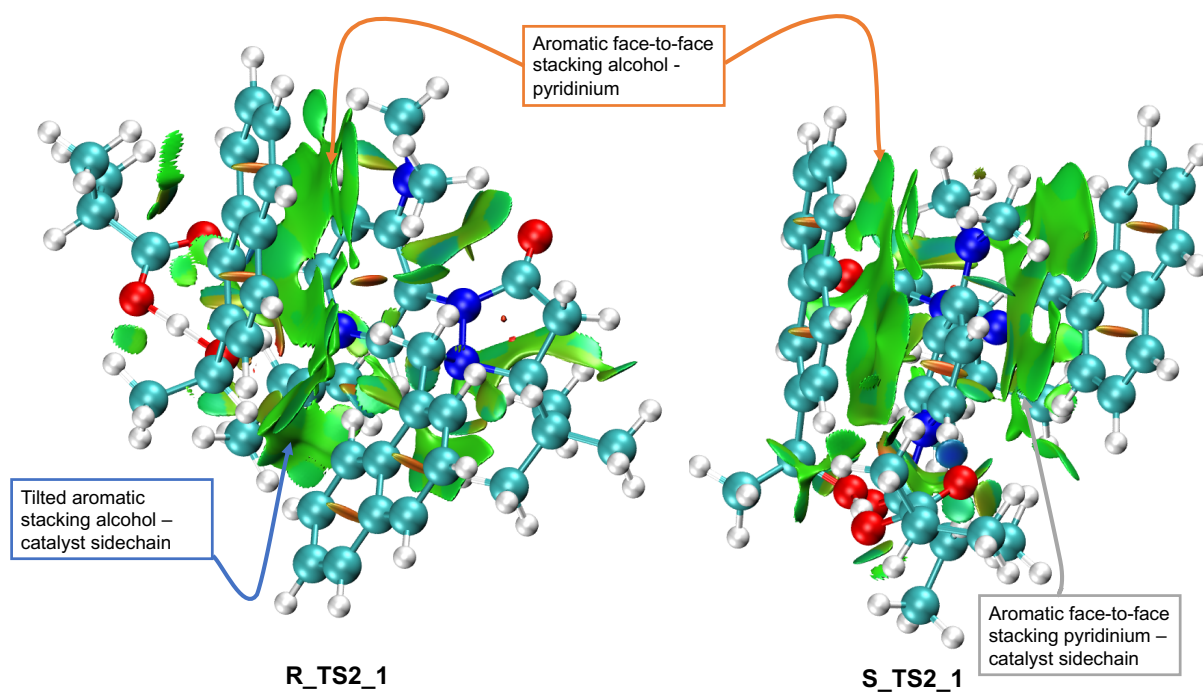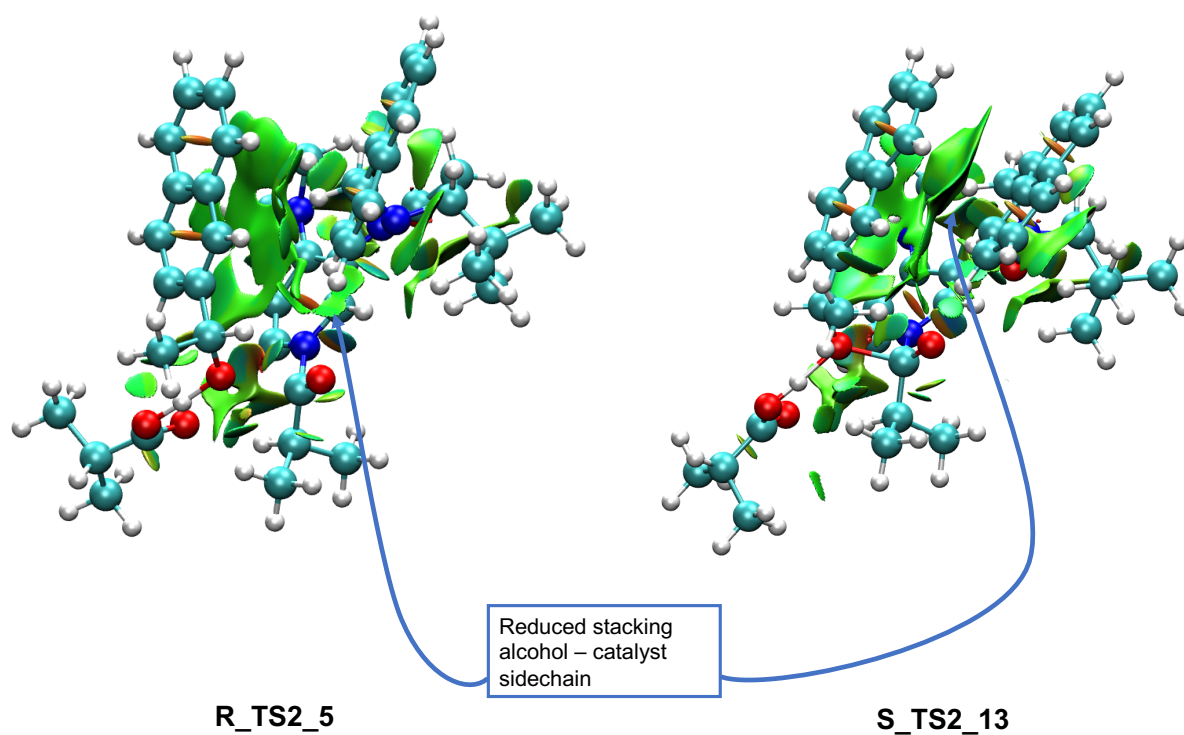
Figure 6.39. NCI plots for **TS2** structures generated from wavefunction at B3LYP-D3/6-31+G(d) level of theory with NCIplot[30] and plotted with VMD[56] with density cutoff at 0.03 au. Colours reflect sign(λ_2)ρ on a scale of -0.03 au (blue) over 0 (green) to +0.03 (red). Accordingly, green surfaces represent van der Waals interaction areas. Colour code: hydrogen (white), carbon (turquoise), nitrogen (blue), oxygen (red).

6.4.9. Analysis of Thermodynamics and Substrate Properties

The design of the experiments in this study rely on the hypothesis that the reactivity of substrate alcohols mainly depends on their strength as dispersion-energy donors (DED). To examine whether other factors impact the reactivity of the different alcohols, several other properties were investigated. Most importantly, the competition experiments with non-aromatic catalyst nBu$_3$P (**6**) show that acylation of all alcohols occurs at similar reaction rates (see chapter 6.2.7). In addition, the thermodynamics of the acylation of the different alcohols was analysed in order to exclude a thermodynamic control of selectivity. Therefore, reaction free energies for the acylation were calculated. **Table 6.38** reports reaction free energies calculated from Boltzmann averaged free energies of substrates and products. Reaction free energies are almost identical for all of the investigated reactions. Thus, a thermodynamic control of selectivity can be excluded.
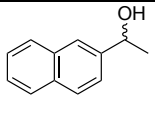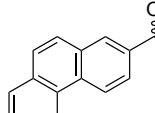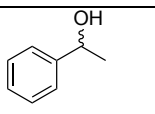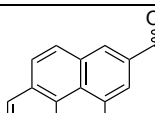
Table 6.38. Reaction free energy for the acylations of the alcohols used in this project.

Reaction	$\Delta G_{223.15}$ CCSD(T)/def2-TZVPP// SMD(Et$_2$O)/B3LYP-D3/6-31+G(d) [kJ mol^{-1}]
1a **2** **4a** **S1**	**-51.1**
1b **2** **4a** **S1**	**-51.5**
1c **2** **4c** **S1**	**-49.4**
1d **2** **4d** **S1**	**-50.6**

As in selectivity determining **TS2** (see **Scheme 6.24**) the partial charge of the oxygen atom as well as the acidity of the hydroxyl proton could influence the reactivity of the alcohol, those two factors were also analysed with DFT methods. The natural charge of the oxygen atom was determined by natural bond orbital (NBO) calculations on the optimized alcohols at SMD(Et$_2$O)/B3LYP-D3/6-31+G(d) level. From the natural population analysis, the natural charge of the oxygen was obtained

and Boltzmann-averaged over the conformers. **Table 6.39** shows that natural charges on the oxygen atoms are almost identical for all four alcohols used in the experiment.

Table 6.39. Results of natural bond order analysis of alcohol substrates.

Alcohol	Conformer	Natural Charge Oxygen	Natural population				Boltzmann factor (see Chapter 6.5)	**Boltzmann averaged natural charge**
			Core	Valence	Rydberg	Total		
1b (OH)	SNp_2	-0.7885	1.9998	6.7702	0.0184	8.7885	1.00	**-0.7880**
	SNp_1	-0.7867	1.9998	6.7687	0.0182	8.7867	0.44	
	SNp_4	-0.7893	1.9998	6.7709	0.0187	8.7893	0.11	
	SNp_3	-0.7885	1.9998	6.7695	0.0193	8.7885	0.08	
	SNp_7	-0.7831	1.9998	6.7654	0.0178	8.7831	0.03	
1c (OH)	SPhant_1	-0.7883	1.9998	6.7700	0.0184	8.7883	1.00	**-0.7881**
	SPhant_3	-0.7890	1.9998	6.7705	0.0187	8.7890	0.04	
	SPhant_7	-0.7809	1.9998	6.7630	0.0180	8.7809	0.03	
1a (OH)	SPhe_1	-0.7887	1.9998	6.7704	0.0184	8.7887	1.00	**-0.7884**
	SPhe_3	-0.7892	1.9998	6.7705	0.0190	8.7892	0.16	
	SPhe_7	-0.7807	1.9998	6.7634	0.0175	8.7807	0.05	
1d (OH)	SPyr_1	-0.7880	1.9998	6.7697	0.0184	8.7880	1.00	**-0.7880**
	SPyr_4	-0.7888	1.9998	6.7700	0.0190	8.7888	0.15	
	SPyr_7	-0.7832	1.9998	6.7653	0.0181	8.7832	0.01	

Another factor describing reactivity of the alcohols is the acidity of the hydroxyl group. As reactions are conducted in anhydrous diethyl ether, the investigation of aqueous pK_a values is not appropriate. The calculation of pK_a values is very dependent on the solvent and should ideally be performed with an explicit solvation model.[57] As the accurate determination of absolute pK_a values is not needed in this context, the reaction free energies for isodesmic proton transfer reactions with reference alcohol **1b** are reported in **Table 6.40**. The acidity increases in the order phenyl < phenanthryl < naphtyl < pyrenyl. The calculated energy differences are quite small and lie within the limits of confidence of the chosen theoretical approach. Furthermore, the order of relative acidities does not fit the experimentally observed relative rates.

Table 6.40. Reaction free energies for isodesmic proton transfer reactions to estimate acidity of the hydrogen protons.

Isodesmic reaction	$\Delta G_{223.15}$ [kJ mol^{-1}] (DLPNO-CCSD(T)/ SMD(Et2O)/B3LYP-D3/ 6-31+G(d))
	+3.5
	+0.5
	-1.4

Analysis of the substrates confirms that the main difference between investigated alcohols is the size of DED groups.

6.5. Tables of Energies, Free Energies and Enthalpies

6.5.1. Conformers of TS2

Table 6.41. Overview of energies of all conformers of **TS2**. Column 1 gives name as used in the manuscript, column 2 refers to categories as defined in Chapter 6.4.5., the single negative frequency (in cm^{-1}) is reported in column 3. Total energy, enthalpy and free energy calculated at SMD(Et$_2$O)/B3LYP-D3/6-31+G(d) and at DLPNO-CCSD(T)/def2-TZVPP are reported for all conformers of **TS2**. All enthalpies are corrected for a quasi-harmonic rotor, free energies with a free-rotor approximation (for details see Chapter 6.4.1). Solvation energy was calculated from the difference of single point calculations in gas phase and total energy with SMD model on B3LYP-D3/6-31+G(d) level of theory and added to enthalpy and free energy at coupled cluster calculations. Differences in free energy are reported relative to the best conformer R_TS2_1 in kJ mol^{-1} for both methods. The geometries of all listed conformers are provided as SDF file.

Name	Category	neg. freq. [cm^{-1}]	E_{tot} [Hartree]	$H_{223.15}$ [Hartree]	$G_{223.15}$ [Hartree]	$\Delta\Delta G^{\ddagger}_{223.15}$ [kJ mol^{-1}]	Grimme-D3 correction [kJ mol^{-1}]	solvation energy [kJ mol^{-1}]	E_{tot} [Hartree]	$H_{223.15, sol}$ [Hartree]	$G_{223.15, sol}$ [Hartree]	$\Delta\Delta G^{\ddagger}_{223.15}$ [kJ mol^{-1}]
			SMD(Et$_2$O)/B3LYP-D3/6-31+G(d)						DLPNO-CCSD(T)/def2-TZVPP			
R_TS2_1	1	-605.2	-2343.943762	-2342.987297	-2343.067809	0.00	-456.20	-129.64	-2339.6314779	-2338.7243919	-2338.8049039	0.00
R_TS2_2	1	-790.7	-2343.944273	-2342.987557	-2343.067520	0.76	-456.50	-130.10	-2339.6318998	-2338.7247358	-2338.8046988	0.54
R_TS2_3	1	-603.2	-2343.943565	-2342.986935	-2343.067531	0.73	-455.29	-129.98	-2339.6309954	-2338.7238734	-2338.8044694	1.14
R_TS2_4	1	-761.2	-2343.944191	-2342.986515	-2343.067337	1.24	-456.20	-130.21	-2339.6315717	-2338.7234907	-2338.8043127	1.55
R_TS2_5	1	-763.1	-2343.940108	-2342.983262	-2343.065842	5.16	-443.44	-135.22	-2339.6256115	-2338.7202695	-2338.8028495	5.39
R_TS2_6	1	-816.2	-2343.940278	-2342.984201	-2343.064481	8.74	-447.47	-135.58	-2339.6267504	-2338.7223114	-2338.8025914	6.07
R_TS2_7	1	-826.8	-2343.939581	-2342.983538	-2343.064615	8.39	-443.60	-136.07	-2339.6250004	-2338.7207834	-2338.8018604	7.99
R_TS2_8	1	-362.3	-2343.940306	-2342.982902	-2343.062445	14.08	-451.00	-137.33	-2339.6256638	-2338.7205658	-2338.8001088	12.59
R_TS2_9	1	-844.6	-2343.938085	-2342.980911	-2343.059826	20.96	-469.62	-135.99	-2339.6260457	-2338.7206687	-2338.7995837	13.97
R_TS2_10	2	-849.6	-2343.935906	-2342.977990	-2343.058398	24.71	-467.68	-134.37	-2339.6254076	-2338.7186686	-2338.7990766	15.30
R_TS2_11	2	-695.8	-2343.935063	-2342.978683	-2343.058668	24.00	-458.73	-138.03	-2339.6225253	-2338.7187183	-2338.7987033	16.28
R_TS2_12	2	-658.6	-2343.935036	-2342.978666	-2343.059091	22.89	-450.52	-142.85	-2339.6198897	-2338.7179267	-2338.7983517	17.20
R_TS2_13	2	-866.8	-2343.936139	-2342.979839	-2343.058358	24.81	-455.35	-139.00	-2339.6230849	-2338.7197289	-2338.7982479	17.48
R_TS2_14	2	-846.0	-2343.936093	-2342.979480	-2343.057798	26.28	-454.59	-139.24	-2339.6227413	-2338.7191633	-2338.7974813	19.49
R_TS2_15	7	-913.0	-2343.936213	-2342.978440	-2343.058041	25.65	-473.27	-125.26	-2339.6264948	-2338.7164308	-2338.7960318	23.29
R_TS2_16	3	-689.4	-2343.930187	-2342.973273	-2343.055630	31.98	-414.44	-149.28	-2339.6104712	-2338.7104152	-2338.7927722	31.85

		SMD(Et$_2$O)/B3LYP-D3/6-31+G(d)						DLPNO-CCSD(T)/def2-TZVPP			
Name	Cate-gory	neg. freq. [cm^{-1}]	E_{tot} [Hartree]	$H_{223.15}$ [Hartree]	$G_{223.15}$ [Hartree]	$\Delta\Delta G^{\ddagger}_{223.15}$ [kJ mol^{-1}]	Grimme-D3 correction [kJ mol^{-1}]	solvation energy [kJ mol^{-1}]	E_{tot} [Hartree]	$H_{223.15,\,sol}$ [Hartree]	$G_{223.15,\,sol}$ [Hartree]	$\Delta\Delta G^{\ddagger}_{223.15}$ [kJ mol^{-1}]
R_TS2_17	3	-636.3	-2343.930378	-2342.974133	-2343.055908	31.25	-414.63	-150.42	-2339.6099266	-2338.7109736	-2338.7927486	31.91
R_TS2_18	6	-912.4	-2343.930151	-2342.972814	-2343.055273	32.91	-436.78	-142.51	-2339.6131484	-2338.7100914	-2338.7925504	32.43
R_TS2_19	6	-844.0	-2343.930052	-2342.972917	-2343.054817	34.11	-435.67	-143.97	-2339.6128509	-2338.7105509	-2338.7924509	32.70
R_TS2_20	6	-868.1	-2343.929690	-2342.972649	-2343.054717	34.37	-432.23	-142.17	-2339.6131707	-2338.7102807	-2338.7923487	32.96
R_TS2_21	3	-226.9	-2343.931421	-2342.973511	-2343.052976	38.94	-427.62	-149.05	-2339.6135723	-2338.7124333	-2338.7918983	34.15
R_TS2_22	3	-188.3	-2343.931886	-2342.972865	-2343.053530	37.49	-432.07	-149.96	-2339.6130567	-2338.7111527	-2338.7918177	34.36
R_TS2_23	3	-881.3	-2343.926932	-2342.970970	-2343.052417	40.41	-416.73	-151.69	-2339.6084744	-2338.7102874	-2338.7917344	34.58
R_TS2_24	3	-188.1	-2343.931513	-2342.973479	-2343.053384	37.87	-430.73	-148.19	-2339.6133695	-2338.7117765	-2338.7916815	34.72
R_TS2_25	3	-848.0	-2343.926742	-2342.969634	-2343.052554	40.05	-413.64	-150.49	-2339.6085378	-2338.7087498	-2338.7916698	34.75
R_TS2_26	3	-185.3	-2343.931489	-2342.972329	-2343.052939	39.04	-432.26	-148.60	-2339.6134463	-2338.7108863	-2338.7914963	35.20
R_TS2_27	3	-185.3	-2343.931488	-2342.972330	-2343.052941	39.04	-432.26	-148.61	-2339.6134160	-2338.7108590	-2338.7914700	35.27
R_TS2_28	3	-625.7	-2343.930451	-2342.973793	-2343.054602	34.67	-416.09	-152.09	-2339.6093086	-2338.7105776	-2338.7913866	35.49
R_TS2_29	6	-930.4	-2343.930757	-2342.973549	-2343.052736	39.57	-448.58	-141.47	-2339.6148231	-2338.7114991	-2338.7906861	37.33
R_TS2_30	3	-864.8	-2343.927182	-2342.969592	-2343.051336	43.25	-421.10	-146.05	-2339.6102724	-2338.7083104	-2338.7900544	38.99
R_TS2_31	3	-383.4	-2343.927917	-2342.970513	-2343.052733	39.58	-425.23	-152.12	-2339.6072361	-2338.7077721	-2338.7899921	39.15
R_TS2_32	3	-655.0	-2343.926665	-2342.970197	-2343.052888	39.18	-406.21	-154.75	-2339.6045072	-2338.7069822	-2338.7896732	39.99
R_TS2_33	4	-928.3	-2343.927797	-2342.970164	-2343.050946	44.27	-428.50	-154.20	-2339.6076619	-2338.7087599	-2338.7895419	40.33
R_TS2_34	3	-796.1	-2343.926665	-2342.969986	-2343.052374	40.52	-406.02	-151.44	-2339.6061041	-2338.7071061	-2338.7894941	40.46
R_TS2_35	3	-144.4	-2343.930186	-2342.969226	-2343.048491	50.72	-471.66	-132.77	-2339.6205668	-2338.7101748	-2338.7894398	40.60
R_TS2_36	3	-688.8	-2343.926778	-2342.969982	-2343.052503	40.19	-405.00	-153.46	-2339.6050368	-2338.7066898	-2338.7892108	41.20
R_TS2_37	3	-378.5	-2343.927332	-2342.969945	-2343.050174	46.30	-422.31	-151.34	-2339.6084954	-2338.7087504	-2338.7889794	41.81
R_TS2_38	6	-923.4	-2343.927307	-2342.970546	-2343.050811	44.63	-442.02	-136.61	-2339.6131851	-2338.7084571	-2338.7887221	42.49
R_TS2_39	5	-1036.8	-2343.928608	-2342.971273	-2343.051708	42.27	-450.33	-150.97	-2339.6078224	-2338.7079904	-2338.7884254	43.26

		SMD(Et$_2$O)/B3LYP-D3/6-31+G(d)							DLPNO-CCSD(T)/def2-TZVPP			
Name	Cate-gory	neg. freq. [cm^{-1}]	E_{tot} [Hartree]	$H_{223.15}$ [Hartree]	$G_{223.15}$ [Hartree]	$\Delta\Delta G^{\ddagger}_{223.15}$ [kJ mol^{-1}]	Grimme-D3 correction [kJ mol^{-1}]	solvation energy [kJ mol^{-1}]	E_{tot} [Hartree]	$H_{223.15,\,sol}$ [Hartree]	$G_{223.15,\,sol}$ [Hartree]	$\Delta\Delta G^{\ddagger}_{223.15}$ [kJ mol^{-1}]
R_TS2_40	5	-564.9	-2343.929464	-2342.971027	-2343.050927	44.32	-456.42	-135.06	-2339.6154760	-2338.7084810	-2338.7883810	43.38
R_TS2_41	3	-539.2	-2343.926583	-2342.969424	-2343.049776	47.35	-425.90	-153.04	-2339.6068067	-2338.7079357	-2338.7882877	43.63
R_TS2_42	3	-300.8	-2343.927442	-2342.970122	-2343.050496	45.46	-426.65	-149.73	-2339.6076505	-2338.7073595	-2338.7877335	45.08
R_TS2_43	6	-937.7	-2343.927205	-2342.969542	-2343.049167	48.94	-433.82	-137.27	-2339.6131482	-2338.7077702	-2338.7873952	45.97
R_TS2_44	6	-914.9	-2343.925677	-2342.967816	-2343.049661	47.65	-436.01	-133.96	-2339.6120309	-2338.7051919	-2338.7870369	46.91
R_TS2_45	6	-940.8	-2343.925689	-2342.968843	-2343.048945	49.53	-424.06	-140.24	-2339.6102744	-2338.7068414	-2338.7869434	47.16
R_TS2_46	6	-964.0	-2343.927421	-2342.970089	-2343.049635	47.72	-447.02	-135.18	-2339.6127628	-2338.7069198	-2338.7864658	48.41
R_TS2_47	3	-279.5	-2343.925799	-2342.967946	-2343.047209	54.09	-430.27	-151.03	-2339.6069468	-2338.7066188	-2338.7858818	49.94
R_TS2_48	3	-278.7	-2343.925800	-2342.967939	-2343.047191	54.13	-430.28	-151.03	-2339.6069384	-2338.7066034	-2338.7858554	50.01
R_TS2_49	6	-887.1	-2343.924704	-2342.967334	-2343.049110	49.09	-426.63	-137.31	-2339.6090915	-2338.7040215	-2338.7857975	50.16
R_TS2_50	3	-735.3	-2343.919181	-2342.962870	-2343.046410	56.18	-412.03	-159.72	-2339.5974794	-2338.7020024	-2338.7855424	50.83
R_TS2_51	6	-907.0	-2343.924621	-2342.967909	-2343.048081	51.80	-426.18	-135.47	-2339.6100547	-2338.7049397	-2338.7851117	51.96
R_TS2_52	3	-934.2	-2343.922308	-2342.966079	-2343.047795	52.55	-395.60	-158.61	-2339.5990887	-2338.7032727	-2338.7849887	52.29
R_TS2_53	4	-866.8	-2343.922716	-2342.965688	-2343.047986	52.05	-418.16	-154.91	-2339.6004123	-2338.7023873	-2338.7846853	53.08
R_TS2_54	4	-911.5	-2343.925098	-2342.967687	-2343.047070	54.45	-435.42	-150.22	-2339.6053392	-2338.7051422	-2338.7845252	53.50
R_TS2_55	6	-643.5	-2343.924598	-2342.966849	-2343.045636	58.22	-463.34	-126.84	-2339.6143608	-2338.7049208	-2338.7837078	55.65
R_TS2_56	4	-904.9	-2343.923283	-2342.966108	-2343.046288	56.50	-422.33	-151.92	-2339.6022247	-2338.7029137	-2338.7830937	57.26
R_TS2_57	6	-951.8	-2343.922279	-2342.965043	-2343.044703	60.66	-437.24	-131.97	-2339.6100984	-2338.7031264	-2338.7827864	58.07
R_TS2_58	6	-820.2	-2343.924247	-2342.965924	-2343.044228	61.91	-454.12	-129.39	-2339.6130265	-2338.7039845	-2338.7822885	59.38
R_TS2_59	2	-739.1	-2343.934803	-2342.978023	-2343.057999	25.76	-460.36					
R_TS2_60	2	-822.3	-2343.935824	-2342.978160	-2343.057576	26.87	-465.14			n.d.		
R_TS2_61	6	-877.2	-2343.929735	-2342.972683	-2343.054763	34.25	-431.66					
R_TS2_62	1	-898.8	-2343.929854	-2342.975254	-2343.054069	36.07	-437.25					

| | | SMD(Et₂O)/B3LYP-D3/6-31+G(d) | | | | | | DLPNO-CCSD(T)/def2-TZVPP | | | |
Name	Cate-gory	neg. freq. [cm⁻¹]	E_{tot} [Hartree]	$H_{223.15}$ [Hartree]	$G_{223.15}$ [Hartree]	$\Delta\Delta G^{\ddagger}_{223.15}$ [kJ mol⁻¹]	Grimme-D3 correction [kJ mol⁻¹]	solvation energy [kJ mol⁻¹]	E_{tot} [Hartree]	$H_{223.15, sol}$ [Hartree]	$G_{223.15, sol}$ [Hartree]	$\Delta\Delta G^{\ddagger}_{223.15}$ [kJ mol⁻¹]
R_TS2_63	2	-831.6	-2343.930279	-2342.972648	-2343.053834	36.69	-448.50					
R_TS2_64	3	-161.4	-2343.930808	-2342.971306	-2343.051711	42.27	-464.08					
R_TS2_65	7	-897.8	-2343.929147	-2342.971633	-2343.051203	43.60	-443.35					
R_TS2_66	3	-157.7	-2343.931282	-2342.971428	-2343.051138	43.77	-465.71					
R_TS2_67	3	-150.6	-2343.929832	-2342.969173	-2343.048615	50.39	-471.04					
R_TS2_68	3	-144.6	-2343.930186	-2342.969226	-2343.048495	50.71	-471.67					
S_TS2_1	3	-893.4	-2343.937881	-2342.980430	-2343.061011	17.85	-461.76	-133.96	-2339.6274930	-2338.7210640	-2338.8016450	8.56
S_TS2_2	3	-879.8	-2343.936887	-2342.980251	-2343.062107	14.97	-445.60	-139.18	-2339.6231105	-2338.7194865	-2338.8013425	9.35
S_TS2_3	3	-915.5	-2343.937789	-2342.980847	-2343.061341	16.98	-443.59	-138.25	-2339.6245273	-2338.7202413	-2338.8007353	10.94
S_TS2_4	3	-808.2	-2343.936702	-2342.979004	-2343.060192	20.00	-463.60	-135.70	-2339.6254136	-2338.7194026	-2338.8005906	11.32
S_TS2_5	3	-858.6	-2343.936397	-2342.979993	-2343.060065	20.33	-462.29	-132.90	-2339.6262607	-2338.7204767	-2338.8005487	11.43
S_TS2_6	3	-858.8	-2343.936397	-2342.979995	-2343.060052	20.37	-462.31	-132.91	-2339.6262560	-2338.7204750	-2338.8005320	11.48
S_TS2_7	3	-895.5	-2343.937587	-2342.980326	-2343.060001	20.50	-461.17	-134.13	-2339.6269707	-2338.7207977	-2338.8004727	11.63
S_TS2_8	3	-895.4	-2343.937587	-2342.980325	-2343.059972	20.58	-461.18	-134.13	-2339.6269222	-2338.7207472	-2338.8003942	11.84
S_TS2_9	3	-908.5	-2343.937746	-2342.980919	-2343.060739	18.56	-442.53	-138.61	-2339.6240499	-2338.7200179	-2338.7998379	13.30
S_TS2_10	3	-907.8	-2343.937773	-2342.981010	-2343.060612	18.90	-442.75	-138.65	-2339.6240868	-2338.7201338	-2338.7997358	13.57
S_TS2_11	3	-812.3	-2343.936728	-2342.979588	-2343.058937	23.29	-463.56	-135.50	-2339.6253869	-2338.7198559	-2338.7992049	14.96
S_TS2_12	3	-767.4	-2343.937063	-2342.979310	-2343.058960	23.23	-457.70	-137.59	-2339.6246193	-2338.7192733	-2338.7989233	15.70
S_TS2_13	1	-162.2	-2343.938155	-2342.979319	-2343.059840	20.92	-467.34	-127.06	-2339.6288338	-2338.7183938	-2338.7989148	15.72
S_TS2_14	3	-755.1	-2343.936436	-2342.979121	-2343.058611	24.15	-462.51	-135.16	-2339.6249573	-2338.7191203	-2338.7986103	16.52
S_TS2_15	3	-698.9	-2343.935194	-2342.977798	-2343.058844	23.54	-463.12	-134.73	-2339.6234622	-2338.7173822	-2338.7984282	17.00
S_TS2_16	1	-184.4	-2343.933857	-2342.976068	-2343.057229	27.78	-434.45	-141.81	-2339.6175647	-2338.7137887	-2338.7949497	26.13
S_TS2_17	1	-913.3	-2343.932489	-2342.974761	-2343.055433	32.49	-436.78	-146.85	-2339.6160100	-2338.7142150	-2338.7948870	26.30

		SMD(Et₂O)/B3LYP-D3/6-31+G(d)						DLPNO-CCSD(T)/def2-TZVPP			
Name	Cate-gory	neg. freq. [cm⁻¹]	E_{tot} [Hartree]	$H_{223.15}$ [Hartree]	$G_{223.15}$ [Hartree]	$\Delta\Delta G^{\ddagger}_{223.15}$ [kJ mol⁻¹]	Grimme-D3 correction [kJ mol⁻¹]	solvation energy [kJ mol⁻¹]	E_{tot} [Hartree]	$H_{223.15, sol}$ [Hartree]	$G_{223.15, sol}$ [Hartree]	$\Delta\Delta G^{\ddagger}_{223.15}$ [kJ mol⁻¹]
S_TS2_18	5	-924.5	-2343.934645	-2342.977384	-2343.056193	30.50	-469.84	-128.46	-2339.6238565	-2338.7155245	-2338.7943335	27.75
S_TS2_19	1	-157.8	-2343.933451	-2342.976355	-2343.055971	31.08	-437.53	-140.73	-2339.6181927	-2338.7146977	-2338.7943137	27.80
S_TS2_20	1	-907.7	-2343.932389	-2342.975167	-2343.054834	34.07	-436.91	-146.57	-2339.6158194	-2338.7144224	-2338.7940894	28.39
S_TS2_21	1	-929.6	-2343.930721	-2342.973667	-2343.055669	31.87	-420.18	-146.84	-2339.6116657	-2338.7105407	-2338.7925427	32.45
S_TS2_22	1	-929.7	-2343.930721	-2342.973669	-2343.055677	31.85	-420.17	-146.84	-2339.6116489	-2338.7105269	-2338.7925349	32.47
S_TS2_23	1	-838.8	-2343.931485	-2342.974381	-2343.053814	36.74	-432.68	-144.46	-2339.6148052	-2338.7127222	-2338.7921552	33.47
S_TS2_24	6	-875.3	-2343.931464	-2342.974150	-2343.053836	36.69	-452.82	-123.49	-2339.6224788	-2338.7121998	-2338.7918858	34.18
S_TS2_25	7	-439.0	-2343.931372	-2342.973476	-2343.053580	37.36	-474.87	-124.81	-2339.6219383	-2338.7115813	-2338.7916853	34.71
S_TS2_26	1	-895.8	-2343.931183	-2342.974606	-2343.055007	33.61	-415.32	-147.94	-2339.6114980	-2338.7112680	-2338.7916690	34.75
S_TS2_27	8	-116.9	-2343.932658	-2342.972549	-2343.052287	40.75	-474.73	-126.10	-2339.6221757	-2338.7100957	-2338.7898337	39.57
S_TS2_28	1	-566.5	-2343.927998	-2342.971531	-2343.050262	46.07	-429.63	-144.79	-2339.6117403	-2338.7104223	-2338.7891533	41.35
S_TS2_29	1	-566.8	-2343.927999	-2342.971526	-2343.050255	46.09	-429.63	-144.80	-2339.6117267	-2338.7104047	-2338.7891337	41.40
S_TS2_30	1	-821.4	-2343.928670	-2342.971145	-2343.050928	44.32	-424.71	-150.33	-2339.6089766	-2338.7087086	-2338.7884916	43.09
S_TS2_31	1	-765.6	-2343.926850	-2342.969568	-2343.051290	43.37	-402.52	-152.65	-2339.6055133	-2338.7063743	-2338.7880963	44.13
S_TS2_32	1	-134.1	-2343.929728	-2342.968688	-2343.048070	51.82	-457.51	-134.06	-2339.6183341	-2338.7083531	-2338.7877351	45.08
S_TS2_33	2	-884.0	-2343.924225	-2342.966518	-2343.047759	52.64	-418.73	-158.18	-2339.6026715	-2338.7052105	-2338.7864515	48.45
S_TS2_34	4	-129.7	-2343.918823	-2342.958822	-2343.039314	74.81	-429.49	-150.85	-2339.5982761	-2338.6957301	-2338.7762221	75.30
S_TS2_35	3	-720.3	-2343.935699	-2342.978741	-2343.058283	25.01	-464.61					
S_TS2_36	3	-837.8	-2343.935912	-2342.980603	-2343.058222	25.17	-461.85					
S_TS2_37	3	-805.6	-2343.930166	-2342.973722	-2343.054282	35.52	-453.22		n.d.			
S_TS2_38	3	-453.9	-2343.929162	-2342.971672	-2343.052951	39.01	-459.65					
S_TS2_39	3	-729.5	-2343.930317	-2342.973197	-2343.052817	39.36	-455.06					
S_TS2_40	1	-872.9	-2343.927194	-2342.970344	-2343.051198	43.61	-417.72					

| Name | Category | neg. freq. [cm^{-1}] | SMD(Et$_2$O)/B3LYP-D3/6-31+G(d) | | | | | | DLPNO-CCSD(T)/def2-TZVPP | | | |
			E_{tot} [Hartree]	$H_{223.15}$ [Hartree]	$G_{223.15}$ [Hartree]	$\Delta\Delta G^{\ddagger}_{223.15}$ [kJ mol^{-1}]	Grimme-D3 correction [kJ mol^{-1}]	solvation energy [kJ mol^{-1}]	E_{tot} [Hartree]	$H_{223.15, sol}$ [Hartree]	$G_{223.15, sol}$ [Hartree]	$\Delta\Delta G^{\ddagger}_{223.15}$ [kJ mol^{-1}]
S_TS2_41	1	-879.5	-2343.924513	-2342.967490	-2343.048088	51.78	-410.35					
S_TS2_42	1	-921.5	-2343.923793	-2342.966912	-2343.047700	52.80	-420.56					
S_TS2_43	2	-152.3	-2343.928696	-2342.969087	-2343.047696	52.81	-470.98					
S_TS2_44	2	-716.6	-2343.924438	-2342.967078	-2343.047417	53.54	-435.77					
S_TS2_45	2	-715.0	-2343.924437	-2342.967077	-2343.047412	53.55	-435.78					
S_TS2_46	2	-885.5	-2343.924652	-2342.967145	-2343.047230	54.03	-416.00					
S_TS2_47	6	-582.7	-2343.924316	-2342.966907	-2343.046947	54.77	-439.86					
S_TS2_48	6	-768.1	-2343.925267	-2342.968286	-2343.046942	54.79	-445.90					
S_TS2_49	1	-930.9	-2343.921990	-2342.964440	-2343.045423	58.77	-425.58					
S_TS2_50	2	-889.8	-2343.919702	-2342.962770	-2343.043912	62.74	-416.97					
S_TS2_51	2	-793.1	-2343.920340	-2342.963087	-2343.042980	65.19	-433.73					
S_TS2_52	6	-793.3	-2343.921838	-2342.962836	-2343.041680	68.60	-463.75					
S_TS2_53	6	-424.1	-2343.921987	-2342.963176	-2343.040601	71.43	-454.96					
S_TS2_54	4	-127.9	-2343.919015	-2342.959466	-2343.038740	76.32	-431.49					
S_TS2_55	4	-128.0	-2343.919015	-2342.959461	-2343.038734	76.34	-431.48					

Table 6.42. Single point energies for best three **TS2** conformers (based on B3LYP-D3/6-31+G(d) energies) on different levels of theory.

| Single point method | Single point energies [Hartree] | | | | |
	B3LYP/6-31+G(d)	DLPNO/CCSD(T)	B3LYP/6-311+G(d,p)	M06-2x/6-311+G(d,p)	wB97XD/6-311+G(d,p)
S_TS2_1	-2343.937363	-2339.627500	-2344.409500	-2343.306200	-2343.532100
S_TS2_2	-2343.936338	-2339.623100	-2344.407900	-2343.303700	-2343.529200
S_TS2_3	-2343.937223	-2339.624500	-2344.408700	-2343.304800	-2343.529800
R_TS2_1	-2343.943332	-2339.631500	-2344.415100	-2343.310500	-2343.535400

| R_TS2_2 | -2343.943738 | -2339.631900 | -2344.415300 | -2343.310000 | -2343.536000 |
| R_TS2_3 | -2343.943020 | -2339.631000 | -2344.414800 | -2343.310200 | -2343.535100 |

Table 6.43. Single point energies for **TS2** structures (column 1) compared to energies of H-capped structures **TS2**-HC (column 2) as shown in **Scheme 6.25** for all conformers populated to more than 5% and the best category-I-*(S)*-conformer at DLPNO-CCSD(T)/def2-TZVPP level of theory. Difference of relative energies compared to R_TS2_1 gives the difference of non-covalent interaction energy (column 6) between naphthyl moiety of the alcohol and the rest of transition state structure.

name	E_{tot} (full **TS2**) [Hartree]	E_{tot} (H-capped **TS2_HC**) [Hartree]	$\Delta\Delta E_{tot}$ (full **TS2**) relative to R_TS2_1 [kJ mol^{-1}]	$\Delta\Delta E_{tot}$ (H-capped **TS2_HC**) relative to R_TS2_1 [kJ mol^{-1}]	$\Delta E_{non-covalent\ interactions}$ relative to R_TS2_1 [kJ mol^{-1}]
R_TS2_1	-2339.6314779	-1955.6298980	0.00	0.00	0.00
R_TS2_2	-2339.6318998	-1955.6308586	-1.11	-2.52	1.41
R_TS2_3	-2339.6309954	-1955.6298939	1.27	0.01	1.26
R_TS2_4	-2339.6315717	-1955.6308136	-0.25	-2.40	2.16
R_TS2_5	-2339.6256115	-1955.6248157	15.40	13.34	2.06
R_TS2_6	-2339.6267504	-1955.6253533	12.41	11.93	0.48
S_TS2_1	-2339.6274930	-1955.6300808	10.46	-0.48	10.94
S_TS2_2	-2339.6231105	-1955.6272284	21.97	7.01	14.96
S_TS2_3	-2339.6245273	-1955.6273449	18.25	6.70	11.55
S_TS2_4	-2339.6254136	-1955.6268408	15.92	8.03	7.90
S_TS2_5	-2339.6262607	-1955.6294994	13.70	1.05	12.65
S_TS2_6	-2339.6262560	-1955.6295027	13.71	1.04	12.67
S_TS2_7	-2339.6269707	-1955.6299134	11.83	-0.04	11.87
S_TS2_8	-2339.6269220	-1955.6299526	11.96	-0.14	12.10
S_TS2_13	-2339.6288338	-1955.6298110	6.94	0.23	6.71

6.5.2. Energy Profile

Table 6.44. Overview of energies of all species used for the calculation of **Figure 6.25.** Column 1 gives the name as used in the manuscript. Total energy, enthalpy and free energy calculated at SMD(Et$_2$O)/B3LYP-D3/6-31+G(d) and at DLPNO-CCSD(T)/def2-TZVPP are reported. All enthalpies are corrected for a quasi-harmonic rotor, free energies with a free-rotor approximation (for details see Chapter 6.4.1). Solvation energy was calculated from the difference of single point calculations in gas phase and total energy with SMD model on B3LYP-D3/6-31+G(d) level of theory and added to enthalpy and free energy at coupled cluster calculations. Differences in free energy are reported relative to the best conformer of each species. **Figure 6.25** gives Boltzmann-averaged values for the reported species. The geometries of all listed conformers are provided as SDF file.

	neg. freq. [cm^{-1}]	SMD(Et$_2$O)/B3LYP-D3/6-31+G(d)			DLPNO-CCSD(T)/def2-TZVPP			
		E_{tot} [Hartree]	$H_{223.15}$ [Hartree]	$G_{223.15}$ [Hartree]	E_{tot} [Hartree]	$H_{223.15, sol}$ [Hartree]	$G_{223.15, sol}$ [Hartree]	$\Delta\Delta G^{\ddagger}_{223.15}$ [kJ mol^{-1}]
1-(2-Napthyl)ethanol 1b								
Np_2		-539.792410	-539.577163	-539.609665	-538.7728677	-538.5737047	-538.6062067	0.00
Np_1		-539.791981	-539.576699	-539.609081	-538.7725927	-538.5734537	-538.6058357	0.97
Np_4		-539.790532	-539.575469	-539.608124	-538.7708248	-538.5727048	-538.6053598	2.22
Np_3		-539.790500	-539.575357	-539.607892	-538.7709622	-538.5725092	-538.6050442	3.05
Np_6		-539.790599	-539.575184	-539.607147	-538.7705978	-538.5722728	-538.6042358	5.17
Np_5		-539.790526	-539.575033	-539.607378	-538.7698245	-538.5718155	-538.6041605	5.37
Np_7		-539.790541	-539.575093	-539.607175	-538.7707620	-538.5718830	-538.6039650	5.89
Isobutyric anhydride 2								
BuAnh_5		-539.041217	-538.819860	-538.857278	-538.1227585	-537.9165355	-537.9539535	0.00
BuAnh_9		-539.040379	-538.818801	-538.856018	-538.1223955	-537.9158285	-537.9530455	2.38
BuAnh_13		-539.040086	-538.818309	-538.855310	-538.1223625	-537.9153995	-537.9524005	4.08
BuAnh_17		-539.039895	-538.819309	-538.855856	-538.1213231	-537.9157881	-537.9523351	4.25
BuAnh_8		-539.040070	-538.819199	-538.855445	-538.1217371	-537.9158821	-537.9521281	4.79
BuAnh_24		-539.040343	-538.818726	-538.855916	-538.1206501	-537.9148161	-537.9520061	5.11
BuAnh_11		-539.040676	-538.819962	-538.855205	-538.1221099	-537.9165669	-537.9518099	5.63
BuAnh_1		-539.040111	-538.818504	-538.854446	-538.1217500	-537.9146200	-537.9505620	8.90
BuAnh_19		-539.040186	-538.819415	-538.854166	-538.1210363	-537.9157523	-537.9505033	9.06
BuAnh_3		-539.039887	-538.818123	-538.853978	-538.1215155	-537.9143255	-537.9501805	9.91
BuAnh_36		-539.037689	-538.816112	-538.853061	-538.1198159	-537.9127909	-537.9497399	11.06

	SMD(Et₂O)/B3LYP-D3/6-31+G(d)			DLPNO-CCSD(T)/def2-TZVPP			
	neg. freq. [cm⁻¹]	E_{tot} [Hartree]	$H_{223.15}$ [Hartree]	$G_{223.15}$ [Hartree]	E_{tot} [Hartree]	$H_{223.15, sol}$ [Hartree]	$G_{223.15, sol}$ [Hartree]	$\Delta\Delta G^{\ddagger}_{223.15}$ [kJ mol⁻¹]
Catalyst 3								
Np1cat_2		-1265.084160	-1264.555993	-1264.610351	-1262.7091374	-1262.2134454	-1262.2678034	0.00
Np1cat_8		-1265.084137	-1264.555968	-1264.610158	-1262.7091179	-1262.2133669	-1262.2675569	0.65
Np1cat_1		-1265.084308	-1264.556116	-1264.609641	-1262.7088450	-1262.2129840	-1262.2665090	3.40
Np1cat_9		-1265.082111	-1264.554261	-1264.608164	-1262.7085405	-1262.2125905	-1262.2664935	3.44
Np1cat_15		-1265.080951	-1264.552957	-1264.605804	-1262.7081570	-1262.2128750	-1262.2657220	5.46
Np1cat_4		-1265.082441	-1264.554186	-1264.607223	-1262.7086104	-1262.2125964	-1262.2656334	5.70
Np1cat_10		-1265.079887	-1264.551856	-1264.606398	-1262.7050302	-1262.2108552	-1262.2653972	6.32
Np1cat_7		-1265.081501	-1264.553177	-1264.605999	-1262.7074145	-1262.2120565	-1262.2648785	7.68
Np1cat_12		-1265.080970	-1264.552825	-1264.607439	-1262.7045538	-1262.2095268	-1262.2641408	9.62
Np1cat_16		-1265.078409	-1264.550184	-1264.603510	-1262.7030736	-1262.2078236	-1262.2611496	17.47
Np1cat_13		-1265.075620	-1264.548928	-1264.600180	-1262.7057730	-1262.2090880	-1262.2603400	19.60
Np1cat_11		-1265.077245	-1264.548887	-1264.601938	-1262.7022462	-1262.2069922	-1262.2600432	20.37
Np1cat_14		-1265.073393	-1264.545026	-1264.598403	-1262.6983454	-1262.2042604	-1262.2576374	26.69
rc (reactant complex)								
TS1_int1_7		-1804.136592	-1803.391751	-1803.461219	-1800.8478986	-1800.1426916	-1800.2121596	0.00
TS1_int1_2		-1804.132816	-1803.388199	-1803.456308	-1800.8456756	-1800.1411076	-1800.2092166	7.73
TS1								
TS1_7	-108.3	-1804.120081	-1803.374404	-1803.441224	-1800.8222098	-1800.1212708	-1800.1880908	0.00
TS1_29	-90.5	-1804.117960	-1803.371568	-1803.437141	-1800.8217588	-1800.1209588	-1800.1865318	4.09
TS1_2	-103.3	-1804.116977	-1803.371197	-1803.437486	-1800.8193990	-1800.1200180	-1800.1863070	4.68
TS1_5	-73.1	-1804.116886	-1803.371104	-1803.437977	-1800.8200986	-1800.1193066	-1800.1861796	5.02
TS1_30	-87.2	-1804.117912	-1803.372080	-1803.436669	-1800.8220158	-1800.1215858	-1800.1861748	5.03
int1								

	neg. freq. [cm^{-1}]	SMD(Et$_2$O)/B3LYP-D3/6-31+G(d)			DLPNO-CCSD(T)/def2-TZVPP			$\Delta\Delta G^{\ddagger}_{223.15}$ [kJ mol^{-1}]
		E_{tot} [Hartree]	$H_{223.15}$ [Hartree]	$G_{223.15}$ [Hartree]	E_{tot} [Hartree]	$H_{223.15, sol}$ [Hartree]	$G_{223.15, sol}$ [Hartree]	
TS1_int2_2		-1804.128126	-1803.381081	-1803.448480	-1800.8243260	-1800.1247270	-1800.1921260	0.00
TS1_int2_1		-1804.126601	-1803.380166	-1803.447055	-1800.8209411	-1800.1239831	-1800.1908721	3.29
TS1_int2_4		-1804.123038	-1803.376947	-1803.444131	-1800.8141043	-1800.1236373	-1800.1908213	3.43
TS1_int2_5		-1804.120496	-1803.374240	-1803.443338	-1800.8108111	-1800.1205441	-1800.1896421	6.52
TS1_int2_7		-1804.123245	-1803.377103	-1803.445157	-1800.8169188	-1800.1202538	-1800.1883078	10.02
TS1_int2_8		-1804.120625	-1803.374621	-1803.441784	-1800.8123244	-1800.1201414	-1800.1873044	12.66
TS1_int2_6		-1804.119890	-1803.373927	-1803.441719	-1800.8064232	-1800.1185942	-1800.1863862	15.07
int1·(R)-1b								
R_TS2_2_int1		-2343.956718	-2342.993737	-2343.075732	-2339.6395214	-2338.7310974	-2338.8130924	0.00
R_TS2_1_int1		-2343.955291	-2342.992558	-2343.074046	-2339.6377416	-2338.7295366	-2338.8110246	5.43
R_TS2_10_int1		-2343.947723	-2342.985765	-2343.066304	-2339.6332081	-2338.7266931	-2338.8072321	15.39
R_TS2_29_int1		-2343.947605	-2342.983939	-2343.065333	-2339.6302057	-2338.7220637	-2338.8034577	25.30
R_TS2_18_int1		-2343.940014	-2342.977574	-2343.060428	-2339.6184913	-2338.7138393	-2338.7966933	43.06
R_TS2_33_int1		-2343.937157	-2342.974958	-2343.056376	-2339.6106117	-2338.7133847	-2338.7948027	48.02
R_TS2_39_int1		-2343.936733	-2342.975406	-2343.056613	-2339.6096403	-2338.7118473	-2338.7930543	52.61
int1·(S)-1b								
S_TS2_13_int1		-2343.953411	-2342.991685	-2343.072235	-2339.6356956	-2338.7312156	-2338.8117656	0.00
S_TS2_4_int1		-2343.950929	-2342.988107	-2343.070083	-2339.6353026	-2338.7282276	-2338.8102036	4.10
S_TS2_2_int1		-2343.948371	-2342.986316	-2343.068935	-2339.6298045	-2338.7254555	-2338.8080745	9.69
S_TS2_1_int1		-2343.949060	-2342.986139	-2343.068152	-2339.6339291	-2338.7270211	-2338.8090341	7.17
S_TS2_29_int1		-2343.946897	-2342.984120	-2343.066568	-2339.6297438	-2338.7243568	-2338.8068048	13.02
S_TS2_19_int1		-2343.940691	-2342.978717	-2343.059653	-2339.6165278	-2338.7174448	-2338.7983808	35.14
R_TS2								
See **Table 6.41**								

		SMD(Et$_2$O)/B3LYP-D3/6-31+G(d)			DLPNO-CCSD(T)/def2-TZVPP			
	neg. freq. [cm^{-1}]	E_{tot} [Hartree]	$H_{223.15}$ [Hartree]	$G_{223.15}$ [Hartree]	E_{tot} [Hartree]	$H_{223.15, sol}$ [Hartree]	$G_{223.15, sol}$ [Hartree]	$\Delta\Delta G^{\ddagger}_{223.15}$ [kJ mol^{-1}]
S_TS2								
*See **Table 6.41***								
R_pc								
R_TS2_1_int2		-2343.974700	-2343.012104	-2343.094978	-2339.6732150	-2338.7568760	-2338.8397500	0.00
R_TS2_2_int2		-2343.974442	-2343.011945	-2343.094312	-2339.6719276	-2338.7567226	-2338.8390896	1.73
R_TS2_29_int2		-2343.971849	-2343.010294	-2343.093945	-2339.6721305	-2338.7541405	-2338.8377915	5.14
R_TS2_10_int2		-2343.967484	-2343.005615	-2343.087545	-2339.6677751	-2338.7520611	-2338.8339911	15.12
R_TS2_17_int2		-2343.970220	-2343.009474	-2343.090229	-2339.6633827	-2338.7521297	-2338.8328847	18.02
R_TS2_29_int2		-2343.969169	-2343.007718	-2343.089382	-2339.6601197	-2338.7507977	-2338.8324617	19.14
R_TS2_33_int2		-2343.964178	-2343.002805	-2343.084458	-2339.6589181	-2338.7475431	-2338.8291961	27.71
S_pc								
S_TS2_2_int2		-2343.970247	-2343.008684	-2343.092002	-2339.6696016	-2338.7540366	-2338.8373546	0.00
S_TS2_1_int2		-2343.968537	-2343.006608	-2343.089413	-2339.6686379	-2338.7529299	-2338.8357349	4.25
S_TS2_4_int2		-2343.968799	-2343.006270	-2343.088895	-2339.6678364	-2338.7518124	-2338.8344374	7.66
S_TS2_13_int2		-2343.970588	-2343.008901	-2343.089003	-2339.6676108	-2338.7528468	-2338.8329488	11.57
S_TS2_29_int2		-2343.963205	-2343.001708	-2343.084024	-2339.6589355	-2338.7479865	-2338.8303025	18.52
S_TS2_19_int2		-2343.963093	-2343.001218	-2343.083299	-2339.6583631	-2338.7455261	-2338.8276071	25.59
1-(2-Napthyl)ethyl isobutyrate 4b								
BuNp_14		-771.110150	-770.796010	-770.839042	-769.6780170	-769.3845640	-769.4275960	0.00
BuNp_2		-771.110858	-770.797639	-770.837966	-769.6794698	-769.3863198	-769.4266468	2.49
BuNp_1		-771.110424	-770.797145	-770.837627	-769.6789633	-769.3858923	-769.4263743	3.21
BuNp_3		-771.110059	-770.795888	-770.837536	-769.6784682	-769.3844592	-769.4261072	3.91
BuNp_12		-771.109814	-770.795745	-770.837623	-769.6776864	-769.3839374	-769.4258154	4.67
BuNp_16		-771.108858	-770.794544	-770.837378	-769.6765941	-769.3829261	-769.4257601	4.82

	neg. freq. [cm^{-1}]	SMD(Et$_2$O)/B3LYP-D3/6-31+G(d)			DLPNO-CCSD(T)/def2-TZVPP			$\Delta\Delta G^{\ddagger}_{223.15}$ [kJ mol^{-1}]
		E_{tot} [Hartree]	$H_{223.15}$ [Hartree]	$G_{223.15}$ [Hartree]	E_{tot} [Hartree]	$H_{223.15,\,sol}$ [Hartree]	$G_{223.15,\,sol}$ [Hartree]	
BuNp_5		-771.109277	-770.795994	-770.837167	-769.6780016	-769.3845626	-769.4257356	4.88
BuNp_4		-771.110007	-770.796619	-770.836558	-769.6784931	-769.3852561	-769.4251951	6.30
BuNp_6		-771.109393	-770.796156	-770.835922	-769.6778903	-769.3847053	-769.4244713	8.20
BuNp_13		-771.109092	-770.795860	-770.836234	-769.6771990	-769.3840740	-769.4244480	8.26
BuNp_7		-771.110084	-770.797481	-770.835483	-769.6782621	-769.3863051	-769.4243071	8.63
BuNp_11		-771.110435	-770.797676	-770.835688	-769.6784988	-769.3861368	-769.4241488	9.05
Isobutyric acid S1								
BuAc_2		-307.744967	-307.621513	-307.648003	-307.2388891	-307.1255001	-307.1519901	0.00
BuAc_4		-307.744470	-307.620544	-307.647407	-307.2378954	-307.1242164	-307.1510794	2.39

6.5.3. Analysis of Substrates and Products

Table 6.45. Overview of energies of all species used for the calculation of thermodynamics in Chapter 6.4.9. Column 1 gives name as used in the manuscript. Total energy, enthalpy and free energy calculated at SMD(Et$_2$O)/B3LYP-D3/6-31+G(d) and at DLPNO-CCSD(T)/def2-TZVPP are reported. All enthalpies are corrected for a quasi-harmonic rotor, free energies with a free-rotor approximation (for details see Chapter 6.4.1). Solvation energy was calculated from the difference of single point calculations in gas phase and total energy with SMD model on B3LYP-D3/6-31+G(d) level of theory and added to enthalpy and free energy at coupled cluster calculations. Differences in free energy are reported relative to the best conformer of each species. In Chapter 6.4.9 Boltzmann-averaged values are reported. The geometries of all listed conformers are provided as SDF file.

	SMD(Et$_2$O)/B3LYP-D3/6-31+G(d)			DLPNO-CCSD(T)/def2-TZVPP			
	E_{tot} [Hartree]	$H_{223.15}$ [Hartree]	$G_{223.15}$ [Hartree]	E_{tot} [Hartree]	$H_{223.15, sol}$ [Hartree]	$G_{223.15, sol}$ [Hartree]	$\Delta\Delta G^{\ddagger}_{223.15}$ [kJ mol^{-1}]
1-(2-Naphtyl)ethanol 1b							
See **Table 6.44**							
1-Phenylethanol 1a							
Phe_1	-386.133758	-385.966887	-385.995840	-385.4197194	-385.2649814	-385.2939344	0.00
Phe_3	-386.132004	-385.965270	-385.994554	-385.4178981	-385.2639991	-385.2932831	1.71
Phe_7	-386.131881	-385.964735	-385.993667	-385.4164389	-385.2627149	-385.2916469	6.01
1-(2-Phenanthryl)ethanol 1c							
Phant_1	-693.452764	-693.189073	-693.225403	-692.1290715	-691.8853695	-691.9216995	0.00
Phant_3	-693.450935	-693.187321	-693.223165	-692.1271056	-691.8842896	-691.9201336	4.11
Phant_7	-693.450890	-693.186997	-693.222991	-692.1258997	-691.8833687	-691.9193627	6.14
1-(2-Pyrenyl)ethanol 1d							
Pyr_1	-769.692444	-769.415726	-769.451915	-768.2180779	-767.9627269	-767.9989159	0.00
Pyr_4	-769.690634	-769.414178	-769.450575	-768.2162984	-767.9618824	-767.9982794	1.67
Pyr_7	-769.690088	-769.414020	-769.448598	-768.2152306	-767.9610546	-767.9956326	8.62
1-(2-Napthyl)ethyl isobutyrate 4b							
See **Table 6.44**							
1-Phenylethyl isobutyrate 4a							
BuPhe1	-617.452392	-617.186437	-617.224894	-616.3261749	-616.0765269	-616.1149839	0.00
BuPhe12	-617.451160	-617.185253	-617.224543	-616.3245000	-616.0749470	-616.1142370	1.96
BuPhe3	-617.451410	-617.185356	-617.223276	-616.3250736	-616.0752836	-616.1132036	4.67

	SMD(Et₂O)/B3LYP-D3/6-31+G(d)			DLPNO-CCSD(T)/def2-TZVPP			
	E_{tot} [Hartree]	$H_{223.15}$ [Hartree]	$G_{223.15}$ [Hartree]	E_{tot} [Hartree]	$H_{223.15, sol}$ [Hartree]	$G_{223.15, sol}$ [Hartree]	$\Delta\Delta G^{\ddagger}_{223.15}$ [kJ mol⁻¹]
1-(2-Phenanthryl)ethyl isobutyrate 4c							
BuPhant2	-924.771182	-924.408763	-924.453948	-923.0353478	-922.6971158	-922.7423008	0.00
BuPhant01	-924.770870	-924.408976	-924.453024	-923.0349477	-922.6972287	-922.7412767	2.69
BuPhant3	-924.770211	-924.408629	-924.453005	-923.0344924	-922.6968014	-922.7411774	2.95
BuPhant14	-924.770757	-924.408947	-924.452942	-923.0346513	-922.6971273	-922.7411223	3.09
BuPhant12	-924.770130	-924.408233	-924.452131	-923.0338320	-922.6961000	-922.7399980	6.05
1-(2-Pyrenyl)ethyl isobutyrate 4d							
BuPyr_4	-1001.009716	-1000.634346	-1000.680978	-999.1234426	-998.7732866	-998.8199186	0.00
BuPyr_7	-1001.010997	-1000.635323	-1000.680270	-999.1247086	-998.7744416	-998.8193886	1.39
BuPyr01	-1001.010643	-1000.635667	-1000.679896	-999.1244784	-998.7749534	-998.8191824	1.93
BuPyr_3	-1001.009657	-1000.634323	-1000.680169	-999.1233822	-998.7732492	-998.8190952	2.16
BuPyr_12	-1001.009746	-1000.634892	-1000.678510	-999.1228592	-998.7735672	-998.8171852	7.18

Table 6.46. Overview of energies of all species used for the calculation of alcoholates for isodesmic proton transfer reactions in Chapter 6.4.9. Column 1 gives name as used in the manuscript. Total energy, enthalpy and free energy calculated at SMD(Et$_2$O)/B3LYP-D3/6-31+G(d) are reported. All enthalpies are corrected for a quasi-harmonic rotor, free energies with a free-rotor approximation (for details see Chapter 6.4.1). Differences in free energy are reported relative to the best conformer of each species. In Chapter 6.4.9 Boltzmann-averaged values are reported.

	SMD(Et$_2$O)/B3LYP-D3/6-31+G(d)		
	E_{tot} [Hartree]	$G_{223.15,\,sol}$ [Hartree]	$\Delta\Delta G^{\ddagger}_{223.15}$ [kJ mol^{-1}]
1-(2-Naphtyl)ethanolat 1b-			
Np_1_anion	-539.259586	-539.091001	0.00
Np_4_anion	-539.258750	-539.090213	2.07
Np_7_anion	-539.256635	-539.087902	8.14
1-Phenylethanolat 1a-			
Phe_1_anion	-385.599818	-385.476182	0.00
Phe_7_anion	-385.551226	-385.429096	123.62
1-(2-Phenanthryl)ethanolat 1c-			
Phant_anion	-692.919475	-692.707197	0.00
Phant_anion	-692.919511	-692.706576	1.63
Phant_anion	-692.871727	-692.659734	124.61
1-(2-Pyrenyl)ethanolat 1d-			
Pyr_3_anion	-769.160263	-768.934461	0.00
Pyr_7_anion	-769.111143	-768.886677	125.46

6.6. Supplementary References

[1]   H. B. Kagan, J. C. Fiaud, *Top. Stereochem.* **1988**, *18*, 249-300.
[2]   C. E. Muller, P. R. Schreiner, *Angew. Chem. Int. Ed.* **2011**, *50*, 6012-6042.
[3]   G. Ma, J. Deng, M. P. Sibi, *Angew. Chem. Int. Ed.* **2014**, *53*, 11818-11821.
[4]   a) H. F. Klare, M. Oestreich, *Angew. Chem. Int. Ed.* **2007**, *46*, 9335-9338; b) M. D. Greenhalgh, J. E. Taylor, A. D. Smith, *Tetrahedron* **2018**, *74*, 5554-5560.
[5]   S. Hoops, S. Sahle, R. Gauges, C. Lee, J. Pahle, N. Simus, M. Singhal, L. Xu, P. Mendes, U. Kummer, *Bioinformatics* **2006**, *22*, 3067-3074.
[6]   I. Vasilief, QtiPlot 0.9.8.9, **2011**.
[7]   S. F. Musolino, O. S. Ojo, N. J. Westwood, J. E. Taylor, A. D. Smith, *Chem. Eur. J.* **2016**, *22*, 18916-18922.
[8]   M. Marin-Luna, B. Pölloth, F. Zott, H. Zipse, *Chem. Sci.* **2018**, *9*, 6509-6515.
[9]   a) K. Naemura, M. Murata, R. Tanaka, M. Yano, K. Hirose, Y. Tobe, *Tetrahedron: Asymmetry* **1996**, *7*, 3285-3294; b) W. H. Pirkle, S. D. Beare, *J. Am. Chem. Soc.* **1967**, *89*, 5485-5487.
[10]   M. P. Sibi, K. Kawashima, L. M. Stanley, *Org. Lett.* **2009**, *11*, 3894-3897.
[11]   F. Fernandez, C. Gonzalez, G. Gomez, C. Lopez, L. Medina, J. M. Calleja, E. Cano, *Arch. Pharm.* **1990**, *323*, 239-242.
[12]   A. Davis, J. Casas-Solvas, T. Mooibroek, S. Sandramurthy, J. Howgego, *Synlett* **2014**, *25*, 2591-2594.
[13]   J. Malmquist, P. Ström, *J. Labelled Compd. Radiopharm.* **2012**, *55*, 387-392.
[14]   R. G. Harvey, M. Konieczny, J. Pataki, *J. Org. Chem.* **1983**, *48*, 2930-2932.
[15]   P. Toy, S. Ma, *Synlett* **2016**, *27*, 1207-1210.
[16]   K. Fujii, K. Mitsudo, H. Mandai, S. Suga, *Bull. Chem. Soc. Jpn.* **2016**, *89*, 1081-1092.
[17]   a) A. D. Becke, *J. Chem. Phys.* **1993**, *98*, 1372 -1377; b) C. Lee, W. Yang, R. G. Parr, *Phys. Rev. B* **1988**, *37*, 785-789; c) S. Grimme, *J. Chem. Phys.* **2006**, *124*, 034108.
[18]   A. V. Marenich, C. J. Cramer, D. G. Truhlar, *J. Phys. Chem. B* **2009**, *113*, 6378-6396.
[19]   S. Grimme, *Chem. Eur. J.* **2012**, *18*, 9955-9964.
[20]   Y.-P. Li, J. Gomes, S. Mallikarjun Sharada, A. T. Bell, M. Head-Gordon, *J. Phys. Chem. C* **2015**, *119*, 1840-1850.
[21]   G. Luchini, J. V. Alegre-Requena, Y. Guan, I. Funes-Ardoiz, R. S. Paton, GoodVibes 3.0.0, **2019**.
[22]   a) C. Riplinger, B. Sandhoefer, A. Hansen, F. Neese, *J. Chem. Phys.* **2013**, *139*, 134101; b) C. Riplinger, F. Neese, *J. Chem. Phys.* **2013**, *138*, 034106; c) F. Weigend, R. Ahlrichs, *Phys. Chem. Chem. Phys.* **2005**, *7*, 3297-3305.
[23]   A. Hellweg, C. Hättig, S. Höfener, W. Klopper, *Theor. Chem. Acc.* **2007**, *117*, 587-597.
[24]   M. Marin-Luna, P. Patschinski, H. Zipse, *Chem. Eur. J.* **2018**, *24*, 15052-15058.
[25]   G. W. T. M. J. Frisch, H. B. Schlegel, G. E. Scuseria, M. A. Robb, J. R. Cheeseman, G. Scalmani, V. Barone, B. Mennucci, G. A. Petersson, H. Nakatsuji, M. Caricato, X. Li, H. P. Hratchian, A. F. Izmaylov, J. Bloino, G. Zheng, J. L. Sonnenberg, M. Hada, M. Ehara, K. Toyota, R. Fukuda, J. Hasegawa, M. Ishida, T. Nakajima, Y. Honda, O. Kitao, H. Nakai, T. Vreven, J. A. Montgomery, Jr., J. E. Peralta, F. Ogliaro, M. Bearpark, J. J. Heyd, E. Brothers, K. N. Kudin, V. N. Staroverov, T. Keith, R. Kobayashi, J. Normand, K. Raghavachari, A. Rendell, J. C. Burant, S. S. Iyengar, J. Tomasi, M. Cossi, N. Rega, J. M. Millam, M. Klene, J. E. Knox, J. B. Cross, V. Bakken, C. Adamo, J. Jaramillo, R. Gomperts, R. E. Stratmann, O. Yazyev, A. J. Austin, R. Cammi, C. Pomelli, J. W. Ochterski, R. L. Martin, K. Morokuma, V. G. Zakrzewski, G. A. Voth, P. Salvador, J. J. Dannenberg, S. Dapprich, A. D. Daniels, O. Farkas, J. B. Foresman, J. V. Ortiz, J. Cioslowski, and D. J. Fox,, Gaussian 09, Revision D.01, Wallingford CT, **2010**.
[26]   F. Neese, *Comput. Mol. Sci.* **2012**, *2*, 73-78.
[27]   Maestro 12.2.012, New York, **2019**.
[28]   a) E. Larionov, M. Mahesh, A. C. Spivey, Y. Wei, H. Zipse, *J. Am. Chem. Soc.* **2012**, *134*, 9390-9399; b) R. Maji, H. Ugale, S. E. Wheeler, *Chem. Eur. J.* **2019**, *25*, 4452-4459.
[29]   T. Lu, F. Chen, *J. Comput. Chem.* **2012**, *33*, 580-592.
[30]   J. Contreras-Garcia, E. R. Johnson, S. Keinan, R. Chaudret, J. P. Piquemal, D. N. Beratan, W. Yang, *J. Chem. Theory Comput.* **2011**, *7*, 625-632.
[31]   W. Humphrey, A. Dalke, K. Schulten, *J. Molec. Graphics* **1996**, *14*, 33-38.
[32]   E. D. Glendening, A. E. Reed, J. E. Carpenter, F. Weinhold, NBO Version 3.1
[33]   R. Denningtion, A. K. Todd, J. M. Millam, GaussView 5, **2009**.
[34]   C. Y. Legault, CYLview 1.0b, Université de Sherbrooke, **2009**.
[35]   S. Xu, I. Held, B. Kempf, H. Mayr, W. Steglich, H. Zipse, *Chem. Eur. J.* **2005**, *11*, 4751-4757.
[36]   J. M. Keith, J. F. Larrow, E. N. Jacobsen, *Adv. Synth. Catal.* **2001**, *343*, 5-26.
[37]   C. Riplinger, P. Pinski, U. Becker, E. F. Valeev, F. Neese, *J. Chem. Phys.* **2016**, *144*, 024109.
[38]   Y. Zhao, D. G. Truhlar, *Theor. Chem. Acc.* **2007**, *120*, 215-241.
[39]   J. D. Chai, M. Head-Gordon, *Phys. Chem. Chem. Phys.* **2008**, *10*, 6615-6620.
[40]   a) K. E. Riley, M. Pitonak, P. Jurecka, P. Hobza, *Chem. Rev.* **2010**, *110*, 5023-5063; b) T. M. Parker, L. A. Burns, R. M. Parrish, A. G. Ryno, C. D. Sherrill, *J. Chem. Phys.* **2014**, *140*, 094106.
[41]   G. Bringmann, A. J. Price Mortimer, P. A. Keller, M. J. Gresser, J. Garner, M. Breuning, *Angew. Chem. Int. Ed.* **2005**, *44*, 5384-5427.
[42]   a) J. W. Hwang, P. Li, K. D. Shimizu, *Org. Biomol. Chem.* **2017**, *15*, 1554-1564; b) C. R. Martinez, B. L. Iverson, *Chem. Sci.* **2012**, *3*, 2191; c) A. J. Neel, M. J. Hilton, M. S. Sigman, F. D. Toste, *Nature* **2017**, *543*, 637-646.
[43]   C. Reichardt, "ET(30) Werte", Philipps-Universität Marburg, https://www.uni-marburg.de/de/fb15/arbeitsgruppen/ag-reichardt/et30-werte-prof-reichardt, accessed at 14.04.2020.
[44]   T. J. Seguin, T. Lu, S. E. Wheeler, *Org. Lett.* **2015**, *17*, 3066-3069.
[45]   S. Grimme, J. Antony, S. Ehrlich, H. Krieg, *J. Chem. Phys.* **2010**, *132*, 154104.
[46]   S. Grimme, R. Huenerbein, S. Ehrlich, *ChemPhysChem* **2011**, *12*, 1258-1261.
[47]   S. Malakar, S. V. Shree Sowndarya, R. B. Sunoj, *Org. Biomol. Chem.* **2018**, *16*, 5643-5652.
[48]   T. Lu, R. Zhu, Y. An, S. E. Wheeler, *J. Am. Chem. Soc.* **2012**, *134*, 3095-3102.
[49]   R. A. Klein, *Chem. Phys. Lett.* **2006**, *425*, 128-133.
[50]   R. F. Bader, *J. Phys. Chem. A* **2010**, *114*, 7431-7444.
[51]   R. F. W. Bader, *Acc. Chem. Res.* **1985**, *18*, 9-15.
[52]   R. G. A. Bone, R. F. W. Bader, *J. Phys. Chem.* **1996**, *100*, 10892-10911.
[53]   S. J. Grabowski, *J. Phys. Chem. A* **2001**, *105*, 10739-10746.
[54]   T. Maity, H. Mandal, A. Bauzá, B. C. Samanta, A. Frontera, S. K. Seth, *New J. Chem.* **2018**, *42*, 10202-10213.
[55]   E. R. Johnson, S. Keinan, P. Mori-Sanchez, J. Contreras-Garcia, A. J. Cohen, W. Yang, *J. Am. Chem. Soc.* **2010**, *132*, 6498-6506.
[56]   W. Humphrey, A. Dalke, K. Schulten, *J. Mol. Graphics* **1996**, *14*, 33-38.
[57]   a) B. Thapa, H. B. Schlegel, *J. Phys. Chem. A* **2015**, *119*, 5134-5144; b) P. G. Seybold, G. C. Shields, *Wiley Interdiscip. Rev. Comput. Mol. Sci.* **2015**, *5*, 290-297.

Chapter 7. Conclusions on Size-Induced Rate Accelerations in Organocatalysis.

London dispersion forces and resulting non-covalent interactions (NCI) were discovered and explored already in the early days of chemical research.[1] Nonetheless, if contemporary organic chemists discuss steric or size-effects, this is very often synonymous to repulsive effects. Only in the last decade, a serious reconsideration of steric effects in terms of molecular attraction started in diverse fields of organic chemistry, like catalysis, compound stability, and enantioselectivity.[2] This discussion was strongly aided by the development of correction schemes fixing the lack of DFT methods in describing long-ranged interactions correctly.[3] A broad variety of theoretical studies investigated dispersion effects[4] and also the influence on thermodynamics was elucidated accurately.[5] In contrast, kinetic studies are rare[6] despite the fact that attractive NCIs should stabilize transition states and in terms of the transition state theory thus accelerate reactions. Herein, the influence of big aromatic moieties on reaction rates was investigated in different organocatalysed protecting group reactions.

7.1. Methodology

As most of the investigated effects on rates are rather small, a suitable sensitive yet robust experimental approach needed to be developed. The following points were found to be critical:

- Competition experiments are clearly preferable over direct kinetics as through identical reaction conditions the relative rates are much more robust than absolute rates. The consequent use of a small and structurally similar reference allows nonetheless to relate the rates of all substrates to each other.

- Substrates used should be as similar as possible. If substrates differ too much the origins of rate deviations become difficult to distinguish. We found it most suitable to use sets of reactants with systematically increasing π-systems as this guarantees similar (flat) geometries of reagents, while largely retaining the original conformational space.

- Every model system should be controlled for its suitability in measuring size-effects. Competition experiments with small reagents without aromatic moieties allow to estimate the baseline reactivity of the different substrates. Ideally, relative rates of the different substrates should be similar for small reagents. By this approach we found, for example, that neighbouring CH-bonds that are parallel to the reaction vectors strongly decrease relative rates, e.g. *peri*-hydrogens in 1-naphthyl or 9-anthracyl substituted reactants (Chapter 3). Especially the reactivity of compounds with several of these CH-bonds showed a strongly reduced reactivity. 2-Substituted alcohols or ketones were, in contrast, found to react with similar or at least comparable rates e.g. with trimethyl silyl chloride, triethylsilane

or with isobutyric anhydride catalysed by tri(*n*-butyl)phosphane and are thus suitable model compound sets.

- There are several strong reasons to measure chemoselectivity and enantiomeric excess at several conversion points and not only at 50%: 1) It gives an internal control, if the preconditions for the use of the Kagan formulas[7] are met (irreversible pseudo first-order kinetics yielding stable products). 2) Deviations at different conversion points can indicate the existence of two competing pathways. 3) Multiple measurements give in general more robust values.

- For high selectivity values ($s > 30$), the results obtained by standard competition experiments become error-prone. Here, the influence of the conversion value on calculated selectivity values becomes critical. In this case, NMR-determined conversions are not suitable and it is strongly recommendable to calculate conversions from the chemoselectivity/enantiomeric excess of products and reactants. Furthermore, the use of linear regression analysis gives superior results. Therefore, it would be a proper standard method to determine high selectivity values (see Chapter 6).

Appropriate model reaction setup for the investigation of size-dependent rate-accelerations
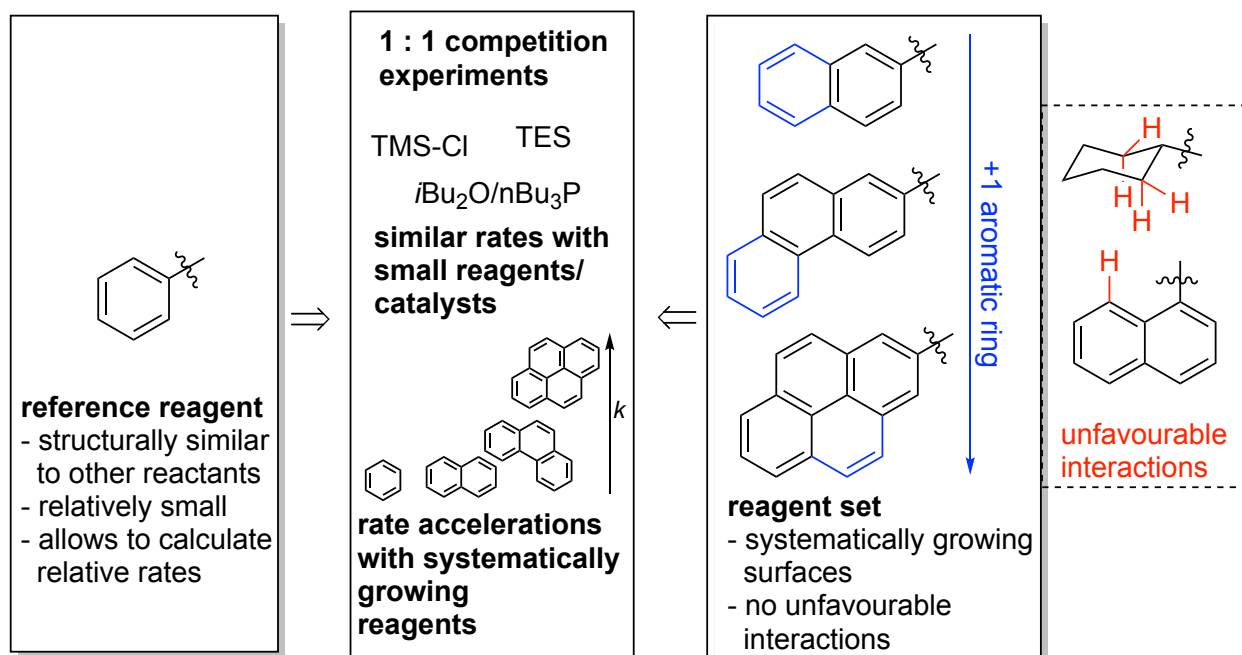
Figure 7.1. Graphical outline of methodological aspects for measuring size-induced rate accelerations. 1 : 1 competition experiments of a reference compound and a set of systematically growing surface without introduction of unfavourable interactions were found to be a proper model setup for the investigation of size-related rate changes.

7.2. Rate-Accelerations

With the developed methods we were able to investigate relative rates in the Lewis base-catalysed silylation of alcohols (Chapter 3), the Lewis acid-catalysed hydrosilylation of ketones yielding the same silyl ether products as the first reaction (Chapter 4) and the Lewis base-catalysed acylation of alcohols (Chapter 6). In all cases, the rate increased notably with increasing substrate size. In

the silylation and hydrosilylation reactions, rate accelerations by a factor of up to four were caused by attractive π-π interactions of reagent and reactant. In acylation reactions, cation-π interactions between catalyst and reagent resulted in rate accelerations of up to ten for DMAP. For chiral catalysts rate differences of up to 400 (resp. 40 regarding only one enantiomer) were measured due to a network of attractive interactions. The major differences in the extent of size-effects can be on the one hand rationalized by the different strengths of neutral π-π interactions and cation-π interactions. On the other hand, it shows that networks of attractive NCIs can stabilize transition states very strongly due to the additivity of dispersion forces. In computational studies for the silylation and hydrosilylation reactions no reasonable relation of relative reaction free energies and relative rates was found. However, Grimme-D3 dispersion energy contributions to the stability of the products correlated well with rate accelerations. The most favourable conformation of products includes tilted aromatic-aromatic stacking. A detailed analysis of the transition states in the asymmetric acylation of alcohols revealed that energy differences are caused by non-covalent interactions, involving cation-π, π-π and CH-π interactions. These results strongly support the hypothesis that attractive non-covalent interactions are an important control element in organocatalysed reactions. These insights can help to systematically design more efficient and selective catalysts or reagents.

Size-Induced Rate Accelerations
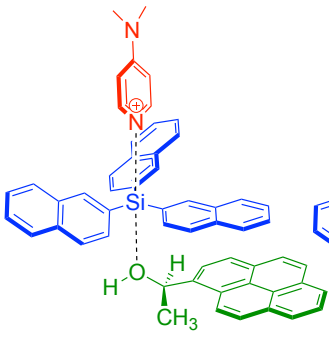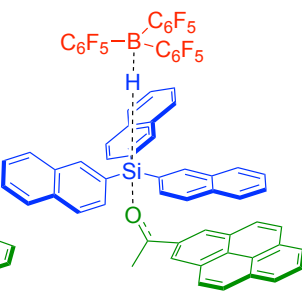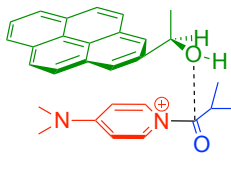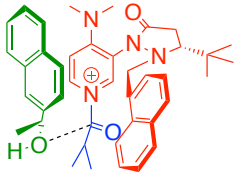
Figure 7.2. Graphical conclusion on size-induced rate accelerations in organocatalysed reactions. For each investigated reaction type the proposed or calculated transition state, maximal experimental rate accelerations and the most important findings on solvent effects and computational results highlighting the role of attractive NCIs are given.

7.3. Solvent Effects

In all of the systems rate accelerations were found to depend crucially on the nature of the solvent. Multi-parameter fits were used to elucidate critical solvent parameters. For the different reaction types different solvent parameters were found to mainly influence selectivities:

- solvent polarity ($E_T(30)$) in the asymmetric acylation reaction;
- the hydrogen bond donor ability α of the solvent in the silylation of alcohols;
- polarizability and hydrogen bond acceptor quality in the hydrosilylation of ketones.

A general explanation comprises the competing solvent-solute interactions that are lost if dispersion complexes are formed. Thus, the gain of dispersion energy in the transition state is diminished as all newly formed solute-solute interactions come at the cost of cancelled solvent-solute interactions. The nature of solvent-solute interactions can comprise (weak) hydrogen-bonding, dipole and van der Waals interactions and crucially depends on the structure and properties of reagents and transitions states. Thus, the critical parameter in determining their strength are unique for each reaction. Another factor that could influence rates are solvophobic effects based on solvent-solvent interactions. However, dispersion effects are generally strongly diminished in solution as compared to computed (gas-phase) energies. Current computational solvation models do not properly reflect the various interactions. As the problem of an accurate calculation of dispersion interaction is more or less solved, attempts are needed to provide notably improved solvation models.[8] A better understanding of solvent effects is probably the most pushing question in this area of research.[9]
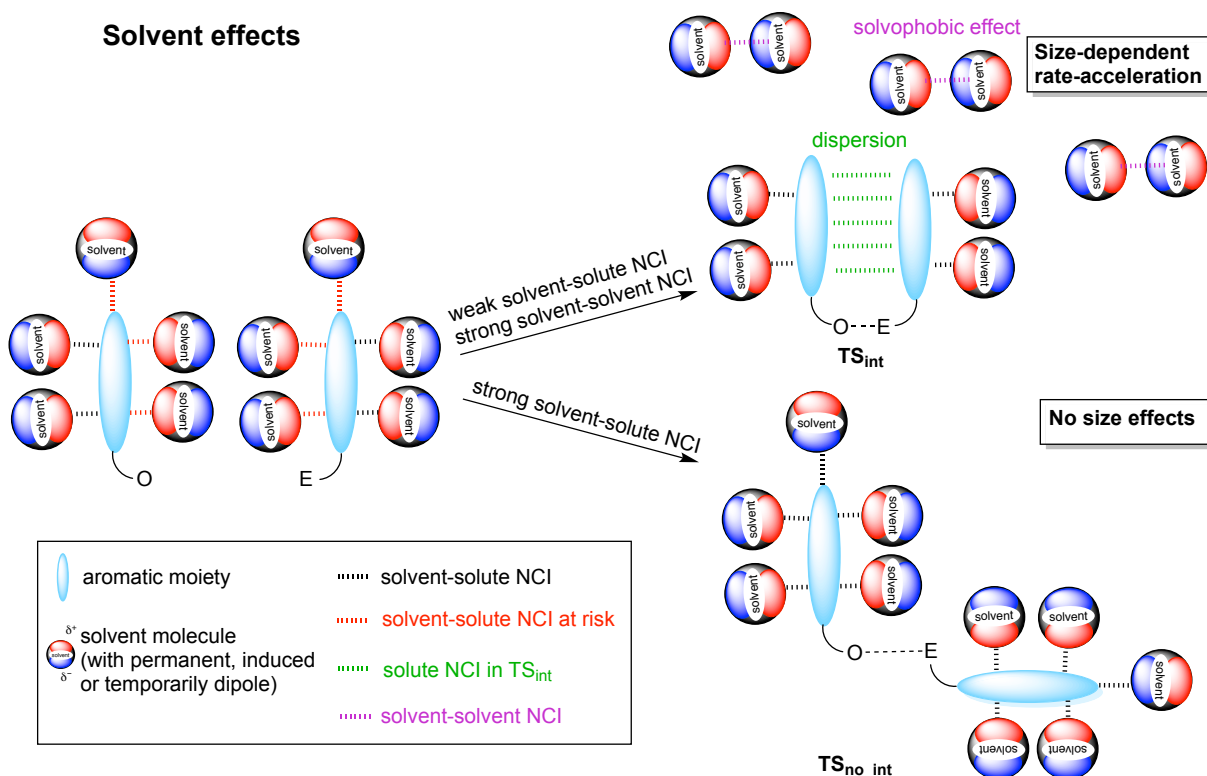
Figure 7.3. Graphical conclusion on solvent effects on relative rates. Depending on the strength and nature of solvent-solute interactions, desolvation either takes place and leads to a gain of NCI energy or solvent-solute interactions are kept and no size effects on relative rates occur.

However, the main reason why dispersion forces are diminished in solution phase is conceptual: The same forces that are responsible for solvation itself are competitors of attractive solute-solute NCIs. Nature, however, managed to exploit non-covalent interactions for achieving near to perfect selectivity for a very broad variety of reactions.[10] Significantly, many enzymes perform catalysis under exclusion of solvent molecules[10] or in poorly polarizable water.[2c, 11] The synthesis of macromolecular organocatalysts mimicking enzymes[4b] and providing solvophobic cavities for the reaction is a promising but also very challenging way to amplify dispersive interaction. More general approaches could comprise solvent-free synthetic methods[12] or the implementation of molecular containers as reaction compartments.[13]

In conclusion, we showed herein for several examples, that attractive steric effects can notably increase reaction rates, if the geometry of the transition state and solvent effects are properly considered. A targeted use of these interactions provides new opportunities for a rational design of selective organocatalysts.

7.4. References

[1]   a) J. D. van der Waals, *Over de continuïteit van den gas - en vloeistoftoestand.*, Sijthoff, **1873**; b) F. London, *Trans. Faraday Soc.* **1937**, *33*, 8-26.
[2]   a) R. R. Knowles, E. N. Jacobsen, *Proc. Natl. Acad. Sci. USA* **2010**, *107*, 20678-20685; b) E. H. Krenske, K. N. Houk, *Acc. Chem. Res.* **2013**, *46*, 979-989; c) J. P. Wagner, P. R. Schreiner, *Angew. Chem. Int. Ed.* **2015**, *54*, 12274-12296.
[3]   a) S. Grimme, *J. Comput. Chem.* **2004**, *25*, 1463-1473; b) S. Grimme, J. Antony, S. Ehrlich, H. Krieg, *J. Chem. Phys.* **2010**, *132*, 154104.
[4]   a) S. E. Wheeler, T. J. Seguin, Y. Guan, A. C. Doney, *Acc. Chem. Res.* **2016**, *49*, 1061-1069; b) D. Yepes, F. Neese, B. List, G. Bistoni, *J. Am. Chem. Soc.* **2020**, *142*, 3613-3625.
[5]   a) L. Yang, J. B. Brazier, T. A. Hubbard, D. M. Rogers, S. L. Cockroft, *Angew. Chem. Int. Ed.* **2016**, *55*, 912-916; b) J. W. Hwang, P. Li, K. D. Shimizu, *Org. Biomol. Chem.* **2017**, *15*, 1554-1564; c) S. Grimme, P. R. Schreiner, *Angew. Chem. Int. Ed.* **2011**, *50*, 12639-12642.
[6]   a) J. Helberg, M. Marin-Luna, H. Zipse, *Synthesis* **2017**, *49*, 3460-3470; b) S. Lin, E. N. Jacobsen, *Nat. Chem.* **2012**, *4*, 817-824.
[7]   H. B. Kagan, J. C. Fiaud, *Top. Stereochem.* **1988**, *18*, 249-300.
[8]   C. Goedecke, S. Grimme, *ChemViews* **2019**, 10.1002/chemv.201900014.
[9]   S. E. Wheeler, J. W. Bloom, *J. Phys. Chem. A* **2014**, *118*, 6133-6147.
[10]   S. J. Benkovic, S. Hammes-Schiffer, *Science* **2003**, *301*, 1196-1202.
[11]   S. M. Ngola, D. A. Dougherty, *J. Org. Chem.* **1996**, *61*, 4355-4360.
[12]   a) D. E. Crawford, *Beilstein J. Org. Chem.* **2017**, *13*, 65-75; b) C. Falenczyk, B. Pölloth, P. Hilgers, B. König, *Synth. Commun.* **2014**, *45*, 348-354; c) F. Gomollón-Bel, *Chem. Int.* **2019**, *41*, 12-17.
[13]   a) R. Warmuth, J.-L. Kerdelhué, S. Sánchez Carrera, K. J. Langenwalter, N. Brown, *Angew. Chem. Int. Ed.* **2002**, *41*, 96-99; b) T. C. Lee, E. Kalenius, A. I. Lazar, K. I. Assaf, N. Kuhnert, C. H. Grun, J. Janis, O. A. Scherman, W. M. Nau, *Nat. Chem.* **2013**, *5*, 376-382.

Part II: An Online Video Library for the Organic Chemistry Laboratory.

Empirical studies.

Chapter 8. Development of a Modular Online Video Library for the Introductory Organic Chemistry Laboratory.

Benjamin Pölloth, Ieva Teikmane, Stefan Schwarzer, Hendrik Zipse

J. Chem. Ed., **2020**, *97*, 338 – 343. DOI: 10.1021/acs.jchemed.9b00383

Online video library:
Benjamin Pölloth, Hendrik Zipse "VidBibOCP" available free of charge at
https://www.cup.uni-muenchen.de/oc/zipse/vidbibocp/

Author contributions: The concept for the online video library was conceived by B.P. and H.Z. The online video library was produced by B.P., I.T. and Fabian Zott. The manuscript was jointly written by B.P., S.S., and H.Z.

Development of a Modular Online Video Library for the Introductory Organic Chemistry Laboratory

Benjamin Pölloth, Ieva Teikmane, Stefan Schwarzer, and Hendrik Zipse*

Department of Chemistry, LMU Muenchen, Butenandtstrasse 5-13, Muenchen, 81377, Germany

S *Supporting Information*

ABSTRACT: A modular and target-group oriented online video library with 48 videos was developed and produced in order to reduce the complexity of an introductory organic chemistry laboratory class. The library comprises three different types of videos: "Tutorials" explaining fundamental laboratory techniques, "Do nots" pointing students in a humorous way to typical mistakes, and videos demonstrating complete syntheses in a "Step-by-Step" fashion. This report describes the principles, development, production, and presentation of this video library.

KEYWORDS: *Second-Year Undergraduate, Laboratory Instruction, Organic Chemistry, Multimedia-Based Learning, Synthesis*

INTRODUCTION

In introductory organic chemistry laboratory courses, students with little practical experience have to use unfamiliar equipment and substances to perform equally unfamiliar techniques in order to understand new chemistry topics. These challenges make the laboratory a complex learning environment,[1−3] and especially at the beginning of introductory organic chemistry laboratory courses students have a hard time performing experiments properly. Sweller postulated that the working memory can only handle a certain number of cognitive processes simultaneously.[4] Students will react to cognitive overload in laboratory work typically by focusing on issues that are of immediate relevance, but will neither reflect on the underlying scientific core ideas nor put their experimental observations into context with the accompanying lecture courses.[2,3] One way to reduce the complexity of laboratory environments is an improved preparation.[3,5−8] The documentation of laboratory courses is commonly limited to printed laboratory manuals briefly describing the experiments. Qualitative interviews with students and teaching assistants (for further information see below) during earlier laboratory courses at our institution showed that many students have problems translating the technical language of the instructions to specific experimental actions. For example, many beginning students are unable to translate the term "The solvent is evaporated" to the specific operation of a rotary evaporator, for example, knowing which control elements to use in which order. Students are thus unable to prepare themselves properly for that specific task. When the utilization of the rotary evaporator is finally demonstrated once in the laboratory by a teaching assistant, students may not be able to memorize all necessary information immediately. In the following steps this

lack of ability can keep students from performing more complex procedures properly, safely, and in an adequate time. Moreover, students often "cook" through given laboratory procedures without reflecting on the underlying chemical processes, despite the fact that theoretical aspects of the reactions performed in the laboratory are discussed in a lecture course running in parallel (at least at our institution).[9,10] Reducing cognitive load caused by experimental work thus offers the potential of making learning more meaningful,[11,12] provided that the design of the laboratory course itself emphasizes student engagement in scientific practices.[13] Hence, it seems that a printed script is neither able to present specific laboratory techniques in a ready-to-replicate manner nor to prepare students sufficiently well for laboratory work.

Recent statistics reveal that globally people aged 18−25 watch on average more than 9 h of online videos per week,[14] and that 60% of German adolescents use the video portal *YouTube* at least several times a week.[15] This dominance of online media as well as the ubiquitous availability of Internet connection and smartphones urge for the implementation of online media in laboratory course settings under the condition that this step has additional educational benefits. Bandura proposed in his social cognitive theory that practical skills as well as behavior can be triggered through the active observation of models,[16,17] either in reality or in media sources and moving images.[18] The most reliable models for experimental work are experienced chemists that work in their authentic environment. Additionally, videos can provide

338

much more information than a written text and allow students to easily mimic operations seen before.

A wide variety of different online media for the preparation of laboratory courses at universities are already available: laboratory techniques are explained by voice-over PowerPoint slides,[19] by first person view videos recorded with an action cam[20] or student-generated videos.[21,22] Moreover, scenes from popular culture movies were used to point out security instructions,[23] animated tutorials to demonstrate the use of chemical software,[24] augmented reality technology to document the operation of analytical instruments,[25] and complex concepts in analytical chemistry were explained in videos using pen and paper imitating private lessons.[26] Box et al. used a set of three different types of student-generated videos,[6] whereas Creswell et al. made teaching videos available in the laboratory through the utilization of tablets.[27] One of the biggest resources of online videos for professionals as well as students is the *Journal of Visualized Experiments* (JoVE), that comprises at the moment more than 10 500 video articles from various fields of physical and life science.[28] Furthermore, videos of students on their own laboratory processes were used for self- and peer-assessment of their laboratory work and for rewarding student's progress by digital badges.[29,30]

In view of the above we implemented an online video library in the introductory organic chemistry laboratory course at our institution. Herein we describe the principles for the development of the online video library and give insights into its structure, presentation, and production. The videos are available online free of charge.[31] The results of chemical educational research on the utilization and benefits of the video library are reported in a companion publication (10.1021/acs.jchemed.9b00647).

■ DESCRIPTION OF THE LABORATORY COURSE

The introductory organic chemistry laboratory course at our institution is held at the beginning of the second year of the bachelor program. In their first year of studies the students gained some prior experience and knowledge from a basic inorganic laboratory course and an introductory organic chemistry lecture course. The laboratory course extends over a period of 10 weeks, running 4 days a week for 5 h in the afternoon. The first 2 weeks of the laboratory course (termed "Pre-Course") focus on fundamental organic chemistry laboratory techniques and include laboratory instructions of "expository" and "inquiry" type[13] (e.g., students get instructions on how to perform a Soxhlet-extraction and are then asked to compare the caffeine-content of green and black tea). In the preparative part of the laboratory course (20 h per week over 8 weeks) students are asked to synthesize 30 compounds following established procedures, which include actual synthesis, workup, and analytical characterization. This part of the course is closely synchronized with an accompanying organic chemistry lecture course (5 h per week), in which theoretical foundations of the reactions performed in the laboratory are presented. The lecture course is complemented by small-group exercise sessions. Students are expected to document their experimental laboratory work in written protocols, which form the basis for feedback discussions with their respective teaching assistants.

■ PRINCIPLES FOR THE DEVELOPMENT OF THE ONLINE VIDEO LIBRARY

In many of the inventions mentioned above video production focused on one specific part of the laboratory course. The goal of the project described here is to cover the entire laboratory course with instructional videos and thus offer the students a resource for improved preparation and a virtual teaching assistant for frequently asked questions. This goal was approached through a modular design principle: Experiments of the laboratory course were divided into basic laboratory techniques, composite operations, and finally full synthetic sequences. Videos from these three classes can then be combined to highlight various aspects of a given laboratory experiment. For example, one video offers a general overview of the synthesis of a compound, which is then complemented by videos providing further details on single steps of the experiment such as glassware assembly, product extraction, evaporation of solvent, and purification through recrystallization. This modular design allows students to get a complete overview over all relevant techniques and sequences quickly and in a targeted manner, which is, in the end, also the functionality expected from a virtual teaching assistant.

Chemistry students should not be seen as a homogeneous cohort, but as a group of diverse individuals.[32,33] Their various personalities, learning behaviors and strategies, prior knowledge, and abilities to learn also demand versatile learning tools. Student characteristic-based differences in the appreciation and utilization of multimedia approaches were found for example, for gender or family background.[34−36] The combination of video tutorials with traditional teaching aids such as printed laboratory manuals and teaching assistants may thus lead to an improved learning experience for a diverse student body. If the videos themselves differ in content and style of presentation, it is even more likely that they serve the specific needs of different students. Therefore, we decided to produce three basically different types of videos as described below. Popular analysis of online video use indicates that viewer attention starts to decrease after 2 to 3 min.[37] Respecting daily life habits of students concerning video consumption is critical in producing target-group oriented learning videos. Consequently, the online videos in this project aim to be as short as possible, recorded in high quality, and easily accessible from mobile devices. In videos for first-timers in experimental organic chemistry the use of nonauthentic equipment can become critical. For example, in our experience even minor differences in the handling of different rotary evaporators can pose a problem for students working in an organic chemistry laboratory for the first time. To avoid these problems and to maximize the benefit of the online video library, all videos were recorded in the original teaching laboratories, where actual laboratory course equipment was used to provide students with an authentic impression of laboratory work.[38]

In view of the general considerations outlined above the following principles guided the production of the online video library: modularity, versatility, target-group orientation, and authenticity.

■ DESCRIPTION OF THE ONLINE VIDEO LIBRARY

The library comprises 48 videos of various types covering the main tasks of the laboratory course, and is divided up in the three categories "Tutorials", "Do nots", and "Step-by-Step-
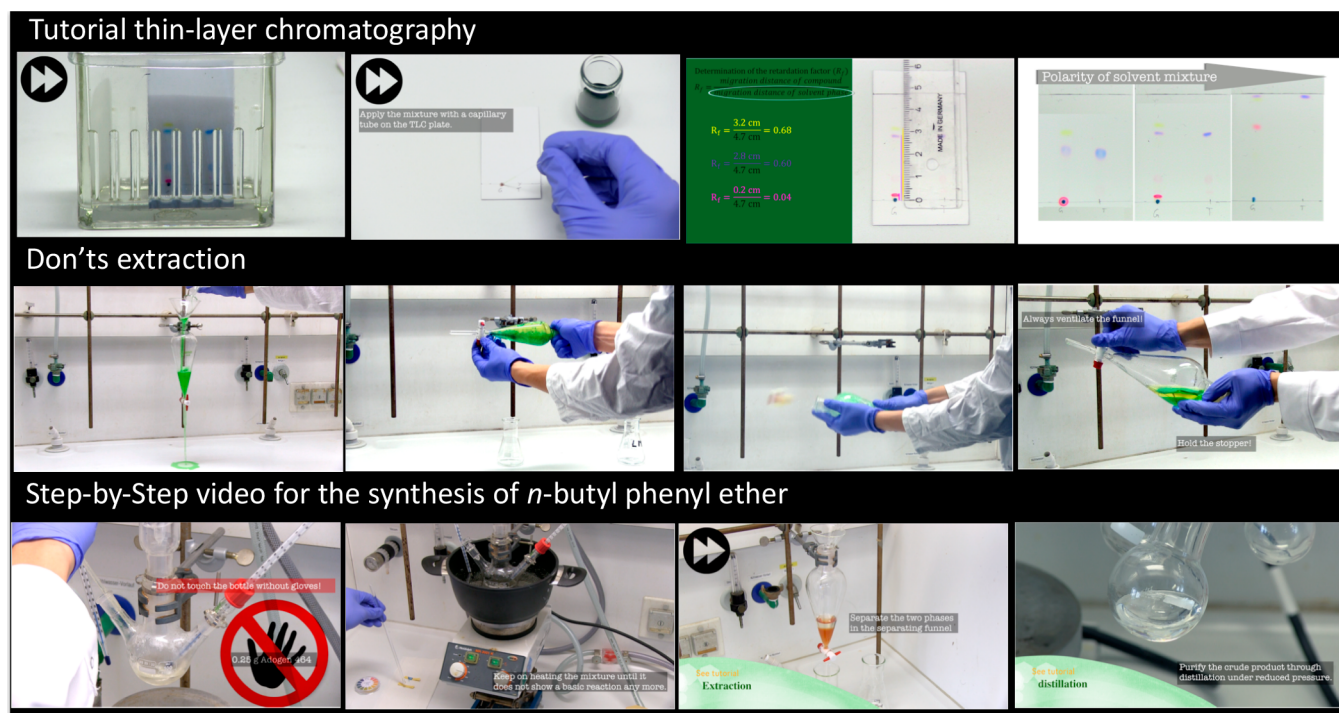
Figure 1. Screenshots of representative videos of the three video types. "Tutorial" thin-layer chromatography using mixtures of dyes (1st row, left to right): General principle of TLC (fast forward development of a TLC); practical preparation of a TLC; determination of the retention factor (R_f); impact of solvent mixtures on R_f. "Do nots" extraction (2nd row, left to right): no Erlenmeyer flask under the extraction funnel; funnel filled too high; extraction without ventilating the funnel; correct procedure. "Step-by-Step" video for the preparation of *n*-butyl phenyl ether (3rd row, left to right): addition of reactants with special hazards; reaction control via pH value measurements; extraction of the reaction mixture including cross-link to the relevant "tutorial"; purification of the product by distillation including cross-link to the "tutorial". The content is here translated to English, the original language is German.

Videos". For each video category screenshots of one representative example are presented in Figure 1.

"Tutorials" for 17 basic organic chemistry laboratory techniques (e.g., standard reaction assemblies, extraction, recrystallization, distillation) show and explain all relevant practical details of a certain experimental procedure. Furthermore, they provide a brief explanation of the underlying theory in order to allow the students to focus on the most important aspects when applying the laboratory technique. Most videos are also modular in themselves starting with an explanation of the fundamental chemical idea of the technique and then focusing on fundamental practical operations. "Add-ons" such as a drying tube on top of a reflux condenser as well as answers of typical questions are presented in the progress of the video. Structural elements of the videos are slides introducing the question of the following section. Often dyes or colored compounds were used to make processes visible, the extraction of a compound from the aqueous to the organic phase being a typical example. All relevant steps and theoretical backgrounds are explained verbally, key information is also provided in text-in-image boxes. During editing, text boxes, graphical elements, and video effects such as transitions, fast forwarding, and sounds were used to make the videos as short and entertaining as possible without affecting completeness or accuracy. Changes in speed are indicated by a special symbol. The resulting video length is about 2 to 5 min, mirroring the typical length of online videos consumed by students in their everyday lives.

Eight "Do nots" illustrate in a humorous way typical mistakes in experimental work as well as their possible undesirable outcomes. Subsequently, the correct working manner is explained. "Do nots" are structured by music, sound, and video effects, and are complementary to the straightforward explanations in "Tutorials" by addressing important aspects of practical laboratory work in an entertaining way. "Do nots" are shorter than "Tutorials" with a duration of approximately 1 to 2 min.

In "Step-by-Step" videos, the experimental procedures for selected syntheses of the laboratory course are demonstrated starting from the assembly of the reaction apparatus, the addition of reactants, followed by actually running and stopping the reaction, all the way to the isolation and purification of the product. Condensing a several hours long experiment into 1 to 3 min of video is achieved by focusing on key steps, fast forwarding, and links to relevant "Tutorials" providing further information on specific operations. Where necessary, specific hazards and tips on certain steps are emphasized. "Step-by-Step" videos are thought to act as worked examples,[39,40] giving the students a realistic impression on experimental work. These videos were produced for 23 of the 42 experiments, mostly those from the beginning of the laboratory course. However, students given too detailed instructions may feel a loss of autonomy and may thus give up their role as active learners.[41] To avoid this effect and to lead students to independent experimental work, for the second half of the laboratory course "Step-by-Step" videos were produced only for selected, more demanding experiments (e.g., Grignard reactions).

PRODUCTION OF THE ONLINE VIDEO LIBRARY

The authenticity of an online video library, which will depend on "Step-by-Step" videos, the appropriateness of content, and the consistency of equipment used in the videos and laboratory course curriculum can only be assured if the library is tailored to a specific laboratory course at a specific institution. Instructions and practical guidelines for the realization of similar projects are provided in the following section:

1. Identification of relevant laboratory techniques, of common difficulties and problems, and of experiments with special requirements: teaching assistants active in a laboratory course of similar design were asked to take notes on common student questions, difficulties, and mistakes. This information was collected daily, and the assistants were interviewed on further details. Additionally, at the end of the laboratory course a group of five students was interviewed on common problems or challenges they or others encountered during the laboratory course. The gathered information was clustered by keywords, and relevant topics for "Tutorials" and "Do nots" were defined. Particular experiment-specific challenges were discussed in detail. On the basis of those reported difficulties and specific practical demands the experiments for "Step-by-Step" videos were selected.

2. Scripting: In our experience, detailed scripting of the videos is crucial for their successful recording. Scripts should ideally include an overall sequence of events for the final video, approximate timing, and appropriate camera positions for time-efficient recording sessions.

3. Recording: Videos were recorded by two experienced chemists in an authentic teaching laboratory using the same equipment, environment, and chemicals as in the laboratory course. Videos were recorded in the 1080p HD standard using a camcorder and professional tripods.

4. Editing: Videos were edited using FinalCutPro.[42] Standardized elements such as intro and outro slides, text boxes, cross-linking, and graphical elements were used to structure the videos and implement a consistent design. Fast forwarding and slow motion became a key element in editing to keep the videos short and focused.

5. Reviewing: During the whole process videos were regularly reviewed by co-workers as well as undergraduate students in order to guarantee the quality and relevance of the videos.

PRESENTATION OF THE ONLINE VIDEO LIBRARY

The modular design principle requires that experiments and videos are clearly assigned to each other. In a first test run of the online video library only a single list with links to each video was presented to students. Students watched videos rarely and seemed to be either not willing or not able to find the relevant videos for an experiment within the list. The presentation of videos was therefore improved through the creation of subpages for each experiment on the electronic learning platform of our institution. Each subpage presents the appropriate "Step-by-Step" video and all relevant "Tutorials" and "Do nots" in the chronological order of the course for this experiment (see Figure 2). This presentation led to a dramatical increase of viewing rates (for numerical proof see the empirical study on this video library). To simplify access to
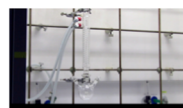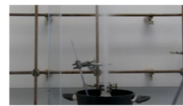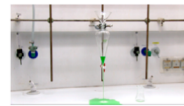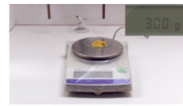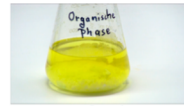
Figure 2. Presentation of the relevant videos for a sample compound. The "Step-by-Step" video is presented on top, followed by "Tutorials" and "Do nots" in chronological order of the experimental procedure. "Do nots" are highlighted in red. The description is here translated to English, the original language is German.

the videos, QR codes linking experiments to the relevant subpages were eventually added to the printed laboratory manual.[22]

Recent surveys indicate that 79% of German adolescents use mainly their smartphone for accessing the Internet.[15] Thus, it is also crucial to optimize webpages and videos for mobile access. The online video library uses responsive web design for both the webpages and the videos to ensure accessibility from different devices.

DISCUSSION

During our laboratory course taken by 114 students we observed 6231 video views; the top viewed videos are presented in Figure 3. The students using the video library rated the whole project with a mean grade of 1.56 on the typical German school grading scale from 1 (very good) to 6 (insufficient). Rating the quality of the video library on a scale from 0 (do not agree at all) to 3 (fully agree), students stated that the video library content was easy to understand (2.76), that all relevant activities were covered (2.35), that access to the videos was user-friendly (2.64), and that the videos were not too long (2.40). The top six viewed videos were four tutorials and the two "Step-by-Step" videos for the first experiments in both parts of the laboratory course, precourse, and compound syntheses (see Figure 3, for all view rates see Supporting Information). These numbers confirm that the design and realization of the online video library is suitable for its purpose and well accepted by students. Student evaluations at the end of the laboratory class indicated significant interest
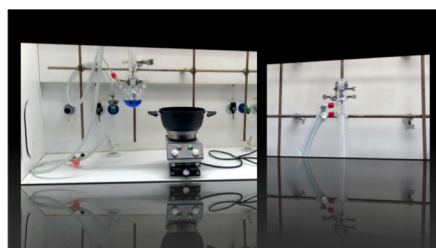
Tutorial
Reaction assembly with reflux cooler
359 views
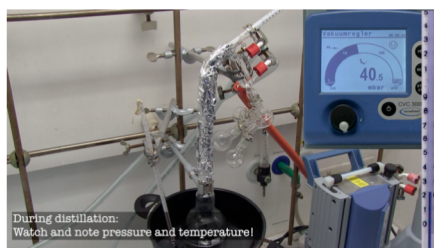
Tutorial
Distillation
358 views
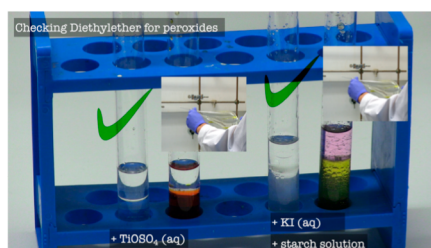
Step-by-Step (1st experiment pre-course)
Purification and drying of diethyl ether
216 views

Tutorial
Column chromatography
203 views

Tutorial
Recrystallization
185 views
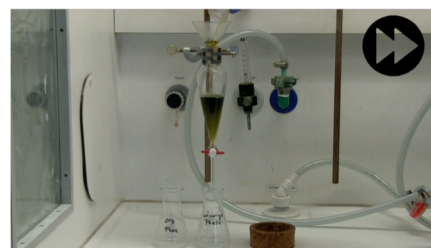
Step-by-Step (1st compound preparation)
Cyclohexyl chloride
179 views

Figure 3. Top six of the most viewed videos in the period of the three investigated laboratory courses (5 months, total of 114 basic organic chemistry laboratory students). View rates were counted by the video server. During the observed time period access to the videos was only granted to laboratory students.

in additional videos covering analytical methods, and therefore "Tutorials" on eight standard analytic methods such as NMR, UV, and IR spectroscopy, mass spectrometry, and melting point determination were additionally produced and implemented.

Further details on the utilization of the videos, their impact on undergraduates' prelaboratory knowledge and attitude with a special focus on student diversity are reported in an empirical study (10.1021/acs.jchemed.9b00647) based on this online video library.

CONCLUSION

Motivated by the previously observed insufficient preparation for laboratory work and the need for additional assistance of the students in the basic organic chemistry laboratory course at our institution an online video library was developed. Three different types of videos were produced in order to cover different aspects of laboratory experiments: the library comprises 25 laboratory technique "Tutorials" and 8 "Do nots" on the execution and the underlying theory of fundamental laboratory techniques, as well as "Step-by-Step" videos for 23 compound preparations of the laboratory course. All videos are presented in a ready-to-use manner and in chronological order for every laboratory course experiment. Special attention in developing the videos was paid to students' daily life habits for online media and to the use of the authentic laboratory course environment. An empirical study on the utilization and benefits of the online library is reported in a companion paper (10.1021/acs.jchemed.9b00647). The video library is available at http://www.cup.uni-muenchen.de/oc/zipse/vidbibocp/ (accessed November 25, 2019).

ASSOCIATED CONTENT

Ⓢ Supporting Information

The Supporting Information is available at https://pubs.acs.org/doi/10.1021/acs.jchemed.9b00383.

List of all videos with relevant viewing numbers (PDF).

AUTHOR INFORMATION

Corresponding Author

*E-mail: zipse@cup.uni-muenchen.de.

ORCID

Benjamin Pölloth: 0000-0001-7777-9903
Stefan Schwarzer: 0000-0002-4134-5684
Hendrik Zipse: 0000-0002-0534-3585

Notes

The authors declare no competing financial interest.

REFERENCES

(1) Johnstone, A. H.; Sleet, R. J.; Vianna, J. F. An Information-Processing Model of Learning - Its Application to an Undergraduate Laboratory Course in Chemistry. *Stud. High. Educ.* **1994**, *19* (1), 77−87.

(2) Johnstone, A. H.; Wham, A. J. B. The demands of practical work. *Educ. Chem.* **1982**, *19* (3), 71−73.

(3) Agustian, H. Y.; Seery, M. K. Reasserting the role of prelaboratory activities in chemistry education: a proposed framework for their design. *Chem. Educ. Res. Pract.* **2017**, *18* (4), 518−532.

(4) Sweller, J. Cognitive Load During Problem Solving: Effects on Learning. *Cogn. Sci.* **1988**, *12* (2), 257−285.

(5) Rollnick, M.; Zwane, S.; Staskun, M.; Lotz, S.; Green, G. Improving pre-laboratory preparation of first year university chemistry students. *Int. J. Sci. Educ.* **2001**, *23* (10), 1053−1071.

(6) Box, M. C.; Dunnagan, C. L.; Hirsh, L. A. S.; Cherry, C. R.; Christianson, K. A.; Gibson, R. J.; Wolfe, M. I.; Gallardo-Williams, M. T. Qualitative and Quantitative Evaluation of Three Types of Student-Generated Videos as Instructional Support in Organic Chemistry Laboratories. *J. Chem. Educ.* **2017**, *94* (2), 164−170.

(7) Nadelson, L. S.; Scaggs, J.; Sheffield, C.; McDougal, O. M. Integration of Video-Based Demonstrations to Prepare Students for the Organic Chemistry Laboratory. *J. Sci. Educ. Technol.* **2015**, *24* (4), 476−483.

(8) Stieff, M.; Werner, S. M.; Fink, B.; Meador, D. Online Prelaboratory Videos Improve Student Performance in the General Chemistry Laboratory. *J. Chem. Educ.* **2018**, *95* (8), 1260−1266.

(9) Hofstein, A.; Lunetta, V. N. The laboratory in science education: Foundations for the twenty-first century. *Sci. Educ.* **2004**, *88* (1), 28−54.

(10) Galloway, K. R.; Bretz, S. L. Video episodes and action cameras in the undergraduate chemistry laboratory: eliciting student perceptions of meaningful learning. *Chem. Educ. Res. Pract.* **2016**, *17* (1), 139−155.

(11) Bretz, S. L. Novak's Theory of Education: Human Constructivism and Meaningful Learning. *J. Chem. Educ.* **2001**, *78* (8), 1107.

(12) Winberg, T. M.; Berg, C. A. R. Students' cognitive focus during a chemistry laboratory exercise: Effects of a computer-simulated prelab. *J. Res. Sci. Teach.* **2007**, *44* (8), 1108−1133.

(13) Domin, D. S. A Review of Laboratory Instruction Styles. *J. Chem. Educ.* **1999**, *76* (4), 543−547.

(14) The state of online video 2018. https://www.limelight.com/resources/white-paper/state-of-online-video-2018/ (accessed November 25, 2019).

(15) Feierabend, S.; Rathgeb, T.; Reutter, T. *JIM 2018 Jugend, Information, Medien*; Medienpädagogischer Forschungsverbund Südwest: Stuttgart, 2018.

(16) Bandura, A. Self-efficacy: Toward a Unifying Theory of Behavioral Change. *Psychol. Rev.* **1977**, *84*, 191−215.

(17) Bandura, A. Social Cognitive Theory: An Agentic Perspective. *Annu. Rev. Psychol.* **2001**, *52*, 1−26.

(18) Bandura, A. Social Cognitive Theory of Mass Communication. *Media Psychol.* **2001**, *3*, 265−299.

(19) Chaytor, J. L.; Al Mughalaq, M.; Butler, H. Development and Use of Online Prelaboratory Activities in Organic Chemistry To Improve Students' Laboratory Experience. *J. Chem. Educ.* **2017**, *94* (7), 859−866.

(20) Fung, F. M. Using First-Person Perspective Filming Techniques for a Chemistry Laboratory Demonstration To Facilitate a Flipped Pre-Lab. *J. Chem. Educ.* **2015**, *92* (9), 1518−1521.

(21) Jordan, J. T.; Box, M. C.; Eguren, K. E.; Parker, T. A.; Saraldi-Gallardo, V. M.; Wolfe, M. I.; Gallardo-Williams, M. T. Effectiveness of Student-Generated Video as a Teaching Tool for an Instrumental Technique in the Organic Chemistry Laboratory. *J. Chem. Educ.* **2016**, *93* (1), 141−145.

(22) Benedict, L.; Pence, H. E. Teaching Chemistry Using Student-Created Videos and Photo Blogs Accessed with Smartphones and Two-Dimensional Barcodes. *J. Chem. Educ.* **2012**, *89* (4), 492−496.

(23) Matson, M. L.; Fitzgerald, J. P.; Lin, S. Creating Customized, Relevant, and Engaging Laboratory Safety Videos. *J. Chem. Educ.* **2007**, *84* (10), 1727−1728.

(24) D'Ambruoso, G. D.; Cremeens, M. E.; Hendricks, B. R. Web-Based Animated Tutorials Using Screen Capturing Software for Molecular Modeling and Spectroscopic Acquisition and Processing. *J. Chem. Educ.* **2018**, *95* (4), 666−671.

(25) Naese, J. A.; McAteer, D.; Hughes, K. D.; Kelbon, C.; Mugweru, A.; Grinias, J. P. Use of Augmented Reality in the Instruction of Analytical Instrumentation Design. *J. Chem. Educ.* **2019**, *96* (3), 593−596.

(26) He, Y.; Swenson, S.; Lents, N. Online Video Tutorials Increase Learning of Difficult Concepts in an Undergraduate Analytical Chemistry Course. *J. Chem. Educ.* **2012**, *89* (9), 1128−1132.

(27) Cresswell, S. L.; Loughlin, W. A.; Coster, M. J.; Green, D. M. Development and Production of Interactive Videos for Teaching Chemical Techniques during Laboratory Sessions. *J. Chem. Educ.* **2019**, *96* (5), 1033−1036.

(28) Journal of Vizualized Experiments. https://www.jove.com/about/ (accessed November 25, 2019).

(29) Hennah, N.; Seery, M. K. Using Digital Badges for Developing High School Chemistry Laboratory Skills. *J. Chem. Educ.* **2017**, *94* (7), 844−848.

(30) Hensiek, S.; DeKorver, B. K.; Harwood, C. J.; Fish, J.; O'Shea, K.; Towns, M. Improving and Assessing Student Hands-On Laboratory Skills through Digital Badging. *J. Chem. Educ.* **2016**, *93* (11), 1847−1854.

(31) Zipse, H.; Pölloth, B. VidBibOCP-Videothek. https://www.cup.uni-muenchen.de/oc/zipse/vidbibocp/ (accessed November 25, 2019).

(32) Goethe, E. V.; Colina, C. M. Taking Advantage of Diversity within the Classroom. *J. Chem. Educ.* **2018**, *95* (2), 189−192.

(33) Laursen, S. L.; Weston, T. J. Trends in Ph.D. Productivity and Diversity in Top-50 U.S. Chemistry Departments: An Institutional Analysis. *J. Chem. Educ.* **2014**, *91* (11), 1762−1776.

(34) Fischer, C.; Zhou, N.; Rodriguez, F.; Warschauer, M.; King, S. Improving College Student Success in Organic Chemistry: Impact of an Online Preparatory Course. *J. Chem. Educ.* **2019**, *96* (5), 857−864.

(35) Niemeyer, E. D.; Zewail-Foote, M. Investigating the Influence of Gender on Student Perceptions of the Clicker in a Small Undergraduate General Chemistry Course. *J. Chem. Educ.* **2018**, *95* (2), 218−223.

(36) Dousay, T. A.; Trujillo, N. P. An examination of gender and situational interest in multimedia learning environments. *Br. J. Educ. Technol.* **2019**, *50* (2), 876−887.

(37) Fishman, E. How Long Should Your Next Video Be? https://wistia.com/learn/marketing/optimal-video-length (accessed November 25, 2019).

(38) Stamer, I.; Pönicke, H.; Tirre, F.; Laherto, A.; Höffler, T.; Schwarzer, S.; Parchmann, I. Development & validation of scientific video vignettes to promote perception of authentic science in student laboratories. *Res. Sci. Technol. Educ.* **2019**, 1−17.

(39) Paas, F. G. W. C.; Merienboer, J. J. G. V. Variability of Worked Examples and Transfer of Geometrical Problem-Solving Skills: A Cognitive-Load Approach. *J. Educ. Psychol.* **1994**, *86*, 122−133.

(40) Crippen, K. J.; Earl, B. L. Considering the Efficacy of Web-based Worked Examples in Introductory Chemistry. *J. Comput. Math. Sci. Teach.* **2004**, *23* (2), 151−167.

(41) Galloway, K. R.; Malakpa, Z.; Bretz, S. L. Investigating Affective Experiences in the Undergraduate Chemistry Laboratory: Students' Perceptions of Control and Responsibility. *J. Chem. Educ.* **2016**, *93* (2), 227−238.

(42) *Final Cut Pro*, version 10.4.2; Apple Inc.: 2018.

Chapter 9. Student Individuality Impacts Use and Benefits of an Online Video Library for the Organic Chemistry Laboratory.

Benjamin Pölloth, Stefan Schwarzer, Hendrik Zipse

Online video library:

Benjamin Pölloth, Hendrik Zipse "VidBibOCP" available free of charge at

https://www.cup.uni-muenchen.de/oc/zipse/vidbibocp/

Author contributions: The concept for the online video library was conceived by B.P. and H.Z. The empirical study was conceived by B.P., S.S. and H.Z. and performed and analyzed by B.P. The manuscript and supporting information was jointly written by B.P., S.S., and H.Z.

Additional information: The herein printed Supporting Information (SI) are an altered version of the published SI. The original SI files can be accessed online under the depicted DOIs or on the electronic attachment of this thesis.

Student Individuality Impacts Use and Benefits of an Online Video Library for the Organic Chemistry Laboratory

Benjamin Pölloth,[ID] Stefan Schwarzer,[ID] and Hendrik Zipse*[ID]

Department of Chemistry, LMU Muenchen, Butenandtstrasse 5-13, Muenchen, 81377, Germany

S *Supporting Information*

ABSTRACT: An online video library comprising three different types of videos was used intensively by bachelor-level students before and throughout an introductory organic chemistry laboratory course, when presented and assigned to the experiments appropriately. An empirical study ($N = 103$) revealed that the utilization of videos and preferences for video types depend crucially on individual student characteristics, such as gender, study course, intrinsic motivation, and the self-perception of conscientiousness. Student assessment of the video library, a positive impact on students' self-concept of ability, and an increase of knowledge in know-how tests on laboratory techniques of up to 100% indicate the benefits of the online video library on students' cognitive, affective, and psychomotor learning in a laboratory course.

KEYWORDS: Chemical Education Research, Second-Year Undergraduate, Laboratory Instruction, Organic Chemistry, Multimedia-Based Learning

FEATURE: Chemical Education Research
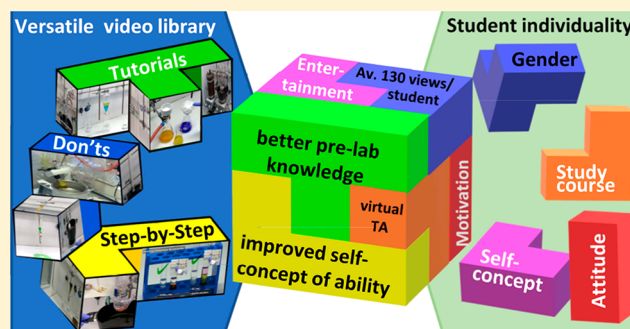
INTRODUCTION

Digital media play an ever increasing role in daily life especially for young people.[1] Recent statistics for Germany indicate that 99% of the 18- to 19-year-olds own a smartphone, 60% of the 12- to 19-year-olds watch *YouTube* videos at least several times a week,[2] and for 47% of them *YouTube* videos play an important role for topics discussed in high school.[3] German citizens aged 18 and older spend an average of 5.0 h per week watching online videos, while globally 6.8 h and in the United States 8.4 h of video content per week were consumed in 2018.[4] These developments cannot be ignored when developing contemporary teaching methods for chemistry at the university level. One of the many ways that the teaching of chemistry can be refined through digitalization is the employment of online media in chemistry studies. For chemistry lectures the efficiency of the implementation of online videos, for example, in flipped-classroom strategies[5−7] or as supporting information,[8−10] was investigated in several studies. For chemistry laboratory courses already a wide variety of online media are being employed,[11−20] and the video data bank of the *Journal of Visualized Experiments* (JoVE) offers more than 10,500 videos of experimental work for professionals and students.[21] At our institution we have recently developed a modular and versatile online video library with 48 videos (2−5 min) and tested their integration into the introductory organic chemistry laboratory course. The library comprises videos of three different types: "Tutorials" explaining key aspects and theoretical foundations of selected basic organic chemistry laboratory techniques, "Do nots" illustrating

in a humorous way typical mistakes of beginners in experimental work, and "Step-by-Step" videos demonstrating complete experimental procedures for the syntheses of target compounds. For every experiment a web page on the central electronic learning platform of our institution provides links to all relevant videos in the chronological order of the experiments.[22] More details as well as insights into principles that were used for the development and production of the videos are outlined in a preceding publication (10.1021/acs.jchemed.9b00383).

LITERATURE BACKGROUND

Videos in Chemistry Laboratory Courses

The benefits of instructional videos for chemistry laboratory courses have been investigated by several studies. Additional videos in organic chemistry laboratories increased the number of correct answers in pre-experimental questionnaires significantly.[11,12] In an extensive study by Stieff et al.[13] two activities in the general chemistry laboratory were explained by teaching assistants (TAs) while two comparable activities were introduced by online videos. The preparation with online videos provided a better understanding of the reactions and reduced the time for completing experiments by 10%, while the number of asked questions during the laboratory course

was not affected. Similarly, when students were instructed for a laboratory course exclusively by student-generated videos, their knowledge about laboratory techniques was found to be higher compared to students instructed by teaching assistants and the number of asked questions was reduced by 37%.[14] Despite those different findings with respect to student questions, Winberg and Berg[23] showed for the implementation of a computer-simulated prelaboratory in a general chemistry laboratory course that the focus of student questions shifts from a practical toward a reflective-theoretical focus. This shift is crucial as Galloway et al.[24] observed that undergraduate students were not able to explain the purpose of the experimental steps in videos of themselves working in the laboratory. As they were focused on psychomotor learning they dismissed major parts of the cognitive benefits of the laboratory course.

Rationales for Videos: Cognitive Load Theory and Meaningful Learning

These findings can be rationalized by the cognitive load theory. Sweller postulates that only a small number of cognitive processes can be handled at the same time due to limits of working memory.[25] Especially in complex environments such as the first organic chemistry laboratory course for under-graduates,[26−28] students mostly focus on practical questions regarding experimentation. This cognitive overload keeps students from reflecting on theoretical and fundamental questions related to the experiments and laboratory techniques. Thus, one way to improve meaningful learning in the laboratory course is to reinforce its preparation.[28,29] New knowledge can then be linked to the prior knowledge that was generated through appropriate preparation.[30−32] Besides prior knowledge, also affective components are critical in achieving meaningful learning of psychomotor abilities.[33−38] Novak emphasizes in his theory of education that meaningful learning can only occur if the cognitive (thinking), affective (feeling), and psychomotor (doing) domains are addressed at the same time.[31,37] Therefore, it is not only the method of teaching itself that has a huge impact on the learning outcome,[39] but it is also crucial how the method activates the different domains of students. Galloway and Bretz[34] found in a national study on learning in undergraduate chemistry courses that expectations for cognitive and affective learning in the laboratory course differ a lot among the student cohort, and that these expectations can also act as self-fulfilling prophecies. Several other studies have also pointed out the importance of addressing the affective domain in prelaboratory activities,[28,34,40,41] where it was found that students felt better prepared through online videos[15,42] or that their positive attitude toward experimentation was increased through simulations.[40] However, there is a wide range of different affections that influence learning. Rather than summarizing affective factors into a single construct such as "attitude", it seems clearly preferable to investigate the role of specific factors[43] such as interests and intrinsic motivation,[44,45] students' self-concept,[43,46] or personality traits of students.[47]

Utilization of Online Videos during Laboratory Courses

Obviously, online media can impact learning in a laboratory course only if they are being used. Preparation for laboratory courses is an unpopular task for many students, and some of them invest little to no time toward this end.[15,45] One limitation of many of the projects quoted above is that videos were only produced for a specific section of a laboratory course,[11−14,17] while other reports mention the need of obligatory quizzes in order to make students use online media for preparation.[15,16] It is therefore essential to investigate whether students are willing to spend extra time and effort in watching preparatory videos. This question is especially important for a video library that covers most of a several months long laboratory course and is offered as an additional, voluntary preparation aid. A major advantage of online videos is that they can be (re)watched anytime, and they are thus not only a tool for laboratory course preparation, but can also serve as a virtual assistant during the course. While most studies focused on using videos for laboratory preparation, Creswell et al.[17] showed recently that interactive videos can also be employed successfully during the laboratory session if tablets are provided to watch them while experimenting. In the study described here videos were optimized for mobile access through smartphones, and Wi-Fi connectivity available in the teaching laboratories thus enabled the students to watch the videos at any time. In the following we will therefore analyze whether students prefer to watch the videos prior or during the laboratory course and how this utilization pattern changes during the progress of the course.

Student Diversity and Online Media

During the last decades the diversity of chemistry students has grown slowly but steadily.[48−51] Higher diversity as well as different capabilities of students necessitate a larger variation in teaching methods. Interestingly, Fischer et al. showed recently that minorities or low-income students benefit from online preparatory courses for an organic chemistry lecture commensurately to their non-at-risk counterparts, and that female students used the online course more than male students.[52] Similarly, electronic "clickers" in undergraduate chemistry courses were more appreciated by female students than by their male counterparts.[53] Gender-related differences have also been reported in the preferences for the design of multimedia tools.[54] Addressing all students with their individual personalities, learning strategies, prior knowledge, and other personal characteristics demands therefore an individualization and differentiation of learning.[55] The implementation of online material and videos as additional teaching methods in the laboratory course is one step toward this goal in teaching chemistry. Moreover, students are enabled to freely choose the material depending on their personal preferences and needs where various and versatile types of online teaching material or videos are offered. Box et al.[11] used a set of three different types of student-generated videos and found that videos explaining the use of instrumentation enhanced the knowledge of students most compared to a control group, while videos on experimental techniques were ranked most helpful by students. Schmidt-McCormack et al.[16] found that videos showing experimental procedures were more vital to students than theoretical prelaboratory videos. In the following we therefore analyze how the individuality of students influences the utilization and preferences for online teaching videos in a chemistry laboratory.

■ RESEARCH QUESTIONS

This study aims to empirically address the following questions:

1. When and how often do students use an online video library in the context of an introductory organic chemistry laboratory course?

Table 1. Scales for Testing Student Characteristics prior to the Laboratory Course

Student Characteristics	Statements for Response[a]	Cronbach's α Values,[b] N = 103	
		Prelab	Postlab[c]
Intrinsic Laboratory Course Motivation	Lab courses are a reasonable part of studies in chemistry.	0.786	0.846
	If I did not have to, I would rather not participate in the organic chemistry lab course.[d]		
	I am looking forward to the OC lab.		
	I expect that my interest in experimental work will be strengthened by this lab course in organic chemistry.		
	I think that I will learn a lot by attending the basic lab course in organic chemistry.		
Self-Concept of Ability in Experimental Laboratory Work	I am more skilled in experimental work than most of my fellow students.	0.770	0.681
	While experimenting, I often feel overstrained.[d]		
	I think that the experiments in the basic lab course will not pose a major problem for me.		
	I am very skilled in experimental work.		
Self-Perception of Conscientiousness	I think that I am more conscientiousness in studying than the average of my fellow students.	0.807	0.684
	I am very diligent in my studies.		
	I complete tasks for university meticulously.		
	I always fulfill my duties in a planned manner.		

[a]Statements translated into English by the authors. See the Supporting Information Chapter 1.1 for the original German-language scales. [b]All items were rated using the following scale: "Fully agree"; "Partially agree"; "Rather not agree"; "Do not agree". [c]Items for the postlaboratory survey were carefully adjusted to past tense. (see the Supporting Information). [d]These items were reverse coded.

2. How does student diversity influence the utilization and preferences within a modular and versatile online video library?

3. How does an online video library influence students' prelaboratory knowledge and their affective laboratory course experience?

■ METHODS AND FRAMEWORKS

Sample description

The video library was evaluated in two introductory organic chemistry laboratory courses for bachelor students with 76 and 12 students, respectively, in the winter semester 2017/2018 at LMU Munich (for further descriptive statistics see Supporting Information (SI) Chapter 2.1). Students gained some prior knowledge from an introductory organic chemistry lecture course and fundamental experimental experiences from an inorganic laboratory course. The laboratory course was running for 10 consecutive weeks, 4 days a week. During the first 2 weeks students were trained in fundamental laboratory techniques performing simple reactions (the "precourse" period). In the remaining part of the course the students synthesized 30 target compounds following known procedures. One teaching assistant was usually in charge of supervising 12 students. The video library was also tested in an introductory organic chemistry laboratory course for students aiming for a teacher's degree with 26 students. The teacher's degree laboratory course is similar to the one for bachelor students, but slightly shortened and modified. If those differences should prove to be critical, the sample would be restricted to bachelor students. Prior to this study the online video library was tested in two laboratory classes (for further information on the pretest see SI Chapter 1.2). One main finding in these preliminary tests was that students barely accessed the videos when no information was provided on how each of the laboratory experiments connect to the relevant videos. This information was subsequently provided through an improved presentation linking videos and experiments in the correct chronological order of appearance in the laboratory class (for

details see preceding publication, 10.1021/acs.jchemed.9b00383).

Survey

In the laboratory courses described above, paper-based surveys were conducted on the day before the laboratory course started and then again toward the end of the laboratory course. Both questionnaires consisted of scales evaluating the intrinsic motivation for the introductory organic chemistry laboratory course, the self-concept of ability in experimental chemistry, and students' self-perception of conscientiousness. Additionally, the prelaboratory questionnaire included a scale on the use of video tutorials in daily life and expectations toward an online video library. The postlaboratory questionnaire probed the utilization of the video library, allowed the students to rate the library, and to assess the impact of the videos on their laboratory course preparedness, motivation, and affective experiences. Items are loosely based on literature scales[56−58] and were adapted to the introductory organic chemistry laboratory course. The actual scales were pretested in an earlier laboratory course with 22 students. Reliabilities were validated by the calculation of Cronbach's α values[59] as presented in Table 1 (complete scales are listed in original German language and translated to English in the SI Chapter 1.1). Questionnaires were anonymous and standardized, and analyses were performed with SPSS.[60] Of 114 students, 103 students (90%) answered at least one survey; 50 were female and 51 were male; 80 aimed for a bachelor degree, 23 for a teaching degree; the mean age was 21.0 years. Incomplete questionnaires were excluded case-wise for each analysis; therefore, the number of participants varies. All participants were informed that by completing the survey they agree on the publication of the results.

Know-How Tests

In addition, know-how tests were performed on 3 days during the first 2 weeks of the laboratory course. Students had to answer those tests prior to any explanation through the laboratory assistant in order to control their prelaboratory preparation. Know-how tests consisted of fundamental questions related to a laboratory technique that was employed

for the first time in the corresponding experiment. As an example, questions on the laboratory technique "extraction" were as follows (for all questions and expected answers see SI Chapter 1.3):

- Which layer in the separating funnel is the organic one?
- What can you do if the layers do not separate properly?
- Give a short reason why the funnel has to be vented regularly during the extraction process.

Additionally, students were asked to state which of the relevant videos they watched. All tests were evaluated by the same neutral person following a predefined scheme.

Analysis of Online Video Use

Besides the surveys, utilization rates of the online video library were analyzed. During this study only course participants were able to watch the videos and no external access was allowed. "Views" of each video were provided by the video server. Those views cannot be personalized and a minor number of views is also caused by administrators. All relevant videos for one experiment were presented at one webpage for every experiment and provided the only access option to the videos. The personalized access rates of students to each of those webpages were analyzed as a second independent data source. Even if it is reasonable to assume that students watched at least one video when visiting those webpages, minor exceptions cannot be excluded nor the number of watched videos per webpage visit can be determined. Despite the mentioned limitations, both numbers can serve as an approximate, but robust estimate of video utilization.

■ FINDINGS

In this section the results from the different surveys and analysis of online video use are presented structured by the addressed research question.

Question 1: When and How Often Do Students Use an Online Video Library in the Context of an Introductory Organic Chemistry Laboratory Course?

Of the students in this study, 62% stated having used the video library on a regular basis, while only 7% did not watch a single video (for full survey results see SI Chapter 2.2). The overall 114 students visited the 31 video web pages presenting the videos during the period of the laboratory courses 4196 times (averaging 37 visits per student), which resulted in 6231 video views (averaging 55 views per student). It should be emphasized that there may be smaller errors in these numbers as mentioned in the methods section, but the major trends are nevertheless clear: The majority of students used the additional online video library regularly and even watched on average more than one movie for the preparation of a single experiment. This intense use is especially striking compared to the preliminary tests of the online video library, where students watched on average only one to four of 48 videos. The major difference in these preliminary tests was that the videos were listed on a single webpage and not assigned to the individual experiments. Thus, the presentation of the videos is crucial for their utilization. Table 2 shows that the 114 students watched all three video types quite extensively. Videos of "Tutorial" type were accessed most frequently, and the videos gathering the largest absolute number of views were "reactions under reflux" (359 views) and "distillation" (358 views, for complete ranking see SI Chapter 3).

Table 2. Total View Rates of the Online Video Library during the Laboratory Course

Video Type	Videos, N	Total Views, N^a	Median Views per Video, N^a
Tutorials	17	2556	97
Do nots	8	822	79
Step-by-Step	23	2853	95
Overall	**48**	**6231**	**87**

^{a}Data from 114 students.

As shown in Figure 1 video views are not distributed uniformly over the time of the laboratory course. Highest
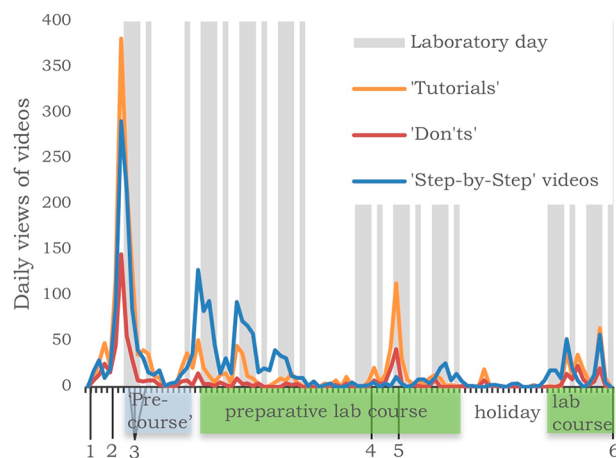
Figure 1. Daily views of the videos of the online video library in the bachelor degree laboratory course I ($N = 76$). Gray fields highlight days when students worked in the laboratory. Data was gathered from the online counter of the server hosting the videos. Numbers mark special events during the laboratory course: 1. first lecture (with first introduction of the online video library); 2. prelaboratory evaluation; 3. know-how tests; 4. midterm exam; 5. final evaluation; 6. end of lab course.

access rates were observed on the day before the beginning of the laboratory class as well as the first day of class. On these 2 days 1310 video views were counted, which represents 27% of all views during the laboratory class. It is furthermore remarkable that "Tutorials" and "Do nots" were mainly watched at the beginning of the laboratory course or when new laboratory techniques were introduced. In later stages of the course student focus then shifted to the more specific "Step-by-Step" videos. Eventually, viewing maximizes regularly on laboratory-free days (white fields in Figure 1) right before actual laboratory days (gray fields). This is in line with results from the postlab survey, where 96% of the students stated having watched videos before the actual laboratory course day, 44% in the laboratory and 6% after the laboratory day (multiple answers possible). Closer examination of the viewing rates presented in Figure 1 also shows that external factors (evaluations of the online video library, written exams in the accompanying lecture course, holiday breaks) triggered additional video access.

Question 2: How does Student Diversity Influence the Utilization and Preferences within a Modular and Versatile Online Video Library?

Despite those general findings, a more detailed analysis of viewing rates reveals striking differences within the student cohort due to student diversity.

The personalized analysis of the video access data in Figure 2 shows that some students accessed the video library rarely or
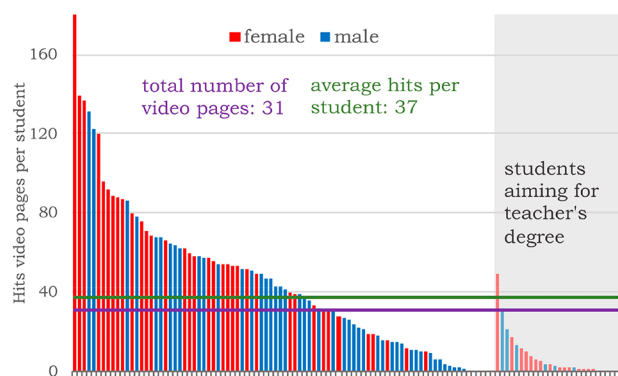
Figure 2. Access rates to the 31 video web pages per student in the three investigated laboratory courses ($N = 114$). A red bar represents a female student, a blue bar a male student, the gray shaded field represents students aiming for a teacher's degree. Distribution curves of the access rates by subgroup are presented in the SI Chapter 2.3.

never, whereas others accessed the video web pages extensively and repeatedly. To further investigate the influence of gender and study course as well as other student characteristic on the use of videos, independent sample t tests or respectively Pearson correlations (Table 3) were calculated. Students

Table 3. Correlation of Student Characteristics and Video Utilization

Student Characteristic	r	p	N
Performance in organic chemistry lecture I[a]	0.331[b]	0.005	70
Use of video tutorials in daily life (Pre)	0.341[b]	0.002	83
Expectations of an online video library (Pre)	0.373[b]	0.001	83
Intrinsic motivation (Pre)	0.334[b]	0.002	83
Self-concept of ability (Pre)[a]	−0.351[b]	0.002	74
Self-perception of conscientiousness (Pre)	0.548[c]	<0.001	83

[a]Bachelor degree students only. [b]Pearson correlation coefficient values are significant at the 0.010 level. [c]Pearson correlation coefficient values are significant at the 0.001 level.

aiming for a teacher's degree used the video library significantly less frequently than bachelor students ($t(93) = 5.60$, $p < 0.001$, $d = 1.38$), while female bachelor students were more likely to use the video library than their male counterparts ($t_{Welch}(55.9) = 4.15$, $p < 0.001$, $d = 0.95$, $N = 72$). For both interdependencies Cohen's d values imply a large effect size.[61] As the influence of the study course appeared too dominant, the sample was restricted to bachelor students for several correlations in Table 3 (for statistical details for both groups see SI Chapter 2.6). Unsurprisingly, students that

consider themselves as conscientious and highly motivated were more likely to use the video library frequently. Students who use video tutorials in daily life were more likely to utilize the videos. Also, the expectations students have toward the video library are directly linked to their usage pattern and thus act as a self-fulfilling prophecy. A good grade in the introductory organic chemistry lecture leads to an above-average usage of the video library. This is, surprisingly, also found to be the case for students with a low self-concept of ability. Possible reasons for gender-related differences may include that female bachelor students assessed themselves prior to the laboratory course as being more conscientious ($t(76) = -2.02$, $p = 0.047$, $d = 0.46$), but less self-confident of their abilities ($t(76) = 2.01$, $p = 0.048$, $d = 0.46$) than their male counterparts. After the laboratory course none of these gender-related differences could be observed anymore. The low video utilization rates for teacher degree students originate most likely from their much lower intrinsic motivation for the laboratory course ($t(93) = 5.49$, $p < 0.001$, $d = 1.36$) compared to bachelor degree students.

The students using the video library were also asked to rate the benefits of the three different video types on a scale from 1 (very good) to 6 (insufficient). Female students rated the whole video library ($t(76) = 3.67$, $p < 0.001$, $d = 0.83$) as well as "Tutorials" ($t(76) = 3.20$, $p = 0.002$, $d = 0.73$) and "Do nots" ($t(76) = 3.40$, $p = 0.001$, $d = 0.77$) approximately half a grade better than their male counterparts, while no such differences were observed for "Step-by-Step" videos (see Figure 3). Interestingly, highly motivated and conscientious
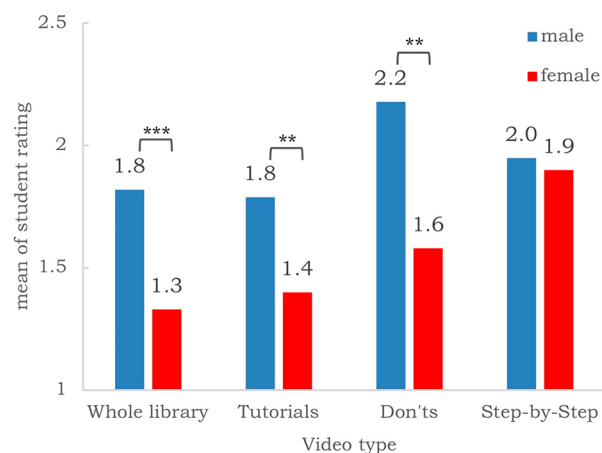
Figure 3. Mean of student rating ($N = 78$) by gender on the benefit of the video library and the different video types on a scale from 1 (very good) to 6 (insufficient). Independent t tests were performed to validate statistical significance. ***Effects are significant at the 0.001 level. **Effects are significant at the 0.010 level.

Table 4. Correlation of Student Characteristics and Ratings of Different Video Types

Video Type	Intrinsic Motivation (Pre)			Self-Concept of Ability (Pre)			Self-Perception of Conscientiousness (Pre)		
	r	p	N	r	p	N	r	p	N
Tutorials	0.271[a]	0.021	73	−0.037	0.767	65	0.207	0.079	73
Do nots	0.330[b]	0.004	73	−0.042	0.739	65	0.239[a]	0.042	73
Step-by-Step	0.389[b]	0.001	71	0.076	0.549	64	0.365[b]	0.002	71
Whole Library	0.264[a]	0.024	73	−0.018	0.890	65	0.161	0.175	73

[a]Pearson correlation coefficient values are significant at the 0.050 level. [b]Pearson correlation coefficient values are significant at the 0.010 level.

students appreciated "Step-by-Step" and "Do nots" videos above average. In contrast, the influence of those characteristics on the rating of "Tutorials" and the whole library is much weaker (see Table 4). For other student characteristics correlations did not turn out to be significant (for all correlations see SI Chapter 2.8).

Question 3. How Does the Video Library Influence Students' Prelaboratory Knowledge and Their Affective Laboratory Course Experience?

The prelaboratory knowledge of students was assessed by know-how tests (see methods section). Figure 4 shows that
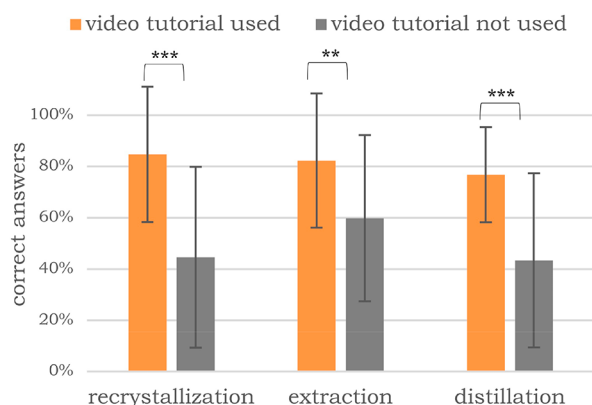
Figure 4. Percentage of correct answers of students ($N = 45-54$) in know-how test on selected laboratory techniques. Independent sample t tests were performed to prove statistical significance. ***Effects are significant at the 0.001 level. **Effects are significant at the 0.010 level.

students, who stated that they have watched the relevant tutorials, answered up to twice as many questions in know-how tests correctly as compared to their fellow students. The know-how tests focus in this case on the topics "recrystallization" ($t(52) = 4.78$, $p < 0.001$, $d = 1.32$), "extraction" ($t(51) = 2.78$, $p = 0.008$, $d = 0.78$), and "distillation" ($t_{Welch}(22) = 3.73$, $p = 0.001$, $d = 1.31$). In view of the Cohen's d values found here the impact of online video tutorials on the quality of student laboratory course preparation is thus quite significant (for full statistical details see SI Chapter 2.7).[61]

Student response to the statements listed in Figure 5 can be employed to estimate the influence of the video library on affective factors of the laboratory course. Online videos seem to have a positive impact on students' feeling of preparedness (Figure 5, items 1−3) and their self-concept of ability in working experimentally (Figure 5, items 4, 5), to the highest extent for "Tutorial" type videos. The impact on the motivation appears to be smaller, but still approximately two-thirds of students agree that watching the videos increased their motivation and their interest in working experimentally (Figure 5, items 6, 7). The attitude toward the videos themselves was found to be very positive, for example, 86% of the students enjoyed watching "Tutorials" and 75% of them were entertained by "Do nots" videos (Figure 5, items 8, 9). In their free format answers students especially praised design, access, and presentation of the videos, while several demanded "Step-by-Step" videos for all experiments and more detailed videos (for all comments see SI Chapter 4). In more general terms the students emphasized the benefits of the video library
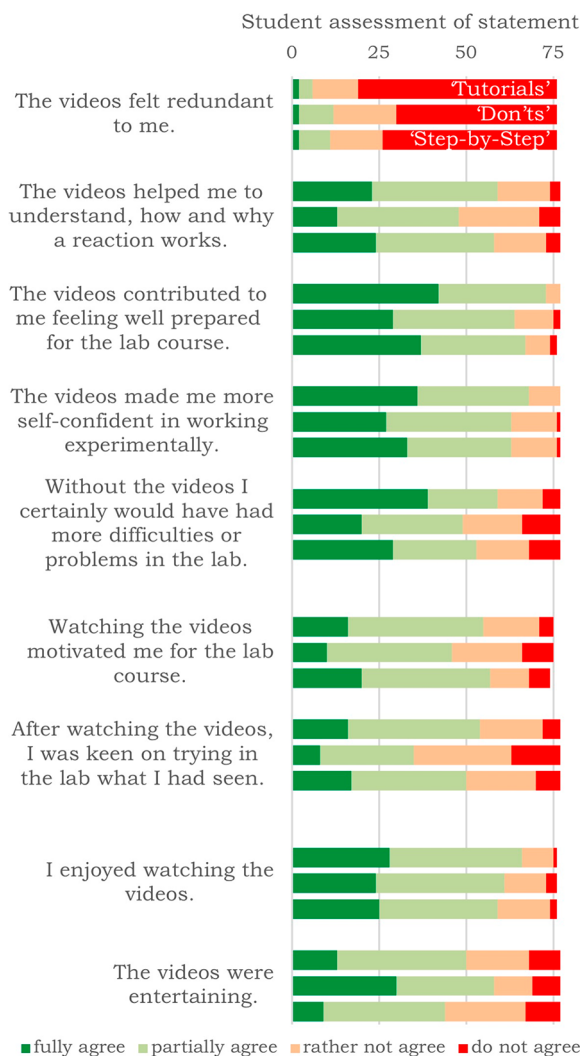
Figure 5. Student assessment of different items evaluating their feeling of being prepared, self-confidence, and motivation for the laboratory course as well as their attitude toward the videos. Every item was rated separately for videos of the type "Tutorial", "Do nots" and "Step-by-Step" videos (top-down). Only students who used the video library were invited to rate these items ($N = 77$).

in successfully learning in the laboratory course, as the following examples illustrate:

- [The videos] gave a good insight into the principles of processes/methods and the use of technical equipment.
- The videos make learning notably easier. The "Do nots" often point out things oneself would not have thought about, thus making experimental work faster and more efficient.
- Experimental setup and procedures got always very clear, one also got a good idea of an experiment (e.g., color of product).

Will positive student ratings of the video library also lead to measurable changes in their motivation, self-concept of ability, and their self-perception of conscientiousness? To answer this question, we grouped students that declared having used the online video library "often" or "sometimes" as frequent video users and those watching the videos "barely" or "never" as sporadic video users. From the pre- and postlaboratory course characteristics collected in Figure 6 we see that changes in
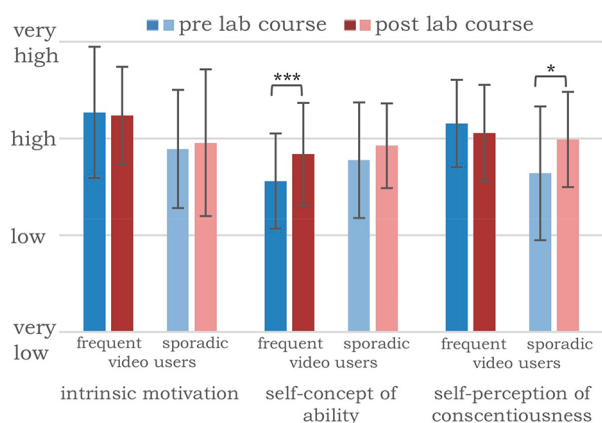
Figure 6. Comparison of student personality properties before and after the laboratory course. Students stating having used the video library "very often" to "sometimes" are grouped as frequent video users ($n = 53$), whereas students using videos "rarely" to "never" are grouped as sporadic video users ($n = 28$). ***Effects are significant at the 0.001 level. *Effects are significant at the 0.050 level.

motivation did not become statistically significant for any of the groups. However, for frequent video users the self-concept of ability in experimental work increased during the laboratory course significantly with a medium effect size ($t(52) = 4.23$, $p < 0.001$, $d = 0.58$). For sporadic users the change in their self-concept of ability is not significant. Interestingly, the self-perception of conscientiousness of the sporadic video users group ($t(27) = 2.45$, $p = 0.021$, $d = 0.46$) grows significantly during the laboratory course and eventually almost reaches the level of frequent video users (for full statistical data see SI Chapter 2.4). Accomplishing a laboratory course successfully thus appears to level internalized self-perceptions of the students.

■ LIMITATIONS

The study was situated in the concrete setting of the described laboratory course and focused on the impact of one specific online video project. Therefore, results can only be generalized with caution. Limitations of the evaluation of online video access are discussed in the method section. As in many other empirical studies the analysis of the temporal course of viewing rates indicates that also surveys themselves can influence test results (here: the viewing rates). As this study did not utilize a blind group design, it cannot be controlled whether the same factors that favor video utilization also influence performance characteristics such as the results of know-how tests. The design of this study does also not allow for a comparison of the benefits of the online video library with other potential laboratory course preparation methods.

■ IMPLICATIONS FOR CHEMISTRY LEARNING

First of all, it should be emphasized that a high percentage of the students invested additional time for the preparation of the laboratory course through using video library. It thus seems that the development of online media tailored to fit particular student requirements are quite effective in raising student motivation.[62] As has already been observed in similar projects,[16] the development of a ready-to-use presentation and the clear assignment of relevant videos to each experiment are critical for this result. When videos are presented without clear structure, students are not able or not willing to search for

the relevant videos for a specific experiment or a particular question. Instructional videos of general type are watched more frequently by students at the beginning of a laboratory course, while views of videos providing specific reaction information such as the "Step-by-Step" videos are accessed at a constant level throughout the laboratory course. It is therefore crucial to identify the prelab knowledge and experience of students in order to offer targeted support through online media. Students choose the time of video utilization themselves (for preparation as well as during the laboratory class), which represents an element of self-regulated learning. This may be supported by, for example, offering additional access possibilities in teaching laboratories.[17]

Analogous to other contemporary teaching methods[52,53] female students appreciate the online video library significantly more than their male counterparts. The fact that gender-related differences in the self-perception of experimental ability and conscientiousness were found in this study before but not after the laboratory course indicates that those differences are likely to be caused by internalized gender stereotypes.[63,64] The significantly higher appreciation of modern media and teaching methods by female students thus points to their potential in deconstructing unproductive clichés. Intrinsic motivation is a key factor for the use of video tutorials and could also explain the low utilization of the videos by students aiming for a teachers' degree. The rather alarming finding on their low motivation to work experimentally certainly deserves further attention. Possible factors such as the personal prerequisites of students choosing to become teachers, but also the teacher training programs in science and their ability to fit specific student needs should be investigated in detail.[65]

Most students seem to prefer more general video types such as the "Tutorials". Nonetheless, especially students that consider themselves as highly conscientious and motivated were likely to value more specific instructions as offered by "Step-by-Step" videos. In addition, preferences for the various video types differ significantly between female and male students. The design of this study does not allow identification of the origins of these differences, but it should be emphasized that different preferences for the design of multimedia tools were also found in other projects.[11,16,54] It thus seems important to create versatile and diverse online teaching tools to increase the chance of meeting the diverse needs and preferences within a heterogeneous student cohort.

In agreement with other studies[11,12,14] prelaboratory knowledge is improved significantly for students utilizing the online video library. This increased prior knowledge is one key factor in reducing the cognitive overload in introductory laboratory courses.[25,28] Furthermore, it reinforces students' individual feeling of preparedness[15] and their self-perceptions.[33] Interestingly, objectively underperforming students (as far as reflected by grades) were more unlikely to watch the videos, whereas students with a (subjective) lower self-concept of ability used the additional help of the online video library above average, triggering a targeted increase of self-concept of ability. Other affective factors such as the intrinsic motivation is relatively stable over the period of the laboratory course and seems to be self-reinforcing. As the less motivated students also tend to invest less time in preparation,[29] they use potentially motivating methods such as the video library less frequently. One way to reach poorly motivated students and students overestimating their abilities could be the implementation of extrinsic motivation factors such as obligatory quizzes.[15,16]

Nonetheless, in this study approximately two-thirds of the students used the online video library on a regular basis even without external obligation. The rather surprising finding that the overwhelming majority of students "enjoyed" watching the movies indicates that respecting and adapting to the (digital) daily life reality of young adults in creating teaching tools is a promising approach to activate and motivate students. Students acknowledged the positive impact of the online video library on their intrinsic motivation, individual feeling of preparedness, and self-concept of ability. Thus, the utilization of online media is a suitable method in making learning meaningful[31,34] and should become a contemporary standard for laboratory courses.

CONCLUSION

In this study, the implementation of an online library composed of "Tutorials", "Do nots", and "Step-by-Step" videos in an introductory organic chemistry laboratory course was explored by an empirical study ($N = 103$). The participating students ($N = 114$) watched more than 6000 videos when these were presented in a ready-to-use manner. The online library was used most frequently at the beginning of the laboratory period. Students watched the videos mostly for the preparation of the laboratory course, but also quite frequently during laboratory hours. Utilization rates differed dramatically among subgroups of the student cohort. Students with a high self-perception of conscientiousness and motivation, but also those with a low self-concept of ability are most likely to watch the videos. Also, female students used the video library on average more frequently than their male counterparts, while students aiming for a teacher's degree used it substantially less frequently. Furthermore, individual preferences for specific video types are affected by gender, motivation, and perception of conscientiousness. Therefore, the use of different video types improves the differentiation and individualization of chemistry teaching. The use of the videos increased the number of correct answers in prelaboratory know-how tests by up to 100% and correlates significantly with the increase of self-concept of ability. Those results together with student assessment of the intervention indicate a positive influence of the online video library on cognitive, affective, and psychomotor learning in laboratory courses. The video library is available at http://www.cup.uni-muenchen.de/oc/zipse/vidbibocp/.

ASSOCIATED CONTENT

Ⓢ Supporting Information

The Supporting Information is available at https://pubs.acs.org/doi/10.1021/acs.jchemed.9b00647.

> Survey instruments, full statistics, video utilization rates, and free format comments (PDF)

AUTHOR INFORMATION

Corresponding Author

*E-mail: zipse@cup.uni-muenchen.de.

ORCID Ⓘ

Benjamin Pölloth: 0000-0001-7777-9903
Stefan Schwarzer: 0000-0002-4134-5684
Hendrik Zipse: 0000-0002-0534-3585

REFERENCES

(1) Jandrić, P.; Knox, J.; Besley, T.; Ryberg, T.; Suoranta, J.; Hayes, S. Postdigital science and education. *Educ. Philos. Theory* **2018**, *50* (10), 893−899.

(2) Feierabend, S.; Rathgeb, T.; Reutter, T. *JIM 2018 Jugend, Information, Medien*; Medienpädagogischer Forschungsverbund Südwest: Stuttgart, 2018.

(3) Jebe, F.; Konietzko, S.; Lichtschlag, M.; Liebau, E. *Jugend/Youtube/Kulturelle Bildung. Horizont 2019*; Rat für Kulturelle Bildung: Essen, 2019.

(4) The state of online video 2018. https://www.limelight.com/resources/white-paper/state-of-online-video-2018/ (accessed November 25, 2019).

(5) Weaver, G. C.; Sturtevant, H. G. Design, Implementation, and Evaluation of a Flipped Format General Chemistry Course. *J. Chem. Educ.* **2015**, *92* (9), 1437−1448.

(6) Obradovich, A.; Canuel, R.; Duffy, E. P. A Survey of Online Library Tutorials: Guiding Instructional Video Creation to Use in Flipped Classrooms. *J. Acad. Librariansh.* **2015**, *41* (6), 751−757.

(7) Liu, Y.; Raker, J. R.; Lewis, J. E. Evaluating student motivation in organic chemistry courses: moving from a lecture-based to a flipped approach with peer-led team learning. *Chem. Educ. Res. Pract.* **2018**, *19* (1), 251−264.

(8) He, Y.; Swenson, S.; Lents, N. Online Video Tutorials Increase Learning of Difficult Concepts in an Undergraduate Analytical Chemistry Course. *J. Chem. Educ.* **2012**, *89* (9), 1128−1132.

(9) Richards-Babb, M.; Curtis, R.; Smith, V. J.; Xu, M. Problem Solving Videos for General Chemistry Review: Students' Perceptions and Use Patterns. *J. Chem. Educ.* **2014**, *91* (11), 1796−1803.

(10) Ranga, J. S. Customized Videos on a YouTube Channel: A Beyond the Classroom Teaching and Learning Platform for General Chemistry Courses. *J. Chem. Educ.* **2017**, *94* (7), 867−872.

(11) Box, M. C.; Dunnagan, C. L.; Hirsh, L. A. S.; Cherry, C. R.; Christianson, K. A.; Gibson, R. J.; Wolfe, M. I.; Gallardo-Williams, M. T. Qualitative and Quantitative Evaluation of Three Types of Student-Generated Videos as Instructional Support in Organic Chemistry Laboratories. *J. Chem. Educ.* **2017**, *94* (2), 164−170.

(12) Nadelson, L. S.; Scaggs, J.; Sheffield, C.; McDougal, O. M. Integration of Video-Based Demonstrations to Prepare Students for the Organic Chemistry Laboratory. *J. Sci. Educ. Technol.* **2015**, *24* (4), 476−483.

(13) Stieff, M.; Werner, S. M.; Fink, B.; Meador, D. Online Prelaboratory Videos Improve Student Performance in the General Chemistry Laboratory. *J. Chem. Educ.* **2018**, *95* (8), 1260−1266.

(14) Jordan, J. T.; Box, M. C.; Eguren, K. E.; Parker, T. A.; Saraldi-Gallardo, V. M.; Wolfe, M. I.; Gallardo-Williams, M. T. Effectiveness of Student-Generated Video as a Teaching Tool for an Instrumental Technique in the Organic Chemistry Laboratory. *J. Chem. Educ.* **2016**, *93* (1), 141−145.

(15) Chaytor, J. L.; Al Mughalaq, M.; Butler, H. Development and Use of Online Prelaboratory Activities in Organic Chemistry To Improve Students' Laboratory Experience. *J. Chem. Educ.* **2017**, *94* (7), 859−866.

(16) Schmidt-McCormack, J. A.; Muniz, M. N.; Keuter, E. C.; Shaw, S. K.; Cole, R. S. Design and implementation of instructional videos

for upper-division undergraduate laboratory courses. *Chem. Educ. Res. Pract.* **2017**, *18* (4), 749−762.

(17) Cresswell, S. L.; Loughlin, W. A.; Coster, M. J.; Green, D. M. Development and Production of Interactive Videos for Teaching Chemical Techniques during Laboratory Sessions. *J. Chem. Educ.* **2019**, *96* (5), 1033−1036.

(18) Fung, F. M. Using First-Person Perspective Filming Techniques for a Chemistry Laboratory Demonstration To Facilitate a Flipped Pre-Lab. *J. Chem. Educ.* **2015**, *92* (9), 1518−1521.

(19) Benedict, L.; Pence, H. E. Teaching Chemistry Using Student-Created Videos and Photo Blogs Accessed with Smartphones and Two-Dimensional Barcodes. *J. Chem. Educ.* **2012**, *89* (4), 492−496.

(20) Matson, M. L.; Fitzgerald, J. P.; Lin, S. Creating Customized, Relevant, and Engaging Laboratory Safety Videos. *J. Chem. Educ.* **2007**, *84* (10), 1727−1728.

(21) *Journal of Vizualized Experiments*. https://www.jove.com/about/ (accessed November 25, 2019).

(22) Zipse, H.; Pölloth, B. VidBibOCP-Videothek. https://www.cup.uni-muenchen.de/oc/zipse/vidbibocp/ (accessed November 25, 2019).

(23) Winberg, T. M.; Berg, C. A. R. Students' cognitive focus during a chemistry laboratory exercise: Effects of a computer-simulated prelab. *J. Res. Sci. Teach.* **2007**, *44* (8), 1108−1133.

(24) Galloway, K. R.; Bretz, S. L. Video episodes and action cameras in the undergraduate chemistry laboratory: eliciting student perceptions of meaningful learning. *Chem. Educ. Res. Pract.* **2016**, *17* (1), 139−155.

(25) Sweller, J. Cognitive Load During Problem Solving: Effects on Learning. *Cogn. Sci.* **1988**, *12* (2), 257−285.

(26) Johnstone, A. H.; Sleet, R. J.; Vianna, J. F. An Information-Processing Model of Learning - Its Application to an Undergraduate Laboratory Course in Chemistry. *Stud. High. Educ.* **1994**, *19* (1), 77−87.

(27) Johnstone, A. H.; Wham, A. J. B. The demands of practical work. *Educ. Chem.* **1982**, *19* (3), 71−73.

(28) Agustian, H. Y.; Seery, M. K. Reasserting the role of pre-laboratory activities in chemistry education: a proposed framework for their design. *Chem. Educ. Res. Pract.* **2017**, *18* (4), 518−532.

(29) Rollnick, M.; Zwane, S.; Staskun, M.; Lotz, S.; Green, G. Improving pre-laboratory preparation of first year university chemistry students. *Int. J. Sci. Educ.* **2001**, *23* (10), 1053−1071.

(30) Cracolice, M. S.; Busby, B. D. Preparation for College General Chemistry: More than Just a Matter of Content Knowledge Acquisition. *J. Chem. Educ.* **2015**, *92* (11), 1790−1797.

(31) Bretz, S. L. Novak's Theory of Education: Human Constructivism and Meaningful Learning. *J. Chem. Educ.* **2001**, *78* (8), 1107.

(32) Grove, N.; Bretz, S. L. CHEMX: An Instrument To Assess Students' Cognitive Expectations for Learning Chemistry. *J. Chem. Educ.* **2007**, *84* (9), 1524.

(33) Nieswandt, M. Student affect and conceptual understanding in learning chemistry. *J. Res. Sci. Teach.* **2007**, *44* (7), 908−937.

(34) Galloway, K. R.; Bretz, S. L. Measuring Meaningful Learning in the Undergraduate Chemistry Laboratory: A National, Cross-Sectional Study. *J. Chem. Educ.* **2015**, *92* (12), 2006−2018.

(35) Galloway, K. R.; Bretz, S. L. Development of an Assessment Tool To Measure Students' Meaningful Learning in the Undergraduate Chemistry Laboratory. *J. Chem. Educ.* **2015**, *92* (7), 1149−1158.

(36) Galloway, K. R.; Malakpa, Z.; Bretz, S. L. Investigating Affective Experiences in the Undergraduate Chemistry Laboratory: Students' Perceptions of Control and Responsibility. *J. Chem. Educ.* **2016**, *93* (2), 227−238.

(37) Novak, J. D. Human constructivism: A unification of psychological and epistemological phenomena in meaning making. *J. Constr. Psychol.* **1993**, *6* (2), 167−193.

(38) Savelsbergh, E. R.; Prins, G. T.; Rietbergen, C.; Fechner, S.; Vaessen, B. E.; Draijer, J. M.; Bakker, A. Effects of innovative science

and mathematics teaching on student attitudes and achievement: A meta-analytic study. *Educ. Res. Rev.* **2016**, *19*, 158−172.

(39) Deslauriers, L.; Schelew, E.; Wieman, C. Improved learning in a large-enrollment physics class. *Science* **2011**, *332* (6031), 862−4.

(40) Supasorn, S.; Suits, J. P.; Jones, L. L.; Vibuljan, S. Impact of a pre-laboratory organic-extraction simulation on comprehension and attitudes of undergraduate chemistry students. *Chem. Educ. Res. Pract.* **2008**, *9* (2), 169−181.

(41) Mayer, R. E. Using multimedia for e-learning. *J. Comput. Assist. Learn.* **2017**, *33* (5), 403−423.

(42) D'Ambruoso, G. D.; Cremeens, M. E.; Hendricks, B. R. Web-Based Animated Tutorials Using Screen Capturing Software for Molecular Modeling and Spectroscopic Acquisition and Processing. *J. Chem. Educ.* **2018**, *95* (4), 666−671.

(43) Bauer, C. F. Beyond "Student Attitudes": Chemistry Self-Concept Inventory for Assessment of the Affective Component of Student Learning. *J. Chem. Educ.* **2005**, *82* (12), 1864.

(44) Cicuto, C. A. T.; Torres, B. B. Implementing an Active Learning Environment To Influence Students' Motivation in Biochemistry. *J. Chem. Educ.* **2016**, *93* (6), 1020−1026.

(45) Pogacnik, L.; Cigic, B. How To Motivate Students To Study before They Enter the Lab. *J. Chem. Educ.* **2006**, *83* (7), 1094.

(46) Lewis, S. E.; Shaw, J. L.; Heitz, J. O.; Webster, G. H. Attitude Counts: Self-Concept and Success in General Chemistry. *J. Chem. Educ.* **2009**, *86* (6), 744.

(47) Clark, G. J.; Riley, W. D. The Connection between Success in a Freshman Chemistry Class and a Student's Jungian Personality Type. *J. Chem. Educ.* **2001**, *78* (10), 1406.

(48) Goethe, E. V.; Colina, C. M. Taking Advantage of Diversity within the Classroom. *J. Chem. Educ.* **2018**, *95* (2), 189−192.

(49) Laursen, S. L.; Weston, T. J. Trends in Ph.D. Productivity and Diversity in Top-50 U.S. Chemistry Departments: An Institutional Analysis. *J. Chem. Educ.* **2014**, *91* (11), 1762−1776.

(50) Widener, A. Chemist diversity in the US. *C&EN Global Enterprise* **2019**, *97* (15), 16−16.

(51) Knezz, S. N. Drawing a New Scientist: Why I Come Out to My Chemistry Class. *J. Chem. Educ.* **2019**, *96* (5), 827−829.

(52) Fischer, C.; Zhou, N.; Rodriguez, F.; Warschauer, M.; King, S. Improving College Student Success in Organic Chemistry: Impact of an Online Preparatory Course. *J. Chem. Educ.* **2019**, *96* (5), 857−864.

(53) Niemeyer, E. D.; Zewail-Foote, M. Investigating the Influence of Gender on Student Perceptions of the Clicker in a Small Undergraduate General Chemistry Course. *J. Chem. Educ.* **2018**, *95* (2), 218−223.

(54) Dousay, T. A.; Trujillo, N. P. An examination of gender and situational interest in multimedia learning environments. *Br. J. Educ. Technol.* **2019**, *50* (2), 876−887.

(55) Trautmann, M.; Wischer, B., Das Konzept der Inneren Differenzierung — eine vergleichende Analyse der Diskussion der 1970er Jahre mit dem aktuellen Heterogenitätsdiskurs. In *Perspektiven der Didaktik: Zeitschrift für Erziehungswissenschaft*; Meyer, M. A., Prenzel, M., Hellekamps, S., Eds.; VS Verlag für Sozialwissenschaften: Wiesbaden, 2009; pp 159−172.

(56) Satow, L. Big-Five-Persönlichkeitstest (B5T): Test- und Skalendokumentation. https://www.drsatow.de/tests/persoenlichkeitstest/ (accessed November 25, 2019).

(57) Wilde, M.; Bätz, K.; Kovaleva, A.; Urhahne, D. Überprüfung einer Kurzskala intrinsischer Motivation (KIM). *Z. Didaktik Nat.* **2009**, *15*, 31−45.

(58) Glowinski, I. *Molekularbiologie als interessenfördernde Lernumgebungen*; Christian-Albrechts-Universität zu Kiel: Kiel, 2007.

(59) Cronbach, L. J. Coefficient Alpha And The Internal Structure of Tests. *Psychometrika* **1951**, *16*, 297−334.

(60) *IBM SPSS Statistics 25*; IBM Corp.: 2017.

(61) Cohen, J. *Statistical Power Analysis for the Behavioral Sciences*, 2 ed.; Lawrence Erlbaum Associates: New York, 1988.

(62) Stamer, I.; Pönicke, H.; Tirre, F.; Laherto, A.; Höffler, T.; Schwarzer, S.; Parchmann, I. Development & validation of scientific

video vignettes to promote perception of authentic science in student laboratories. *Res. Sci. Technol. Educ.* **2019**, 1−17.

(63) Miyake, A.; Kost-Smith, L. E.; Finkelstein, N. D.; Pollock, S. J.; Cohen, G. L.; Ito, T. A. Reducing the gender achievement gap in college science: a classroom study of values affirmation. *Science* **2010**, *330* (6008), 1234−7.

(64) Nosek, B. A.; Smyth, F. L.; Sriram, N.; Lindner, N. M.; Devos, T.; Ayala, A.; Bar-Anan, Y.; Bergh, R.; Cai, H.; Gonsalkorale, K.; Kesebir, S.; Maliszewski, N.; Neto, F.; Olli, E.; Park, J.; Schnabel, K.; Shiomura, K.; Tulbure, B. T.; Wiers, R. W.; Somogyi, M.; Akrami, N.; Ekehammar, B.; Vianello, M.; Banaji, M. R.; Greenwald, A. G. National differences in gender-science stereotypes predict national sex differences in science and math achievement. *Proc. Natl. Acad. Sci. U. S. A.* **2009**, *106* (26), 10593−7.

(65) Kaub, K.; Karbach, J.; Biermann, A.; Friedrich, A.; Bedersdorfer, H.-W.; Spinath, F. M.; Brünken, R. Berufliche Interessensorientierungen und kognitive Leistungsprofile von Lehramtsstudierenden mit unterschiedlichen Fachkombinationen. *Z. Pädagog. Psychol.* **2012**, *26* (4), 233−249.

9.1. Short Overview of Basic Statistic Parameters

Statistic methods are crucial for a scientific evaluation of innovations in chemical education. To help the reader to interpret the reported analysis a short introduction and overview of statistic parameter is given. This overview is **not** intended to be a reasonable or comprehensive introduction to statistic methods but the shortest possible compilation of methods used in this study. For a more detailed introduction see the quoted literature.[1] The goal of statistic methods is to get information about a **population**. The population is a set of similar items or persons, e.g. all chemistry students at a certain university. As it is in general impossible to investigate the whole population, a subset is chosen as the **sample** with sample size N. Statistics allow to control how reliable this gathered information is. A **scale** $X = (x_1, x_2, \ldots, x_n)$ is a set of n data points. A survey in an empirical study is usually built from several **items** (e.g. questions, statements). Several related items can be numerically coded and yield a metric scale that describes a property (e.g. motivation) of a participant. To verify the **reliability** of the scale, the internal consistency is tested e.g. by calculation of Cronbach's alpha values.[2] The scatter of a parameter is commonly described by the **standard deviation** (Eq. 9.3), that is the root square of the **variance** (Eq. 9.2). In practice, it is very often of major interest in how far two scales X and Y depend linear on each other. A standardized description gives the Pearson correlation r_{XY} (Eq. 9.5).

Table 9.1. Overview of basic statistic parameter.[1b]

Parameter	Equation		meaning
arithmetic mean	$\bar{x} = \dfrac{1}{n}\displaystyle\sum_{i=1}^{n} x_i$	Eq. 9.1	average value of parameter in the sample
variance[a]	$\tilde{s}^2 = \dfrac{1}{n-1}\displaystyle\sum_{i=1}^{n}(x_i - \bar{x})^2$	Eq. 9.2	scatter of the parameter
standard deviation[a]	$\tilde{s} = \sqrt{\tilde{s}^2}$	Eq. 9.3	scatter of the parameter
empirical covariance[a]	$\tilde{s}_{XY} = \dfrac{1}{n-1}\displaystyle\sum_{i=1}^{n}(x_i - \bar{x})(y_i - \bar{y})$	Eq. 9.4	Describes the degree of linear dependency of two parameters; not standardized
Pearson's correlation coefficient	$r_{XY} = \dfrac{\tilde{s}_{XY}}{\tilde{s}_X \tilde{s}_Y}$	Eq. 9.5	z-standardized linear dependency of two parameters r = +1: parameters correlate positively r = 0: parameters are independent r = -1: parameters correlate negatively

[a]valid for a sample; for the entire population: $\frac{1}{n}$ instead of $\frac{1}{n-1}$ is used

One of the most central questions in statistics is then, whether a found correlation is accidental for the sample or representative for the whole population, that is **significant**. Therefore, the following question is investigated: "If one presumes that the two investigated parameters are independent in the whole population, how probable is it these test statistics are found within the sample?" This **null**

hypothesis indicates that the scatter of the investigated parameters is normal distributed, or more exactly *t-distributed* within the population. To answer this question the test statistic *t* (see below) of the obtained correlation is calculated and compared to the test statistic T of a *t*-distributed population. Dependent on the degrees of freedom (often sample size -1) the **p-value** displays then how likely it is that the observed differences are accidental. If $p > 0.05$ (that is: there is a 5% chance that correlations are accidental) results should not be discussed, results with $p < 0.05$ are **statistically significant** (commonly marked with *), for $p < 0.01$ they are called very significant (**) and for $p < 0.001$ highly significant (***). The central statistic descriptor is thus the **test statistic *t***. Generally, it is defined as the ratio of estimator and standard error. However, for different analysis methods the test statistic is calculated in different ways as shown in **Table 9.2**.

Table 9.2. Overview of different possibilities to calculate test statistic t.[1]

Statistical	Equation		Analysis of…
Pearson correlation	$t = \dfrac{r\sqrt{n-2}}{\sqrt{1-r^2}}$	Eq. 9.6	the linear dependence of two scales.
Independent samples t-test[a]	$t = \dfrac{\bar{X}-\bar{Y}}{\sqrt{\dfrac{(n_x-1)s_x^2 + (n_y-1)s_y^2}{n_x+n_y-2}}\sqrt{\dfrac{1}{n_x}+\dfrac{1}{n_y}}}$	Eq. 9.7	the mean of a parameter in two sub groups.
Paired samples t-test[a]	$t = \dfrac{\bar{D}}{\dfrac{S_D}{\sqrt{n}}}$ $with\ D = (x_{i_{t_2}} - x_{i_{t_1}})$	Eq. 9.8	the change of a parameter x over time t_1 to t_2.

[a]for two equally contributed samples as controlled by Levene's test. For not equally contributed samples a Welch test should be performed instead.

A significant test does not imply how strong the correlation is. This **effect size** can be, for example, described by **Cohen's *d*** as the ratio of the mean difference to the standard deviation (in the simplest cases). As a rule of thumb effects with *d < 0.20* are small, with *d > 0.80* large and with *d > 1.20* very large.[3]

9.2. Survey Instruments

9.2.1. Pre- and Post-Laboratory Questionnaire: Scales and Reliability

The pre-lab questionnaire was answered by students the day before the lab course started, the post-lab questionnaire was answered towards the end of the 3 months lab course. All questionnaires were coded in order to retain anonymity and to identify related pre- and post-lab-questionnaires as well as know-how tests. The scales were pretested with a sample group of 22 students of another lab course. Several items were formulated following the literature[4].

Table 9.3. Scales of the pre-lab questionnaire with items in original language German and its translation into English with the relevant Cronbach's alpha values. Items in italic were coded inverse. Every item could be rated by "Fully agree", "Partially agree", "Rather not agree" or "Do not agree".

Intrinsic lab course motivation	α=.786

Praktika sind ein sinnvoller Teil des Chemiestudiums.

Lab courses are a reasonable part of the studies in chemistry.

Wenn ich nicht müsste, würde ich nicht am OC-Grundpraktikum teilnehmen.

If I did not have to I would rather not participate in the organic lab course.

Ich freue mich auf das OC-Grundpraktikum.

I am looking forward to the OC lab course.

Ich erwarte, dass durch das OC-Praktikum mein Interesse am experimentellen Arbeiten gestärkt wird.

I expect that my interest in experimental work will be strengthened by this lab course in organic chemistry.

Ich denke, dass ich durch das OC-Grundpraktikum viel lernen werde.

I think that I will learn a lot by attending the basic lab course in organic chemistry.

Self-concept of ability in experimental lab work	α =.770

Ich bin im experimentellen Arbeiten geschickter als die meisten meiner Kommilitonen.

I am more skilled in experimental work than most of my fellow students.

Beim Experimentieren fühle ich mich oft überfordert.

While experimenting I often feel overstrained.

Ich denke, dass die Experimente im Grundpraktikum kein großes Problem für mich darstellen werden.

I think that the experiments in the basic lab course will not pose a major problem for me.

Ich bin beim Experimentieren sehr begabt.

I am very skilled in experimental work.

Self-perception of self-conscientiousness	α =.807

Ich denke, dass ich im Studium gewissenhafter als der Durchschnitt meiner Kommilitonen bin.

I think that I am more conscientiousness in studying than the average of my fellow students.

Ich bin im Studium sehr pflichtbewusst.

I am very diligent in my studies.

Aufgaben für die Uni erledige ich immer sehr genau.

I complete tasks for university meticulously.

Ich erledige meine Aufgaben immer planvoll.

I always fulfill my duties in a planned manner.

Use of video tutorials in daily life	α =.734

Ich nutze regelmäßig Video-Tutorials (z. B. zu Rezepten, PC-Problemen, Beauty-Tipps...).

I frequently use video tutorials (e.g. for recipes, computer problems, beauty tips….).

Wenn ich mich im Internet über ein Alltagsproblem informiere, schaue ich lieber ein Video an als einen Text zu lesen.

If I look for information about a daily problem in the internet I watch a video rather than reading a text

Verstehe ich im Studium etwas nicht, nutze ich Erklärvideos auf YouTube oder vergleichbaren Plattformen.

I use explanation videos on YouTube or similar platforms if I have problems understanding some content in my studies.

Expectations of an online video library	α =.666

Ich finde, ein Online-Video-Tutorial zum OC-Grundpraktikum ist eine gute Idee.

I think an online-video tutorial for the organic lab course is a good idea.

Ein Video-Tutorial zum OC-Grundpraktikum empfinde ich als überflüssig.

I think a video tutorial for the organic lab course is redundant.

Ich werde mir wohl eher nicht die Zeit nehmen, die Videos des Online-Video-Tutorials anzuschauen.

I think I will not invest the time watching the online-video tutorial videos.

Von einem Online-Video-Tutorial zum Grundpraktikum erwarte ich laborpraktische Arbeitsweisen verständlich erklärt zu bekommen.

From an online-video tutorial for the basic lab course I expect that lab techniques are explained comprehensibly.

Von einem Online-Video-Tutorial zum Grundpraktikum erwarte ich, dass ich mich nach dem Anschauen der Videos beim Experimentieren selbstsicherer fühle.

From an online-video tutorial for the basic lab course I expect, that I feel more confident in working experimentally after watching the videos.

Table 9.4. Scales of the post lab questionnaire with items in original language German and its translation into English with the relevant Cronbach's alpha values. Items in italic were coded inverse. Every item could be rated by "Fully agree", "Partially agree", "Rather not agree" or "Do not agree".

Intrinsic lab course motivation	α =.846

Das Grundpraktikum war ein sinnvoller Teil des Chemiestudiums.
The lab course was a reasonable part of the studies in chemistry.

Ich habe am Praktikum nur teilgenommen, weil ich musste.
I only participated in the lab course, because I had to.

Ich freue mich auf das nächste Praktikum.
I am looking forward to the next lab course.

Durch das OC-Praktikum wurde mein Interesse am experimentellen Arbeiten gestärkt.
My interest in experimental work was strengthened by this lab course in organic chemistry.

Ich denke, dass ich im OC-Grundpraktikum viel gelernt habe.
I think that I learned a lot by attending the basic lab course in organic chemistry.

Self-concept of ability in experimental lab work	α =.681

Ich war im experimentellen Arbeiten geschickter als die meisten meiner Kommilitonen.
I was more skilled in experimental work than most of my fellow students.

Die Experimente im Grundpraktikum haben kein großes Problem für mich dargestellt.
The experiments in the basic lab course did not pose a major problem for me.

Ich bin beim Experimentieren sehr begabt.
I am very skilled in experimental work.

Self-perception of conscientiousness	α =.684

Ich war im Grundpraktikum gewissenhafter als der Durchschnitt meiner Kommilitonen bin.
I was in the lab course more conscientiousness than the average of my fellow students.

Ich habe im Grundpraktikum sehr pflichtbewusst gearbeitet.
I worked very diligent in the lab course.

Die Experimente im Grundpraktikum habe ich sehr genau erledigt.
I completed the experiments in the lab course meticulously.

9.2.2.Pretest of Questionnaires

Pre- and post-lab questionnaires were pretested in an introductory organic chemistry laboratory course for biology students with 22 students. Students were asked to mark questions in the survey, that were difficult to understand. Answers of students were analyzed with SPSS, and Cronbach alpha values were calculated to check the reliability of the scales. As a representative example we show here the changes made for the scale "intrinsic motivation for the lab course".

New item	Old item	Remark
Praktika sind ein sinnvoller Teil des Chemiestudiums. Lab courses are a reasonable part of the studies in chemistry.	Praktika sind ein sinnvoller Teil des Chemiestudiums. Lab courses are a reasonable part of the studies in chemistry.	
Wenn ich nicht müsste, würde ich nicht am OC-Grundpraktikum teilnehmen. *If I had not to I´d rather not participate in the organic lab course.*	*Es ärgert mich, dass ich meine Nachmittage für das Praktikum investieren muss.* *It annoys me that I have to invest my afternoons for the lab course.*	Old item not consistent with scale.
Ich freue mich auf das OC-Grundpraktikum. I am looking forward to the OC lab course.	Ich freue mich auf das OC-Grundpraktikum. I am looking forward to the OC lab course.	
Ich erwarte, dass durch das OC-Praktikum mein Interesse am experimentellen Arbeiten gestärkt wird. I expect that my interest in experimental work will be strengthened by this lab course in organic chemistry.	Ich erwarte, dass durch das OC-Praktikum mein Interesse am experimentellen Arbeiten gestärkt wird. I expect that my interest in experimental work will be strengthened by this lab course in organic chemistry.	
Ich denke, dass ich durch das OC-Grundpraktikum viel lernen werde. I think that I will learn a lot by attending the basic lab course in organic chemistry.		Item added.

9.2.3. Lab Technique Know-How Tests

Conduction of know-how tests: Before any explanation through the lab assistant was given, students had to answer simple questions related to the lab techniques needed for this day's experiment, like "Where do you (ideally) find impurities after recrystallization?" or "What can you do if the phases (in the separating) funnel do not separate properly?" to control if the student's preparation for the lab course allowed them to fully understand, how certain lab techniques work. Furthermore, utilization and rating of related videos was requested. Subsequently the tests were evaluated by one senior master student following a strict model solution (answer correct 1 point; correct, but incomplete answer 0.5 points; incorrect or no answer 0 points) and over-all points were calculated.

Table 9.5. Know-how tests for tutorials recrystallization, extraction and distillation in original language German and its translation into English. A rubric for grading is presented below.

Recrystallization

Wo befinden sich die Verunreinigungen (im Idealfall) **nach** einer Umkristallisation?
Where are impurities (ideally) **after** recrystallization?
Accepted answers: mother liquor, liquid phase, solvent, in the filtring flask.

Nennen Sie Strategien, um eine Auskristallisation anzustoßen.
Name several strategies to initiate the crystallization process.
At least two strategies of the following (if only one: 0.5 points): cooling, addition of a seed crystal, scratching at the glass surface.

Extraction

Welche Phase im Scheidetrichter ist die organische Phase?
Which layer in the separating funnel is the organic one?
    Die obere Phase/The upper phase
    Die untere Phase/The lower phase
    Abhängig von den verwendeten Lösungsmitteln/This depends on the solvents used
Correct answer: 3

Was können Sie tun, falls sich die Phasen nicht trennen?
What can you do if the layers are not separating properly?
At least one of the following: add saturated NaCl solution; drain already separated lower phase.

Begründen Sie knapp, weshalb beim Extrahieren regelmäßig belüftet werden muss.
Give a short reason why the funnel has to be vented regularily during the extraction process.
Accepted answer: To avoid overpressure in the funnel.

Distillation

Erklären Sie, was man bei einer Destillation unter dem Vorlauf versteht.
Explain the fore shot of a distillation.
Minimum requirement for answer: The first condensed liquid before the boiling temperature is stable.

Wann sollte der Vorlagekolben bei einer fraktionierten Destillation gewechselt werden?
When should you change the receiver during a fractional distillation?
Accepted answer: As soon as the boiling temperature changes.

Welchen Vorteil hat es unter vermindertem Druck zu destillieren?
What advantage gives distilling under reduced pressure?
At least one of the following: A lower boiling temperature is needed; thermic instable compounds can be easier distilled; works faster.

Was können Sie konkret tun, wenn ihre Apparatur bei der Vakuumdestillation undicht ist?
Which steps do you take if your apparatus for distillation under reduced pressure leaks of air?
At least two of the following: check glassware for damages, check all grindings, grease all grindings, use clamps for grindings.

9.2.4.Informed Consent

All participants of the study were informed that all parts of the study are intended to publication. The original wording for the instruction at the beginning of the survey was:

"Liebe Studentinnen und Studenten,

seit diesem Jahr steht Ihnen zur Unterstützung im OC-Grundpraktikum eine Video-Bibliothek mit Tutorials zu den wichtigsten Arbeitstechniken und den meisten Versuchen über Moodle zur Verfügung.

Diese Videos sollen dazu beitragen, Ihnen den Einstieg in die experimentelle organische Chemie zu erleichtern. Wir können aber nur mit Ihrer Hilfe herausfinden, ob das gelungen ist und darauf aufbauend das Angebot verbessern. Bitte nutzen Sie deshalb die Video-Bibliothek und nehmen Sie an der zugehörigen Evaluation teil! Die Ergebnisse dieser Studie sollen auch in einer Fachzeitschrift veröffentlicht werden.

Hinweise zum Ausfüllen des Fragebogens:
- Kreuzen Sie bitte jeweils **die Aussage** an, die am besten auf Sie zutrifft. Setzen Sie keine Kreuze zwischen den Kästchen.
- Es gibt keine richtigen oder falschen Antworten, es kommt alleine darauf an, wie Sie die Dinge einschätzen.
- Die Erhebung ist komplett **anonym** und hat keinen Einfluss auf die Benotung.
- Der **Teilnehmercode** dient dazu, die verschiedenen Fragebogen einander zuzuordnen.
- Bei Unklarheiten können Sie jederzeit nachfragen.

Durch Ihre Mithilfe unterstützen Sie die Verbesserung der Lehre für die nachfolgenden Semester!

Vielen Dank dafür!"

9.3. Statistics of Survey

9.3.1. Basic Descriptive Statistics

Statistical data of the 103 students being part of the study:

- Sex: 50 female, 51 male, 2 not specified
- Semester: 3 (76), 5 (20), 6 (1), 7 (4), 9 (1)
- Average grade basic organic chemistry lecture: 2.9 (on a scale of 1-5)
- Academic goal: bachelor of science (80), teacher's degree (23)

Table 9.6. Age distribution of students in survey

18	19	20	21	22	23	24	25	26	27	29	missing
4	23	30	18	6	6	5	2	4	2	2	1

As the study consists of five independent surveys, participant numbers vary. Know-how tests were conducted only in the first lab course for students aiming for the bachelor's degree.

9.3.2. Utilization and Rating of Videos
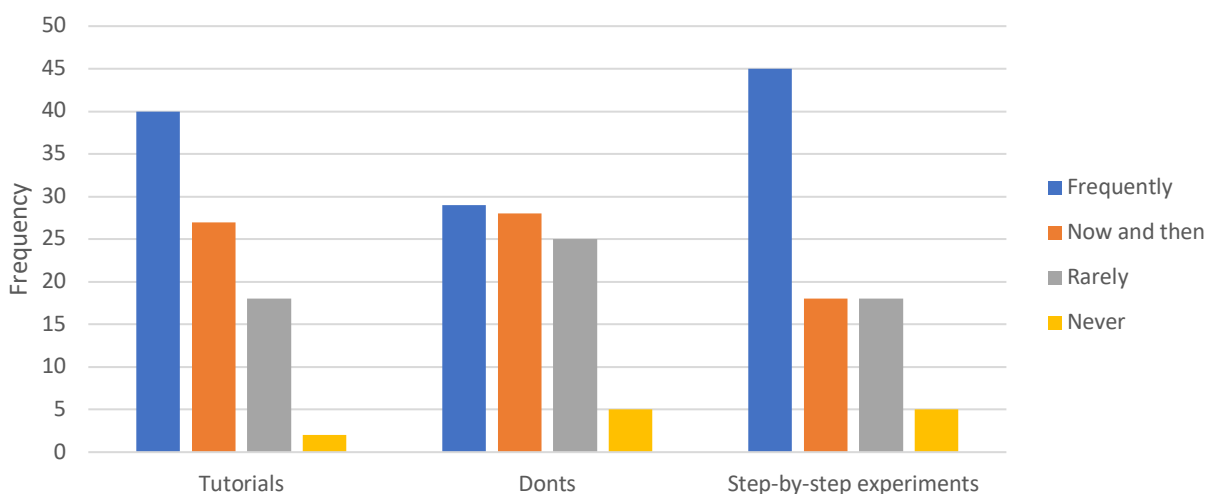
Figure 9.1. Frequency of answers on question "How often did you use the different video types?" (N = 87)
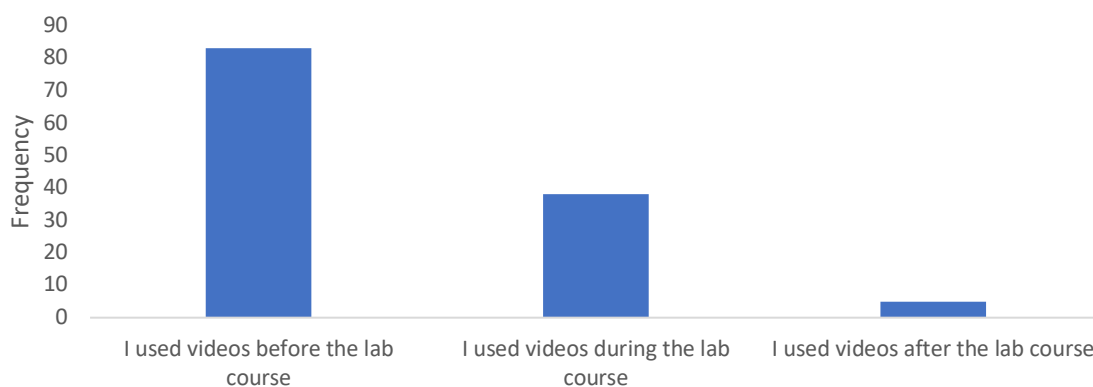
Figure 9.2. Frequency of answers on question "When did you use the videos?" (N = 87)
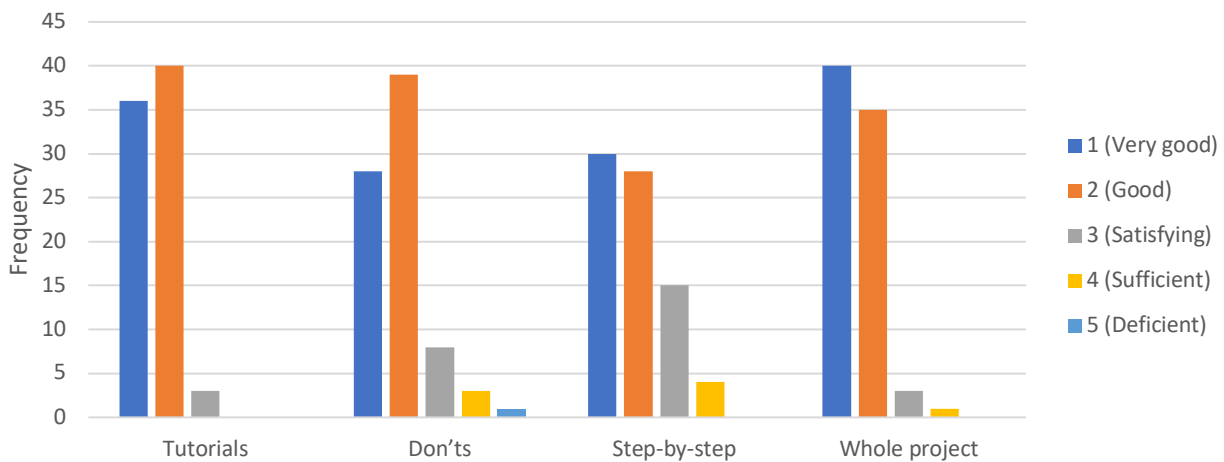
Figure 9.3. Frequency of answers on question "Please rate the overall impression of videos with school grades (1-6)." (*N* = 79)

Table 9.7. Frequency of rating on items related to the quality of the videos. (*N* = 79)

	Fully agree	Partly agree	Rather not agree	Do not agree
The content of the videos was very comprehensible	64	20	0	0
The technical realization of the videos (video/audio/cut) was inadequate.	2	3	30	49
All relevant steps were shown in the videos.	34	45	3	1
The videos were too long.	1	7	33	43
Access to the videos was very user-friendly.	58	23	2	1

9.3.3. Distribution Curves of Access Rates

The descriptive analysis of access rates to the video web pages shown in Fig. 2 of the main text can also be analyzed by calculating distribution curves for the total of the sample and the different subgroups (male/female, bachelor's degree/teacher's degree). Averages and standard deviations are presented in Table 9.8, the curves itself in Figure 9.4.

Table 9.8. Averages and standard deviations of the access rates to the 31 video web pages in the three investigated laboratory courses (*N* = 114).

	Total sample	Bachelor's degree students	Teacher's degree students	Female students	Male students
Average access rate	36.8	45.5	7.5	44.4	30.0
Standard deviation	36.2	36.5	11.2	41.0	29.6
n	114	88	26	54	60
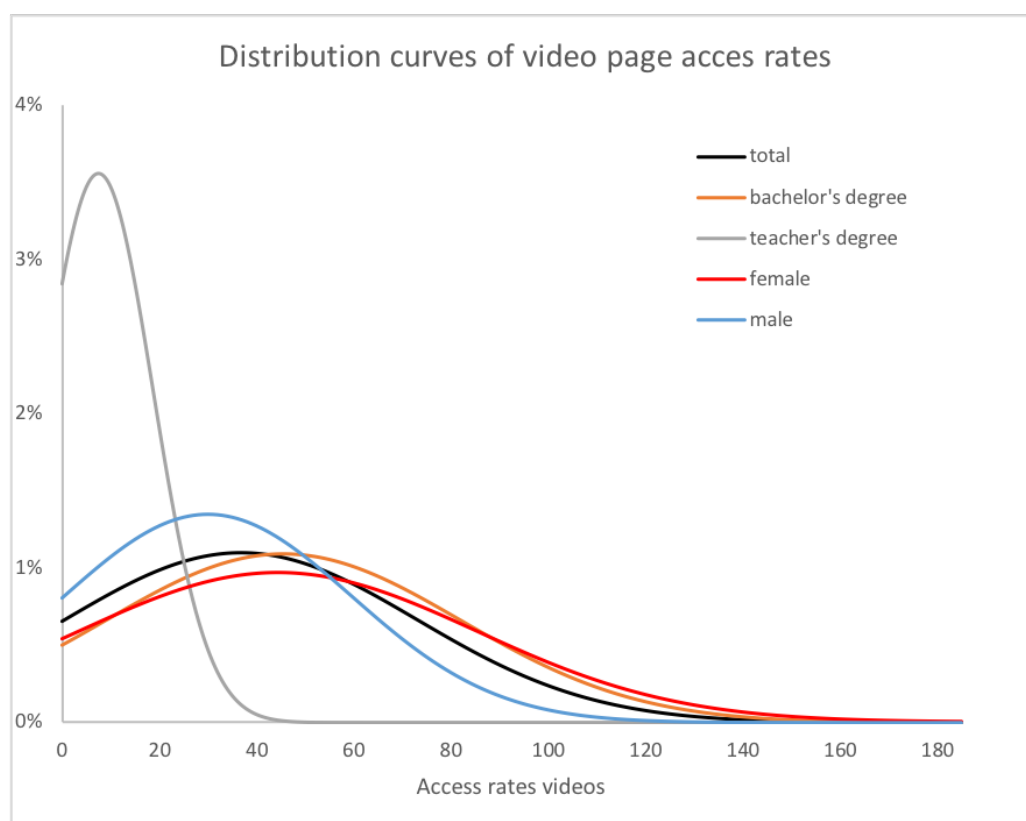
Figure 9.4. Distribution curves for the access rates to the 31 video web pages in the three investigated laboratory courses (*N* = 114) for the total sample and for the subgroups.

9.3.4.t-Test of Pre- and Post-Lab Measured Personality Traits

One aim of the study was to examine the influence of the lab course on personality traits. Therefore, a dependent t-test of the pre- and post-lab personality traits was performed (see **Table 9.9**). In order to identify the influence of the use of the online video library the same t-test was performed after grouping the students by their video watching behavior (see **Table 9.10**). Students that stated to use the whole library as well as the different videos types in average "often" or "sometimes" are considered as frequent video users, students stating "rarely" or "never" as sporadic video users.

Table 9.9. Results of the t-test of pre- and post-lab measurements of personality traits for the complete sample (N = 81).

	Paired Differences							
	Mean	Std. Deviation	Std. Error Mean	95% Confidence Interval of the Difference		*t*	*p*	Cohen's *d*
				Lower	Upper			
Intrinsic motivation for lab course	.001	.518	.058	-.113	.116	.021	.983	
Self-concept of ability	.236	.482	.054	.129	.342	4.398	.000	.490
Self-perception of conscientiousness	.056	.666	.074	.092	.203	.751	.455	

Table 9.10. Results of the t-test of pre- and post-lab measurements (for scales see Table 9.3 and Table 9.4) of personality traits for students having used the online video "often" or "sometimes" (*n* = 53).

	Mean	Std. Deviation	Std. Error Mean	95% Confidence Interval of the Difference		*t*	*p*	Cohen's *d*
Paired Differences								
				Lower	Upper			
Intrinsic motivation for lab course	-.032	.469	.064	-.161	.097	-.498	.621	
Self-concept of ability	.280	.481	.066	.147	.413	4.234	.000	.582
Self-perception of conscientiousness	-.099	.564	.077	-.254	.056	-1.279	.207	

Table 9.11. Results of the t-test of pre- and post-lab measurements (for scales see Table 9.3 and Table 9.4) of personality traits for students having used the online video library "barely" or "never" (*n* = 28).

	Mean	Std. Deviation	Std. Error Mean	95% Confidence Interval of the Difference		*t*	*p*	Cohen's *d*
Paired Differences								
				Lower	Upper			
Intrinsic motivation for lab course	.064	.604	.114	-.170	.298	.563	.578	
Self-concept of ability	.152	.481	.091	-.035	.338	1.669	.107	
Self-perception of conscientiousness	.348	.753	.142	.056	.640	2.448	.021	.462

9.3.5. Independent Sample t-Tests for Gender/Study Course

Table 9.12. Group statistics of video utilization (1 = often, 4 = never) of students by study course (*N* = 95).

	study course	*N*	Mean	Std. Deviation	Std. Error Mean
Video utilization	teachers' degree	21	2.845	.995	.217
	bachelor	74	1.706	.769	.089

Table 9.13. Results of the independent samples t-test of video utilization of students grouped by study course (*N* = 95).

		Levene's Test for Equality of Variances		t-test for Equality of Means		Sig. (2-tailed)	Mean Difference	Std. Error Difference	95% Confidence Interval of the Difference		Effect size
		F	Sig.	t	df	p			Lower	Upper	Cohen's d
Video utilization	Equal variances assumed	3.486	.065	5.599	93	.000	1.139	.203	.735	1.543	1.384
	Equal variances not assumed			4.850	27	.000	1.139	.235	.657	1.621	

Table 9.14. Group statistics of video utilization (1 = often, 4 = never) of students by gender (*N* = 72). The sample was restricted to bachelor students.

	sex	N	Mean	Std. Deviation	Std. Error Mean
Video utilization	female	34	1.353	.431	.074
	male	38	2.007	.857	.139

Table 9.15. Results of the independent samples t-test of video utilization of students grouped by gender (*N* = 72). The sample was restricted to bachelor students.

		Levene's Test for Equality of Variances		t-test for Equality of Means		Sig. (2-tailed)	Mean Diffe-rence	Std. Error Diffe-rence	95% Confidence Interval of the Difference		Effect size
		F	Sig.	t	df				Lower	Upper	Cohen's d
Video utilization	Equal variances assumed	15.89	.000	-4.013	70	.000	-.654	.163	-.979	-.329	0.947
	Equal variances not assumed			-4.150	55.89	.000	-.654	.158	-.969	-.338	

Table 9.16. Group statistics of chosen personality traits of students by gender (*N* = 72). The sample was restricted to bachelor students.

	sex	N	Mean	Std. Deviation	Std. Error Mean
Self-perception of conscientiousness pre lab course	female	37	1.881	.489	.080
	male	41	2.130	.590	.092
Self-perception of conscientiousness post lab course	female	34	1.931	.506	.087
	male	37	2.047	.523	.086
self-concept of ability pre lab course	female	37	2.451	.488	.080
	male	41	2.207	.570	.089
self-concept of ability post lab course	female	34	2.186	.480	.082
	male	38	2.048	.544	.088

Table 9.17. Results of the independent samples t-test of chosen personality traits of students of students grouped by gender (*N* = 72). The sample was restricted to bachelor students.

		Levene's Test for Equality of Variances		t-test for Equality of Means		Sig. (2-tailed)	Mean Differ-ence	Std. Error Differ-ence	95% Confidence Interval of the Difference		Effect size
		F	Sig.	t	df				Lower	Upper	Cohen's d
Self-perception of conscientious-ness pre lab course	Equal variances assumed	.810	.371	-2.021	76.00	.047	-.249	.123	-.495	-.004	.458
	Equal variances not assumed			-2.041	75.47	.045	-.249	.122	-.493	-.006	
Self-perception of conscientious-ness post lab course	Equal variances assumed	.029	.866	-.947	69.00	.347	-.116	.122	-.360	.128	
	Equal variances not assumed			-.949	68.81	.346	-.116	.122	-.360	.128	

		Levene's Test for Equality of Variances		t-test for Equality of Means					95% Confidence Interval of the Difference		Effect size
self-concept of ability pre lab course	Equal variances assumed	1.326	.253	2.012	76.00	.048	.243	.121	.002	.484	.456
	Equal variances not assumed			2.028	75.81	.046	.243	.120	.004	.482	
self-concept of ability post lab course	Equal variances assumed	.061	.806	1.136	70.00	.260	.138	.121	-.104	.380	
	Equal variances not assumed			1.144	69.99	.256	.138	.121	-.103	.379	

Table 9.18.Group statistics of motivation of students by study course (*N* = 95).

	Study course	N	Mean	Std. Deviation	Std. Error Mean
motivation lab course pre lab course	teacher's degree	11	2.509	.616	.186
	bachelor	80	1.766	.517	.058
motivation lab course post lab course	teacher's degree	21	2.591	.700	.153
	bachelor	74	1.789	.557	.065

Table 9.19. Results of the independent samples t-test of motivation of students by study course (*N* = 95).

		Levene's Test for Equality of Variances		t-test for Equality of Means					95% Confidence Interval of the Difference		Effect size
		F	Sig.	t	df	Sig. (2-tailed)	Mean Differ-ence	Std. Error Differ-ence	Lower	Upper	Cohen's d
motivation lab course pre lab	Equal variances assumed	.054	.816	4.367	89.00	.000	.743	.170	.405	1.081	1.404
	Equal variances not assumed			3.821	12.02	.002	.743	.194	.319	1.166	
motivation lab course post lab	Equal variances assumed	1.248	.267	5.488	93.00	.000	.801	.146	.511	1.091	1.357
	Equal variances not assumed			4.830	27.59	.000	.801	.166	.461	1.141	

9.3.6. Correlations of the Utilization of Videos

Table 9.20. Correlation of the average video utilization rate (1 = often, 4 = never) with personality traits of students. Due to the big influence of the academic goal correlations were recalculated for the group of bachelor's students only (right columns). ** Correlation is significant at the 0.01 level (2-tailed). * Correlation is significant at the 0.05 level (2-tailed).

	complete sample			bachelor's students only		
	Pearson Correlation r	p (2-tailed)	N	Pearson Correlation r	p (2-tailed)	N
academic goal (0=teacher's degree, 1=bachelor)	-.502**	<.001	95			
Sex (0=female, 1=male)	.166	.111	93	.432**	<.001	72
grade lecture organic chemistry	.183	.083	91	.331**	.005	70
motivation for lab course pre	.334**	.002	83	.235*	.044	74
self concept of ability pre	-.201	.069	83	-.351**	.002	74
self-perception of conscientiousness pre	.548**	<.001	83	.534**	<.001	74
use of videos in daily life	.341**	.002	83	.317**	.006	74
motivation for lab course post	.423**	<.001	95	.138	.241	74
self concept of ability post	.032	.757	95	-.164	.163	74
self-perception of conscientiousness post	.161	.122	93	.077	.516	73
Expectations of an online video library	.373**	.001	83	.377**	.001	74

9.3.7. Interdependency of Know-How Tests and Videos

To analyze the results of know-how tests answers of the questions (see **Table 9.5**) were marked with 1 point, if it was correct and complete, 0.5 points if the answer was correct but an aspect was missed and 0 points if the answer was wrong or no answer was given. Points were added up for each tutorial (recrystallization, extraction and distillation). Students also stated if they saw the tutorial or not in preparation of the reaction and were grouped accordingly in order to perform an independent t-test (see **Table 9.21** to **Table 9.26**).

Table 9.21. Group statistics of mean points in the know-how tests for "recrystallization" grouped by self-assessment on the utilization of tutorial "recrystallization".

recrystallization	n	Mean points know-how test (max. possible: 2 points)	Std. Deviation	Std. Error Mean
tutorial not watched	23	0.891	0.706	0.147
tutorial watched	31	1.694	0.527	0.095

Table 9.22. Independent samples t-test of mean points in the know-how tests for "recrystallization" grouped by self-assessment on the utilization of tutorial "recrystallization".

	Levene's Test		t-test for Equality of Means					95% Confidence Interval of the Difference		Effect size
	F	Sig.	t	df	Sig.	Mean Difference	Std. Error Difference	Lower	Upper	Cohen's d
Equal variances assumed	3.612	0.063	-4.783	52	.000	-0.802	0.167	-1.139	-0.466	1.316
Equal variances not assumed			-4.581	39.05	.000	-0.802	0.175	-1.156	-0.448	

Table 9.23. Group statistics of mean points in the know-how tests for "extraction" grouped by self-assessment on the utilization of tutorial "extraction".

extraction	n	Mean points know-how test (max. possible: 3 points)	Std. Deviation	Std. Error Mean
tutorial not watched	22	1.795	.971	.207
tutorial watched	31	2.468	.784	.141

Table 9.24. Independent samples t-test of mean points in the know-how tests for "extraction" grouped by self-assessment on the utilization of tutorial "extraction".

	Levene's Test		t-test for Equality of Means					95% Confidence Interval of the Difference		Effect size
	F	Sig.	t	df	Sig.	Mean Difference	Std. Error Difference	Lower	Upper	Cohen's d
Equal variances assumed	2.030	.160	-2.783	51	.008	-.672	.242	-1.157	-.187	0.776
Equal variances not assumed			-2.683	39.07	.011	-.672	.251	-1.179	-.166	

Table 9.25. Group statistics of mean points in the know-how tests for "distillation" grouped by self-assessment on the utilization of tutorial "distillation".

distillation	n	Mean points know-how test (max. possible: 4 points)	Std. Deviation	Std. Error Mean
tutorial not watched	17	1.735	1.359	.330
tutorial watched	28	3.071	.742	.140

Table 9.26. Independent samples t-test of mean points in the know-how tests for "distillation" grouped by self-assessment on the utilization of tutorial "distillation".

	Levene's Test		t-test for Equality of Means					95% Confidence Interval of the Difference		Effect size
	F	Sig.	t	df	Sig.	Mean Difference	Std. Error Difference	Lower	Upper	Cohen's d
Equal variances assumed	13.276	.001	-4.276	43	.000	-1.336	.312	-1.966	-.706	1.315
Equal variances not assumed			-3.730	21.88	.001	-1.336	.3582	-2.079	-.593	

9.3.8. Correlations with Student Grading on Different Video Types

Students were asked to grade their overall impression of the whole online library as well as of each video type individually on a scale from 1 (very good) to 6 (deficient) (see Table 9.30). Correlations of those grades with students' personality traits and sex (see Table 9.27) were calculated, the results for the gender was proved by independent sample t-tests (see Table S25 and S26).

Table 9.27. Pearson correlation of student's grading on the different video types and the video library as a whole with gender and selected pre-lab personality traits.

		sex	motivation lab course	Self-concept of ability	self-perception of conscientiousness
Tutorials	Pearson Correlation	.345**	.271*	-.037	.207
	Sig. (2-tailed)	.002	.021	.767	.079
	N	78	73	65	73
Don'ts	Pearson Correlation	.364**	.330**	-.042	.239*
	Sig. (2-tailed)	.001	.004	.739	.042
	N	78	73	65	73
Step-by-step	Pearson Correlation	.027	.389**	.076	.365**
	Sig. (2-tailed)	.814	.001	.549	.002
	N	76	71	64	71
Whole project	Pearson Correlation	.388**	.264*	-.018	.161
	Sig. (2-tailed)	.000	.024	.89	.175
	N	78	73	65	73

Table 9.28. Group statistics student's grading of the different video types and the video library as a whole grouped by gender.

	sex	*n*	Mean	Std. Deviation	Std. Error Mean
Grade Tutorials	male	38	1.790	.528	.086
	female	40	1.400	.545	.086
Grade Don'ts	male	38	2.180	.766	.124
	female	40	1.580	.813	.129
Grade Step-by-step	male	37	1.950	.743	.122
	female	39	1.900	1.021	.163
Grade whole project	male	38	1.820	.652	.106
	female	40	1.330	.526	.083

Table 9.29. Independent samples t-test of sex and student's grading of the different video types and the video library as a whole.

		Levene's Test for Equality of Variances		t-test for Equality of Means					95% Confidence Intervall of the Difference		
		F	*Sig.*	*t*	*df*	Sig. (2-tailed)	Mean Difference	Std. Error Difference	Lower	Upper	Cohen's *d*
Grade Tutorials	Equal variances assumed	1.974	.164	3.202	76	.002	.389	.122	.147	.632	.725
	Equal variances not assumed			3.204	75.971	.002	.389	.122	.147	.632	
Grade Don'ts	Equal variances assumed	1.852	.178	3.402	76	.001	.609	.179	.253	.966	.771
	Equal variances not assumed			3.408	75.996	.001	.609	.179	.253	.965	
Grade Step-by-step	Equal variances assumed	9.268	.003	.236	74	.814	.049	.206	-.361	.458	
	Equal variances not assumed			.238	69.452	.813	.049	.204	-.359	.456	
Grade whole project	Equal variances assumed	.046	.832	3.670	76	.000	.491	.134	.224	.757	.831
	Equal variances not assumed			3.650	71.104	.000	.491	.134	.223	.759	

9.3.9. Coding Scheme and Coded Data

Table 9.30. Raw results of survey part I: general information, utilization and grading of video library.

Case N°	Study course[a]	Sex[b]	Grade basic lecture organic chemistry[c]	Utilization of the video library[d]					Grading video library[e]			
				Views Tutorials	Views Don'ts	Views Step-by-Step	Views total	Mean views	Grade Tutorials	Grade Don'ts	Grade Step-by-Step	Grade total
1	1	1	2.0	2	2	1	1	1.50	2	1	3	2
2	1	0	2.7	2	2	1	1	1.50	1	1	1	1
3	1	1	3.7	3	3	4	3	3.25	2	2	3	1
4	1	0	3.3	1	1	1	1	1.00	1	1	1	1
5	1	1	1.0	2	3	2	1	2.00	1	4	1	2
6	1	1	3.0	2	3	3	3	2.75	2	3	2	2
7	1	1	4.0	2	2	2	2	2.00	2	2	2	2
8	1	0	1.3	1	1	1	1	1.00	2	1	1	1
9	1	0	2.0	1	1	1	1	1.00	1	1	2	1
10	1	1	2.7	3	3	2	2	2.50	2	2	2	2
11	1	1	1.7	1	2	1	1	1.25	1	2	2	1
12	1	1	2.0	1	2	2	1	1.50	1	1	2	1
13	1	0	2.7	2	2	1	1	1.50	1	1	1	1
14	1	0	1.3	1	2	2	1	1.50	1	2	2	1
15	1	1	2.7									
16	1	1	2.0	1	1	1	1	1.00	1	2	2	2
17	1	1		3	2	1	1	1.75	3	2	2	2
18	1	0	1.3	1	1		1	1.00	1	1	3	1
19	1	1	2.3	1	2	1	1	1.25	2	3	1	2
20	1	0	2.3	1	1	1	1	1.00	1	1	1	1
21	1	0	2.7	1	1	1	1	1.00	1	1	1	1
22	1	1	3.7									
23	1	1	1.7	2	2	1	1	1.50	1	2	2	1
24	1	0	1.7	1	1	1	1	1.00	1	1	1	1
25	1	1	3.7	4	3	3	2	3.00				
26	1	1	2.3	2	4	1	2	2.25	2	5	2	2
27	1	0	2.3	1	1	1	1	1.00	1	1	1	1
28	1		3.0	1	1	1	1	1.00	1	1	1	1
29	1	1	2.0	1	2	3	1	1.75	2	2		2
30	1	1	2.7	4	4	4	3	3.75				
31	1	1	2.3	3	3	3	1	2.50	1	1	2	1
32	1	1	2.3	1	1	1	1	1.00	2	2	2	4
33	1	0	1.3	1	1	1	1	1.00	1	1	1	1
34	1	1	3.0	1	1	1	1	1.00				
35	1	0	2.3									
36	1	0	3.0	1	2	1	1	1.25	1	2	1	1
37	1	0	2.7									
38	1	1	3.7	2	2	2	1	1.75	2	2	2	1
39	1	1	2.7	1	2	1	1	1.25	2	3	1	1
40	1	1	2.0	2	2	2	2	2.00	2	2	2	2
41	1			3	3	3	3	3.00				
42	1	0	2.0	1	1	2	1	1.25	2	1	2	2
43	1	0	3.3	2	2	3	1	2.00	2	2	3	1
44	1	0	4.0	1	1	1	1	1.00	1	1	1	1
45	1	1	2.7									
46	1	1	2.7	1	1	1	1	1.00				
47	1	0	3.3	1	1	3	1	1.50	1	4	3	1

				Utilization of the video library[d]					Grading video library[e]			
Case N°	Study course[a]	Sex[b]	Grade basic lecture organic chemistry[c]	Views Tutorials	Views Don'ts	Views Step-by-Step	Views total	Mean views	Grade Tutorials	Grade Don'ts	Grade Step-by-Step	Grade total
48	1	1	1.7	1	2	1	1	1.25	2	2	1	1
49	1	0	3.7	1	1	1	1	1.00	1	2	2	1
50	1	0	2.3	2	3	1	1	1.75	1	1	1	1
51	1	0	3.0	3	3	2	1	2.25	2	2	1	2
52	1	1	3.3	1	2	1	1	1.25	2	3	2	2
53	1	0	2.0	1	1	1	1	1.00	1	2	2	1
54	1	0	3.3									
55	1	0	2.7	1	1	1	1	1.00	1	1	1	1
56	1	1		2	1	1	1	1.25	2	1	2	1
57	1	1	4.0	2	2	1	1	1.50	2	2	2	3
58	1	0	1.7	1	1	1	1	1.00	2	2	4	2
59	1	1	1.3	2	2	1	1	1.50	2	2	2	2
60	1	0	2.7	3	3	3	2	2.75				
61	1	1	2.3	3	3	2	2	2.50	2	2	1	2
62	1	0		2	2	1	1	1.50	2	2	3	2
63	1	1	2.7	2	3	3	1	2.25	1	3	1	2
64	1	1	1.7	2	3	3	2	2.50	2	2	2	2
65	1	0	4.0	2	2	1	2	1.75	1	1	1	1
66	1	1	4.0	1	1	1	1	1.00	2	2	2	1
67	1	0	1.7	1	1	1	1	1.00	1	1	1	1
68	1	0	2.0	2	3	1	1	1.75	2	2	1	1
69	1	0	5.0	2	2	1	1	1.50	1	1	1	1
70	1	0	5.0	1	3	1	1	1.50	1	1	3	1
71	1	0	5.0	1	1	2	1	1.25	2	2	2	2
72	1	0	5.0	1	1	2	1	1.25	1	2	2	2
73	1	0	5.0	2	2	2	2	2.00	3	1	3	2
74	1	1	5.0	4	4	4	4	4.00				
75	1	1	5.0	3	4	3	2	3.00	1	2	1	2
76	1	1	5.0	1	3	1	1	1.50	2	2	1	2
77	1	1	5.0	3	3	2	2	2.50	2	2	3	2
78	1	1	5.0	3	3	3	2	2.75				
79	1	1	5.0	4	4	4	4	4.00				
80	1	0	5.0	1	2	1	1	1.25	1	1	1	1
81	0	1	2.7	4	4	4	4	4.00				
82	0	1	3.3	1	1	2	1	1.25	2	2	3	2
83	0	0	3.3	2	1	3	1	1.75	2	1	2	2
84	0	0	3.3	4	4	4	4	4.00				
85	0	0	4.0	3	3	3	2	2.75	1	1	3	2
86	0	1	3.3									
87	0	0	3.7	3	3	3	3	3.00				
88	0	0	1.3	1	2	2	1	1.50	2	2	3	2
89	0	0	1.7	4	4	4	4	4.00				
90	0	0	1.7									
91	0	0	3.0	3	4	4	3	3.50	2	3	3	1
92	0	1	2.3	3	3	3	3	3.00	3	2	3	2
93	0	1	4.0	2	3	2	2	2.25	2	2	3	2
94	0	0	3.0	2	3	3	3	2.75	2	4		3
95	0	1	4.0	1	1	1	1	1.00	1	2	1	1
96	0	0	2.7	4	4	4	4	4.00				
97	0	0	3.2	3	3	4	3	3.25				

Case N°	Study course[a]	Sex[b]	Grade basic lecture organic chemistry[c]	Utilization of the video library[d]					Grading video library[e]			
				Views Tutorials	Views Don'ts	Views Step-by-Step	Views total	Mean views	Grade Tutorials	Grade Don'ts	Grade Step-by-Step	Grade total
98	0	0	3.0	3	4	4	3	3.50	2	3	4	2
99	0	1	1.7	2	2	2	2	2.00	1	2	1	2
100	0	1	3.3	4	4	4	3	3.75	2	2	2	2
101	0	1	3.0	2	2	1	2	1.75	2	3	4	3
102	0	0	2.3	3	3	3	2	2.75	2	2	4	1
103	0	1	2.0	4	4	4	4	4.00				

[a]0=teacher's degree, 1=bachelor; [b]0=female, 1=male; [c] 1=very good, 2=good, 3=satisfying, 4=sufficient, 5=not passed; [d]1=often, 2=sometimes, 3=rarely, 4=never; [e]1=very good, 2=good, 3=satisfying, 4=sufficient, 5=poor, 6=insufficient

Table 9.31. Raw results of survey part II: pre- and post-laboratory survey of personality traits, motivation and use of videos in daily life (for instruments see Chapter 9.2.1).

Case N°	Pre-laboratory survey[f]				Post-laboratory survey[f]		
	Motivation for lab course	Self-concept of ability in experimen-tal chemical work	self-perception of conscientious-ness	Use of video tutorials in daily life	Motivation for lab course	Self-concept of ability in experimen-tal chemical work	self-perception of conscientious-ness
1	1.00	2.50	1.75	2.67	1.60	2.33	2.00
2	1.00	1.75	1.50	2.00	1.00	1.67	2.00
3	2.60	2.00	3.25	2.00	2.80	2.67	2.50
4	1.00	2.75	1.75	1.67	1.40	2.00	2.25
5	1.00	1.25	1.00	3.67	1.40	1.67	1.50
6	1.80	1.75	3.75	2.00	2.00	1.33	1.25
7	1.20	1.50	2.25	2.00	1.40	1.67	2.25
8	1.60	2.25	1.00	1.67	2.20	2.67	1.00
9	1.40	2.75	2.00	1.33	1.40	2.00	1.75
10	1.00	2.50	1.50	2.00	1.00	1.33	1.25
11	1.40	2.00	1.75	1.33	1.80	2.67	2.25
12	1.40	2.00	2.25	2.33	1.20	1.67	2.00
13	1.40	2.25	1.75	1.00	2.40	2.67	2.25
14	1.40	2.25	2.00	2.33	1.80	2.67	1.25
15	1.60	2.25	2.00	2.00			
16	1.60	2.50	2.25	2.00	1.60	2.00	2.25
17	1.60	2.75	2.00	3.00	1.40	3.00	2.25
18	2.20	3.00	1.75	2.33	2.00	2.33	3.00
19	2.00	3.50	2.75	2.67	1.60	3.00	2.50
20	1.40	2.33	1.00	1.00	1.60	2.33	2.00
21	1.20	2.50	2.00	2.00	1.40	2.00	2.00
22	2.00	2.50	2.25	1.33			
23	1.00	2.75	1.75	1.67	1.00	2.00	1.00
24	1.60	2.00	1.25	2.00	1.00	1.67	1.00
25	1.80	2.00	2.00	3.00	2.60	2.00	1.75
26	3.00	1.75	2.25	2.67	2.20	2.00	2.75
27	1.20	2.00	1.75	1.33	1.00	1.67	1.75
28	1.40	1.67	1.50	1.00	1.80	2.00	1.75
29	1.80	3.25	1.50	2.00	2.60	3.33	2.00
30	1.40	1.00	2.25	3.33	1.00	1.00	1.25
31	2.00	2.25	2.25	2.67	2.60	2.00	2.00
32	2.00	2.75	1.75	1.33	2.00	2.00	1.25
33	2.00	2.50	1.25	3.00	2.20	2.00	1.50
34	1.40	2.00	1.50	2.67	1.00	2.00	2.00
35	1.00	1.25	2.25	1.67			
36	1.80	2.25	1.00	2.00	1.20	1.67	1.25

Case N°	Pre-laboratory survey[f]				Post-laboratory survey[f]		
	Motivation for lab course	Self-concept of ability in experimen-tal chemical work	self-perception of conscientious-ness	Use of video tutorials in daily life	Motivation for lab course	Self-concept of ability in experimen-tal chemical work	self-perception of conscientious-ness
37	1.00	2.25	2.00	1.00			
38	1.80	1.75	2.50	1.33	1.40	1.67	2.00
39	1.60	3.00	1.25	1.00	1.60	2.00	2.25
40	1.80	1.50	3.00	2.33	2.60	2.00	3.25
41	2.60	2.50	2.50	3.00	1.00	2.00	2.00
42	3.00	2.00	1.50	3.67	2.00	2.00	2.00
43	2.40	2.25	2.25	3.33	2.00	2.33	2.00
44	2.00	3.50	1.75	1.33	1.60	2.33	1.50
45	1.40	2.00	1.75	1.33			
46	1.40	2.00	1.75	1.33	1.60	1.33	1.75
47	2.40	2.50	2.00	1.33	1.20	1.67	2.75
48	1.60	2.75	1.50	2.67	2.00	2.33	2.50
49	2.20	2.25	2.50	1.67	3.00	2.00	2.00
50	1.00	2.00	2.00	3.00	1.00	2.00	1.50
51	1.80	2.25	2.50	3.00	1.40	1.67	1.75
52	2.40	2.25	2.00	1.33	2.40	2.00	2.50
53	2.80	2.50	2.25	3.67	2.40	3.33	3.00
54	2.00	3.25	2.00	3.33			
55	1.60	2.25	1.00	3.67	1.40	2.00	1.50
56	1.40	1.75	1.75	1.33	2.80	2.67	2.75
57	2.00	2.00	2.50	2.33	1.60	1.33	2.00
58	2.00	3.00	1.75	1.33	1.60	3.00	1.75
59	1.80	2.00	2.00	2.67	1.80	1.50	2.00
60	2.20	2.75	2.75	1.67	1.60	1.67	2.25
61	2.60	1.50	1.25	2.00	2.40	2.00	2.50
62	2.00	2.00	2.00	1.67	2.00	2.00	2.25
63	1.00	3.00	2.25	3.00	1.00	2.67	2.00
64	1.40	2.50	2.25	3.00	1.80	2.33	2.25
65	1.60	3.00	2.50	2.00	1.60	2.67	2.25
66	2.20	3.25	2.33	1.00	1.80	2.33	1.75
67	2.00	2.33	1.50	2.33	2.00	2.00	2.00
68	1.80	2.75	2.25	1.33	1.80	2.33	2.00
69	1.80	2.00	2.25	1.33	1.80	2.00	1.67
70	1.50	2.50	2.67	2.00	2.20	1.67	1.25
71	2.60	3.25	2.75	1.33	2.20	2.00	2.25
72	2.20	3.50	1.75	1.33	2.40	3.33	2.25
73	2.20	2.00	1.75	1.33	1.20	2.00	2.00
74	2.20	2.00	3.25	2.33	1.20	2.33	2.75
75	1.60	2.00	3.00	2.00	2.00	2.00	2.25
76	1.60	1.75	1.50	2.33	1.80	1.00	1.00
77	2.00	3.00	2.75	1.33	2.20	2.67	2.50
78	2.60	2.00	2.50	3.67	3.00	2.00	
79	2.80	1.75	2.25	2.33	3.20	2.00	1.75
80	1.20	2.75	1.67	2.33	1.60	3.00	2.75
81					3.60	1.67	2.25
82	1.60	2.25	1.50	2.33	1.80	1.67	1.50
83					1.40	1.33	1.00
84					3.60	3.00	2.75
85	2.80	3.00	2.00	2.67	2.80	2.33	1.75
86	2.80	1.75	3.00	3.00			
87					2.60	1.67	2.25

Case N°	Pre-laboratory survey[f]				Post-laboratory survey[f]		
	Motivation for lab course	Self-concept of ability in experimen-tal chemical work	self-perception of conscientious-ness	Use of video tutorials in daily life	Motivation for lab course	Self-concept of ability in experimen-tal chemical work	self-perception of conscientious-ness
88	2.60	3.00	2.00	2.33	2.60	2.00	
89					2.80	2.33	2.25
90	1.20	1.67	2.00	1.33			
91					2.80	3.00	2.75
92					3.00	2.00	2.00
93	2.40	2.50	2.25	1.33	1.80	2.67	1.25
94	2.80	2.50	2.00	2.00	3.40	2.33	1.75
95	2.80	2.25	2.25	1.00	2.80	2.00	2.00
96					2.20	2.00	2.00
97	3.40	3.25	3.50	2.67	4.00	2.33	1.75
98	2.80	3.00	3.00	3.00	2.80	2.67	2.00
99	2.40	3.00	1.00	2.00	1.80	2.33	2.00
100					1.80	1.67	2.25
101					1.80	2.00	2.25
102					2.60	2.33	1.50
103					2.40	3.33	2.50

[f]coding: 1=high to 4=low

Table 9.32. Raw results of survey part III: number of correct answers in know-how-tests and statements if relevant tutorials were watched. Know-how tests were only performed in the bachelors' lab course.

Case N°	Correct answers know-how tests[g]			Video tutorial watched[h]		
	Recrystallization (2 questions)	Extraction (3 questions)	Distillation (4 questions)	Tutorial recrystallization	Tutorial extraction	Tutorial distillation
1	2.0	2.5	4.0	1	1	1
2	2.0	3.0	3.5	1	1	1
3						
4	0.0	1.5	2.5	0	0	1
5	1.0	3.0	3.0	0	0	1
6			4.0			0
7	2.0	3.0		1	0	
8	1.5	3.0	3.0	1	0	1
9	1.0	1.0	0.0	0	0	0
10	1.5	3.0	3.0	0		1
11	2.0	2.0	3.5	1	1	0
12	2.0	2.0	2.5	1	1	1
13	1.5	3.0	2.0	0		0
14	0.5	3.0	0.0	0	0	
15	0.0	0.0	0.0	0	0	0
16	0.5	3.0	4.0	0	1	1
17						
18	1.0	3.0	2.5	1	1	1
19						
20	2.0	2.5	3.5	1	1	1
21	2.0	2.0	3.5	1	1	1
22	2.0	3.0	3.5	1	1	1
23	2.0	3.0	3.5	1	1	1
24						
25	0.5			0		
26		1.5	3.0		1	1
27	0.5	3.0	3.5	1	1	1
28	1.0	2.5	2.5	1	1	1
29						

	Correct answers know-how tests[g]			Video tutorial watched[h]		
Case N°	Recrystallization (2 questions)	Extraction (3 questions)	Distillation (4 questions)	Tutorial recrystallization	Tutorial extraction	Tutorial distillation
30	0.5	2.0	3.0	0	0	0
31	2.0	3.0	2.5	1	1	1
32						
33						
34						
35	2.0			0		
36						
37	0.0	1.0	1.0	0	0	0
38	0.5	0.0	0.0	0	0	0
39	2.0	3.0	4.0	1	1	1
40	2.0	3.0	3.5	0	1	0
41						
42	2.0	3.0		1	1	
43	1.0	1.0	2.0	0	0	1
44	0.0	0.0	0.5	1	1	1
45	0.0	2.0	2.5	0	1	1
46	1.5	1.5		0	0	
47	2.0			1		
48	2.0	3.0	4.0	1	1	1
49	1.0	3.0	3.5	1	1	1
50	0.0			0		
51	1.5	1.0	3.0	1	1	1
52	2.0	3.0	3.0	1	1	1
53	0.5	1.0	1.0	0	0	0
54	1.5	3.0		1	1	
55	2.0	3.0	1.0	1	1	0
56	2.0	1.5	3.5	1	1	1
57	1.0	2.0	2.0	0	0	0
58	1.5	3.0		1	1	
59						
60	1.0	2.0	3.0	1	0	0
61	2.0			0		
62	2.0	1.0	2.5	1	0	0
63						
64	1.5	2.0			0	
65	2.0	3.0	0.0	0	1	0
66	2.0	2.0	3.0	1	1	1
67	2.0	3.0	3.5	1	1	1
68						
69		3.0	2.0		0	0
70	1.0			0		
71						
72						
73						
74		3.0			0	
75	2.0	2.5	1.0	1	0	0
76						
77						
78		1.0			0	
79		2.0			0	
80		1.0			1	

[g]1 point for correct answer, 0.5 for incomplete but correct answer, 0 for wrong answer; [h] 0=not watched, 1=watched

9.4. Analysis of Video Usage

Table 9.33. Complete list of videos in the online library with original and English title in order of descending views. View rates were gained from the website hosting the videos for the period from 16.10.17-16.03.2018. In this period the three lab courses happened at our university. No public access was granted to videos during this time. The last columns specifies the video type, for step-by-step videos the order of experiments in the pre-course resp. the compound preparation number is given.

Name	Translation	Views	Video Type
Rückflusskühler	Reflux condenser	359	tutorial
Destillation	Distillation	358	tutorial
Reinigen und Trocknen von Diethylether	Purification and drying of diethyl ether	216	step-by-step pre-course 1
Säulenchromatographie	Column chromatography	203	tutorial
Umkristallisation	Recrystallization	185	tutorial
Cyclohexylchlorid	Cyclohexyl chloride	179	step-by-step compound 1
(-)-Menthyltosylat	(-)-Menthyl tosylate	176	step-by-step compound 4
n-Butylphenylether	n-Butyl phenylether	173	step-by-step compound 3
Wasserdampfdestillation	Steam distillation	163	tutorial
Trocknen von Lösungen	Drying of solutions	158	tutorial
Benzyltriphenylphosphoniumbromid	Benzyltriphenylphosphonium bromide	156	step-by-step compound 2
(2R*,3S*)-Dibrombernsteinsäurediethylester	Diethyl (2R*,3S*)-dibromosuccinate	150	step-by-step compound 7
Racemattrennung 1-Phenylethylamin	Resolution of racemic 1-phenyl ethyl amine	149	step-by-step pre-course 7
Isolierung von (R)-(+)-Limonen	Isolation of (R)-(+)-limonene	141	step-by-step pre-course 8
Don'ts Rückflusskühler	Don'ts: reflux condenser	135	don'ts
1,1-Dichlor-2-phenylcyclopropan	1,1-Dichloro-2-phenylcyclopropane	132	step-by-step compound 9
Dünnschichtchromatographie	Thin layer chromatographie	131	tutorial
Soxhlet-Extraktion	Soxhlet Extraction	127	tutorial
Quenchen und Desaktivieren	Quenching and Deactivation	126	tutorial
Isolierung von Trimyristin	Isolation of trimyristin	124	step-by-step pre-course 5
Trennung 3-Stoffgemisch	Separation of a mixture of three compounds	123	step-by-step pre-course 6
Filtration	Filtration	123	tutorial
Extraktion (Scheidetrichter)	Extraction (separatory funnel)	121	tutorial
Isolierung von Eugenol und Derivatisierung	Isolation and derivatization of eugenol	119	step-by-step pre-course 9
Reinigung und Trocknen von Methanol	Purification and drying of methanol	119	step-by-step pre-course 2
Diels-Alder-Reaktion	Diels-Alder reaction	118	step-by-step compound 10
Don'ts Heizen und Kühlen	Don'ts: Heating and cooling	115	don'ts

Name	Translation	Views	Video Type
Don'ts Extraktion (Scheidetrichter)	Don'ts: Extraction (separatory funnel)	**114**	don'ts
Don'ts Filtration	Don'ts: Filtration	**114**	don'ts
Rotationsverdampfer	Rotary evaporator	**112**	tutorial
4-Methyl-4'-nitrobenzophenon	4-Methyl-4'-nitrobenzophenone	**104**	step-by-step compound 14
Fetten von Schliffen	Greasing of ground joints	**103**	tutorial
Reinigen und Trocknen von Aceton	Purification and drying of acetone	**101**	step-by-step pre-course 4
Reinigen und Trocknen von Methanol/Ethanol	Purification and drying of methanol/ethanol	**100**	step-by-step pre-course 3
Don'ts Destillation	Don'ts: Distillation	**97**	don'ts
Don'ts Säulenchromatographie	Don'ts: Column chromatography	**93**	don'ts
cis- und *trans*-Stilben	*cis*- and *trans*-stilbene	**92**	step-by-step compound 27
1-(*N*-Morpholino)cyclohexen	1-(*N*-Morpholino)cyclohexen	**88**	step-by-step compound 26
Wiegen und Pipettieren	Weighing and pipetting	**88**	tutorial
GC-MS Analytik Alkohole	GC-MS analysis of alcohols	**80**	step-by-step
Azeotrope Destillation (Wasserabscheider)	Azeotropic distillation	**80**	tutorial
1,3-Dinitrobenzol	1,3-Dinitrobenzene	**79**	step-by-step compound 12
Grignard-Reaktion	Grignard reaction	**78**	step-by-step compound 28
Don'ts Rotationsverdampfer	Don'ts: Rotary evaporator	**77**	don'ts
Don'ts Dünnschichtchromatographie	Don'ts: Thin layer chromatography	**77**	don'ts
Trocknen im Exsikkator	Drying in a desiccator	**61**	tutorial
Befüllen NMR-Röhrchen	Filling of NMR tubes	**58**	tutorial
1,5-Diphenyl-1,4-dien-3-on	1,5-Diphenyl-1,4-diene-3-one	**56**	step-by-step compound 24

Table 9.34. List of tutorials produced after the lab course.

Name	Translation	Video Type
Schmelzpunkt	Melting point	tutorial
Brechungsindex	Refraction index	tutorial
Massenspektrometrie	Mass spectrometry	tutorial
NMR: Messung	NMR: measurement	tutorial
NMR: Auswertung	NMR: analysis of spectra	tutorial
UV/Vis-Spektroskopie	UV/Vis-spectroscopy	tutorial
IR-Spektroskopie	IR spectroscopy	tutorial
Drehwinkel	Specific rotation	tutorial

9.5. Free Format Comments

In the following the free format comments are quoted uncorrected in their original form in German. They were grouped and assigned by categories. Comments in bold were quoted in a translated version in the main text.

Praise
Easy and user-friendly access to movies

- Der schnelle Zugriff im Labor
- mobile Version
- benutzerfreundliche Gestalltung;
- dass man die Videos auch auf dem Handy problemlos ansehen konnte.
- Benutzerfreundlich
- Einfache Bedienung

Design of the videos

- Knapp und kurz alles wichtige erklärt 2. verständlich 3. gut gestaltet
- gut produziert/geschnitten;kurz gehakten, spulen bei längeren phasen kurze prägnante Zusammenfassung
- Videos mit Stimme
- Auch Gestaltung und Machart waren sehr gut und hilfreich
- Übersichtlich gestaltet, ansprechende sehr lehrreiche Video
- Videos sind super gemacht und helfen sehr für die Vorbereitung

Profound explanations in videos

- Lob: guter Überblick, Zusammenfassend, Text, Video, Sprache,Moderation
- Die ruhige sachliche Erklärung
- sehr gut erklärt
- Hat vieles deutlich klarer gemacht

Clear presentation of videos

- Gute Übersichtliche Struktur
- Gut und klar strukturiert, man konnte Handgriffe nach denen man gesucht hat schnell finden
- Übersichtlich
- Die übersichtliche und anschauliche Darstellung
- Übersichtlich

Short duration of videos

- kurz und prägnant
- gute, informative Videos, nicht zu lang

General praise for video library:

- Unklarheiten klären
- generell gute Idee mit Videos da manche eher der visuelle Typ sind
- Lange gewünschter Schritt der LMU in Richtung Digitalisierung und Medien
- Mehr Videos für die ersten Präparate gut, da am Anfang unsicher
- Sehr viel Mühe, großes Angebot, sehr sinnvoll.
- Ganz gut
- Sehr Hilfreich!
- Die Videos sind super
- eine gute Idee, ich werde sie in Zukunft zur Vorbereitung verwenden
- mit, fühle ich mich vorbereitet
- Sehr gute Vorbereitung und nützliche Tipps
- Passt so!
- Sehr nice , soundtrack manchnmal zu funky
- Anschaulich erklärt,

- Ansonsten sehr hilfreich
- all good
- Sehr Hilfreich!
- Super
- Sehr hilfreich
- Videos sind Super
- alles gut
- Ich finde es für die Vorbereitung anschaulich mit den Videos zu arbeiten
- Tolle Videos

Praise for lab technique 'tutorials'

- Neue Arbeitstechniken erklärt (Aufbau, etc.)
- Arbeitsmethoden waren sehr gut und Verständlich erklärt
- Hilfreich, neue Methoden und Geräte kennenlernen
- sowie die Videos zu den Arbeitsmethoden, da man gerade am Anfang noch shr unsicher war
- **Einblicke in die Funktionsweise von Vorgängen/Methoden und Benutzung der Geräte**
- Tipps, wenn die kristallisation nicht funktioniert
- Einführung in die organisch-chemische Laboratoriumstechnik + Methoden (Lehrbuch ungleich Praxis)
- die Apparaturen werden anschaulich erklärt
- Hinweise zu Phasenlage (oben/unten) bei Extraktion

Praise for 'Don'ts' videos

- Unterhaltsam
- Dass die DONTS lustig gestalltet waren
- Lob: vor allem die donts sind hilfreicg und teilweise echt wichtig;
- **Die Videos machen das Lernen deutlich einfacher. Die Videos zu den DONTS weisen oft auf Dinge hin, an die man selbst nicht gedacht hätte, wodurch das Experimentieren schneller und effizienter verläuft**

Praise for 'Step-by-Step' videos

- Vorstellung von den Versuchen zu bekommen
- **Versuchsaufbau und Durchführung waren immer gut ersichtlich 2. Man konnte sich auch immer ein gutes Bild von einem Versuch machen (z.B. Farbe des Präparats)**
- Präparat Videos als Vorberietung; Vorkurs Videos
- Sehr genaue Versuchsbeschreibungen,
- Vorgehensweisen bei Präparaten-Farbe, Konsistenz der Reaktionsmischung-Frühzeitige Erkennung ob Reaktion (korrekt) abläuft;
- Im Vorraus sehen wie die Versuche gehen 2. Vorbereitung/Sicherheit
- Gute Vorbereitung um Vorstellung vom Ablauf zu gewinnen
- Es war gut, dass wichtige Details des Versuchsablaufes gezeigt wurden, die so im Skript nicht beschrieben waren
- Versuchsaufbauten anschauen, Vorstellungen des Versuchs bekommen, Tipps
- Die Vorkursvieos, da sie besonders ausführlich und und Schritt für Schritt Anleitungen waren,
- Für Protokolle und komplexe Verusche waren die Videos hilfreich
- Vor dem ersten Praktikumstag sind die Videos hilfreich um ein wenig zu verstehen, wie es funktioniert.
- Alle schritte wurden erklärt
- Verständlich erklärt, Schritt für Schritt
- Sehr deutlich und Schritt für Schritt, beantworten die aufkommenden Fragen

Criticism

All Videos (also 'step-by-step' videos) should provide voice-over

- Alle Videos sollten Ton haben
- Ton bei Präparatvideos/ alle Präparate
- Stimmen zu den Videos vervollständigen

- Immer mit Stimme anleiten, Bitte
- Alle Videos sollten Ton haben bzw eine kurze mündliche Erklärung liefern wie ein Versuch genau funktioniert
- vtl. teilweise Erklärungen
- Teilweise kein Ton.
- Alle Videos mit Ton.
- Überall Ton einfügen wäre gut
- Bitte alle Viedos mit Ton
- Ton hat gefehlt
- Fehlender Ton
- Kein Ton
- Verbesserung: in den Experiementen auch mit Sprache /Moderation arbeiten
- Versuchsvideos auch mit Stimme anleiten,

'Step-by-Step' videos for all experiments

- Für 7a war ein Video zu finden aber für 7b nicht
- Zu allen Präparaten Videos (Auch wenn es sich doppelt)
- Vielleicht für jede Versuchsdruchführung ein seperates Video (haben bei manchen Präparaten gefehlt)
- evtl für jedes Präparat ein Video
- Bei den späteren Präparatvideos: dass keinVideo 7b gedreht wurde, obwohl das Vorgehen teilweise unterschiedlich war
- Videos zu den fehlenden Präparaten nachliefern (siehe Verfolgung des Reaktionsfortschritts)
- Auch an den weiteren Versuchen Videos zur Verfügung stellen
- Noch mehr Videos zu Präparaten, dafür weniger Verlinkung zu "DONTs" bei späteren Präpararten
- Alle Präparate zur Verfügung stellen
- Zu allen Versuchen Videos
- Es fehlen noch Videos zu einigen Präparaten
- Eventuell zu allen Präparaten Videos drehen, damit man weiß, welche Farbe etwas haben soll usw.
- Videos für fast alle Präparate
- Zu jedem Verusch 1 Video

Videos should be sometimes slower/more detailed:

- Mehr Ausführlichkeit
- Etwas langsameres Tempo
- Manchmal geht der Versuchnzu schnell.
- Etwas langsamer, da man teilweise nicht so schnell mitlesen kann; ebtl mehr Sicherheitshinweise
- Bei manchen Versuchen fehlen entscheidende Details.
- Etwas unübersichtlich, bei Videos besser evtl. gesamten Versuch zeigen
- Zu schneller ablauf der Videos!
- Manchmal zu schnell vorgespult bei Versuchsaufbauten
- teilweise sehr knapp und zu wenige Dos/Donts
- manchmal zu schneller textwechsel
- Vielleicht etwas langsameres Tempo damit man dem Inhalt besser folgen kann
- Reaktionsgleichungen in den Videos wären sehr hilfreich
- Erklärung der Reaktionen: Was macht was?
- Kommentar bei den Arbeitsmethoden

Videos should be shorter:

- Videos kürzer

Videos should provide security information:

- mehr Sicherheitshinweise

- Mehr Sicherheitshinweise
- Worauf man im Verusch noch besonders achten sollte z.B. Giftigkeit von Stoffen

Specific Criticism on design of videos:

- Etwas mehr "Ernst" in den "DONts" (Soundeffekt oft nicht passend; gleiches gilt für Videoeffekt),
- Mit Musik unterlegen
- weniger Bild-/videoeffekte

Content of videos:

- oftmals wurden Szenen im Video gezeigt, die "anscheinend" falsch waren, bzw die wir anders machen sollten - aufpassen!!!
- Verbesserung: Die Assistenten meinten wir sollen die Schläuche an Rückflusskühler, anders herum anschließen damit das Wasser langsam wärmer werden kann und dann wenn es an heißesten ist sofort abgekühlt wird.
- Das Wasser beim Durchflusskühler wurde falsch angeschlossen

Videos for analytical methods/more lab techniques:

- An Moodle, Strukturierung, Anordnung; wie führt man NMR-Analysen durch, Schritt für Schritt mit Mestre Nova; Wie führt man GCMS aus?
- Mehr Arbeitsmethoden, wie abrotieren, Vakuumdestillieren (auch technisches, wie was muss ich einstellen)
- Tipps wie man mit Verunreinigungen (z.B. beim Umkristallisieren) oder anderen Problemen die für das Praktikum typisch sind umzugehen hat. (Teilweise in DONTs Videos enthalten)

Technical equipment:

- WLAN im Labor
- 2. am Anfang gab es Tablet für die Videos, dann nicht mehr?? 3. WLAN im Labor
- WLAN im Praktikumssaal
- Studenten sollten Laptop mit ins Labor bringen und während dem Experiment Dinge nachschauen.

Comments due to differences in-between bachelor course and teacher's degree course:

- Die Präparatvideos haben teilweise nicht 100% mit den Versuchen im Praktikum übereingestimmt. (LA)
- Die Methoden in den Videos sollen mit denen der Versuche übereinstimmen (LA)
- Videos haben nicht exakt zur Vorgabe im Praktikumsskript gepasst. (LA)
- Wäre gut, wenn der Assistent die Versuche kennt und auch tatäschlich da ist.
- Teilweise hat das Video zum Präparat nicht zum Versuch gepasst. (LA)

Miscellaneous:

- Sortierung der DO/DONTS
- Leider noch nicht ansehen können, da technische Defekte am eigenen Laptop
- Noch nicht die Videos sehen können, aufgrund technischer Probleme
- Es wäre hilfreich, alle videos noch unabhängig von den Versuchen aufgelistet zu haben, das Exsikatorvideo habe ich bspsw nicht gefunden
- Versuchsanleitungen müssen übersichtlicher warden

9.6. List of Common Statistical Parameters

α	Cronbach's alpha for reliability
d	Cohen's measure of effect size
df	degrees of freedom
F	F-ratio
n	number in subsample
N	total number in sample
p	probability <u>or</u> statistical significance
Sig.	significance
r	pearson correlation
$\tilde{s}^2$	variance
$\tilde{s}$, *SD*	standard deviation
t	test statistic

9.7. Supplementary References

[1]   a) B. Both, *SPSS-Skript für Einsteiger Version 1.2*, Johannes-Gutenberg Unviersität Mainz, **2016**; b) T. C. Stocker, I. Steinke, *Statistik: Grundlagen und Methodik*, De Gruyter, Oldenbourg, **2016**.

[2]   a) L. J. Cronbach, *Psychometrika* **1951**, *16*, 297-334; b) M. Tavakol, R. Dennick, *Int. J. Med. Educ.* **2011**, *2*, 53-55.

[3]   S. S. Sawilowsky, *J. Mod. Appl. Stat. Methods* **2009**, *8*, 597-599.

[4]   a) I. Glowinski, *Molekularbiologie als interessefördernde Lernumgebungen*, Christian-Albrechts-Universität zu Kiel (Kiel), **2007**; b) L. Satow, "Big-Five-Persönlichkeitstest (B5T): Test- und Skalendokumentation.", https://www.drsatow.de/tests/persoenlichkeitstest/, accessed at 25.11.2019, **2012**; c) M. Wilde, K. Bätz, A. Kovaleva, D. Urhahne, *Zeitschrift für Didaktik der Naturwissenschaften* **2009**, *15*, 31-45.

Abbreviations

Ac	acetyl	iProp	isopropanol
AIM	atoms in molecules	IR	infrared
Ar	aryl	KR	kinetic resolution
B3LYP	hybrid DFT method with *Becke*'s three-parameter exchange functional and *Lee-Yang-Parr*'s correlation functional	Me	methyl
		mp	melting point
bcp	bond critical point	NBO	natural bond orbital
BSSE	basis set superposition error	NCI	non-covalent interaction
Bu	butyl	NMR	nuclear magnetic resonance spectroscopy
calc.	calculated	Np	naphthyl
CBS	complete basis set extrapolation	Ph	phenyl
CCDC	Cambridge Crystallographic Data Centre	Phenant	phenanthryl
CCSD(T)	coupled cluster theory with single, double and perturbative triple excitations	Pyr	pyrenyl
		rt	room temperature
ced	cohesive energy density	SAPT	symmetry adapted perturbation theory
CIP	Cahn-Ingold-Prelog priorities	SdP	solvent dipolarity
conv.	conversion	SMD	continuum solvent model density
DCC	dicyclohexylcarbodiimid	SP	solvent polarizability
DCM	dichloromethane	SP	single point calculation
DED	dispersion energy donor	SPP	solvent polarity-polarizability
DFT	density functional theory	St.dev.	standard deviation
DINSCL	diisopropylnaphtylsilyl chloride	T	temperature
DLPNO	domain based local pair natural orbital	TBDMSCI	tert-butyldimethylsilyl chloride
DMAP	4-Dimethylaminopyridine	TCAP	9-azajulolidine
DMF	dimethyl formamid	TES	triethylsilane
DMPSCI	dimethylphenylsilyl chloride	THF	tetrahydrofuran
DMSO	Dimethyl sulfoxide	TIPSCI	triisopropylsilyl chloride
EDC	1-ethyl-3-(3-dimethylaminopropyl)carbodiimide	TLC	thin-layer chromatography
ee	enantiomeric excess	TMSCI	trimethylsilyl chloride
EI	electron ionization	TN*SCI	tris(5-chloro-6-methoxynaphthalen-2-yl)silyl chloride
eq	equivalent		
ESI	electrospray ionization	TNSCI	tris(2-naphthyl)silyl chloride
Et	ethyl	TPS	triphenylsilane
Et_2O	diethyl ether	TPSCI	triphenylsilyl chloride
EtOAc	ethyl acetate	TS	transition state
GC	gas chromatography	UV	ultraviolet light
Hex	hexane	UV/Vis	ultraviolet and visual light
HPLC	high-performance liquid chromatography		
HRMS	high resolution mass spectrometry		